MICHAL LEBL

Peptides

BUILDING BRIDGES: THE PROCEEDINGS OF THE
TWENTY-SECOND AMERICAN PEPTIDE SYMPOSIUM

22ND AMERICAN PEPTIDE SYMPOSIUM

JUNE 25-30, 2011

HARBOR ISLAND, SAN DIEGO

CALIFORNIA

Peptides: Building Bridges

Proceedings of the Twenty-Second American Peptide Symposium

Peptides:
Building Bridges

Proceedings of the Twenty-Second American Peptide Symposium

Peptides:

Building Bridges

Proceedings of the
Twenty-Second American Peptide Symposium
June 25 - 30, 2011, San Diego, CA, U.S.A.

Introduction

The American Peptide Society returned its Symposium to sunny San Diego following trips to Montreal, Quebec and Bloomington, Indiana. The theme of this 22nd Symposium was "Building Bridges" symbolizing the important role that peptide science currently plays in so many other disciplines. The program of this Symposium explored the potential impact of peptides in scientific fields that have yet to fully realize the utility of these wonderful molecules. The Symposium brought together investigators of varying backgrounds and fostered stimulating discussions, and hopefully catalyzed future multidisciplinary collaborations.

Young investigators are an important element of our Society and their enthusiasm was clearly displayed through the unexpected enrollment of over 200 students in the poster competition. Many of these students also participated in a new Symposium event: Rapid-Fire oral poster presentations (3 slides, 5 min each) held during the first two lunch breaks of the Symposium. In addition, the main program featured Bert Schram Young Investigator oral presentations, highlighting the work of several of our most promising young researchers in peptide science. We were pleased to be able to support the attendance of many of these young scientists through approximately $50,000 in travel grants. In addition, the Bert Schram foundation helped to support a round-table professional development luncheon followed by a stimulating presentation and discussion on the future of peptide science.

The scientific program for 2011 was filled with distinguished lectures delivered by some of the most prominent peptide scientists in the world. The symposium was opened with an unexpected distinguished lecture by Richard Houghten and closed with the chemistry and philosophy of Barry Sharpless. Keeping with the Symposium theme, Building Bridges, approximately 57 of the 78 speakers had not previously presented their work at the APS, and many were attending our conference for the first time in their career. The Symposium highlighted presentations from APS award winners, including Richard DiMarchi (Merrifield Award), Jeffery Kelly (Makineni Award), Victor Hruby (Goodman Award) and, for the first time at the APS Symposium, the two duVigneaud Award winners, Morten Meldal and Fernando Albericio. The final session of the symposium, Building Bridges, was dedicated to emerging areas not traditionally associated with the peptide field such as renewable biofuels and synthetic biology.

The meeting was held at the Sheraton Hotel and Marina on Harbor Island, which served as an outstanding venue to facilitate scientific interaction by mixing posters, exhibitors and social and professional networking. The opening reception was held on the hotel's front lawn overlooking the beautiful San Diego Harbor and the iconic Coronado Bay Bridge. Following San Diego APS tradition, the speakers' dinner was held at the Scripps Aquarium where attendees were treated to a beautiful sunset overlooking the shores of La Jolla. In between sessions, attendees enjoyed several beautiful pools, a picturesque harbor, baseball games, casino trips, excellent restaurants and prime views of an evening sailing regatta in San Diego Bay. The meeting was capped with the closing banquet that included dinner and dancing.

We are deeply indebted to numerous individuals who assisted in the organization, execution and funding of the meeting, including members of the Scientific Committee, Student Affairs Committee and Travel Award Committee. It was our pleasure and honor to have chaired this Symposium and with the best of luck to the organizers of the 2013 Symposium.

Joel Schneider
Co-chair

Philip Dawson
Co-Chair

Editor's Remarks

American Peptide Society used the same production team (scientific and technical editor) as in 2009. And again, manuscripts were accepted through the internet page, entered into the database which allowed creating indexes on the fly and simplified communication with authors. Processed manuscripts were available for proofing – helping us to correct blunders made by us and authors in the rush to deliver the book as soon as possible. The finalized book was available on the website for downloading 8 weeks after the symposium ended. The "real book" is available from "just in time" printing process at www.lulu.com. Due to the fact that the American Peptide Society is a nonprofit organization, there is no margin charged for the book, and all members can order it for production cost.

Our thanks go to all authors who delivered manuscripts of a high technical quality before the deadline. This time we had minimal number of authors trying to "squeeze in" three pages of text on two pages of manuscript, or modifying the template of the text file. Time to time we were amused by scientists leaving the parts of the original template text in their manuscripts, but in general, we received papers of reasonable quality. Due to the time constraints, we were not able to redo the graphical components of the manuscripts – graphs and illustrations – authors have to understand that some of the graphs looking good at the poster size are far from ideal for book page size. We believe that the quality of the figures and schemes is a part of the presentation skills of the authors and we let them show it.

In the past we were insisting on the delivery of only monochromatic graphics with large enough details (fonts). However, since only less than 5% of all distributed books were produced in paper form (95% of proceeding books from the last symposium were downloaded free by the public as pdf file), we believe that we can slightly relax this requirement. Downloaded file can be displayed in "zoomed" version allowing even details, not distinguishable in printed version due to its color or size, be clearly seen.

We hope to be able to produce the proceedings of the next symposia even faster than this volume. The ultimate goal is to deliver the proceedings during the symposium. It is actually achievable – the crude, unedited, version can be produced from manuscripts delivered (electronically) at the time of the symposium by our semi-automated process. The final, edited, version would be available several weeks after your return home. The requirement of delivery of your manuscript at the time of the symposium is not that draconic – it was done like that in the past when you had to deliver the hard copy of your paper.

We would like to hear your comments.

Roseann Story-Lebl
Technical Editor
rpstory@gmail.com

Michal Lebl
Scientific Editor
m@5z.com

Message from the President of the American Peptide Society

My term as President of the American Peptide Society (APS) is now complete, and I'd like to discuss where the Society stands today. The 22nd American Peptide Symposium was held June 25 - 30, 2011 at the Sheraton Hotel and Marina in San Diego, and was co-chaired by Phil Dawson and Joel Schneider. I congratulate Phil and Joel along with their staff and the organizing and program committees for a terrific meeting on the timely theme "Building Bridges."

The APS was proud to award at the Symposium the prestigious R. Bruce Merrifield, Vincent du Vigneaud, Murray Goodman Scientific Excellence & Mentorship, and the Rao Makineni Lecture Awards. The recipient of this year's Merrifield Award was Richard DiMarchi (Indiana University), the recipients of this year's two du Vigneaud Awards were Fernando Albericio (IRB Barcelona) and Morten Meldal (University of Copenhagen and Carlsberg Laboratory), and the recipient of the year's Goodman Award was Victor Hruby (University of Arizona). It is also a pleasure to recognize that Jeffery Kelly (The Scripps Research Institute) was chosen to present this year's Rao Makineni Lecture.

Registration for the American Peptide Symposium included a number of amenities such as complimentary lunches, complimentary social events, including the closing banquet, and participation in an NIH Proposal Writing Seminar. Additionally, if you wished to accept it, your registration included two years' complimentary membership in the APS. This included a print and electronic subscription to our Society's official journal, *Biopolymers (Peptide Science)*. The journal publishes both original articles and reviews covering all aspects of peptide science. The Editor-in-Chief is Joel Schneider. He welcomes your manuscript submissions. Members also have free access to the Society's continually evolving web site (www.americanpeptidesociety.org/) where the latest information on APS activities and developments in peptide science may be found. Free professional position and resume posting is offered at the site. Through the membership of the American Peptide Society in the Federation of American Societies for Experimental Biology (FASEB), our members have a strong voice advocating for support of biomedical research.

The Society is on excellent financial ground, and is further investing in the support of young scientists, the presentation of peptide science at large symposia, and the preservation of peptide science history. The APS has increased the visibility of its Awards. The APS has stepped forward to improve representation of peptide-based research on the Synthetic and Biological Chemistry B (SBC-B) Study Section within the Center for Scientific Review of the NIH. DeAnna Long is overseeing the (Herculean) digital conversion of the complete American Peptide Symposium Proceedings (1968-present). I am pleased to recognize David Lawrence and Marcey Waters from The University of North Carolina at Chapel Hill as co-organizers of the 23rd American Peptide Symposium, to be held in 2013.

Finally, I wish to thank outgoing Society Officers Robin Offord (Secretary) and Richard Houghton (Past President). Robin was invaluable for providing precise and thorough guidelines for APS actions, while maintaining exceptional humor throughout all of it, while Richard's insight allowed me to continue the stability previously achieved for the APS. A special thank you goes to Becci Totzke, Association Manager of the APS. Without her incredible assistance, I fear that I would have been hopelessly lost! It has been both a pleasure and an honor the serve as the APS President, and I welcome Ben Dunn as the next APS President.

Gregg B. Fields
Torrey Pines Institute for Molecular Studies

22ⁿᵈ AMERICAN PEPTIDE SYMPOSIUM

June 25-30, 2011
San Diego, California

Co-Chairs

Philip Dawson
Department of Chemistry
The Scripps Research Institute
La Jolla, CA 92037

Joel Schneider
National Institute of Health
Chemical Biology Lab
Frederick, MD 21702

The Scientific Committee

Christian Becker
Technical University of Munich
David Craik
University of Queensland
Richard DiMarchi
Indiana University
Gregg Fields
University of Texas Health Science Center
Jeffery Kelly
Scripps Research Institute
William Lubell
University of Montreal
Dek Woolfson
University of Bristol

The Student Affairs Committee

Jung-Mo Ahn, Co-chair
University of Texas at Dallas
Audrey Kelleman, Co-chair
Grace Davison Discovery Sciences/Synthetech
Bikash Manandhar
University of Texas, Dallas
Michael Giano
National Institute of Health
Elizabeth Girnys
University of Michigan
Wendy Hartsock
University of Colorado, Denver
Erica Haslach
University of Florida
Kaiulani Houston
University of North Carolina, Chapel Hill
Finith Jernigan
University of North Carolina, Chapel Hill
Timothy Reichart
The Scripps Research Institute

The Travel Award Committee

Bradley Nilsson, (Chair)
University of Rochester
 Carrie Haskell-Leuvano, Ph.D.,
University of Minnesota

List of 22nd American Peptide Symposium Sponsors

The 22nd American Peptide Symposium was made possible through the generous support of the following organizations:

Gold:

AMERICAN PEPTIDE COMPANY
Total Peptide Management ™

INNOVATIVE TECHNOLOGIES FOR PEPTIDE SYNTHESIS AND PURIFICATION
Biotage

IPSEN
Innovation for patient care

aappтec
advanced automated peptide protein technologies

CS
C S Bio Co.
People Who Know Peptides

PolyPeptide
GROUP

Silver:

CovX

FERRING
PHARMACEUTICALS

AILERON
THERAPEUTICS

Bronze:

BACHEM

CEM
Leaders in Microwave Peptide Synthesis

Ironwood

PEPTIDE SCIENCE EXPERTISE
MIDWEST BIO-TECH INCORPORATED

M
EMD MILLIPORE

Additional Sponsors:

Ambrx

NEW ENGLAND BioLabs Inc.

NEP
New England Peptide ™

novo nordisk

Roche

Protein Technologies, Inc.

RSP Amino Acids, LLC

List of 22nd American Peptide Symposium Exhibitors

aapptec
Advantar Laboratories, Inc.
AkzoNobel/Kromasil
Almac
American Peptide Company, Inc.
AnaSpec, Eurogentec Group
Aviv Biomedical, Inc.
Bacham Americas, Inc.
Biopeptek, Inc.
Bio-Synthesis, Inc.
Biotage
C.A.T. GmbH&Co Chromatographic und Analysentechnik KG
Cambridge Research Biochemicals
CEM Corporation
CMDBioscience
CPC Scientific Inc.
Creosalus
CS Bio Co.
EMD Millipore
FASEB MARC
GL Biochem (Shanghai) Ltd.
Hybio Pharmaceutical Co., Ltd.
Intavis, Inc.
IRIS Biotech GmbH
Neuland Laboratories, Inc.
New England Peptide LLC
Peptide Scientific Inc.
Peptide International, Inc.
Peptisyntha SA
Phenomenex, Inc.
PolyPeptide Group
Protein Technologies, Inc.
Rapp Polymere GmbH
Senn Chemicals
Sussex Research
Synthetech/Grace Davison Discovery Sciences
Tianjinj Nankai Hecheng Science & Technology Co. LTD
Wiley-Blackwell
YMC America, Inc.

The American Peptide Society

The American Peptide Society (APS), a nonprofit scientific and educational organization founded in 1990, provides a forum for advancing and promoting knowledge of the chemistry and biology of peptides. The approximately one thousand members of the Society come from North America and from more than thirty other countries throughout the world. Establishment of the American Peptide Society was a result of the rapid worldwide growth that has occurred in peptide-related research, and of the increasing interaction of peptide scientists with virtually all fields of science.

A major function of the Society is the biennial American Peptide Symposium. The Society also sponsors the Journal of Peptide Research and Biopolymers (Peptide Science), recommends awards to outstanding peptide scientists, works to foster the professional development of its student members, interacts and coordinates activities with other national and international scientific societies, sponsors travel awards to the American Peptide Symposium, and maintains a website at www.ampepsoc.org.

The American Peptide Society is administered by Officers and Councilors who are nominated and elected by members of the Society. The Officers are: President: Ben Dunn, University of Florida, President Elect: Robin Offord, Mintaka Foundation for Medical Research, Secretary: DeAnna Wiegandt-Long, Jefferson Community and Technical College, Treasurer: Pravin Kaumaya, The Ohio State University, Past President: Gregg B. Fields, Torrey Pines Institute for Molecular Studies. The councilors are: Maria Bednarek, MedImmune Ltd, Waleed Danho, Retired, Phil Dawson, Scripps Research Institute, Charles Deber, Hospital for Sick Kids, Carrie Haskell-Luevano, University of Minnesota, Emanuel Escher, Institute de Pharmacology, University of Sherbrooke, Michal Lebl, Illumina Inc., John Mayer, Eli Lilly and Co., Henry I. Mosberg, University of Michigan, Tom Muir, Rockefeller University, Laszlo Otvos, Temple University, Joel Schneider, National Institute of Health.

Membership in the American Peptide Society is open to scientists throughout the world who are engaged or interested in the chemistry or biology of peptides and small proteins. Categories of membership include General Member, Postdoc Member, Student Member, Emeritus Member and Honorary Member. For application forms or further information on the American Peptide Society, please visit the Society web site at www.americanpeptidesociety.org or contact Becci Totzke, Association Manager, P.O.Box 13796, Albuquerque, NM 87192, U.S.A., tel (505) 459-4808; fax (775) 667-5332; e-mail "APSmanager@americanpeptidesociety.org".

American Peptide Symposia

1st 1968 Saul Lande & Boris Weinstein Yale University, New Haven, CT
2nd 1970 F. Merlin Bumpus, Cleveland Clinic, Cleveland, OH
3rd 1972 Johannes Meienhofer, Children's Cancer Research Foundation, Boston, MA
4th 1975 Roderich Walter, The Rockefeller University, New York, NY
5th 1977 Murray Goodman, University of California-San Diego, San Diego, CA
6th 1979 Erhard Gross, Georgetown University, Washington, DC
7th 1981 Daniel H. Rich, University of Wisconsin-Madison, Madison, WI
8th 1983 Victor J. Hruby, University of Arizona, Tucson, AZ
9th 1985 Kenneth D. Kopple & Charles M. Deber University of Toronto, Ontario, Canada
10th 1987 Garland R. Marshall, Washington University, St. Louis, MO
11th 1989 Jean E. Rivier, University of California-San Diego, San Diego, CA
12th 1991 John A. Smith, Massachusetts Institute of Technology, Cambridge, MA
13th 1993 Robert S. Hodges, Edmonton Convention Center, Edmonton, Alberta, Canada
14th 1995 Pravin T.P. Kaumaya, The Ohio State University, Columbus, OH
15th 1997 James P. Tam, Nashville Convention Center, Nashville, TN
16th 1999 George Barany & Gregg B. Fields, Minneapolis Convention Center, Minneapolis, MN
17th 2001 Richard A. Houghten & Michal Lebl, Town and Country Resort Hotel, San Diego, CA
18th 2003 Michael Chorev & Tomi K. Sawyer, Marriott Copley Place, Boston, MA
19th 2005 Jeffery W. Kelly & Tom W. Muir Town and Country Resort, Hotel, San Diego, CA
20th 2007 Emanuel Escher & William D. Lubell, Palais des congres de Montreal, Quebec, Canada
21st 2009 Richard DiMarchi & Hank Mosberg, Indiana University, Bloomington, IN
22nd 2011 Philip Dawson & Joel Schneider, Sheraton San Diego Hotel and Marina, San Diego, CA

The Merrifield Award

(previously the Alan E. Pierce Award)

The Merrifield Award was endowed by Dr. Rao Makineni in 1997, in honor of R. Bruce Merrifield (1984 Nobel Prize in Chemistry), inventor of solid phase peptide synthesis. Previously, it was called the Alan E. Pierce Award and was sponsored by the Pierce Chemical Company from 1977-1995.

Richard DiMarchi

The American Peptide Society is very pleased to announce that Richard DiMarchi of Indiana University has been chosen to receive the R. Bruce Merrifield Award for 2011. DiMarchi is cited for "discovery, development and advances in the field of peptide-based medicines". This award was presented during the 22nd APS Symposium held in San Diego, California on June 25-30, 2011.

Richard DiMarchi has distinguished himself in pharmaceutical, academic, and biotechnology circles of scientific investigation. The majority of his career has been conducted while a scientist and executive at Lilly Research Laboratories. In 2003, he joined the Chemistry Department at Indiana University as a Cox Professor and Gill Chair in Biomolecular Sciences. Additionally, he has co-founded two start-up biotechnology companies. The first with Dr. Pete Schultz named Ambrx, and the second titled Marcadia with Dr. Gus Watanabe.

The most visible therapeutic contributions from DiMarchi's laboratory pertain to the field of endocrinology, and more specifically diabetes. He made vital contributions to the development and commercialization of some of the first rDNA-based medicines, specifically Humulin® and Humatrope®. He exceeded these successes by cleverly designing the first rDNA-derived human peptide analog approved as a medicine, Humalog®. This work was built upon an indepth understanding of diabetes care and the therapeutic deficiencies inherent to the native human insulin sequence. The design of this analog was inspired by the prior biosynthesis and biophysical characterization of human IGF-1. This biosynthesis was made possible by his development of selective chemical cleavage following tryptophan with preservation of integrity in the methionine and multiple cysteine residues. Through a subtle change in amino sequence of native insulin a LysPro insulin analog emerged as a much more precise drug for glucose control. This single molecule currently represents a life-saving daily therapy for more than a million patients. More importantly it established a precedent that has been replicated through other chemical modifications with protein drugs.

DiMarchi's early work demonstrated the ability to successfully immunize agricultural animals against viral challenge with virulent virus, without the utilization of carrier protein. The nature of the immune response as a function of chemical structure across multiple serotypes of FMOV was elucidated. Separately, the group explored methods in rapid parallel synthesis of peptide inhibitors. In 1991 his laboratory demonstrated the ability to identify a nanomolar peptide inhibitor of HIV protease within a highly heterogeneous, but defined peptide mixture. The structure-activity relationship contributed to the initial structure-based drug design program that eventually yielded Viracept®. Some of the first reports in characterization of leptin action in rodent models of diabetes and obesity emerged from his research collaborations. Additionally, the native hormone was stabilized for clinical development as a crystalline analog and its structure reported in Nature. This work provided a foundation for pharmacology currently ongoing at Ambrx with site-specific leptin analogs of sustained action, in combination with peptide-based therapeutics.

Throughout the decade of the 1990s, DiMarchi served as the executive leader as Lilly expanded its interests from insulin to a broader base of diabetes based medicine, and in particular skeletal diseases. The endocrine group at Lilly during his tenure was generally regarded as the most influential and successful in forging scientific direction in the pharmaceutical industry. Under his leadership, Forteo® (parathyroid hormone 1-34) and Evista® emerged as two drugs that have transformed the treatment of osteoporosis and advanced commercial research interests in diseases of women's health. Arguably, Forteo represents the best example of a regenerative medicine where functional bone is restored late in life to dramatically diminish the occurrence of bone fracture. It serves as a prime example of the miraculous medicinal properties possible in peptide based medicines.

Richard DiMarchi has been extremely active in advancing biotechnology in academic and commercial ventures, especially as it relates to macromolecules and in particular peptides, proteins and anti-sense. He has coauthored of more than one hundred scientific papers and an additional one hundred patents. He maintains international recognition in peptides, rDNA biosynthesis and endocrinology. At Lilly under his leadership the product development group successfully developed the commercial process for biosynthes is of Xigris®, one of the most molecular complex proteins produced. Its successful development against the disease of sepsis was viewed as a benchmark achievement in medical sciences. He has been a scientific advocate for RNA-based antisense drug candidates in collaboration with the Isis Corporation, where he currently serves a member of the board of directors.

His current work at Indiana University is likely to be the crowning achievement in an already distinguished career. His research group has discovered a set of incretin peptides that demonstrate unprecedented activity in preclinical *in vivo* models of diabetes and obesity. The central elements to success has been the chemistry to install within single peptides simultaneous agonism at related G-protein coupled receptors, and the counterintuitive discovery that glucagon and GIP agonism could synergize the proven efficacy of GLP-I in the treatment of the metabolic syndrome. A set of drug candidates differing in biochemical character have been pharmacologically assessed in rodents and primate disease models. They are independently being advanced clinically by three separate pharmaceutical companies.

Independent of the research at IU and Marcadia, DiMarchi has teamed with Dr. Peter Schultz to launch a company focused on chemical biotechnology, termed Ambrx. The simultaneous mutation of tRNAs and the synthetases that charge amino acids to them has demonstrated that amino acids previously restricted to synthetic approaches can be successfully prepared by rDNA biosynthetic methods. At Ambrx, DiMarchi served as part-time CEO, CSO and chair of the SAB as the core technology matured to commercial expression levels and several proteins advanced towards clinical study. A sustained-acting growth hormone is currently in Ph II clinical study. Structurally optimized versions of beta-IFN, FGF-21 and leptin are also in advanced study.

Richard DiMarchi has demonstrated scientific excellence in the laboratory, as an executive administrator, and a distinguished teacher. Dr. DiMarchi is the recipient of numerous awards including the 2005 AAPS Career Research Achievement Award in Biotechnology, the 2006 ACS Barnes Award for Leadership in Chemical Research Management, the 2006 ACS Esselen Award for Chemistry in the Service of Public Interest, the 2007 Carothers Award for Excellence in Polymer Sciences, and the 2009 Watanabe Award for Life Sciences Research. He is readily accessible to collaborators, students, and a passionate public speaker in support of biotechnology, diabetes, obesity and peptides. He has served on a number of scientific boards, most notably the national BIO organization, the American Peptide Society, Chairman of the Peptide Therapeutic Foundation, and co-chaired the 21st APS symposium.

2011 - Richard DiMarchi, Indiana University
2009 - Stephen Kent, University of Chicago
2007 - Isabella Karle, Naval Research Laboratory, D.C.
2005 - Richard A. Houghten Torrey Pines Institute for Molecular Studies
2003 - William F. DeGrado, University of Pennsylvania
2001 - Garland R. Marshall, Washington University Medical School
1999 - Daniel H. Rich, University of Wisconsin-Madison
1997 - Shumpei Sakakibara, Peptide Institute, Inc.
1995 - John M. Stewart, University of Colorado-Denver
1993 - Victor J. Hruby, University of Arizona
1991 - Daniel F. Veber, Merck Sharp & Dohme
1989 - Murray Goodman, University of California-San Diego
1987 - Choh Hao Li, University of California-San Francisco
1985 - Robert Schwyzer, Swiss Federal Institute of Technology
1983 - Ralph F. Hirschmann, Merck Sharp & Dohme
1981 - Klaus Hofmann, University of Pittsburgh, School of Medicine
1979 - Bruce Merrifield, The Rockefeller University
1977 - Miklos Bodansky, Case Western Reserve University

The Vincent du Vigneaud Award

Sponsored by BACHEM Inc.

Fernando Albericio

Fernando Albericio was born in Barcelona, Spain in 1953. He received his Ph.D. in Chemistry at the University of Barcelona, in 1981 under the supervision of Ernest Giralt. Following postdoctoral work with Victor A. Naljar at Tufts University (Boston), Jurphaas van Rietschoten at the Universite d'Aix Marseille (France), and George Barany at the University of Minnesota (1981-1984), he returned to Barcelona as Associate Professor. During the 1992-1994 period, he was Director of Peptide Research with Milligen/Biosearch at Boston. He rejoined the University of Barcelona, where he was promoted to Professor in 1995. Nowadays, he is holding a triple appointment as General Director of the Barcelona Science Park, Professor at the University of Barcelona, and Group Leader at the Barcelona Biomedical Research Institute.

Fernando's major research interests cover practically all aspects of peptide synthesis and combinatorial chemistry methodologies, as well as synthesis of peptides and small molecules with therapeutic activities. Thus, main programs in his research are devoted to the synthesis and structure-activity relationship studies of antitumoral compounds isolated from the sea.

Fernando has published over 500 papers, several review articles, more than forty patents, and co-author of the books, Chemical Approaches to the Synthesis of Peptides and Proteins and Solid-Phase Synthesis, A Practical Guide. He is currently editor of International Journal of Peptide Research and Therapeutics. He received the Leonidas Zervas award from the European Peptide Society in 1994. Recently, Fernando Albericio has been honored with a Doctorate Honoris Causa by the Universidad de Buenos Aires (Argentina).

Morten Meldal

Professor Morten Meldal has dedicated his scientific life to the development of novel methods, supports, instruments and chemical tools for the peptide scientist at large. Amongst the prominent new chemical reactions introduced in peptide chemistry by Meldal is "Click" chemistry and reactions. Meldal has introduced peptide based transition metal carbelle / phosphine catalysts and he has developed a vast array of assays and combinatorial techniques as tools in peptide chemistry and biology.

Meldal has headed synthesis at Carlsberg Laboratory in Copenhagen through twenty exciting years of research where he directed a Centre of Combinatorial Chemistry and Molecular Recognition. He was recently appointed Professor of Nano Science at the Nano Science Center of Copenhagen University. He has a PhD degree in Chemistry of Oligo saccharides from Technical University of Denmark. He did a Post-Doctoral stay in Cambridge with Dr. R.C. Sheppard at M. R. C. where he studied peptide synthesis. He has received many awards and is member or board member of several Danish and international scientific societies. He is on the editorial advisory board of major journals in the field. He cofounded Society of Combinatorial Sciences in 1999, which he is currently chairing. His research areas cover: sugar and oligosaccharide chemistry, combinatorial chemistry, "click" chemistry, polymer chemistry, organic synthesis, automation in synthesis, artificial receptors and enzymes, nano-assays, bio-molecular recognition, enzyme activity, cellular assays, molecular immunology, nano-scale MS and NMR, res in-encoding, catalysis and material sciences.

Meldal addressed the need for a solid phase for both peptide- and peptide-organic chemistry and for on-resin analysis for chemical biology and protein chemistry. He invented several PEG-based resins (i.e. PEGA, SPOCC, POEPOP, ULTRAMINE) unique in their amphipatic nature and investigated properties of these by physical methods.

In 2001, at the APS in San Diego, Meldal presented the highly cited Cu-catalyzed chemical "click" ligation (cycloaddition) of acetylenes and azides (CuAAC) currently widely used in peptide and protein conjugations, in polymers and in materials sciences. His group also showed this reaction to be completely orthogonal to most other chemistries.

The PEG-based resins have allowed Meldal to merge organic and peptide chemistry on solid support, as well demonstrated by a large range of novel methods based on the highly specific generation of N-acyl iminium ions involving backbone or side-chain amides to yield complex large heterocyclic systems from peptides upon intramolecular cascade reaction with C-, N-, O- and S-nucleophiles. Meldal also developed live cell on bead assays using the biocompatible PEG-resins and has shown that GPCR's can be screened using a fluorescent reporter gene assay in a conventional split mix format. Combinatorial libraries of heterocycles were generated and screened for GPCR active substances in cell-based on-bead screening using functionalized PEGA supports.

Pioneering the concept of organozymes, Meldal has created peptide-organic molecules that fold around transition metals and chelate these through phosphines, carbenes and heterocycles and act as enzyme like chiral catalysts on solid support. Similarly, he has developed peptide based cage like receptors that can recognize sugars in water. Otherwise inaccessible and sterically hindered, peptide oligomers were synthesized by Meldal using azide protection of the amines. The azido acids also facilitated orthogonal chemistries required for glycopeptide assembly. Meldal has developed chemistry for synthesis of all known types of N, O and C-linked glycopeptides and used these in the study of cancer related mucins.

Meldal has pioneered many technological developments and instruments for peptide synthesis, including a carousel amino acid delivery system and the first realtime on-resin spectrophotometric monitoring of peptide coupling. He developed the first multiple column synthesizer and instrumentation for assembly of split - mix libraries. He also developed many fluorescence based screening to study e. g. protease specificity and inhibition and this technique is currently active in a large effort to characterize the biological function of plant proteases. He developed combichem of peptides containing phosphinic acid as transition state analogs and identified nanomolar selective inhibitors for metallo-proteases. Recently Meldal has developed the first practical optical encoding technique for beaded solid supports for tracking chemical identity during synthesis and screening at high rate and with a large encoding potential, particularly in combinatorial chemistry.

2011 - Fernando Albericio, University of Barcelona
2011 - Morten Meldal Carlsberg Laboratory, Copenhagen
2010 - Phil Dawson, Scripps Research Institute
2010 - Reza Ghadiri, Scripps Research Institute
2008 - Jeffery W. Kelly, Scripps Research Institute
2008 - Tom W. Muir, Rockefeller University
2006 - Samuel H. Gellman, University of Wisconsin
2006 - Barbara Imperiali, Massachusetts Institute of Technology
2004 - Stephen B. H. Kent, University of Chicago
2004 - Dieter Seebach, Swiss Federal Institute of Technology, Zurich
2002 - Horst Kessler, Technical University of Munich
2002 - Robert Hodges, School of Medicine, University of Colorado
2000 - Charles M. Deber, University of Toronto
2000 - Richard A. Houghten, Torrey Pines Institute for Molecular Studies
1998 - Peter W. Schiller, Clinical Research Institute of Montreal
1998 - James A. Wells, Genentech, Inc
1996 - Arthur M. Felix, Hoffmann-La Roche, Inc.
1996 - Richard G. Hiskey, University of North Carolina
1994 - George Barany, University of Minnesota, Minneapolis
1994 - Garland R. Marshall, Washington University Medical School, St. Louis
1992 - Isabella L. Karle, Naval Research Laboratory
1992 - Wylie W. Vale, The Salk Institute for Biological Studies
1990 - Daniel H. Rich, University of Wisconsin-Madison
1990 - Jean E. Rivier, The Salk Institute for Biological Studies
1988 - William F. De Grado, DuPont Central Research
1988 - Tomi K. Sawyer, The Upjohn Company
1986 - Roger M. Freidinger, Merck Sharpe & Dohme
1986 - Michael Rosenblatt, Massachusetts General Hospital
1986 - James P. Tam, The Rockefeller University
1984 - Betty Sue Eipper, The Johns Hopkins University
1984 - Lila M. Gierasch, University of Delaware
1984 - Richard E. Mains, The Johns Hopkins University

The 2011 Makineni Lectureship

Endowed by PolyPeptide Laboratories and Murray and Zelda Goodman (2003)

Jeffery W. Kelly

Dr. Kelly received his Ph.D. in organic chemistry from the University of North Carolina at Chapel Hill (1986) and performed post-doctoral research at The Rockefeller University in the area of chemistry and biology. After rising through the ranks in the chemistry department at Texas A&M University he joined the Department of Chemistry at The Scripps Research Institute in 1997 as the Lita Annenberg Hazen Professor of Chemistry. He served as Dean of Graduate Studies and Vice President of Academic Affairs from 2000-2006 and is currently Chair of Molecular and Experimental Medicine at The Scripps Research Institute. His research focuses on the physical basis of protein folding, misfolding and aggregation and the influence of small molecules on these processes *in vivo*. Dr. Kelly and his research group have studied the synergy between the hydrophobic effect and backbone-backbone hydrogen bonding in β-sheet folding employing side-chain as well as amide-to-ester and amide-to-olefin backbone mutations. His laboratory is currently exploring the effects of glycosylation on the energetics of protein folding. His laboratory also studies the etiology of neurodegenerative diseases, including Alzheimer's disease, Parkinson's disease, and the familial gelsolin and transthyretin-based amyloidosis - publishing over 200 papers in this area to date. Two small molecules discovered by the Kelly laboratory are now being tested in placebo-controlled human clinical trials for the amelioration of peripheral neuropathy caused by amyloidosis. These small molecules selectively bind to the native state of transthyretin and serve as native state kinetic stabilizers- allowing scrutiny of the hypothesis that prevention of amyloidogenesis will ameliorate a neurodegenerative disease. One of these molecules has successfully completed a Phase II/III trial and is expected to receive FDA approval in 2011. The Kelly Laboratory has also made considerable progress in discerning the biochemical basis of Gaucher's disease, a loss of function misfolding disease. This mechanistic insight has been used to develop small molecule pharmacologic chaperones that could be useful in ameliorating this lysosomal storage disease. Another current focus of the Kelly group is to restore the protein homeostasis capacity that protects us from numerous diseases similar to those mentioned above when we are young utilizing "proteostasis regulators", small molecules that adapt stress responsive signaling pathways to restore normal cellular balance. They have demonstrated the efficacy of this approach in both gain- and loss-of-function diseases.

The Kelly group has also discovered functional amyloid structures in humans, revealing the fine line between pathology and physiology. Kelly has won numerous awards including the American Chemical Society Arthur C. Cope Scholar Award, The Peptide Society Vincent du Vigneaud Award and the Emil Thomas Kaiser Award, the State University of New York at Fredonia Alumni Distinguished Achievement Award, the Protein Society - Dupont Young Investigator Award, The Biophysical Society National Lecturer Award, the Texas A&M University Honors Program Teacher / Scholar Award, the Camille Dreyfus Teacher-Scholar Award, and the Searle Scholar Award, to name a few.

2011 - Jeffery W. Kelly, The Scripps Research Institute
2009 - William DeGrado, University of Pennyslvania
2007 - Ronald T. Raines, University of Wisconsin - Madison
2005 - Robin E. Offord, Centre Medical Universitaire, Switzerland
2003 - James P. Tam, Vanderbilt University

The 2011 Murray Goodman Scientific Excellence & Mentorship Award

The Goodman Award recognizes an individual who has demonstrated career-long research excellence in the field of peptide science. In addition, the selected individual should have been responsible for significant mentorship and training of students, post-doctoral fellows, and/or other co-workers. The Awards Committee may also take into account any important contributions to the peptide science community made by the candidate, for example through leadership in the American Peptide Society and/or its journals. Endowed by Zelda Goodman (2007).

Victor J. Hruby

Professor Victor J. Hruby is Regents Professor in the Department of Chemistry and Biochemistry at the University of Arizona. Dr. Hruby was born in Valley City. North Dakota and received his B.S. and M.S., with A. William Johnson, at the University of North Dakota. He then went to Cornell University where he received his Ph.D. with A. T. Blomquist, and then was an Instructor at Cornell University Medical College with Vincent duVigneaud, Nobel Laureate. He moved to the University of Arizona in 1968 as an Assistant Professor.

Professor Hruby's research has been primarily in the chemistry, conformation-biological activity relationships, and molecular mechanisms of information transduction and of molecular diseases associated with peptide hormones and neurotransmitters and their receptors that modulate health, disease and human behavior. Specific hormones and neurotransmitters of interest include the opioids, the melanotropins, CCK, glucagon, substance P, oxytocin and related compounds and receptors. Specific methods and approaches used in this research include: de novo design of biologically active peptides and peptidomimetics; asymmetric synthesis; design and asymmetric synthesis of novel amino acids; computational chemistry; conformational analysis using NMR, X-ray crystallography and other biophysical tools; combinatorial chemistry; conformation-biological activity relationships, especially as they relate to the design of conformationally and topographically constrained peptide, peptidomimetic and peptide mimetic hormone and neurotransmitter agonists and antagonists for exploring the chemical-physical basis for information transduction in biological systems; the design, synthesis and biological evaluation of peptide and peptide mimetic ligands that affect pain, addictions, feeding behaviors, pigmentation, sexual behavior and motivation, glucose homeostasis, cancer and other biological effects; the chemical-physical basis for behavior; the mechanisms of hormone and neurotransmitter action; peptide mimetic design; and the structure-function of G-protein coupled receptors.

The Hruby group also is developing new synthetic methodologies for the assembly of multimeric ligands for the detection and treatment of pain, cancer and other diseases; a new approach to design of ligands for disease states involving the concept of overlapping pharmacophores to address several receptors simultaneously in a single small molecular ligand for the treatment of neuropathic pain without tolerance or addiction and which cross the blood-brain-barrier; and a new biophysical method, plasmon waveguide resonance spectroscopy, which allows one for the first time to examine the structures, thermodynamics and kinetics of GPCRs and other integral membrane proteins on interactions with ligands, modulatory proteins, enzymes, parallel and perpendicular to the membrane bilayer independently. Professor Hruby has published over 1000 articles, reviews, chapters, commentaries and editorials and has over 25 patents and patent filings.

Victor Hruby has received numerous awards and honors, including a Guggenheim Fellowship (1984), the Alan E. Pierce Award (now the Merrifield Award) (1993), a Senior Humboldt Fellowship (1999-2000) and the American Chemical Society Arthur C. Cope Scholar Award (2009). He was awarded a Doctor of Science, Honoris Causa from the Free University of Brussels (1989) and was named Regents Professor at the University of Arizona (1989). Additional awards include the American Chemical Society Ralph F. Hirschmann Award (2002), The Jacob Javits Neuroscience Award (1987), the NIH MERIT Award (1988). Sommer Award (2003) and Arizona Innovator of the Year (2009).

2011 - Victor J. Hruby, University of Arizona
2009 - Charles M. Deber, University of Toronto, Hospital for Sick Children

Young Investigators' Competition

Oral Presentation Winners

Weichen Xu, University of North Carolina, Chapel Hill, A Correlation Between Src Kinase Activity and Prostate Cancer Cell Invasiveness as Revealed by Src Kinase Peptide Sensor and Capillary Electrophoresis

Bryan Meade, University of California, San Diego, Peptide Transduction Domain of Macromolecules: Tackling the siRNA Delivery Problem

Leah S. Cohen, City University of New York, Studies on Large Fragments of a G Protein-Coupled Receptor in Membrane Mimetic Media

Poster Competition

1st Place Winners

Jason Arsenault, SNARE Based Peptide Linking as an Efficient Strategy to Retarget Botulinum Neurotoxin's Enzymatic Domain to Specific Neurons Using Diverse Neuropeptides as Targeting Domains

Renee Roodbeen, Understanding Peptide-Protease Interactions: Rational Design of a Bicyclic Peptide as Protease Inhibitor

Fazel Shahbanpoor, Structural Minimization of the Neuropeptide, Relaxin-3, Confers Selectivity at Its Rxfp3 Receptor

Charles M. Rupert-Perez, A Collagen Peptide-Based Hydrogel for Cell Encapsulation

V.G. Nadeau, Pro-Gly Mutations in The Loop of a Eukaryotic Transmembrane Alpha-Helical Hairpin Peptide Convert It to a Beta-Hairpin

Liat Spasser, Total Chemical Synthesis of All di-Ubiquitin Chains

Kerry-Anne Perkins, Myristoylation of Protein Kinase C Beta II/Zeta Peptide Inhibitors, or Caveolin-1 Peptide Facilitates Rapid Attenuation of Phorbol 12-Myristate 13-Acetate

S. Chattopadhyay, Collagen Mimetic Peptides Enable Cutaneous Wound Assessment and Expedite Healing

2nd Place Winners

Graeme Kelly, Polymeric Combination Therapy Based on Host Defense Peptides Targeting Cancer Cells

Charles Robertson, Orally-Bioavailable Galanin Analogs with Analgesic Activities

F. Rechenmacher, First Coating of Titanium with αvβ3 or α5β1 Selective Peptidomimetics: Design, Synthesis and Biological Evaluation

Katelyn J. Nagy, Enhancement of Material Properties and Control of Degradation Through Utilization of Enantiomeric Peptide Hydrogels

A.A Beharry, Azobenzene Photo-Switches for Cellular Applications

John C. Shimko, Generation of a Fully Synthetic Modified Histone H3 Library

Todd M. Doran, Probing the Effect of Turn Nucleation on Amyloid Self-Assembly Using B-Turn Peptidomimetics

A. Elliott, Protein Hijack to Produce Cyclic Peptides

Contents

Adventures in Peptides and Science with Students! The Joys of Research

Victor J. Hruby

University of Arizona, Tucson, AZ, 85721, U.S.A.

Introduction

It is a great honor to receive the Murray Goodman Award for Scientific Excellence and Mentorship. I believe it is primarily a reflection of the tremendous scientific abilities, productivities, and accomplishments of my Graduate Students and Postdoctoral Associates both while in my laboratory and since. It also is tremendous to be associated in this way with Murray Goodman who was a good friend and colleague. He gave me much good advice in numerous aspects of my career. We also shared some important adventures as consultants for the United Nation's Development Program, and the in the development of the American Peptide Symposium and American Peptide Society.

It is very daunting to reflect on my life as a Professor and mentor, since I have had so many outstanding graduate students and postdoctoral associates including 20 Masters students, 65 Ph.D. students and over 90 Postdoctoral Associates, most of whom have published multiple papers with me. How can I summarize their tremendous efforts and accomplishments when associated with me and my laboratory? I have tried to solve this problem by simply illustrating how our thoughts and sciences have evolved on a few joint accomplishments we have had in the 42 plus years I have been a mentor. Hopefully they will illustrate my philosophy as a teacher and mentor (Figure 1).

1. Every person is unique; help them find their uniqueness.
2. Everyone needs to take ownership of their research. Make the most of your ideas.
3. Collaboration within the group and with our biological colleagues is encouraged and often necessary for excellence.
4. Good ideas and creativity can come from everyone, but generally by choosing to solve a difficult problem.
5. Failure is critical to success in research, so don't be afraid to fail. It is often the best road to success.
6. The best scientists are the hardest working scientists.
7. Have fun! Enjoy the moment!

Fig. 1. My philosophy of mentorship.

In so doing there is much I will not talk about including: 1) use of ^{2}H, ^{13}C, etc. NMR to examine peptide-protein interactions; 2) computational chemistry and peptide drug design; 3) asymmetric synthesis of novel amino acids and β-turn mimetics; 4) peptide synthesis; 5) oxytocin conformation-activity relationships; 6) development of combinatorial chemistry and the selectide process; 7) glucagon - development of pure antagonists, inverse agonists and multiple signaling pathways; 8) substance P, CCK, melanocyte concentrating hormone and other neurotransmitters; and 9) conversion of somatostatin to a highly selective mu opioid antagonist.

Results and Discussion

<u>Melanotropin Peptides and Mimetics, Melanocortin Receptors and Biological Activities.</u> Our initial efforts in studying the melanotropin peptides (α-MSH, β-MSH, γ-MSH) was to obtain an analogue of α-MSH that was more stable for *in vivo* studies. Based on chemical, biochemical and pharmacological studies done primarily by Tomi Sawyer in my lab and Chris Hewart in Mac Hadley's lab, we designed [Nle^4, D-Phe^7] α-MSH(NDP-α-MSH)(MT-I) which was highly potent, stable *in vivo* (hours vs minutes for α-MSH) and had extraordinary prolonged activity (days to weeks) [1,2]. Modeling building based on the Ramachandran plot led to the concept of a β-turn in the vicinity of the D-Phe^7 residue, and then to the concept of cyclization of a linear

peptide. c[Cys^4,Cys^{10}] α-MSH [3] was designed which also was a potent analog with high *in vivo* stability. Extensive structure-activity studies and NMR analysis by several graduate students and postdocs led Fahad Al-Obeidi to do extensive computational studies which led to the design of the truncated cyclic lactam analogue of α-MSH Ac-Nle^4-c[Asp^5, D-Phe^7, Lys^{10}]-α-MSH(4-10)-NH$_2$ (MT-II)[4,5]. These two peptides along with the first discovered melanocortin 3 receptor (MC3R) and melanocortin 4 receptor (MC4R) antagonist Ac-Nle^4-c[Asp^5, D-Nal(2')^7, Lys^{10}]α-MSH(4-10)-NH$_2$ (SHU-9119) [6] have been the cornerstone peptides for very extensive and exciting studies on the chemistry, biology, and medical applications by hundreds of academic and industrial laboratories worldwide. The discoveries in the 1990's as part of the human genome project, that there were 5 melanocortin receptors, four of which utilized the basic pharmacophore His-Phe-Arg-Trp [7] were transformational. These receptors were found to be involved in most of the key behaviors and biological process related to survival in animals including feeding behavior, sexual behavior, response to stress, pigmentation, fear-flight learning behavior, immune response, etc. It was also found that they were involved in numerous diseases including obesity anorexia, metabolic syndrome, pigmentary disorders, erectile dysfunction, cancer, premature labor and many others.

The continuing creative efforts of many students in my research group led to several critical contributions to this still exciting and ongoing area of research of which a few examples follow. Work of Shubh Sharma led to one of the first demonstrations that multivalent conjugated ligands could be used for the microscopic visualization and characterization of melanoma, of melanocortin receptor trafficking including patching, internalization, and recycling of these receptors [8]. Many biologists, endocrinologists, and physiologists were particularly interested in determining the underlying mechanism(s) of the prolonged actions of NDP- α-MSH(MT-I) and MT-II, and we provided numerous laboratories with the peptides and in some cases, the animals or tissues, for their studies. Though we were able to demonstrate that these were cAMP and Ca^{+2} dependent bioactivities, further insights into the mechanism of the prolonged bioactivity (as if the ligand had made a "constitutively active" receptor; a novel hypothesis) have not been forthcoming, and so with Carrie Haskell-Luevano, Lackmal Boteju and others in my research group we decided to see if we could determine the chemical (conformational and topographical structure) basis for this novel biological function. For this purpose, we turned to our concepts of topographic space as it relates to biological activity (for an earlier review see [9]). We first examined the use of the 4 isomers β-methyl-phenylalanine in the D-Phe^7 position since the D-Phe^7 residue was so critical to bioactivity, but no new insights were obtained. However, when we turned to use the 4 isomers of β-MeTrp [10] exciting new insights were obtained. All four isomers of β-MeTrp [(25,23) (2S,3R), (2R,3S) and (2R,3R)] were incorporated into MT-II in the 9 position (for Trp^9). Evaluation of prolonged bioactivity of all 4 diastereoisomers of MT-II demonstrated that the [(2R,3R)-β-MeTrp^9]-MT-II analogue was as prolonged acting as MT-II, the (2S,3S)-β-MeTrp derivative was intermediate and the other 2 isomers had no prolongation. Extensive NMR studies demonstrated that the [(2R,3R)-β-MeTrp^9]MT-II had unique topographic relationships for the 4 key pharmacophore side chain residues which could account for its prolonged biological activity [11].

From a biological/medical perspective, we were the first to demonstrate, in collaboration with Roger Cone, using the superagonist MT-II and the MC3R/MC4R antagonist SHU-9119, that a single dose of MT-II could dramatically reduce food intake in both normal mice and obese mice and the effect was completely reversible with the antagonist SHU-9119 [12]. Prolonged application of MT-II led to weight loss. In collaboration with our biological and medical colleagues, we have performed several clinical trials in humans on the biological effects of MT-I and MT-II. Among other findings, we demonstrated that MT-I (and later MT-II) led to pigmentation throughout the body without sun [13,14] and that this hormone-induced pigment could reduce U.V. radiation-induced DNA damage in humans. Equally exciting was the finding that MT-II, in a double blind, placebo controlled, clinical trial could lead to erectile function in men with non-organic erectile dysfunction [15] when given peripherally. These compounds may soon be in clinical medicine.

Conformational and Topographical Considerations in the Design of Novel Ligands for Pain and Addiction. Another area of research which has been of great interest to us for many years is that of pain and addiction, and many outstanding students and postdocs have made significant contributions in this area. Here we will discuss a few key discoveries along the way. The discovery that the peptide enkephalin (H-Tyr-Gly-Gly-Phe-Leu(Met)-OH) is the natural endogenous opioid in animals, opened a new era in pain research, as did the discovery of three

opioid receptors μ, δ, and κ. Since the non-peptide plant natural product, morphine (an alkaloid) was shown to be selective for the μ opioid receptor, the search for delta selective ligands has been a key aspect of opioid research. Our efforts were again based on conformational considerations which lead Hank Mosberg and Robin Hurst in my group, informed by our considerations of cyclic melanotropins to the design and synthesis of the cyclic, conformationally constrained 14-membered cyclic analogue of enkephalin c[D-Pen[2], D-Pen[5]] Enkepalin (Tyr-c[D-Pen-Gly-Phe-D-Pen] (DPDPE) which was a highly selective agonist for the delta opioid receptor [16] using penicillamine residues (β,β-dimethyl-cystine) as conformational constraints due to geminal dimethyl transannular effect in medium sized rings. Subsequently extensive NMR, computational and eventually X-ray crystal structure analysis of DPDPE established that DPDPE had similar conformation in aqueous and DMSO solutions and the crystal [e.g. 17]. However, still this left unknown the topographical requirement of the exocyclic Tyr[1] residue, a key pharmacophore for the opioid receptor. To examine this problem led Xinhua Qian, Ding Jiao, K.C. Russell and Mark Shenderovich in my group to the synthesis of all 4 isomers of [2S3S, 2S3R, 2R3S, 2R3R] β-methyl-3',5'-dimethyltyrosine (TMT) [18] which are highly biased in chi-1 conformation (g(-), g(+) or trans) depending upon the isomer. All 4 isomers were incorporated into DPDPE and their conformational and biological properties examined with the expectation that if the delta opioid receptor preferred a particular topography only one of four isomers would mimic DPDPE in its potency and selectivity. Indeed it was found that only the [2S,3R]TMT[1]-DPDPE analogue had both high affinity and high selectivity for the delta opioid receptor [19,20]. Interestingly, this same analogue turned out to be an antagonist at the mu opioid receptor albeit a weak antagonist. Though we tried to publish it all in a single paper in the J. Am. Chem. Soc. (synthesis, conformational analysis, biological properties), the JACS editor and a referee made us take out much of the biological data. Though we vigorously objected that this was an excellent example addressing how chemical thinking could explain biology, we did not prevail. The myopia of chemists, even chemical leaders, is unfortunate and has greatly limited progress in both chemistry and biology. In any case, with these results in hand with Mark Shenderovich, Subo Liao and Jose Alfaro-Lopez, we decided we could utilize these results to design *de novo* a non-peptide peptide mimetic of DPDPE. This involved conformational and topographic evaluation of key pharmacophores in 3D vector space in conjunction with analysis of simple organic templates as a possible scaffold for the key pharamacophore moieties. This led to the design of SL-3111 as shown in Figure 2 [21] which had binding and second messenger activity properties very similar to DPDPE but not as other similar piperazine analogues in the literature.

Fig. 2. De novo design of non-peptide mimetic of a δ-opioid agonist.

Recent New Directions in Peptide Structure Based Drug Design. Though we have had many other exciting adventures in peptide chemistry, biophysics, biology and medicine, I will end my brief discussion of the journey I have taken with my students in the past 40 plus years, with a brief outline of our more recent adventures that are still in progress and for which we are very excited.

In our view, current methods of drug design and development for many of our most prevalent diseases are inadequate or ill advised. Modern genomics, proteomics, etc. have demonstrated that many degenerative diseases result from multiple changes in the expressed genome. Thus we must re-examine our methods of drug design to address and eventually cure

the disease state. In most cases, our analyses indicate that ligands with multiple bioactivities are needed.

In this regard, our efforts to address the problem of prolonged and neuropathic pain for which medications for acute pain such as morphine are either relatively ineffective, or actually counter indicated are very relevant. These pain states involve up regulation of a number of stimulatory neuropeptides and their receptors in pain pathways. Thus we have suggested [e.g. 22] that drug design for these pain states should require design and development of multivalent ligands. To address this hypothesis, a number of design approaches are possible including: design of multivalent ligands with overlapping pharmacophores; adjacent pharmacophores; or template separated pharmacophores for the various receptors. In our many studies to date, we have designed bifunctional ligand [e.g. 23], trifunctional [e.g. 24,25] and tetrafunctional ligands [e.g 26] and thus far have obtained a number of ligands that have unique biological profiles against pain states in which opiates and other current drugs for pain have minimal or no efficacy, using standard doses, and with little or no toxicity [e.g. 27]. Some of these peptides and peptidomimetics are stable against proteolytic breakdown and can cross the blood-brain barrier. We are vigorously pursuing these compounds or enhanced analogues toward clinical trials.

Another major new area of research is toward the detection and treatment of cancer utilizing multivalency. Since cancer involves major changes in the expressed genome, our major goal is to develop a scaffold which can have multivalent ligands that will allow the synthetic construct to distinguish normal from cancer cells [e.g. 28,29]. Both heteromultivalent and homomultivalent ligands may turn out to be useful, though it seems that heteromultivalency will be the most likely to be successful *in vivo*.

Finally, we have been developing ligands that can interact with allosteric sites on G Protein Coupled Receptors (GPCRs). It has been postulated that development of such ligands (instead of orthosteric ligands) should have greater selectivity of biological activity and fewer side effects. We have several very good leads especially for the melanocortin receptors [e.g. 30] and we plan to pursue these vigorously into the future.

Acknowledgments

References

1. Sawyer, T.K., et al. *Proc. Natl. Acad. Sci. U.S.A.* **77**, 5754 (1980).
2. Hadley, M.E., et al. *Science* **213**, 1025 (1981).
3. Sawyer, T.K., et al. *Proc. Natl. Acad. Sci. U.S.A.* **79**, 175 (1982).
4. Al-Obeidi, F., Hadley, M.E., Pettitt, R.M., Hruby, V.J. *J. Am. Chem. Soc.* **111**, 3413 (1989).
5. Al-Obeidi, F., et al. *J. Med. Chem.* **32**, 2555 (1989).
6. Hruby, V.J., et al. *J. Med. Chem.* **38**, 3454 (1995).
7. Hruby, V.J., et al. *J. Med. Chem.* **30**, 2126 (1987).
8. Sharma, S.D., et al. *Proc. Natl. Acad. Sci. U.S.A.* **93**, 13715 (1996).
9. Hruby, V.J., Al-Obeidi, F., Kazmierski, W.M. *Biochem. J.* **268**, 249 (1990).
10. Boteju, L., et al. *Tetrahedron* **50,** 2391 (1997).
11. Haskell-Luevano, C., et al. *J. Med. Chem.* **38**, 4720 (1995).

12. Fan, W., et al. *Nature* **384**, 165 (1997).
13. Levine, N., et al. *J. Am. Med. Assoc*. **266**, 2730 (1991).
14. Hadley, M.E., et al. *Ann. N.Y. Acad. Sci.* **680**, 424 (1993).
15. Wessells, H., et al. *J. Urology* **160,** 389 (1998).
16. Mosberg, H.I., et al. *Proc. Natl. Acad. Sci. U.S.A.* **80,** 587 (1983).
17. Flippen-Anderson, J.L., et al. *J. Am. Chem. Soc*. **116,** 7523 (1994).
18. Qian, X., Russell, K.C., Boteju, L.W., Hruby, V.J. *Tetrahedron* **51**, 1033 (1995).
19. Qian, X., et al. *J. Am. Chem. Soc.* **118,** 7280 (1996).
20. Bilsky, E.D., et al. *J. Pharm. Exp. Therap*. **293**, 151, (2000).
21. Liao, S., et al. *J. Med. Chem.* **41,** 4767 (1998).
22. Hruby, V.J., et al. *Am. Assoc. Pharm. Sci. J.* **8**, E450-E460 (2006).
23. Lee, Y.S., et al. *J. Med Chem.* **54**, 382 (2011).
24. Hruby, V.J., et al. *Life Sciences* **73**, 699 (2003).
25. Yamamoto, T., et al. *J. Med. Chem*. **50,** 2779 (2007).
26. Lee, Y.S., et al. *Bioorg. Med. Chem. Letters* **51,** 748 (2010).
27. Largent-Milnes, T., et al. *Brit. J. Pharmacol*. **161**, 986 (2010).
28. Gillies, R.J., Hruby, V.J. *Expert Opin. Ther. Targets* **7** 137 (2003).
29. Vagner, J., et al. *Angew. Chem. Int. Ed*. **47**, 1685 (2008).
30. Cain, J.P., et al. *Bioorg. Med. Chem. Letters* **16**, 5462 (2006).

Nano-Particle-Peptide-Synthesis (NPPS): A Novel Dimension for Merrifield Synthesis and Biological Applications

Raz Khandadash, Victoria Machtey, and Gerardo Byk

Laboratory of Nano-Biotechnology, Department of Chemistry, Bar Ilan University, Ramat Gan-52900, Israel

Introduction

Functionalizing nano-hydrogels with biological signals is critical for many applications ranging from cell sensing to drug delivery. While most synthetic monomers allow creating and engineering gels with carefully tuned structures and desired matrix properties, synthetic bio-compatible polymers lack any biologically recognized functionality, and at best, facilitate non-specific interactions that can be exploited with limited control. Thus, there is a great deal of interest in the development of strategies to tether biological signals or therapeutic molecules to nanometric hydrogel systems. Although many of the available nano-hydrogels are cross-linked, most of them contain highly degradable functional groups such as alkyl-esters [1]. They cannot be easily modified on their surfaces using multistep organic reactions. The currently available methods for nanoparticle modifications include so far conjugation with a single molecule such as protein, antibody, or enzyme, via a single click reaction followed by dialysis or ultra-centrifugation for removal of reagents. In the context of our efforts for synthesizing substituted nanoparticles for live cells applications, we have designed and synthesized cross-linked nanoparticle hydrogels (NPHG's) that can be functionalized with biological signaling molecules by a novel Merrifield multistep reaction approach suitable for nanometric particles. The process has been automated using a multiple organic synthesis robot for parallel synthesis bringing about a novel dimension to Merrifield synthesis where the synthesized peptides remain linked to the nanoparticles for biological applications. We called the approach NPPS, Nano-Particle-Peptide-Synthesis.

Results and Discussion

Cross-linked monodispersed PEG nanohydrogels of different sizes were obtained by free radical dispersion polymerization using mixtures containing low molecular weight PEG-diamine substituted with mono and diacrylamide and N-isopropylacrylamide (NIPAAM) that nucleates growth for the polymerization and formation of the nanospheres thanks to its low critical solution temperature (LCST) [1]. Thus, NPHG's sized 20, 50, 80, 100, 130, 250, 300 nm were obtained. In order to allow the Merrifield synthesis, nanohydrogels were embedded into magnetite and magnetic susceptibility was used for repeated reactions and washings. Briefly, magnetite was generated as previously shown [2] but in the presence of the NPHG's that were thus embedded into the magnetic matrix. XRD and TGA analyses of magnetite and magnetite-embedded NPHG's demonstrated the embedment of the particles (see Figure 1, left panel).
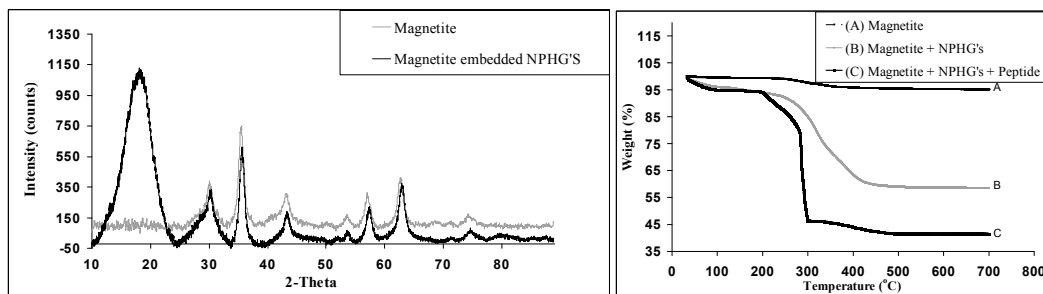
Fig. 1. Left panel: XRD analysis of magnetite (grey) and magnetite-embedded NPHG's (black). Right panel: Thermo-gravimetric analysis of magnetite (A), magnetite embedded NPHG's(B) and magnetite embedded NPHG's after peptide synthesis (C).

As proof of feasibility, we have synthesized a nuclear localization sequence (NLS) peptide which is composed of the sequence PKKKRKV [3]. This and similar peptides have been shown to penetrate into cells and localize in the nuclei. The cell penetration process can be observed if the synthesized NLS-modified NPHG's include a fluorescent label that allows intracellular tracking after incubation with cells using microscopy. An Advanced ChemTech 496MOS robot was adapted to the NPPS by placing cylindrical magnets (N50) on both sides of each reaction well so that the magnetic matrix adheres to the walls of the reaction well permitting the contact of solvents and reagents with the matrix and appropriate evacuation of solvents/reagents through the filter (see Figure 2).
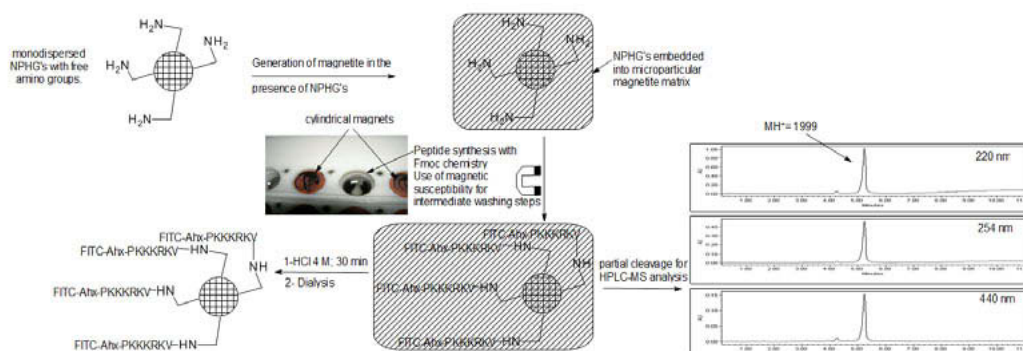
Fig. 2. Nanoparticle peptide synthesis of FITC-Ahx-KKKRKV nuclear localization sequence.

Peptides were synthesized using classical Fmoc chemistry with coupling reagent BOP/HOBT. At the N-terminal position an amino-hexanoyl (Ahx) spacer was placed and reacted with FITC to give the final labeled NLS-NPHG's. The linker HMBA allowed partial cleavage of the peptide by hydrolysis of the ester bond for HPLC-MS analysis of the fully protected peptide. The product was compared to the crude obtained using the same chemistry but on conventional solid supports and was of high quality (see Figure 2). Thermo-gravimetric analysis of the magnetite embedded NPHG's with the peptide disclosed a substantially different pattern than that observed for magnetite or magnetite embedded unmodified NPHG's (see Figure 1, right panel). Finally the FITC-NLS-NPHG's were recovered from the matrix after treatment with HCl for 30 minutes followed by addition of EDTA, neutralization to pH=7 and single dialysis process to remove iron-EDTA soluble complex. The NLS-NPHG's were used for intracellular trafficking studies disclosed in a separate presentation in this proceedings book [4].

Acknowledgments

References

1. Leobandung, W., Ichikawa, H., Fukumori, Y., Peppas, N.A. *J. Appl. Polym. Sci.* **87**, 1678-1684 (2003).
2. Zhiya, M.A., Yueping, G., Huizhou, L. *J. Polym. Sci. A: Polym. Chem.* **43**, 3433-3439 (2005).
3. Kaihatsu, K., Huffman, K.E., Corey, D.R. *Biochemistry* **43**, 14340-14347 (2004).
4. Machtey, V., et al. *in this Proceedings Book*.

Development of a Novel Liquid-Phase Peptide Synthesis (LPPS) on Anchors Bearing a Long Aliphatic Chain: AJI-PHASE™

Daisuke Takahashi

Research Institute for Bioscience Products and Fine Chemicals, Ajinomoto Co., Inc.,
Yokkaichi, Mie, 510-0885, Japan

Introduction

Until recently, peptide drug manufacturing has mainly used Solid-Phase Peptide Synthesis (SPPS). Alternatively, Liquid-Phase Peptide Synthesis (LPPS) is a promising procedure for the large-scale synthesis of high-quality peptides since the product can be purified and characterized at each step in the reaction. However, LPPS has traditionally had the disadvantages of being applicable only to short peptides and involving long synthetic timescales. Some methods that try to overcome the disadvantages of LPPS have been reported [1-3]. We also developed a novel form of liquid phase peptide synthesis AJI-PHASE™ which overcomes the weak points of LPPS. This procedure combines the advantageous features of both SPPS and LPPS methods in that stepwise elongation and segment condensation reactions which can be performed in a homogeneous liquid phase with the aid of a soluble anchor having long aliphatic chains. This not only facilitates isolation of the product from the reaction mixture by precipitation but also drives the coupling reaction to completion by using equimolar amounts of the *N*-/*C*-components, enabling the whole process to be performed at lower cost.

Results and Discussion

The method uses soluble and precipitation anchor supports, 9-bromo-2-[12-(docosyloxy)-dodecyloxy]-9-(3-fluorophenyl)-9*H*-fluorene **1** and *bis*[4-(docosyloxy)phenyl]methylamine **2** which we have developed, compatible with Fmoc chemistry to prepare peptide-acids and amides, respectively. The long aliphatic chain can help the anchored peptides not only be readily dissolved in a halogenated solvent but also to be easily recovered and purified by simple precipitation with a polar solvent.

Particularly, this method accomplished to prepare fully protected peptide segments with a free α-carboxyl group that can be used for convergent LPPS to obtain large peptides. The peptide-ester linked to 1 was completely stable during isolation using MeOH, which causes significant degradation of the peptide-ester on a trityl-type anchor [4], but was selectively cleavable by treatment with 2% TFA or HFIP in CHCl₃. Additionally, stepwise elongation onto 1 was not accompanied by the formation of a diketopiperazine even in the case of peptides that contain Pro or *N*-alkylated amino acids in the *C*-terminal dipeptide sequence.
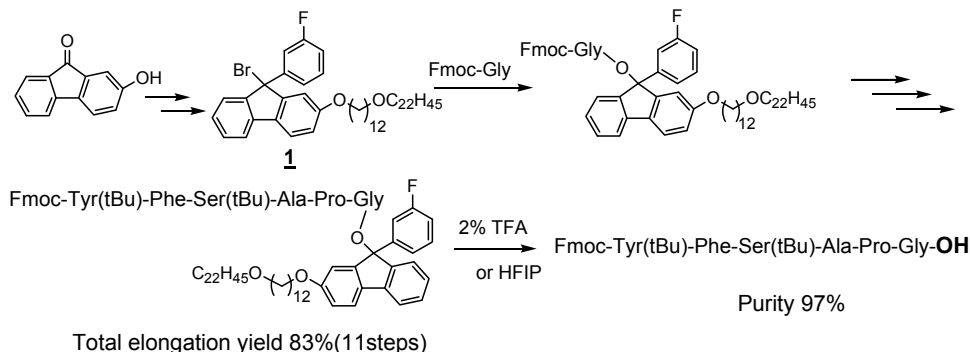
Fig. 1. Procedure of the protected peptide acid using fluoren anchor.

The elongation of C-terminus amide peptides, which are found in most of peptide drugs, was also accomplished by using diphenylmethyl type anchor 2. This anchor was able to load amino acid easily and to be detached with standard TFA condition in final deprotection step.
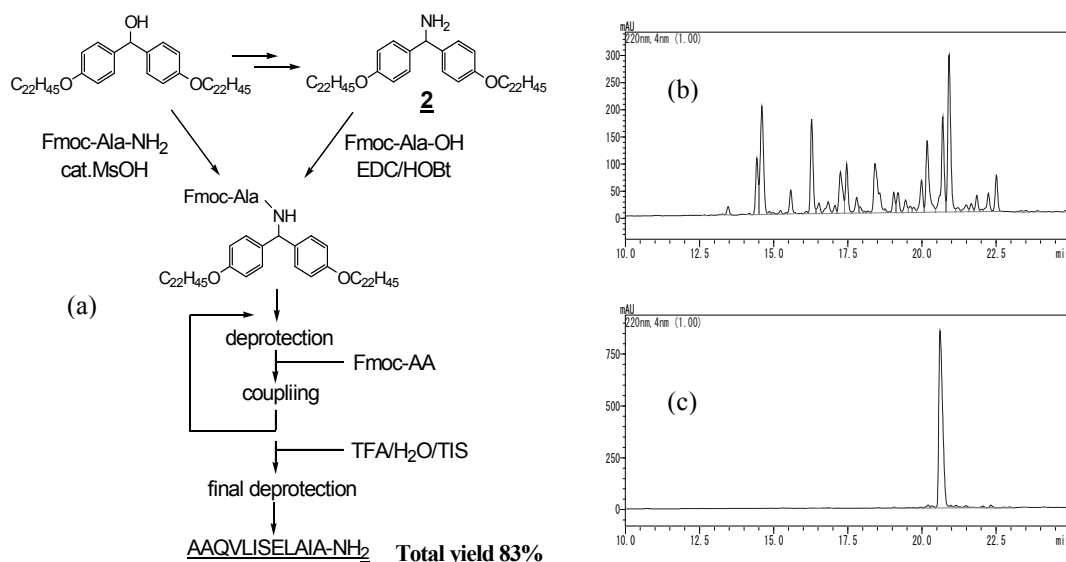
Fig. 2. (a) Synthetic scheme for anchors and 12mer peptide by AJI-PHASE, (b) HPLC chart of deprotected 12mer peptide synthesized by SPPS, (c) synthesized by AJI-PHASE method.

It is noteworthy that a 12-mer peptide having hydrophobic amino acid residues (AAQVLISELAIA-NH$_2$) was synthesized by our methodology with Fmoc strategy in much higher purity and efficiency than SPPS method.

We have already synthesized various peptides including hydrophobic peptides, more than 40 mer long sequence of peptides without any deletion products. These results demonstrated the usefulness of anchors for LPPS. This work is subject of patent applications WO2010/104169 and US2010/0249374.

Acknowledgements

References

1. Narita, M., Itsuno, S., Hirata, M., Kusano, K. *Bull. Chem. Soc. Jpn.* **53**, 1028 (1980).
2. Tamiaki, H., Obata, T., Toma, K. *Peptide Science 1998* 125-128, (1999).
3. Mizuno, M., Goto, K., Miura, T., Hosaka, D., Inazu. T. *Chem. Comm.* 972, (2003).
4. Chiba, K., Kim, S., Kohno. Y. WO2007/122847.

A Simple and Efficient Approach to Prepare One-Bead One-Compound Cyclic Peptide Libraries for Ligands Identification

Anick Girard[1,2], François Bédard[1,2], and Eric Biron[1,2]

[1]*Faculty of Pharmacy, Université Laval, Québec (QC), G1V 0A6, Canada;* [2]*Laboratory of Medicinal Chemistry, CHUQ Research Center, Québec (QC), G1V 4G2, Canada*

Introduction

The controlled interference of protein-protein interactions (PPI) with chemical compounds has great potential for the discovery of novel therapeutics. Considering the nature of the interaction, cyclic peptides represent a template of choice to mimic protein secondary structures and modulate PPI. Besides increased conformational rigidity and improved proteolytic stability, they offer a great degree of molecular complexity and diversity to fully exploit this great chemical diversity, the combinatorial one-bead one-compound (OBOC) approach is a very powerful approach [1]. However, its use with cyclic peptides is limited by difficulties in sequencing hit compounds by Edman degradation or MS/MS due to the lack of free N-terminal amine and complicated fragmentation patterns, respectively. This problem has been overcome by Pei and coworkers by using a bead segregation strategy [2,3] (Figure 1). Initially introduced by Lam et al. [4], the topological segregation offers the opportunity to synthesize two compounds per bead. Based on previous results, our objective was to study the effects of various parameters on bead segregation in order to control the exterior versus interior ratio in a reproducible manner.

Results and Discussion

Bead segregation is usually performed on PEG-based resins such as TentaGel (TG). The approach is based on the compatibility of the solid support with aqueous and organic media. The strategy is to create a biphasic environment after swelling the beads with water (Figure 1). After filtration, only the surface of the TG beads is exposed to organic solvent that contains the derivatizing reagent, while the interior of the bead remains in water without any derivatizing reagent. We have observed that the outer/inner ratio could depend on many parameters such as reagent nature, solvent mixture, reaction time, linker or spacer and resin type. The outer/inner ratio was determined by dosing the Fmoc group [5] after segregation (partial loading) and capping with Fmoc-Glu(tBu)-OH, HCTU and N-methylmorpholine (NMM) (total loading).

The segregation step is usually performed with an OSu derivative such as Fmoc-OSu or Fmoc-Xaa-OSu in CH_2Cl_2/Et_2O (55:45) (Figure 1) [2-4]. This solvent mixture is optimal for TG beads segregation. Variation of Fmoc-Glu(OSu)-Oall equivalents showed that the beads can be segregated in a linear manner. Unfortunately, some of the Fmoc-Xaa-OSu derivatives suffer poor stability during long term storage. To overcome this problem, different activated ester derivatives were tested. Surprisingly, very good segregation has been achieved with the amino acid derivative Fmoc-Glu-Oall, HCTU and NMM (4 equiv versus HCTU) (Table 1).
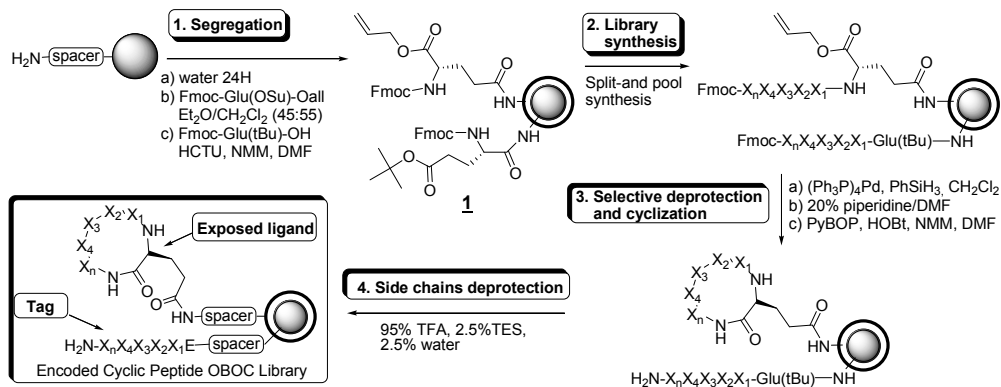
Fig. 1. Synthesis of encoded OBOC cyclic peptide libraries (X=variable amino acid Xaa) [2].

Table 1. Topological bead segregation evaluation in various conditions with TentaGel resin

Reagent	equiv[a]	time (min)	Partial loading (mmol/g)	Total loading (mmol/g)	Ratio ext vs int
Fmoc-Glu(OSu)-Oall	0.2	30	0.061	0.281	22%
	0.4	30	0.089	0.269	33%
	0.6	30	0.136	0.276	49%
	0.8	30	0.172	0.264	66%
	1	30	0.181	0.251	72%
Fmoc-Glu-Oall and HCTU	0.25	5	0.036	0.251	14%
		15	0.061	0.250	24%
		30	0.066	0.244	27%
	0.5	5	0.046	0.247	19%
		15	0.072	0.246	31%
		30	0.110	0.251	44%
	1	2	0.037	0.244	15%
		5	0.057	0.235	25%
		15	0.121	0.245	49%
		30	0.175	0.244	72%
		60	0.196	0.237	82%
		120	0.199	0.232	86%

[a]Equivalents calculations are based on the theorical loading of TentaGel S NH$_2$ 130µm of 0.29mmol/g

For the preparation of encoded OBOC cyclic peptides libraries, we usually target a 30% outer/inner ratio. The study performed with various amount of derivatizing reagents at different reaction time (Table 1) showed that 0.4 equiv of Fmoc-Glu(OSu)-Oall for 30 min and 0.5 equiv of Fmoc-Glu-Oall with HCTU and NMM for 15 min would allow us to achieve the aimed outer/inner ratio. The results also showed that almost complete bead saturation is achieved with 1 equiv of Fmoc-Glu-Oall/HCTU for 2h. This result was unexpected because it was anticipated that the presence of water inside the bead would hydrolyze an important portion of the activated esters penetrating the bead. This observation suggests that after some time reagents will migrate inside the beads and that water can eventually be displaced by the organic solvent.
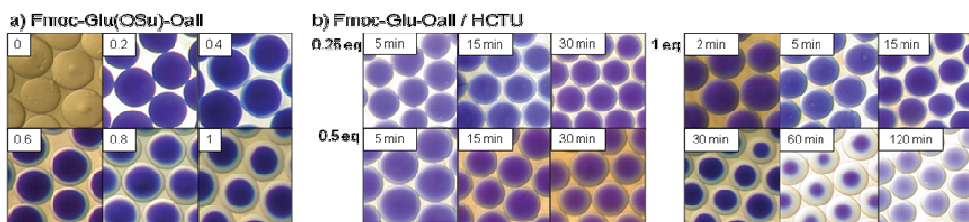
Fig. 2. Microscope view of segregated TG beads treated with Bromophenol Blue.

The results obtained in the described study showed that bead segregation can be achieved with Fmoc-protected amino acids and HCTU in CH$_2$Cl$_2$/Et$_2$O (55:45) in a wide variety of controllable and predictable outer versus inner ratios. The described procedure reduces the need to synthesize and use OSu derivatives for bead topological segregation. It also allows a simple and efficient first step to prepare encoded OBOC cyclic peptide libraries by bead segregation.

Acknowledgments

References

1. Lam, K.S., Krchnak, V., Lebl M. *Chem. Rev.* **97**, 411-448 (1997).

Critical Evaluation of *In Situ* Coupling Reagents for SPPS

Raymond Behrendt[1], A. Brünner[1], and P. White[2]

[1]*Novabiochem, Merck & Cie, Schaffhausen, 8200, Switzerland;* [2]*Novabiochem, Merck Chemicals Ltd., Beeston, Notts, NG9-2JR, U.K.*

Introduction

With the plethora of coupling reagents available for mediating amide bond formation in peptide synthesis, making a rational decision as to the optimal reagent for a given application can be difficult. Herein we compare a wide range of novel and commercially available coupling reagents for solubility, solution stability, and efficiency, with a view to simplifying the selection of coupling reagents.

Results and Discussion

The coupling reagents tested in this study are shown in Figure 1 [1-6]. Novel and standard coupling reagents forming HOBt, Cl-HOBt, HOAt and Oxyma Pure active esters highly viable for SPPS were selected.
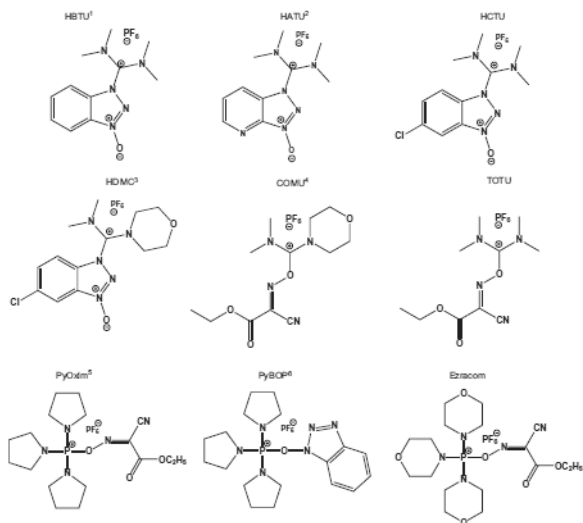
Fig. 1. Coupling reagents examined in this study.

First the solubility of coupling reagents was tested by placing 2.5 mmol of coupling reagent in a measuring cylinder and adding DMF in 10 ml aliquots until a clear solution was obtained. Solubilities above 1.5 M were not tested. With the exception of Ezracom, all Oxyma Pure based coupling reagents demonstrated superior solubility compared to the hydroxybenzo-triazole based coupling reagents.

The solution stabilities of the tested coupling reagents were evaluated in open and closed vials by ^{1}H-NMR time course studies in d$_7$-DMF. The closed vial stability closely mimics the conditions employed on synthesizers such as the ABI 433 or PTI Symphony.

As expected, solutions of uronium coupling reagents are stable under both open and closed vial conditions for more than 7 days. Thus, uronium coupling reagents appear to be a good choice for use with synthesizers based on an open XY platform. On the other hand, phosphonium reagent solutions can only be safely used up to 7 days if stored in closed vials. Surprisingly, and in contradiction of published results, COMU appeared to be highly unstable in solution.

The stabilities of solutions of coupling reagents in DMF containing DIPEA were also tested by the NMR method. HBTU/DIPEA and PyBOP/DIPEA mixtures were found to be sufficiently stable to be usable after 2 days.

Three peptides selected from the literature [2,3] were used as models to evaluate the efficiency of the coupling reagents (*Peptide 1:* H-Tyr-Sar-Sar-Phe-Leu-NH$_2$; *Peptide 2:* H-Tyr-Aib-Aib-Phe-Leu-NH$_2$; *Peptide 3:* H-Tyr-MeLeu-MeLeu-Phe-Leu-NH$_2$). The peptides were assembled in an ABI 433A on Rink amide resin. Couplings were performed by Fmoc-Aaa-OH:Coupling reagent:DIPEA (4:4:8) and deprotection by 20% piperidine in DMF. In every case the C-terminal three residues were coupled for 1 h. In the case of *peptides 1* and *3* the final two residues were coupled for 5 mins to exaggerate the differences in efficiencies between the coupling reagents under test. With *peptide 2*, a 1 h coupling time was used for all residues. The final cleavage was carried out by a mixture of TFA/water/TIS (95:2.5:2.5) for 3 h.

Table 1. Composition of products obtained using selected coupling reagents in the synthesis of peptide 3

Sequence	PyBOP	PyOxim	HBTU	TOTU	HCTU	HATU	COMU	Ezra-com	HDMC
MeLFL	60	10	57	5	31	0	9	9	24
YMeLFL	31	45	31	58	35	16	47	50	46
MeLMeLFL	5	5	8	2	9	7	4	5	7
YMeLMeLFL	4	40	4	35	25	77	40	26	31

In our hands, only *peptide 3* proved useful as a tool for evaluating these coupling reagents: *peptide 1* was efficiently assembled by all reagents tested; with *peptide 2*, the des-Aib peptide could not be baseline resolved from the desired pentapeptide using three different HPLC columns; whereas with *peptide 3*, all the by-products from synthesis were fully resolved and the peptide appears to be highly discriminating between coupling reagents. Table 1 summarizes the results obtained using *peptide 3* as the model. These data reveal remarkably consistent trends. The nature of the coupling reagent leaving group appears to be the most important factor influencing efficiency. The activating moiety appears to have little influence. HATU was the most efficient reagent for amide bond formation. All three Oxyma-based reagents, COMU, PyOxim and Ezracom, gave very similar results and were more effective than Cl-HOBt and HOBt-based reagents. HOBt-based reagents were the least effective.

In conclusion PyOxim appeared to combine high reactivity and solubility with moderate stability, making it an excellent choice of coupling reagent for synthesizers employing closed-bottle reagent storage. Furthermore, unlike uronium-based coupling reagents, it will not give rise to guanidinylated by-products, making it ideal for coupling of slow-to activate amino acids, cyclizations and fragment condensations.

HATU was the most effective coupling reagent of those tested, but its high cost limits its use to special applications.

For synthesizers employed open-vials, uronium-based reagents should be employed owing to their high stability.

References

1. Knorr, R., et al. *Tetrahedron Lett.* **30**, 1927 (1989).
2. Carpino, L.A., et al. *J. Am. Chem. Soc.* **115**, 4397 (1993).
3. El-Faham, A., Albericio, F. *J. Org. Chem.* **73**, 2731(2008).
4. El-Faham, et al. *Chem. Eur. J.* **15**, 9404 (2009).
5. Subiros-Funosas, R., et al. *Org. Biomol. Chem.* **8**, 3665 (2010).
6. Coste, J., et al. *Tetrahedron Lett.* **31**, 205 (1990).

A Green Strategy for the Synthesis of Cysteine-Containing Peptides

Miriam Góngora-Benítez[1,2], Alessandra Basso[3], Thomas Bruckdorfer[4], Judit Tulla-Puche[1,2], and Fernando Albericio[1,2,5]

[1]*Institute for Research in Biomedicine, Barcelona Science Park, Baldiri Reixac 10, 08028, Barcelona, Spain;* [2]*CIBER-BBN, Networking Centre on Bioengineering, Biomaterials and Nanomedicine, Barcelona Science Park, 08028, Barcelona, Spain;* [3]*SPRIN S.p.A., c/o BIC Incubatori FVG, via Flavia 23/1, 34148, Trieste, Italy;* [4]*IRIS Biotech GmbH, Waldershofer Str. 49-51, D-95615, Marktredwitz, Germany;* [5]*Department of Organic Chemistry, University of Barcelona, 08028, Barcelona, Spain*

Introduction

The appropriate choice of cysteine-protecting groups and their corresponding removal conditions is often crucial for the formation of disulfide bridges as a final stage in peptide synthesis. Phenylacetamidomethyl [1] (Phacm) is a protecting group compatible with both Boc and Fmoc synthetic strategies, which can be removed in similar conditions than acetamidomethyl (Acm) and, in addition, by the action of the enzyme penicillin amidohydrolase (PGA, E.C.3.5.1.11). As PGA is selective to the phenylacetyl moiety, Phacm can be smoothly deblocked, while the resulting thioaminal is hydrolyzed to the free Cys residue.

In this work, the combination of Pham and a PGA from *E. coli,* which is covalently immobilized on an amino acrylic resin, exhibits promising applications in peptide synthesis and opens new perspectives for further purposes. The reliability and versatility of Phacm as a protecting group and its removal by the immobilized-PGA is discussed herein.

Results and Discussion

The Phacm removal by an immobilized-PGA and the subsequent disulfide bridge formation have been thoroughly investigated and compared with the commonly used Acm protection strategy for the synthesis of the urotensin II-related peptide (URP) (Figure 1).

URP is an 8-residue peptide which contains a disulfide bridge (Cys^2-Cys^7) and presents in its sequence Tyr and Trp residues. Two parallel synthesis of URP following Fmoc/tBu strategy with both Phacm and Acm protection strategies have been carried out. Linear peptides were manually synthesized on a 2-chlorotrityl chloride resin using DIPCDI and Oxyma in DMF, with 5 min preactivation, for 1h at RT to incorporate the Cys residues. These conditions assure a total absence of racemization [2,3]. The other amino acids were coupled using COMU and DIEA in DMF for 1h at RT.
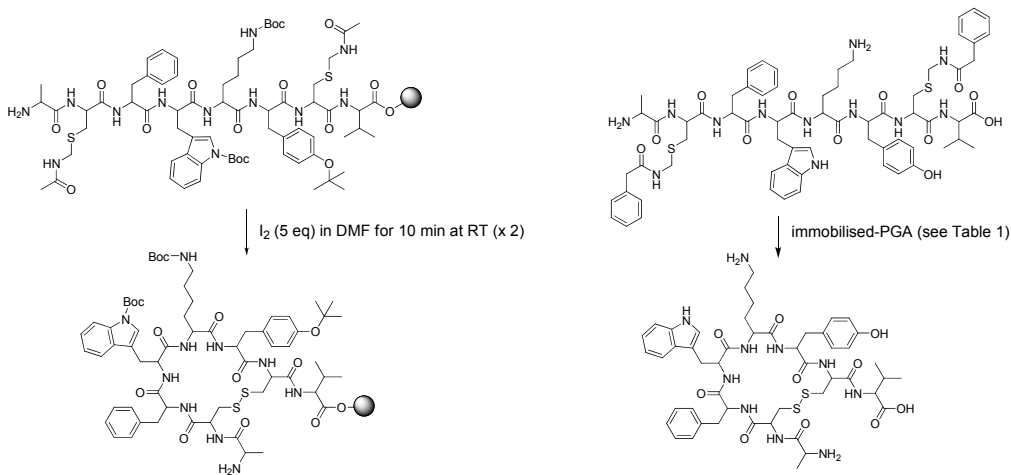
Fig. 1. Acm protection strategy for URP (left); Phacm protection strategy for URP (right).

The quality of the crude product using Phacm was superior to the one prepared with Acm. Possibly, the extra peaks in the Acm strategy correspond to Trp and Tyr modified by the Acm group. Additionally, the use of co-solvents in aqueous media [4] and the effect of pH have been widely examined (Table 1).

Table 1. Effect of co-solvents and pH. [peptide]: 8 x 10^{-5} M; 25 mg (3 EU) SPRIN imibond PGA – Immobilized Penicillin G Amidas, (hydrolytic activity U/g$_{wet}$ 130) at 37°C for 24h

	Reaction Media	pH	totally deprot.	fully oxidized
1	H_2O	7.0	OK	-
2	H_2O/DMSO (95/5)	7.0	OK	OK
3	H_2O/MeCN (95/5)	7.0	OK	-
4	H_2O/MeOH (95/5)	7.0	OK	-
5	H_2O/2-propanol (95/5)	7.0	OK	-
6	H_2O/DMF (95/5)	7.0	OK	-
7	0.1 mM phosphate	7.8	OK	-
8	0.1 mM phosphate/DMSO (95/5)	7.8	OK	OK
9	0.1 mM phosphate	5.3	OK	-
10	0.1 mM phosphate/DMSO (95/5)	5.3	OK	OK

The enzymatic activity and stability of the immobilized-PGA remained intact in the presence of an extended variety of organic co-solvents. A further advantage is that a wide range of pH is tolerated by the immobilized-PGA enzyme.

Conclusions

The Phacm group is a promising alternative to the conventional Acm protection, which prevents undesired side products that are associated with the removal of the Acm groups with iodine. The immobilized-PGA demonstrates a high efficiency under a wide range of reaction conditions. The use of DMSO as a co-solvent promotes oxidation of thiols to disulfide.

Acknowledgments

References

1. Royo, M., Alsina, J., Giralt, E., Slomcyznska, U., Albericio, F. *J. Chem. Soc. Perkin Trans.* **1**, 1095-1102 (1995).
2. Han, Y., Albericio, F., Barany, G. *J. Org. Chem*. **62**, 4307-4312 (1997).
3. Angell, Y.M., Alsina, J., Albericio, F., Barany, G. *J. Peptide Res.* **60**, 292-299 (2002).
4. Kim, M.G., Lee, S.B. *J. Mol. Catal. B: Enzym.* **1**,181-190 (1996).

Practical Tips on the Use of Oxyma: An Exhaustive Stability Assay

Lidia Nieto-Rodriguez[1], Magda Carceller[1], Ramon Subirós-Funosas[1,4], Gerardo A. Acosta[1,4], Marta Paradís Bas[1], Ayman El-Faham[1,2], and Fernando Albericio[1,3,4]

[1]*Institute for Research in Biomedicine, Barcelona Science Park, Baldiri Reixac 10, 08028, Barcelona, Spain;* [2]*Department of Chemistry, Faculty of Science, Alexandria University, Ibrahimia, 21321, Alexandria, Egypt;* [3]*Department of Organic Chemistry, University of Barcelona, Martí i Franquès 1-11, 08028, Barcelona, Spain;* [4]*CIBER-BBN, Networking Centre on Bioengineering, Biomaterials and Nanomedicine, Barcelona Science Park, Baldiri Reixac 10, 08028, Barcelona, Spain*

Introduction

The thermal and mechanical unstability exhibited by *N*-hydroxybenzotriazoles, such as HOBt, 6-Cl-HOBt, HOAt and the corresponding aminium salts is of great importance to methodology of peptide synthesis [1]. A few years ago, some of these reagents were regarded as Class 1 explosive substances. This has imposed severe transport limitations, especially overseas, thereby hampering commercial availability [1]. Consequently, the need for alternative potent, efficient and safe additives and onium salts led recently to the reevaluation of ethyl 2-cyano-2-(hydroxyimino) acetate (Oxyma, Figure 1, left), standing as a suitable *N*-hydroxylamine

Fig. 1. Structure of Oxyma, COMU and PyOxim.

scaffold for developing new coupling reagents [2]. Its high acidity and low bulkiness results in enhancement of solubility, epimerization suppression and coupling efficiency in demanding sequences, together with a considerably safer decomposition profile. This extraordinary behavior as additive to carbodiimides prompted the design of derived coupling reagents, like the uronium salt COMU (Figure 1, center) or the phosphonium salt PyOxim (Figure 1, right), which generally performed at a similar level than HOAt-based analogues [3]. However, solutions of *N*-hydroxylamines are usually stored long time, especially when employed to assist peptide bond formation in automated synthesizers. Moreover, in basic media oximes can shift to their nitroso tautomer, which in this case would result in inactivity as peptide bond-assisting moiety [4]. Herein, an exhaustive study of the stability and chemical integrity of Oxyma is reported.

Results and Discussion

In order to study the stability of Oxyma in different solvents (DMF, CH_3CN and NMP) with time and temperature, 0.5M solutions at room temperature and at 40ºC were scrutinized by HPLC, HPLC-MS and IR. Using the two former techniques, no changes were observed regardless of temperature and solvent, up to 30 days after preparation of the corresponding solutions.
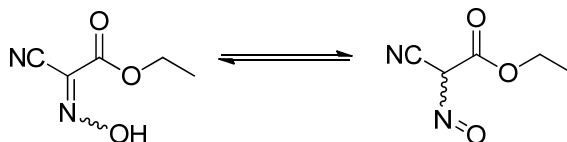
Fig. 2. Tautomeric equilibrium between Oxyma and its nitroso form.

One hypothetic event was the possibility of a tautomeric equilibrium of Oxyma in solution to the nitroso form, which is inactive as additive to carbodiimides (Figure 2). In order to check the likeliness of this dramatic tautomeric shift, solutions of Oxyma in DMF at rt and at 40ºC were evaporated 34 days after their preparation, and samples were analyzed by FT-IR. In all experiments the characteristic oxime bands, that is N-O st (1004 cm^{-1}), C=N st (1630 cm^{-1}) and associated O-H st (3127 cm^{-1}) were observed, in contrast to the absence of typical nitroso bands, such as N-O st (1280, 1550 cm^{-1}), resulting in identical spectra to that of a fresh Oxyma. These experiments confirm that long-term stored solutions of Oxyma retain the oxime form.

With the purpose to unequivocally determine the efficiency of solutions of Oxyma in DMF, experiments at room temperature for 40 days and at 40ºC for 57 days, were tested in the conversion of Z-Aib-OH into the Oxyma ester. Compared to freshly prepared solutions of Oxyma in DMF, the long-term stored samples performed with similar efficiency, affording quantitatively the ester in only 2 hours.

Acknowledgments

References

1. Wehrstedt, K.D., Wandrey, P.A., Heitkamp, D. *J. Hazard. Mat*. **A126**, 1 (2005).
2. Subirós-Funosas, R., Prohens, R., Barbas, R., El-Faham, A., Albericio, F. *Chem. Eur. J.* **15,** 9394 (2009).
3. Subiros-Funosas, R., El-Faham, A., Albericio, F. "*N*-hydroxylamines for Peptide Synthesis", *Patai's Chemistry of Functional Groups*, *Ed. John Wiley & Sons*, **2 (2)**, 623 (2011).
4. Eddings, D., Barnes, C., Gerasimchuk, N., Durham, P., Domasevich, K. *Inorg. Chem*. **43**, 3894 (2004).

Novel Applications of Oxyma: Minimization of Base-Driven Side Reactions

Ramon Subirós-Funosas[1,4], Ayman El-Faham[1,2], and Fernando Albericio[1,3,4]

[1]*Institute for Research in Biomedicine, Barcelona Science Park, Baldiri Reixac 10, 08028, Barcelona, Spain;* [2]*Department of Chemistry, Faculty of Science, Alexandria University, Ibrahimia, 21321, Alexandria, Egypt;* [3]*Department of Organic Chemistry, University of Barcelona, Martí i Franquès 1-11, 08028, Barcelona, Spain;* [4]*CIBER-BBN, Networking Centre on Bioengineering, Biomaterials and Nanomedicine, Barcelona Science Park, Baldiri Reixac 10, 08028, Barcelona, Spain*

Introduction

Benzotriazole-based additives and coupling reagents have prevailed in the past decades over other *N*-hydroxylamine scaffolds such as benzotriazines, succinimides, triazoles or pyridinones. However, consecutive nitrogens contained in these structures derive in explosive profiles, seriously compromising their overseas transport and consequently, their commercial availability [1]. Alternatively, oxime-based templates such as ethyl 2-cyano-2-(hydroxyimino)acetate (Oxyma, Figure 1) stand as a reliable, efficient and safe family of coupling reagents, displaying enhanced solubility and increased reactivity, superseding even HOAt in demanding sequences [2]. However, the scope of application of *N*-hydroxylamines in peptide synthesis is not restricted to traditional methods of assisting peptide bond formation. Thus, the extraordinary acidity of *N*-hydroxylamines prompted their use in the minimization of base-catalyzed side reactions in Fmoc/*t*Bu chemistry. Our main objectives in the present communication consist in finding novel applications of Oxyma, including the ability to reduce the impact of aspartimide formation and Pro-mediated overcoupling in comparison to benzotriazoles.

Results and Discussion
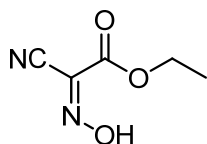
Fig. 1. Structure of Oxyma.

The intramolecular cyclization and subsequent ring-opening by nucleophiles occurring in Asp residues is one of the most detrimental side reactions in peptide synthesis [3]. Although found either in acidic and basic conditions, the impact of aspartimides/piperidides is more severe in the Fmoc/*t*Bu approach, where these byproducts may appear after every N^α-deprotection cycle once Asp has been incorporated in the sequence. Among various strategies described to overcome this problem, addition of acidic *N*-hydroxylamines such as HOBt, HOSu and electron-deficient phenols stands as a cost-saving, simple, universal and efficient strategy to minimize the impact of the undesired cyclization. Herein, the effect of Oxyma in 20% piperidine/DMF
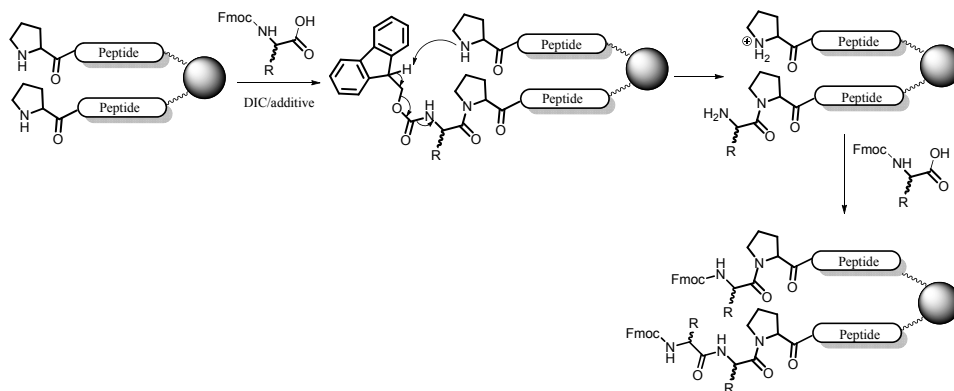
Fig. 2. Mechanism of Pro-based overcoupling in Fmoc/tBu chemistry.

Table 1. Reduction of aspartimides and derived byproducts after 6+6 hour treatments of Fmoc-Ala-Orn-Asp-Gly-Tyr-Ile-resin with 20% piperidine/DMF, including N-hydroxylamines at various concentrations

Concentration of additive in 20% piperidine/DMF	additive	α-peptide	β-peptide	aspartimide	piperidides
--	--	55.62	0.23	11.06	33.09
0.1M	Oxyma	62.75	0.26	9.36	27.62
	HOBt	59.72	0.38	9.88	30.02
	HOAt	60.59	0.22	10.43	28.76
0.5M	Oxyma	74.74	0.51	8.08	16.67
	HOBt	65.87	0.23	12.75	21.16
	HOAt	67.11	0.26	13.54	19.08
1M	Oxyma	85.59	0.10	9.60	4.67
	HOBt	79.00	0.25	14.03	6.72
	HOAt	79.68	0.13	14.36	5.82

cocktails has been tested in the Fmoc removal of a hexapeptide containing a known sensitive sequence towards this side reaction (Fmoc-Ala-Orn-Asp-Gly-Tyr-Ile-resin) [4]. Table 1 highlights the increasing reduction of aspartimide and ring-opening byproducts, mainly piperidides, with more concentrated solutions of *N*-hydroxylamines in 20% piperidine/DMF. Thus, purity can be raised from 55% to 86% by addition of 1M Oxyma to Fmoc deprotection cocktails, superseding the contribution of HOBt/HOAt to the minimization of this side reaction, regardless of conditions tested.

Proline is the only proteinogenic amino acid containing a *N*-terminal secondary amine, which confers to this moiety an unusual high basicity, close to that exhibited by DIEA and piperidine. Consequently, this residue is involved in the premature N^{α}-deprotection of recently incorporated Fmoc-amino acids, causing their overcoupling (Figure 2). Our goal was focused on investigating the occurrence of this unreported side reaction and the envisaged advantageous effect of peptide-resin treatments, when Pro is the *N*-terminal residue, with acidic *N*-hydroxylamines. Therefore, resin bound tripeptide H-Pro-Phe-Leu was mixed with a solution of Fmoc-Pro/Tyr-OH for 2h prior to addition of coupling cocktail, in order to promote this side reaction. Alternatively, resin was treated with 0.1M solutions of HOAt, HOBt and Oxyma before conducting the experiment. Although this protocol induced the appearance of only 3-4% overcoupling-derived hexapeptides, the beneficial effect of *N*-hydroxylamines was clearly observed. Thus, Oxyma reduced the premature Fmoc removal to a greater extent than HOBt.

Acknowledgments

References

1. Wehrstedt, K.D., Wandrey, P.A., Heitkamp, D. *J. Hazard. Mat*. **A126**, 1-7 (2005).
2. Subirós-Funosas, R., Prohens, R., Barbas, R., El-Faham, A., Albericio, F. *Chem. Eur. J.* **15,** 9394-9403 (2009).
3. Martinez, J., Bodanszky, M. *Int. J. Pept. Protein Res.* **12**, 277-283 (1978).
4. Nicolas, E., Pedroso, E., Giralt, E. *Tetrahedron Lett.* **30**, 497-500 (1989).

Peptide Modifications at the *C*-terminus in Solid Phase Synthesis with Side Chain Peptide Attachment onto Chlorotrityl Resin

Anna Kwiatkowska, Marc-André Bonin, Xue Wen Yuan, and Witold A. Neugebauer

Département de Pharmacologie de Sherbrooke, Université de Sherbrooke, Sherbrooke, J1H 5N4, Québec, Canada

Introduction

Many biologically active peptides exhibit higher potency and specificity when chemically modified at their *C*-terminus. Here, we are presenting a useful solid phase synthesis strategy with *C*-terminal peptide modification. This strategy allows for *C*-terminal coupling of:

-aliphatic amines,

-aromatic amines,

-reactive amino acids derivatives (chloromethyl ketones),

otherwise impossible to start by a regular solid phase peptide synthesis procedure.

Results and Discussion

The method presented here applies to peptide sequences with *C*-terminal lysine or other *bis*-amino acid such as: ornitine, 2,4-diaminobutric acid, 2,3-diaminopropionic acid or *bis*-carboxyl amino acids (Asp, Glu). The first Fmoc amino acid α-carboxyl allyl ester was attached to 2-chlorotrityl chloride (Cl-Trt) resin *via* its side chain function (Figure. 1) [1,2].
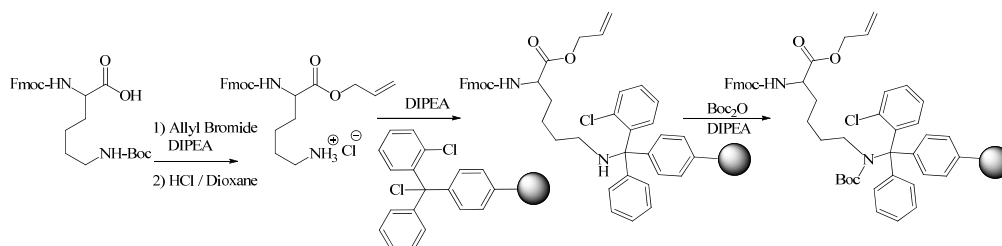
Fig. 1. Attachment of a protected lysine derivative Fmoc–Lys(OAll)–OH to 2-chlorotrityl chloride (Cl-Trt) resin.

The secondary amine linking lysine (*bis*-amino acids) and chlorotrityl resin was protected by Boc protecting group. For relatively inert amides, allyl esters are removed on the resin with Pd(PPh$_3$)$_4$ tetrakis (triphenylphosphine)palladium(0) / 5,5-dimethyl-1,3-cyclohexanedione. Amidation of Fmoc-Lys(2-Cl-Trt resin)-OH (or ornitine) was performed with DPPA or COMU activation to couple aliphatic or aromatic amine at $^\alpha$*C*-terminus. The elongation of the peptide (up to 7 amino acids) was carried out using the Fmoc/*t*Bu strategy. All peptides were synthesized using a continuous flow peptide synthesizer (Pioneer). For the chemically reactive amides, lysine (or other) allyl ester on the resin was used to complete the peptide sequence and then allyl ester was removed followed by an amidation procedure with DPPA or COMU. Both strategies are presented in picture (Figure 2). A solution of TFA/H$_2$O/TIPS (95:2.5:2.5) was used to cleave peptides from the resin and to remove the side-chain protection groups from the amino acids. Liquid was precipitated dropwise in anhydrous ethyl ether, centrifuged and lyophilized. Peptide salt was then purified on reversed phase (C18) chromatography. The purity and identity of each peptide were determined by analytical RP-HPLC and confirmed by MALDI TOF mass spectrometry.
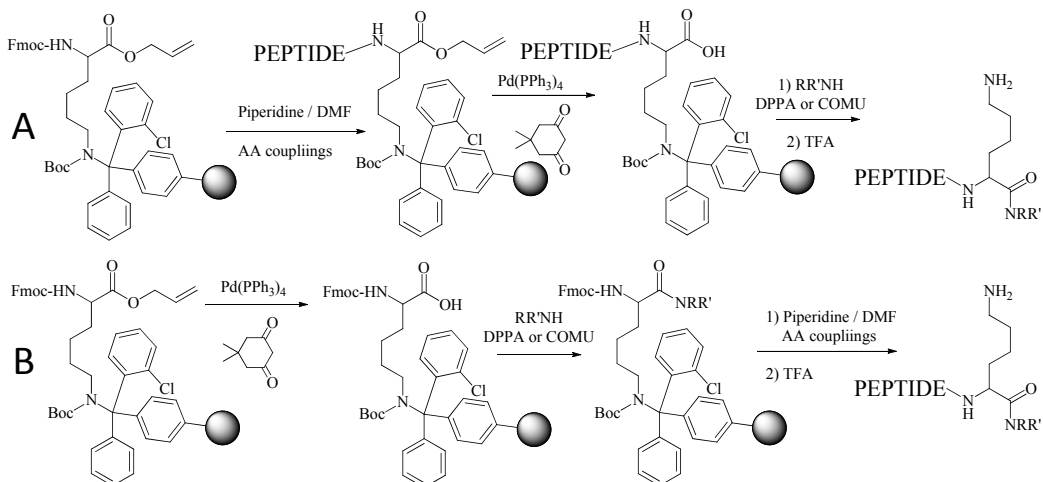
Fig. 2. Solid-phase synthesis of C-terminal-modified peptides containing **A** relatively inert amides and **B** chemically reactive amides.

In our studies, several different amines (Figure 3) were coupled as desired *C*-terminal amides, including:

aromatic arginine mimetic with amidine moiety (4-Amba, 2,4-Apaa),
amino acid's chloromethyl ketone (Arg(Pbf)-CH$_2$Cl),
amino acid coumarin derivative (Arg(Pbf)-AMC).

| 4-Amba | 2,4-Apaa | Arg(Pbf)-AMC | Arg(Pbf)-CH$_2$Cl |

4-(aminomethyl)benzimidamide 2-(4-aminophenyl)acetimidamide
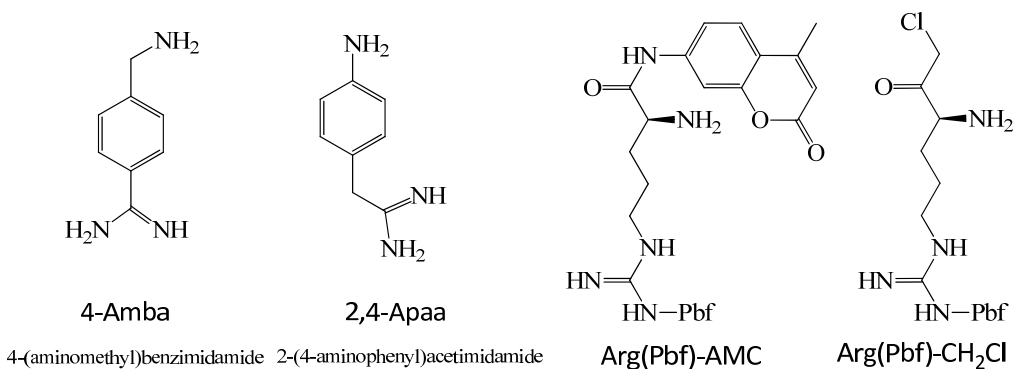
Fig. 3. Structure of C-terminal modifications.

All of these peptides were obtained in pure form in good yield (between 40 to 70%). In our opinion, this synthetic strategy can be successfully applied for the preparation of a variety *C*-terminally modified peptides.

Acknowledgments

References

1. Thieriet, N., Alsina, J., Giralt, E., Guibé, F., Albericio, F. *Tetrahedron Lett.* **38**, 7275-7278 (1997).
2. Bernhardt, A., Drewello, M., Schutkowski, M. *J. Peptide Res.* **50**, 143-152 (1997).

A New Solid-Supported SH-specific Biotinylation Reagent for the Efficient Biotin-labeling of Small Molecules

Kentarou Fukumoto[1,2], Kumi Adachi[1], Akihiro Kajiyama[1], Yuri Yamazaki[1], Fumika Yakushiji[1], and Yoshio Hayashi[1]

[1]*Department of Medicinal Chemistry, School of Pharmacy, Tokyo University of Pharmacy and Life Sciences, Tokyo, 193-0392, Japan;* [2]*Kokusan Chemical, Co., Ltd., Tokyo, 103-0023, Japan*

Introduction

In the life science research, a biotinylation of bioactive compounds such as peptides, proteins or other molecules is a well-known process to analyze their biological role and function. In general, covalently biotinylated molecules of interest are detected or isolated via the binding to avidin with an extremely high affinity and specificity to biotin. Biotinylation is unlikely to perturb the natural function of the molecule due to the small molecular size of biotin (MW 244.31). In most cases, biotinylation can be performed rapidly and specifically to the particular functional groups of the target molecules with specific reagents [1-4]. In general, the biotinylation reagent is excessively used to the target molecule for increasing reaction efficacy. Hence, after the labeling, the unreacted reagent or by-products produced during the reaction have to be removed by purification usually using a gel-filtration. However, in the case of biotinylation of small molecules, more complex and advanced purification methods such as avidin affinity chromatography or reverse-phase HPLC were required due to a similar molecular weight of the target molecules to biotin. To avoid such laborious purification steps, solid-phase chemistry seems to be beneficial because the unreacted biotinyl unit can be kept on the solid support, which can be easily removed by filtration. Therefore, in the present study, we designed and synthesized a new solid-supported and SH-selective biotinylation reagent as shown in Figure 1.
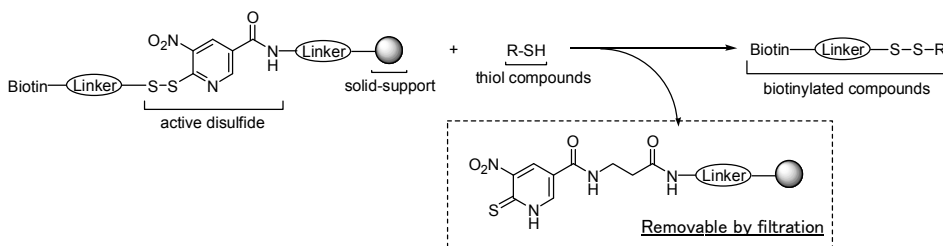
Fig. 1. Design of the SH selective solid-supported biotinylation reagent.

Results and Discussion

In the design of new biotinylation reagent, an Npys (3-nitro-2-pyridinesulfenyl)-type active disulfide structure was adopted on the solid support via a hydrophilic polyethyleneglycol linker to realize the biotinylation reaction in either aqueous or organic solution, and then biotin unit was connected to the active disulfide to be selectively introduced to the SH group of the target molecules. Based on this concept, the SH selective solid-supported biotinylation reagent (**1**) was successfully synthesized in 10 steps from a commercially available 6-hydroxynicotinic acid (**2**), (Figure 2).

To examine the property of **1**, the biotinylation of a small SH-containing amide was performed using captopril. In filtration tube, captopril and **1** (4 equiv., the molar quantity is based on the NH_2 content on the resin) were mixed, and the mixture was stirred for 12 h in DMF/H_2O (1:1) as solvents. After the completion of reaction, monitored by reverse phase HPLC, the solid-supported reagent was removed from the reaction mixture by filtration. The biotinylated captopril was obtained in high yield and purity without any further purification. Therefore, it was concluded that this reagent can perform the efficient biotinylation of small
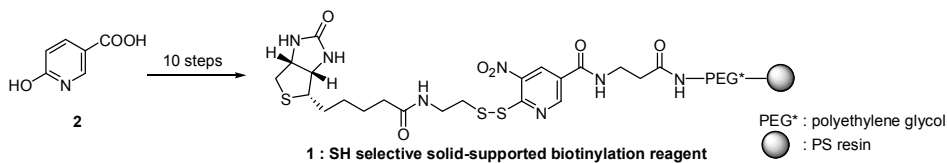
Fig. 2. Synthesis of a SH selective solid-supported biotinylation reagent.

molecules with a similar molecular size to biotin as well as peptides and proteins without any laborious purification steps.

References

1. Oda, Y., Nagasu, T., Chait, B.T. *Nature Biotech.* **19,** 379-382 (2001).
2. Sutoh, K., Yamamoto, K., Wakabayashi, T. *J. Mol. Biol.* **178,** 323-339 (1984).
3. Ghebrehiwet, B., Bossone, S., Erdei A., Reid, K.B.M. *J. Immunol. Methods* **110,** 251-260 (1988).
4. Hayashi, Y., Ezawa, K. *Jpn. Kokai Tokkyo Koho*. JP 63246382 (1988).

DTNP as a Gentle and Effective Method of Deprotection for Side-Chain Protectants on Commercially-Available Cys and Sec SPPS Derivatives

Stevenson Flemer Jr, Alayne L. Schroll, and Robert J. Hondal

Department of Biochemistry, University of Vermont College of Medicine, B415 Given Bldg, 89 Beaumont Ave, Burlington, VT, 05405, U.S.A.

Introduction

The use of cysteine (Cys) and selenocysteine (Sec) building blocks in solid phase peptide synthesis requires the judicious selection of orthogonal blocking protocol between standard Fmoc or Boc N^α protection and their reactive thiol and selenol sidechain functionalities. Many of the existing commercially-available Cys and Sec derivatives require relatively harsh conditions to effect the removal of their side chain protectants. In a previously-reported account by our research group [1], we introduced a gentler protocol for the removal of Acm and Mob S- and Se-protection using the conditions of 2,2'-dithiobis(5-nitropyridine) (DTNP) in a TFA/thioanisole solvent system. Based upon these initial successes, we have now expanded this study to include a comprehensive evaluation of these conditions to mediate the removal of many acid-stable commercially-available Cys and Sec side chain protectants.
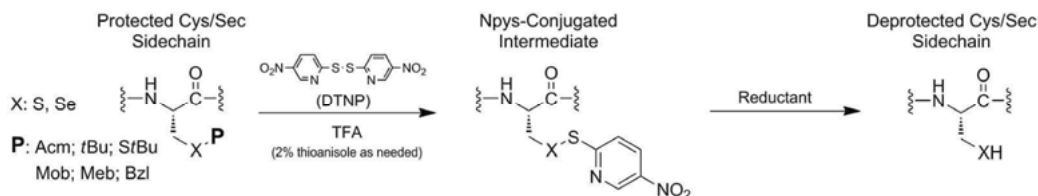
Fig. 1. DTNP Deprotection sequence on common commercially-available Cys & Sec derivatives.

Results and Discussion

Six commercially-available *S*-protected Fmoc-Cys derivatives as well as three *Se*-protected Fmoc-Sec derivatives (Mob, Meb, and Bzl) were subjected to a deprotection assay using the conditions listed in Figure 2. The Sec(Meb) and Sec(Bzl) derivatives, while their N^α-Boc conjugates are known compounds [2,3], have never been reported as their corresponding N^α-Fmoc counterparts. Since it would be informative to track the deprotective potential of this methodology against the full range of benzyl-templated Sec blocking groups, we elected to synthesize these compounds as their N^α-Fmoc derivatives [4,5]. These derivatives, along with those from commercial sources, were incorporated into various test peptides for analysis.

Initial deprotection profile comparisons were carried out through the incorporation of the various Cys and Sec derivatives into a 6-mer test peptide sequence (Figure 2). These peptides were then assayed as to their deprotection facility at differing DTNP concentrations under standard deprotection conditions (1 hr; 25°C), with the results of each assay followed by comparison of HPLC peak areas. The measured deprotection product of the Cys peptide was its corresponding 5-Npys conjugate. The Sec peptide initially afforded a more complex deprotection HPLC profile, and the isolated product required reduction with $NaBH_4$ as a second step yielding (upon AcOH quench and exposure to air) the diselenide as the measured deprotection product.

Of the Cys protectants, the Bzl and Meb protecting groups were robust to the deprotection conditions, showing limited removal. In the presence of thioanisole, Mob, Acm, and S*t*Bu groups were quite labile, although in the absence of thioanisole they were much more robust. The deprotection profile of the *t*Bu group showed equal efficiency whether thioanisole was used or not. The three benzyl-templated Sec protectants showed high lability to the deprotection conditions, with Mob and Meb removal being a facile process regardless of thioanisole addition. Sec(Bzl) removal had a high dependence upon the presence of thioanisole, however.
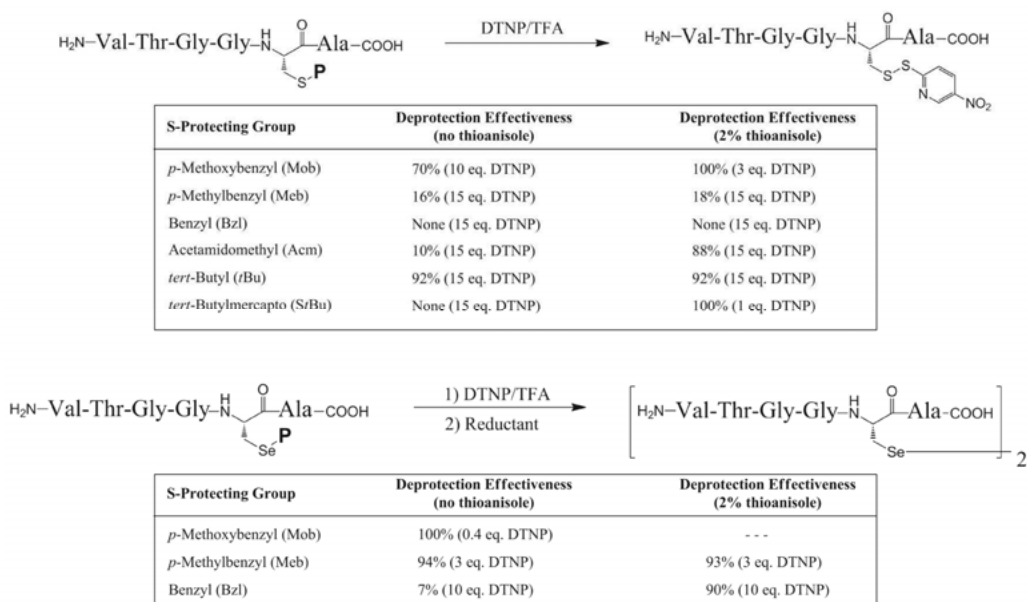
Fig. 2. Tabulation of different Cys and Sec protecting groups' lability to the DTNP conditions.

Cys apamin and Sec Lys16A peptide models (Figure 3) were utilized as templates for the iterative construction of two-disulfide and two-diselenide systems respectively. Initial disulfide installation in apamin was accomplished with high DTNP concentration in the absence of thioanisole followed by selective reduction with 1 eq. DTT. Following purification, this intermediate was treated with DTNP at similar concentration in the presence of thioanisole followed by reduction with 1 eq. DTT to afford native apamin.

Sequential diselenide formation in Sec Lys16A was carried out by first treating the peptide with 1 eq. DTNP in the absence of thioanisole to induce spontaneous first diselenide formation. Following purification, the single-diselenide intermediate was treated with 10 eq. DTNP in the presence of thioanisole followed by reduction with excess DTT to afford fully-cyclized Lys16A.
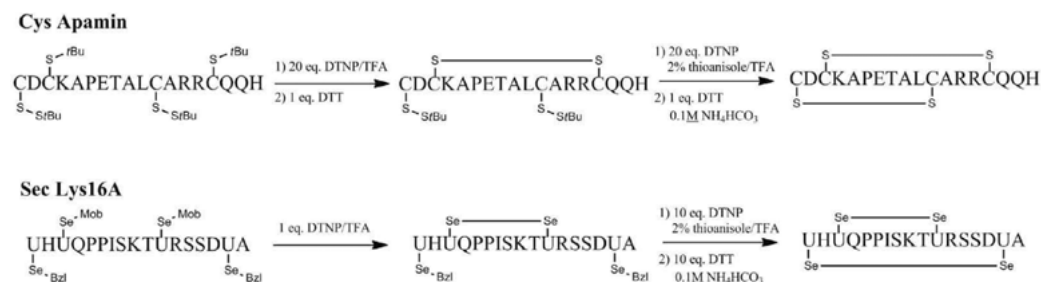
Fig. 3. Sequential deprotection and disulfide/diselenide formation on Apamin & Lys16A models.

References

1. Harris, K.M., Flemer, S., Hondal, R.J. *J. Peptide Sci*. **13**, 81-93 (2007).
2. Oikawa, T., Esaki, N., Tanaka, H., Soda, K. *Proc. Natl. Acad. Sci*. **88**, 3057-3059 (1991).
3. Walter, R., du Vigneaud, V. *J. Am. Chem. Soc*. **87**, 4192-4193 (1965).
4. Gieselman, M.D., Xie, L., van der Donk, W.A. *Org. Lett*. **3**, 1331-1334 (2001).
5. Metanis, N., Keinan, E., Dawson, P.E. *J. Am. Chem. Soc*. **128**, 16684-16691 (2006).

Imidazole-Promoted Cyclization of Peptide Thioester to Cyclic Depsipeptide and Cyclic Peptide

Yangmei Li, Marc Giulionatti, and Richard A. Houghten

Torrey Pines Institute for Molecular Studies, Port St. Lucie, FL, 34987, U.S.A.

Introduction

An imidazole promoted cyclization strategy for the synthesis of cyclic depsipeptide has been developed. Non-protected peptide thioester CH_3CO-Ser-Ala-Phe-Tyr-Gly-SCH_2Ph has been used as the linear precursor. The cyclization was performed at a concentration of 1 mM in 1.5 M imidazole in acetonitrile at room temperature. The macrolactonization was complete after 24 h with a yield over 95%. This cyclization strategy has been successfully applied to the synthesis of several natural cyclic depsipeptides such as Kahalalides and Sansalvamide A. This imidazole promoted cyclization strategy also works for the synthesis of Gramicidin S, a natural cyclic peptide.

Results and Discussion
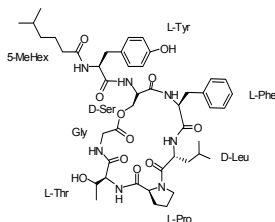
Fig. 1. Kahalalide B.

Bioactive cyclic peptides and depsipeptides which are isolated from natural sources provide a range of lead structures for the design of new drugs. Biosynthesis of cyclic depsipeptides through peptide synthetase has been reported by using peptide thioester as substrate. Studies of different peptide synthetase systems suggest the possibility that a histidine residue functions as a catalyst of condensation/elongation/cyclization reaction in the peptide synthesis [1]. Imidazole has been reported as a catalyst mimicking the histidine residues of enzymes hydrolyzing the ester bond and the thioester bond [2]. The generally accepted mechanism of the imidazole-catalysis involves the reaction intermediates of acyl imidazole and the acyl imidazolium cation, which are formed by the direct attack of imidazole on the carbonyl group. This mechanism can be envisioned for the formation of a cyclic depsipeptide by macrolactonization and a cyclic peptide by macrolactamization. The mild imidazole-catalytic condition may also eliminate the risk of racemization during acyl activation. Herein, we report an imidazole-catalytic approach for the synthesis of cyclic depsipeptides by macrolactonization of peptide thioesters and the use of this application in the synthesis of Kahalalide B (Figure 1) and its analogues.

The stepwise synthesis of the linear peptides starts with functionalized mercaptomethylphenyl silica gel **1** as the "volatilizable" support (Scheme 1) [3]. Boc-glycine was coupled on the resin based on the structure of Kahalalide B. After removal of the Boc group with 55% TFA, threonine, proline, D-leucine, phenylalanine, D-serine, tyrosine, and 5-methylhexanoic acid were coupled stepwise to form the on-resin synthetic precursor of Kahalalide B **3a**. The resin-bound **3a** was then treated with anhydrous HF for 2 h at 0°C. Following evaporation of the anhydrous HF with a gaseous nitrogen stream, the unprotected peptide thioester **4a** was obtained following lyophlization [4].
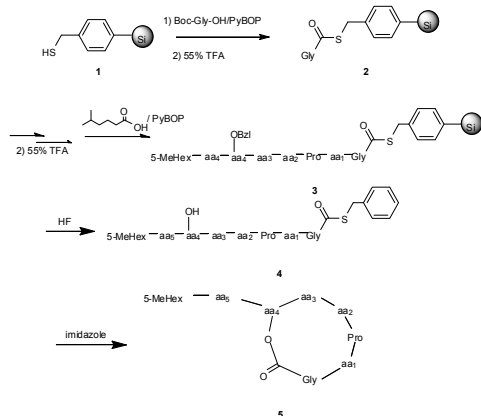
Scheme 1. Synthesis of Kahalalide B and Analogs.
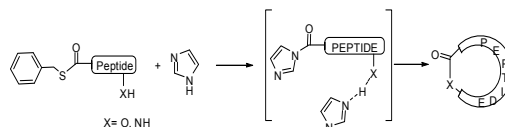
Scheme 2. Mechanism of imidazole-promoted cyclization.

Table 1. Kahalalide B and Analogs

Entry	AA_1	AA_2	AA_3	AA_4	AA_5	Yield %[a]
5a	Thr	D-Leu	Phe	D-Ser	Tyr	98
5b	Ser	D-Leu	Tyr	D-Ser	Tyr	90
5c	Ser	D-Ala	Phe	D-Ser	Phe	85
5d	Thr	D-Ala	Tyr	D-Ser	Phe	80
5e	Thr	D-Leu	Tyr	D-Thr	Phe	92

[a]Yield is based on the weights of purified cyclic products and their purified linear peptide thioesters

The cyclization was performed by macrolactonization in acetonitrile using imidazole as a catalyst. The effect of imidazole on catalytic esterification and cyclization was at first tested using an N-acetyl pentapeptide thioester Ac-Xxx-Ala-Phe-Tyr-Gly-SCH$_2$Ph, where Xxx were Ser and Thr. It was found the concentration of imidazole significantly affected the macrolactonization. Macrolactonization by the hydroxyl on the serine residue was complete after a 24 h reaction at room temperature with a yield over 95% when the concentration of imidazole was 1.5 M; but failed even after reacting for 10 days when the concentration was 0.15 M. The need for a high concentration of imidazole probably suggested the formation of the imidazolyl intermediate as rate limiting (Scheme 2). The formation of kahalalide B (**5a**) was tested using 1 mM of **4a** and 1.5 M imidazole in acetonitrile at room temperature for 24 h. It was found the cyclic depsipeptide of kahalalide B was quantitatively converted. Analogues of kahalalide B (5b-e) were synthesized by selectively changing residues at positions AA$_1$, AA$_2$, AA$_3$, AA$_4$, and AA$_5$. Residues of glycine and proline were reserved in the cyclic product. The yield and purity of Kahalalide B and its analogues are shown in Table 1.

Natural cyclic despipeptide Sansalvamide A has been synthesized by using this imidazole-promoted cyclization method. Linear thioester HO-Leu-Val-Leu-Phe-Leu-SCH$_2$Ph has been synthesized and then cyclized under microwave irradiation at 60 °C for 120 min. The yield of cyclization is around 80%, along with about ~20% hydrolysis byproduct forming (Figure 2). Natural cyclic peptide Gramicidin S has also been synthesized by using imidazole-promoted cyclization method. Unprotected linear peptide thioester D-Phe-Pro-Val-Orn-Leu-D-Phe-Pro-Val-Orn-Leu-SCH$_2$Ph has been cyclized in 0.188 M imidazole in acetonitrile-water (7:1 in volume) solution at r.t. overnight, forming desired cyclic Gramicidin S (Figure 3) [5].
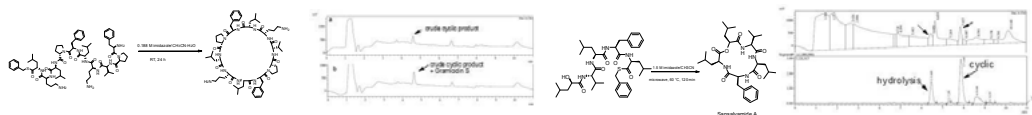
Fig. 2. HPLC of cyclization of Sansalvamide A.   Fig. 3. HPLC of cyclization of Gramicidin S.

In summary, we present here a novel imidazole-promoted cyclization method to the synthesis of cyclic depsipeptides and cyclic peptides from their linear thioesters. This method is promising for the synthesis of the natural cyclic products.

Acknowledgments

References

1. Kohli, R.M., Walsh, C.T., Burke, M.D. *Nature* **418**, 658 (2002).
2. Bruice, T.C., Schmir, G.L. *J. Am. Chem. Soc.* **79**, 1663 (1957).
3. Li, Y., Yu, Y., Giulianotti, M., Houghten, R.A. *J. Comb. Chem.* **10**, 613 (2008).
4. Li, Y., Giulianotti, M., Houghten, R.A. *Org. Lett.* **12**, 2250 (2010).
5. Li, Y., Yongye, A., Giulianotti, M., Martinez-Mayorga, K., Yu, Y., Houghten, R.A. *J. Comb. Chem.* **11**, 1066 (2009).

Macrocyclization of Linear Peptides Enabled by Amphoteric Molecules

Andrei K. Yudin

Davenport Research Laboratories, Department of Chemistry, University of Toronto, 80 St. George Street, Toronto, Ontario, Canada, M5S 3H6

Introduction

Cyclic peptides are known for their capacity to stabilize secondary structures such as α-helices, β-turns, γ-turns, and β-sheets. We have applied amphoteric molecules, namely aziridine aldehydes, towards the macrocyclization of linear peptides. Our method efficiently yields macrocycles with high chemo- and stereoselectivities and exhibits no signs of epimerization, cyclodimerization, or oligomerization. The reaction products contain an electrophilic aziridine "handle" that can be used for late stage structural modification.

Results and Discussion

A number of naturally occurring cyclic peptides are known. Peptide macrocycles often exhibit many favourable characteristics of larger protein medicines (e.g. antibodies), such as high target specificity. They also overcome some deficiencies of this therapeutic class, such as instability and high cost. The laboratory synthesis of macrocycles from linear peptide precursors has remained a challenge for a number of years [1]. We have developed a method that employs amphoteric aziridine aldehydes to effect macrocyclization of linear peptides. Amphoteric aziridine aldehydes were described in a recent report from our laboratory and are now commercially available from Sigma-Aldrich [2]. These materials can also be easily accessed from readily available feedstocks (Figure 1).
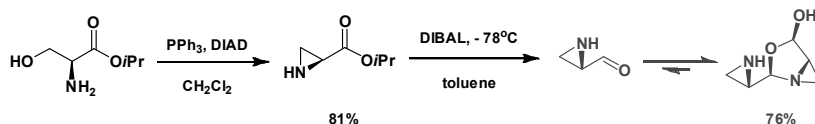
Fig. 1. Synthesis of bench-stable, unprotected amino aldehydes for use in peptide macrocyclization.
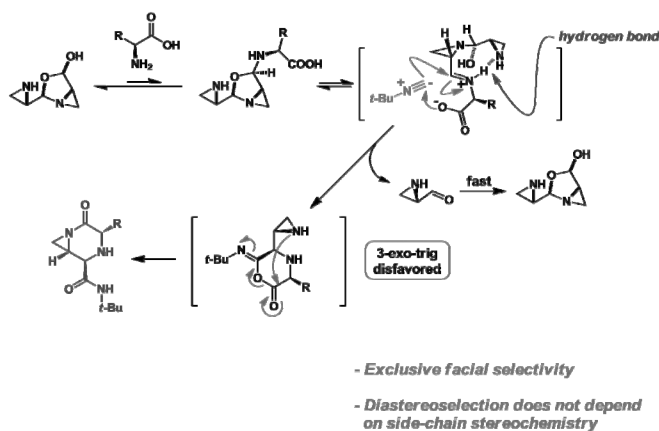
Fig. 2. Mechanism of cyclization shown on an amino acid example.
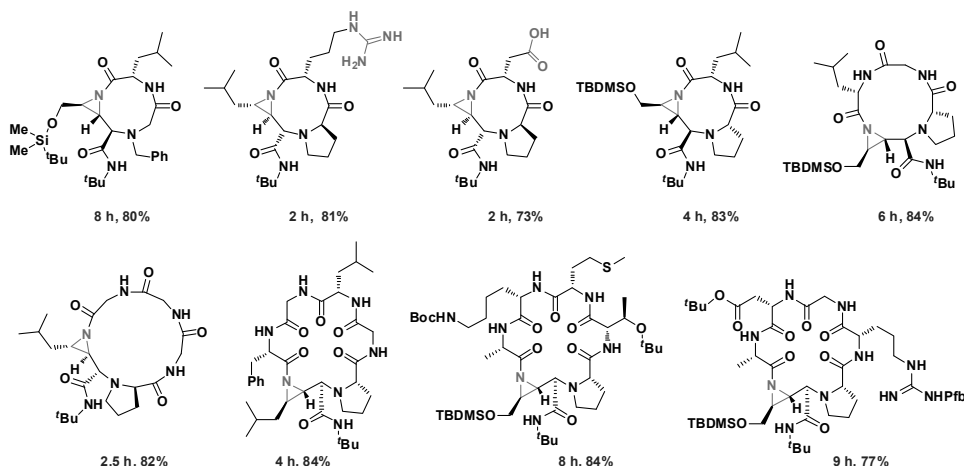
Fig. 3. The cyclization reaction scope.

Figure 2 highlights the mechanistic underpinnings of the process, whereas Figure 3 shows the reaction scope. Notably, macrocycles can now be produced within short reaction times and without any cyclodimerization by-products [3,4].

The presence of a nucleophilic center at the α-position of an amphoteric aziridine aldehyde is responsible for high yields and stereoselectivities observed in our chemistry. The molecules of macrocycles can now be assembled with high chemoselectivities from amino acids or linear peptides, isocyanides, and amphoteric aziridine aldehydes in a simple one-step process. The analytically pure product of the reaction can be isolated by precipitation from the reaction mixture or by using preparative HPLC. Most importantly, the resulting molecules possess useful structural features that allow specific modification at defined positions via straightforward aziridine ring-opening. Control elements such as fluorescent tags, conformation-tuning substituents, and liphophilic control elements, are amenable to incorporation into macrocycle frameworks at late stages of synthesis. Given the prevalence of macrocycles in chemistry and biology, our reaction should find utility in many areas.

Acknowledgments

References

1. White, C., Yudin, A.K. *Nature Chem.* **3**, 509-524 (2011).
2. Hili, R., Yudin, A.K. *J. Am. Chem. Soc.* **128,** 14772-14773 (2006).
3. Hili, R., Rai, V., Yudin, A.K. *J. Am. Chem. Soc.* **132**, 2889-2891 (2010).
4. Rotstein, B., Rai, V., Hili, R. *Nature Protocols* **5**, 1813 (2010).

Microwave Assisted Lactam Cyclization of Peptides

Vinod V. Kulkarni, Nabila Brabez, Christine Salibay, Heather J. Harteis, Channa De Silva, and Victor J. Hruby

Department of Chemistry and Biochemistry, University of Arizona, Tucson, AZ, 85719, U.S.A.

Introduction

Microwave-Assisted Peptide Synthesis (MAPS) is routinely used to synthesize peptides in high purity and shorter times. Based on microwave dielectric heating which converts electromagnetic waves into instant heat, microwave based chemistry is an emerging field in the areas of chemistry related sciences. The mechanisms of dipolar polarization and ionic conductance in microwave irradiation offer a unique way in enhancing organic synthetic reactions in solution phase as well as solid phase. Thus microwave based chemistry [1] offers diversity in conducting chemical reactions.

Fetching two termini of a large molecule to proximity for the formation of a chemical bond has always been an interesting and demanding problem. Cyclic peptides are important molecules whether derived from their parent linear peptides or from nature. They offer constrained and limited conformational features, which are highly desirable for the development of highly selective and profiled biological ligands. Due to the high flexibility of a linear peptide, cyclizations of peptides are generally challenging in their synthesis and obtaining them in high purity. Generally, lactam based cyclizations on solid phase are performed for hours to days to undergo completion, thus affecting the overall purity of the final peptide. The purity is further compromised if the desired peptide needs further addition of amino acids.

Lactam based cyclization on solid phase using microwave technique has been previously reported [2]. However, choice of solvents, coupling reagent and power requirements for microwave has not been explored further. Ac-Nle-c[Asp-His-D-Phe-Arg-Trp-Lys]-NH$_2$ **(MT-II)**, Ac-Nle-c[Asp-His-D-Nal(2′)-Arg-Trp-Lys]-NH$_2$ **(SHU9119)**, Ac-Nle-c[Asp-Pro-D-Nal(2′)-Arg-Trp-Lys]-NH$_2$ **(PG901)** and c[Nle-Val-D-Nal(2′)-Arg-Trp-Glu]-NH$_2$ **(AVM127)** are all well-known cyclic peptides specific towards melanocortin receptors. They are cyclized via a lactam bridge from side chain to side chain functional groups bearing a carboxylic acid and amine termini except for **AVM127**, which is cyclized from side chain to N-terminus. We here demonstrate the application of microwave technology in synthesizing the above cyclic peptides bridged by a lactam formation. Low temperature and shorter reaction times with microwave conditions have been developed to synthesize the above melanocortin-based ligands with high purity. The methodology established may be applied towards any lactam based cyclic peptides.

Results and Discussion

The linear peptide corresponding to **MT-II**, **SHU9119**, **PG901** and **AVM127** were synthesized manually using the standard Fmoc/*t*Bu strategy for solid phase peptide synthesis. Rink amide MBHA resin (0.68 mmol/g) was used. The synthesis was performed until the precursor of the peptide required for lactam cyclization, which is usually towards the last amino acid of N-terminus. N$^\alpha$-Fmoc of Asp for **MT-II**, **SHU9119** and **PG901** was maintained while for **AVM127** the N$^\alpha$-Fmoc was deprotected. Upon completion of these linear precursors the resin was vacuum dried and re-swollen in dry dichloromethane. Addition of phenylsilane and tetrakis (triphenylphosphine) palladium(0) under Argon bubbling for 15 minutes was performed twice to deprotect selectively the orthogonal protection from Lysine, Aspartic acid and Glutamic acid. 5% Solution of sodium diethyldithiocarbamate trihydrate in DMF was used to remove any traces of palladium. The peptide-resin was then subjected to lactam cyclization with the following procedure. To the above peptide-resin solvent was added followed by the coupling reagent and base, *N,N*-diisopropylethylamine. The mixture was stirred for a minute and then subjected to -78°C. Finally, microwave energy was irradiated for a fixed amount of time and repeated, by reducing the starting temperature of the mixture back to -78°C. The final temperature of the peptide-resin mixture was measured to be not more than 45°C in any performed choice of solvent, coupling agent, microwave power (W) and time subjected to microwave irradiation. Table 1 shows the conditions used and total time required to achieve

Table 1. Microwave conditions used for lactam cyclization of the peptides

	Microwave Conditions: Maximum Applied Power (W), time in seconds (s) per cycle[1]			
	25W, 60s cycle[1]	*50W, 30s cycle[1]*	*100W, 15s cycle[1]*	*200W, 8s cycle[1]*
Coupling Reagent: HBTU Solvent ⇓	Total time required in seconds (s) for completion of cyclization			
DMF	480s	360s	180s	32s
DMF:DCM(4:1)	480s	360s	180s	32s
DMF:THF(1:1)	480s	360s	180s	128s
NMP	480s[i]	360s[i]	180s[i]	64s[i]
Coupling Reagent: HCTU				
Solvent Conditions[2]	480s[i]	360s[i]	180s[i]	128s[i]

[i]*Incomplete cyclization (linear precursor of the peptide observed in HPLC);* [1]*A cycle refers to a continuous exposure of microwave irradiation for the mentioned amount of time in seconds. Note: Temperature is not constant and rises with time for the corresponding maximum power applied. Max. Temp. measured is 45 °C;* [2]*All solvent conditions mentioned for HBTU were tested but didn't result in completed cyclization*
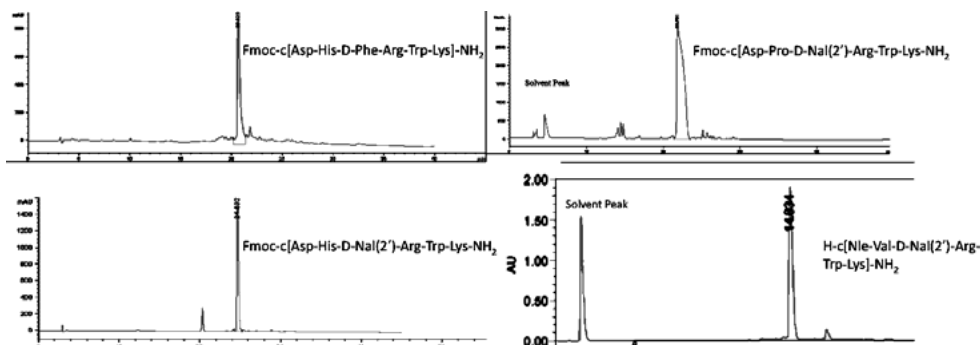
Fig. 1. HPLC profiles of the lactam cyclized precursor peptides at 200W.

completion of the lactam cyclization reaction which is monitored by Kaiser test and Reverse Phase High Pressure Liquid Chromatography (HPLC) (Figure 1).

Thus it can be concluded that among solvents, DMF alone and in combination with DCM or THF produce the best results for cyclization by drastically shorter times and higher yields (>90% for all peptides). Also coupling reagent HBTU in any solvent combination gave pure cyclized products as compared to HCTU. This is not clearly understood since HCTU is a stronger reagent compared to HBTU. In terms of the power requirement for microwave irradiation, 200W is the most optimum but a minimum power of 25W also gave the same HPLC profiled results as 200W. This is indicative that the power requirements for cyclization should be structure dependent due to their conformational features. Microwave irradiation thus represents a powerful technique for cyclization of peptides.

Acknowledgments

References

1. Kappe, O.C. *Angew. Chem. Int. Ed.* **43**, 6250-6284 (2004); Al-Obeidi, F., et al. *Mini-Reviews in Medicinal Chemistry* **3**, 449-460 (2003); Collins, J.M., Leadbeater, N.E. *Org. Biomol. Chem.* **5**, 1141-1150 (2007).
2. Monroc, S., et al. *SYNLETT* **9**, 1131-1134 (2006); Mason, C., Singh, S., Douglas, A., Williamson, E., Vanier, G. *Poster Presentation 21st American Peptide Symposium,* (2009).

Microwave-Assisted Synthesis of a Glycine-Rich Difficult Peptide Sequence, the C-terminal Amidated Portion of Acanthoscurrin

Vinícius M.R. Milan[1], Diego P. Santos[2], Márcia L.A. Temperini[2], and M. Terêsa Machini[1*]

[1]*Departments of Biochemistry;* [2]*Fundamental Chemistry, Institute of Chemistry, University of São Paulo, São Paulo, SP, 05508-000, Brazil*

Introduction

Besides studying chemistry, structure and mode of action of antimicrobial peptides (AMP), we have been investigating solid-phase peptide synthesis (SPPS) at elevated temperatures. We have shown that our protocols at 60ºC using conventional heating are effective and economical for high-speed stepwise synthesis of a variety of peptides by Fmoc or Boc strategy [1]. We have also demonstrated the adequacy of such protocols to microwave-assisted SPPS [2].

Acanthoscurrin is a glycine-rich protein (GRP) isolated from the hemocytes of the Brazilian spider *Acanthoscurria gomesiana*. This GRP, also an AMP, is released to the hemolymph when the spider is infected [4]. The two existing isoforms of the protein contains 130 and 132 amino acid residues. The last has net charge +8 at physiological pH, an isoelectric point of 10, a C-terminal portion with 32 amino acid residues [*acantho(101-132)]*, an N-terminal portion containing 22 amino acid residues [*acantho(1-22)]* and a central portion that comprises three repeats of 26 amino acid residues [*acantho(23-48), (49-74) and (75-100)*] [3].

In 2009, we demonstrated that *acantho(101-132)* is a typical difficult peptide sequence as its synthesis was achieved by Fmoc strategy only when our protocols at 60ºC using conventional heating were used in combination with CLEAR amide resin of low substitution degree, chaotropic salt and amide backbone protection (Hmb group) [4]. The present study aimed to verify whether, under such experimental conditions, microwave irradiation minimizes peptide aggregation in stepwise solid-phase synthesis of *acantho(101-132)* to the point of avoiding amide backbone protection.

Results and Discussion

Microwave-assisted stepwise peptide assembly on resin (Rink Amide or CLEAR amide of substitution level of 0.40 or 0.33 mmol/g, respectively) employed Fmoc amino acid and a SPS Discover[TM] system (CEM Corporation®, Charlotte/ NC, EUA). The set temperature used in all steps (washing, deprotection and coupling) was 60°C. Coupling (in DMF containing 2.5 fold excess of incorporating amino acid and DIC/HOBt for 15 min) and deprotection (in 20-30% piperidine for 6 min) reactions occurred under N_2 atmosphere and were monitored by the ninhydrin test [1,2]. When needed, recoupling was performed under the same conditions or with the replacement of DIC/HOBt by TBTU/DIPEA. Washings pre- and post-deprotection or coupling employed 20% DMSO/NMP, MeOH, 20% DMSO / NMP, MeOH and DCM (for Rink amide resin) or 20% DMSO/NMP isopropanol, 20% DMSO / NMP, isopropanol and DCM (for CLEAR amide).

Samples of the growing-peptide resins were examined by Raman spectroscopy.

Peptide full deprotection/detachment from resin was performed in TFA:water:*m*-cresol:TIS (92.5:2.5:2.5:2.5; v/v/v/v) for 4h at 37°C under orbital shaking. Product isolation followed procedure previously described [5]. While peptide analysis and purification were done by RP-HPLC, peptide identification employed LC/ESI-MS.

H-Gly[105]-Gly-Gly-Arg-Gly-Gly-Gly-Tyr-Gly-Gly[114]-Gly-Gly-Gly-Tyr-Gly-Gly-Gly-Tyr-Gly-Gly-Gly-Tyr-Gly-Gly-Gly-Lys-Tyr-Lys[132]-NH_2

Fig. 1. Amino acid sequences of the peptides obtained by using Rink amide resin [acantho(114-132)] and CLEAR amide [acantho(105-132)].

---

* Previously M. Terêsa M. Miranda or M.T.M. Miranda

The results obtained (Figures 1-3) confirmed our prior observation [5] that, at least on resin, glycine-rich peptides derived from *acantho(101-132)* present early tendency to assume β-sheet structures typical for peptide aggregation. In fact, this phenomenon was not entirely avoided during peptide microwave-assisted assembly on RINK amide resin (data not shown) or CLEAR amide at high temperature even in presence of LiCl, as confirmed by Raman spectroscopy analysis of the growing peptide-resins (Figure 2). On the other hand, the fact that microwave-assisted synthesis of *acantho(105-132)* was achieved without requiring the use of Fmoc-Gly(Hmb)-OH is a further, and more importantly, unequivocal demonstration that microwave irradiation can drastically minimize peptide aggregation in solid-phase synthesis of difficult peptides.

1   2
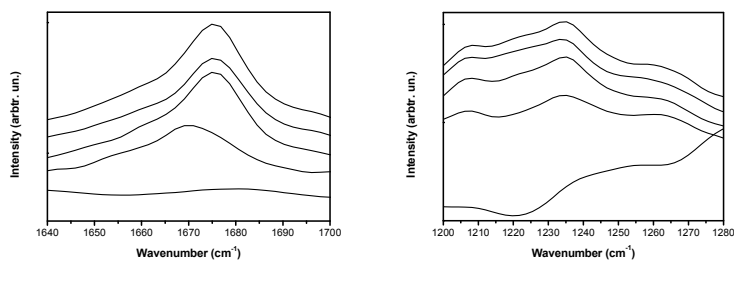
Fig. 2. Raman spectra in the amide I (1) and amide III (2) regions of CLEAR amide and of the growing peptide-CLEAR amide. From bottom to top: H-acantho(126-132)-, Fmoc-acantho(118-132)-, H-acantho(112-132)- and H-acantho(106-132)-CLEAR amide.
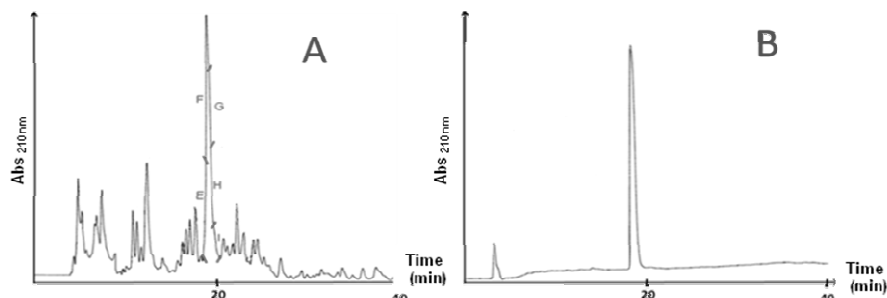
Fig. 3. RP-HPLC profile of the crude (A) and purified (B) H-acantho(105-132). Semi-preparative RP-HPLC conditions (A): volume of crude peptide solution injected: 100 μL, column: Vydac C$_{18}$ (1 X 25 cm, 300 Å), solvents A: 0.1% TFA/H$_2$O, B: 40% ACN/0.1 % TFA/ H$_2$O, λ: 210 nm, flow: 3.0 mL/min, linear gradient: 30% - 50% B in 40 min. Analytical RP-HPLC (B): volume of crude peptide solution injected: 20 μL, column: Vydac C$_{18}$ (0.46 X 25.0 cm, 300 Å), solvents A: 0.1% TFA/H$_2$O, B: 40% ACN/0.1% TFA/ H$_2$O, λ: 210 nm, flow: 1.0 mL/min, linear gradient: 5% - 95% B in 30 min.

References
1. Varanda, L.M., Miranda, M.T.M. *J. Pept. Res*. **50**(2), 102-108 (1997). Rivier, J.E., Miranda, M.T.M., *Synthesis of Peptides and Peptidomimetics*, **4**, 806-813 (2001). Souza, M.P., et al. *Tetrahedron* **60**, 4671-4681 (2004).
2. Loffredo, et al. *J. Pept.Sci.* **15** (12), 808-817 (2009).
3. Silva, P.I., Jr., et al. *J. Biol. Chem*. 275, 33464-33470 (2000).
4. Lorenzini, D., et al. *Dev. Comp. Immunol.* **27**, 781-791 (2003).
5. Remuzgo, et al. *Biopolymers* 92, 65-75 (2009).

Optimizing the Synthesis of 4(5)-Benzyl-L-Histidine and Analogues

D. David Smith[1,2], Audrey T. Gallagher[1,3], Wayne Gergens[3], Vincent M. Crowley[1,3], Peter W. Abel[2], and Martin Hulce[1,3]

[1]Department of Biomedical Sciences; [2]Department of Pharmacology; [3]Department of Chemistry, Creighton University, Omaha, NE, 68178, U.S.A.

Introduction

The amino acid residue of 4(5)-benzyl-L-histidine is found in the potent, human selective calcitonin gene-related peptide (CGRP) antagonists N-α-benzyl-[4(5)-benzylhistidyl][10]-CGRP(8-37) **1** and N-α-benzoyl-[4(5)-benzylhistidyl][10]-CGRP(8-37) [1,2] **2**. The key step in the synthesis of these antagonists, namely the global benzylation of the assembled, resin-bound, protected peptide to benzylate the C4 position of the imidazole ring of the BOM-protected histidyl residue in position 10, proceeds in a 40% yield resulting in a poor isolated yield of 6% for the antagonists. Consequently, recent efforts to improve the yield of **1** and **2** focused on the synthesis of the amino acid 4(5)-benzyl-L-histidine [3,4].

Results and Discussion

Two literature reports describe a two-step synthesis of 4(5)-benzyl-L-histidine from L-histidine. Briefly, L-histidine undergoes a Pictet-Spengler condensation with benzaldehyde under basic conditions to yield a mixture of *cis* and *trans* isomers of L-4-phenylspinacine, which undergoes hydrogenolysis to cleave the doubly benzylic C-N bond yielding 4(5)-benzyl-L-histidine (Figure 1). Efforts to reproduce these methods proved challenging with unreacted starting material present after each step and so a complete review of the synthesis was undertaken to improve the reproducibility of the synthetic methods and improve the isolated yield of 4(5)-benzyl-L-histidine.

Initial efforts explored the reaction time and amount of potassium hydroxide needed to promote the Pictet-Spengler reaction. The reaction was repeated with two [3] and three [4] equivalents of potassium hydroxide and its progress monitored by RP-HPLC. Upon completion, ethanol was removed *in vacuo* and the resulting aqueous solution was neutralized to pH of 6.8, the pI value of spinacine, and cooled to 0°C. Two equivalents of potassium hydroxide yielded phenylspinacine in an 81% yield in agreement with literature reports [3] but the reaction required up to 24 hours to be complete. Three equivalents of potassium hydroxide gave an improved yield of 91% and the reaction was complete in one hour. Similar results were obtained using a variety of mono-fluoro-substituted benzaldehydes to yield the corresponding fluorinated phenyl-spinacines.

Previously, hydrogenolysis of 4-L-phenylspinacine was accomplished using hydrogen gas at atmospheric pressure over 25% Pd/C [4]. Unfortunately, this catalyst is not readily available and when this reaction was repeated using 10% Pd/C, hydrogenolysis was incomplete after 18 hours. Catalytic transfer hydrogenolysis using ammonium formate in methanol at ambient temperature gave similar results [5], however, when the reaction was performed under reflux [6]
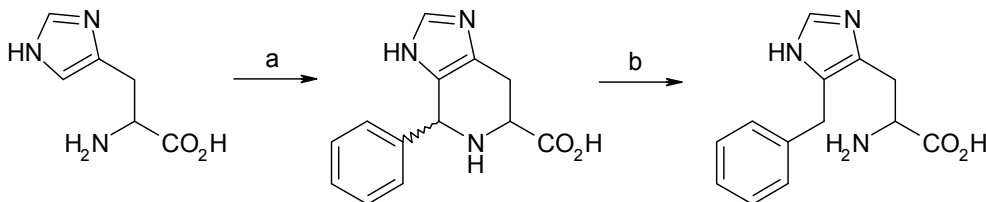
Fig. 1. Synthesis of 4(5)-benzyl-L-histidine. Reagents & conditions: a) benzaldehyde (1eq.), KOH (2 or 3 eq.), refluxing ethanol/water (1/2, v/v). b) H₂, 25% Pd/C, methanol/acetic acid (1/1, v/v).

Table 1. Reduction of 4-L-phenylspinacine

Reagents	Solvent	Temp (°C)	Time (hr)	Yield (%)	% Purity
H_2 (40 psi), 10% Pd/C	Methanol	Ambient	18	80[a]	80
$NH_4^+HCO_2^-$, 10% Pd/C	Methanol	Ambient	18	80[a]	80
$NH_4^+HCO_2^-$, 10% Pd/C	Methanol	65	0.25	92[b]	93
$NH_4^+HCO_2^-$, 10% Pd/C	Trifluoroethanol	78	0.25	93	>97
$NH_4^+HCO_2^-$, 10% Pd/C	Water	100	0.25	58[c]	>93

[a]*20% recovered starting material.* [b]*57% isolated yield after recrystallisation from water.* [c]*Crystallised from water.*

no starting material was observed after 15 minutes by RP-HPLC. Similar results were obtained using trifluoroethanol and water as solvents (Table 1).

In summary, we have optimized the synthesis of 4(5)-L-benzylhistidine. Use of three equivalents of potassium hydroxide in the Pictet-Spengler reaction reduced the reaction time from 24 hours to one hour and improved the isolated yield of 4-L-phenylspinacine to 91%. Catalytic transfer hydrogenolysis at elevated temperatures resulted in complete cleavage of the doubly benzylic C-N bond of phenylspinacine in less than 15 minutes over a 10% Pd/C catalyst. These improvements significantly reduced the total reaction time for the synthesis of 4(5)-L-benzylhistidine and substantially increased the yield over the two steps from L-histidine from 62% (81% for step 1 [3] and 77% for step 2 [4]) to 85% (91% for step 1 and 93% for step 2).

Acknowledgments

References

1. Smith, D.D., Saha, S., Fang, G., Schaffert, C., Waugh, D.J., Zeng, W., Toth, G., Hulce, M., Abel, P.W. *J. Med. Chem.* **46**, 2427-2435 (2003).
2. Taylor, C.K., Smith, D.D., Hulce M., Abel, P.W. *J. Pharmacol. Exp. Ther.* **319**, 749-757 (2006).
3. Guzman, F., Cain, M., Larscheid, P., Hagen, T., Cook, J.M., Schweri, M., Solnick, P., Paul, S.M. *J. Med. Chem.* **27**, 564-570 (1984).
4. Yutilov, Y.M., Abramyants, M.G., Smolyar, N.N. *Russian Journal of Organic Chemistry* **37**, 119-124 (2001).
5. Anwer, M.K., Spatola, A.F. *Synthesis* 929 (1980).
6. Ram, S., Spicer, L. *Synthetic Communications* **22**, 2673-2681 (1992).

One-Pot Synthesis of LHRH Agonists Using Tetraphenylborate Salts

Karel Decroos, Naima Benzitouni, Etienne Moniotte, and Roland Callens

Peptisyntha Process Development and Scale-up, Brussels, B-1120, Belgium

Introduction

The work-up after synthesis of peptides containing unprotected arginine residues can be very troublesome due to the low solubility in organic solvents. However, their tetraphenylborate (TPB) salt is insoluble in water but soluble in a wide range of organic solvents, allowing an extractive and cost effective work-up [1]. TPB is introduced as sodium tetraphenylborate (Figure 1) to an aqueous solution of a water-soluble salt of an arginine containing peptide. The formed TPB salt precipitates and can be recovered by filtration or extraction.
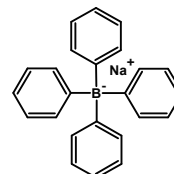
Fig. 1. Sodium tetraphenyl borate (NaTPB).

Lutein Hormone Releasing Hormone (LHRH) or Gonado-tropin Releasing Hormone (GnRH) agonists are a family of therapeutic peptides of commercial interest. They are analogues of the natural decapeptide with modifications on position 6 and 10 (Table 1) which render them more resistant to enzymatic degradation while maintaining biological activity. They are used in several therapeutic domains of which the treatment of hormone-dependent cancers and control of fertility are the most important [2].

Our goal was to develop a novel common LPPS strategy for different LHRH agonists using the TPB technology and benefiting as much as possible from the sequence similarity to obtain an economically interesting process by using common building blocks.

Table 1. Sequence of some LHRH agonists synthesized here with the TPB technology

	1	2	3	4	5	6	7	8	9	10
Natural LHRH	pGlu -	His -	Trp -	Ser -	Tyr -	Gly -	Leu -	Arg -	Pro -	Gly-NH$_2$
Triptorelin	pGlu -	His -	Trp -	Ser -	Tyr -	(D)Trp -	Leu -	Arg -	Pro -	Gly-NH$_2$
Goserelin	pGlu -	His -	Trp -	Ser -	Tyr -	(D)Ser(OtBu)-	Leu -	Arg -	Pro -	azaGly-NH$_2$
Leuprorelin	pGlu -	His -	Trp -	Ser -	Tyr -	(D)Leu -	Leu -	Arg -	Pro -	N-Et

Results and Discussion
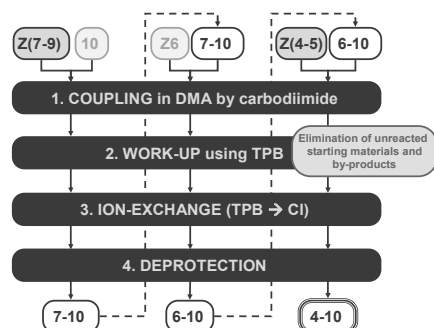
Fig. 2. General scheme for the one-pot synthesis of the 4-10 fragment of LHRH agonists. Only the 4-10 fragment is isolated by precipitation.

We opted for a 1-3 + 4-10 strategy giving the following common building blocks: the (1-3) fragment, the Z(7-9) and Z(4-5) fragment.

In a first step we coupled the coupled Z(7-9) to the residue in position 10. After work-up using the TPB technology, ion exchange on resin and deprotection, the 7-10 fragment was obtained in solution at high purity, making purification by precipitation or crystallization unnecessary. The 7-10 fragment was thus not isolated and coupled directly to the Z6 amino acid according to the same procedure and the obtained 6-10 fragment was again not isolated but coupled directly to the Z(4-5) fragment to yield the 4-10 fragment that was precipitated (Figure 2).

This procedure showed to be applicable to the three LHRH agonists we tested and gave excellent results in terms of yield and purity (Table 2) and was easy to scale-up.

Table 2. Results (purity and yield) for the different stages in the synthesis of the 4-10 fragment of LHRH agonists

	triptorelin		goserelin		leuprorelin	
Fragment	HPLC purity (%)	Yield (%)	HPLC purity (%)	Yield (%)	HPLC purity (%)	Yield (%)
7-10	98	83	99	79	97	85
6-10	97	89	97	91	94	90
4-10	96	88	97	87	94	86
Total yield (%)	65		62		66	

Conlusion

We developed a one-pot LPPS protocol for the synthesis of the 4-10 fragment of LHRH agonists using TPB technology. By applying the same synthetic procedure repetitively we obtained the 4-10 fragment with excellent purity and yield. The protocol was applicable to three examples of LHRH agonists and is ready for other members of this family. This process constitutes an economically appealing approach for the synthesis of different LHRH agonists using common building blocks and optimal inventory management strategies.

The TPB technology showed to be a powerful tool for the in process purification of arginine-containing peptides, in such a manner that isolation of intermediates, which can be very time-consuming at industrial scale, can be avoided.

References

1. Callens, R., Jeannin, L. WO 2009/153294 A9.
2 Moreau, J.P., Delavault, P., Blumberg, J. *Clinical Therapeutics* **28**, 1485-1508 (2006).

Synthesis and Application of Tetrasubstituted Alkene-type Dipeptide Isosteres as *N*-Methylamide Equivalent

Kazuya Kobayashi, Shinya Oishi, Ryoko Hayashi, Kenji Tomita, Tatsuhiko Kubo, Noriko Tanahara, Hiroaki Ohno, and Nobutaka Fujii

Graduate School of Pharmaceutical Sciences, Kyoto University, Kyoto, 606-8501, Japan

Introduction

We previously identified a highly potent CXCR4 antagonist, FC131 [*cyclo*(-D-Tyr[1]-Arg[2]-Arg[3]-Nal[4]-Gly[5]-)], by downsizing study of an anti-HIV peptide derived from horseshoe crabs, polyphemusin II [1]. The structure-activity relationship study on FC131 demonstrated that replacement of Arg[2] with MeArg, D-Arg, or D-MeArg affected orientation of the D-Tyr-Arg peptide bond and/or antagonist activity. For example, in most potent FC122 [*cyclo*(-D-Tyr[1]-D-MeArg[2]-Arg[3]-Nal[4]-Gly[5]-)], 30% *cis*-conformer of the *N*-methylated peptide bond between D-Tyr[1] and D-MeArg[2] was observed. This *cis/trans* isomerization was induced mainly by steric effects of Arg[2] chirality and *N*-methyl group [2]. To identify the predominant conformer that contributes to bioactivity of FC122, we employed alkene-type dipeptide isosteres for the D-Tyr[1]-Arg[2] peptide bond in FC131. A structure-activity relationship study was carried out using di- and tri-substituted alkene isosteres mimicking the planar structure of a peptide bond, and a tetra-substituted alkene isostere as an equivalent of an *N*-methyl peptide bond. In this paper, we report the synthesis of a series of alkene-type isosteres for the D-Tyr-L/D-Arg dipeptide, and the application to FC131 derivatives.

Results and Discussion

FC131 derivatives **5-8** containing di-, tri-, and tetra-substituted alkene-type isostere were synthesized as previously reported [3]. Tyr-Orn-type alkene dipeptide isosteres **1-4** were synthesized via organocopper-mediated S_N2' reaction of γ-activated α,β-enoate derived from D-tyrosine [4-6]. The resulting isosteres were incorporated into FC131 then the δ-amino group of Orn was converted into the guanidine functional group of Arg (Scheme 1).

To evaluate the biological activity of cyclic peptides **5-8**, the inhibitory potency against [125I]SDF-1 binding to CXCR4 was assessed (Table 1). Whereas all derivatives exhibited lower potency compared with FC131 [IC_{50}(FC131), 0.084 ± 0.037 μM], a series of isostere-containing peptides showed similar bioactivity profile to the parent peptides. For example, D-Tyr-L-Arg tetra-substituted alkene isostere-containing peptide **7** showed low activity (IC_{50}, 2.5 ± 1.0 μM). On the other hand, D-Tyr-D-Arg-type tetra-substitute alkene isostere-containing peptide **8** had nearly equipotent activity to FC131 (IC_{50}, 0.10 ± 0.029 μM). These results suggest that: (1) the peptide bond between D-Tyr and Arg in bioactive conformations of FC131 exists as a *trans*
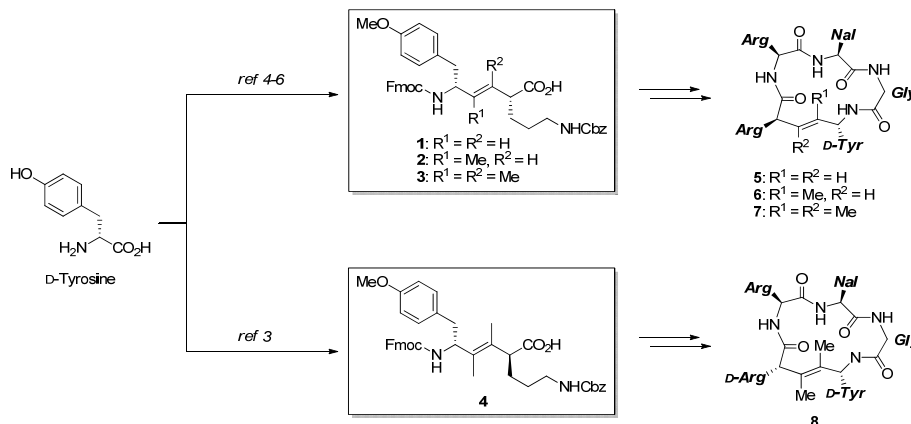
Scheme 1. Synthesis of FC131 derivatives containing alkene-type isostere.

Table 1. Biological activity of FC131 and its derivatives

Compound	Sequence	IC_{50} (μM)[a]
FC131	*cyclo*(-D-Tyr^1-L-Arg^2-L-Arg^3-L-Nal^4-Gly^5-)	0.084
5	*cyclo*(-D-Tyr^1-[(*E*)-CH=CH]-L-Arg^2-L-Arg^3-L-Nal^4-Gly^5-)	0.33
6	*cyclo*(-D-Tyr^1-[(*E*)-CMe=CH]-L-Arg^2-L-Arg^3-L-Nal^4-Gly^5-)	0.50
7	*cyclo*(-D-Tyr^1-[(*E*)-CMe=CMe]-L-Arg^2-L-Arg^3-L-Nal^4-Gly^5-)	2.5
8	*cyclo*(-D-Tyr^1-[(*E*)-CMe=CMe]-D-Arg^2-L-Arg^3-L-Nal^4-Gly^5-)	0.10
FC162[2]	*cyclo*(-D-Tyr^1-L-MeArg^2-L-Arg^3-L-Nal^4-Gly^5-)	0.29
FC122[2]	*cyclo*(-D-Tyr^1-D-MeArg^2-L-Arg^3-L-Nal^4-Gly^5-)	0.063

[a]*IC_{50} values are based on inhibition of [^{125}I]SDF-1 binding to CXCR4 transfectant of CHO cells*

isomer; (2) the dipole of the D-Tyr-Arg peptide bond contributes little to the activity; and (3) tetra-substituted alkene dipeptide isostere mimics *N*-methylated peptide bond.

To understand the structure-activity relationship of the derivatives, conformational analysis was carried out by using molecular dynamics simulation with NMR data. Molecular dynamics simulations were performed by MacroModel using the Merck Molecular Force Field (MMFFs). Pseudoatoms were defined for the CH_3 protons on alkene of **6**, **7**, and **8**, and methylene protons of D-Tyr^1, D/L-Arg^2, Arg^3, and Nal^4. The dihedral φ angle constraints were calculated based on the Karplus equation. Lower and upper angle errors were set to 15°. The NOESY spectrum with a mixing time of 200 ms was used for the distance restraints between protons. The NOE intensities were classified into three categories based on contour lines in the cross-peaks to define the upper-limit distance restraints. A total of 100,000 random structures were generated by molecular dynamic simulation starting with any initial structure in water. The structures matched with the restraints from the NMR data were then selected. The structure in the lowest potential energy was defined as the most stable structure in solution. The backbone structure of FC131 was similar to that calculated in our previous report [2]. Although the orientation of all peptide bonds in FC131 derivatives **5-8** was consistent with that in FC131, local conformations around Arg^2, Arg^3, and Nal^4 were slightly different among FC131 and the derivatives. Based on the calculated structures, binding mode analysis of these peptides to CXCR4 is now in progress.

Acknowledgments

References

1. Fujii, N., Oishi, S., et al. *Angew. Chem., Int. Ed.* **42**, 3251-3253 (2003).
2. Ueda, S., Oishi, S., Fujii, N., et al. *J. Med. Chem.* **50**, 192-198 (2007).
3. Kobayashi, K., Fujii, N., et al. *PEPTIDE SCIENCE 2010*, 120 (2011).
4. Ibuka, T., Fujii, N., et al. *Angew. Chem., Int. Ed.* **29**, 801-803 (1990).
5. Oishi, S., Fujii, N., et al. *Org. Lett.* **4**, 1055-1058 (2002).
6. Oishi, S., Fujii, N., et al. *J. Chem. Soc., Perkin. Trans.* **1**, 1786-1793 (2002).

Modified Synthesis of Safety Catch Acid-Labile (SCAL) Linker

Marketa Lebl-Rinnova, Hai N. Tran, and Michal Lebl

Spyder Institute, LLC, 3550 General Atomics Ct., San Diego, CA, U.S.A.

Introduction

SCAL linker (CAS 147046-64-8) was introduced by Patek and Lebl [1,2] twenty years ago in order to increase orthogonality and to enable synthesis of branched or cyclic peptides with C-terminal amide function. The linker in the oxidized form is stable to a wide range of chemical conditions (e.g. strong acids, TFA, HF). It is compatible with Fmoc, Boc and Alloc peptide chemistry protocols. However, when sulfoxides are reduced (SiCl$_4$, PPh$_3$/Me$_3$SiCl, Me$_3$SiBr, HBr/AcOH) to sulfides the transformed linker becomes labile to TFA. The linker has been used, for its stability and versatility, by many research groups for a variety of applications, e.g. chemical ligations [3,4], glycoconjugate- [5] and glycopeptide- [6] syntheses and cyclizations [7,8]. Due to continuous demand and recent unavailability (Sigma-Aldrich Cat. No. 84607) of the linker, we decided to reevaluate the procedure and make this unique precursor available again. The original synthetic protocol consisted of 14 steps. Using our new strategy the linker is built in 9 synthetic steps.

Results and Discussion

A central benzophenone scaffold was originally constructed using Friedel-Crafts acylation in the 8th step of the synthesis. In the new procedure (Scheme 1) we were able to optimize Fries rearrangement of a readily available ester 2. Following O-alkylation of the benzophenone 3, a substitution of aromatic fluoride using NaSMe was trouble-free in NMP (reacts already at room temperature) yielding an intermediate 5. Attempts to introduce SMe group earlier in a presence of free hydroxyl group, directly on benzophenone 3 provided low yields and only after using various high temperatures (90-170°C). Following hydrolysis of an ester group to yield an intermediate 6, an amino group was generated from oxime 7 in aqueous ammonia in a presence of zinc dust. Protection of amine by Fmoc-group using a standard procedure, followed by oxidation of sulfides resulted in the final product, the SCAL linker.

The procedure involves certain limitations and some steps have required substantial optimization. Mainly the Fries rearrangement protocol needed extensive experimentation with reaction conditions and work-up. To some extent the solvent free reaction in AlCl$_3$ causes decomposition of an ester intermediate 2 and the major product 3 of the reaction is hard to quantitatively extract from an aqueous phase in the following work-up. We were able to
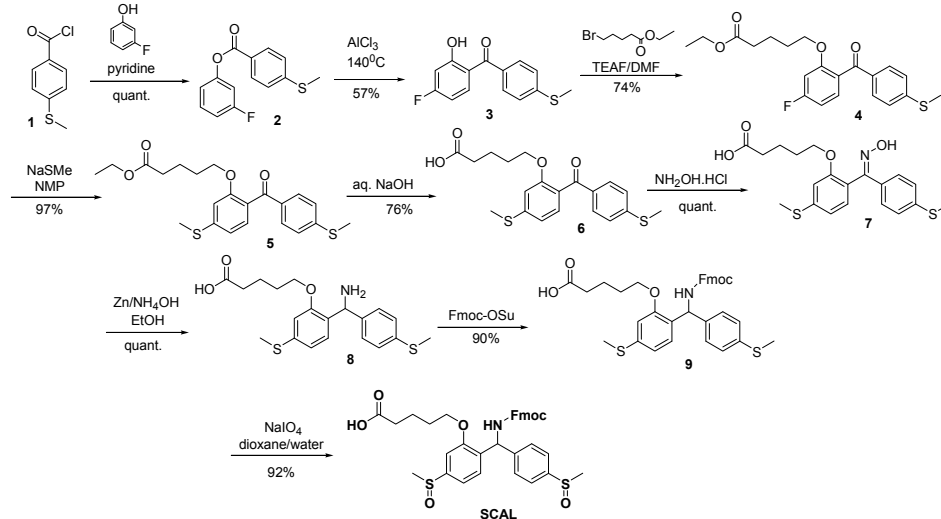
Scheme 1. New synthetic procedure.

improve yield (57%) from the originally isolated low 30%, together with purity. This intermediate could be used after optimized work-up without further purification in the next step. The final step, the oxidation of sulfides to sulfoxides, is time consuming (4-5 days) but provides a clean product.

Conclusion

The presented synthesis was developed in order to facilitate the preparation of the SCAL linker on a larger scale that would accommodate demand from the peptide/glycopeptide-synthetic community. We were able to shorten the original 14 steps synthetic protocol to 9 steps and make the synthesis and its scale-up feasible.

Acknowledgments

References

1. Patek, M., Lebl, M. *Tetrahedron Lett.* **32**, 3891-3894 (1991).
2. Patek, M., Lebl, M. 1997. Patent US005684131A.
3. Brik, A., Keinan, E., Dawson, P.E. *J. Org. Chem*. **65**, 3829-3385 (2000).
4. Moyle, P.M.,Olive, C., Ho, M.F., Burgess, M., Karpati, L., Good, M.F., Toth, I. *J. Org. Chem.* **71**, 6846-6850 (2006).
5. Katajisto, J., Karskela, T., Heinonen, P., Lonnberg, H. *J. Org. Chem.* **67**, 7995-8001 (2002).
6. Katajisto, J., Lonnberg, H. *Eur. J. Org. Chem.* 3518-3525 (2005).
8. Muttenhaller, M., Nevin, S.T., Grishin, A.A., Ngo, S., Choy, P.T., Daly, N.L., Hu, S.H., Amirshaw, C.J., Wang, C.I.A., Lewis, R.J., Martin, J.L., Noakes, P.G., Craik, D.J., Adams, D.J., Alewood, P.F. *J. Am. Chem. Soc.* **132**, 3514-3522 (2010).
9. Brust, A., Tickle, A.E. *J. Pept. Sci.* 13, 133-141 (2007).

Simultaneous Fmoc and Boc Synthesis of a Contryphan Positional Scanning Library and the Conotoxin Prialt on the Overture™ Robotic Peptide Library Synthesizer

James P. Cain, Christina A. Chantell, Michael Onaiyekan, Ogaga Ojameruaye, and Mahendra Menakuru

Protein Technologies, Inc. Tucson, AZ, 85714, U.S.A. Web: www.ptipep.com, Email: info@ptipep.com

Abstract

The Overture™ (Figure 1) is the only robotic peptide library synthesizer that can perform Boc and Fmoc chemistry at the same time. In this contribution, the flexible Overture™ Library Design Tools are used to generate a focused positional scanning library of contryphans. This contryphan library is then synthesized using Fmoc chemistry, while the conotoxin drug, Prialt is synthesized using Boc chemistry in the same synthesis. This has never been seen before on a peptide synthesizer.

Introduction

Like standard peptide library generation tools, the Overture™'s Library Design Tools can be used to generate positional scanning libraries utilizing all 20 standard amino acids. However, only the Overture™ software has the added flexibility to generate focused scanning libraries using amino acids selected by the user. In this way, it is possible to generate positional scanning libraries containing only

Fig. 1. The Overture™ Robotic Peptide Library Synthesizer from Protein Technologies, Inc.

hydrophobic, basic, acidic, or even non-standard amino acids. In this article, the Overture™ software is used to generate a positional scanning library based on Contryphan-Vn [1], varying position 2 to include the acidic amino acids and their amides (D, E, N, Q) (Figure 2).

Contryphan-Vn: GDCPwKPWC-NH$_2$
D2E analog: G**E**CPwKPWC-NH$_2$
D2N analog: G**N**CPwKPWC-NH$_2$
D2Q analog: G**Q**CPwKPWC-NH$_2$

Fig. 2. Positional scanning library based on Contryphan-Vn, where w = D-Trp. Substitutions are shown in bold.

In addition, the Overture™ is the only commercially available peptide synthesizer on which Fmoc and Boc chemistry can be run simultaneously. Most routine syntheses today are run using Fmoc chemistry, however, certain peptides have been optimized to run with greater success using Boc chemistry. These peptides include thioesters for native chemical ligation applications, and the conotoxin, Prialt [2]. The Overture™ is the only peptide synthesizer that can run different protocols simultaneously, including Fmoc and Boc chemistry. With its 96 reaction vessels, the Overture™ increases productivity by eliminating the need to perform two separate syntheses every time a different chemistry is required. In this paper, the positional scanning library of Contryphan-Vn was synthesized using Fmoc chemistry, while the conotoxin Prialt was synthesized using Boc chemistry all in the same synthesis on the Overture™.

Results and Discussion

A positional scanning library based on the Contryphan-Vn sequence was synthesized using Fmoc chemistry alongside the conotoxin peptide, Prialt, synthesized using Boc chemistry in the same synthesis on the Overture™. The HPLC results for the crude peptides are shown in Figures 3 and 4.
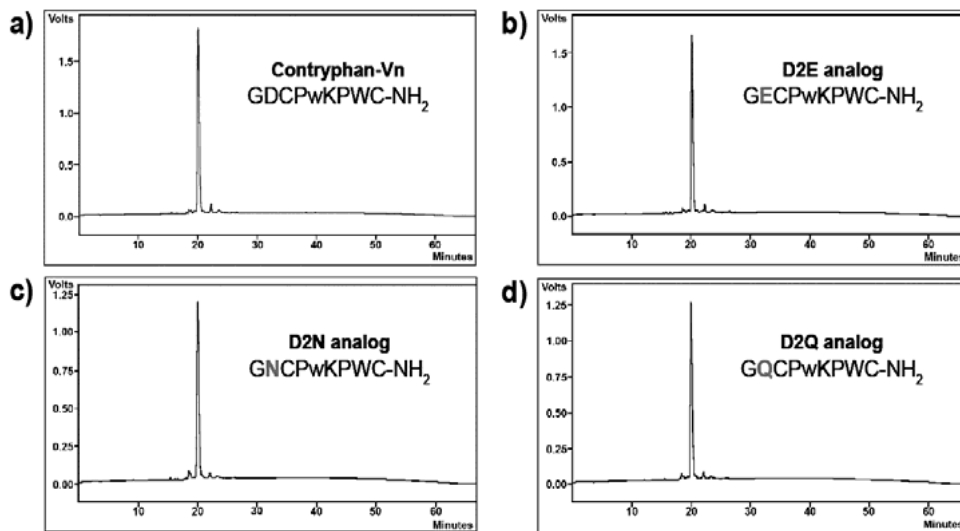
Fig. 3. HPLC results for Contryphan-Vn positional scanning library crude peptides synthesized using Fmoc chemistry on the Overture™. Substitutions are shown in grey bold.
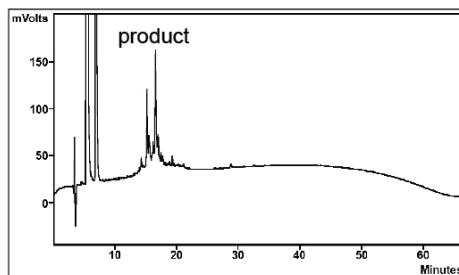
Fig. 4. HPLC results for crude Prialt synthesized using Boc chemistry on the Overture™. The product elutes at 16.5 min. The peaks with RT < 9 min are due to DTT and background.

Conclusions

Using the Overture™ Robotic Peptide Library Synthesizer, we have successfully synthesized Prialt using Boc chemistry and a small positional scanning library based on Contryphan-Vn with Fmoc chemistry in the same synthesis. Unlike existing robotic platforms, the Overture™ is an extremely flexible platform for generating focused peptide libraries and running different chemistries at the same time.

Acknowledgments

References

1. Massilia, G.R., et al. *Biochem. Biophys. Res. Comm.* **303**, 238-246 (2003).
2. Chung, D., et al. *Int. J. Peptide Protein Res.* **46**, 320-325 (1995).

Synthesis of Peptides with Different Lengths and Modification Positions on the Overture™ Robotic Peptide Library Synthesizer

Christina A. Chantell, Ogaga Ojameruaye, James P. Cain, Michael Onaiyekan, and Mahendra Menakuru

Protein Technologies, Inc. Tucson, AZ, 85714, U.S.A.; Web: www.ptipep.com, Email: info@ptipep.com

Introduction

In nature, post translational modifications such as methylation, acetylation, phosphorylation and ubiquitination can affect protein function [1]. In the case of histone proteins (which are associated with DNA in chromatin), post translational modifications can affect gene expression as well as other DNA-templated processes in the cell [1]. In addition to the modifications found in nature, synthetic peptides often include modifications such as biotinylation, pegylation, and fluorescent labels for use in biological assays.

Fig. 1. The Overture™ Robotic Peptide Library Synthesizer from Protein Technologies, Inc.

Typically, robotic peptide library synthesizers must run the same program in all reaction vessels during a synthesis. If special programs are necessary to synthesize a modified peptide, only peptides with modifications in the same position can be synthesized at the same time. It is also not possible to efficiently synthesize peptides of different lengths in the same synthesis. The Overture™ Robotic Peptide Library Synthesizer (Figure 1) was designed to overcome these shortcomings, and can easily synthesize different length peptides with modifications in different positions all in the same synthesis.

To illustrate this, four histone peptides of varying lengths (Figure 2) were synthesized on a 2x2 reaction vessel block on the Overture™. Modifications included biotinylation, pegylation, and acetylation, which occurred in different positions within the sequences. Sequences were selected from a combinatorial library of 110 modified histone peptides originally synthesized by Dr. Brian Strahl's laboratory at the University of North Carolina, School of Medicine [1].

66: Ac-SGRGK(Ac)GGKGLGKGGAKRHRKVLR-PEG-Biotin
70: Ac-SGRGK(Ac)GGKGLGK(Ac)GGAKRHRKVLR-PEG-Biotin
72: Ac-SGRGK(Ac)GGK(Ac)GLGK(Ac)GGAKRHRKVLR-PEG-Biotin
301: Ac-SGRGK(Ac)QGGK(Ac)ARAK(Ac)AK(Ac)TR-PEG-Biotin

Fig. 2. Modified histone peptide sequences synthesized on the Overture™. The numbers to the left correspond to the sequence labels on Dr. Brian Strahl's website [2].

Experimental

Materials: Biotin-PEG NovaTag resin and Fmoc-Lys(Ac)-OH were purchased from Novabiochem (Boston, MA). TFA, HATU, NMM and solvents were provided by Protein Technologies, Inc. (Tucson, AZ).

Synthesis: The peptides were synthesized at the 20 µmol scale on an Overture™ Robotic Peptide Library Synthesizer on Biotin-PEG NovaTag resin (0.47 mmol/g). Deprotection: 20% piperidine/DMF 2x7 min. Coupling: 1:1:2 0.2 M AA/0.2 M HATU/ 0.4 M NMM/DMF (10x excess) for 50 min (standard amino acids), or for 2 x 50 min (Fmoc-Lys(Ac)-OH couplings). Cleavage: 95/2.5/2.5 TFA/TIS/water for 2 hours.

Analysis: Crude peptides were precipitated in ice cold ether, dissolved in water and analyzed on a Varian ProStar HPLC using a C18, 300 Å, 5 µm, 250 x 4.6 mm column (Varian

Microsorb-MV), over 60 minutes with a flow rate of 1 mL/min, and using a gradient of 5-95% B, where Buffer A was 0.1% TFA in water and Buffer B was 0.1% TFA in acetonitrile. Detection was at 214 nm. Mass analysis was performed on a Shimadzu LCMS-2020 Single-Quad mass spectrometer, equipped with a C18, 100 Å, 2.6 µm, 50 x 2.1 mm column (Phenomenex Kinetex), over 7 minutes with a flow rate of 1 mL/min and using a gradient of 5-50% B where Buffer A was 0.1% formic acid in water and Buffer B was 0.1% formic acid in acetonitrile.

Results and Discussion

Four modified histone peptides were synthesized on the Overture™ in a single synthesis on a single 2x2 reaction vessel block. The peptides ranged in length from 17 to 23 amino acids and contained 1, 2, 3, or 4 modified lysine residues, which were coupled under different conditions than the standard amino acids. Mass analysis verified the main peak was the product peptide in each case, allowing for easy purification (data not shown). HPLC data is shown in Figure 3.
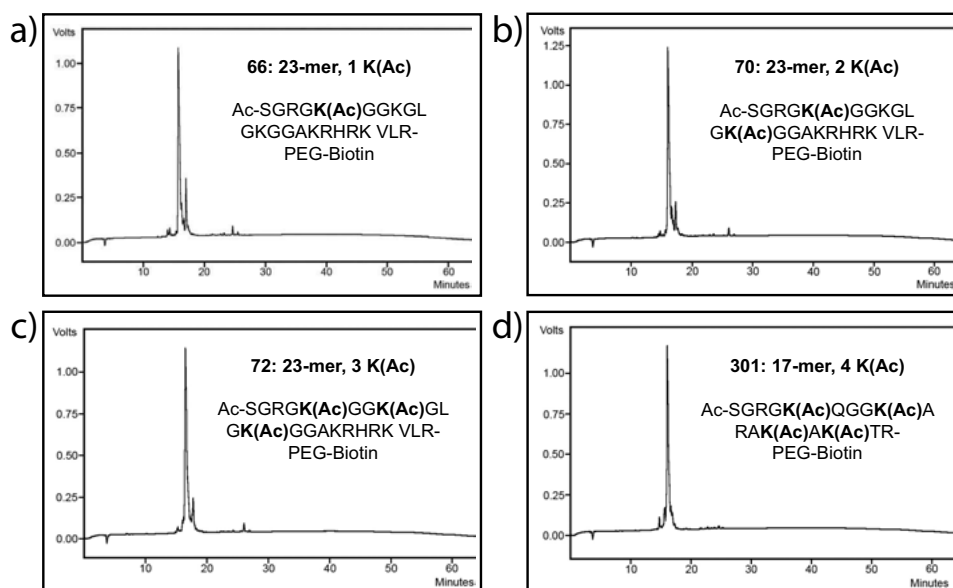
Fig. 3. HPLC results for crude peptides.

Conclusions

Unlike existing robotic platforms, the Overture™ is an extremely flexible platform for synthesizing modified peptides. Peptides of different lengths with modifications in different positions can be successfully synthesized in one synthesis.

Acknowledgments

References

1. Fuchs, S.M., Krajewski, K., Baker, R.W., Miller, V.L., Strahl, B.D. *Curr. Biol.* **21**, 53-58 (2011).
2. Online Analytical Data: http://www.med.unc.edu/~bstrahl/Arrays/Pep_t.htm

Synthesis of Long Peptides and Multiple Scales on the Overture™ Robotic Peptide Library Synthesizer

Christina A. Chantell, Michael Onaiyekan, Ogaga Ojameruaye, James P. Cain, and Mahendra Menakuru

Protein Technologies, Inc. Tucson, AZ, 85714, U.S.A.; Web: www.ptipep.com, Email: info@ptipep.com

Introduction

The Overture™ (Figure 1) is a new and powerful robotic peptide library synthesizer from Protein Technologies, Inc. designed to overcome the shortcomings of existing robotic synthesizers. One of the limitations of existing robotic synthesizers is that only one program can be run at a time on all reaction vessel positions for a synthesis. The Overture™ has 6 independent reaction vessel blocks which can run different protocols simultaneously, and special software that also allows different protocols to be run within the same reaction vessel block.

Fig. 1. The Overture™ Robotic Peptide Library Synthesizer from Protein Technologies, Inc.

Another limitation of existing robotic synthesizers is the inability to synthesize peptides longer than 15-20 amino acids in length with good crude purity. This is due to septa failure and cross contamination issues, as well as inconsistent deliveries across the reaction vessels which prevent good chemistry for higher numbers of cycles. The Overture™ was designed to eliminate these issues, so it can synthesize peptides greater than 20 amino acids long in excellent crude purities similar to non-robotic units.

In this paper, we demonstrate the simultaneous synthesis of a modified version of the luteinizing hormone releasing hormone (G-LHRH: GHWSYGLRPG-NH$_2$) at the 2 and 20 μmol scales, and the 65-74 fragment of the acyl carrier protein ([65-74]ACP: VQAAIDYING-OH) at the 100 μmol and 1 mmol scales on the Overture™. We also compare the crude results of two long peptides (31-mer C-peptide: EAEDLQVGQV ELGGGPGAGS LQPLALEGSL G-OH and 68-mer SDF-1α: KPVSLSYRCP CRFFESHVAR ANVKHLKILN TPNCALQIVA RLKNNNRQVC IDPKLKWIQE YLEKALNK-OH) synthesized on the Overture™ and non-robotic synthesizers.

Results and Discussion

Multiple Scales: Multiple scales were successfully synthesized at the same time on the Overture™ in different sized reaction vessels (Figure 2). The 2 μmol scale was synthesized at a 50x excess and the 20 μmol scale was synthesized at a 5x excess using 250 μL deliveries of amino acid and activator solution, and 1 mL deliveries for deprotection and washes. The 100 μmol scale was synthesized at a 5x excess using 1.5 mL deliveries of amino acid and activator solution, and 3 mL deliveries for deprotection and washes. The 1 mmol scale was synthesized at a 5x excess using 7.5 mL deliveries of amino acid and activator solution, and 15 mL deliveries for deprotection and washes. Results for the 2 μmol and 20 μmol scales for G-LHRH and the 100 μmol and 1 mmol scales for [65-74]ACP were extremely pure and largely similar (Figure 3), demonstrating the ability of the Overture™ to produce crude peptides from large to small scales with high purities.
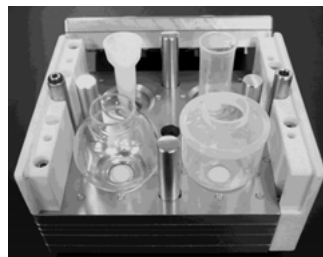
Fig. 2. 2x2 Overture™ reaction vessel block containing different sized reaction vessels. Clockwise from upper left: 1.3 mL (2 μmol scale), 10 mL (20 μmol scale), 40 mL (100 μmol scale), 45 mL (1 mmol scale).
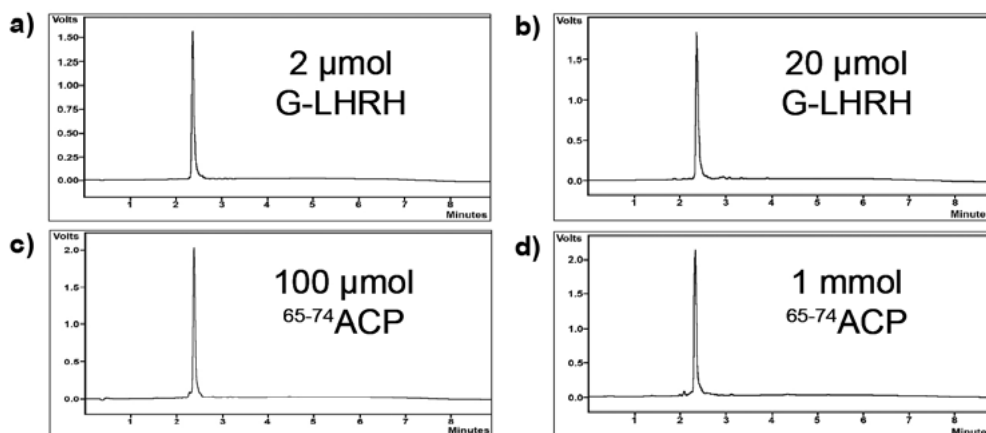
Fig. 3. HPLC results for crude peptides synthesized simultaneously on the Overture™ at different scales. a) G-LHRH: 2 μmol scale; b) G-LHRH: 20 μmol scale; c) $^{65-74}$ACP: 100 μmol scale; d) $^{65-74}$ACP: 1 mmol scale.
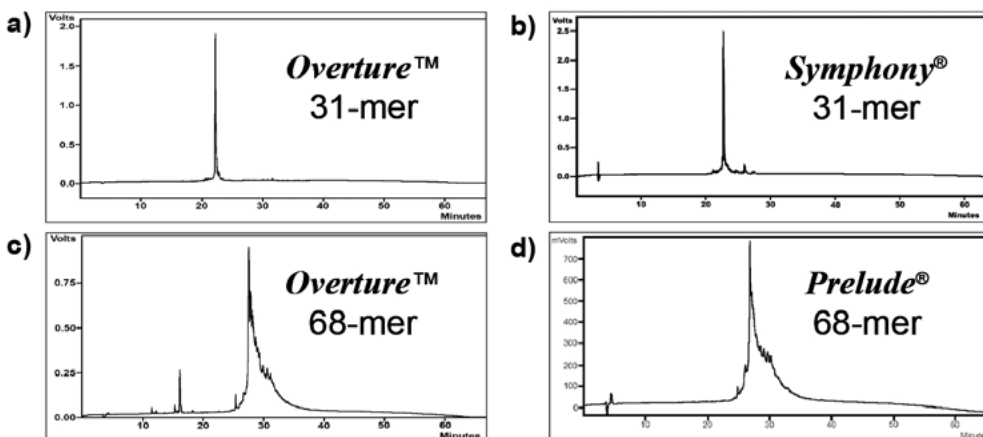
Fig. 4. HPLC results for the 31-mer C-peptide synthesized on the a) Overture™ and b) Symphony®, and the 68-mer chemokine SDF-1α synthesized on the c) Overture™ and d) Prelude®.

Long Peptides: The Overture™ was able to produce long peptides at similar purities to non-robotic platforms. The 31-mer C-peptide was successfully synthesized on the Overture™ and the non-robotic Symphony® with similar crude purities, and the 68-mer chemokine, SDF-1α, was successfully synthesized on the Overture™ and the non-robotic Prelude® with similar crude purities (Figure 4).

Conclusions

G-LHRH was synthesized at the 2 and 20 μmol scales simultaneously with $^{65-74}$ACP at the 100 μmol and 1 mmol scales all on the same reaction vessel block on the Overture™ with good crude purities, demonstrating the ability of the Overture™ to synthesize multiple scales at the same time and produce high purity peptides from large to small scales.

The 31-mer C-peptide was also synthesized on the Overture™ with a similar crude purity to the non-robotic Symphony®, and the 68-mer chemokine, SDF-1α, was synthesized on the Overture™ with a similar crude purity to the non-robotic Prelude®, demonstrating the ability of the robotic Overture™ platform to produce high purity long peptides similar to non-robotic units.

Synthesis, Physico-Chemical Properties and Applications of Chiral PNAs

Tatyana Dzimbova and Tamara Pajpanova

Institute of Molecular Biology "Roumen Tsanev", Bulgarian Academy of Sciences, 1113, Sofia, Bulgaria

Introduction

In 1991, Nielsen, Egholm, Berg and Buchardt [1] reported the synthesis of peptide nucleic acids (PNAs), new completely artificial DNA/RNA analogues, in which the backbone is a pseudopeptide rather than a sugar. First, PNAs were based upon an N-(2-aminoethyl)glycine pseudopeptide backbone. The bases (corresponding to A, G, C, T) are attached to the backbone via a methylene carbonyl linker. Their structure completely mimics the structure of DNA or RNA, and they are able to form very stable complexes with complementary DNA and RNA.

The development of new molecules able to efficiently bind specific nucleic acid sequences is of the hot topics in the field of nucleic acid chemistry. Improved DNA and/or RNA recognition is actually mandatory for many diagnostic and therapeutic applications [2].

In order to obtain more potent DNA/RNA mimetics we synthesized several chiral PNAs. They contain chiral backbone on the base of basic amino acids arginine and lysine. Their properties were compared to original PNA with N-(2-aminoethyl)glycine containing backbone.

New analogues are presented on Figure 1.
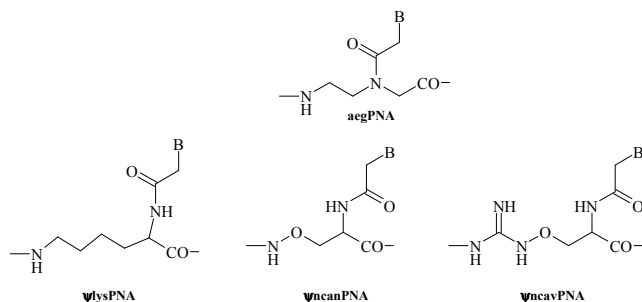
Fig. 1. Structures of chiral PNAs.

Results and Discussion

Total synthesis of PNA is divided into three synthetic steps:
- Synthesis of amino acid analogues;
- Synthesis of PNA monomer;
- SPPS of PNA.

We developed new method for preparation of mono-Fmoc-ethylendiamine, that allows us to perform this process in one step (till now this product have been synthesized in two-step reaction), and to increase yield and purity. For the next steps of the scheme different approaches were evaluated. Along with method in solution, we applied both microwave assisted method, and method in solution with sonochemical irradiation.

PNA oligomer was made by synthesis in solution, conventional SPPS, SPPS with sonochemical and microwave irradiation, using both Fmoc-Aeg(T) or Boc-Aeg(T) [3].

For the synthesis of PNA with a chiral backbone, we applied two different strategies – preparation of monomers followed by SPPS of PNA, or SPPS of the pseudopeptide chain and consequent coupling with nucleobases [4].

For the preparation of two of our unnatural amino acid analogues we use SPPS – conventional and MWA. Scheme representing the synthesis is shown on the Figure 2A. In conditions of MWA SPPS on the first and second stages, reaction is carried out at 40 degrees and irradiation time of 2 minutes. Introduction of guanidine group was made also under a condition of MWA synthesis at 40 degrees and irradiation time of 5 minutes.
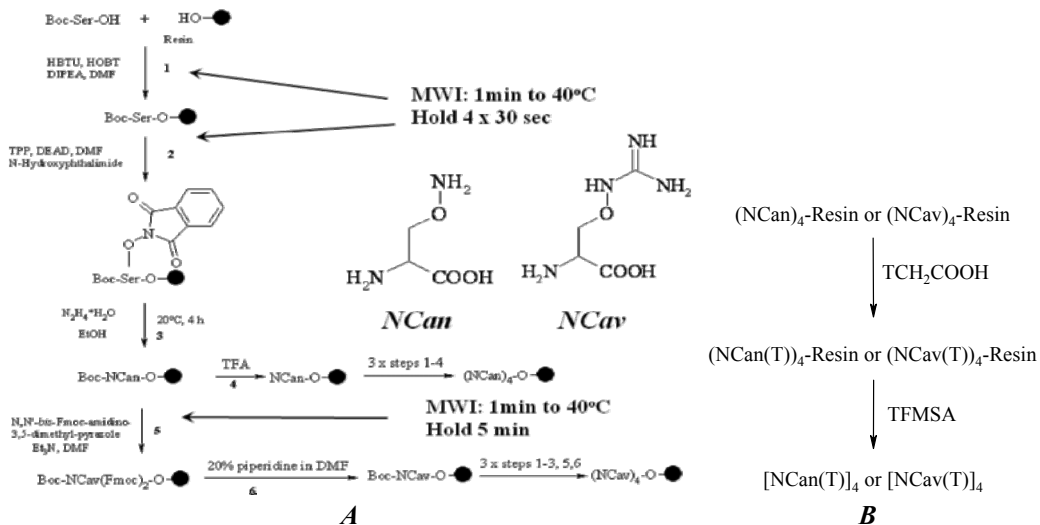
Fig. 2. Synthesis of ncanPNA and ncavPNA.

For the synthesis of pseudopeptide fragments shown on Figure 2B by conventional SPPS, 11 hours are needed. With the help of MWA SPPS we shorten reaction time to 1 hour and 15 minutes.

PNA oligomers were made by SPPS of the backbone followed by coupling with thymine bases. Similar approach was used for synthesis of lysPNA. Protected amino acids were involved in SPPS of pseudopeptide backbone. After removal of protecting groups on side chain, acetylated thymine was used for synthesis of this new types of PNAs.

Acknowledgments

References

1. Nielsen, P.E., Egholm, M., Berg, R.H., Buchardt, O. *Science* **254**, 1497-1500 (1991).
2. Calabretta, A., Tedeschi, T., Corradini, R., Marchelli, R., Sforza, S. *Tetrahedron Lett.* **52**, 300-304 (2011).
3. Dzimbova, T., Pajpanova, T. *Proceedings of the 31st European Peptide Symposium,* M. Lebl, M. Meldal, K. J. Jensen, T. Hoeg-Jensen (Editors), European Peptide Society (2010).
4. Dzimbova, T., Pajpanova, T. *Trakia Journal of Sciences* **8**, Suppl. 2, 98-101 (2010).

A Flexible Approach for Attachment of Peptides to Oligonucleotides

Malgorzata Wenska, Margarita Alvira, and Roger Strömberg

Department of Biosciences and Nutrition, Karolinska Institutet, Novum, Huddinge, SE-141 83, Sweden

Introduction

Delivery is a seriously limiting factor for antisense, siRNA and gene therapy *in vivo* [1-3]. One approach to enhance nucleic acid uptake into cells is to utilize cell penetrating peptides (CPPs) either in the form of complexes or in the form of covalent conjugates, which also protects from digestion by intracellular enzymes [4]. A recent successful example involves a CPP-conjugate of a morpholino phosphorodiamidate oligomer that when given in low doses leads to efficient splice switching and production of therapeutically useful levels of dystrophin in skeletal and heart muscles, which makes this a promising approach for treatment of Duchenne muscular dystrophy (DMD) [5]. A reaction that would seem ideal for conjugation of peptides and oligonucleotides, due to the compatibility with many other functional groups, is the copper (I) catalyzed 1,3-dipolar cycloaddition between an azide and an alkyne, commonly referred to as click chemistry [6,7].

Results and Discussion

A versatile method for the synthesis of multiple types of peptide-oligonucleotide conjugates (POCs) that can be performed on solid support in sub-micromole scale with commercially available oligonucleotide and peptide derivatives has been developed [8]. Convenient handling and efficient reaction at low concentration under mild room temperature conditions is enabled by use of a new activated triple bond donor and by performing reaction on solid support. To increase the reaction rate of the click reaction we developed a linker with an activated triple bond donor, α-(N-propynoylamino)-*p*-toluic acid (PATA, Figure 1, C, the electron withdrawing carbonyl vicinal to the triple bond makes it considerably more reactive in the Cu(I) catalyzed cycloaddition). Convenient and efficient conversion of peptides into clickable derivatives also contributes to making the concept user friendly.

For conversion of peptides into clickable derivatives two approaches were developed depending on the site of attachment (Figure 1, A and B). An N-terminal azido-derivatized peptide could be readily made from a solid support bound commercial peptide by condensation with 2-(2-azidoethyl)ethoxyacetic acid followed by cleavage from support (Figure 1, A) [8]. This peptide-azide can be optionally trifluoroacetyl-protected on amino groups, if needed [8]. C-Terminal azido derivatized peptides can be obtained from non-supported fully deprotected peptides by intermediate TFA protection and subsequent attachment of an azide containing linker (Figure 1, B) [9]. For the studies on synthesis of POCs we used DNA and locked nucleic acid (LNA) as well as 2'-O-methylRNA oligonucleotides, purchased still attached to controlled pore glass CPG or polystyrene PS support and carrying either 2-(aminoethoxy)ethyl phosphate (aminomodifier Am5) or aminohexyl phosphate (aminomodifier C6) as amino linkers (initially MMT-protected). The PATA reagent was then coupled to the solid supported aminolinker-oligonucleotide. Subsequent Cu(I) catalyzed cycloaddition under mild conditions with a peptide azide gives corresponding oligonucleotide peptide conjugate (Figure 1, C) [8]. The POC is deprotected/cleaved from support by conc. ammonia at 55°C and then isolated by RP-HPLC.

An alternative approach for solid phase conjugation of peptides to oligonucleotides is based on purchasing oligonucleotides on support and then attaching an aminolinker manually followed by conjugation to the peptide. This lowers the amount of side product with N-acetylated aminolinker and keeps the overall cost down, while still enabling POC synthesis without the need to employ a DNA/RNA synthesizer. Methods for synthesis of POCs by use of "click chemistry" enhanced by the PATA moiety have been developed. Locked nucleic acid (LNA) conjugates with the N-terminal of a C-myc derived peptide as well as with the C-terminal of the MIF peptide were prepared on solid support (CPG). DNA-peptide conjugates with the C-myc peptide were made on both polystyrene and CPG supports. Apart from the oligoether amino linker (Am5) an aminohexylphosphate linker (C6) was also used.

COMMERCIAL PEPTIDES

A

B

C

COMMERCIAL OLIGONUCLEOTIDE
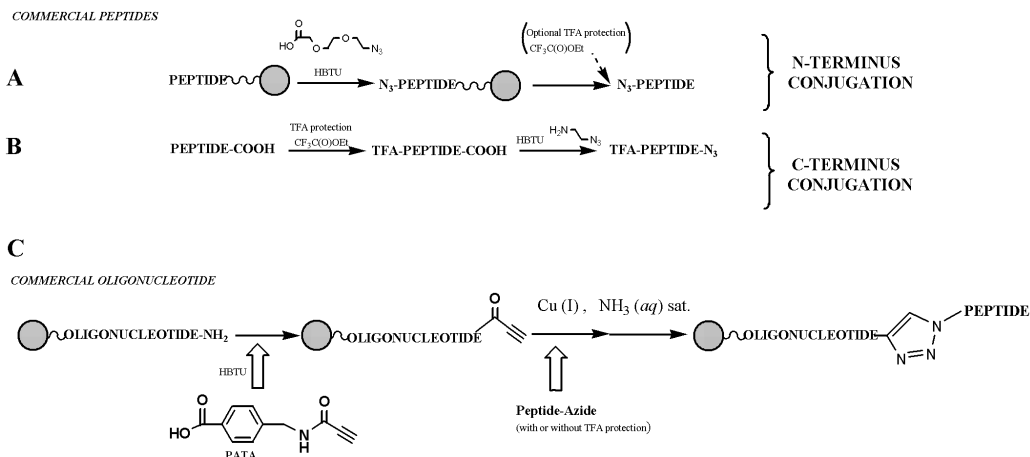
Fig. 1. Schematic representation of: A: Synthesis of azido-derivatives of peptides for N-terminal conjugation; B: Synthesis of azido-derivatives of peptides for C-terminal conjugation; C: Scheme for POC (peptide-oligonucleotide conjugates) synthesis on solid support using commercial oligonucleotides.

The methodology should be highly suitable for parallel synthesis of libraries of POCs in which either or both components are varied. Use of the 1,3-dipolar cycloaddition with an activated alkyne should also make the approach suitable for conjugation with other biomolecules or labels thus enabling the use of a single type of conjugation method in synthesis of different conjugates.

Acknowledgments

References

1. Akhtar, S., Hughes, M.D., Khan, A., Bibby, M., Hussain, M., Nawaz, Q., Double, J., Sayyed, P. *Advanced Drug Delivery Reviews* **44**, 3-21 (2000).
2. Lundin, P., Johansson, H., Guterstam, P., Holm, T., Hansen, M., Langel, Ã., El Andaloussi, S. *Bioconjugate Chemistry* **19**, 2535-2542 (2008).
3. Lebleu, B., Moulton, H.M., Abes, R., Ivanova, G.D., Abes, S., Stein, D.A., Iversen, P.L., Arzumanov, A.A., Gait, M.J. *Advanced Drug Delivery Reviews* **60**, 517-529 (2008).
4. Frederic, H., May Catherine, M., Gilles, D. *British Journal of Pharmacology* 157, 195-206 (2009).
5. Jearawiriyapaisarn N., Moulton H.M., Buckley B., Roberts J., Sazani P., Fucharoen S. Iversen P.L., Kole, R. *Mol. Ther.* **16**, 1624-1629 (2008).
6. Kolb, H.C., Finn, M.G., Sharpless, K.B. *Angew. Chem., Int. Ed.* **40**, 2004-2021 (2001); Kolb, H.C., Sharpless, K.B. *Drug Discovery Today* **8**, 1128-1137 (2003).
7. Meldal, M., Tornoe, C.W. *Chem. Rev.* **108**, 2952-3015, (2008); Tornoe, C.W., Christensen C., Meldal, M. *J. Org. Chem.* **67**, 3057-3064, (2002).
8. Wenska, M., Alvira, M., Steunenberg, P. Stenberg, Å., Murtola, M., Strömberg, R. *Nucleic Acid Research* (2011), DOI: 10.1093/nar/gkr603.
9. Steunenberg, P., Wenska M., Strömberg, R. *Nature Protocols* DOI: 10.1038/nprot.2010.94, (2010).

Application of Ring-Closing Metathesis to Grb2 SH3 Domain-Binding Peptides

Wenjian Qian[1], Fa Liu[1,4], Alessio Giubellino[2], Philip Simister[3], Michael C. Giano[1], Stephan M. Feller[3], Donald P. Bottaro[2], and Terrence R. Burke, Jr.[1]

[1]*Chemical Biology Laboratory, Molecular Discovery Program, Center for Cancer Research, NCI-Frederick, National Institutes of Health, Frederick, MD, 21702,U.S.A.;* [2]*Urologic Oncology Branch, National Cancer Institute, National Institutes of Health, Bethesda, MD, 20989, U.S.A.;* [3]*Cell Signalling Group, Weatherall Institute of Molecular Medicine, University of Oxford, Oxford, OX3 9DS, UK;* [4]*Currently with Lilly Research Laboratories, Indianapolis, IN, 46285, U.S.A.*

Introduction

The growth factor receptor-bound protein 2 (Grb2) is a mediator of receptor tyrosine kinase signaling, which is a potential target for anticancer therapeutic development [1]. Grb2 contains N- and C-terminal SH3 domains that bind to Polyproline II (PPII) helices [2]. These are commonly involved with protein-protein interactions in cellular signal transduction [3]. Although numerous examples exist of stabilizing α-helices using ring closing metathesis (RCM), there are few reports on the stabilization PPII helices by this approach [4]. Our current work was undertaken to examine the effects of RCM on stabilizing PPII motifs in the context of Grb2-SH3 domain-binding peptides.

Results and discussion

The Sos1-derived peptide "Ac-V1-P2-P3-P4-V5-P6-P7-R8-R9-R10-amide" (1) is known to bind to the Grb2 N-terminal SH3 domain [5]. Based on the NMR solution structure of 1 bound to the target Grb2 N-terminal SH3 domain (PDB: 3GBQ) [6], the P4 and P7 residues were chosen as sites for introducing functionality needed for RCM macrocyclization. This was accomplished by appending alkenyloxy groups of different lengths off the P4 and P7 pyrrolidine rings. We designed and synthesized the necessary proline analogues in protected form (2 and 3a-3c, Figure 1) and utilized them for the solid-phase synthesis of peptides 5a-5c and 7a-7c (Scheme 1).
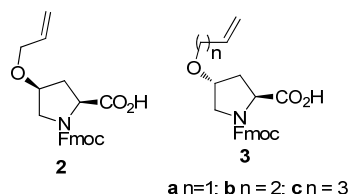
Fig. 1. Protected proline analogues employed in this study.
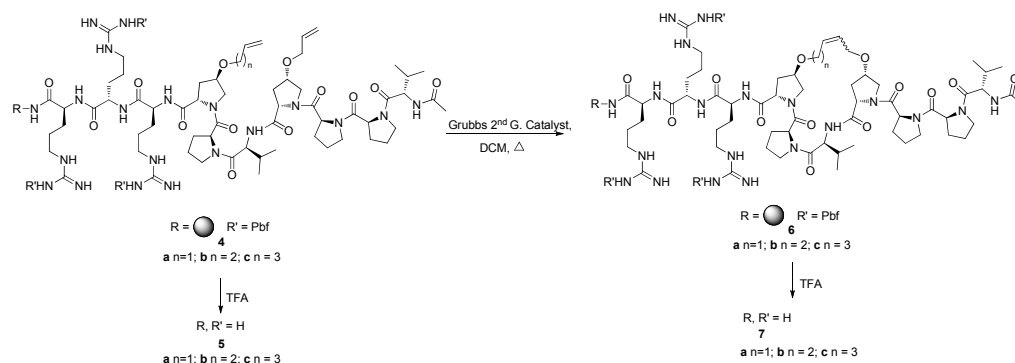
Scheme 1. Solid-phase peptide synthesis and RCM macrocyclization.

We used a Trp-fluorescence assay to determine the binding affinity of the synthetic peptides to the Grb2 N-terminal SH3 domain protein [7]. While the wild-type peptide **1** and the open-chain peptides **5a-5c** showed similar binding affinities, the cyclopeptides **7a-7c** failed to exhibit improved affinities. As indicated by circular dichroism data [8], the cyclopeptides **7a-7c** displayed slightly increased PPII helical character. We also examined the ability of certain of these synthetic peptides to block the binding of Sos1 to full length Grb2 in cell lysate pull-down assays [9], where the IC_{50} values of **7b** and **7c** were approximately 300 nM – 1μM. The most effective analogue (**7a**) had an apparent IC_{50} value between approximately 100 nM and 300 nM. Although the reasons for the apparent inconsistency of the *in vitro* fluorescence binding data as compared to the data using whole cell lysates are not yet clear, the current study represents a rare application of RCM macrocyclization to biologically active PPII helical peptides. Of note are the findings that RCM macrocyclization can increase PPII helicity and enhance the ability of peptides to block Grb2 – Sos1 interactions.

Acknowledgements

References

1. a) Dharmawardana, P.G., Peruzzi, B., Giubellino, A., Burke, T.R., Jr., Bottaro, D.P. *Anti-Cancer Drugs* **17,** 13 (2005); b) Giubellino, A. Burke, T.R., Jr; Bottaro, D.P. *Expert Opinion Therap. Targ.* **12,** 1021 (2008).
2. Harkiolaki, M., Tsirka, T., Lewitzky, M., Simister, P.C., Joshi, D., Bird, L.E., Jones, E.Y., O'Reilly, N., Feller, S.M. *Structure* **17**, 809 (2009).
3. a) Jacobsen, O., Klaveness, J., Rongved, P. *Molecules* **15**, 6638 (2010); b) Siligardi, G., Drake, A.F. *Biopolymers* **37**, 281 (1995); c) Kay, B.K., Williamson, M.P., Sudol, P. *FASEB J.* **14**, 231 (2000).
4. Liu, F., Stephen, A.G., Waheed, A.A., Freed, E.O., Fisher, R.J., Burke, T.R., Jr. *Bioorg. Med. Chem. Lett.* **20**, 318 (2010).
5. a) Yuzawa, S., Yokochi, M., Hatanaka, H., Ogura, K., Kataoka, M, Miura, K.-I., Mandiyan, V., Schlessinger, J., Inagaki, F. *J. Mol. Biol.* **306,** 527 (2001); b) McDonald Caleb, B., Seldeen Kenneth, L., Deegan Brian, J., Farooq, A. *Biochemistry* **48**, 4074 (2009).
6. a) Simon, J., Schreiber, S.L. *Chem. Biol.* **2,** 53 (1995); b) Wittekind, M., Mapelli, C., Lee, V., Goldfarb, V., Friedrichs, M.S., Meyers, C.A., Mueller, L. *J. Mol. Biol.* **267,** 933 (1997).
7. Posern, G., Zheng, J., Knudsen, B.S., Kardinal, C., Muller, K.B., Voss, J., Shishido, T., Cowburn, D., Cheng, G., Wang, B., Kruh, G.D., Burrell, S.K., Jacobson, C.A., Lenz, D.M., Zamborelli, T.J., Adermann, K., Hanafusa, H., Feller, S.M. *Oncogene* **16,** 1903 (1998).
8. Helbecque, N., Loucheux-Lefebvre, M.H. *Int. J. Peptide Protein Res.* **19,** 94 (1982).
9. Shi, Z.-D., Liu, H., Zhang, M., Worthy, W.M., Bindu, L., Yang, D., Fisher, R.J., Burke, T.R., Jr. *Bioorg. Med. Chem.* **15**, 4200 (2005).

Cu(I)- and Ru(II)-Mediated "Click" Cyclization of Tripeptides: Toward Vancomycin-Inspired Mimics

Jinqiang Zhang, Johan Kemmink, Dirk T.S. Rijkers, and Rob M.J. Liskamp

Medicinal Chemistry & Chemical Biology, Utrecht Institute for Pharmaceutical Sciences, Department of Pharmaceutical Sciences, Faculty of Science, Utrecht University, 3508 TB, Utrecht, The Netherlands

Introduction

Reduction of conformational flexibility is important to increase the affinity of a peptide for its natural receptor. A first convenient approach to achieve this goal is head-to-tail cyclization. However, Nature has found many other covalent constraints to reduce the flexibility of a peptide, and even beyond this, in the creation of cavity or shell-like structures. The cavity of the vancomycin antibiotics induced by the biaryl ether bridge is an outstanding example in this respect. In our previous approaches [1,2] we have used ring-closing metathesis for a side-chain knotted pentapeptide inspired by vancomycin, as well as the Sonogashira reaction for the preparation of alkyne-bridged cyclic tripeptides as mimics of vancomycin. As a new attractive alternative for the biaryl ether bridge in vancomycin, we report here on the successful introduction of the 1,4- and 1,5-disubstituted triazole moiety in cyclic tripeptides toward the synthesis of vancomycin-inspired peptidomimetics.

Results and Discussion

The syntheses started with L-4-hydroxyphenyl glycine, which was, after introduction of the Boc-group, converted into its corresponding methyl amide to suppress racemization during subsequent peptide coupling steps [3]. Methylation of the phenolic hydroxyl group with MeI/K_2CO_3 in DMF led to the methyl ether (83% yield) and was followed by iodination using I_2 in the presence of CF_3COOAg (87% yield) [4]. Next, the desired alkyne moiety was introduced via a Pd-catalyzed Sonogashira cross-coupling using TBDMS-protected acetylene in an excellent yield (94%). After Boc-group removal by TFA, Boc-D-Ala-OH was coupled with BOP, to give the dipeptide in good yield (80%). At this point, the optimal length of the side chain of the azido-amino acid needed for cyclization by CuAAC [5,6] or RuAAC [7] was not known. Therefore, after removal of the Boc-group, four different azido-amino acids were introduced, which were conveniently accessible in a diazotransfer reaction using imidazole-1-sulfonyl azide [8]. Finally, the TBDMS-group was removed by TBAF and the "click" precursors **1a-d** were obtained in high yields.

In the CuAAC reactions, 1.5 equiv of the soluble Cu(I) catalyst $Cu(CH_3CN)_4PF_6$ was used at a diluted precursor concentration (1 mM). Under these conditions, the "click" macrocyclization proceeded with complete conversion after 24 h at room temperature. Not unexpectedly, cyclization of the precursors **1a-c** led to the formation of dimers and even trimers in an appreciable yield (up to 57%), while macrocycles **2a-c** could not be isolated from the reaction mixture, as was judged by HPLC and MALDI-TOF. Gratifyingly, the precursor containing the lysine-derived azide **1d** led to formation of the desired macrocycle **2d** as the major product (46%), together with its corresponding dimer as the minor product (15%).

These results are indicative of the scope of the preparation of small cyclic peptides containing the 1,4-disubstituted triazole ring system. Access to a 1,5-disubstituted triazole moiety via RuAAC, in which the substitutents are positioned under a smaller angle, might be beneficial for achieving a more easily obtainable bent site in the said macrocycles. Marcaurelle and co-workers recently described the Ru(II)-catalyzed synthesis of 1,5-disubstituted triazole *N*-methyl lactams [9], which seemed very attractive for application on "click" precursors **1a-d**.

[Cp*RuCl]₄ was selected as a catalyst since it leads to a good regioselectivity toward the 1,5-disubstituted triazole moiety. Attempts with the shortest azide-containing side chain precursor **1a** were already successful. Complete conversion was achieved after 24 h at 50ºC using a precursor concentration of 5 mM in the presence of 15 mol % catalyst. In addition to the dimer (31%), the desired monocycle **3a** was obtained in an encouraging yield of 14%. Using this protocol, precursors **1b-d** were subjected to Ru(II)-catalyzed cyclization, which resulted in

exclusive formation of the desired monocycles **3b-d** in attractive yields for these relatively small macrocyclic tripeptides, without the detection of any dimers.
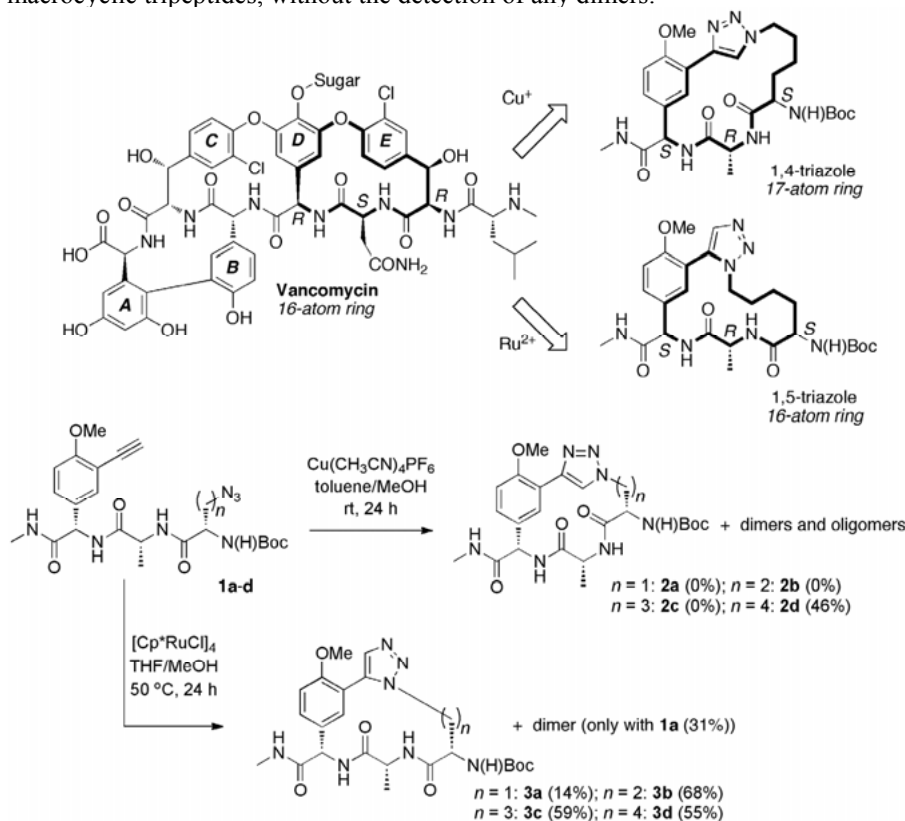
These results demonstrated clearly that the geometry of the triazole moiety determines to a large extent the outcome of the "click" macrocyclization [10]. Since the 1,4-disubstituted triazole is extended, predominantly cyclic dimers were formed. Only when the ring size is 17 atoms (**2d**), a cyclic monomer was formed. Because of its β-turn-like conformation, the 1,5-disubstituted triazole favored the formation of cyclic monomers and allowed the formation of a highly constrained ring structure of 13 atoms in **3a**.

Acknowledgments

References

1. ten Brink, H.T., Rijkers, D.T.S., Kemmink, J., Hilbers, H.W., Liskamp, R.M.J. *Org. Biomol. Chem.* **2**, 2658-2663 (2004).
2. ten Brink, H.T., Rijkers, D.T.S., Liskamp, R.M.J. *J. Org. Chem.* **71**, 1817-1824 (2006).
3. Grimm, J.B., Wilson, K.J., Witter, D.J. *Tetrahedron Lett.* **48**, 4509-4513 (2007).
4. Nicolaou, K.C., Boddy, C.N.C., Li, H., Koumbis, A.E., Hughes, R., Natarajan, S., Jain, N.F., Ramanjulu, J.M., Brase, S., Solomon, M.E. *Chem. Eur. J.* **5**, 2602-2621 (1999).
5. Tornøe, C.W., Christensen, C., Meldal, M. *J. Org. Chem.* **67**, 3057-3064 (2002).
6. Rostovtsev, V.V., Green, L.G., Fokin, V.V., Sharpless, K.B. *Angew. Chem. Int. Ed.* **41**, 2596-2599 (2002).
7. Zhang, L., Chen, X.G., Xue, P., Sun, H.H.Y., Williams, I.D., Sharpless, K.B., Fokin, V.V., Jia, G.C. *J. Am. Chem. Soc.* **127**, 15998-15999 (2005).
8. Goddard-Borger, E.D., Stick, R.V. *Org. Lett.* **9**, 3797-3800 (2007).
9. Rowley Kelly, A., Wei, J., Kesavan, S., Marié, J.-C., Windmon, N., Young, D.W., Marcaurelle, L.A. *Org. Lett.* **11**, 2257-2260 (2009).
10. Zhang, J., Kemmink, J., Rijkers, D.T.S., Liskamp, R.M.J. *Org. Lett.* **13**, 3438-3441 (2011).

Synthetic Studies toward Lucentamycin A and 3-Alkyl-4-Alkylideneprolines via Enolate-Claisen Rearrangement

Sujeewa Ranatunga[1,2], Jinsoo Kim[1], and Juan R. Del Valle[1]

[1]Drug Discovery Department, H. Lee Moffitt Cancer Center and Research Institute, Tampa, FL, 33612, U.S.A.; [2]Department of Chemistry and Biochemistry, New Mexico State University, Las Cruces, NM, 88003, U.S.A.

Introduction

Lucentamycins A-D are non-proteinogenic tripeptides isolated from the marine bacteria *Nocardiopsis lucentensis* [1]. The most biologically active of these structures, lucentamycin A, exhibits significant cytotoxicity toward HCT-116 human colon cancer cells *in vitro* (IC_{50} = 0.20 µM). Structural elucidation based on NMR experiments and Marfey analysis of degradation products revealed unique tripeptides composed of an *N*-acylated homoarginine (Har), a *C*-terminal leucine or tryptophan, and a central 4-ethylidene-3-methylproline (Emp) residue unprecedented in the natural product literature. We employed an ester enolate-Claisen rearrangement to install the stereochemistry of proposed Emp core of lucentamycin A [2] and have extended this methodology to synthesize related analogs and diastereopure 3-alkyl-4-alkylideneprolines.

Results and Discussion

We designed a general approach toward 3,4-disubstituted prolines by way of a linear allylglycine precursor (Figure 1). We envisioned that the desired linear amino acid could be accessed via a stereoselective ester enolate-Claisen rearrangement as shown in Figure 1. On the basis of a chair transition state model [3], the appropriate ester starting material should possess an *S* configuration and *E* alkene geometry to afford the desired Emp isomer. We used (−)-ethyl lactate as a chiral progenitor to furnish the desired residue. Further elaboration to introduce a *C*-terminal leucine and *N*-terminal acylated homoarginine (Har) afforded the putative structure of lucentamycin A (Figure 2) [2]. The anticipated stereochemical outcome of our key rearrangement reaction was confirmed by a combination of NOE studies and X-ray diffraction of the final tripeptide. A number of NMR chemical shift discrepancies between our tripeptide and natural lucentamycin A confirmed the need for a structural revision. In addition, the synthetic material exhibited much weaker activity against HCT-116 cells (37% growth inhibition at 10 µM) compared to the natural product.

We then synthesized Bz-Har-(8*R*,9*S*,10*Z*)Emp-Leu, a *cis*-Emp diastereomer of the proposed structure, following the same synthetic route starting from (+)-methyl lactate. Analogs with a *trans*-Emp relationship were also prepared from an ester substrate bearing a *Z* alkene geometry [4]. Each of the enolate-Claisen rearrangement proceeded with high dr and yield, irrespective of alkene configuration. Unfortunately, the spectral data of all four tripeptide diastereomers failed to match that of the natural product.
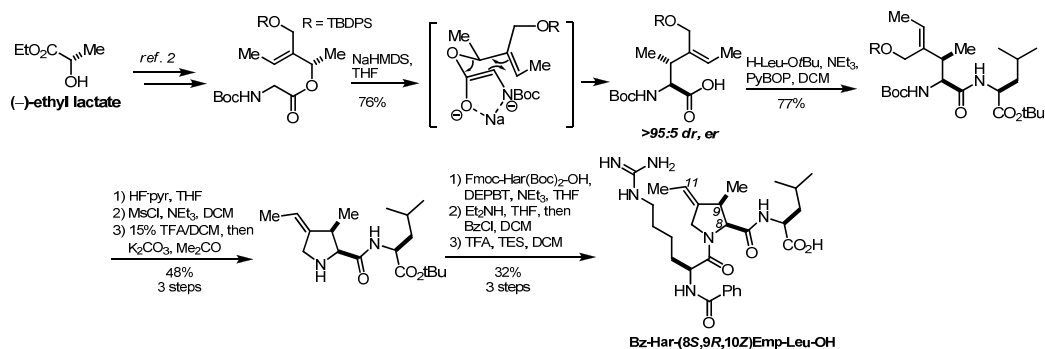
Fig. 1. An ester enolate-Claisen route to proposed Lucentamycin A.
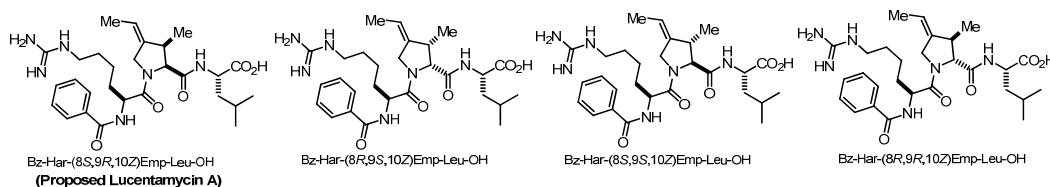
Fig. 2. Proposed Lucentamycin A and other synthesized stereoisomers.

In an effort toward diversely substituted lucentamycin analogs, we extended our ester enolate-Claisen methodology to access highly substituted prolines. By introducing different R^1, R^2, and R^3 groups onto the allylic ester, a series of new substrates was prepared and subjected to the rearrangement (Figure 3). The diastereomeric ratios of resulting acid products were analyzed by HPLC. The utility of this synthetic route to access highly substituted prolines was confirmed through the synthesis of the selected prolyl dipeptides shown in Figure 3.

R^1	R^2	R^3	acid dr[a]	acid yield[b]	R^1	R^2	R^3	acid dr[a]	acid yield[b]
Me	Me	H	>95:5	76	Et	Ph	H	88:12	76
Me	H	Me	>95:5	78	iPr	Ph	H	60:40	54
Me	n-pentyl	H	>95:5	77	tBu	Ph	H	78:12	61
Et	n-pentyl	H	91:9	60	Ph	Ph	H	73:27	69
iPr	n-pentyl	H	90:10	62	Ph	Me	H	>95:5	78
tBu	n-pentyl	H	83:17	52	Me	Et	H	>95:5	89
Ph	n-pentyl	H	87:13	74	H	Me	H	>95:5	82
Me	Ph	H	>95:5	85	H	H	Me	94:6	65
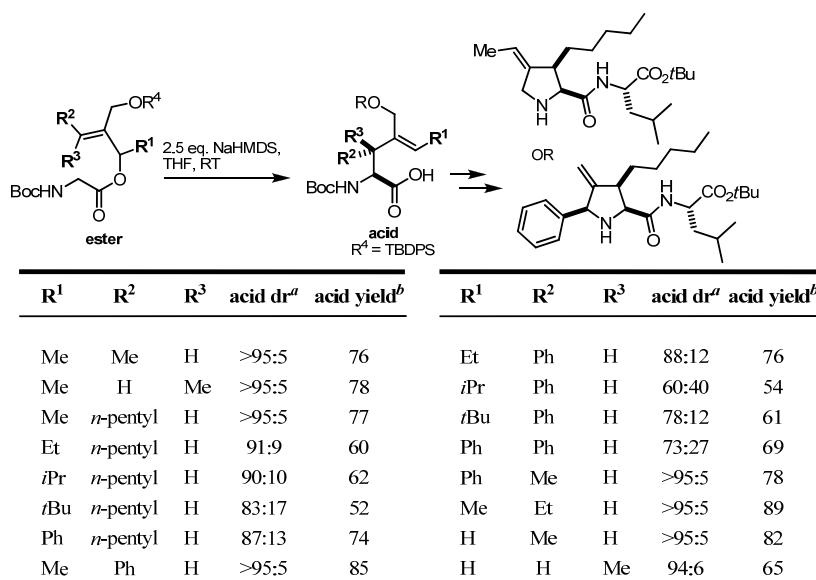
[a]Determined by HPLC of semi-crude product mixture; [b]Combined isolated yield of diastereomeric mixture; [c]R_4 = TIPS

Fig. 3. Substituent effects on enolate-Claisen rearrangement diastereoselectivity.

We are currently investigating application of this methodology to furnish other constrained amino acids and highly substituted proline derivatives for various biological applications.

Acknowledgement

References

1. Cho, J.Y., Williams, P.G., Kwon, H.C., Jenson, P.R., Fenical, W. *J. Nat. Prod.* **70,** 1321-1328 (2007).
2. Pal, U., Ranatunga, S., Ariyarathna, Y., Del Valle, J.R. *Org. Lett.* **11**, 5298-5301 (2009).
3. Kazmaier, U., Hiersemmann, M., Nubbemeyer, U. (Eds.) *The Claisen Rearrangement*, Wiley-VCH Verlag Gmbh & Co., Weinheim, Germany, 2007, p. 233.
4. Cha, J.H., Pae, A.N., Choi, K.I.I., Cho, Y.S., Koh, H.Y., Lee, E. *J. Chem. Soc. Perkin Trans.* **1**, 2079-2081 (2001).

A Novel Side Reaction in Fmoc-SPPS:
Formation of Cyclo(-Xaa-Asp)-Yaa Peptides

Daniel Samson and Günther Loidl

Bachem AG, 4416, Bubendorf, Switzerland

Introduction

Chain termination at the Xaa-Asp-Yaa motif caused by formation of cyclo(-Xaa-Asp)-Yaa peptides has been identified as a side reaction during Fmoc-SPPS, which is not limited to Asp β-benzyl esters as initially described in [1]. In contrast to the well-known aspartimide (Asi) formation at the Asp-Yaa site [2-5], the resulting cyclo(-Xaa-Asp)-Yaa peptides are not acylated during further SPPS and are generally detected as truncated sequences only after TFA cleavage in the crude product of the SPPS (Figure 1 shows a typical HPLC trace). These cyclic by-products are formally obtained by cyclization via nucleophilic attack of the free amino group of the Xaa residue at either the β-carboxy group of Asp or the α- and β-carbonyl groups of the Asi intermediate after deprotection of Fmoc-Xaa-peptide-resin.

Fig. 1. HPLC of Ac-DDGAKF-NH$_2$.

It is conceivable that both a 7-membered ring (diketodiazepine, 'DKD') following pathways A or B in Scheme 1 and/or a 6-membered ring (diketopiperazine, 'DKP') following pathway C in Scheme 1 can be formed. The peptide sequence Ac-Xaa-Asp-Yaa-Ala-Lys-Phe-NH$_2$ has been used to investigate the influence of different parameters such as the flanking amino acid residues Xaa and Yaa, the Fmoc cleavage conditions and the Asp β-carboxy protecting group on the side reaction.

Results and Discussion

Influence of the Flanking Residues Xaa and Yaa
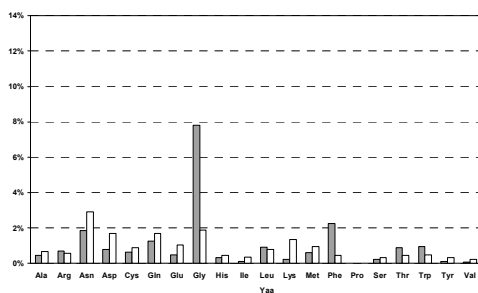
Fig. 2. Amount of by-products with varying Yaa.

Two peptide series were synthesized with Xaa = Gly and Yaa = all 20 natural amino acids (Figure 2) or Xaa = all 20 natural amino acids and Yaa = Gly (Figure 3). The obtained amounts of cyclo(-Xaa-Asp)-Yaa peptide (grey bars) and the corresponding aspartimides (white bars) are depicted relative to linear target.

Within the Xaa = Gly series, chain termination was most prominent with Yaa = Gly (8% of cyclo(-Gly-Asp) peptide detected, see Figure 2). As expected for N-alkyl amino acids, no aspartimide by-product was found for Yaa = Pro or when Yaa = Gly was incorporated as backbone-protected Fmoc-
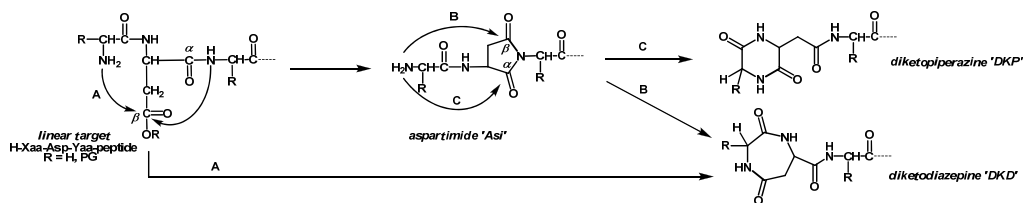
Scheme 1. Possible chain termination pathways A, B and C.

(Dmb)Gly-OH. Furthermore, no cyclo(-Gly-Asp) peptides were observed in these cases. Thus, chain termination via pathway A in Scheme 1 can be excluded.

The diketopiperazine cyclo(-Gly-Asp)-Gly peptide was synthesized independently. HPLC co-elution of this reference compound with the corresponding truncated sequence indicates that chain termination occurs via pathway C (see Scheme 1).
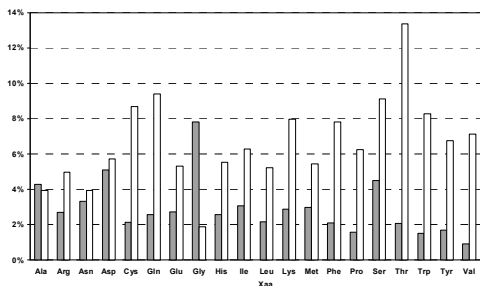
Fig. 3. Amount of by-products with varying Xaa.

In the series with constant Yaa = Gly, the 'worst case motif' for aspartimide formation, highest levels of cyclo(-Xaa-Asp) peptides were obtained for Xaa = Gly and Asp (grey bars in Figure 3). Additionally, the corresponding aspartimides (white bars in Figure 3) were detected in amounts ranging from 2 to 13%. Hence, the nature of the residue Xaa unexpectedly influences the level of aspartimide formed at the Asp-Yaa motif. Xaa also determines the extent of subsequent truncated peptide formation via aspartimide ring opening by its N-terminal amino function.

Influence of Asp β-carboxy Protecting Group and Fmoc Deprotection Reaction Time
The peptide Ac-G-D-G-A-K-F-NH$_2$ was synthesized using OtBu or OMpe as Asp side-chain protecting groups and different reaction times for Fmoc removal. Compared to OtBu, OMpe reduces formation of aspartimide [3] and consequently of cyclo(-Gly-Asp) peptide. Longer Fmoc cleavage reaction times lead to increasing levels of aspartimide and of the truncated cyclo(-Gly-Asp) peptide. A detailed evaluation of the reaction mechanism yielding cyclo(-Xaa-Asp)-Yaa peptides with structure elucidation of these truncated by-products and the influence of residue Xaa on aspartimide formation is ongoing and will be presented elsewhere in due course.

Summary

Chain termination during Fmoc-SPPS at the Xaa-Asp-Yaa motif is described. The resulting by-product is most likely the corresponding N-terminal diketopiperazine (DKP). An independently synthesized DKP-reference substance co-elutes on HPLC with the according by-product. It is proposed that the truncated cyclo(-Xaa-Asp) peptides are formed via nucleophilic attack of N-terminal Xaa amino function at the aspartimide intermediate (pathway C, Scheme 1). The extent of chain termination can be reduced by diminishing aspartimide formation, *e.g.* by
- short Fmoc deprotection times
- Asp β-carboxy protection with OMpe
- backbone protection at Yaa, as in Asp-(Dmb)Gly.

Experimental Procedures

All peptides were synthesized on Ramage resin (150 µmol scale). Couplings were performed with amino acid derivative or AcOH and TBTU/DIPEA. If not stated otherwise, Asp was introduced as Fmoc-Asp(OtBu)-OH and Fmoc was removed using 20% piperidine in DMF (2x15 min). The crude peptides were obtained after cleavage with aqueous TFA and analyzed with rapid HPLC (Waters Acquity C18, 1.7 µm; linear gradient of ACN in 0.1% TFA; flow 0.4 mL / min, λ = 220 nm). Peak assignment was performed using LC-MS analysis of the crude peptides.

References

1. Süli-Vargha, H., Schlosser, G., Ilaš, J. *J. Peptide Sci.* **13**, 742-748 (2007).
2. Bodanszky, M. *Principles of Peptide Synthesis* Springer-Verlag, Berlin, 1984.
3. Mergler, M., Dick, F., Sax, B., Weiler, P., Vorherr, T. *J. Peptide Sci.* **9**, 36-46 (2003).
4. Mergler, M., Dick, F., Sax, B., Stähelin, C. Vorherr, T. *J. Peptide Sci.* **9**, 518-526 (2003).
5. Mergler, M., Dick, F. *J. Peptide Sci.* **11**, 650-657 (2005).

On the Mechanism of Degradation of Oxytocin and its Analogues in Aqueous Solutions

Kazimierz Wiśniewski, Jens Finnman, Marion Flipo, Robert Galyean, and Claudio D. Schteingart

Ferring Research Institute Inc., San Diego, CA, 92121, U.S.A.

Introduction

Oxytocin (OT, **1**) is a nonapeptide containing a 20-member, six amino acid ring closed by a disulfide bridge between cysteines in position one and six. OT is used clinically as a labor inducing agent and is parenterally administered in an aqueous formulation of low pH. Although the stability of OT in common liquid formulations has been extensively studied [1], and a room temperature stable liquid formulation has been proposed [2], neither the degradation mechanism, nor the identity of the degradation products have been adequately described in the literature. In a recent stability study, monomeric polysulfides and dimeric products were identified as the major degradation products. The dimeric degradants were not fully characterized, but were postulated to derive from β-elimination with concurrent deamidation and dimerization reactions [3].
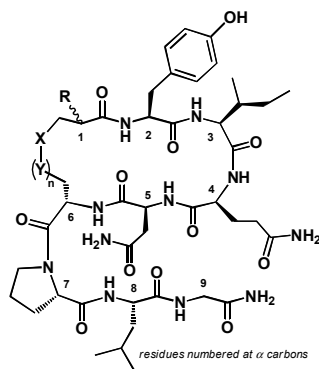
Fig. 1. Structure of compounds synthesized in this study.

To further understand this process we prepared a series of OT analogues mono- or di-N-alkylated on the Cys^1 residue and a second series with selenium or ^{34}S replacing the sulfur atom in the Cys^1 and/or Cys^6 residues (Figure 1). Initially, **1** was incubated in aqueous solutions in the 3.8-8.2 pH range and the degradation rates were determined. All analogues were then incubated at physiological pH and the degradation reactions were followed by HPLC and LCMS.

Here we present a preliminary account on this study with the focus on identifying structural features responsible for the rather poor stability of OT in near-neutral aqueous solutions, and the evidence demonstrating that β-elimination is a key step of the OT degradation process.

Results and Discussion

Peptides **1-14** were synthesized manually by standard Fmoc SPPS. The N-terminal alkylations were achieved on resin by Mitsunobu reaction (**8**, **10**) or reductive alkylation (**9**, **11**). To synthesize the ^{34}S labeled analogues **6** and **7**, Fmoc-[^{34}S]Cys-(Mob)-OH was prepared from ^{34}S as described earlier [4].

The degradation rate of **1** increased with pH, suggesting that the rate-determining step involves proton subtraction. Monomeric polysulfides (peaks b-d) and dimeric compounds (peaks e-g) were observed in the incubation solutions at pH 7.4 (Figure 2). Synthetic oxytocin trisulfide **14** coeluted with the corresponding degradation product represented by peak b. Sulfur atoms inserted to form polysulfides come exclusively from the Cys^1 residues (Figure 2).

Compound	Observed M+H+ for peaks a-g						
	a	*b*	*c*	*d*	*e*	*f*	*g*
1 (OT)	1007.3	1039.3	1071.2	1103.3	1949.5	1949.5	1981.5
6	1009.3	1043.3	1077.2	1111.2	1949.5	1949.5	1983.5
7	1009.3	1041.2	1073.2	1105.1	1953.4	1953.5	1985.4

Fig. 2. LCMS trace of the OT degradation mixture at day 7, pH 7.4 and MH+ observed for peaks a-g. Identical traces were obtained for ^{34}S labeled compounds 6 and 7.

Table 1. Structure and stability of compounds synthesized in this study

Compound	Conf at Cα carbon of Aaa[1]	R	X	Y	n	Stability (% remaining after 28 days)
		Structure (see Figure 1)				
1	R	NH_2	S	S	1	12.6
2	R	NH_2	Se	S	1	3.3
3	R	NH_2	S	Se	1	20.5
4	S	NH_2	CH_2	S	1	96.3
5	S	NH_2	CH_2	CH_2	1	97.5
6	R	NH_2	^{34}S	S	1	NT[a]
7	R	NH_2	S	^{34}S	1	NT[a]
8	R	$NHCH_2CHEt_2$	S	S	1	35.3
9	R	NMe_2	S	S	1	14.3
10	R	NHMe	S	S	1	2.3
11	R	NH-iPr	S	S	1	39.9
12	R	H	S	S	1	90.1
13	S	NH_2	S	S	1	50.9
14	R	NH_2	S	S	2	NT[a]

[a]*NT, not tested*

This was also true for mixed selenium/sulfur bridges. Oxytocin, **1,** and its D-Cys[1] analogue **13** resulted in sets of polysulfides with different retention times, indicating that they are formed from their parent compounds without affecting the chirality of the position 1 α-carbon. Dimers represented by peaks e, f (Figure 2) contain sulfur atoms solely from Cys[6], while the sulfur atoms from both Cys[1] appear to have been lost. Surprinsingly, compounds **8-11** produced identical dimers to those from **1** and **13**, showing that the N-terminal amino functionality is also lost in the dimers. The degradation rates of compounds **8-11** appear to depend on the basicity of the nitrogen and the size of the N-alkyl substituent. In the absence of an amino functionality (**12**) the degradation rate becomes very slow, suggesting that the N-terminal group is an integral part of the degradation mechanism. The sensitivity of the degradation rate to pH and the faster degradation rate observed for the Sec[1] compound **2** than for **1** (Table 1) suggest that the rate determining step may occur within the Aaa[1] residue and is consistent with C-S(Se) bond breakage via β-elimination of a persulfide (perselenide is a better leaving group than persulfide). The presence of both N-terminal amino functionality and the disulfide bridge is required for fast degradation as removal of any one of these structural features in **4, 5,** and **12** led to much more stable compounds. Further experiments are being conducted to find out the origin of the polysulfides, the fate of the putative persulfide intermediates, and to elucidate the structure of the dimeric degradants.

These data suggest that it is possible to design OT analogues with enhanced stability in liquid formulations by elimination of one or both structural features responsible for OT instability.

References

1. Trissel, L.A., Zhang, Y., Douglass, K., Kastango, E. *Int. J. Pharm. Comp.* **10**, 156-158 (2006).
2. Avanti, C., et al. *AAPS J.* **13**, 284-290 (2011).
3. Hawe, A., et al. *Pharm. Res.* **26**, 1679-1688 (2009).
4. Rooseboom, M., et al. *Chem. Res. Toxicol.* **15**, 1610-1618 (2002).

Investigation of Gamma Irradiation Effect upon Several Physiologically Relevant Peptides

Renata F.F. Vieira[1], Daniela T. Nardi[1], Nanci Nascimento[2], Jose C. Rosa[3], and Clovis R. Nakaie[1]

[1]*Department of Biophysics, Federal University of Sao Paulo, Sao Paulo, 04044020, Brazil;* [2]*Institute for Energy Research and Nuclear Science (IPEN), University of Sao Paulo, Sao Paulo, 05508000, Brazil;* [3]*Protein Chemistry Center and Department of Molecular and Cell Biology, School of Medicine of Ribeirao Preto, University of Sao Paulo, Ribeirao Preto, 14049900, Brazil*

Introduction

The reaction products and mechanisms involved in the radiolysis of macromolecules of biological relevance are object of several studies [1]. These factors (mainly the oxidation induced by free radicals) are known to be involved in many pathological disorders such as diabetes, cancer, Alzheimer's and Parkinson's diseases [2]. Following with previous studies related to the vasoactive peptides angiotensin II (DRVYIHPF, AII) [3] and bradykinin (RPPGFSPFR, BK) [4] and aiming at unravel the potential of strong electromagnetic irradiation strategy for peptide structure modifications, several physiologically relevant peptides were submitted to Co^{60} gamma irradiation in aqueous solution (doses ranging from 1 to 15 kGy).

Results and Discussion

The gamma irradiation process induced, regardless of the peptide sequence, a non-linear and progressive degradation of all peptides assayed. Figure 1 shows for example, the time-course degradation process of *α-MSH* and *Substance P,* respectively. Of note, the rate of this structural modification induced possibly by generated free radicals in aqueous solution was typically sequence- and position-dependent. For instance, under this strong electromagnetic irradiation condition, BK and AII and some of their related peptides such as the Pro^4-BK or (1-7) AII and AI (DRVYIHPFHL) were more stable than the melanocyte-stimulating hormone (Ac-SYSMEHFRWGKPV-amide, *α-MSH*) or *Substance P* (RPKPQQFFGLM-amide).
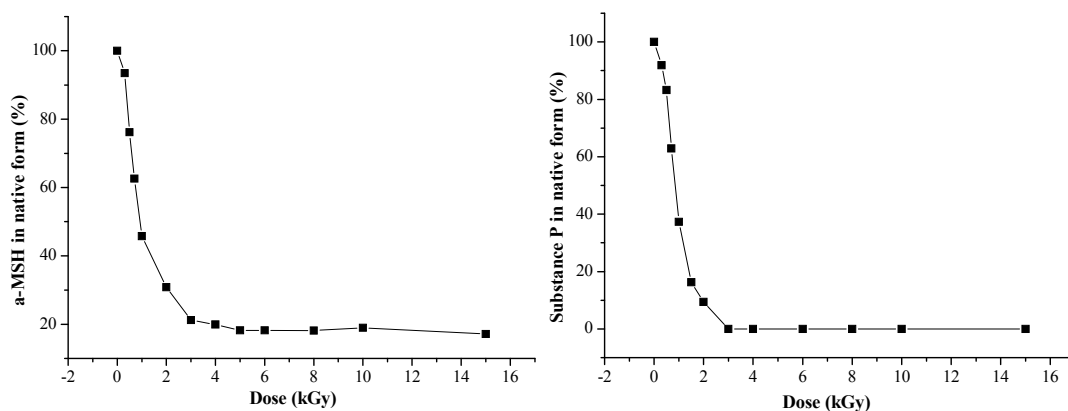
Fig. 1. Remaining α-MSH (a) and Substance P (b) quantities (in percentage) as a function of the gamma irradiation dose.

Table 1. Peptides and its possible fragments formed under gamma radiation

Peptides	Sequence	Dose (kGy)	MW (Da)	Possible fragments
AII	D-R-V-Y-I-H-P-F-OH	1	532	+17 Da (1Phe/1Tyr)
		2	532	+17 Da (1Phe/1Tyr)
BK	R-P-P-G-F-S-P-F-R-OH	2	539	+16 Da (1Phe/1Tyr)
		4	539	+16 Da (1Phe/1Tyr)
α-MSH	Ac-S-Y-S-M-E-H-F-R-W-G-K-P-V-NH$_2$	1	841	+16 Da (1Phe/1Tyr)
		2	841	+16 Da (1Phe/1Tyr)
Substance P	R-P-K-P-Q-Q-F-F-G-L-M-NH$_2$	1	690	+33 Da (2Phe/2Tyr)
			683	+17 Da (1Phe/1Tyr)
		2	691	+33 Da (2Phe/2Tyr)
			683	+17 Da (1Phe/1Tyr)

The main products generated by gamma irradiation were examined by means of Edman sequencing method coupled to the electrospray triple-quadrupole tandem mass spectrometry applying the daughter ion scanning by collision induced dissociation (CID-MS/MS) method (data not shown).

Usually, the most prominent derivatives generated from this experimental protocol revealed that they are likely induced by oxidation process, yielding a variation of +16 Da in their molecular weight. Our data revealed that the Phe oxidation is due to hydroxyl moiety insertion at *o*-, *m*- or *p*- positions of its aromatic side chain (checked by amino acid analysis), generating in the latter case, the Tyr residue. This was the case of AII [3] and BK [4]. A similar hydroxylation of Phe residue also seemed to have occurred with the *α-MSH*, producing an analogue with increase of 16 Da in its molecular weight. This increase would be possibly derived either from the Phe or Met residues oxidation (Table 1).

In complement, other side-products were also detected such as that with an increment of + 33 Da in its molecular weight observed for *Substance P*. This finding seems to be likely due to oxidation of the two Phe residues present in its sequence (Table 1). Of relevance, one can stress that even in small peptide structures, this experimental protocol applying strong electromagnetic radiation seems to induce a clear residue- and sequence-dependent effect in the peptide backbone.

Indeed, the main objective of this innovative approach lies in the feasibility of generating unusual peptide analogues, not easily obtained by conventional synthesis methods. Classical structure-function study of purified analogues obtained in some cases, with uncommon structures, is currently in progress.

References
1. Garrison, W.M. *Chem. Rev*. **87**, 381-398 (1987).
2. Simic, M.G. *Cancer Res*. **54**, 1918-1923 (1994).
3. Nardi, D.T., Casare, M.S., Teixeira, L.G.D., Nascimento, N., Nakaie, C.R. *Int. J. Radiat. Biol*. **84**, 937-944 (2008).
4. Nardi, D.T., Rosa, J.C., Jubilut, G.N., Miranda, A., Nascimento, N., Nakaie, C.R. *Int. J. Pept. Res. Ther*. **16**(2), 71-78 (2010).

Synthesis and Structure Activity Relationship Study of Didehydro-derivatives of a Natural Diketopiperazine Tryprostatin

Yuki Shinozaki, Yoshihiko Yamamoto, Haruka Takeno, Yuri Yamazaki, Fumika Yakushiji, and Yoshio Hayashi

Department of Medicinal Chemistry, School of Pharmacy, Tokyo University of Pharmacy and Life Sciences, Tokyo, 192-0392, Japan

Introduction

Tryprostatins A (**1**) and B (**2**) are cyclic dipeptides (diketopiperazine, DKP), which were isolated from *Aspergillus fumigatus* BM939 by Osada's group in 1995 (Figure 1) [1]. They inhibited cell cycle progression of tsFT210 cells in the M phase with mild IC_{50} values of 78.7 and 18.8 µM, respectively [2]. In our previous study focused on another natural DKP phenylahistin (PLH/halimide), a mild microtubule depolymerization agent, we succeeded in creating a highly potent vascular disrupting agent Plinabulin which is in Phase II clinical trials as an anticancer drug [3]. In the structural optimization of PLH, the conversion to the dehydro-structure was a key for increasing the cytotoxic activity. Hence in the present study, we focused on tryprostatins and synthesized didehydro-derivatives having a potent cytotoxic activity (Figure 1). The cytotoxicity of derivatives was evaluated against human colon cancer cell line HT-29 by the XTT assay.

Tryprostatin A (**1**); R = OMe
Tryprostatin B (**2**); R = H

3
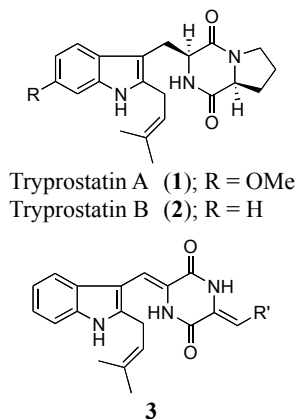
Fig. 1. Structure of tryprostatins and their didehydro-derivative 3.

Results and Discussion

To develop the didehydro-derivatives from relatively potent tryprostatin B (**2**), a synthetic route with 8 steps was planned as depicted in Scheme 1. Protection of the 1*H*-indole nitrogen in **4** with the phenylsulfonyl (besyl) group followed by introduction with the prenyl group at the C(2) position of the indole ring afforded 2-prenylindole **6**. After deprotection of the besyl group under microwave condition [4], the product was formylated by the Vilsmeier reaction and the 1*H*-indole nitrogen was protected with the Boc group again to obtain indolealdehyde **9** in moderate yield. Then, the aldol condensation of **9** was carried out towards *N,N'*-diacetylpiperazine-2,5-dione **10**, followed by the easy deprotection of the Boc group under heating condition with silica-gel to obtain DKP derivative **12** in good yield. This DKP **12** was used as a common intermediate for the synthesis of the didehydro-derivatives. Namely, by the additional aldol condensation with a variety of aryl aldehydes, we could obtain a series of didehydro-derivatives of tryprostatin B (**3a-n**, Scheme 1).

The cytotoxic activity of didehydro-derivatives **3a-n** was evaluated by the XTT assay against HT-29 cells and the IC_{50} values are summarized in Table 1. Compounds **3h** and **3k**, which have a methoxy or hydroxyl group at the 2-position of the phenyl ring, respectively, exhibited relatively potent cytotoxic activity with the IC_{50} values of 6.6 and 32.6 µM. In addition, 1-naphthyl derivative **3l** exhibited more potent activity (0.6 µM) than phenyl derivatives **3h** and **3k**. Hence, the methoxy group was inserted at the same position in the naphthyl derivative **3l**, and resulted in the most potent derivative **3n** among all derivatives synthesized in the present study. The results suggested that modification of the R' position was important for the activity in the didehydro-tryprostatin derivatives and the existence of oxygen at the 2-positon was effective for the potent activity, which may probably interact with the target protein via a hydrogen bonding. Substitution at the *m*-position with CH_3 or Br (**3c**, **3f**) was tolerable for the activity and no activity was observed with the substitutions at the *p*-position.
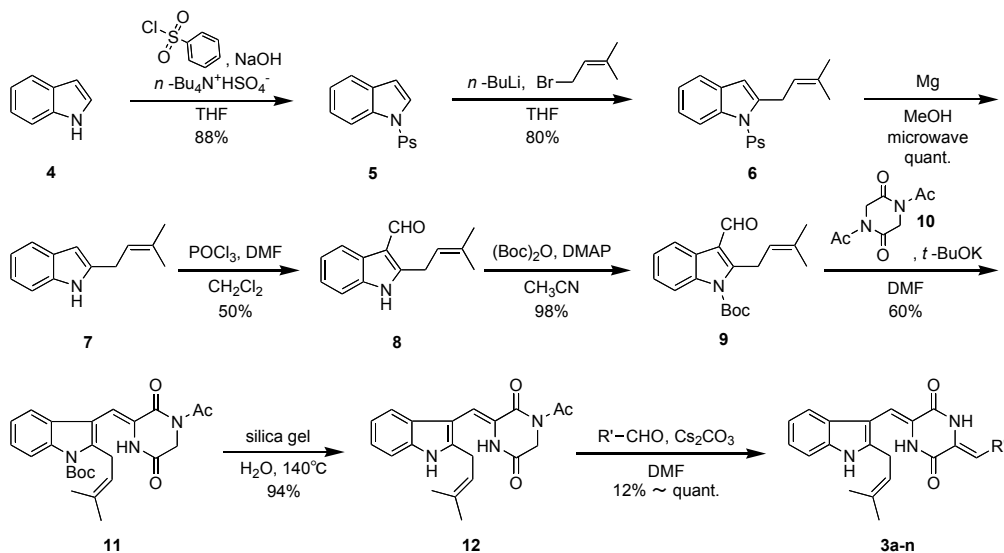
Scheme 1. Synthesis of didehydro-derivatives of tryprostatin B via the Boc group.

Therefore, it is concluded that the conversion to the didehydro-structure in tryprostatin was effective to develop the potent cytotoxic compound such as **3n**. Moreover, it is suggested that the planar structure around the didehydroDKP ring might be a proper template for the protein molecule recognition. In addition, since slight change in the chemical structure of DKP **3** drastically influenced the activity, highly constrained conformation of this DKP might target to a specific cellular molecule for the cytotoxicity. The detailed study of the biological mechanism is currently under investigation.
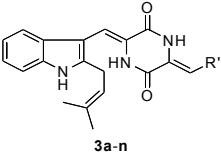
Acknowledgments

References

1. Cui, C.-B., et al. *J. Antibiot.* **48**, 1382-1384 (1995).
2. Cui, C.-B., et al. *J. Antibiot.* **49**, 527-533 (1996).
3. Nicholson, B., Lloyd, G.K., Miller, B.R., Palladino, M.A., Kiso, Y., Hayashi, Y., Neulteboom, S.T.C. *Anti-Cancer Drugs* **17**, 25-31 (2006).
4. Jernej, W., et al. *Synthesis* **9**, 1436-1442 (2008).

Table 1. Cytotoxicity of didehydro-derivatives

3a-n

Compounds	R—	IC_{50} (µM)
a	Phenyl	> 100
b	o-CH$_3$-Phenyl	> 100
c	m-CH$_3$-Phenyl	17.2 ± 1.0
d	p-CH$_3$-Phenyl	> 100
e	o-Br-Phenyl	> 100
f	m-Br-Phenyl	35.5 ± 2.4
g	p-Br-Phenyl	> 100
h	o-MeO-Phenyl	6.6 ± 0.2
i	m-MeO-Phenyl	> 100
j	p-MeO-Phenyl	> 100
k	o-OH-Phenyl	32.6 ± 1.3
l	1-Naphthyl	0.60 ± 0.02
m	2-Naphthyl	> 100
n	2-MeO-1-Naphthyl	0.41 ± 0.01

IC_{50} = Mean ± SD (HT-29 cells)

Total Synthesis of Phalloidin

Jianheng Zhang, Xuejing Xu, Qingzheng Wang, and Baosheng Liu

American Peptide Company, Inc., 777 E. Evelyn Ave., Sunnyvale, CA, 94086, U.S.A.

Introduction

Phalloidin, a bicyclic heptapeptide, is one major component of a group of fungal toxins isolated from poisonous mushroom *Amanita phalloides*. Its structural features include a thioether bridge linking Cys[3] and Trp[6], a *cis* epimer of 4-hydroxy-L-proline (*cis*-Hyp[4]), an unusual amino acid (2S,4R)-4,5-dihydroxy-L-leucine (Figure 1). Phalloidin and its fluorescent analogs can selectively bind to filamentous actin, therefore, phalloidin derivatives are commonly used as a very convenient tool in imaging applications for labeling F-actin in fixed cells, permeabilized cells and cell-free experiments. Since the structure of these fungal toxins has been recognized, a lot of synthetic work on natural and non-natural analogues of these bicyclic peptides has been carried out, especially in Wieland's laboratory [1]. However, the total synthesis of phalloidin has not yet been completed before. We have developed a method for the synthesis of phalloidin derivatives, which combines the solid-phase and solution phase peptide synthesis techniques. A feature of the method is the efficient preparation of linear heptapeptides, the precursor of the phalloidin derivatives, through a solid-phase approach. Another feature of the method is post-cleavage cyclization of the heptapeptide and subsequent direct thionation of indole ring of tryptophan by iodine oxidation in solution to form bicyclic peptides in good yields [2]. The first total synthesis of phalloidin has been achieved via this route successfully.
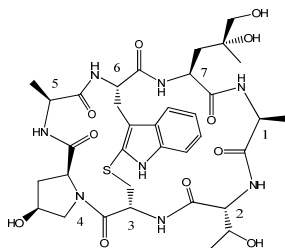
Bicyclic(Ala[1]-DThr[2]-Cys[3]-cis-4-hydroxy-Pro[4]-Ala[5]-2-mercapto-Trp[6]-4,5-dihydroxy-Leu[7])(S-3→6)

Fig. 1. Structure of Phalloidin.

Results and Discussion

The unusual amino acid (2S,4R)-4,5-dihydroxy-L-Leucine is a key building block for the total synthesis. The Sharpless asymmetric dihydroxylation of Fmoc-Leu(4,5-dehydro)-Ala-OH with AD-mix α or AD-mix β gives a mixture of diasteromers of Fmoc-Leu(4,5-di-OH)-Ala-OH with 4R or 4S configuration. The results showed that dihydroxylation with both AD-mix α and AD-mix β cannot give the dipeptide with a steroisomerically pure 4,5-dihydroxyleucine. However, each AD-mix dihydroxylation favors one of the two diasteromers respectively and both dipeptides are synthetically useful (Figure 2, Table 1) [3].

The linear heptapeptide has been synthesized by using Fmoc-strategy solid phase peptide synthesis. First, Fmoc-*trans*-4-hydroxy-proline was loaded to 2-chloro trityl chloride (CTC) resin via the C-terminal attachment. By using 3,5-dinitrobenzoic acid, the configuration of *trans*-4-hydroxy-proline was inverted under the Mitsunobu reaction condition on-resin. After the reaction was complete, the resulting Fmoc-*cis*-Hyp(3,5-dinitrobenzoyl)-CTC resin was easily obtained by washing off the excess reagents. The resin was treated with 20% piperidine in DMF to remove Fmoc and the resulting H-*cis*-Hyp(3,5-dinitrobenzoyl)-CTC resin was coupled with selected amino acids and the dipeptide to assemble the desired linear heptapeptide by using standard Fmoc chemistry. DIC/HOBt was employed as coupling reagents. After the couplings were complete, the N-terminal Fmoc and side chain protecting group 3,5-dinitrobenzoyl on

A: Fmoc-(2S,4R)-Leu(4,5-di-OH)-Ala-OH   **B:** Fmoc-(2S,4S)-Leu(4,5-di-OH)-Ala-OH
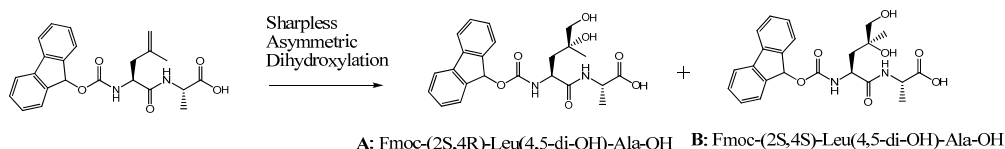
Fig. 2. Sharpless asymmetric dihydroxylation of Fmoc-Leu(4,5-dehydro)-Ala-OH.

Table 1. Sharpless asymmetric dihydroxylation of Fmoc-Leu(4,5-dehydro)-Ala-OH

Reaction condition	Ratio of product (based on HPLC)	
	A	B
AD mix-α (0 ^{o}C)	3	1
AD mix-α (RT)	2	1
AD mix-β (0 ^{o}C)	1	9
AD mix-β (RT)	1	7

hydroxyproline were removed simultaneously by 2% hydrazine in DMF. Then the linear peptide was cleaved from resin using the cocktail mixture consisting of TFE/HOAc/DCM (2/2/6). Next, head to tail coupling reaction of linear peptide was carried out in dilute DMF solution with PyBOP/DIEA to afford cyclic peptide in high yield. Finally, the formation of thioether, the key step of phalloidin synthesis, was achieved by direct thionation of indole ring of tryptophan by iodine oxidation [4,5] (Figure 3).
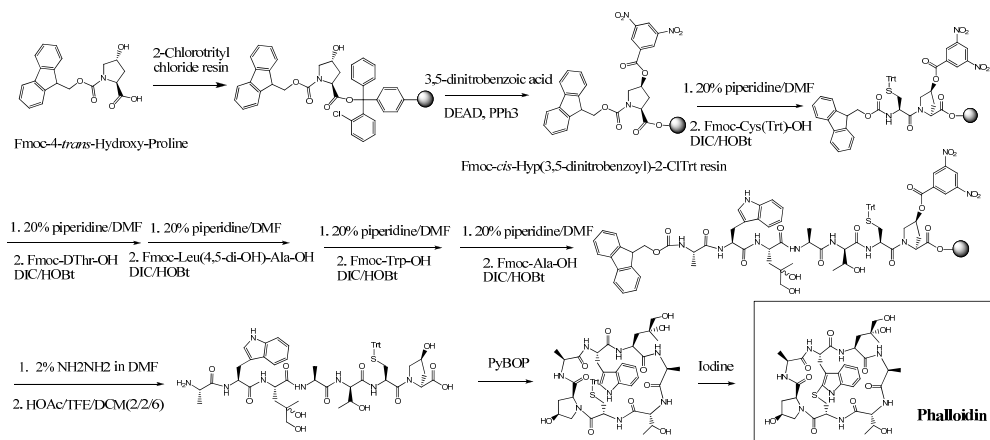
Fig. 3. Synthesis of Phalloidin.

Reverse phase-HPLC purification of the crude gives the desired phalloidin over 95% purity. The overall yield of phalloidin is 8.4% based on the initial resin loading. HPLC, MS and circular dichroism (CD) analysis showed that the synthetic phalloidin is identical to the natural phalloidin (Figure 4).
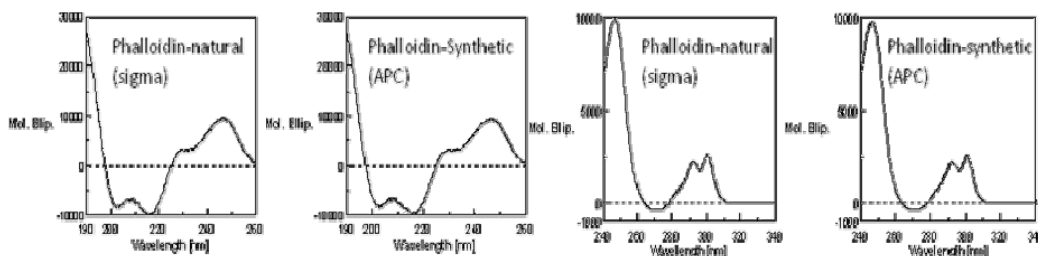
Fig. 4. Far and near UV circular dichroism (CD) spectra of natural Phalloidin (Sigma) and synthetic Phalloidin (APC) in water (0.5 mg/mL).

References

1. Wieland, T. *Peptides of Poisonous Amanita mushrooms*, Springer-Verlag: New York, 1986.
2. Liu, B., Zhang, J. *US Provisional patent application*, US 61/463,422. Feb. 2011.
3. Edagwa, B.J., Taylor, C.M. *J. Org. Chem.* **74**, 4132-4136 (2009).
4. Sieber, P., Kamber, B., Riniker, B., Rittel, W. *Helv. Chim. Acta.* **63**, 2358-2363(1980).
5. Schuresko, L.A., Lokey, R.S. *Angew. Chem. Int. Ed.* **46**, 3547-3549(2007**)**.

Peptidomimetic Ligation

Naila Assem, Aditya Natarajan, and Andrei K. Yudin

Davenport Research Laboratories, Department of Chemistry, University of Toronto, 80 St. George Street, Toronto, Ontario, Canada, M5S 3H6

Introduction

The three-dimensional folding of peptides and proteins determines a broad range of their properties [1]. Structural modification of the amino acid sequence has become increasingly important in the study of biological processes. In this regard, unnatural α-amino acids are useful elements of functional control that can determine the conformational preferences of peptides. Insertion of unnatural amino acids has been simplified through the use of site directed mutagenesis and native chemical ligation [2]. However, α-amino acids do not impose constitutional changes over the polyamide core. Replacing peptide bonds with their isosteres can bring about such changes. Despite significant advances in chemical synthesis, installation of a peptidomimetic bond is plagued with the need for protecting groups. To avoid such problems we have developed a peptidomimetic ligation during which a reduced peptide bond can be selectively placed at a cysteine, alanine, phenylalanine, or substituted cysteine residue of a peptide chain.

Results and Discussion
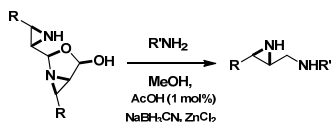
The concentration of free aldehyde is negligible ⟹ no overalkylation

Scheme 1. Reductive conjugation.

To introduce the amino methylene-containing backbone fragment into a peptide chain, we sought to employ the recently developed unprotected aziridine aldehydes [3]. The first step of our method is reductive conjugation between an aziridine aldehyde and a peptide (Scheme 1). This epimerization-free [4] reaction was run on a series of peptides. By using 1 equivalent excess of aziridine aldehyde, a simple wash with a saturated solution of sodium bicarbonate followed by extraction with ethyl acetate removes any excess aziridine aldehyde, affording the corresponding peptide conjugates. The reaction proceeds via partially dissociated dimeric amino aldehyde species which, upon condensation and subsequent reduction, produces one equivalent of the peptide conjugate and one equivalent of the free amino aldehyde, which rapidly re-dimerizes. This reductive amination is favourable not only because it is epimerization free, but over-alkylation is not a problem either.

With the NH aziridine-containing peptide conjugates in hand, we tested the feasibility of chemoselective peptidomimetic ligation using thio amino acids. We hypothesized that aziridine ring-opening would trigger an S-to-N acyl group transfer. Mechanistically, the reaction was projected to occur via a five-membered ring intermediate reminiscent of Kent's native chemical ligation [5]. The thio-amino acids required in order to put this idea to test were prepared through activation of the carboxylic acid end of the peptide with carbonyldiimidazole followed by the addition of sodium sulfide. This synthetic route was found to be practical as it did not employ the difficult to handle gaseous hydrogen sulfide. Furthermore, no purification was found to be necessary after workup with hydrochloric acid. We were gratified that the thio amino acids and the corresponding COSH-containing peptides did undergo clean ring-opening of the aziridine peptide conjugates, delivering a single addition/rearrangement product in every reaction we tried.

Remarkably, the reaction is compatible with water and tolerates unprotected secondary amine functionality. Indeed, we have seen no evidence for the 6-membered ring formation via competitive attack of the secondary amine moiety. We also did not observe any competition from the aza-Payne rearrangement. In addition, the peptidomimetic ligation was found to be free of epimerization. The ring opening was selective for the less hindered carbon (C2 position). This type of regioselectivity was not observed by Tam et al. due to the electron withdrawing carbonyl group on the hindered side which gave a 6:4 selectivity favouring the less hindered carbon [6]. Since there is no electron withdrawing group in our system, we only observe one
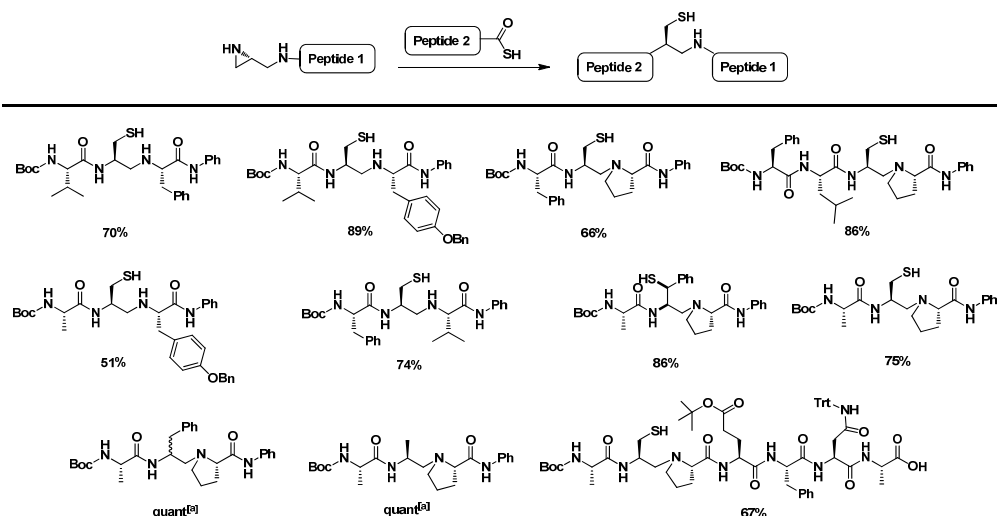
Fig. 1. Scope of peptidomimetic ligation.

isomer. We have found it possible to make ligated peptides of various sizes. Post ligation modification is made possible through Raney nickel to afford a new ligation site. Further diversification of ligation site is also made possible through the use of differently substituted aziridine aldehydes. As a result, ligation at alanine, phenylalanine, and substituted cysteine was demonstrated. (Figure 1) [7].

In summary, the first example of chemoselective peptidomimetic ligation has been made possible using thio aminoacids and NH aziridine-terminated peptides. Our methodology employs readily accessible thio amino acids and enables incorporation of a reduced amide bond at the site of ligation. This technique proceeds free of epimerization and has significant potential for further expansion and development.

Acknowledgments

References

1. Kimmerlin, T. Seebach, D. *J. Pept. Res*. **65**, 229-260 (2005).
2. Muir, T.W., Kent, S.B.H. *Curr. Opinion. Chem. Biol*. **10**, 487 (2006).
3. Hili, R., Yudin, A.K. *J. Am.Chem. Soc*. **128**, 14772-14773 (2006).
4. Li, X., Yudin, A.K. *J. Am. Chem. Soc*. **129**, 14152-14153 (2007).
5. Dawson, P.E., Muir, T.W., Clark-Lewis, I., Kent, S.B. *Science* **266**, 776-779 (1994).
6. Tam, J.P., Lu, Y.A., Liu, C.F., Shao, J. *Proc. Natl. Acad. Sci*. **92**, 12485-12489 (1995).
7. Assem, N. Natarajan, A., Yudin, A.K. *J. Am. Chem. Soc*. **132**, 10986-10987 (2010).

Synthesis of IGF-1 through Native Chemical Ligation

Maria L. Ufret[1], Deborah M. Rothman[2], Nicholas Prairie[1], Jundong Zhang[1], John Eynon[1], Jeanne Comstock[1], Natia Tsomaia[1], and Jesse Z. Dong[1]

[1]*IPSEN/Biomeasure Incorporated, Milford, CT, 01757, U.S.A.;* [2]*Novartis Institute for BioMedical Research, Cambridge, MA, 02139, U.S.A.*

Introduction

IGF-1 is a 70 amino acid polypeptide hormone having insulin-like and mitogenic growth biological activities. This hormone enhances growth of cells in a variety of tissues including musculoskeletal systems, liver, kidney, intestines, nervous system tissues, heart, and lung. Disruption of IGF-1 action may contribute to a number of physiological disorders such as ALS, muscular dystrophy, multiple sclerosis, osteoarthritis, osteoporosis, rheumatoid arthritis and ischemic injuries to organs such as the heart, brain, or liver. As a consequence, IGF-1 could have therapeutic potential for the treatment of the neurodegenerative disorders listed above and others such as stroke, epilepsy, Parkinson's disease, Alzheimer's disease, etc. IGF-1 has also been associated with the treatment of conditions such as insulin resistance, reduced renal function, wound healing, cardiac disorders, intestinal disorders and others. Increlex® is the first rhIGF-1 treatment approved in the United States for the treatment of growth disorders in children with severe primary IGF-1 deficiency.

IGF-1 binds to the insulin/IGF family of receptors (IGF-1R, IR-A and IR-B, the last two being insulin receptors) activating their tyrosine kinase domain activities. The activated receptors initiate signaling cascades resulting in the regulation of a number of biological responses.

Wild-type IGF-1 has three disulfide bridges comprising residues Cys6-Cys48, Cys47-Cys52, and Cys18-Cys61. Native IGF-1 and several analogs have been successfully synthesized through native chemical ligation [1] (see Figure 1a), and then folded into the native structure, dictated by the formation of the correct disulfide bridges. The compounds were tested *in vitro* in receptor binding and bioactivity assays (see Figure 1b).

Results and Discussion

Protein Ligation

Human IGF-1 was synthesized through native chemical ligation from two fragments. The N-terminal thioester fragment IGF-1(1-47)-SR was synthesized using Boc chemistry. The C-terminal fragment IGF-1(48-70) was synthesized using standard Fmoc chemistry. The two fragments were dissolved in ligation buffer (6 M guanidine-HCl in 200 mM sodium phosphate, pH 8.5), to which TCEP and MPAA were added. The reaction was monitored by LC/MS. Upon completion, the reaction was quenched, the product purified by RP-HPLC and lyophilized.

Protein Folding

Folding of the purified ligated protein was performed using three different conditions. The first method involved using a glutathione redox pair, the ligated lyophilized protein was dissolved in
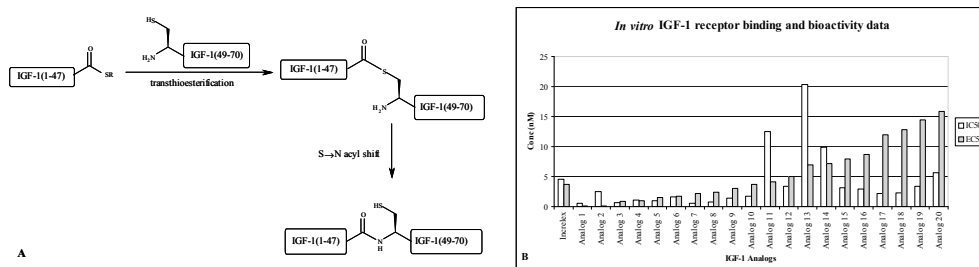
Fig. 1. a) Native chemical ligation of IGF-1. b) In vitro binding and bioactivity data.

ligation buffer to a concentration of 1 mg/mL. Three volumes of folding buffer (100 mM Tris, pH 8.5, 1 mM oxidized glutathione, 10 mM reduced glutathione) were added to bring the protein concentration to 0.25 mg/mL. Folding was monitored by RP-HPLC, and quenched by decreasing the pH. The folded protein was isolated by RP-HPLC and lyophilized.

Alternatively, the protein was folded using a cysteine/cystine pair. In this case, the ligated product was dissolved in 20 mM Tris, pH 7.8, 5 M guanidine-HCl to a concentration of 10 mg/mL. Folding buffer (20 mM Tris, pH 7.8, 1 mM cystine, 8 mM cysteine) was added to bring the final protein concentration to 1 mg/mL. Again, the folding was monitored by RP-HPLC and quenched by decreasing the pH. The folded product was isolated by RP-HPLC.

In a third method, the protein was folded using a copper/oxygen redox pair. The ligated protein was dissolved in 20 mM glycine, pH 10.5, 2 M Urea, 1 M NaCl, 20% ethanol, to a concentration of 1 mg/mL. Copper (II) bromide was added to a concentration of 0.5 μM and the folding monitored by RP-HPLC. The folded protein was isolated by RP-HPLC.

We were able to isolate the desired folded product using the three folding methods described; however, a higher yield was obtained when a thiol donor was not present in the folding mixture, as no disulfide adducts are formed. Thus method three using copper (II) bromide gave the highest yield. The obtained native IGF-1 and several analogs were tested and found to bind to the IGF-1 receptor in an *in vitro* receptor binding assay. The compounds were also active when tested in a thymidine incorporation assay.

In vitro receptor binding assay

Membranes were prepared for radioligand binding studies by homogenization of human MCF-7 cells expressing the native IGF-1 receptor in 20 mL of ice-cold 50 mM Tris-HCl with a Brinkman Polytron. The homogenates were washed twice by centrifugation and the final pellets were resuspended in 50 mM Tris-HCl containing 2.5 mM $MgCl_2$ and 0.1% BSA.

For the assay, aliquots were incubated with 0.05 nM [^{125}I]IGF-1. Unlabeled competing test peptides were sometimes included. The final assay volume was 0.25 mL. After a 120 minute incubation period, the bound [^{125}I]IGF-1 was separated from the free radioactive particles by centrifugation. The supernatant was decanted and the radioactive particles trapped in the pellet were counted by gamma spectroscopy. Specific binding was defined as the total [^{125}I]IGF-1 bound minus that bound in the presence of 100 nM IGF-1.

In vitro IGF-1 bioactivity assay

Mouse 3T3/R cells (obtained from Dr. E. Rozengurt at UCLA) were cultured on a 24-well plate and maintained for 2 days in culture. The media was removed and the cells were washed once with serum-free media. The serum was then starved for 24h. After starvation, [^{3}H]thymidine and IGF-1 peptides were added. The cells were then incubated for 24h at 37°C.

At the end of the incubation period, the media was aspirated and the cells were washed with an ice-cold 0.9% NaCl solution. An ice-cold 5% TCA solution was then added for a 30 minute incubation at 4°C. The TCA was aspirated and the wells were incubated with 95% ethanol for 4h. The media was then transferred to a liquid scintillation vial for radioactivity counting. *In vitro* IGF-1 bioactivity data (EC50 values) are presented in Figure 1b.

Conclusions

Human IGF-1 has been synthesized through native chemical ligation from two synthetic peptidic fragments; the ligated product was purified by RP-HPLC and properly folded into its active form. Multiple folding conditions were tested to reduce the number of misfolded isomers and increase product yield. Folding conditions were selected to reduce the number of disulfide adducts; the properly folded protein was isolated by RP-HPLC. hIGF-1 has been tested *in vitro* for receptor binding and activation.

References

1. Dawson, P.E., Muir, T.W., Clark-Lewis, I., Kent, S.B. *Science* **266**, 776-779 (1994).

N-Sulfanylethylanilide Derivative as a Peptide Thioester Equivalent

Kohei Sato, Shugo Tsuda, Kohei Tsuji, Ken Sakamoto, Akira Shigenaga, and Akira Otaka

Institute of Health Biosciences and Graduate School of Pharmaceutical Sciences, The University of Tokushima, Tokushima, 770-8505, Japan

Introduction

Native chemical ligation (NCL) is the most widely used chemoselective ligation technique in the chemical synthesis of proteins [1]. Here, facile preparation of peptide thioesters based on solid-phase peptide synthesis (SPPS) is indispensable for the success of the NCL. Nowadays, Fmoc SPPS has prevailed in preparation of peptides; however, the use of piperidine for Fmoc removal has hampered the application of the Fmoc protocol to the preparation of peptide thioester. To overcome this problem, we have developed *N*-sulfanylethylanilide (SEAlide) peptide as a thioester precursor [2]. Developed SEAlide peptides can be synthesized by standard Fmoc SPPS and converted to corresponding thioesters under acidic conditions (Figure 1). However, such acidic treatment sometimes caused side reactions including epimerization. Therefore, efforts to achieve the conversion to the thioester without accompanying side reactions have been continued.
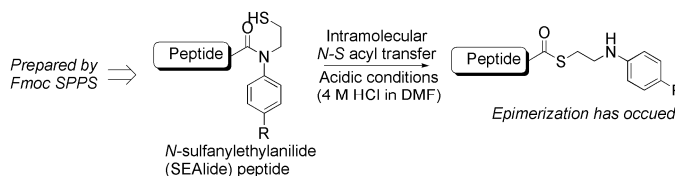
Fig. 1. N-S Acyl-transfer-mediated synthesis of peptide thioester using SEAlide peptide.

Results and Discussion

Several attempts finally disclosed that the SEAlide peptide itself could directly participate in NCL with N-terminal cysteinyl peptide without pre-conversion to the corresponding thioester to yield a ligated product [3] (Figure 2). Furtheremore, the participation in NCL was found to be enhanced in the presence of phosphate salt, that is, NCL of the SEAlide peptide with slow reaction rate in HEPPS buffer was proved to be greatly accelerated by the addition of phosphate salt into the reaction mixture. These result promoted us to envision that one-pot, multi-fragment NCL in a kinetically controlled fashion should be achieved by the use of the SEAlide peptides.
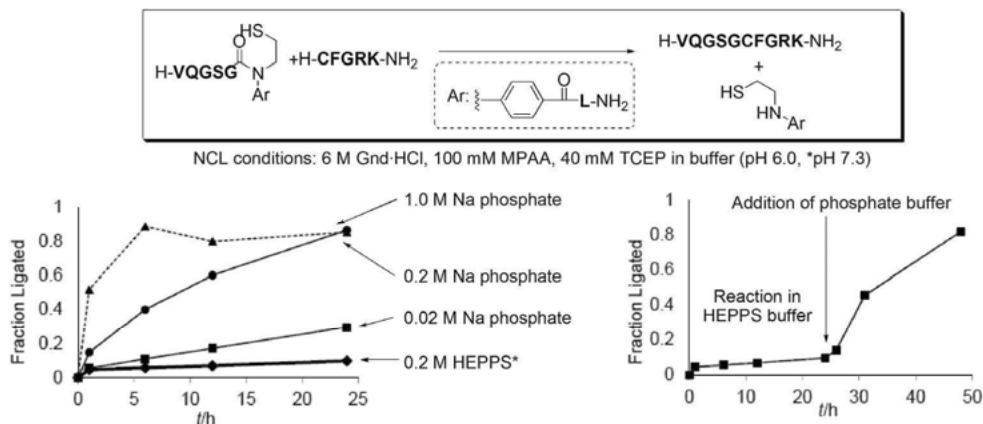
Fig. 2. Influence of ligation buffer in model ligation of SEAlide peptide with cysteinyl peptide. The fraction ligated was determined by integration of ligated product (integ. product) as a fraction of the sum of unreacted cysteinyl peptide + integ. product.

The kinetically controlled ligation, developed by Kent and co-workers, is known as a one-pot, three-fragment NCL, which relies on the different reactivity between arylthioester and alkylthioester peptides [4]. This protocol has afforded great success in sequential NCL-mediated protein syntheses. Despite this advance, difficulties still exist due to the fact that N-terminal cysteinyl Gly-alkyl thioester peptides have not shown enough kinetic selectivity. Therefore, we envisioned that the SEAlide peptide should be used as an alternative to the alkyl thioesters in the kinetically controlled ligation. An applicability of the SEAlide peptide to the kinetically controlled NCL was comfirmed through the preparation of human atrial natriuretic peptide (hANP) as shown in Figure 3. The first NCL between **5** and **6** (1 mM each) in HEPPS buffer almost completed within 3 h to give the corresponding intermolecular NCL product (**5** + **6**) without detectable amount of cyclic peptide resulting from the intramolecular NCL of fragment **6**. Subsequent addition of fragment **7** in Na phosphate (1.0 M) to the reaction mixture allowed the SEAlide moiety to work as the thioester yielding desired 2Cys-SH hANP (**8**) efficiently. In this synthesis, almost complete kinetic controll was achieved albiet using Gly-alkylthioester equivalent. We attempted the application of Kent's protocol to hANP synthesis; however, no sufficient kinetic resolution was achieved because of the relatively high reactivity of the Gly-alkyl thioester.

Next, an unprecedented one-pot, four-fragment NCL was attempted by using a combination of our method and Kent's kinetic protocol. Four-fragment NCL was demonstrated by the synthesis of 4Cys-SH α-conotoxin ImI (^{11}Ala) obtaining the ligation product in high purity (data not shown).

In conclusion, we revealed that the *N*-sulfanylethylanilide (SEAlide) peptide efficiently works as a thioester equivalent in the presence of phosphate salts. On the basis of this attractive feature, the efficient kinetically controlled NCL was accomplished. Combination of our methodology and Kent's kinetic NCL permitted an unprecedented one-pot, four-fragment NCL. Application of the SEAlide peptides to the synthesis of more complex proteins will be presented in due course.
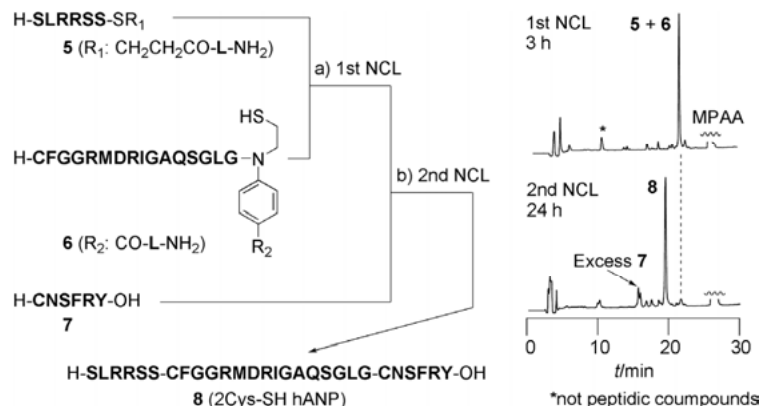
*Fig. 3. Sequential NCL-mediated assembly of 2Cys-SH hANP **8** utilizing the SEAlide peptide **6**. a) 6 M guanidine, 0.2 M HEPPS, 40 mM TCEP, 30 mM MPAA (pH 7.3), 37°C. b) addition of 1 M Na phosphate (pH 6.4). (Final concentration: 3 M guanidine, 0.1 M HEPPS, 0.5 M Na phosphate, 20 mM TCEP, 15 mM MPAA), 37°C.*

Acknowledgments

References

1. Dawson, P.E., Muir, T.W., Clark-Lewis, I., Kent, S.B.H. *Science* **266**, 776-779 (1994).
2. Tsuda, S., Shigenaga, A., Bando, K., Otaka, A. *Org. Lett.* **11**, 823-826 (2009).
3. Sato, K., Shigenaga, A., Tsuji, K., Tsuda, S., Sumikawa, Y., Sakamoto, K., Otaka, A. *ChemBioChem* in press.
4. Bang, D., Pentelute, B.L., Kent, S.B.H. *Angew. Chem. Int. Ed.* **45**, 3985-3988 (2006).

Synthesis of CXCL14 and Its Derivatives Utilizing C to N or N to C Directive Sequential NCL Protocol

Kohei Tsuji[1], Yoshitake Sumikawa[1], Kosuke Tanegashima[2], Akira Shigenaga[1], Takahiko Hara[2], and Akira Otaka[1]

[1]*Institute of Health Biosciences and Graduate School of Pharmaceutical Sciences, The University of Tokushima, Tokushima, 770-8505, Japan;* [2]*Stem Cell Project Group, The Tokyo Metropolitan Institute of Medical Science, Setagaya-ku, 156-8506, Japan*

Introduction

CXCL14, also known as BRAK, BMAC, or Mip-2g, belongs to the CXC chemokine family and was originally found via cloning of its corresponding gene [1]. Human CXCL14 consists of 77 amino acid residues including four cysteine residues (Figure 1). CXCL14 shows chemotactic activity for immature dendric cells, activated macrophages, and activated natural killer cells. Although some biological functions of CXCL14 have emerged, its physiological significance remains to be obscure. Additionally, the receptor responsible for mediating CXCL14 activities

Fig. 1. Primary amino acid sequence of human CXCL14.

has yet to be identified. Therefore, we decided to synthesize CXCL14 derivatives including native one to reveal the biological significance of CXCL14.

Native chemical ligation (NCL) is the most widespread method for chemical synthesis of proteins [2]. NCL allows the chemoselective ligation between an unprotected peptide thioester and an unprotected N-terminal cysteinyl peptide. Sequencial NCL using more than two fragments is widely used for synthesis of multi cysteinyl peptide such as CXCL14. In the sequential NCL utilizing three fragments, peptide elongation with the use of an N-terminal cysteine protected peptide thioester has been commonly employed (Figure 2, C to N direction). This method is suitable for diversification of N-terminal fragment. On the other hand, we previously reported sequential NCL in N to C direction utilizing N-terminal unprotected cysteinyl peptide thioacid [3], and it seems to be suitable for introduction of diversity in C-terminal fragment (Figure 2, N to C direction). To achieve the diversity oriented synthesis of CXCL14, we examined synthesis of CXCL14 and its derivatives by two distinct directive sequential NCL.

Results and Discussion

Native CXCL14 was successfully synthesized utilizing the C to N directive sequential NCL protocol. On the other hand, an attempt at the preparation of the native form by N to C protocol met with failure due to the rapid hydrolysis of intermediary thioester fragment (CXCL14 1-49 [49]His thioester). This result prompted us to examine the replacement of [49]His with Gly for suppressing the thioester hydrolysis. And attempted
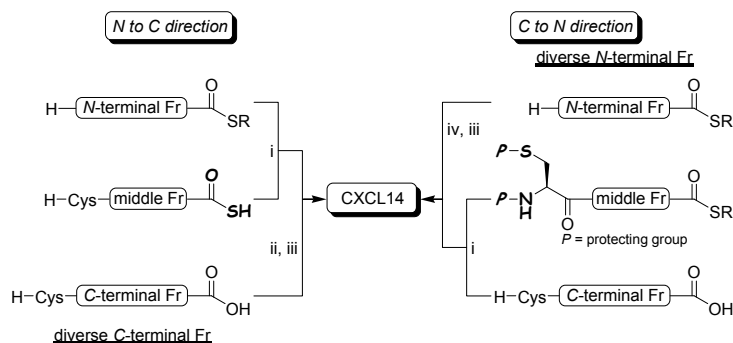
Fig. 2. Two distinct Native Chemical ligation (NCL) protocols for synthesis of CXCL14 proteins: (i) 1st NCL; (ii) thioesterification; (iii) 2nd NCL, followed by oxidation; (iv) deprotection (Fr = fragment).

replacement resulted in successful synthesis of CXCL14 (^{49}Gly) in the N to C fashion (Figure 3, analog **1**). A fluoroscein-5-thiocarbonyl (FTC)-incorporated CXCL14 (^{49}Gly) (analog **2**) was also synthesized in N to C-directive sequential NCL to visualize the CXCL14 receptor. These synthetic materials had chemotactic activity almost equal to native one (Figure 3).

In conclusion, CXCL14 and its derivatives were successfuly synthesized in either N to C- or C to N-directive sequential NCL protocol [4]. In particular, the use of the N to C-directive manner allowed introduction of diversity on the C-terminal fragment. The significant chemotactic activity of the CXCL14 (^{49}Gly) (analog **2**) suggests the potential for C-terminal modification of CXCL14. Because the FTC-incorporated analog showed activity comparable to CXCL14, it will behave as a molecular probe to disclose location of CXCL14 receptors and its physiological role. Uncovering the biological significance of CXCL14 using CXCL14 analogs is being undertaken in our laboratory.
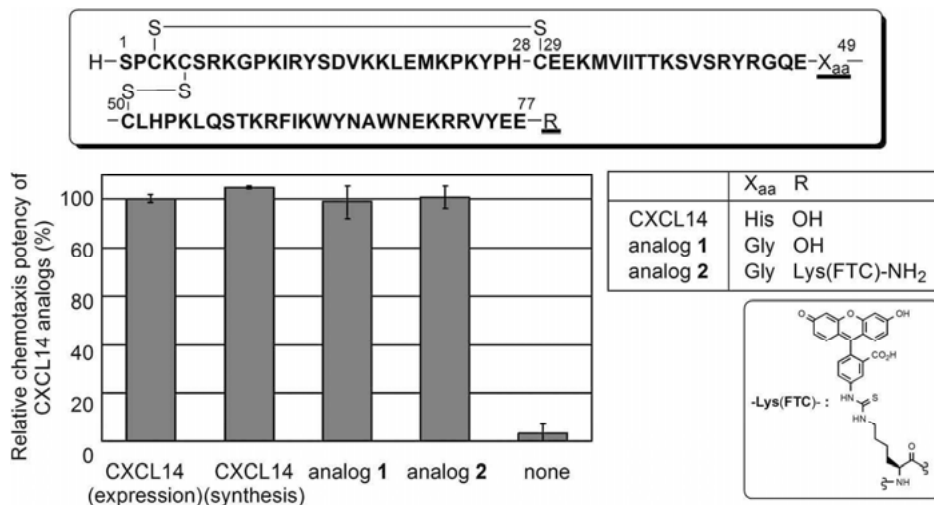
Fig. 3. Chemoattractant activity of CXCL14 proteins.

Acknowledgments

References

1. Hromas, R., Broxmeyer, H.E., Kim, C., Nakshatri, H., Christopherson, K., II., Azam, M., Hou, Y.-H. *Biochem. Biophys. Res. Commun.* **255**, 703-706 (1999).
2. Dawson, P.E., Muir, T.M., Clark-Lewis, I., Kent, S.B.H. *Science* **266**, 776-779 (1994).
3. Shigenaga, A., Sumikawa, Y., Tsuda, S., Sato, K., Otaka, A. *Tetrahedron* **66**, 3290-3296 (2010).
4. Tsuji, K., Shigenaga, A., Sumikawa, Y., Tanegashima, K., Sato, K., Hara, T., Otaka, A. *Bioorg. Med. Chem.* **19**, 4014-4020 (2011).

Selective Labeling of Lysine-Containing Biologically Active Peptides at the N-Terminus with Alexa Fluor Dye

Dziuleta Cepeniene[1], Randall Irvin[2], Robert S. Hodges[1], and Lajos Gera[1]

[1]*Department of Biochemistry and Molecular Genetics, University of Colorado, School of Medicine, Aurora, CO, 80045, U.S.A.;* [2]*Department of Medical Microbiology and Immunology, University of Alberta, Edmonton, Alberta, T6G 2H7, Canada*

Introduction

Pseudomonas aeruginosa readily binds to stainless steel to form highly recalcitrant, organized communities (known as biofilms). These in turn can cause major problems, namely, hospital-acquired infections in susceptible (e.g. immunocompromised or burn) patients with medical implants including catheters, prosthetics and stainless steel implants [1]. *P. aeruginosa* has polar type IV pili which are made up of thousands of homogenous pilin monomers assembled in a helical array. The pilus-associated epithelial cell receptor binding domain (RBD) is located in the well–structured C-terminal end within residues 128-144 of the C-terminal region of the pilin structural protein of the *P. aeruginosa* strain PAK as a 14-residue disulfide loop**.** Binding studies demonstrated that a synthetic peptide of PAK pilin epithelial cell receptor binding domain [PAK(128-144)ox] [(Ac-KCTSDQDEQFIPKGCSK-OH)ox] binds directly to steel with high affinity. The interaction of pili with steel was specifically inhibited by this peptide [1]. Therefore, it seemed reasonable to investigate the binding ability of *P. aeruginosa* K122-4 wild-type strain RBD peptide [(ACTSNADNKYLPKTCQT-NH$_2$)ox] to stainless steel using fluorescence microscopy. Amine-reactive fluorescent probes are widely used to label peptides at the N-terminal α-amino group or lysine side-chains. We chose Alexa Fluor 350 to label our K122-4 peptide, because the Alexa Fluor dye conjugates are more readily visualized and more photostable than most other fluorescent conjugates and remain highly fluorescent over a broad pH range [2].

Results and Discussion

Recently, an Alexa Fluor 680-glycylglycylglycine-bombesin[7-14]NH$_2$ peptide was developed for optical imaging of tumors with overexpressed GRP receptors [3]. The Alexa Fluor 680 N-hydroxysuccinimide (NHS) ester in dimethylformamide was added to a sodium bicarbonate solution (pH 8.5) of NH$_2$-G-G-G-BN[7-14]NH$_2$ at room temperature. In our first synthesis attempt we tried this dye labeling method in spite of the presence in our peptide of two lysine residues and consequently three possible labeling sites. Besides the Alexa Fluor 350 labeling process, we also had to form an intrachain disulfide bridge. The peptide was manually synthesized on a solid phase using standard Fmoc-chemistry and Rink amide MBHA-resin. The glycine-linked [K122-4] crude peptide was purified by reversed-phase high-performance liquid chromatography (RP-HPLC). The intrachain disulfide bond was formed by dissolving the synthetic peptide in 0.1 M ammonium bicarbonate, pH 8.0, at a peptide concentration of 0.5 mg/mL and overnight incubation at 25°C. The lyophilized intrachain disulfide-bridged peptide was dissolved in 0.1 M sodium bicarbonate buffer (pH 8.3) for conjugation with the fluorescence label. The Alexa Fluor 350 NHS ester (CAS Registry Number: 200554-19-4) in DMF was added to the peptide solution, and the reaction mixture was allowed to incubate at room temperature for 5 h in the dark. The acylation of the N-terminal amino group with Alexa Fluor 350 NHS ester in the presence of ε-amino groups of the two lysines was not successful and gave a mixture of the labeled peptides at the N-terminal of the peptide and the ε-amino positions of the two lysines. Attempts to label the amine terminus using buffer closer to neutral pH, as the pKa of the N-terminal amine is lower than of the lysine ε-amino group, also gave mixtures of the labeled peptides. We also tried to label our lysine-containing peptide with the Alexa Fluor 350 dye at lower pH using ammonium acetate buffer. The acylation reaction was very slow and also non-selective. To solve this problem, we developed a selective N-terminal Alexa Fluor labeling method for lysine-containing peptides using Fmoc protection of the ε-amino groups during Alexa Fluor 350 labeling (Figure 1). The peptide was manually synthesized on a solid phase using a Boc/Fmoc orthogonal protecting group strategy and 4-methyl-benzhydrylamine (MBHA) resin. The HF-cleaved crude peptide which had two

Lys(Fmoc) residues was purified by RP-HPLC. After the creation of the intrachain disulfide bond, the peptide was labeled with Alexa Fluor 350 NHS at the N-terminal amino group and the Fmoc-protecting groups were removed from the lysine ε-amino groups. The peptide was dissolved in a mixture of DMF and diethylamine and the reaction was left at room temperature for two hours. The crude peptide was lyophilized and analyzed using LC/MS. This N-terminal Alexa Fluor 350 labeled K122-4 peptide was purified by RP-HPLC and characterized by analytical RP-HPLC and LC-MS. The Boc-amino acid side-chain protecting groups were as follows: Asn(Xan), Asp(OcHx), Cys(4-Me-Bzl), Gln(Xan), Lys(Fmoc), Ser(Bzl), Thr(Bzl) and Tyr(2,6-Cl$_2$-Bzl).
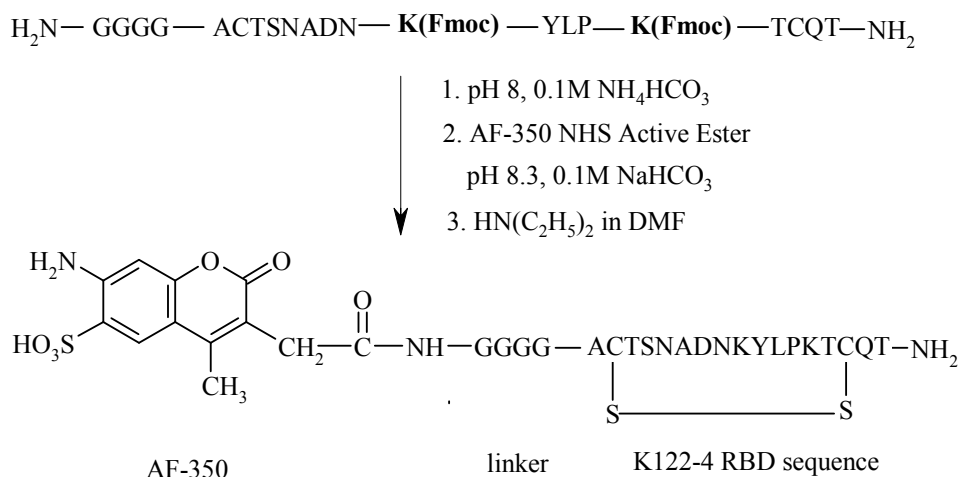
Fig. 1. Synthesis of [AF-350]-GGGG-[K122-4] RBD peptide.

The controlled acylation of the N-terminal amino group of the GGGG-[K122-4] peptide with Alexa Fluor 350 NHS ester in solution in the presence of the ε-amino groups of the two lysines at pH 8.3 or lower pH was not successful and yielded a mixture of the dye-labeled peptides. At a pH higher than the optimal 8.3 hydrolysis of the Alexa Fluor 350 NHS ester was rapid and the product yield diminished. At low pH the amino groups were protonated and no significant modification took place. The Boc/Fmoc orthogonal synthesis strategy provided the desired α-amino Alexa Fluor 350 labeled peptide and the overall yield was approximately 15%. A new synthetic approach for the [AF-350]-GGGG-[K122-4] peptide with an aim to improve the overall yield is in progress and includes the selective acylation of the N-terminal α-amino acids with the Alexa Fluor dye by solid-phase synthesis.

References

1. Giltner, C.L., van Schaik, E.J., Audette, G.F., Kao, D., Hodges, R.S., Hassett, D.J., Irvin, R.T. *Mol. Microbiol.* **59**, 1083-1096 (2006).
2. Panchuk-Voloshina, N., Haugland, R.P., Bishop-Stewart, J., Bhalgat, M.K, Millard, P.J., Mao, F., Leung, W-Y., Haugland, R.P. *J. Histochem. Cytochem*. **47**, 1179-1188 (1999).
3. Ma., L., Yu, P., Veerendra, B., Rold, T.L., Retzloff, L., Prasanphanich, A., Sieckman, G., Hoffman, T.J., Volkert, W.A., Smith., C.J. *Mol. Imaging* **6**, 171-180 (2007).

Submonomer Solid-Phase Synthesis of Aza-Glu Peptides

David Sabatino[1,2] and William D. Lubell[1]

[1]*Department of Chemistry, Université de Montréal, C.P. 6128 Downtown Station, Montréal, Québec, H3C 3J7, Canada;* [2]*Department of Chemistry and Biochemistry, Seton Hall University, South Orange, NJ, 07079, U.S.A*

Introduction

Constrained peptide mimics (peptidomimetics) containing glutamate residues have adopted widespread use in medicinal chemistry programs aimed to modulate the activity of target receptors by selective ionic interactions [1]. Azapeptides constitute an important class of constrained peptidomimetics that pre-organize some types of β-turn structures and improve pharmacokinetic properties of bio-active peptides for potential therapeutic applications [2]. An inherent limitation to study the biological activity of azapeptides is the tedious solution phase preparation of the aza-amino acid monomer prior to incorporation within peptide sequences by solid-phase peptide synthesis (SPPS). This is particularly the case in aza-Glu containing azapeptides which required iterative protection and deprotection steps for selectively differentiating the two hydrazine nitrogen atoms prior to the incorporation of the side chain [3]. In order to facilitate the synthesis of azapepetides, we have devised a submonomer method, which builds the aza-residue side chain directly onto the peptide during Fmoc-based solid-phase synthesis [4]. The method is highlighted by the synthesis of aza-Glu containing azapeptides related to the GHRP-6 (i.e. His-D-Trp-Ala-Trp-D-Phe-Lys-NH₂) and the D-Thr-D-Glu-D-Glu-D-Glu-D-Gln-D-Tyr-D-Leu sequences.

Results and Discussion

As proof-of-principle, the Ala[3] position of GHRP-6 was modified to [aza-Glu[3]]-GHRP-6 by submonomer azapeptide synthesis. Azapeptide synthesis was performed on Rink amide Merrifield resin using Trp(Boc)-D-Phe-Lys(Boc) **1** as starting sequence. Incorporation of the *N*-terminal semicarbazone was accomplished by coupling of a benzylidene carbazate **2** onto the dipeptide bound solid support. Michael addition of *tert*-butyl acrylate onto semicarbazone derived peptide resin **3** was next accomplished with *tert*-butylimino-tri(pyrrolidino)phosphorane (BTPP) in 80% conversion as detected by cleavage and deprotection of a small aliquot of resin followed by LCMS analysis. Removal of the semicarbazone from aza-Glu **4** was completed with hydroxylamine-hydrochloride in pyridine. The liberated semicarbazide was then employed in the completion of the azapeptide sequence by standard Fmoc-based SPPS. [aza-Glu[3]]-GHRP-6, **5** was isolated in acceptable yield and purity (10% and 99%, respectively) following cleavage, deprotection (TFA:H₂O:TES 95:2.5:2.5 v/v/v) and purification by reverse-phase HPLC. Azapeptide **5** was characterized by molecular weight following LCMS analysis.
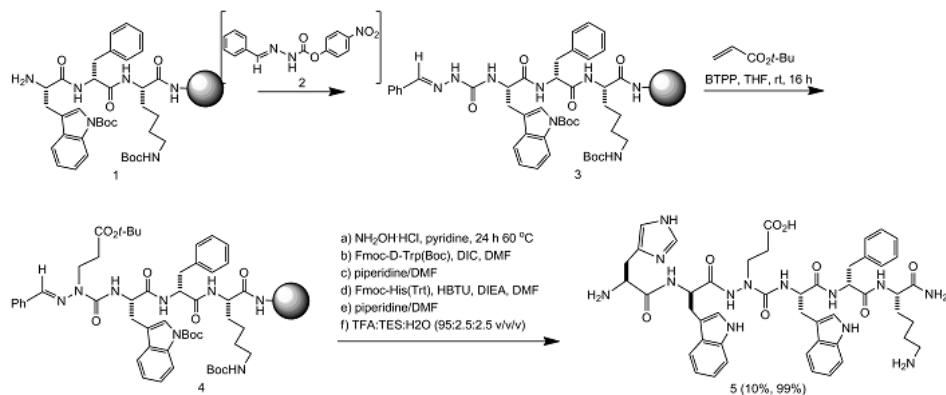
Scheme 1. Submonomer solid-phase azapeptide synthesis of [aza-Glu³]GHRP-6 (5).

With method in hand, we set out to site specifically incorporate aza-Glu residues in the poly-glutamate teeeqyl sequence for potential structure-activity relationship studies. In a split-and-mix approach using Wang resin, semicarbazone aza-Glu(*t*-Bu)-D-Gln(Trt)-D-Tyr(*t*-Bu)-D-Leu, **6** aza-Glu(*t*-Bu)-D-Glu(*t*-Bu)-D-Gln(Trt)-D-Tyr(*t*-Bu)-D-Leu, **8** and aza-Glu(*t*-Bu)-D-Glu(*t*-Bu)-D-Glu(*t*-Bu)-D-Gln(Trt)-D-Tyr(*t*-Bu)-D-Leu, **10**, all were prepared by acylation of the respective peptide with protected aza-Gly and alkylation with *tert*-butyl acrylate. The resulting protected aza-Glu sequences were converted into the desired azapeptides **7**, **9** and **11** as previously described and isolated by purification on HPLC in acceptable yields (5-7%) and 99% purity. Azapeptides **7, 9** and **11** were characterized by molecular weight on LCMS.
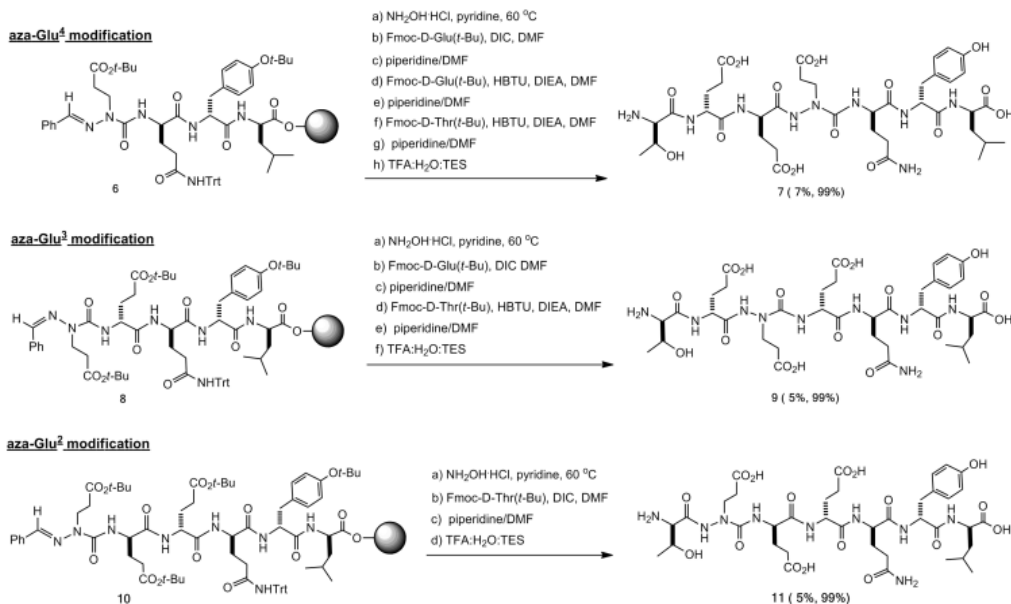
Scheme 2. Aza-Glu scan of teeeqyl.

In sum, submonomer synthesis was effective for preparing aza-Glu containing azapeptides. Opportunity now exists for exploring structure-activity relationships of bio-active azapeptides.

Acknowledgments

References

1. (a) Brauner-Osbourne, H., Egebjerg, J., Neilsen, E.O., Madsen, U., Krogsgaard-Larsen, P. *J. Med. Chem.* **43**, 2609-2645 (2000); (b) Stefanic, P., Dolenc, M.S. *Curr. Med. Chem.* **11**, 945-968 (2004).
2. Proulx, C., Sabatino, D., Hopewell, R., Spiegel, J., Garcia Ramos, Y., Lubell, W.D. *Future Med. Chem.* **3**, 1139-1164 (2011).
3. Hart, M., Beeson, C. *J. Med. Chem.* **44**, 3700-3709 (2001).
4. (a) Sabatino, D., Proulx, C., Bourguet, C. Klocek, S., Boeglin, D., Ong, H., Lubell, W.D. *Org. Lett.* **11**, 3650-3653 (2009); (b) Sabatino, D., Proulx, C., Pohankova, P., Ong, H., Lubell, W.D. *J. Am. Chem. Soc.* **133**, 12493-12506 (2011).

Synthesis of [Azaphenylglycine⁴]- and [Aza-1-phenyl-2,3-triazole-3-alanine⁴]Growth Hormone Releasing Peptide-6 and Comparison of their Conformations with [AzaPhe⁴]GHRP-6

Caroline Proulx and William D. Lubell

Département de Chimie, Université de Montréal, C.P. 6128, Succursale Centre-Ville, Montréal, Québec, H3C 3J, Canada

Introduction

The replacement of an amino acid amide in a peptide by a semicarbazide affords an azapeptide, which may confer increased stability, resistance to proteases, as well as enhanced selectivity relative to the native peptide [1]. In analyses of model azapeptides using X-ray crystallography, NMR spectroscopy, and computation, preferred β-turn conformations were observed due likely to constraints about the phi (φ) and psi (ψ) dihedral angles, respectively from lone pair-lone pair electronic repulsion between the adjacent hydrazine nitrogen atoms and the planar geometry of the urea [1]. The conformational effects of the aza-residue in [azaPhe⁴]Growth Hormone Releasing Peptide-6 (GHRP-6, His-D-Trp-Ala-Trp-D-Phe-Lys-NH₂) have been suggested to account for its relative selectivity for the CD36 over the GHS-R1a receptor [2]. Studying structure-activity relationships (SARs) of [azaPhe⁴]GHRP-6, new methodology for making azapeptides bearing aza-residues with aromatic side chains has been developed by a submonomer approach.

Results and Discussion

Submonomer azapeptide synthesis entails three key steps 1) acylation of the supported peptide with an activated methylidene carbazate, (2) regioselective semicarbazone *N*-modification, and (3) chemoselective semicarbazone deprotection (Figure 1) [2].
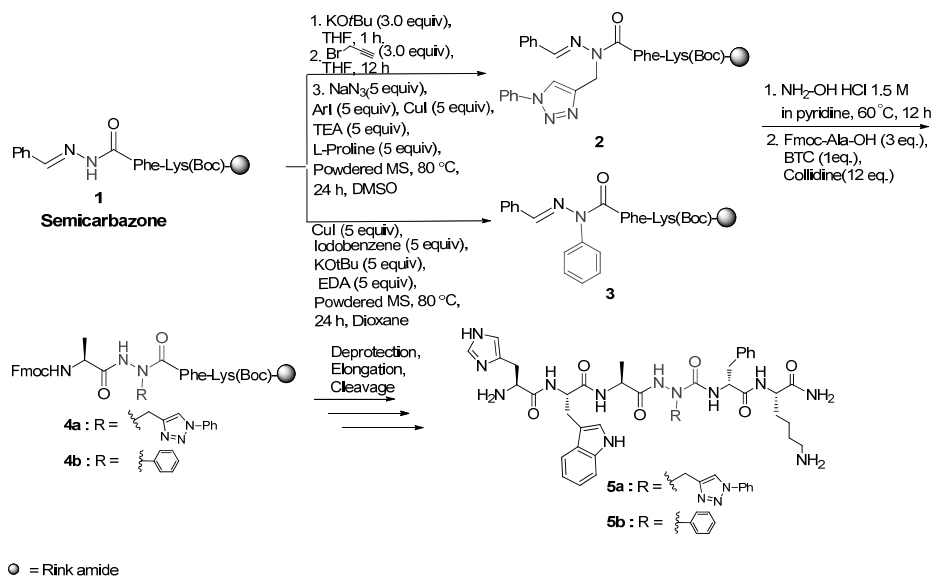
Fig. 1. Submonomer Azapeptide Synthesis.

Employing propargyl bromide as an alkylating agent, protected aza-propargyglycine residue **1** was obtained [2] and further functionalized via a tandem copper-catalyzed aryl azide formation/[1,3] dipolar cycloaddition reaction to give **2** [3]. Aza-1-phenyl-2,3-triazole-3-alanine azapeptide **5a** was obtained after semicarbazone deprotection and sequence elongation and cleavage (Figure 1) [3]. The resin-bound semicarbazone building block was also subjected to conditions allowing for regioselective *N*-arylation (Figure 1). Employing iodobenzene as the aryliodide component, we synthesized [Azaphenylglycine[4]]GHRP-6 **5b** [4]. In comparative studies using circular dichroism (CD) spectroscopy in water, [AzaPhe[4]]GHRP-6, [Aza-1-phenyl-2,3-triazole-3-alanine[4]]GHRP-6 **5a,** and [Azaphenylgly[4]]GHRP-6 **5b** all exhibited CD curves characteristic of β-turn conformations with negative maxima around 230 and 190 nm and a positive maximum at 215 nm (Figure 2), in contrast to native GHRP-6, which exhibited a random coil spectrum exhibiting a negative maximum at 190nm.
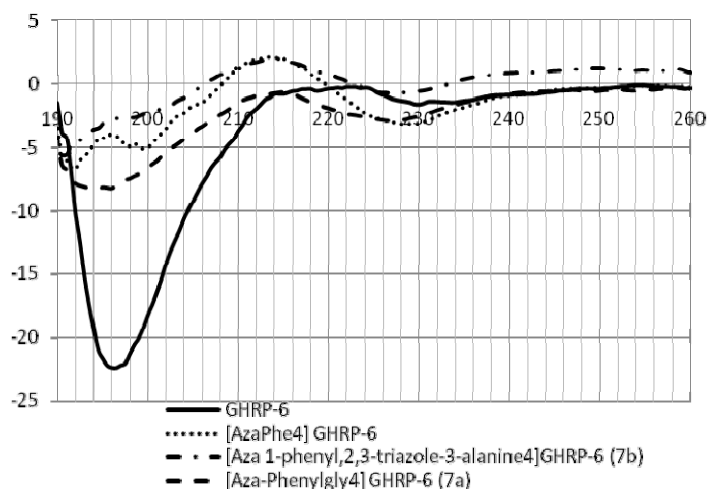
Fig. 2. Comparative circular dichroism spectra of aza-GHRP-6 analogs.

The nature of the side-chain on the aza amino acid residue does not alter significantly the propensity of azaGHRP-6 analogs to adopt turn conformations, albeit subtle differences in the nature of the turn are observed. The values of the affinity of azapeptides for both the GHS-R1a and CD36 receptors will be presented in the near future.

Acknowledgments

References

1. Proulx, C., Sabatino, D., Hopewell, R., Spiegel, J., García Ramos, Y., Lubell, W.D. *Future Medicinal Chemistry* **3**, 1139-1164 (2011).
2. Sabatino, D., Proulx, C., Klocek, S., Bourguet, C.B., Boeglin, D., Ong, H., Lubell, W.D *Organic Letters* **11**, 3650 (2009).
3. Proulx, C., Lubell, W.D. *The Journal of Organic Chemistry* **75**, 5385-5387(2010).
4. Proulx, C., Lubell, W.D. *Organic Letters* **12**, 2916-2919(2010).

On the Nature of Azabicyclo[X.Y.0]alkanone and Aza-Dipeptide Mimicry of Turn Conformations

Carine B. Bourguet and William D. Lubell

Department of Chemistry, Université de Montréal, C.P. 6128 Downtown Station,
Montréal, Québec, H3C 3J7, Canada

Introduction

Peptide mimicry is a broad term, because many strategies exist for creating molecules resembling the fold and function of peptides [1]. For example, "foldamers" are non-natural oligomers displaying discrete folding propensities [1a]. Small molecule scaffolds, such as sugars, may orient the display of side-chains and replicate the biological activity of natural peptides [1b]. The growing impact of peptides in medicine combined with their inherently poor pharmacokinetic properties, such as rapid proteolysis and limited oral bioavailability, fuel design of peptide mimics (peptidomimetics) as means for converting peptidic agents into more drugable molecules. Constrained dipeptide analogs, such as azabicyclo[X.Y.0]alkanone amino acids [1c] and azapeptides [1d], are particularly useful tools for the identification of biologically active turn conformations [2]. The conformational preferences of azabicyclo[X.Y.0]alkanones and azapeptides illustrated in X-ray crystallographic and computational analyses [3,4] have been compared revealing their complementary means for recreating turn geometries.

Results and Discussion

The β-turn reverses a peptide direction by 180° and places the i and $i + 4$ amino acid α-carbons at a distance of less than 7 Å, without inducing a helical geometry [2]. Polar side chains, which are often involved in recognition events, are commonly displayed at turn regions, rather than buried in hydrophobic regions of the peptide. Among the most common β-turn geometries are type I and II; furthermore, their mirror image counterparts type I' and II' have high propensity to nucleate β-hairpin conformations [2].

Azabicyclo[X.Y.0]alkanone amino acids (Figure 1) are dipeptide mimics composed of a bicyclic structure possessing an azacycloalkane α-carboxylate (i.e., proline, pipecolate) fused to an α-amino lactam [1c,3]. The conformation of the azabicyclo[X.Y.0]alkanone amino acid in a peptide is dictated by the configuration of the ring fusion and the stereochemistry of ring substituents, ring size, as well as the number and identity of the ring substituents. The orientation of the amine and the carboxylate substituents on the same side of the bicycle leads to turn conformations. In particular, X-ray structural analyses of azacycloalkanone N-(Boc)amino esters bearing 5,5-, 6,5-, 5,6- and 6,6-fused ring systems have shown that the dihedral angle geometry of the peptide bonds locked within the bicycle are similar to those of the central residues of an ideal type II' β-turn (Table 1) [3].

Azapeptides possess at least one semicarbazide residue in which the α-carbon of an amino acid residue is replaced by nitrogen (Figure) [1d,4]. The combination of diacylhydrazine and urea functionalities in the semicarbazide residue cause significant restrictions of the peptide backbone favoring non-linear conformations. Computational analyses as well as X-ray crystallographic studies of model aza-peptides have demonstrated their preferences for adopting β-turn conformations (Table 2) [4].

In comparing the conformational preferences of azabicycloalkanone and aza-dipeptide mimics, the potential for (3S,6S,9S)-indolizidin-2-one amino acid and aza-Gly-Pro structures to adopt similar conformations has been validated in two unrelated biological systems. For example, studying the antagonist [D[31],P[34],F[35]]CGRP[27-37] of calcitonin gene-related peptide (CGRP), respective replacements of the Gly[33]-Pro[34] residue with an indolizidin-2-one amino acid and with aza-Gly[33]-Pro[34] led to similar efficacy and 7- and 10-fold greater antagonism potencies compared to the parent peptide [5]. Moreover, studying PDC113.824, a negative allosteric modulator of the prostaglandin F2α (PGF2α) receptor (FP) [6], substitution of the indolizidin-2-one amino acid residue with aza-Gly-Pro led to similar reduction of PGF2α–induced myometrial contractions, potentiation of the effect of PGF2α on G_q-mediated ERK1/2 activation and inhibition FP modulation of cell ruffling, a response dependent on the

G_{12}/RhoA/ROCK signaling pathway [6]. Such complementarities of azabicycloalkane and azapeptide mimics suggest their parallel use in exploring peptide conformation.
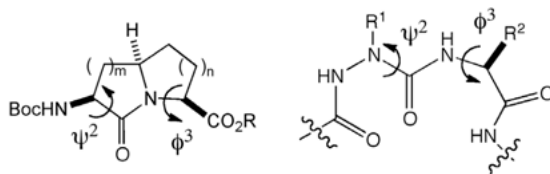
Fig. 1. Azabicyclo[X.Y.0]alkanone N-(Boc)amino Ester and Aza-dipeptide mimics.

Table 1. X-ray data of Azabicyclo[X.Y.0]alkanone N-(Boc)amino ester

Ring system	m	n	R	ψ^2, deg	ϕ^3, deg	ref.
(3S,5R,8S)-pyrrolizidinone	1	1	Me	−149	−45	3a
(3S,6S,9S)-indolizidin-2-one	2	1	Me	−176	−78	3b
(2S,6R,8S)-indolizidin-9-one	1	2	Me	−141	−34	3c
(3S,6R,10S)-quinolizidin-2-one	2	2	t-Bu	−163	48	3d
Ideal Type II' β-turn $i+1$ and $i+2$ residues				−120	−80	2

Table 2. Computational and x-ray data of Aza-dipeptide models

Aza-dipeptide Model	method	ϕ^2, deg	ψ^2, deg	ϕ^3, deg	ψ^3, deg	ref.
Ac-azaGly-L-Ala-NHMe	Comp. Minimum	−74	−23	−102	12	4a
	Min. + 0.9 kJ/mol	59	−153	−90	12	4a
Ac-azaAla-L-Ala-NHMe	Comp. Minimum	−76	−18	−102	12	4a
	Min. + 2.7 kJ/mol	60	−154	−86	9	4a
Boc-azaAla-L-Pro-NHi-Pr	X-ray	−58	−25	−67	−18	4b
Ideal Type I β-turn $i+1$ and $i+2$ residues		−60	−30	−90	0	2
Ideal Type II' β-turn $i+1$ and $i+2$ residues		60	−120	−80	0	2

In sum, indolizidin-2-one amino acid and aza-Gly-Pro dipeptide surrogates exhibit similar conformational preferences for peptide mimicry. Their complementary application to explore peptide structure-activity relationships offers effective means for validating the importance of turn geometry for peptide biological activity.

Acknowledgments

References

1. (a) Gellman, S.H. *Acc. Chem. Res.* **31**, 173-180 (1998); (b) Hirschmann, R.F., et al. *Acc. Chem. Res.* **42**, 1511-1520 (2009); (c) Cluzeau, J., Lubell, W.D. *Biopolymers, Peptide Science* **80**, 98-150 (2005). (d) Proulx, C., et al. *Future Med. Chem.* **3**, 1139-1164 (2011).
2. Wilmot, C.M., Thornton, J.M. *J. Mol. Biol.* **203**, 221-232 (1988).
3. (a) Dietrich, E., Lubell, W.D. *J. Org. Chem.* **68**, 6988-6996 (2003); (b) Lombart, H.-G., Lubell, W.D. *J. Org. Chem.* **61**, 9437-9446 (1996); (c) Gosselin, F., Lubell, W.D. *J. Org. Chem.* **63**, 7463-7471 (1998); (d) Gosselin, F., Lubell, W.D. *J. Org. Chem.* **65**, 2163-2171 (2000).
4. (a) Thormann, M., Hofmann, H.J. *J. Mol. Struct. (Theochem)* **469**, 63-76 (1999); (b) André, F., Boussard, G., Bayeul, D., Didierjean, C., Aubry, A., Marraud, M. *J. Pept. Res.* **49**, 556-562 (1997).
5. Boeglin, D., et al. *J. Med. Chem.* **50**, 1401-1408 (2007).
6. Bourget, C., et al. *J. Med. Chem.* **54**, asap (2011).

Biocatalysis and Superparamagnetic Nanoparticles in Peptide Chemistry

Raphaella M. Fernandes[1], Cleber W. Liria[1], Natália J. Costa[2], Liane M. Rossi[2], and M. Terêsa Machini[1*]

[1]*Departments of Biochemistry;* [2]*Fundamental Chemistry, Institute of Chemistry, University of São Paulo, São Paulo, SP, 05508-000, Brazil*

Introduction

The remarkable ability of enzymes to efficiently catalyze *in vivo* chemical reactions has been extensively studied. As a result, in the last decades, synthetic chemists started using these biocatalysts to make *in vitro* organic reactions more selective, productive and environmentally friendly [1,2].

Optimization of enzyme-catalyzed reactions can be achieved by employing insoluble materials to support the catalysts [3]. Indeed, this type of immobilization may enhance enzyme activity and stability and/or change substrate specificity or pH-activity profile. Moreover, immobilized enzymes can be easily recovered from reaction media and reused. Owing to their high ratio of surface area/volume and easy separation of the reaction medium, magnetic nanoparticles are among the various materials successfully used for such purpose [3].

Here we show that free thermolysin, a protease, and free α-chymotrypsin (αCT), a protease with esterase activity, catalyze two of the three steps required for the synthesis of Ala-Phe, a dipeptide with bitter taste that can be used in food industry as flavoring. We also describe immobilization of αCT on a particular type of superparamagnetic nanoparticles (SPNP) and the properties of the covalently bound enzyme (αCT-SPNP).

Results and Discussion

The synthetic route explored is summarized below:

Step 1: ***Z-Ala-OH + Phe-OMe . HCl → Z-Ala-Phe-OMe + H_2O***

Step 2: ***Z-Ala-Phe-OMe + H_2O → Z-Ala-Phe-OH + MeOH***

Step 3: ***Z-Ala-Phe-OH + H_2/Pd^0 → Ala-Phe + CO_2 + toluene***

Optimization of the coupling between Z-Ala and Phe-OMe catalyzed by free thermolysin in acetate buffer, pH 6, at 50°C provided Z-Ala-Phe-OMe with good yield (68% in 6h). Its precipitation in the reaction medium followed by filtration and washing with water led to chemical homogeneity. Ester hydrolysis catalyzed by free αCT in 30% ACN/Tris.HCl buffer, pH 8, at 37°C furnished Z-Ala-Phe-OH with high purity and yield (77%, 10 min), which was isolated from the reaction medium by extraction. Z-group removal by catalytic hydrogenation at 1 atm in methanol containing 10% palladium on carbon gave Ala-Phe, the desired bitter dipeptide, with high purity and yield (77%, 2h). Elimination of the carbon and alcohol led to a homogeneous material.

In the search for more advantageous synthesis conditions, enzyme immobilization on amino SPNP was then studied. αCT was chosen as model because this is significantly cheaper than thermolysin. Synthesis of amino SPNP, its functionalization by glutaraldehyde and αCT immobilization on it were based on previously described protocols [4]. Since determination of protease amount on a solid material can be problematic (free proteases catalyze autolysis during the immobilization process), the αCT-SPNP obtained was submitted to total acid hydrolysis followed by amino acid analysis of the hydrolyzate using ion exchange HPLC and pulsed amperometry detection. The immobilization yield found was 23% (46.4 mg of αCT/g of αCT-SPNP).

Amidase activity of αCT prior and after immobilization (using the chromogenic substrate Bz-*DL*-Tyr-pNA) was confirmed. Specific activities of free αCT and αCT-SPNP were 79 and 70 U/mg, respectively. When stored in suspension at room temperature or at 4°C, αCT-SPNP (*susp. αCT-SPNP*) was 60% more active than when stored in its dry form at 4°C (Figure 1). Its amidase activity was maintained even after 10 cycles of use.

---

* Previously M. Terêsa M. Miranda or M.T.M. Miranda
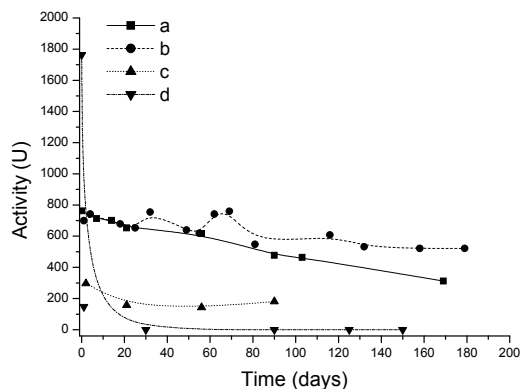
Fig. 1. Chemical stabilities of αCT- SPNP stored in suspension at room temperature (a), in suspension at 4°C (b) and in the dry form at 4°C (c). As control, free αCT was stored in solution at room temperature (d).

Likewise free *αCT, susp. αCT-SPNP* also presented esterase activity as it catalyzed Z-Ala-Phe-OMe ester hydrolysis (Figure 2). More importantly, the immobilized enzyme showed to be selectively recovered and reusable for such purpose without significant loss of activity (only 10% after 4 cycles of reuse).
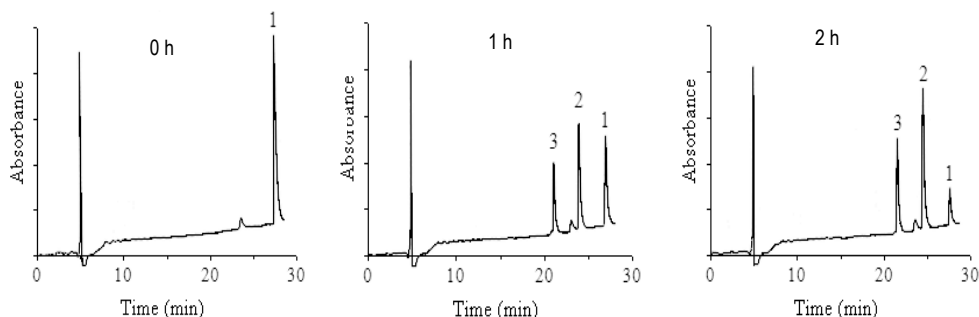
Fig. 2. RP-HPLC monitoring of Z-Ala-Phe-OMe incubation with susp. αCT–SPNP (after 4 cycles of reuse). 1: esterified dipeptide; 2: desired product:[M+H$^+$] (found/calculated)= 371.3/370.4; 3: byproduct most likely resulting from enzyme degradation.

In summary, *(i)* synthesis of Ala-Phe with high yields and no side reactions was achieved using a very selective and clean technology, *(ii)* an alternative magnetic support for immobilizing αCT was found, *(iii)* an alternative and efficient method for determining the efficiency of enzyme immobilization on SPNP was established; *(iv)* storage conditions for active and relatively more stable αCT-SPNP were determined, *(v)* applicability and reusability of αCT-SPNP in dipeptide ester hydrolysis was demonstrated.

Acknowledgments

References

1. Machado, A., et al. *Quim. Nova* **5**, 781-789 (2004).
2. Liria, C.W., et al. *J. Braz. Chem. Soc.* **19**(8), 1574-1581 (2008).
3. Hong, J., et al. *Microporous Mesoporous Mater.* **109**, 470-477 (2008); Lee, J., et al. *J. Mater. Chem.* **19**, 7864-7870 (2009).
4. Rossi, L.M., et al. *Green Chem.* **9**, 379-385 (2007).

Sunflower Trypsin Inhibitor-1: Chemical v. Biological Synthesis

Alysha G. Elliott, David J. Craik, and Joshua S. Mylne

Institute for Molecular Bioscience, The University of Queensland, St Lucia, 4072, Australia

Introduction

Diverse gene-encoded cyclic peptides are produced by species from all three domains of life. The 14-residue, head-to-tail cyclized plant peptide, SFTI-1 (Sunflower Trypsin Inhibitor 1) [1] (Figure 1) has attracted much attention due to its great stability and capability to potently inhibit trypsin (Ki 0.1 nM) as well as the epithelial serine protease matriptase (Ki 0.92 nM) [2], giving it exciting promise as a drug lead and a protein engineering scaffold [2]. Although peptides such as SFTI-1 are routinely produced by chemical synthesis, the biological mechanisms that enable biosynthesis of ribosomally synthesized cyclic peptides are largely unknown.

Recently Mylne *et al.* described the biosynthetic origin of SFTI-1 and a related peptide SFT-L1 [3]. Both emerge from seed storage protein precursors PawS1 and PawS2, respectively, using each seed protein's own maturing protease for their release [3]. We used transgenic constructs in the model plant *Arabidopsis thaliana* combined with proteomics and MALDI mass spectrometry to study this unusual dual-fate for PawS1 and identified the residues that are critical for SFTI-1 maturation and cyclisation [3]. Here we compare best practice for chemical synthesis of SFTI-1 with how plants biologically create the same product.

Fig. 1. Sequence of SFTI-1 (left) and a model of its backbone structure (PDB 1SFI). When chemically synthesized, SFTI-1 ends with an N-terminal Cys, but its biological ligation point is between Gly1 and Asp14.

Results and Discussion

There is a long history of the synthesis of cyclic peptides by manual solid-phase peptide synthesis [4]. Here we describe the optimized synthesis of the 14 residue cyclic peptide, SFTI-1 using BOC (t-butoxycarbonyl) chemistry with *in situ* neutralization, HBTU [2-(1-H-benzotriazol-1-yl)-1,1,3,3-tetramethyluronium hexafluorophosphate] [5] and a C-terminal thioester linker.

Peptides were assembled on a PAM-Gly-Boc (phenylacetamidomethyl-glycine-t-Boc) resin on a 0.5-mmol scale and designed to contain the C-terminal thioester linker, S-trityl-β-mercaptopropionic acid, and an N-terminal cysteine. Peptides were subsequently cleaved from the resin by HF cleavage with p-cresol as the scavenger (9:1 HF:p-cresol by volume). The cleavage reaction was incubated at <5 to 0°C for 90 min; HF was removed under vacuum and the peptide precipitated with diethyl ether, then filtered and re-dissolved in 50% acetonitrile 0.045% TFA and lyophilised. The crude peptide was subsequently purified by RP-HPLC using a gradient of 0–80% acetonitrile 0.045% TFA over 80 min. Analytical HPLC and ESI-MS confirmed peptide purity and mass.

Importantly, the folding for SFTI-1 is a two-step process. The two steps ensure that the more favorable reaction, disulfide bond formation occurs secondarily to cyclization, the less favorable reaction, as the free sulfur donated from the cysteine is required to form a thiol for cyclization.

Firstly, the peptides were reduced and cyclized in 0.1 M ammonium bicarbonate pH 8.2 with 0.5 mg/mL TCEP overnight at room temperature, followed by RP-HPLC purification. Secondly, the peptides were oxidized in 0.1 M ammonium bicarbonate pH 8.2 overnight at room temperature, followed by RP-HPLC purification as above to yield fully folded and pure peptides. From ~200 mg of crude cleaved peptide ~40 mg of over 98% pure fully folded SFTI-1 may be obtained using this method.

Sunflowers produce SFTI-1 with ease. We cloned the precursor gene for SFTI-1, *PawS1,* and were surprised to find that the sequence for SFTI-1 was encoded along with a much larger

protein of entirely different function. PawS1 is a preproalbumin, which encodes a seed storage albumin protein as well as SFTI-1 [3]. Seed storage albumins are matured from proalbumins by the action of a Cys-protease called asparaginyl endopeptidase (AEP, aka legumain, vacuolar processing enzyme). AEP usually cleaves at Asn and, to a lesser extent, at Asp. Within PawS1, SFTI-1 ends with Asp and is preceded by Asn suggesting AEP matures both the albumin and SFTI-1. We used an *Arabidopsis* mutant lacking AEP to confirm that AEP was required to release SFTI-1 at both proto-termini and is the best candidate for the ligation reaction.

Furthermore, an in-depth mutagenesis of *PawS1* and subsequent testing of these constructs *in vivo* revealed residues essential for SFTI-1 processing. These experiments combined with the wealth of information about albumin maturation [6] allowed us to propose a model for the processing of SFTI-1 from within PawS1 (Figure 2) [3].

PawS preproalbumin is sent to the ER where its signal peptide is cleaved and with the aid of hairpin formation from hydrophobic clustering within SFTI-1 the Cys38-Cys46 disulfide bond is formed. The proalbumin is then matured at several points by AEP in multivesicular bodies as they traffic to protein storage vacuoles. During this processing SFTI-1 is released at the N-terminus (PawS1 Gly36) and during the final cleavage at its C-terminal P1 aspartic acid, a reactive, thioester acyl-intermediate is created. Instead of the typical attack by water and bond hydrolysis, we propose this reactive intermediate is instead attacked at its carbonyl carbon by the unmasked amino terminus of the glycine, held in proximity to the thioester by the disulfide bond. This attack results in peptide bond formation and reconstitutes the AEP active site thiol [3].
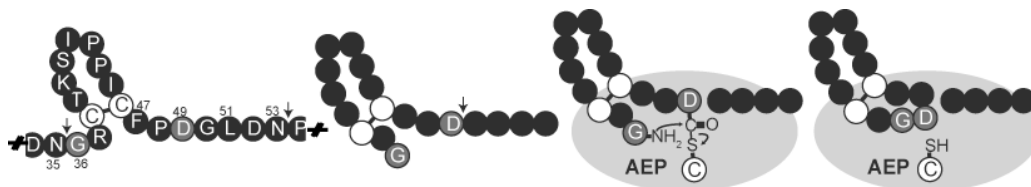
Fig. 2. Proposed model for SFTI-1 biosynthesis (adapted from Mylne et al. 2011) [3]. AEP cleavage occurs firstly at N35 and N53, later at D49 followed by ligation of G36 and D49 (grey) to form the cyclic peptide, SFTI-1.

Solid phase peptide synthesis is the best way to study peptides for applications in drug design. However, to produce them on a large-scale by chemical synthesis becomes costly. We propose to use plants as a cost effective manufacturing process for producing cyclic peptide therapeutics based on molecules produced naturally by plants. To do this, requires an in-depth knowledge of their *in planta* processing so that we may manipulate this processing to vary the peptides produced. To enhance this understanding we will continue to approach this problem by combining synthetic chemistry with plant genetic engineering.

Acknowledgments

References

1. Luckett, S., et al. *J. Mol. Biol.* **290**, 525-533 (1999).
2. Long, Y., et al. *Bioorg. Med. Chem. Lett.* **11**, 2515-2519 (1999); Daly, N., et al. *J. Biol. Chem.* **281**, 23668-23675 (2006); Swedberg, J., et al. *Chem. Biol.* **16**, 633-643 (2009).
3. Mylne, J., et al. *Nat. Chem. Biol.* **7**, 257-259 (2011).
4. White, C., Yudin, A. *Nat. Chem.* **3**, 509-524 (2011).
5. Schnolzer, M., et al. *Int. J. Pept. Protein Res.* **40**, 180-193 (1992).
6. Hara-Hishimura, I., et al. *Plant J.* **4**, 793-800 (1993); Hiraiwa, N., et al. *FEBS Lett.* **447**, 213-216 (1999); Gruis, D., et al. *Plant Cell* **16**, 270-290 (2004); Otegui, M.; et al. *Plant Cell* **18**, 2567-2581 (2006).

Site-Specific Protein Labeling Via Oxime and Hydrazone Ligations Using Protein Farnesyltransferases

Mohammad Rashidian and Mark D. Distefano

Department of Chemistry, University of Minnesota, Minneapolis, MN, 55455, U.S.A.

Introduction

Chemical modification of proteins is important for many applications in biology and biotechnology [1]. Selective functionalization of proteins is challenging because of the large number of reactive functional groups typically present in polypeptides [2,3]. Our laboratory and others have recently exploited the high specificity of the enzyme protein farnesyltransferase (PFTase) to site-specifically modify peptides and proteins. In nature, PFTase catalyzes the transfer of a farnesyl isoprenoid group from farnesyl pyrophosphate (**FPP**, Figure 1a) to a sulfur atom present in a cysteine residue. That residue must be located in a tetrapeptide sequence (denoted as a CAAX-box) positioned at the C-terminus of a protein or peptide to be a PFTase substrate. Here we describe the development and use of an aldehyde-containing substrate for PFTase that can be used to introduce aldehyde functionality into almost any protein.

Results and Discussion
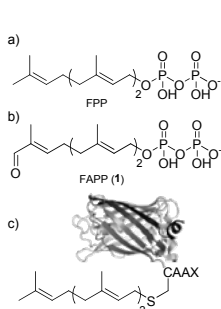
Fig. 1. a) Farnesyl pyrophosphate, farnesyl aldehyde pyrophosphate (FAPP, 1) and a farnesylated protein showing a CAAX-box (CVIA) positioned at the C-terminus of a protein.

To evaluate the ability of PFTase to be used in a protein modification strategy, an aldehyde-functionalized isoprenoid diphosphate analogue was designed for enzymatically modifying proteins via rapid oxime and hydrazone ligations (Figure 1b). Analogue **1** is a derivative of FPP which was prepared in six steps starting from farnesol as previously described [4], with some modifications that significantly improved the overall yield. To evaluate **1** as a substrate for PFTase, a continuous spectrofluorometric assay was employed. Enzymatic studies indicated that analogue **1** was an excellent alternative substrate for the enzyme. Next, we evaluated the utility of the aldehyde analogue for selective protein modification. Accordingly, aldehyde **1** was incubated with GFP-CVIA (**2**) in the presence of PFTase for 2h at 30°C in which the reaction time was based on our earlier observations with a peptide substrate. Reaction completion was confirmed by LC-MS analysis. In comparison to the large peak for GFP-functionalized aldehyde (**3a**) none of free **2** could be detected. Deconvolution of the LC-MS data from the purified protein product showed peak at 27559.0, consistent with the proposed structure of aldehyde-GFP **3a**. Next, in order to fluorescently label the aldehyde-functionalized protein, we chose two sensitive fluorophores, Texas red hydrazide (**4b**) and Alexaflour-488 aminooxy (**4c**). Aldehyde-GFP **3a** was incubated separately with aminooxy **4c** at pH 7 and rt. After 4-6h of reaction, LC-MS analysis revealed no detectable unmodified protein-aldehyde remaining (**3a**) which suggested that the reaction had proceeded to completion. The deconvoluted MS data indicated only the presence of species at 28032.0, consistent with the proposed oxime **3c**. In-gel fluorescence analysis performed under denaturing conditions confirmed covalent attachment of aminooxy **4c** to the aldehyde-containing protein. Unprenylated GFP-CVIA (**2**) failed to show any labeling with the fluorophore **4c**, further confirming that the oxime ligation requires the presence of the introduced aldehyde functionality and that the ligation reaction is actually bioorthogonal. Overall, the oxime ligation reaction appears to be highly efficient since no unligated aldehyde-GFP (**3a**) was observed upon LC-MS analysis of the ligation reaction mixtures (Figure 2b and 2c). Next, aldehyde-functionalized GFP **3a** was incubated with hydrazide **4b** at pH 7 and rt under the same condition used in the oxime ligation reaction. LC-MS analysis of hyrazone formation reaction of **3a** and **4b** after 1h showed approximately 20% conversion of aldehyde **3a** to its respective hydrazone **3b** (Figure 2d).
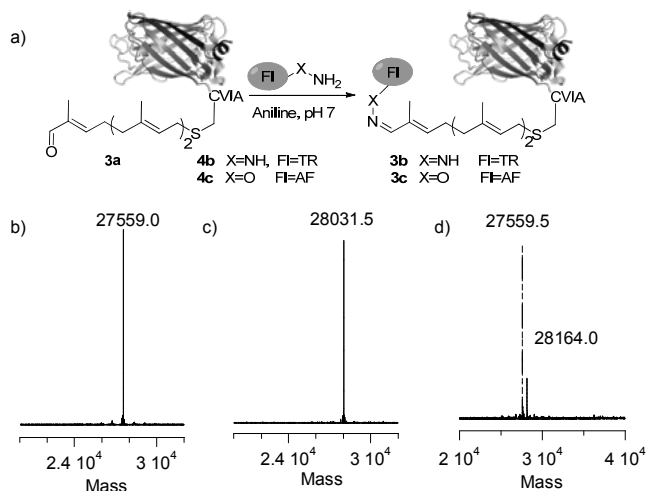
*Fig. 2. a) Schematic representation of oxime and hydrazone ligations of **3a** to yield **3b** and **3c**. b) ESI deconvoluted mass spectra of **3a** and hydrazone/oxime ligation products **3b** and **3c**, showing full conversion for oxime (spectrum c) and ~20% for hydrazone (spectrum d) ligations.*

In conclusion, we have demonstrated that PFTase can be used to introduce an aldehyde group near the C-terminus of a protein, and that the resulting protein can be further functionalized via aniline-promoted hydrazone or oxime formations.

This copper free labeling approach may be particularly useful for live cell studies or in applications where enzymatic activity must be preserved. It should also be noted that this ligation chemistry and the Cu(I)-catalyzed click reaction [5] are bioorthogonal. This opens up the possibility of performing multiple modifications on proteins using different bioorthogonal chemistries. Given that CAAX-box sequences can be appended to the C-termini of almost any protein, the method reported here should be useful for a wide range of applications in protein chemistry.

Acknowledgments

References

1. Wong, L.S., Khan, F., Micklefield, J. *Chem. Rev.* **109**, 4025-4053 (2009).
2. Prescher, J.A., Bertozzi, C.R. *Nat. Chem. Biol*. **1**, 13-21 (2005).
3. Tiefenbrunn, T.K., Dawson, P.E. *Biopolymers* **94**, 95-106 (2010).
4. Rashidian, M., Dozier, J.K., Lenevich, S., Distefano, M.D. *Chem. Commun.* **46**, 8998 (2010).
5. Kolb, H.C., Finn, M.G., Sharpless, K.B. *Angew. Chem. Int. Ed.* **40**, 2004-2021 (2001).

Photocaged Cysteine Peptides for Studying Protein Farnesylation

Daniel Abate-Pella and Mark D. Distefano

Department of Chemistry, University of Minnesota, Minneapolis, MN, 55455, U.S.A.

Introduction

Mutant Ras proteins are responsible for 30% of human cancers, and farnesylation is a key step that activates their oncogenicity [1]. Here we report the synthesis and caging of cysteine in peptides that are substrates of the enzyme protein farnesyltransferase (PFTase). The photoremovable groups bromohydroxy quinoline (BHQ) and bromohydroxy coumarin (bhc) were incorporated into peptides using standard Fmoc SPPS and evaluated for their ability to release uncaged peptide upon photolysis. Kinetic analysis shows that BHQ and bhc uncaging of thiols is significantly more rapid compared to nitrobenzyl-based groups [2,3] although BHQ photolysis results in other photoproducts that reduce the overall efficiency. In addition we show that a bhc-caged peptide is not a substrate for PFTase, but upon irradiation such a peptide is farnesylated by the enzyme.

Results and Discussion

Peptides **1-4** were synthesized using Fmoc-cysteine(MOM-BHQ)-OH (**5**) or Fmoc-cysteine(MOM-bhc)-OH (**6**) as building blocks during SPPS (see Figure 1). Photolysis time courses were carried out for each caged peptide in order to compare decay kinetics. The short peptide **3** had the fastest decay rate, while peptide **2** was the slowest to photolyze. Subsequent analysis to detect the corresponding uncaged forms of each peptide revealed a different picture: peptide **1** converted to a debrominated species that did not undergo further photolysis, and peptide **2** underwent a rearrangement that we speculate was the capture of the bhc group by the electron-rich dansyl moiety. We were able to detect significant amounts of correct peptide

Fig. 1. BHQ and bhc caged peptides 1-4 and SPPS building blocks 5-6.

formed upon analysis of the short peptide **3**, which led us to synthesize the farnesylation sequence peptide **4**. The Fmoc group was left on the N-terminus in order to facilitate analysis by HPLC. Photolysis of this peptide and subsequent quantitation by HPLC revealed a half-life of approximately two minutes (see Figure 2) and an overall conversion efficiency of 70-80%.

Peptide **4** was then tested in an *in vitro* farnesylation assay in order to show that the peptide is not a substrate of PFTase while caged. Upon photolysis it is converted to Fmoc-KKKSKTK-CVIM (**7**) and after processing by PFTase the farnesyl group is attached to the cysteine residue to become Fmoc-KKKSKTKC(farnesyl)VIM (**8**, see Scheme 1). Peptide **4** was subjected to photolysis for 10 minutes utilizing 365 nm light from a Rayonet photoreactor (Figure 3, trace A). Analysis by HPLC shows the disappearance of peptide **4** (not shown). This photolyzed sample was then subjected to the *in vitro* farnesylation conditions and allowed to react over two hours. An aliquot of this reaction analyzed by HPLC shows the formation of farnesylated peptide **8** (trace B).

Fig. 2. Photolysis time course of peptide 4.
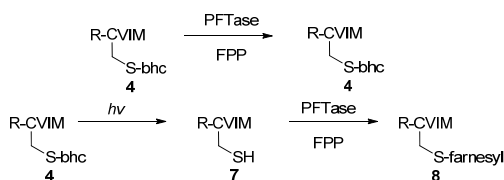
Scheme 1. Photolysis and farnesylation of caged peptide 4.

LC-MS data of each solution was collected in order to confirm the identities of peptides **7** and **8** (not shown). Additionally, caged peptide **4** was subjected to the same farnesylation assay and no farnesylated peptide **8** was detected via HPLC or LC-MS (not shown). Overall this approach shows the versatility and advantages of using caged groups to study protein farnesylation. Further applications to employ these strategies in the study of farnesylation in living cells are under way.
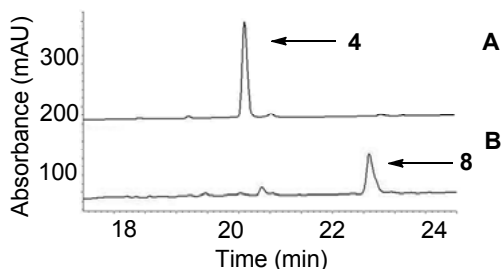
Fig. 3. HPLC traces of the photolysis and farnesylation of caged peptide 4. A) Chromatogram of 4. B) Photolyzed and farnesylated peptide 8.

Acknowledgments

References

1. Ohkanda, J., Knowles, D.B., Blaskovich, M.A., Sebti, S.M., Hamilton, A.D. *Curr. Top Med Chem.* **2**, 303-323 (2002).
2. Pan, P., Bayley, H. *FEBS Lett.* **405**, 81-85 (1997).
3. Specht, A., Loudwig, S., Peng, L., Goeldner, M. *Tet. Lett.* **43**, 8947-8950 (2002).

Synthesis of a-Factor and a-Factor Analogs Using a Cysteine-Anchoring Method

Verónica Díaz-Rodríguez, Daniel Mullen, and Mark D. Distefano

Department of Chemistry, University of Minnesota, Minneapolis, MN, 55455, U.S.A.

Introduction

a-Factor is a dodecapeptide pheromone secreted by a haploid cell of *S. cerevisiae* and is involved in the mating of yeast [1,2]. This peptide contains a farnesylated cysteine and a *C*-terminal methyl ester that have been shown to be crucial for its bioactivity [3]. After secretion, **a**-factor binds to a G protein-coupled receptor initiating a cell signaling cascade. The **a**-factor/receptor system can be used as a simple model to study how farnesylated proteins interact with other proteins in cells. The study of these interactions is important due to the participation of farnesylated proteins in signal transduction pathways and their resulting role in different diseases [4,5]. In this study, a cysteine-anchoring method [6] has been developed for the synthesis of **a**-factor and **a**-factor analogs in which the peptide is grown by Fmoc SPPS via its cysteine side-chain instead of its carboxy terminus.

Results and Discussion

Protein farnesylation is a post-translational modification that consists of the addition of a farnesyl-C_{15} group to a cysteine (Cys) residue near the *C*-terminus of a selective group of proteins. There is a three-step process that a protein must undergo in order to be a mature farnesylated protein: addition of a farnesyl group, proteolysis of the *C*-terminal tripeptide and methylation of the new *C*-terminus of the protein. With each of these transformations the structure of the protein changes from having an acidic *C*-terminal sequence to having a prenylated cysteine methyl ester at the *C*-terminus. While many efforts have been made in order to synthesize prenylated peptides containing a methyl ester, these methods unfortunately include the use of strong acidic [7] or oxidative [8] conditions. Recently, a new peptide synthesis approach was published that introduced a novel side-chain anchoring strategy for Cys [6]. This method consists of attaching a peptide, containing an alkyl ester,
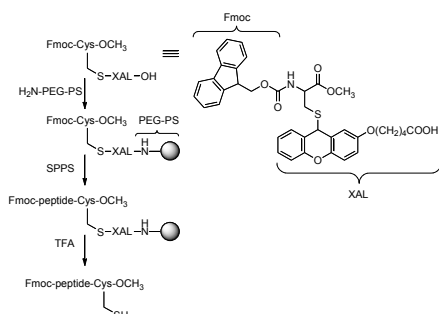
Fig. 1. XAL-Anchoring Method.

to a solid support via the side-chain of a Cys amino acid. It was found that this method produced the desired peptides in high yield, with no risk of racemization, and without the formation of the byproducts observed when using common solid phase peptide synthesis (SPPS) where the *C*-terminal carboxylic group on the peptide is directly attached to the resin.

We utilized a modified version of this method to synthesize peptides containing methyl esters at the *C*-terminus (Figure 1). We first started with the five step chemical synthesis of the XAL handle (Figure 2) followed by the attachment of this handle to an Fmoc-Cys-OMe by a
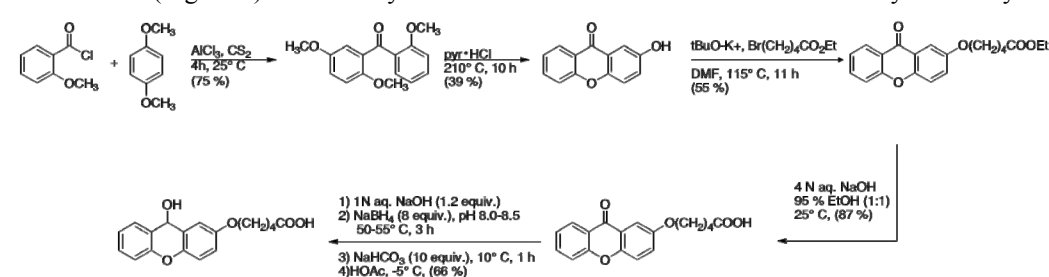
Fig. 2. Synthesis of XAL (5-(9-hydroxyxanthen-2-oxy)valeric acid handle).

condensation reaction in acidic media. Coupling of the Fmoc-Cys(XAL)-OMe onto the amino containing resin was successful with a loading of 82% yield. The synthesis of **a**-factor peptide sequence (YIIKGVFWDPAC-OCH$_3$) was then completed using Fmoc SPPS conditions. Deprotection of the side-chains, including the Cys, which was attached to the resin via the XAL handle, was successfully achieved after treatment of the material with Reagent K. RP-HPLC analysis of the purified material using a C$_{18}$ column shows a peak with a retention time of 37 min. ESI-MS of the purified material confirmed the mass of the desired peptide ([M+2H$^+$]$^{2+}$ = 713.4 m/z calc., 713.3 m/z obs.). This material was then chemically farnesylated in an alkylation reaction between the free cysteine and farnesyl bromide in the presence of Zn(OAc)$_2$ in order to produce the desired **a**-factor (YIIKGVFWDPAC(farnesyl)-OCH$_3$). After analysis using RP-HPLC, it was found that the farnesyl group attached to the peptide caused an increase in the retention time of the peptide. A peak was observed at 63 min and ESI-MS confirmed the expected mass ([M+2H$^+$]$^{2+}$ = 815.5 m/z calc., 815.6 m/z obs.).

After a successful synthesis of **a**-factor utilizing the XAL-anchoring method, the procedure was modified for the synthesis of **a**-factor analogs that will be used to study the interaction of **a**-factor with its receptor. These analogs included an NBD-, a 5-Fam- and a biotin-labeled **a**-factor. For those syntheses, an ivDde-protected lysine was incorporated into the **a**-factor peptide sequence (Figure 3). This group can be orthogonally cleaved using nucleophillic conditions in order to reveal a free side-chain amino group suitable for functionalization with various reporters (fluorophores or biotin). The attachment of the 5-Fam probe to the peptide was successfully achieved and a peptide peak was observed in RP-HPLC with a retention time of 49 min and in ESI-MS with a mass of [M+2H$^+$]$^{2+}$ = 892.4 m/z calc., 892.3 m/z obs. Thus, in summary, we have demonstrated the feasibility of using the XAL-anchoring method for the synthesis **a**-factor and derivatives thereof. Future work will be directed towards employing **a**-factor derivatives in experiments designed to probe the interaction between **a**-factor and its receptor, Ste3p.
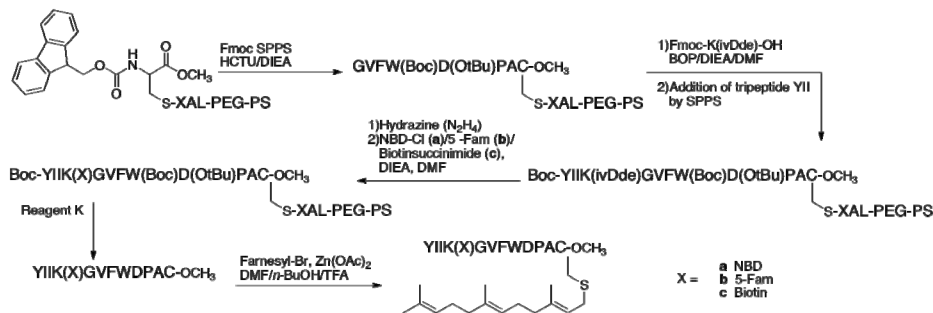
*Fig. 3. Strategy for the synthesis of **a**-factor analogs.*

Acknowledgments

References

1. Xie, H.B., Shao, Y., Becker, J.M., Naider, F., Gibbs, R.A. *J. Org. Chem.* **65** (25), 8552-8563 (2000).
2. Xie, H., Becker, J.M., Gibbs, R.A., Naider, F. *J. Peptide Res.* **55** (5), 372-383 (2000).
3. Dawe, A.L., Becker, J.M., Jiang, Y., Naider, F., Eummer, J.T., Mu, Y.Q., Gibbs, R.A. *Biochemistry* **36** (40), 12036-12044 (1997).
4. Zhang, F.L., Casey, P.J. *Annu. Rev. Biochem.* **65**, 241-269 (1996).
5. Ohkanda, J., Knowles, D.B., Blaskovich, M.A., Sebti, S.M., Hamilton, A.D. *Curr. Top. Med. Chem.* **2** (3), 303-323 (2002).
6. Barany, G., Han, Y.X., Hargittai, B., Liu, R.Q., Varkey, J.T. *Biopolymers* **71** (6), 652-666 (2003).
7. Xue, C.B., Caldwell, G.A., Becker, J.M., Naider, F. *Biochem. Biophys. Res. Commun.* **162** (1), 253-257 (1989).
8. Ludolph, B., Eisele, F., Waldmann, H. *J. Am. Chem. Soc.* **124** (21), 5954-5955 (2002).

Strategies for Biosynthesis of Sizeable Transmembrane Receptor Fragments

Zhanna Potetinova[1], Subramanyam Tantry[1], Jeffrey M. Becker[2], and Fred Naider[1]

[1]*Department of Chemistry, College of Staten Island, The City University of New York, Staten Island, NY, 10314, U.S.A.;* [2]*Department of Microbiology, University of Tennessee, Knoxville, TN, 37996, U.S.A.*

Introduction

Since membrane proteins are major targets for various therapeutics, knowledge of their structure is essential for rational drug design. Investigations on membrane proteins are challenging due to their hydrophobic nature, which results in difficulties in the biosynthesis and purification of the milligram quantities needed for their biophysical analysis. In this work, we developed protocols for the biosynthesis of large portions of Ste2p, a yeast seven transmembrane (7TM) G protein-coupled receptor (GPCR) that recognizes the *Saccharomyces cerevisiae* tridecapeptide pheromone α-factor.

Results and Discussion

The GPCR constructs containing the predicted four or five membrane-spanning Ste2p domains (Table 1) were obtained using two different approaches: 1) our standard TrpΔLE fusion protein protocol [1-3] which requires processing by CNBr and 2) a direct expression approach that simplifies the overall method by eliminating intermediate fusion protein purification and cleavage with the highly toxic CNBr reagent. The N-terminal fragment (4TMN) was expressed as a fusion protein using a modified pMMHa vector, pSW02 [1]. The C-terminal fragments (4TMC and 5TMC) were biosynthesized by direct expression using a pET21a vector. The final plasmids encoding the Met- and Cys-less GPCR fragments contained mutations to replace Met and Cys residues with Ile or Leu and Ser (M54I, M69I, M71I, M165I, M180I, M189I, M218L, M250I, C252S, M294I) and small sequence variations (K77R in 4TMN and A299V in 5TMC) which do not affect bioactivity of Ste2p as indicated by published data [4] or construction of the corresponding mutation in Ste2p. All constructs contained an N-terminal His-Tag that allowed detection of the polypeptides and evaluation of their relative expression levels by Western Blotting in addition to Coomassie Blue analysis.

Fig. 1. Western Blot of 4TMN-FP IB expressed in different BL21 E. coli cells at 30°C for 18-21 h.

Table 1. Composition and characterization of the biosynthesized GPCR fragments

	GPCR construct		Molecular Mass, Da		HPLC[a]
Name		Composition	Expected	Observed	RT, min
4TMN-FP	M-H9-TrpΔLE-M-[Ste2p(G_{31}-A_{198})]		31685	31682	11.6
4TMC	M-H8-[Ste2p(T_{155}-L_{340})]		21375	21399	11.9
5TMC	M-H8-[Ste2p(I_{120}-L_{340})]		25229	25222	13.2

[a]*RP-HPLC conditions: Zorbax 300SB-C3 column (4.6x150mm, 3.5-micron), a flow rate of 1 ml/min, 50-88% linear gradient of MeCN in 0.1%TFA /10%iPro/H_2O for 30 min, T 60°C, λ 220 nm.*
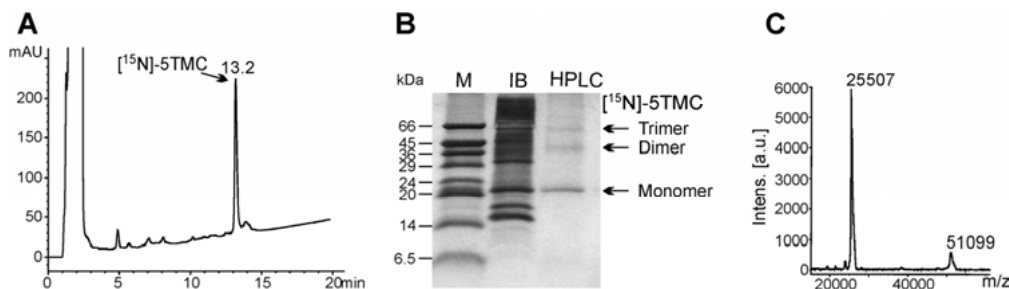
Fig. 2. Biosynthesis and characterization of [15N]-labeled 5TMC. A) HPLC chromatogram of [[15N]-5TMC IBs expressed in the BL21(DE3)/M9 system by induction at ~1.0 OD_{600} with 0.25 mM IPTG with 0.25 mM IPTG at 30°C for 21 h. B) 16% SDS-PAGE Coomassie Blue stained gel of [[15N]-5TMC IBs and [[15N]-5TMC purified by HPLC. Lane M, Sigma Low Range protein marker. C) Positive MALDI-TOF spectrum of [[15N]-5TMC purified by HPLC from isolated IBs.

To develop protocols for biosynthesis of these large Ste2p fragments, the small-scale expression experiments (50 ml) were carried out in rich (LB) and minimal (M9) media supplemented with chloramphenicol and/or ampicillin under different conditions (cell, temperature, OD_{600}, inducer concentrations and time). The best heterologous expression for the fusion and direct expression constructs transformed into various BL21 *E. coli* strains (Invitrogen) was found in IPTG-induced BL21(DE3) cells at 30°C. The 4TMN fusion protein also was expressed at a high protein level in arabinose-induced BL21-AI cells in M9 medium (Figure 1). This contrasted with LB medium where target protein expression was very low. The same observation was made previously for shorter TrpΔLE-fusion Ste2p fragments [3]. There was no difference in expression levels between LB and M9 media for directly expressed 5TMC. Although, increasing the inducer concentration had the opposite effect on the 5TMC expression level in the two media: with increasing IPTG concentration the expression improved in LB whereas it was reduced in M9. The desired products were accumulated in inclusion bodies (IB), purified by RP-HPLC and characterized by SDS-PAGE and MALDI (Table 1, Figure 2). The C-terminal constructs were biosynthesized under optimized conditions and recovered on a preparative scale in multi-milligram amounts. A significant variation in the yield of the directly expressed 4TMC (1.5-2 mg/L) and 5TMC (18-20 mg/L) was observed. To evaluate the His-Tag influence on the expression level of the fragments, the His-Tag residues were moved to the C-terminus where they were expected to have a lower effect on the folding during expression. The change in the location of the His-Tag did not improve the expression; both fragments with the C-terminal His-Tag were produced in the same lower amounts in comparison to the N-terminal tagged 5TMC, suggesting a contribution of the N-terminal polyhistidine region to the high yield of the target 5TMC peptide. We also biosynthesized the largest 5 TM domain fragment in a stable isotope-labeled form. The [15N]-uniformly labeled 5TMC was expressed in M9 medium supplemented with [15N]H_4Cl and purified by HPLC in amounts sufficient to produce NMR samples (9-10 mg per 500 ml, by weight). [15N]-incorporation was 96% as determined from the MALDI spectra for the unlabeled and labeled compounds measured in parallel. In summary, a biosynthetic scheme that provided sufficient quantities of large four and five TM domain-containing fragments of Ste2p in labeled and unlabeled forms to perform biophysical and structural investigations of these GPCR surrogates has been developed.

Acknowledgments

References

1. Arevalo, E., et al. *Biopolymers (Peptide Science)* **71**, 516-531 (2003).
2. Estephan, R., et al. *Biochemistry* **44**, 11795-11810 (2005).
3. Cohen, L.S., et al. *Biopolymer (Peptide Science)* **90**, 117 (2008).
4. Martin, N.P., Celic, A., Dumont, M.E. *J. Mol. Biol.* **317**, 765-788 (2002).

A New Versatile Process for Peptide Purification Using Ion Exchange Centrifugal Partition Chromatography

Leslie Boudesocque[1], Nassima Amarouche[1], Pedro Lameiras[1], Romain Kapel[3], Ivan Marc[3], Jean-Marc Nuzillard[1], Matthieu Giraud[2], John Mc Garrity[2], Francesca Quattrini[2], and Jean-Hugues Renault[1]

[1]*Institut de ChimieMoléculaire de Reims UMR CNRS 6229, Equipe Isolement et Structure; IFR 53 Interactions Cellules Microenvironnement, Université de Reims Champagne-Ardenne, Reims, 51100, France;* [2]*Lonza AG, WalliserWerke, Lonzastrasse, Visp, 3930, Switzerland;* [3]*LRGP UPR CNRS 3349, 13 rue du Bois de la Champelle, Vandoeuvre-lès-Nancy, 54500, France*

Introduction

Centrifugal Partition Chromatography (CPC) is a support-free chromatographic technique, which was particularly developed in the field of phytochemistry [1]. The introduction of the so-called displacement mode expanded the field of CPC applications by allowing an easiest access to ionic or ionizable compounds. Ion-exchange CPC (IXCPC) purification of cationic molecules requires the presence of an exchanger in the organic stationary phase, namely a lipophilic anionic extraction agent. During sample injection, the analytes and the exchanger must preferentially form ion pairs in the organic stationary phase. Then, the displacer-containing aqueous mobile phase is pumped through the stationary phase, and performs the displacement process of the hydrophilic analytes in the mobile phase, thus allowing them to progress in the CPC column as an isotachic train [2] (Figure 1). In this framework, we have developed a preparative purification method devoted to peptide purification and based on strong and/or weak ion-exchange CPC. This method uses a lipophilic cation-exchanger: diethylhexylphosphoric acid (DEHPA), partially deprotonated by triethylamine (TEA) and a couple of displacers: Ca^{2+} and H^+. To define the optimal operating conditions, a model mixture of five dipeptides was initially studied.

Fig. 1. Isotachic train in the CPC ion exchange.

Results and Discussion

A model mixture of five dipeptides - GG, GY, AY, LV and LY - was chosen in order to study the potential of ion exchange CPC for peptide purification. These peptides have very close isoelectric points that range from 6.08 to 6.1, so that they are electrically charged in the same way at the same pH. Nevertheless, they cover a large polarity range, from the very polar GG to the quite apolar LV and LY. Both GY and AY have an intermediate polarity, and are structurally very close. The model mixture we chose thus allowed us to investigate the chromatographic process selectivity in a non-trivial case. Indeed, this mixture is not resolved by the previous published methods using CPC [3]. After optimization of the different experimental parameters, IX CPC, using the quaternary biphasic solvent system MtBE/CH₃CN/n-BuOH/water (2:1:2:5, v/v), was successfully applied to the purification of dipeptides within a five component model mixture as shown by the Figure 2. The optimal separation conditions relied on a Mixed Ion eXchange CPC (MIXCPC) mode, which combined a strong displacer, calcium, and a weak displacer, proton. Moreover, the column was segmented in two parts, in which the exchanger was activated by triethylamine at two different concentrations (see caption of Figure 2). The ¹H and ³¹P DOSY NMR study allowed us to better understand the mechanisms that are involved in the peptide extraction during CPC experiments. We were thus able to
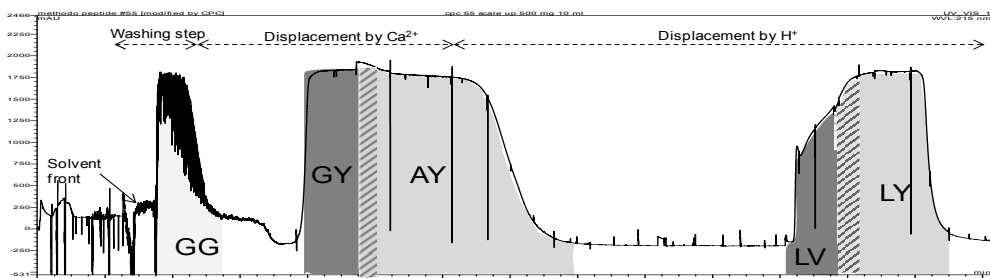
Fig. 2. MIXCPC chromatogram for the purification of 100 mg of each dipeptide. Biphasic solvent system: MtBE/CH₃CN/n-BuOH/water (2:1:2:5, v/v); stationary phase: upper organic phase + DEHPA (75 mM) with 30% (25% of the column volume) then 2.15% of TEA (75% of the column volume); mobile phase: aqueous phase + CaCl₂ 7.2 mM, then HCl 12.5 mM; rotation speed: 1200 rpm; flow rate: 2 mL/min.

confirm the hypothesis of ions pair formation at usual DEHPA concentration conditions.

Secondly, the ion exchange process we developed during this study succeeded to polish a synthetic peptide, the dirucotide, which was longer than those already purified by means of a similar strategy. Dirucotide, a 17-aminoacid peptide, analog of the 82-98 sequence of the myelin basic protein, is a drug candidate for the treatment of multiple sclerosis. The high purity (about 98%) of the obtained dirucotide fractions after IXCPC demonstrated the high selectivity of our process, since most of critical impurities were eliminated in our conditions, although they usually were co-eluted with all the previously tested methods (Figure 3). The presented results strongly suggest that IXCPC will be a very easy-to-use promising alternative to conventional peptide purification protocols.
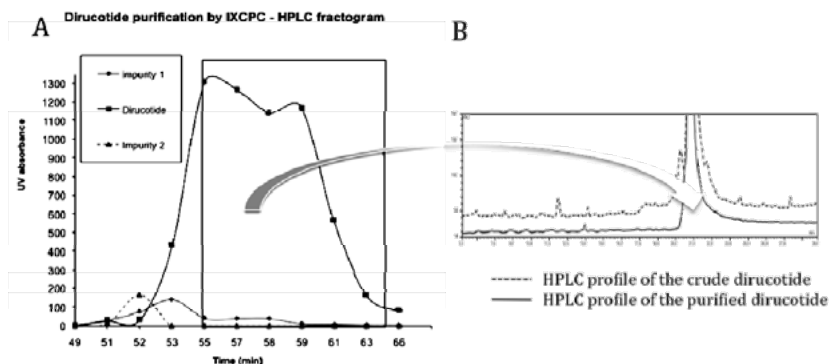
Fig. 3. MIXCPC chromatogram for the purification of 1 g of dirucotide. Biphasic solvent system: MtBE/CH₃CN/n-BuOH/water (2:1:2:5, v/v); stationary phase: upper organic phase + DEHPA (300 mM) with 2.15% of TEA; mobile phase: aqueous phase + CaCl₂ 29 mM; rotation speed: 1200 rpm; flow rate: 2 mL/min.

Acknowledgments

References

1. Pauli, G.F., Pro, S.M., Friesen, J.B. *J. Nat. Prod.* **71**, 1489-1508 (2008).
2. Maciuk, A., Renault, J.-H., Margraff, R., Trébuchet, P., Zèches-Hanrot, M., Nuzillard, J.-M. *Anal. Chem.* **76**, 6179-6186 (2004).

Immobilized Peptide as Affinity Chromatography Ligand for Soybean Peroxidase Purification

Nancy B. Iannucci[1,2], Silvia A. Camperi[1], María V. Miranda[1], Fernando Albericio[3,4,5], and Osvaldo Cascone[1]

[1]*School of Pharmacy and Biochemistry, University of Buenos Aires, Buenos Aires, 1113, Argentina;*
[2]*Therapeutic Peptides Research and Development Laboratory, Chemo-Romikin, Buenos Aires, 1605, Argentina;* [3]*Institute for Research in Biomedicine, Barcelona Science Park, Barcelona, 08028, Spain;*
[4]*CIBER-BBN, Networking Centre on Bioengineering, Biomaterials and Nanomedicine, Barcelona Science Park, Barcelona, 08028, Spain;* [5]*Department of Organic Chemistry, University of Barcelona, Barcelona, 08028, Spain*

Introduction

Affinity chromatography (AC) is a valuable tool for the purification of proteins because it integrates several downstream steps, like isolation and specific purification, in only one step. Integrative procedures provide increasing yield and productivity at the industrial scale [1]. Discovery of biospecific ligands have a key role in AC development, phage display and chemical combinatorial libraries may lead to the development of tailor-made peptide ligands [2]. Successful affinity purification requires a biospecific ligand which can be covalently attached on a chromatographic support [3]. An affinity peptide ligand for the soybean peroxidase (SBP) was identified from the screening of a combinatorial library composed by 130,321 tetrapeptides.

An affinity purification system for SBP was designed by immobilizing the peptide ligand on a suitable support. The purification system was characterized by determining the chromatographic parameters derived from isotherms and the protein recovery was optimized by immobilizing the peptide ligand on different supports.

Results and Discussion
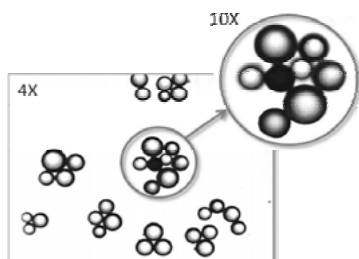
Fig. 1. SBP affinity screening positive bead.

Peptide KVQN was identified from the library as an affinity ligand for SBP. Figure 1 shows a positive bead isolated from the screening; peptide was identified by Edman sequencing. In Table 1 are summarized the most relevant experimental procedures and results obtained from the adsorption isotherms. Peptide KVQN was synthesized on CLEAR^R resin and adsorption isotherms were performed (Figure 2). Elution of SBP with 20 mM AcH/AcNa, pH 4.0, 0.5 M NaCl was not complete because of resin contraction.

In order to improve protein recovery, peptide KVQNC was immobilized on SulphoLink^R resin. This procedure increased the purification yield of SBP from 40 to 90%. SBP purification from a crude extract is shown in Figure 3.

Specificity of the purification system was assessed by loading different proteins, such as bovine serum albumin, lysozyme and horseradish peroxidase (HRP). None of the proteins was adsorbed on the affinity resin. SBP and HRP chromatographic patterns are compared in Figures 4 and 5.

Table 1. Experimental procedures and adsorption isotherms results

Library Design	KVQN-CLEAR^R Isotherms	Isotherms results	KVQNC-SulphoLink^R
Amino PEGA resin was the solid support and the 19L-amino acids (except Cys) were the monomers.	Michaelis Menten equation was used: $q* = c* . qm / c* + Kd$	Maximum capacity qm: 12 mg SBP/ml resin Dissociation constant Kd: 3×10^{-7} M	KVQNC immobilization: 32 mg of peptide reacted with 1 ml resin at RT for 45 min. L-Cys was the quenching reagent.
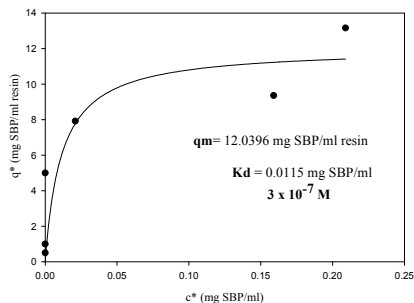
Fig. 2. Adsorption isotherm KVQN-CLEAR Resin.
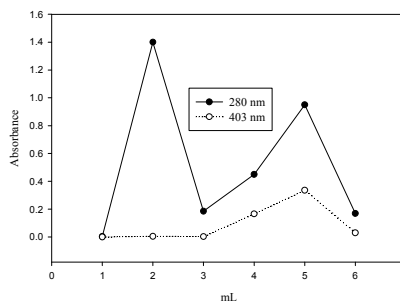
Fig. 3. Affinity chromatography of crude SBP on KVQNC-SulfoLink.
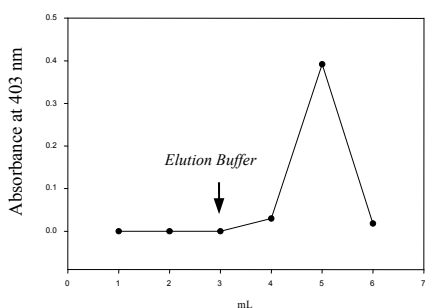
Fig. 4. SBP Adsorption on KVQN-CLEAR resin.
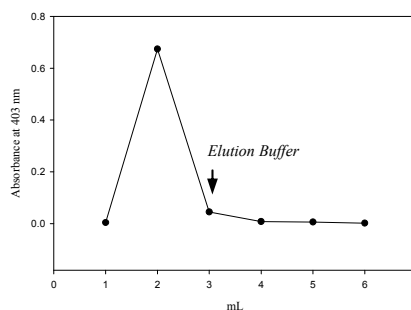
Fig. 5. HRP Adsorption on KVQN-CLEAR resin.

An affinity purification system for SBP with a peptide ligand derived from a library was developed. Chromatographic parameters were comparable to those claimed by commercial systems. The immobilization of peptide KVQNC on SulphoLink[R] resin yielded an optimized protein recovery from 40 to 90% with respect to KVQN-CLEAR[R] resin.

Alternative applications of this system are under study regarding its high affinity for a color-developing enzyme, like the isolation and visualization of SBP labeled proteins.

Acknowledgments

References

1. Thommes, J., Kula, M.R. *Biotechnol. Prog.* **11**, 357-367 (1995).
2. Burnouf, T, Radosevich, M. *J. Biochem. Biophys. Methods* **49**, 575-586 (2001).
3. Clonis, Y.D. *J. Chromatogr. A*. **1101**, 1-24 (2006).

Hierarchic Folding and Assembly of C_N-Symmetric Homo-Oligomers: Demonstration of Chemical and Stereochemical Variables of Polypeptide Structure as the Design Alphabet

Punam Ghosh and Susheel Durani

Department of Chemistry, Indian Institute of Technology Bombay, Mumbai, 400076, India

Introduction

Protein homomers of C_N or D_N point-group symmetry, like C_2-symmetric HIV-protease dimer and D_2-symmetric hemoglobin tetramer, evolve in chemical-sequence space over L-α-amino acids as the biological alphabet [1]. Design of heteropolymer folds and their assemblies over the codes of a specific structural alphabet remains a challenge [2]. With maturation of the theory of biomolecular structure, folding, and assembly, computation has rapidly emerged as a powerful approach to implement the designs. In this study we explore computation of oligopeptide folds and assemblies to the desired stoichiometry as C_N-symmetric structures. Specifically we explore the application of chemical and stereochemical variables over L- and D-α-amino-acid structures as the design alphabet [3]. Stereochemically diverse homopolypeptides are annealed, screened for the variants best adapted as C_N-symmetric oligomers, and inverse optimized in sequence space over side chains, which are applied to L or D stereochemical option as required. Demonstrating the algorithm, we report successful design of octapeptides as C_5-symmetric assemblies. Alternative sequences assembled as homo-pentamers 1, 2, 3 and 4 shown in Figure 1 are made by manual solid-phase synthesis. Results of circular dichroism, nuclear magnetic resonance, fluorescence, differential light scattering, and microscopy are presented as proof that the desired folds and assemblies have successfully been accomplished.

Assembly_1_Seq_1: Ac-^{D}Ser(1)-***^{D}Glu(2)***-^{D}Thr(3)-Trp(4)-Leu(5)-Lys(6)-Tyr(7)-^{D}Val(8)-NH$_2$

Assembly_1_Seq_2: Ac-^{D}Ser(1)-***^{D}Gln(2)***-^{D}Thr(3)-Trp(4)-Leu(5)-Lys(6)-Tyr(7)-^{D}Val(8)-NH$_2$

Assembly_2_Seq_3: Ac-Thr(1)-Lys(2)-^{D}Trp(3)-Phe(4)-Asn(5)-^{D}Glu(6)-^{D}Val(7)-***^{D}Ala(8)***-NH$_2$

Assembly_2_Seq_4: Ac-Thr(1)-Lys(2)-^{D}Trp(3)-Phe(4)-Asn(5)-^{D}Glu(6)-^{D}Val(7)-***^{D}Arg(8)***-NH$_2$

Seq1   Seq2   Seq 3   Seq4

Assembly 1   **Assembly 2**
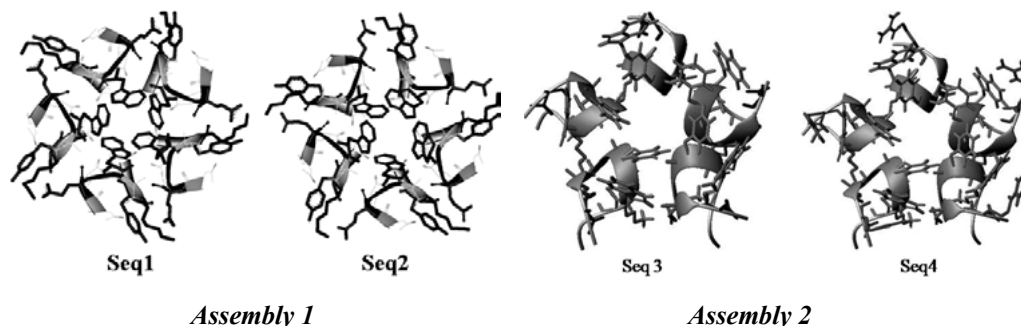
Fig. 1. Cartoon representation of octapeptide sequences in forming two different C_5 assemblies.

Results and Discussion

The designs were accomplished in three steps. Homopolymers were folded over L and D structures as the stereochemical alphabet, the folds were assembled as oligomers of the desired C_N symmetric structure, and the oligomers were inverse optimized to the desired chemical structures over side chains, which were applied to L or D enantiomer structure as required. Stereochemically diverse octa-leucines were folded with simulated-annealing molecular dynamics. The resultant stereochemically diverse folds of random conformational structure were evaluated for self assembly as C_5-symmetric structure with public domain software SymmDock. The folds furnishing the highest scoring C_5 assemblies according to SymmDock

were further tested and screened with molecular dynamics as the variants best adapted as pentamer assemblies. The assemblies were inverse-sequence optimized over the chemical alphabet in side chains. The optimization involving the application of side chains to L or D chiral option was accomplished with our in-house software IDeAS (Inverse Design Algorithm for Sequences). The software provides minimum-energy sequences for the desired assembly by applying identical side chains over symmetry-related positions of the building-block folds. The designs involve Dead End Elimination and Monte Carlo as the search algorithms. The synthesis and characterization of the designed sequences as the targeted assemblies will be discussed.
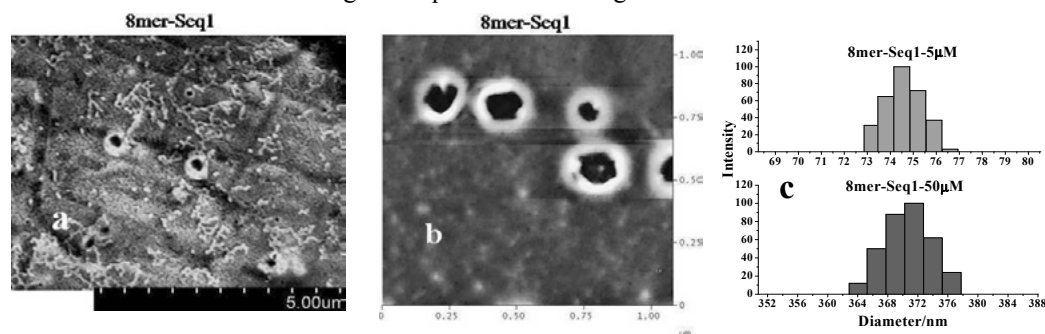
Fig. 2. (a) Scanning electron micrograph (b) Atomic Force Microscopy Image and (c) Dynamic Light Scattering showing the particle size distributions at 5μM and 50μM respectively.

Planned Octapeptides made by solid phase synthesis were proven with MALDI-MS, 1D and 2D NMR. Circular Dichroism shows a concentration dependent variation in molar ellipticity from 5 to 100 μM range, implying the probable formation of self-assembly. Steady state fluorescence measurements were carried out in the range of 20μM to 100μM and the OD corrected spectra obtained indicated fluorescence quenching evidencing self-assembly. Fluorescence anisotropy also varied in a concentration dependent manner in the range of 5 to 100μM concentration indicating self-assembly due to apparent increase in molecular mass. Dynamic light scattering experiments indicated concentration dependent variation in particle size distributions in the range of ~70 and ~370 nm, suggesting the possibility of monomer-pentamer equilibrium. Scanning Electron Microscopy experiments indicated ring like structures at nanometer resolution. We also recorded Atomic Force Microscopy, and the images clearly reflect the formation of spherical nano-ring like structures at nanometer resolution. We scrutinized the peptides computationally by running molecular dynamics in Gromacs at 298 K. The ideal folds were modeled as monomers and pentamers in all of the sequence constructs. Molecular Dynamics was performed for 50 ns with all the monomer and the pentamer folds. We analyzed molecular dynamics trajectories in RMSD and Rg of the polypeptide-main-chain structure, and for the number of peptide hydrogen bonds within monomer and pentamer folds. We concluded that all the monomers are unstable folds. The pentamer folds appear to be stabilized in this sequence due to the strengthening of intermolecular interactions like aromatic-aromatic, cation-π and salt bridge interactions. The pentamer structures appear to be maintained over the full time course of simulation.

Acknowledgments

References

1. Goodsell, D.S., Olson, A.J. *Annu. Rev. Biophys. Biomol. Struct*. **29**, 105-153 (2000).
2. Valery, C., Paternostre, M., Robert, B., et al. *Proc. Natl. Acad. Sci. U.S.A*. **100**, 10258-10262 (2003).
3. Durani, S. *Acc. Chem. Res*. **41**, 1301-1308 (2008).

Playing with Peptides: How to Build a Supramolecular Peptide Nanostructure by Exploiting Helix-Helix Macrodipole Interactions

Emanuela Gatto[1], Alessandro Porchetta[1], Fernando Formaggio[2], Claudio Toniolo[2], Manuela Scarselli[3], Maurizio De Crescenzi[3], and Mariano Venanzi[1]

[1]*Department of Chemical Sciences and Technologies, University of Rome "Tor Vergata", 00133, Rome, Italy;* [2]*ICB, Padova Unit, CNR, Department of Chemistry, University of Padova, 35131, Padova, Italy;* [3]*Department of Physics, University of Rome "Tor Vergata", 00133, Rome, Italy*

Introduction

Biomolecules have been extensively investigated as possible components of nanoscaled supramolecular entities, because of their good self-assembly properties. The key advantage of using self-assembly is that it capitalizes on the formation of non-covalent and reversible interactions. In particular, dipole-dipole interactions are expected to be promising tools for the construction of stable assemblies [1].

In this work, bicomponent, peptide-based, self-assembled monolayers (SAMs) composed of two types of helical peptides were immobilized on gold surfaces. Specifically, the following peptides were studied:

A8Pyr:Z-Aib-Api(CO-Pyr)-L-(αMe)Nva-Aib-L-(αMe)Nva-L-(αMe)Nva-Aib-Api(Boc)-NH*t*Bu
SSA4WA: Lipo-(Aib)$_4$-L-Trp-Aib-O*t*Bu

where Z is benzyloxycarbonyl, Aib is α-aminoisobutyric acid, Api is 4-aminopiperidine-4-carboxylic acid, (αMe)Nva is C$^\alpha$-methyl norvaline, and *t*Bu is *tert*-butyl.

SSA4WA is a lipoic (Lipo) acid-containing peptide, able to bind gold surfaces *via* an Au-S linkage [2] and **A8Pyr** is a pyrene(Pyr)-containing peptide devoid of any gold-binding group. The peptides investigated comprise almost exclusively C$^\alpha$-tetrasubstituted α-amino acids. These non-coded residues, because of their unique conformational properties, force the peptide backbone to attain helical conformations, which form stable SAMs on gold surface [2-4]. Here, we demonstrate that it is possible to build a stable supramolecular peptide nanostructure, where the **A8Pyr** peptide is incorporated into the **SSA4WA** palisade, by exploiting helical dipole·dipole interactions.

Results and Discussion

The presence of both types of peptides on the gold surface was investigated by spectroscopic and electrochemical techniques.
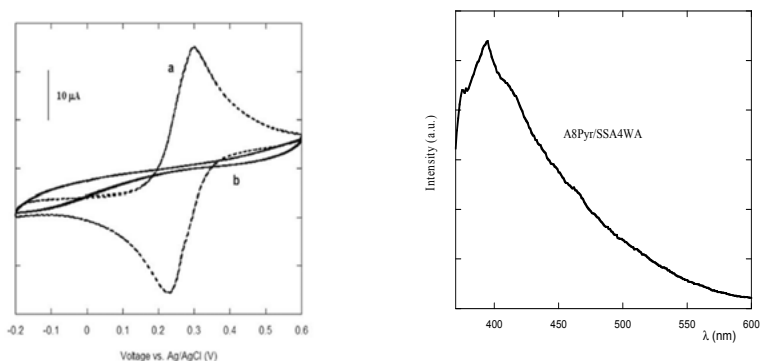
Fig. 1. (Left) Cyclic voltammetry experiments in a 0.50 mM K$_3$[Fe(CN)$_6$] aqueous solution: (a) bare gold electrode; (b) gold electrode modified with the mixed peptide SAM (A8Pyr/SSA4WA). Sweep rate: 50 mV/s. (Right) Fluorescence experiments in the pyrene emission region for the same peptide mixture. Spectra of the gold (5 nm)/glass slide/ mixed peptides SAM. Excitation wavelength: 340 nm.

Cyclic voltammetry experiments showed that after 24-hour incubation of a gold electrode into a 1:1 (mol/mol) **A8Pyr/SSA4WA** peptide solution, a SAM on the gold electrode is formed that is able to inhibit almost completely the $K_3[Fe(CN)_6]$ electrolyte discharge (Figure 1, left).

The fluorescence spectrum of the bicomponent SAM exhibits the typical emission band of the pyrene monomer fluorophore (Figure 1, right), as compared to the absence of any band for the bare gold and the **SSA4WA** SAM in this spectral region. The fluorescence spectrum does not show any excimer-like contribution, thus excluding pyrene· pyrene excited-state interactions in the peptide film. Moreover, this result suggests that the pyrene chromophores are intercalated within the **SSA4WA** palisade homogeneously and quite distant from each other [4].

The morphology of the monolayer was analyzed by scanning tunnelling microscopy (STM). These measurements show holes 0.2-0.3 nm deep and 2-6 nm wide, which are commonly considered as good evidence for the formation of a homogeneous peptide monolayer, chemisorbed on the gold substrate through Au-S linkages. In agreement with the fluorescence measurements, the monolayer is homogeneous and there are no raft domains, *i.e.* segregated single-component regions are absent. Furthermore, the bicomponent SAM does not show stripes, which are typical of surface lying molecules. This finding indicates that both peptides are vertically oriented on the gold surface.

Dots of 1-nm size are clearly observed in the STM images at highly positive bias voltages (Figure 2). The sizes of these spots are always the same from place to place in the flat terraces. The diameter of the dots agrees well with that of a peptide 3_{10}-helix, suggesting that each dot represents a single helix protruding from the surrounding SAM.

Fig. 2. Constant current STM image of the peptide SAM (image recorded at a sample bias of 1.8 V and tunnelling set current of 60 pA). Figure size: 200x200 nm.

In this work, spectroscopy, electrochemistry, and microscopy techniques were employed for the investigation of a bicomponent SAM composed of two short, conformationally constrained, peptides, one bearing a lipoic acid group able to bind a gold surface, and the other having a fluorescent pyrene chromophore but lacking the gold binding group. Our results suggest that the helical peptides are oriented in an antiparallel manner by taking advantage of the favorable dipole··dipole interactions.

References

1. Kimura, S. *Org. Biomol. Chem*. **6**, 1143-1148 (2008).
2. Venanzi, M., Pace, G., Palleschi, A., Stella, L., Castrucci, P., Scarselli, M., De Crescenzi, M., Formaggio, F., Toniolo, C., Marletta, G. *Surface Sci.* **600**, 409-416 (2006).
3. Gatto, E., Venanzi, M., Palleschi, A., Stella, L., Pispisa, B., Lorenzelli, L., Toniolo, C., Formaggio, F., Marletta. G. *Mater. Sci. Engin. C* **27**, 1309-1312 (2007).
4. Gatto, E., Caruso, M., Porchetta, A., Toniolo, C., Formaggio, F., Crisma M., Venanzi, M. *J. Pept. Sci.* **17**, 124-131 (2011).

Helical Peptides with Alternating Aib and Ala Residues are Hydrosoluble!

Alessandro Moretto, Edoardo Longo, Fernando Formaggio, and Claudio Toniolo

ICB, Padova Unit, CNR, Department of Chemistry, University of Padova, 35131, Padova, Italy

Introduction

More than twenty years ago, one of us (C.T.) co-authored a paper [1] which represented the first X-ray diffraction proof for a $3_{10} \rightarrow \alpha$-helix conversion in the crystal state induced by peptide lengthening only. The -(Aib-Ala)$_3$- (Aib, α-aminoisobutyric acid) sequential oligomer was found to be fully 3_{10}-helical, while the -(Aib-Ala)$_4$- octamer was essentially α-helical (it is worth pointing out that the remarkably short peptides found to be helical in these series are heavily based on the strongly helicogenic, non-coded Aib residue). However, it was subsequently reported that the isomeric -(Ala-Aib)$_4$- octapeptide sequence adopts a C-terminally distorted 3_{10}-helix structure in the crystal state [2]. Globally, it was found that, at a main-chain length near the critical size between these two types of helices, even subtle differences in the chemical structure, terminal blocking groups, packing motifs, and co-crystallized solvent molecules, may bias significantly the helix preference. In this same paper [2], it was also shown that the long oligomer -(Ala-Aib)$_8$- is α-helical under the same experimental conditions.

A variety of FT-IR absorption, NMR, and CD publications was devoted to the conformational investigations of consecutive Aib/Ala dipeptide sequences in a number of *organic* solvents. Spectral patterns indicative of a partially developed 3_{10}-helix appear at approximately the 5-mer level, while those characteristic of an α-helix influence are seen at the 7-/8-mer level. Both critical main-chain lengths for secondary structure change depend upon solvent polarity. For an extensive discussion, see reference [3].

Results and Discussion

In the course of our ongoing study on the use of helical peptides with alternating Aib and Ala residues as wires for electron transfer to very long distances (this research was pioneered in a series of papers by Kimura and his associates [4]), we serendipitously discovered that a complete, terminally blocked, sequential oligopeptide series (from dimer to nonamer) based on these two residues is *hydrosoluble*. Therefore, to determine the important missing information, namely the critical main-chain lengths for 3_{10}-helix formation and $3_{10} \rightarrow \alpha$-helix conversion in *water*, we analyzed this series of compounds in aqueous solution by far-UV CD. We carefully checked a variety of parameters, such as nature of the N-terminal protecting (blocking) group (either urethane or amide), presence/absence of an ester moiety and a negative charge at the C-terminus, and temperature (by either heating or cooling). The "borderline" oligopeptides between different (non-helical versus 3_{10}-helical, and 3_{10}-helical versus remarkably developed α-helical) conformations in water seem to be the hexapeptide (Figure 1A) and the octapeptide (Figure 1B), respectively.
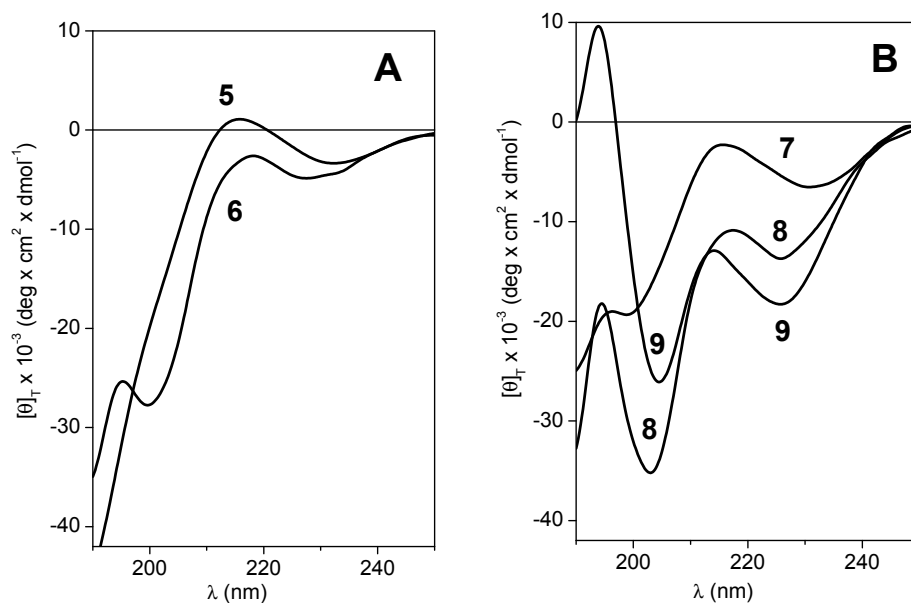
Fig. 1. Far-UV CD spectra of: (A) Ac-Ala-(Aib-Ala)₂-OMe (5) and Ac-(Aib-Ala)₃-OMe (6);
(B): Ac-Ala-(Aib-Ala)ₙ-OMe (n = 3; 7) and (n = 4; 9) and and Ac-(Aib-Ala)₄-OMe (8). All
measurements were recorded in water at 20°C.

References

1. Pavone, V., Benedetti, E., Di Blasio, B., Pedone, C., Santini, A., Bavoso, A., Toniolo, C., Crisma, M., Sartore, L. *J. Biomol. Struct. Dyn.* **7**, 1321-1331 (1990).
2. Otoda, K., Kitagawa, Y., Kimura, S., Imanishi, Y. *Biopolymers* **33**, 1337-1345 (1993).
3. Longo, E., Moretto, A., Formaggio, F., Toniolo, C. *Chirality* (2011) in press.
4. Arikuma, Y., Nakayama, H., Morita, T., Kimura, S. *Langmuir* **27**, 1530-1535 (2011), and references therein.

The Fully-Extended Peptide Conformation: In Search of Stabilizing Features

Fernando Formaggio[1], Gema Ballano[1], Alessandro Moretto[1], Cristina Peggion[1], Marco Crisma[1], Raffaella Lettieri[2], Emanuela Gatto[2], Mariano Venanzi[2], and Claudio Toniolo[1]

[1] *ICB, Padova Unit, CNR, Department of Chemistry, University of Padova, 35131, Padova, Italy;*
[2] *Department of Chemical Sciences and Technologies, University of Rome "Tor Vergata", 00133, Rome, Italy*

Introduction

In the last 25 years the highly crystalline nature of the peptides rich in C^α-tetrasubstituted residues was exploited to characterize at atomic resolution the fully-extended (C_5) conformation (Figure 1A) and the related 2.0_5-helix by X-ray diffraction analyses. In particular, multiple, consecutive C_5 conformations were observed in homo-peptides having two side chains longer than a methyl [1,2]. For instance, this is the case for the achiral Deg ($C^{\alpha,\alpha}$-diethylglycine) (Figure 1B), the residue investigated in this study.

Further evidence for this conclusion came from spectroscopic studies in solution and conformational energy computations [1-4]. Interestingly, the axial translation per residue in the 2.0_5-helix is about 3.70 Å, the longest possible for a single amino acid, thus making this conformation extremely attractive for its use as a spacer or bridge [5]. For review articles on this novel peptide conformation, see refs. [6,7]. More recently, however, Tanaka *et al.* [8] have found that this type of helical structure is not very robust, as subtle perturbations in the chemical structure and environment can induce a dramatic conformational switch to the (40%) shorter 3_{10}-helix.

Results and Discussion

With the aim at detecting the most appropriate chemical structures and experimental conditions for the stabilization of the 2.0_5-helix, we synthesized and characterized in solution and in the crystal state several additional series of Deg homo-peptides, differing by the nature of the N- and/or C-terminal protecting (or blocking) groups. Our findings are as follows:

(i) The N-terminal group most suitable to stabilize the 2.0_5-helix is Tfa (trifluoroacetyl), thanks to its property to generate an additional intramolecular H-bond, F·H-N(N-terminal). Other amide or urethane N-terminal protections may accomplish a similar role, at least in $CHCl_3$ solution.

A **B**
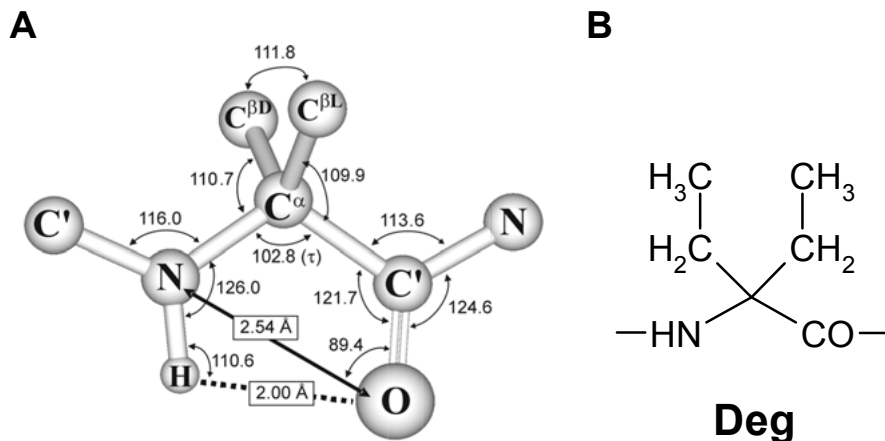
Fig. 1. *(A)Average geometrical parameters for the fully-extended, intramolecularly H-bonded, C_5 conformation from a statistical analysis of the X-ray diffraction structures. (**B**) Chemical formula of Deg.*

(ii) Either an ester (especially a *tert*-butyl ester) or a tertiary amide at the C-terminus is compatible with the 2.0_5-helix. Conversely, primary and secondary amides favor the formation of a 3_{10}-helix (Figure 2).

(iii) The absence or nature of solvent is crucial in governing the Deg homo-peptide conformation. In particular, crystal-packing forces and type of crystallization solvent may induce a 3_{10}-helical structure in an otherwise fully-extended peptide in CDCl$_3$ [9]. Also, we synthesized a $(Deg)_{1-3}$ homo-peptide series with a pyrenylacetyl fluorophore at the N-terminus and a *para*-nitrobenzyloxy quencher at the C-terminus. A preliminary time-resolved fluorescence analysis clearly shows that the peptides are predominantly fully extended in CHCl$_3$, but folded in MeCN or MeOH.
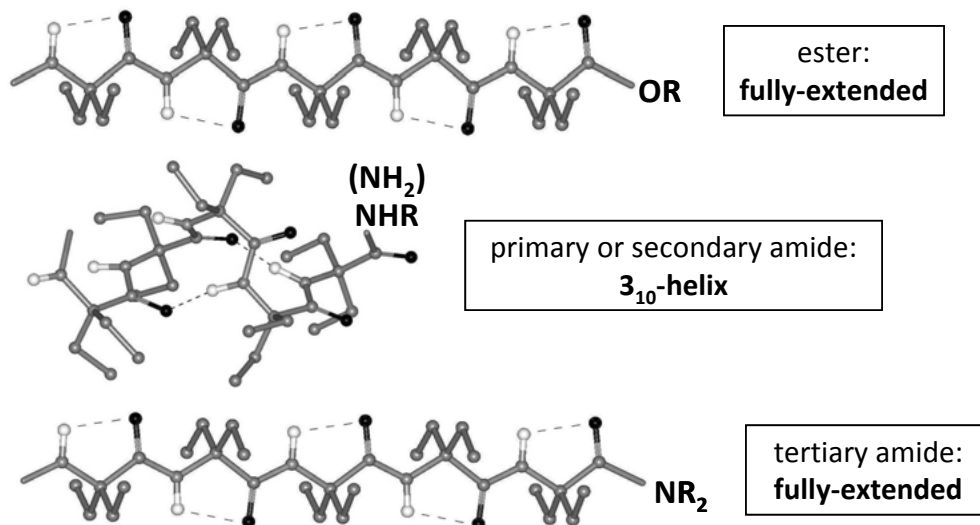
Fig. 2. Effect of the C-terminal protecting (blocking) group on the conformation adopted by the $(Deg)_n$ homo-peptide chain.

Acknowledgments

References

1. Toniolo, C., Benedetti, E. In Balaram, P., Ramaseshan, S. (Eds.) *Molecular Conformation and Biological Interactions*, Indian Academy of Sciences, Bangalore, India, 1991, p. 511.
2. Benedetti, E., Barone, V., Bavoso, A., Di Blasio, B., Lelj, F., Pavone, V., Pedone, C., Bonora, G.M., Toniolo, C., Leplawy, M.T., Kaczmarek, K., Redlinski, A. *Biopolymers* **27**, 357-371 (1988).
3. Toniolo, C., Bonora, G.M., Bavoso, A., Benedetti, E., Di Blasio, B., Pavone, V., Pedone, C., Barone, V., Lelj, F., Leplawy, M.T., Kaczmarek, K., Redlinski, A. *Biopolymers* **27**, 373-379 (1988).
4. Torras, J., Zanuy, D., Crisma, M., Toniolo, C., Betran, O., Alemán, C. *Biopolymers (Pept. Sci.)* **90**, 695-706 (2008).
5. Toniolo, C., Crisma, M., Formaggio, F., Peggion, C., Broxterman, Q.B., Kaptein, B. *Biopolymers (Pept. Sci.)* **76**, 162-176 (2004).
6. Benedetti, E., Di Blasio, B., Pavone, V., Pedone, C., Toniolo, C., Crisma, M. *Biopolymers* **32**, 453-456 (1992).
7. Crisma, M., Formaggio, F., Moretto, A., Toniolo, C. *Biopolymers (Pept. Sci.)* **84**, 3-12 (2006).
8. Tanaka, M., Imawaka, M., Kurihara, N., Suemune, H. *Helv. Chim. Acta* **82**, 494-510 (1999).
9. Crisma, M., Ballano, G., Formaggio, F., Moretto, A., Toniolo, C., unpublished results.

3$_{10}$-Helical Ladder Peptides Using Alkene Metathesis

Matteo De Poli[1], Sheharbano Sangji[2†], Alessandro Moretto[1], Fernando Formaggio[1], Robert H. Grubbs[3], Daniel J. O'Leary[2], and Claudio Toniolo[1]

[1]*ICB, Padova Unit, CNR, Department of Chemistry, University of Padova, 35131, Padova, Italy;*
[2]*Department of Chemistry, Pomona College, Claremont, CA, 91711, U.S.A.;* [3]*Division of Chemistry and Chemical Engineering, California Institute of Technology, Pasadena, CA, 91125, U.S.A.*

Introduction

After having investigated the stereoselectivity and conformational effects of the ring-closing metathesis (RCM) reaction in 3$_{10}$-helical peptides [1], we decided to use the metathesis reaction to generate ladder peptides based on a bundle of two Aib-rich 3$_{10}$-helices held together by two (or more) linkers. The present communication describes the results of the initial phase of this joint project, which was inspired by the Senior Thesis at Pomona College by the late S. Sangji. 3D-structural elucidation of these bundles could offer an important insight into the packing pattern of 3$_{10}$-helical peptides.

Results and Discussion

Our target was to synthesize and chemically and conformationally characterize the parallel ladder peptide shown in Figure 1, by taking advantage of two consecutive alkene metathesis reactions, namely a cross (self)-metathesis followed by RCM (Figure 2), both performed by aid of the second-generation Grubbs' catalyst and using as reactants the O-allylated side chains of two Asp guest residues incorporated at the *i*, *i*+3 internal positions into an Aib host homo-pentapeptide. The two saturated cross-links originate from two hydrogenation reactions on the diastereomeric mixtures resulting from each of the two metathesis reactions. Alternatively, the first (C-terminal) cross-link (peptide **C** in Figure 3) was obtained *via* a two-step *bis*-esterification of the Asp side chain using 1,4-butanediol as the nucleophile.
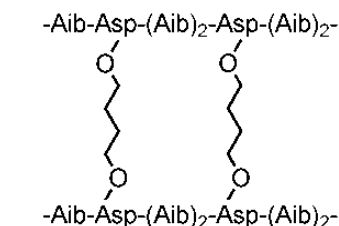
Fig. 1. The target ladder peptide.

The side-chain linked, heptapeptide intermediate dimer (**A**) and the cyclic compound (**B**) are both folded in 3$_{10}$-helix conformations according to our preliminary FT-IR absorption, CD, and NMR analyses.
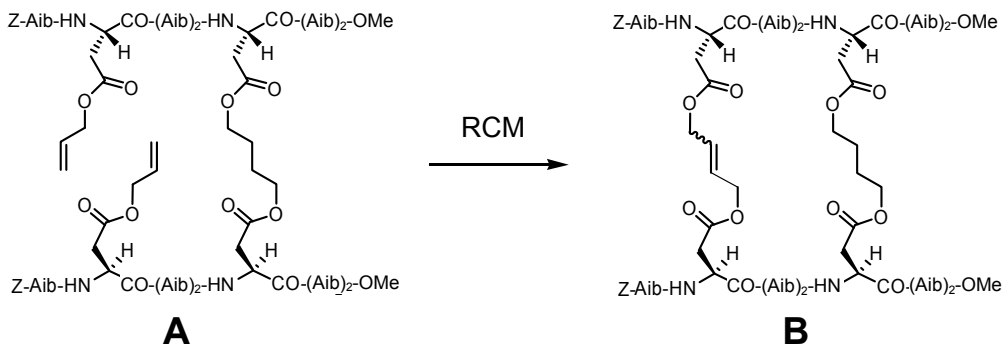
*Fig. 2. Macrocyclization of the peptide intermediate **A** using the second generation Grubbs' catalyst.*

---
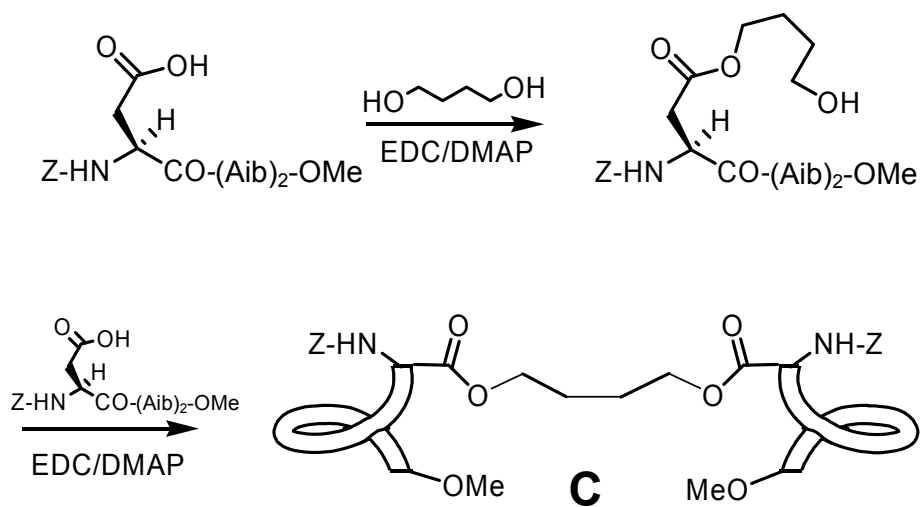
*Fig. 3. Synthesis of the peptide intermediate (**C**) via double esterification with 1,4-butanediol.*

References

1. Boal, A.K., Guryanov, I., Moretto, A., Crisma, M., Lanni, E.L., Toniolo, C., Grubbs, R.H., O'Leary, D.J. *J. Am. Chem. Soc.* **129**, 6986-6987 (2007).

Model Peptide Aggregates: The Role of Aromatic Interactions and Conformational Aspects

Mario Caruso[1], Gema Ballano[2], Fernando Formaggio[2], Claudio Toniolo[2], and Mariano Venanzi[1]

[1]*Department of Chemical Sciences and Technologies, University of Rome "Tor Vergata", 00133, Rome, Italy;* [2]*ICB, Padova Unit, CNR, Department of Chemistry, University of Padova, 35131, Padova, Italy*

Introduction

The study of the early aggregation steps of model peptides is mostly relevant for our understanding of the molecular processes leading to neurological diseases (*e.g.*, Alzheimer and Creutzfeld-Jacob diseases) or the assembly of peptide-based materials (hydrogels, fibrils, nanotubes) [1]. Experimental evidence indicates that aggregation is determined by a complex interplay of interchain interactions and structural effects, with a specific role played by the interaction of aromatic residues. Conformational aspects related to the secondary structure attained by the peptide building blocks and its effect on the formation of the small peptide clusters which nucleate aggregation are also relevant. In this study, the aggregation propensities of two Ala-based pentapeptides [Py-CH$_2$-CO-(L-Ala)$_5$-OtBu (**A5P**) and Py-CH$_2$-CO-(L-Ala)$_3$-Aib-L-Ala-OtBu (**A3UAP**)], both functionalized with a pyrene (Py) aromatic chromophore at the N-terminus, have been investigated in methanol/water solvent mixtures by optical spectroscopies and in dried conditions by atomic force microscopy. In **A3UAP**, an Aib residue, a well-known β-sheet breaker, was inserted in the sequence to study the effect of secondary structure perturbation on the aggregation properties of the peptides investigated.

Results and Discussion

The aggregation propensities of **A5P** and **A3UAP** in solution were investigated by several spectroscopic techniques (UV-Vis absorption, steady-state and time-resolved fluorescence, infrared absorption, electronic circular dichroism), triggering the process by adding increasing fractions of water to a methanol solution. Upon increasing the water content, bathochromic and hypochromic effects on the positions and intensities of the UV-Vis absorption bands of **A5P** were observed, which suggest formation of J-aggregates, *i.e.* stacked arrays of aromatic groups characterized by the slip angle $\alpha = \pi/2$. The spectral shift of the center of mass of the transition, *i.e.* the intensity-weighted maximum wavelength, emphasizes the cooperative character of the process. Fluorescence spectra of **A5P** at increasing peptide concentrations (1-20 μM) show a remarkable decrease of the intensity, also characteristic of J-aggregates. On the contrary, neither the absorption nor the fluorescence spectral features of **A3UAP** in the same concentration range show any significant change.

The aggregation process can also be characterized by fluorescence excitation spectra measured at 390 nm, where the monomer emission predominates, and at 460 nm (excimer emission). While **AUA3P** shows overlapping excitation spectra at both emission wavelengths, **A5P** exhibits a significant bathochromic shift of the (0,0) transition and a general broadening of the spectrum at 460 nm. This result confirms the formation of J-type aggregates in **A5P**, but not in **AU3AP**.

The ATR-IR spectra of the pyrene-functionalized peptides in a (30:70 v/v) water/methanol solution revealed interesting differences, particularly in the amide I region. **A5P** exhibits a strong absorption band at 1631 cm^{-1}, characteristic of peptide groups involved in a β-sheet structure. Conversely, in the ATR-IR spectrum of **AU3AP**, measured under the same conditions, no evidence of such absorption feature could be detected. The CD spectrum of **A5P** in the same water/methanol solution shows formation of chiral aggregates leading to intense dichroic bands in the UV-Vis regions of the amide and pyrene transitions. Significantly, the CD spectrum of **A3UAP** did not reveal any equivalent dichroic feature in the pyrene absorption region, showing only the onset of a negative band at $\lambda < 220$ nm.

AFM measurements, carried out on dried peptide films supported on mica, highlighted that **A3UAP** forms globular structures (Figure 1, left). This morphology is characteristic of an unspecific aggregation, driven by hydrophobic interactions promoted by the presence of the

aromatic moieties. Conversely, **A5P** shows filamentous fibrils, several microns long (Figure 1, right) typical of extended β-sheet domains.

These results confirm the influence of the aromatic groups in the aggregation process, but also emphasize the importance of peptide conformation in generating the small peptide clusters which nucleate the growth of the mesoscopic structures.
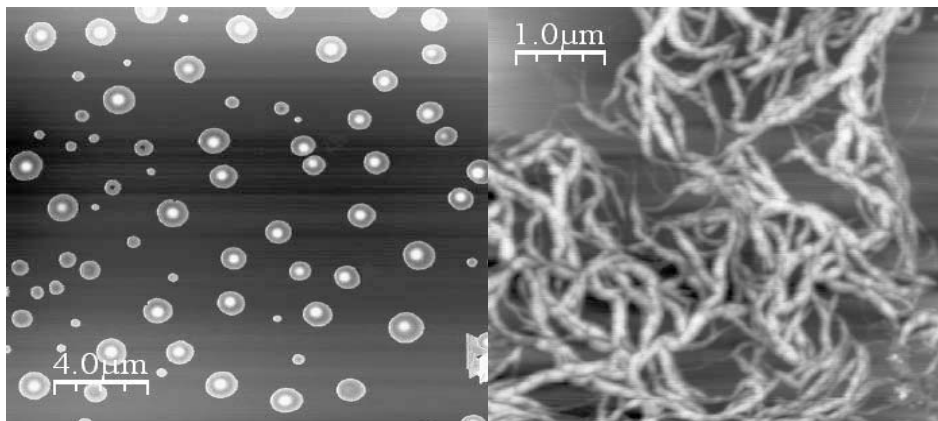
*Fig. 1. AFM image of **A3UAP** (left) and **A5P** (right) dried on a mica surface from a 10 µM 30:70 v/v water/methanol solution.*

References

1. Hamley, I.W., Brown, G.D., Castelletto, V., Cheng, G., Venanzi, M., Caruso, M., Placidi, E., Aleman, C., Revilla-Lopez, G., Zanuy, D. *J. Phys. Chem. B* **114**, 10674-10683 (2010).

A *bis-para*-Carboxylated, *para*-Azobenzene Photoswitchable, Cᵅ-Tetrasubstituted α-Amino Ester Dimer for Supramolecular Applications

Alessandro Moretto[1], Paola Fatás[2], Ana I. Jiménez[2], Carlos Cativiela[2], and Claudio Toniolo[1]

[1]*ICB, Padova Unit, CNR, Department of Chemistry, University of Padova, 35131, Padova, Italy;*
[2]*Department of Organic Chemistry, ICMA, University of Zaragoza-CSIC, 50009, Zaragoza, Spain*

Introduction

We have previously described [1] the synthesis and chemical characterization of the two achiral, Cᵅ-tetrasubstituted α-amino acids, each characterized by two azobenzene moieties covalently linked to their α-carbon atom, namely *bis*[4-(phenylazo)benzyl]Gly (*p*AzoDbg) and its *bis*[3-(phenylazo)benzyl]Gly (*m*AzoDbg) analog. These "albatross-like" compounds were characterized by UV-Vis spectroscopies and one of them by X-ray diffraction as well. Also, we found that they undergo multiple, reversible isomerizations by irradiation with Vis light (to *trans*) or UV light (to *cis*). We also unraveled an intermediate state in the interconversion process, namely the racemate of the *trans/cis* and *cis/trans* configurational isomers.

Since the reversible photoswitch transformation in azobenzene chemical species is useful for various types of applications [2], we have extended our investigation to a *bis-para*-carboxylated *p*AzoDbg (*p*C*p*AzoDbg) α-amino acid derivative.

Results and Discussion

We prepared the ethyl ester of *p*C*p*AzoDbg by treatment with TFA of the side-chain-protected *bis-tert*-butyl ester. Then, this α-amino/α-ester was side-chain *bis*-coupled to the previously prepared, 3₁₀-helical octapeptide H-(Aib-Ala)₄-OMe using HATU. Finally, the resulting molecule was covalently dimerized at its Nᵅ-functionality using fumaric acyl chloride. This final system (**1**) possesses five photoswitchable (*cis* and *trans*) regions, namely four azobenzenes and one fumaric/maleic acid moieties (Figure 1). Compound **1** was characterized by UV-Vis spectroscopies, NMR and mass spectrometry.

We find that even this dimeric compound undergoes a multiple, reversible isomerization of the azobenzene moieties by irradiation with 450 nm Vis light (to *trans*) or 350 nm UV light (to *cis*) (Figure 2).

We are currently extending the study of this complex system **1** to supramolecular chemistry (*e.g.*, rotaxane formation) and to the utilization of the additional *cis/trans* (fumaric/maleic) region.
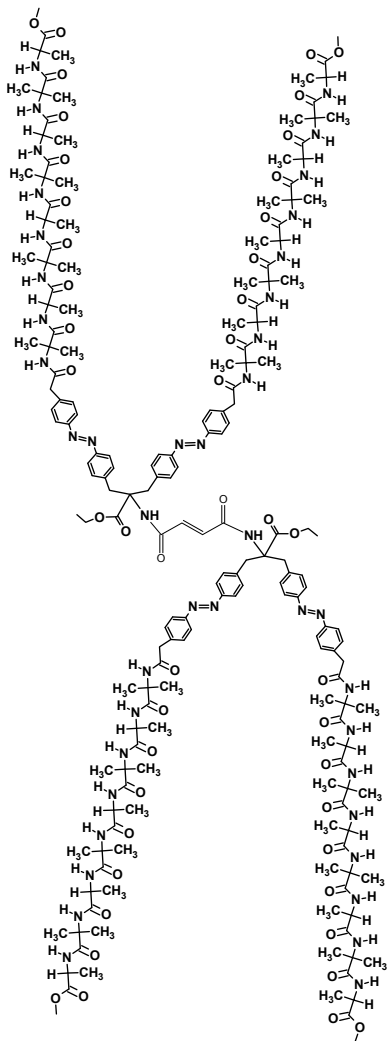
Fig. 1. The dimeric peptide molecule (1) synthesized and studied in this work.
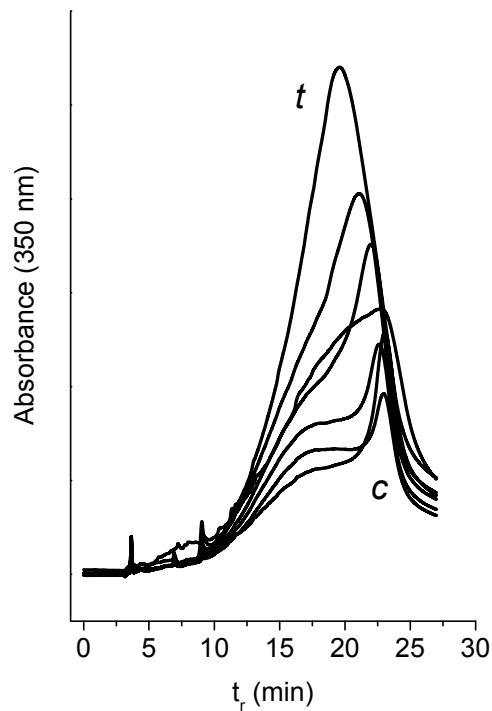
*Fig. 2. Light (350 nm)-driven azobenzene trans-to-cis isomerization kinetics of the fumaric acid dimerized, side-chain bis-substituted, H-pCpAzoDbg-OEt derivative **1** as recorded by HPLC (t indicates the curve of the all-trans compound and c that of the largely prevailing all-cis compound).*

References

1. Moretto, A., Crisma, M., Fatás, P., Ballano, G., Jimenez, A. I., Cativiela, C., Toniolo, C., In Lebl, M., Meldal, M., Jensen, K.J. and Hoeg-Jensen, T. (Eds.) *Peptides 2010: Tales of Peptides (Proceedings of the 31st European Peptide Symposium)*, Prompt Sci. Publ., San Diego, CA, 2010, p. 12.
2. Schrader, T.E., Cordes, T., Schreier, W.J., Koller, F.O., Dong, S.-L., Moroder, L., Zinth, W. *J. Phys. Chem. B* **115**, 5219-5226 (2011).

A 2,5-Dioxopiperazine-Based Molecular Shuttle

Alessandro Moretto, Edoardo Longo, Fernando Formaggio, and Claudio Toniolo

ICB, Padova Unit, CNR, Department of Chemistry, University of Padova, 35131, Padova, Italy

Introduction

2,5-Dioxopiperazines or 2,5-diketopiperazines (DKP) are members of a class of cyclic organic compounds that result from double peptide bond formation between two amino acids to afford a *bis*-lactam. They are the smallest cyclic peptides. Due to their conformationally restricted structure, chiral nature, and varying side chains, DKP are an attractive scaffold for drug design [1,2].

   We are currently interested in rotaxanes, mechanically interlocked molecular architectures in which a central linear molecule (axle) is threaded in the cavity of a macrocycle (wheel). Simple peptido[2]rotaxanes, based on varying -Gly-Xxx- dipeptide stations in the axle, were first reported by Leigh and coworkers [3]. Subsequently, more complex peptido[2]rotaxanes, based on a 3_{10}-helical axle, were described by our group [4]. Our present interest is to expand this field by synthesizing and studying peptido[2]rotaxane molecular shuttles, part of the axle of which is composed of DKP, planned as stations for the reversible motion of a tetrabenzamido macrocycle wheel.

Results and Discussion

We synthesized first the axle of the symmetrical peptido[2]rotaxane using the Boc-Lys-Lys(diphenylacetyl)-OCH$_3$ dipeptide, which was subsequently dimerized *via* reaction of the Lys ε-NH$_2$ functions with fumaric acyl chloride. Then, we assembled the tetrabenzamido wheel developed by Leigh and coworkers [3] on top of the fumardiamide station to obtain rotaxane **1** (Figure 1) having two diphenylacetamido stoppers.
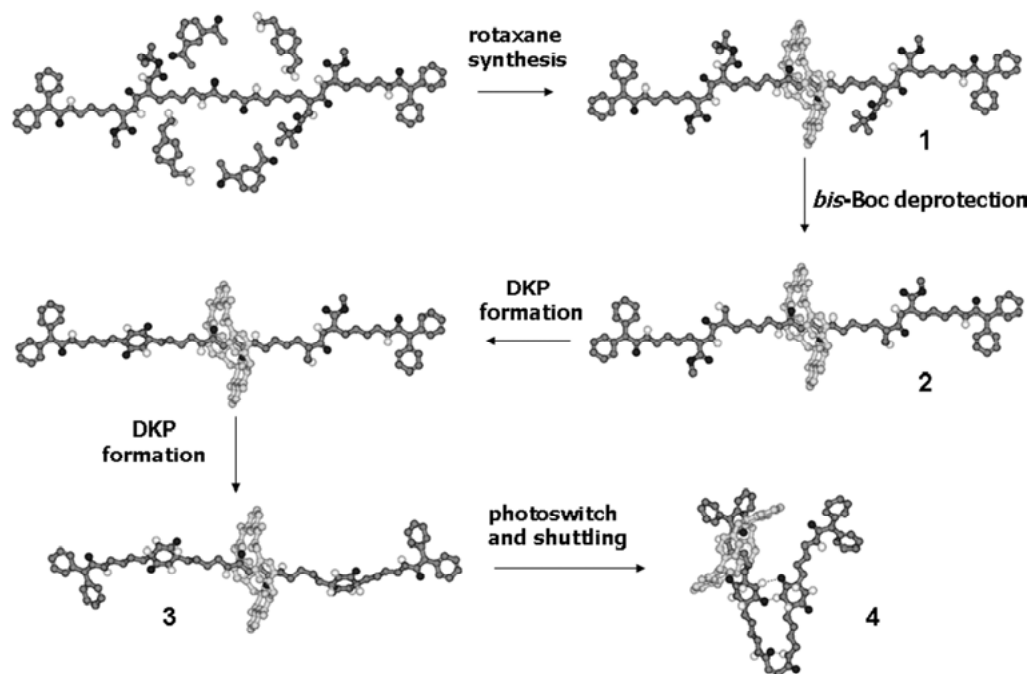
*Fig. 1. The peptido[2]rotaxanes (**1-4**) studied in this work.*

Acidic removal of the two Boc Lys α-amino protections furnished **2**, which was subsequently *bis*-cyclized to the double DKP peptido[2]rotaxane [**3**] using CN⁻-catalysis and heating in MeCN.

Upon irradiation of **3** at 256 nm in DMSO solution, the tetrabenzamido wheel travels along the axle, eventually reaching one of the two DKP stations and providing peptido[2]rotaxane **4**. Both types of stations can interact effectively with the wheel through multiple hydrogen bondings. Figure 2 shows the ^{1}H NMR spectra of peptido[2]rotaxanes **1**, **3**, and **4**, which highlight in particular the differences between the isomeric peptido[2]rotaxanes **3** and **4**.
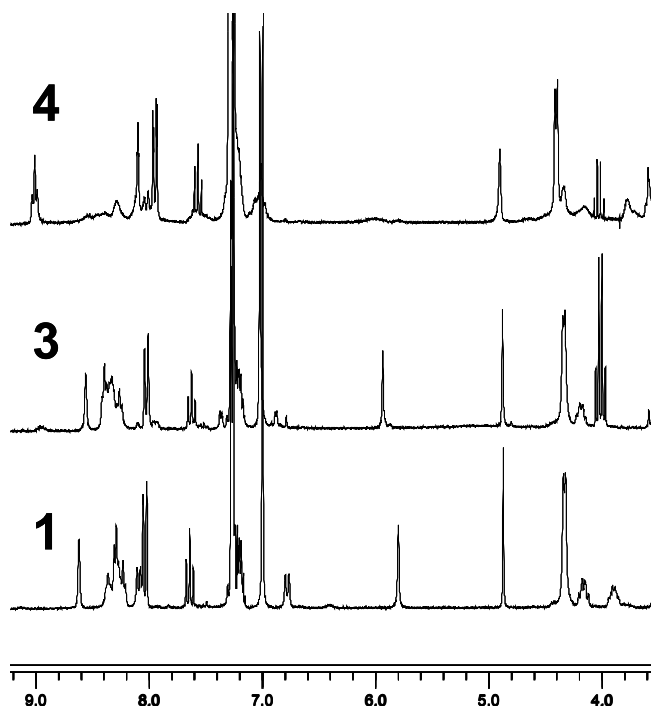
*Fig. 2. Low-field portions of the ^{1}H NMR spectra of peptido[2]rotaxanes **1, 3**, and **4** in DMSO,d$_6$ solution.*

References

1. Martin, M.B., Carvalho, I. *Tetrahedron* **63**, 9923-9932 (2007).
2. Ressurreição, A.S.M., Delatouche, R., Gennari, C., Piarulli, U. *Eur. J. Org. Chem.* 217-228 (2011).
3. Clegg, W., Gimenez-Saiz, C., Leigh, D.A., Murphy, A., Slawin, A.M.Z., Teat, S.J. *J. Am. Chem. Soc.* **121**, 4124-4129 (1999).
4. Moretto, A., Menegazzo, I., Crisma, M., Shotton, E.J., Nowell, H., Mammi, S., Toniolo, C. *Angew. Chem. Int. Ed.* **48**, 8986-8989 (2009).

Oligo(*p*-phenylenevinylene)-Peptide Conjugates in Water: Synthesis and Self-Assembly Properties

Alessandro Moretto[1,2], Miriam Mba[1], Lidia Armelao[1,3], Marco Crisma[1,2], Michele Maggini[1], and Claudio Toniolo[1,2]

[1]*Department of Chemistry, University of Padova, 35131, Padova, Italy;* [2] *ICB-CNR, Padova Unit, Italy;* [3]*ISTM-CNR, INSTM, Italy*

Introduction

Molecular self-organization is a useful approach to prepare soft and flexible, functional micro- and nano-architectures. A practical principle to self-assemble structures is based on simple π-π stacking interactions of π-conjugated oligomers. Self-assembly (SA) of functionalized oligo(*p*-phenylenevinylene)s (**OPV**), for instance, gives organogels with interesting photophysical properties and potential applications in light-emitting diodes, light-harvesting systems or thermal imaging [1]. However, organized, robust molecular structures are difficult to obtain by π-π stacking alone.

Therefore, a variety of promoters able to establish additional noncovalent interactions, such as directional hydrogen bonds, have recently received increasing attention. Among them, peptide amphiphiles, made of a π-conjugated unit and carefully selected peptide sequences, have been investigated in view of their strong tendency to form well-defined secondary structures and to self-assemble in water [2].

Results and Discussion

In this communication, we describe synthesis and SA characteristics of two **OPV**-peptide conjugates (**OPV-1** and **OPV-2**) in which a new **OPV**-based ω-amino acid was incorporated in two different β-sheet forming sequences [3]. The synthesis of the Fmoc-protected **OPV** derivative (**6**) is shown in Scheme 1. The X-ray diffraction structure of the Boc/O*t*Bu amino
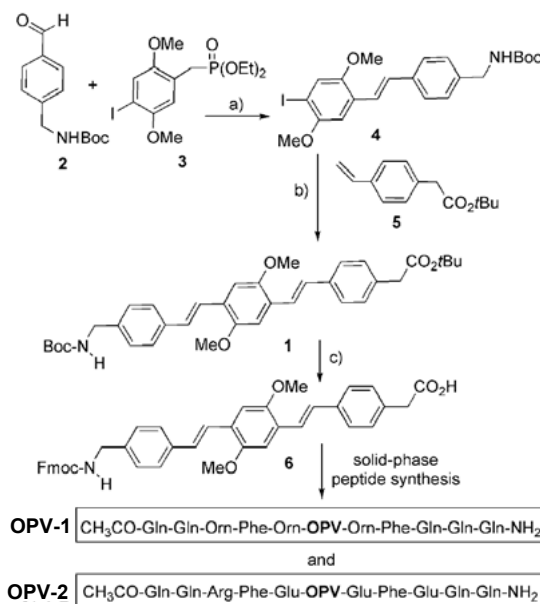
Scheme 1. Synthesis of the Fmoc-protected **OPV** (**6**) derivative and the peptides **OPV-1** and **OPV-2**. Reagents and conditions: a) NaH, THF, 25°C, 6 h, 78%; b) Pd(OAc)$_2$, triethylamine, tri(o-tolyl)phosphine, DMF, 90°C, microwave, 15 min, 63%; c) trifluoroacetic acid, CH$_2$Cl$_2$, 25°C, 2h, then trimethylsilyl chloride, diisopropylethylamine, 9-fluorenylmethyl-chloroformate, 24h, 87%.

acid derivative synthetic intermediate (**1**) is reported in Figure 1. The *trans-trans* configuration of the two C=C bonds is confirmed. As the distance from the N-terminal nitrogen (N1) to the C-terminal carbonyl carbon is 21.2 Å, **OPV** might serve as a replacement for five α-amino acid units in a β-strand. Standard Fmoc-mediated SPPS afforded peptides **OPV-1** and **OPV-2** in about 50% isolated yield after purification.

In these systems, a reversible SA to a stable, fluorescent hydrogel was triggered by changing pH. In particular, as documented by our IR and UV absorption, and CD experiments, the Orn(ornithine)-rich **OPV-1** self-assembles at basic pH, whereas for **OPV-2**, which contains Glu residues, SA occurs at acidic pH. A detailed (TEM and AFM) analysis of the SAs revealed the formation of complex networks in which helical fibers are present [4].
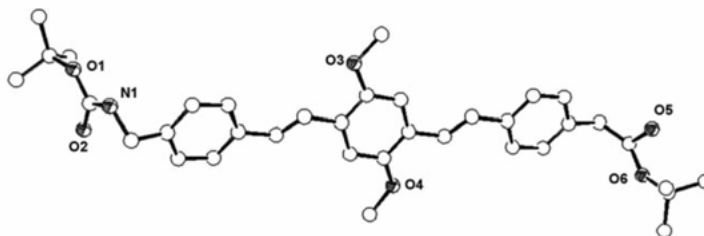
*Fig. 1. X-Ray diffraction structure of the Boc–**OPV**–OtBu amino acid derivative **1** with heteroatom numbering.*

References

1. Srinivasan, S., Babu, P.A., Mahesh, S., Ajayaghosh, A. *J. Am. Chem. Soc.* **131**, 15122-15123 (2009).
2. Babu, S.S., Mahesh, S., Kartha, K.K., Ajayaghosh, A. *Chem. Asian J.* **4**, 824-829 (2009).
3. Davies, R.P.W., Aggeli, A., Beevers, A.J., Boden, N., Carrick, L.M., Fishwick, C.W.G., McLeish, T.C. B., Nyrkova, I., Semenov, A.N. *Supramol. Chem.* **18**, 435-443 (2006).
4. Mba, M., Moretto, A., Armelao, L., Crisma, M., Toniolo, C., Maggini, M. *Chem. Eur. J.* **17**, 2044-2047 (2011).

^{19}F Solid-State NMR Investigations of an Alamethicin F50/5 Analog Carrying a CF$_3$CO- Label

Evgeniy S. Salnikov[1], Jesus Raya[1], Cristina Peggion[2], Gema Ballano[2], Claudio Toniolo[2], Jan Raap[3], and Burkhard Bechinger[1]

[1]*Institute of Chemistry, University of Strasbourg /CNRS-UMR 7177, 67070, Strasbourg, France;* [2]*ICB, Padova Unit, CNR, Department of Chemistry, University of Padova, 35131, Padova, Italy;* [3]*Leiden Institute of Chemistry, Gorlaeus Laboratories, University of Leiden, 2300, RA Leiden, The Netherlands*

Introduction

Peptaibiotics bind to lipid membranes and self-associate into oligomers [1]. In particular, we are currently investigating this phenomenon in a long (19-mer) peptaibiotic alamethicin (Alm) F50/5 analog (a membrane channel former and highly helical peptide). To this goal, we recently synthesized via solution methods a set of Alm analogs bearing the CF$_3$CO-^{19}F probe. In order to investigate oligomer formation, the ^{19}F-labelled [Dab(CF$_3$CO)^9] Alm analog, where Dab is α,γ-diaminobutyric acid, was reconstituted into phospholipid bilayers and the ^{19}F solid-state NMR spectra recorded using MAS. The orientation dependence of the ^{19}F chemical shift interactions is a pre-requisite to count the number of peptides within an oligomeric state using the centerband-only detection of exchange (CODEX) solid-state NMR. This technique was successfully applied to the transmembrane peptide of the M2 protein bound to lipid membranes [2].

Results and Discussion

In order to test the aggregation state of Alm by ^{19}F solid-state NMR methods, slow peptide motions have to be eliminated. To this end, the NMR spectra were recorded at low temperatures. One-dimensional ^{19}F NMR spectra indicate that at 240 K and 250 K the ^{19}F chemical shift anisotropy is 48 ppm, a value similar to the static powder limit for this label [3]. At temperatures > 262 K the [Dab(CF$_3$CO)^9] Alm analog exhibits motional averaging of the ^{19}F chemical shift anisotropy, whereas at 250 K dipolar spin diffusion remains as the only mechanism of magnetization exchange. At the same time, fast rotation of the CF$_3$ group (occurring in the GHz frequency range) makes all three fluorine atoms magnetically equivalent.

Figure 1a shows the CODEX curve of the Alm analog in POPC (1-palmitoyl-2-oleoyl-*sn*-glicero-3-phosphocholine) at 240 K and a representative set of spectra, where in one the signal diminishes under spin-exchange conditions (S), and is compared to another experiment where this process is absent (S$_0$). Uncertainties in the S/S_0 values were estimated from the spectral signal-to-noise ratios. At long exchange mixing times, the initial magnetization is equally distributed among n orientations in the cluster, reducing the CODEX echo intensity to $1/n$. Thus, the equilibrium value of the exchange intensity gives the oligomeric number of aggregating peptide molecules or the number of magnetically inequivalent molecules in a crystal unit cell. The S/S_0 value of the longest mixing time is 0.16 ± 0.04, which is consistent with a transmembrane pentameric bundle. Notably, at 247 K the Alm analog adopts a transmembrane topology when reconstituted into the POPC membrane [4]. To fit the data, a bi-exponential function $S/S_0 = 0.186 + 0.334\ e^{-t/1} + 0.510\ e^{-t/200}$ was used (solid line) which shows an excellent agreement with the experimental data.

The simulated spin diffusion curve with $r = 5.8$ Å fits experimental values at short mixing times, but it falls below the experimental intensities > 50 ms (Figure 1b). On the other hand, the simulated spin diffusion intensity using an inter-^{19}F distance of $r = 7.5$ Å fits the experimental values at long mixing time, but shows little agreement in the beginning of the curve. This discrepancy reflects the bi-exponential nature of the experimental curve. One possible reason for the bi-exponentiality of the curve is structural heterogeneity of the Alm helical bundle. Alternatively, simulation using a Gaussian distance distribution centered at 7 Å gives an almost perfect agreement with both the short- and long-time points of the experimental data (Figure 1c). Another possible reason for the imperfection of a mono-exponential fit is the phenomenological nature of the 1H-driven spin diffusion theory used to simulate the MAS data.

Free fitting with a bi-exponential function gives an equilibrium value of 0.186. This finding implies that hexamers, which would provide an equilibrium value of 0.17, and even heptamers, with an equilibrium value of 0.14, cannot be completely ruled out from the experimental S/S0 value at the longest mixing times. As an example, the simulation with a symmetric heptamer (Figure 1d) fits the experimental curve with a similar quality as that of a symmetric pentamer.
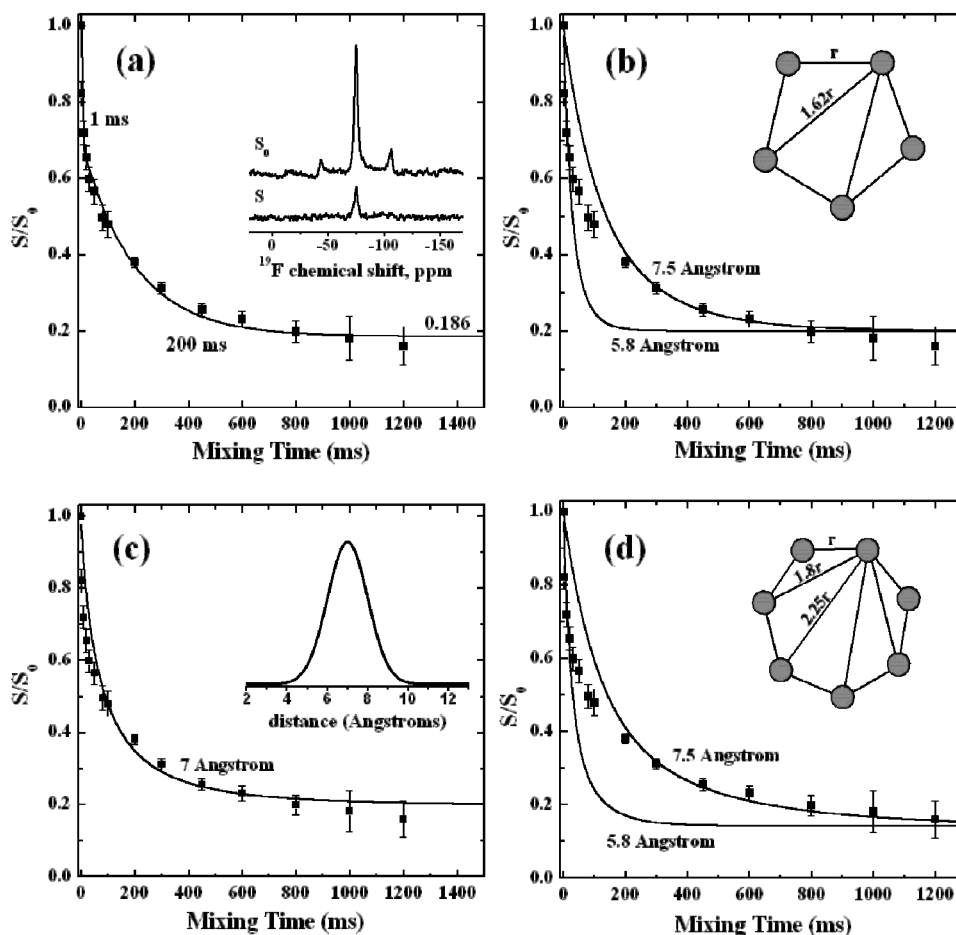
Fig. 1. (a) ^{19}F CODEX data (squares) of the $[Dab(CF_3CO)^9]$ Alm analog in POPC vesicles at 240 K and 15 kHz MAS. The S_0 and S spectra for a mixing time of 600 ms are shown. Unbiased fitting of the data using a bi-exponential gives an equilibrium value of 0.186 ± 0.015. (b) Simulations of the exchange curve (details can be found in ref. [2]) using a symmetric pentamer, which is sketched in the inset. (c) A Gaussian distance distribution centered at 7 Å (inset) for the same pentamer model gives an almost perfect fit for both the short and long mixing times. (d) Simulations of exchange curve with a symmetric heptamer, which is sketched in the inset.

References

1. Toniolo, C., Brückner, H. *Peptaibiotics: Fungal Peptides Containing α-Dialkyl α-Amino Acids,* Wiley-VCD, Weinheim, Germany, 2009.
2. Luo, W., Hong, M. *J. Am. Chem. Soc.* **128**, 7242-7251 (2006).
3. Grage, S.L., Durr, U.H.N., Afonin, S., Mikhailiuk, P.K., Komarov, I.V., Ulrich, A.S. *J. Magn. Reson.* **191**, 16-23 (2008).
4. Salnikov, E.S., De Zotti, M., Formaggio, F., Li, X., Toniolo, C., O'Neil, J.D.J., Raap, J., Dzuba, S.A., Bechinger, B. *J. Phys. Chem. B* **113**, 3034-3042 (2009).

The Structural Features which Explain the Function of Prestin

Sándor Lovas, David Z.Z. He, Marcus P.D. Hatfield, Jason L. Pecka, Oseremen E. Okoruwa, Jie Tang, Shuping Jia, and Kirk W. Beisel

Department of Biomedical Sciences, Creighton University, Omaha, NE, 68178, U.S.A.

Introduction

Prestin is a member of the family of solute carrier 26 (SLC26A) anion transporter proteins [1]. It is the motor protein of the cochlear outer hair cells (OHC) and uniquely functions as a direct voltage-to-force transducer. Prestin is necessary for the electromotility of OHCs and cochlear amplification. Mutations in the prestin gene lead to non-syndromic hearing loss. It is predicted to have a transmembrane helical sulfate transporter (SulpTP) and intracellular STAS domains [1]. Several models have been proposed for the SulpTP topology but these are insufficient to provide a cohesive explanation of the results of site-directed mutagenesis and residue deletions. Furthermore, no experimental structure for any of the SLC26A proteins is available. In this work, we have determined the three-dimensional (3D) structure of the SulpTP domain of rat prestin by combining *ab initio* structure prediction [2], 3D folding recognition by threading [3], homology modeling [4] and molecular dynamics (MD) simulations. Three 100 ns MD simulations of the structure SulpTP domain of prestin was performed in aqueous lipid environment at 300 K, 1 bar atmospheric pressure using the DESMOND package [5]. The protein was embedded in a 1-palmitoyl-2-oleoyl phosphatidyl choline (POPC) lipid bilayer. The predicted transmembrane helical fragment 8 (TM8): Ac-SSLFLGLDYGLITAVIIALLTVIYR-NH$_2$ and the intracellular finger (ICF): Ac-SIGPFAVISLMIGGVAVRLVPDDI-NH$_2$ were synthesized by solid phase peptide synthesis on a CEM Liberty Microwave peptide synthesizer using N^α-Fmoc chemistry. The secondary structure of the fragments in different solvents was determined by electronic circular dichroism (ECD) spectropolarimetry. Wild type and an ICF-truncated version of prestin were expressed in HEK394 cells and their nonlinear capacitance (NLC) were measured.

Results and Discussion

Using the pGenTHREADER 3D fold recognition method [3] nine different structures were identified as possible 3D templates for the SulpTP domain of rat prestin. These proteins could be classified into biologically related and biologically unrelated groups. Using these structures as templates in homology modeling, the resulting structure of SulpTP was similar to that of the bacterial glutamate/aspartate transporter, Glt$_{Ph}$ [6]. The final homology model, therefore, was built solely on all available X-ray structures of Glt$_{Ph}$. The structure from the homology modeling was further refined by three independent 100 ns MD simulations. Trajectories were submitted to cluster analysis and the central structure of the largest cluster (Figure 1) was further characterized. The major structural features of SulpTP domain are 8 transmembrane (TM) spanning domains, TM3 - TM4 loop, two helical pin (HP) re-entry loops and the intracellular finger (ICF). The structure could be further divided into an outer shell represented by TM1 - TM6 and an inner core (HP1, HP2, TM7 and TM8) that could contain the putative transport-associated and charge sensing features of prestin.
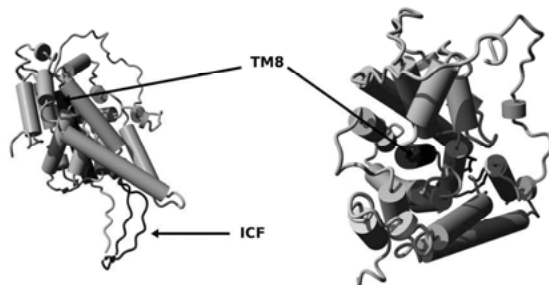
Fig. 1. Central structure of the largest cluster of structures from the trajectories of the simulations. Left, side view; Right, top view. Transmembrane 8 (TM8) and intracellular finger (ICF) are indicated by arrows.
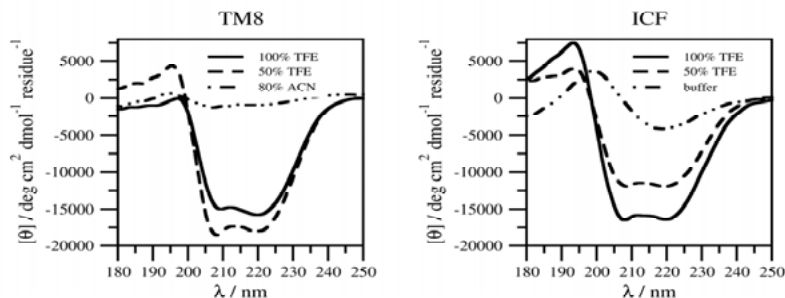
Fig. 2. ECD spectra of fragments of rat prestin in different solutions. Left, TM8 fragment; Right, ICF fragment.
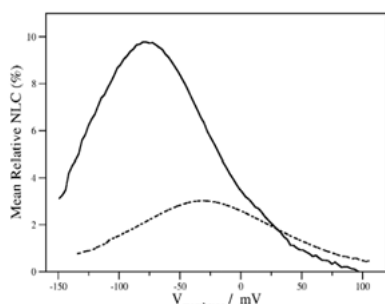
Fig. 3. Non-linear capacitance of prestin (solid line) and ICF-truncated prestin (dashed line).

To support computational findings, regions from TM8 and ICF were selected for solid phase peptide synthesis and subsequent structural characterization using ECD spectropolarimetry. Synthetic fragments were synthesized with N-terminal acetyl and C-terminal amide protections to preserve the electronic structure of the backbone as in prestin.

Molecular dynamics simulations showed that TM8 forms a stable α-helical structure, subsequently, the core region residues 478 to 502 was selected for synthesis. ECD spectra in 80% ACN, 50% TFE and 100% TFE are shown on Figure 2. Since the peptide is part of a TM region and hydrophobic, it was only possible to dissolve it in 80% ACN. The weak signal in this solution could be attributed to either a β-sheet or an aggregated structure. Increasing TFE concentration induced an α-helical conformation which is consistent with structural properties of many well-characterized fragments of different TM proteins.

Residues 133-156 extends into the intracellular regions and during MD simulations form a stabile antiparallel β-sheet structure, hence was it named as ICF. The ECD spectrum of the peptide in 20 mM KH_2PO_4/K_2HPO_4 and 100 mM NaCl (pH 7.0) buffer is same as that of a typical anti-parallel β-sheet structure (Figure 2). The increasing TFE concentration induces conformational change resulting spectra characteristic for mixture of α-helical and β-sheet structures.

Expression of the variant of the rat prestin from which the ICF region missing in HEK394 cells further supports the proposed model that ICF is not part of the TM region of the protein. The substantially decreased non-linear capacitance (Figure 3), however, indicates that ICF is still needed for the full biological activity of prestin.

Acknowledgments

References

1. Dallos, P., Fakler, B. *Nature Rev. Mol. Cell Biol.* **3**, 104-111 (2002).
2. http://bioinf.cs.ucl.ac.uk/psipred/
3. Jones, D.T. *J. Mol. Biol.* **287**, 797-815 (1999).
4. http://www.yasara.org
5. Bowers, K.J., et al. *Proceedings of the ACM/IEEE Conference on Supercomputing (SC06)*, Tampa, Florida, 2006.
6. Yernool, D., Boudker, O., Jin, Y., Gouaux, E. *Nature* **431**, 811-818 (2004).

Structural Importance of the Lid Subdomain of Human Hsp70-1

Marcus P.D. Hatfield and Sándor Lovas

Department of Biomedical Sciences, Creighton University, Omaha, NE, 68178, U.S.A.

Introduction

Heat shock proteins (Hsp) play an important role in the cell by refolding misfolded proteins and participating in numerous housekeeping functions, which allow the cell to survive in stressed environment. The highly conserved 70 kDa Hsp70 chaperones can regulate apoptosis by directly neutralizing the apoptosome or inhibiting caspase-independent cell death effectors [1]. There are eight human isotypes of Hsp70. Cancer cells have increased expression of Hsp70-1. The inhibition of the activity of Hsp70-1 specifically kills cancer cells in cell culture and in xenograft tumor models in mice [2,3].

Hsp70 consists of a nucleotide-binding (NBD) and a substrate-binding domain (SBD) connected by a short inter-domain linker. The SBD consists of a peptide-binding subdomain formed by β-sheets, a lid subdomain formed by α-helices A-E and a tail. The helical lid consists of helix A which connects the β-sheet region to an anti-parallel helical bundle (helices B-E) and serves as a hinge about which the helical bundle can swing.

Although, several X-ray structures for the NBD of human Hsp70 isotypes have been determined, no structures of the entire SBD have been reported so far. Therefore, the structure of the SBD of Hsp70-1 was determined with homology modeling using X-ray structures of DnaK, the bacterial analog of Hsp70, as templates. Homology models were further refined by 50 ns Molecular Dynamics simulations in explicit solvent to examine the stability of the models and to examine the mechanisms of lid movement.

Results and Discussion

The sequence of Hsp70-1 was submitted to YASARA homology modeling [4] using slow modeling speed, 6 PSI-BLAST iterations per template search, a maximum of 10 templates in monomeric form, 5 alignment variations per template, 50 loop samples and a TermExtension of 10 residues.

No hybrid model had a better scoring than the initial models, so the initial model based on the protein with PDB code 1DKX, [5] was used to construct the initial model. 1DKX is a 2 Å resolution structure of the SBD of DnaK in complex with a substrate peptide with a final Z-score of 0.042 and encompassing residues 1 to 235 of the SBD. Since the homology modeling did not provide a structure for residues 236 to 252 of Hsp70-1, further modeling was performed using two methods.

In model **1**, the terminal residues were attached to the homology model in YASARA using random coil dihedrals. The model structure was then subjected to energy minimization and refinement in YASARA.

In model **2**, the tail sequence of residues 227 to 252 of Hsp70-1 was submitted for homology modeling. The PSI-BLAST search for the tail only yielded one hit, a protein with PDB code 3LOF, which is a 2.40 Å resolution structure of the C-terminal domain of human
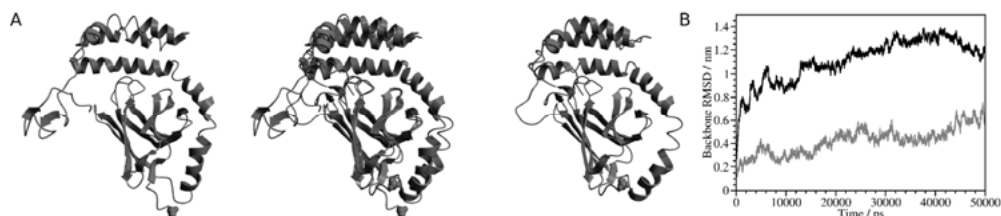
*Fig. 1. A). The middle structures of the largest cluster from the 50 ns trajectories of model **1** (left) and model **2** (right) of Hsp70-1 superimposed (center) along the peptide binding region. B).Backbone RMSD from the starting structure along the trajectory of the 50 ns simulation of model **1** (black) and model **2** (grey).*

Hsp70-1b, which produced a model with a Z-score of -0.315. The tail model was submitted to refinement in YASARA. The refined tail model and model **1** were then subjected to a 10 ns MD simulation. The trajectories of these simulations were subjected to cluster analysis and the middle structures were superimposed using the backbone atoms of residues 229 and 230 of Hsp70-1.

50 ns MD simulations of the structures of models **1** and **2** were performed with the GROMACS 3.3.1 software package [6] and the OPLSAA force field. The SBD was solvated with SPC water at 300 K and 1 bar pressure by coupling the system to an external heat bath using the method of Berendsen [7]. A reaction-field correction was used for long range electrostatic interactions, and a dispersion correction was used for energy and pressure.
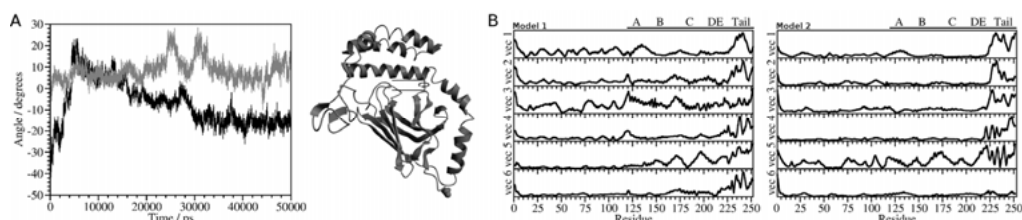
*Fig. 2. A). Orientation of the lid (helix B) to the peptide binding pocket (inner loops) as defined by the dihedral between backbone atoms 1233, 241, 2346 and 2505 for model **1** (black) and model **2** (grey). B). RMSF of the top 6 eigenvectors calculated from the simulations of models 1 and 2. The position of the different helices in the primary structure of the lid and the tail are shown above.*

The representative structures from the simulations (Figure 1A) and the backbone RMSD (Figure 1B) indicate that both models are stable throughout the simulation. The superimposed structure indicates that both models had the same conformation except for a rotation of the tail.

In model **1**, after 5 ns, the angle of the hinge gradually decreases to about -15° indicating a gradual lid movement, while in model **2**, the fluctuation is reduced to 0° to 10° with brief, 3 to 4 ns, increases to 25° to 30° (Figure 2A).

The plots of the RMSF (Figure 2B) of the projection of the trajectory into the top 6 eigenvectors based on essential dynamics analysis showed that most of the peaks occur at the region between helices which allows for movement of the helices relative to each other. Peaks are present in the middle of helix B. In model **1**, this peak is broader than in model **2**. In model **1**, this motion is likely due to the unraveling of the helix, while in model **2**, the eigenvectors are describing the bending of the helix.

The analysis of the 50 ns MD simulations of Hsp70-1indicates that both models are stable, but the lid of model **2** shows a more well-defined movement. The two models showed that the lid can move in relation to the peptide-binding pocket by the unraveling or kinking of helix B, the movement of helix A, or the hinge movement of the residues between helix A and B. These models are the first step in the design of peptides that specifically bind to and inhibit the activity of Hsp70-1.

Acknowledgments

References

1. Galluzzi, L., Giordanetto, F., Kroemer, G. *Mol. Cell*. **36**, 176-177 (2009).
2. Nylandsted, J., Rohde, M., Brand, K., Bastholm, L., Elling, F; Jäättelä, M. *Proc. Natl. Acad. Sci. U.S.A.* **97**, 7871-7876 (2000).
3. Wei, Y.Q., Zhao, X., Kariya, Y., Teshigawara, K., Uchida, A. *Cancer Immunol. Immunother*. **40**, 73-78 (1995).
4. Krieger, E., Koraimann, G., Vriend, G. *Proteins* **47**, 393-402 (2002).
5. Zhu, X., Zhao, X., Burkholder, W.F., Gragerov, A., Ogata, C.M., Gottesman, M.E., Hendrickson, W. A. *Science* **272**, 1606-1614 (1996).
6. Lindahl, E., Hess, B., Van der Spoel, D. *J. Mol. Mod.* **7**, 306-317 (2001).
7. Berendsen, H.J.C., Postma, J.P.M., DiNola, A., Haak, J.R. *J. Chem. Phys.* **81**, 3684-3690 (1984).

Helical Secondary Structures of Oligopeptides Composed of Chiral Five-membered Ring Amino Acids

Masakazu Tanaka[1], Masanobu Nagano[2], Yosuke Demizu[3], Mitsunobu Doi[4], Masaaki Kurihara[3], and Hiroshi Suemune[2]

[1]Graduate School of Biomedical Sciences, Nagasaki University, Nagasaki, 852-8521, Japan; [2]Graduate School of Pharmaceutical Sciences, Kyushu University, Fukuoka, 812-8582, Japan; [3]Division of Organic Chemistry, National Institute of Health Sciences, Tokyo, 158-8501, Japan; [4]Osaka University of Pharmaceutical Sciences, Osaka, 569-1094, Japan

Introduction

Homopeptides composed of achiral cyclic amino acids form 3_{10}-helical structures, in which both right-handed and left-handed screw sense of helices exist [1]. We have reported that homo-chiral homopeptides composed of chiral cyclic amino acid (S,S)-Ac$_5$c^{dOM} having side-chain chiral centers but not having α-carbon chiral centers, preferentially form left-handed (M) helical structures [2]. The left-handed helical-screw sense was exclusively controlled by the side chain chiral centers, without an α-carbon chiral center. Herein, we synthesized two diastereomeric five-membered ring α-amino acids $(1S,3S)$- and $(1R,3S)$-1-amino-3-(methoxy)cyclopentanecarboxylic acids (Ac$_5$c^{OM}), prepared two series of Ac$_5$c^{OM} homo-chiral homopeptides, and studied their preferred secondary structures [3].

Results and Discussion

Two diastereomeric five-membered ring amino acids $(1S,3S)$- and $(1R,3S)$-Ac$_5$c^{OM} were synthesized starting from L-(-)-malic acid (Figure 1). At first, malic acid was converted to a diester, and then the secondary alcohol was converted to a methyl ether. Reduction of diester, followed by substitution of the primary alcohol with iodide gave a diiodide **1**. Dialkylation of dimethyl malonate with **1** produced a cyclopentane diester **2** in 75% yield. Monohydrolysis of **2** under alkaline conditions, followed by Curtius rearrangement with diphenylphophoryl azide afforded two diastereomeric five-membered ring amino acids $(1S,3S)$- and $(1R,3S)$-Ac$_5$c^{OM} in a ratio of 3 : 1 in 85% yield. Oligomers Cbz-{$(1S,3S)$-Ac$_5$c^{OM}}$_m$-OMe {m = 10, up to decamer} and Cbz-{$(1R,3S)$-Ac$_5$c^{OM}}$_n$-OMe {n = 10, up to decamer} were generally prepared by the coupling between N-terminal-free oligomers and N-protected dimer-acid in solution-phase methods. However, elongation of N-terminal-free $(1R,3S)$-Ac$_5$c^{OM} dimer to a tetramer did not work well due to diketopiperazine formation. Thus, the $(1R,3S)$-tetramer was prepared via a trimer, which was derived from an N-terminal-free amino acid and the dimer-acid.
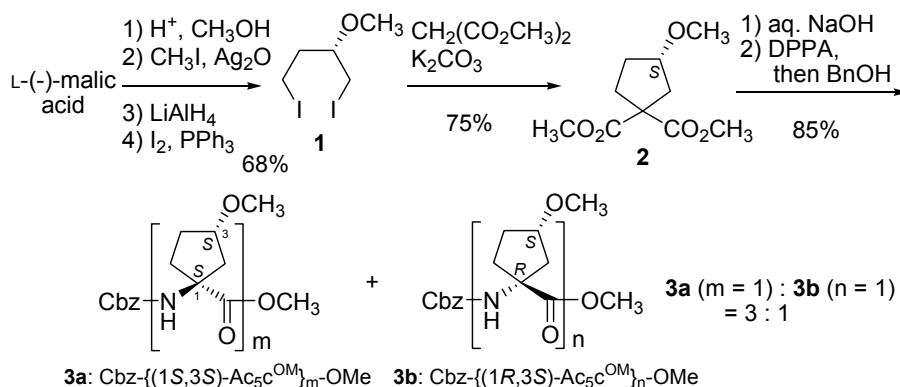
Fig. 1. Synthesis of chiral five-membered ring amino acids.

In the CD spectra, none of tetramers and hexamers in trifluoroethanol solution, neither (1*S*,3*S*)- nor (1*R*,3*S*)-Ac$_5$c^{OM}, showed characteristic maxima (208 and 222 nm) for the helical structure, suggesting the presence of both right-handed (*P*) and left-handed (*M*) helices or disordered structures. By elongation of oligomer length, positive maxima at 208 and 222 nm were observed in the CD spectra of (1*S*,3*S*)-octamer and decamer, while negative maxima were seen in the (1*R*,3*S*)-octamer and decamer. These CD spectra suggest that the dominant conformation of (1*S*,3*S*)-octamer and decamer is a left-handed (*M*) helix, and that of (1*R*,3*S*)-ones is a right-handed (*P*) helix.

The X-ray analysis of (1*S*,3*S*)-Ac$_5$c^{OM} hexamer showed both diastereomeric right-handed (*P*) and left-handed (*M*) 3$_{10}$-helices, and that of (1*S*,3*S*)-octamer showed only left-handed (*M*) 3$_{10}$-helices. In contrast to the (1*S*,3*S*)-Ac$_5$c^{OM} peptides, the diastereomeric (1*R*,3*S*)-Ac$_5$c^{OM} hexamer showed two conformers, which were both right-handed (*P*) 3$_{10}$-helices. The (1*R*,3*S*)-octamer also showed two conformers, both (*P*) 3$_{10}$-helices, in which six consecutive intramolecular H-bonds of the $i \leftarrow i+3$ type ($i = 0 \sim 5$) were found, respectively (Figure 2). By the elongation of peptide-length, the (1*R*,3*S*)-decamer showed two (*P*) α-helices having seven consecutive H-bonds of the $i \leftarrow i+4$ type ($i = 0 \sim 6$), respectively.

These analyses indicated that, up to hexamer, both (1*S*,3*S*)- and (1*R*,3*S*)-chiral five-membered ring amino acid oligomers respectively formed both diastereomeric right-handed (*P*) and left-handed (*M*) helical conformations in solution. In the crystal state, the (1*S*,3*S*)-hexamer assumed both (*P*) and (*M*) 3$_{10}$-helices as in solution, while the (1*R*,3*S*)-hexamer formed only (*P*) helices, probably influenced by the crystal packing force. By the elongation of peptide-length, both (1*S*,3*S*)- and (1*R*,3*S*)-Ac$_5$c^{OM} oligomers were controlled to form one-handed helical-screw structures, *i.e.*, by the increase of chiral centers, the (1*S*,3*S*)-Ac$_5$c^{OM} octamer preferentially formed (*M*) helices and the (1*R*,3*S*)-Ac$_5$c^{OM} octamer and decamer formed (*P*) helices.
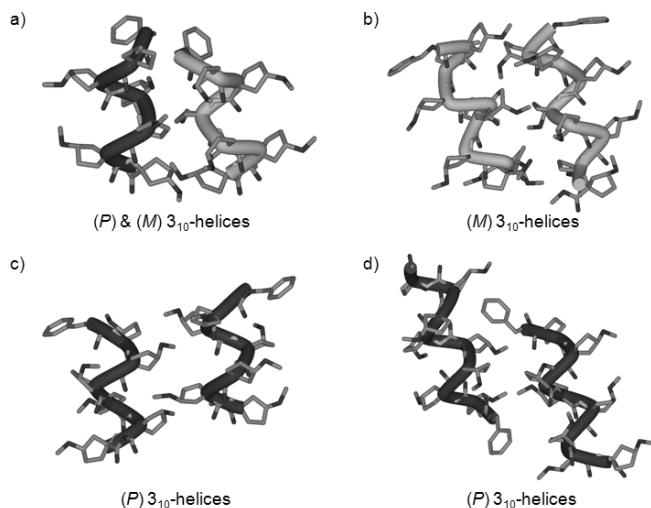
Fig. 2. X-ray crystallographic analyses. a). (1S,3S)-Ac$_5$c^{OM} hexamer. b). (1S,3S)-Ac$_5$c^{OM} octamer. c). (1R,3S)-Ac$_5$c^{OM} hexamer. d). (1R,3S)-Ac$_5$c^{OM} octamer.

Acknowledgments

References

1. Santini, A., Barone, V., Bavoso, A., Benedetti, E., Di Blasio, B., Fraternali, F., Lelj, F., Pavone, V., Pedone, C., Crisma, M., Bonora, G.M., Toniolo, C. *Int. J. Biol. Macromol.* **10**, 292-299 (1988).
2. Tanaka, M., Demizu, Y., Doi, M., Kurihara, M., Suemune, H. *Angew. Chem., Int. Ed.* **43**, 5360-5363 (2004).
3. Nagano, M., Tanaka, M., Doi, M., Demizu, Y., Kurihara, M., Suemune, H. *Org. Lett.* **11**, 1135-1137 (2009).

Design of a Stabilized Short Helical Peptide and Its Application

Masaaki Kurihara[1], Yusuke Demizu[1], Nanako Yamagata[1], Yukiko Sato[1], Yuki Takeuchi[1], Mitsunobu Doi[2], Masakazu Tanaka[3], and Haruhiro Okuda[1]

[1]Division of Organic Chemistry, National Institute of Health Sciences, Tokyo, 158-8501, Japan; [2]Osaka University of Pharmaceutical Sciences, Osaka, 569-1094, Japan; [3]Graduate School of Biomedical Sciences, Nagasaki University, Nagasaki, 852-8521, Japan

Introduction

The *de novo* design of peptides and proteins is of extraordinary importance in the fields of organic chemistry, nanotechnology, and medicinal chemistry. A variety of approaches to controlling the conformations of peptides have been investigated, and the incorporation of α,α-disubstituted α-amino acids [1,2] and cross-linked side chains into peptide sequences is of vital importance for constructing stable helical structures.

Results and Discussion

We speculated that stable helical structures could be constructed using a combination of α,α-disubstituted α-amino acids and a covalent cross-linking system. Here, we have designed and synthesized four L-leucine (L-Leu) based heptapeptides containing an α-aminoisobutyric acid at the 4th position as a helical promoter and L/D-(homo)serine derivatives at the 3rd and 7th positions to produce a cross-linked subunit (Figure 1). Their dominant conformations were studied using IR, NMR, and CD spectra in solution, and X-ray crystallographic analysis in the crystalline state. Stable helical peptides are expected to be catalysts and inhibitors of protein-protein interaction (Figure 2).

$S_{3,7}S$-2, $S_{3,7}R$-2, $R_{3,7}S$-2, $R_{3,7}R$-2, $hS_{3,7}S$-2, $hS_{3,7}R$-2, $hS_{3,7}hS$-2
S: L-Ser derivative, **R**: D-Ser derivative, **hS**: L-Hse derivative
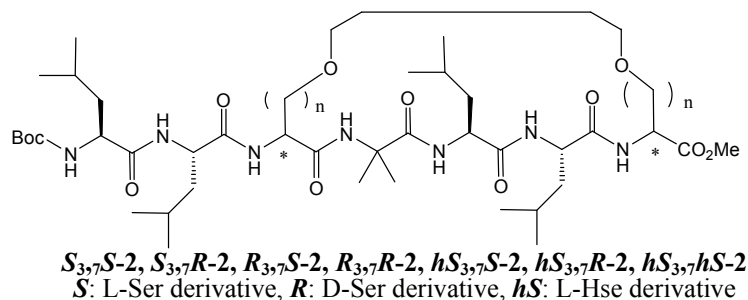
Fig. 1. Design of stabilized short helical peptides using α,α-disubstituted α-amino acids and a covalent cross-linking system.
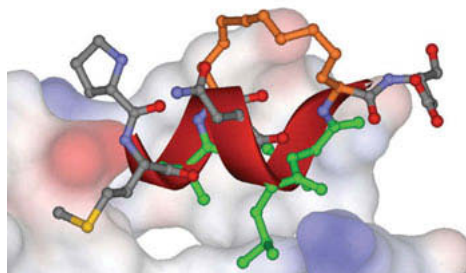
Fig. 2. Model of the interaction between a helical peptide and the surface of nuclear receptor.

We have synthesized L-Leu based heptapeptides that are tethered by L-serine, D-serine, and L-homoserine derivatives at their 3rd and 7th positions. The peptide **hS$_{3,7}$hS-2,** which contained cross-linked L-homoserine derivatives at its 3rd and 7th positions, formed a stable right-handed (*P*) 3_{10}-helix. On the other hand, the peptide **R$_{3,7}$R-2**, which is tethered by D-serine derivatives at the 3rd and 7th positions, formed a (*P*) α-helix (Figure 3).

The peptide R$_{3,7}$R-2 formed suitable crystals for X-ray crystallographic analysis and only one conformer of the peptide molecule was found in the asymmetric unit of the peptide, a right-handed (P) α-helix. Furthermore the peptide inhibited the interaction between vitamin D receptor (VDR) and a coactivator.
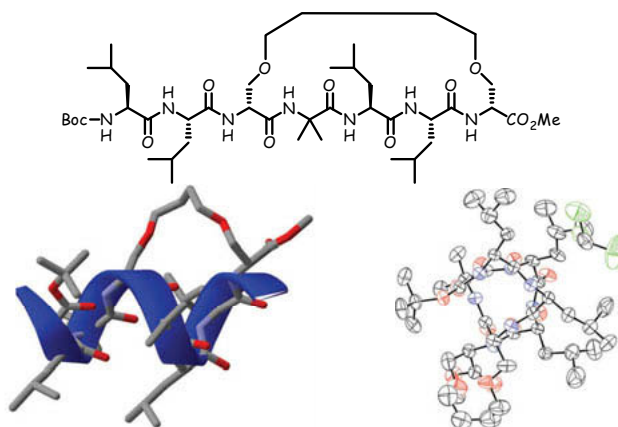
Fig. 3. Right-handed (P)α-helix revealed by x-ray analysis of R$_{3,7}$R-2.

Acknowledgments

References

1. Yamagata, N., Demizu, Y., Sato, Y., Doi, M., Tanaka, M., Nagasawa, K., Okuda, H., Kurihara, M. *Tetrahedron Lett.* **52**, 798-801 (2011).
2. Demizu, Y., Yamagata, N., Nagoya, S., Sato, Y., Doi, M., Tanaka, M., Nagasawa, K., Okuda, H., Kurihara, M., *Tetrahedron,* in press.

The Inherently Risky Folding Landscape of a β-Barrel Protein, CRABP1, in the Test Tube and in the Cell

I. Budyak, B. Krishnan, M. Ferrolino, E.M. Clerico, A. Clouser, K.F. Pobre, A. Zhuravleva, and L.M. Gierasch

Department of Biochemistry & Molecular Biology, Univ. of Massachusetts, Amherst, MA, 01003, U.S.A.

Introduction

Protein misfolding and aggregation are implicated in many pathological states, such as the neurodegenerative disorders - Alzheimer's, Parkinson's, and other amyloid diseases. Hence, there is an urgent need to improve our fundamental grasp of protein folding mechanisms in defined media and to link this knowledge to the cellular context, wherein successful maintenance of functional, folded proteins and avoidance of aggregation is crucial. This goal is challenging because the complexities of the cellular environment present major technical challenges to studies of protein folding and misfolding *in vivo*. We are developing approaches to tackle these challenges using as a case study a predominantly β-sheet protein whose *in vitro* folding we are also exploring in detail, cellular retinoic acid-binding protein 1 (CRABP1) [1,2]. We have examined how aggregation competes with folding of CRABP1 *in vitro* and in cells, and we have begun to elucidate its mechanism of aggregation. In the case of CRABP1, the mechanism of aggregation appears to be the same *in vitro* and *in vivo*, and sequence-predicted aggregation-prone regions correlate closely with those that form the cores of isolated aggregates. Based on our results, we hypothesize that dynamic fluctuations between native and near-native states present an inherent risk of aggregation for CRABP1, and that furthermore, such dynamic fluctuations are critical to the functions of this and many other proteins.

Results and Discussion

CRABP1 is a member of the large family of intracellular lipid-binding proteins, which are structurally homologous. They have a β-barrel architecture with 10 antiparallel strands surrounding an internal cavity, and a helix-loop-helix segment that guards the ligand-binding cavity (Figure 1A). Ligand entry and exit requires dynamical fluctuations of the helical region, and NMR studies show enhanced dynamics in this so-called 'portal' region in the apo-protein versus the holo-protein [3]. Kinetic analysis of refolding of CRABP1 using primarily fluorescence of the three intrinsic tryptophans [4], as well as single-Trp mutants [5], and CD signal and H exchange of backbone NHs led to a description of a folding landscape for CRABP1 [6]. The folding of CRABP1 from denaturant solution begins from an ensemble of states that sample locally folded structure at turns III and IV and the helix-turn-helix based on peptide studies [7,8], then collapses hydrophobically to form an early intermediate ensemble (I_1). Next, native topology forms along with the internal ligand-binding cavity, resulting in an ensemble that has native secondary structure, but lacks specific side chain packing and stable β-sheet hydrogen bonding (I_2). The rate-determining step in folding is the exclusion of solvent from between the strands and the specific side chain packing to form the fully compacted core.

No diseases have been identified in which aggregation of CRABP1 or its close relatives are implicated. However, we have found several conditions [9] and point mutations (for example, [10]) that enhance the aggregation propensity of CRABP1, arguing that while its folding landscape is robust, there are high-risk states visited to some extent during folding and under other conditions. As indicated in Figure 1B, the species that leads to aggregation may be close to the unfolded state, a misfolded off-pathway intermediate, an on-pathway intermediate, or a near-native state that arises from conformational fluctuations. Our current data, taken together, support a model in which aggregation initiates from a near-native state (N* in the figure). For example, many point mutations of CRABP1 cause the protein to be a poorly behaved refolder. After denaturant treatment, under conditions where the wild-type protein refolds in high yield to the native fold, these mutants populate a state that lacks distinct signatures of the native fold, such as the tryptophan blue-shift indicative of hydrophobic side chain burial (Figure 1C). Similar behavior is indicated by CD spectra that show secondary structure but lack native features, for example for a variant, Δ3 CRABP1, which is missing the C-terminal three residues
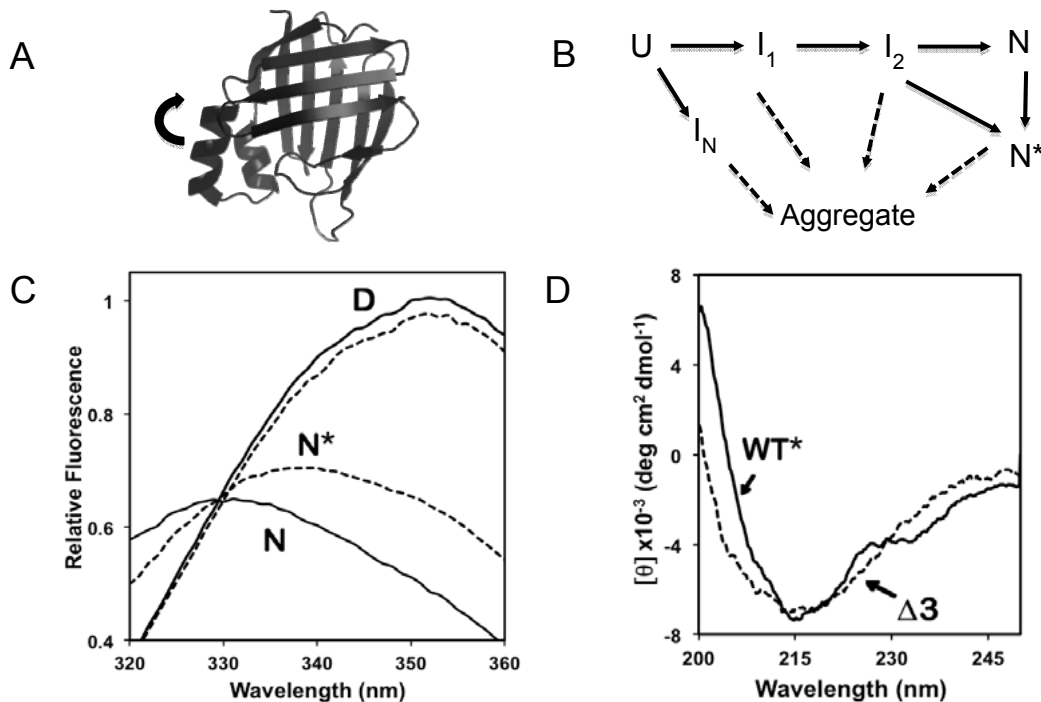
Fig. 1. A) Structure of CRABP1; B) folding pathway with possible routes to aggregation; C) Fluorescence spectra of wild-type (solid lines), and point mutant L118V CRABP1 (dashed lines); D) CD spectra of wild-type (solid line) and Δ3 CRABP1 (dashed line).

(Figure 1D). Acid denaturation followed by salt treatment also leads to a very similar partially folded state [9]. Preliminary analysis of the nature of aggregates formed by all these species has identified the core regions as those strands that surround the opening of the ligand-binding cavity. These strands would be more accessible to intermolecular interaction upon fluctuations of the helical portal region and overall conformational dynamics of the barrel. The very same properties are required for ligand entry and exit from CRABP1 as part of its normal function. Thus, our working hypothesis is that CRABP1 has on its folding landscape a near-native state N* required for binding and release of retinoic acid, which in turn modulates transcription of a specific set of genes. Many perturbations such as mutation, truncation, or alteration of solution conditions can cause over-population of N*, and consequent aggregation, as observed in our work.

We speculate that folding landscapes frequently rely on conformational fluctuations to enable proteins to perform specific functions and thus have near-native minima, which are 'high risk' for aggregation because of the poor solubility of backbone and non-polar side chains.

Acknowledgments

References

1. Ignatova, Z., Gierasch, L.M. *Proc. Natl. Acad. Sci. U.S.A.* **101**, 523 (2004).
2. Ignatova, Z., et al. *Biopolymers* **88**, 157 (2007).
3. Krishnan, V.V., Sukumar, M., Gierasch, L.M., Cosman, M. *Biochemistry* **39**, 9119 (2000).
4. Clark, P.L., Liu, Z.P., Zhang, J., Gierasch, L.M. *Protein Sci.* **5**, 1108 (1996).
5. Clark, P.L., Weston, B.F., Gierasch, L.M. *Fold Des.* **3**, 401 (1998).
6. Clark, P.L., Liu, Z.P., Rizo, J., Gierasch, L.M. *Nat. Struct. Biol.* **4**, 883 (1997).
7. Rotondi, K.S., Gierasch, L.M. *Biochemistry* **42**, 7976 (2003).
8. Sukumar, M., Gierasch, L.M. *Fold Des.* **2**, 211 (1997).
9. Liu, Z.P., Rizo, J., Gierasch, L.M. *Biochemistry* **33**, 134 (1994).
10. Ignatova, Z., Gierasch, L.M. *Biochemistry* **44**, 7266 (2005).

Studies for Optimum Design of Artificial Zinc Finger Recombinases by Evaluation of Effects of DNA Binding Affinity and Linker Components on Recombination Efficiency

Akemi Masuda[1], Wataru Nomura[1], Kenji Ohba[2], Naoki Yamamoto[2], and Hirokazu Tamamura[1]

[1]*Institute of Biomaterials and Bioengineering, Tokyo Medical and Dental University, Tokyo, 101-0062, Japan;* [2] *Yong Loo Lin School of Medicine, National University of Singapore, Singapore, 117597, Singapore*

Introduction

Zinc finger proteins (ZFPs) consist of about 30 amino acids and form a $\beta\beta\alpha$ structure by coordination of zinc ion. Several zinc finger can be applied to chimera enzymes including nucleases [1], recombinases [2,3], and methylases [4]. Artificial recombinases, zinc finger recombinases (ZFRs), however, could have room for improvement of their recombination efficiency. Recombination mechanism of ZFR shows that two dimers form tetramer for strand exchange and the sequence between two target sites is excised from the target gene allele (Figure 1). The resulting sequence could be controlled by this reaction. Therefore, ZFR would be a powerful tool of gene knockout. For the design of highly-active ZFR, effects of DNA binding affinity and linker length of ZFR on recombination efficiency were evaluated.
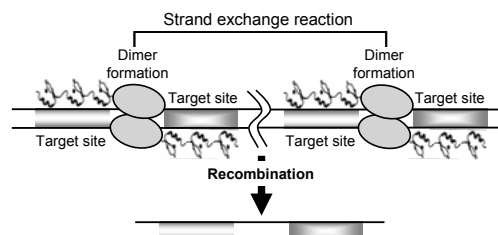
Fig. 1. Reaction mechanism of ZFR.

Table 1. Recombination efficiency of finger-number variants in E. coli

Finger numbers	Ratio of recombination
2 fingers	0
3 fingers	0.68 ± 0.013
4 fingers	1.1 ± 0.0065
5 fingers	1.1 ± 0.0094
6 fingers	1 ± 0.036

Results and Discussion

For construction of artificial recombinases, catalytic domain of Tn3 resolvase was utilized. As catalytic domains and DNA binding domains of serine recombinases, such as Tn3, are structurally separated, members of serine recombinase family are ideal candidates for this fusion study.

The target sites are composed of 20 bp spacer sequence flanked by 18 bp zinc finger binding sites (ZBS) (Figure 1). The spacer sequence, which is recognized by the catalytic domain, has been reported as Z+4 site for NM resolvase [2]. The plasmids encoding 2- to 6-finger modules were constructed. These ZFPs were expressed as a fusion of maltose binding protein

Table 2. Recombination efficiency of linker variants in E. coli

Linker length (6 fingers)	Ratio of recombination	Flexible linker length (6 fingers)	Ratio of recombination
3 a.a.[a]	0.049 ± 0.013	3 a.a.	0.16 ± 0.009
6 a.a.	0.18 ± 0.009	6 a.a.	1.1 ± 0.026
9 a.a.	0.69 ± 0.012	9 a.a.	1.1 ± 0.009
12 a.a.	1.1 ± 0.040	12 a.a.	1.1 ± 0.056
15 a.a.	1.0 ± 0.018	15 a.a.	1.0 ± 0.053
18 a.a.	0.91 ± 0.056	18 a.a.	1.0 ± 0.032
21 a.a.	0.79 ± 0.031		
24 a.a.	0.63 ± 0.067		
27 a.a.	0.64 ± 0.022		
30 a.a.	0.55 ± 0.035		

[a]*a.a.: amino acids*

(ZFP-MBP) in *E. coli*. ZFP-MBP was purified and employed for ELISA to evaluate DNA binding affinity. The results showed that binding affinity increased from 160 to 13 (nM for K_d) which depends on its finger numbers.

Recombination of ZFR in *E. coli* was tested utilizing a plasmid recombination system. The plasmids encoding ZFR variants and their target sequences were constructed. In this system, ZFRs expressed from plasmids recognize target sequences and recombine. After excision of the region between target sites by recombination, a shorter plasmid was produced. The recombination efficiency was evaluated by restriction enzyme assays. The results showed that increase of recombination efficiency depended on the numbers of finger modules (Table 1). Recombination efficiency corresponded to DNA binding affinity of ZFPs. Recombination efficiency of various linkers was also tested (Table 2). The results showed that ZFR with 12 amino acids linker had the highest recombination efficiency and ZFR with more or less than 12 amino acids linker decreased recombination efficiency. ZFR with flexible linker variants indicated high recombination efficiency except 3 amino acids linker.

Furthermore, recombination of ZFR in mammalian cells was also tested. A CHO-K1 strain, which has EGFP flanked by two target sites on its genome, was constructed. The plasmids encoding ZFR and DsRed were transfected into CHO-K1 cells. The sequences between target sites were excised. Therefore, EGFP positive cells before transfection were changed to both EGFP negative and DsRed positive cells. The changes of fluorescence intensity enable semi-quantitative calculation of recombination efficiency. Forty-eight hours after transfection, fluorescence of cells was detected by FACS. The result showed that recombination efficiency of ZFRs with different finger numbers was similar to that in *E. coli*. On the other hand, recombination efficiency of ZFRs with a different linker sequence showed different tendency from that in *E. coli* (Table 3).

A molecular modeling study was performed to understand these results. It found that the 6 amino-acids linker-sequence could be the optimum length for the fusion enzyme (figure not shown). The mammalian recombination system developed in this study could be a feasible method to detect recombination efficiency within 48 hours after introduction of ZFR-expressing plasmids by transient transfection.

These results were supportive information of recombination efficiency of ZFR. It was indicated that recombination efficiency could be improved by the design of ZFR involving finger numbers and linker lengths. ZFR technology would be applied for genetic studies utilizing gene knock-out or gene therapy in near future.

Table 3. Recombination efficiency of finger-number variants and linker length variants in CHO-K1 cells

Finger numbers	Recombination (%)
2 fingers	6.2 ± 0.09
3 fingers	11.8 ± 0.68
4 fingers	16.1 ± 0.24
5 fingers	19.3 ± 0.32
6 fingers	14.9 ± 0.36
non-binding 5 fingers	5.2 ± 0.77

Linker length	Recombination (%)
5 fingers 15 a.a.	13.8 ± 1.3
6 fingers 0 a.a.	14.9 ± 1.6
6 fingers 6 a.a.	18.6 ± 2.2
6 fingers 12 a.a.	13.1 ± 2.1
6 fingers 15 a.a.	12.8 ± 2.2
6 fingers 30 a.a.	11.2 ± 1.1
non-binding 5 fingers 15 a.a.	6.0 ± 0.6

Acknowledgments

References

1. Miller, J.C., et al. *Nat. Biotechnol*. **25**, 778-785 (2007).
2. Akopikan, A., He, J., Boocock, M.R., Stark, W.M. *Proc. Natl. Acad. Sci. U.S.A.* **100**, 8688-8691 (2003).
3. Gordley, R.M., Smith, J.D., Gräslund, T., Barbas, C.F., III. *J. Mol. Biol.* **367**, 802-813 (2007).
4. Nomura, W., Barbas, C.F., III. *J. Am. Chem. Soc*. **129**, 8676-8677 (2007).

Synthesis of HIV Gp41 Trimer Mimics Inducing Neutralizing Antibodies Based on Remodeling of Dynamic Structures of HIV-1 Envelope Proteins

Wataru Nomura[1], Toru Nakahara[1], Chie Hashimoto[1], Kenji Ohba[2], Tetsuo Narumi[1], Naoki Yamamoto[2], and Hirokazu Tamamura[1]

[1]*Institute of Biomaterials and Bioengineering, Tokyo Medical and Dental University, Chiyoda-ku, Tokyo, 101-0062, Japan;* [2]*Yong Loo Lin School of Medicine, National University of Singapore, Singapore, 117597, Singapore*

Introduction

Development of new anti-HIV drugs such as protease inhibitors and integrase inhibitors has contributed to highly active anti-retroviral therapy (HAART) for AIDS. We have also developed several anti-HIV agents including CXCR4 antagonists [1], CD4 mimics [2] and integrase inhinitors [3]. Although practically useful drugs have been discovered, the antibody therapy is still a promising and desirable treatment. To develop effective HIV vaccines, artificial antigen molecules have been synthesized based on HIV-1 envelope proteins such as gp120 and gp41. Gp41 plays a pivotal role in the membrane fusion process of HIV-1 infection, and is divided by the N-terminal helix region (N36) and the C-terminal helix region (C34). In the membrane fusion process, a six-helical bundle structure of gp41 is formed, which consists of a trimeric coiled-coil of N36 surrounded by three strands of C34 in an antiparallel fashion. Thus, it suggests that antibodies, which recognize the N36 trimer and the C34 trimer, might block HIV-1-entry.

Results and Discussion

Initially, to construct an N36 trimer mimic, three strands of the N36 peptides were assembled on a C3-symmetric template with three equivalent linkers by thiazolidine ligation [4] for chemoselective coupling of an N-terminal Cys-containing unprotected N36 peptide with an aldehyde scaffold-containing three arms (Figure 1) [5]. Sera produced by immunization of the synthetic N36 trimer antigen showed structural preference in binding to the N36 trimer (Figure 2) and higher potent neutralizing activity, compared to sera produced by the N36 monomer immunization. As anti-HIV peptides, the N36 trimer and monomer showed modest inhibitory activity, and the trimer is three times more potent than the monomer. Next, to construct a C34 trimer mimic, three strands of the C34 peptides were assembled on another C3-symmetric template with three equivalent linkers by native chemical ligation for chemoselective coupling of a C-terminal-thioester-containing unprotected C34 peptide with Cys-containing three arms. Sera produced by immunization of the synthetic C34 trimer antigen showed structural preference in binding to the C34 trimer and higher potent neutralizing activity, compared to sera produced by the C34 monomer immunization. It is noteworthy that as
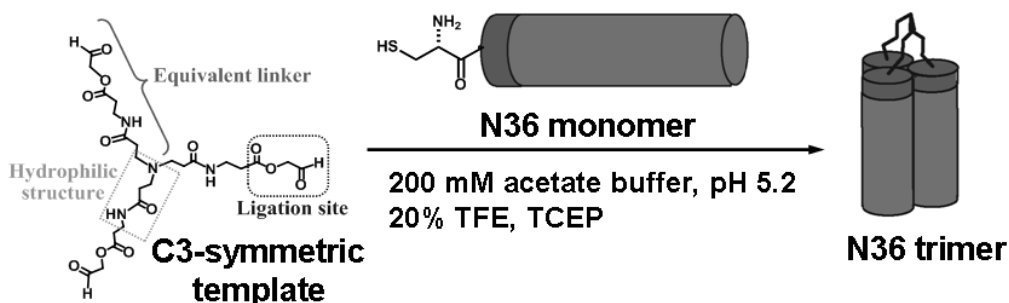
Fig. 1. Synthesis of an N36 trimer assembled on a C3-symmetric template.

anti-HIV peptides, the C34 trimer and monomer showed high inhibitory activity, and that the trimer is 100 times more potent than the monomer (EC$_{50}$ (C34 trimer) = 1.30 nM, EC$_{50}$ (C34 monomer) = 124 nM). The C-region of gp41 such as C34 is known to be critical as fusion inhibitors, and enfuvirtide (Trimeris/Roche) is cross to the C-region. Thus, it can be explained that these C34 monomer and trimer have potent fusion inhibitory activity, but it is difficult to explain the reason for the higher inhibitory activity of the C34 trimer relative to that of the monomer. The elucidation of the detailed action mechanism of the C34 trimer as a fusion inhibitor will be the subject of our future study. There are two advantages in the design of inhibitors and vaccines: The exposed timing of epitopes of the helical region trimers is limited
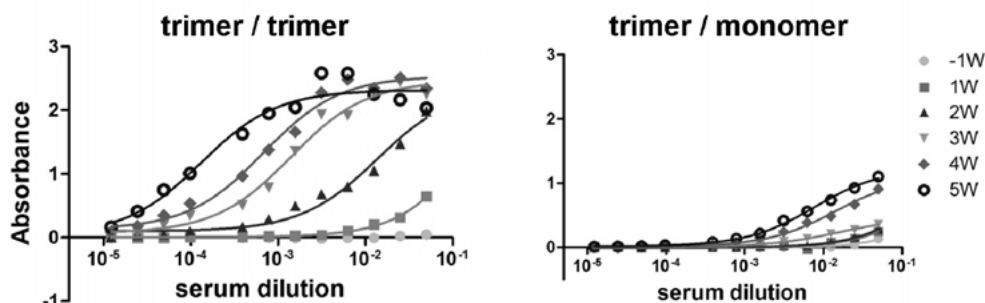
Fig. 2. Results of serum titer ELISA of antisera collected during immunization (from one week before start to five weeks after immunization start) to determine the immunogenicity of designed antigens. The titers were evaluated as followings; antiserum against the N36 trimer binding to the N36 trimer (left) and to the N36 monomer (right).

in the fusion step, and carbohydrates are not included in the amino acid residues of the regions. Burton's group reported the importance of antibody recognition for the trimer form of surface proteins, suggesting the trimer-specific antibodies show broad and potent neutralization [6]. The N36 and C34 trimer-form specific antibodies produced in this study could also obtain the corresponding properties. The elucidation of antibody-producing mechanisms and epitope recognition mode of induced antibodies will be addressed in our future studies. The designs of antigens and inhibitors targeting the dynamic supramolecular mechanism of HIV-1 fusion will be useful for AIDS vaccines and anti-HIV agents.

Acknowledgments

References

1. Liu, C.F., Tam, J.P. *Proc. Natl. Acad. Sci. U.S.A.* **91**, 6584-6588 (1994).
2. Nakahara, T., et al. *Bioconjugate Chem.* **21**, 709-714 (2010).
3. Walker, L.M., et al. *Science* **326**, 285-289 (2009).
4. Tamamura, H., et al. *Biochem. Biophys. Res. Commun.* **253**, 877-882 (1998).
5. Yamada, Y., et al. *Bioorg. Med. Chem. Lett.* **20**, 354-358 (2010).
6. Suzuki, S., et al. *J. Med. Chem.* **53**, 5356-5360 (2010).

Development of Bivalent Ligands for CXCR4 with Rigid Linkers and Application to Detection of Cancer Cells

Wataru Nomura, Tomohiro Tanaka, Akemi Masuda, Tetsuo Narumi, and Hirokazu Tamamura

Institute of Biomaterials and Bioengineering, Tokyo Medical and Dental University, Chiyoda-ku, Tokyo, 101-0062, Japan

Introduction

The chemokine receptor CXCR4 is a membrane protein belonging to the family of G protein-coupled receptors (GPCRs), which are attractive drug targets involving 40% of commercially available drugs. It has been difficult, however, to obtain structural information pertaining to GPCR which is required for drug development. Recent studies have indicated a pivotal role for homo- and hetero-oligomerization of CXCR4 in cancer metastasis and the significance of oligomeric forms of GPCR has been gaining acceptance [1]. In this study, we designed and synthesized novel CXCR4 bivalent ligands consisting of two molecules of [*cyclo*(-D-Tyr-Arg-Arg-Nal-D-Cys-)] (Nal = L-3-(2-naphthyl)alanine) an FC131 analogue [2,3], connected by a poly-L-proline or a PEGylated poly-L-proline linker. Our bivalent ligands with linkers of various lengths were used to determine the distance between two binding sites of ligands consisting of CXCR4 dimers. This approach will expand the utility of the polyproline helix in elucidation of biologically important questions concerning GPCRs. Moreover, by obtaining specificity for the dimeric form of receptors, fluorescent labeling of the ligands would produce a molecular probe specific for oligomerized receptors in cancer diagnosis.

Results and Discussion

Acetamide-capped FC131 (**2**), in which Gly was replaced by D-Cys and the molecule was capped with an acetamide group, was synthesized as a monomer unit of the ligand (Figure 1). Although this substitution causes 2-fold decrease in binding to CXCR4, the binding affinity is still adequate for analyses. In conjugation reaction, the compound **1** was mixed with various proline linkers in ratio of 2:1 in a buffer solution. Poly-L-proline helices are known to maintain a length of 0.9 nm per turn [4]. In this study, polyproline helices covering 2-8 nm of length, and a PEGylated polyproline-type linker covering the same range of length and owing to the PEG moiety, flexible at both ends, were synthesized (Figure 1). The binding affinities of the synthetic ligands were evaluated in a competitive binding assay against [^{125}I]SDF-1α as reported previously [3] (Table 1). It is known [5] that the binding affinities of bivalent GPCR ligands depend on the linker lengths and the binding assay in this study also showed that the binding of bivalent ligands is clearly dependent on the linker lengths. The ligands with the highest affinity in two types of linkers were 20-prolines (**8**) and 12-prolines-PEG (**14**). As monomer controls, FC131 with 6-proline (**17**) or PEG linker (**18**), acetylated at the other end were prepared. In comparison with controls, **8** and **14** showed a 7.3- and 21.2-fold increase of binding affinity, respectively. The results indicate successful bivalent binding of ligands, which has been known to be responsible for an increase in binding affinity. It is of interest that the maximum increase
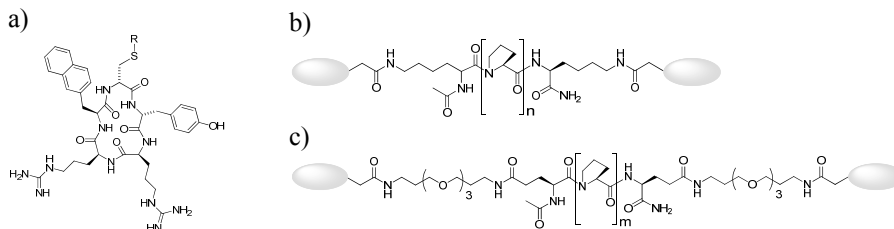
*Fig. 1. Design of bivalent ligands against CXCR4 chemokine receptor. As CXCR4 binding moiety, D-Cys FC131, (R=H, **1**) and acetamide-capped FC131 (R=CH$_2$CONH$_2$, **2**) were prepared (a). Two kinds of linkers, poly-L-proline (b, **3-10**) and PEG-conjugated poly-L-proline (c, **11-16**), with CXCR4 binding moieties on both ends (shown as ovals).*

Table 1. Results of binding assay of ligands by [^{125}I]SDF-1α competition assay

Entry	Ki (nM)	linker length (nm)	Entry	Ki (nM)	linker length (nm)
FC131	31.5	-	**10** (27pro FC131b)	45.8	8.1
2 (Acetamide FC131)	53.4	-	**11** (3proPEG FC131b)	87.2	3.8
3 (6pro FC131b)	51.2	1.8	**12** (6proPEG FC131b)	45.6	4.7
4 (9pro FC131b)	45.4	2.7	**13** (9proPEG FC131b)	17.8	5.6
5 (12pro FC131b)	64.4	3.6	**14** (12proPEG FC131b)	13.9	6.5
6 (15pro FC131b)	59.5	4.5	**15** (15proPEG FC131b)	49.3	7.4
7 (18pro FC131b)	13.2	5.4	**16** (18proPEG FC131b)	83.3	8.3
8 (20pro FC131b)	9.9	6	**17** (Ac6pro FC131)	72	-
9 (23pro FC131b)	22.5	6.9	**18** (AcPEG FC131)	294	-

in binding was observed for linkers of similar length (ca. 5.5-6.5 nm). Molecular modeling studies of the binding site of FC131 suggest that amino acids in transmembrane 7 are important for FC131 binding. Utilizing the rhodopsin structure, it was revealed that in TM4-5 assembly form the distance between ligand binding sites is 5.3 nm. The changes in binding affinity are relatively moderate and the existence of different assembly forms is possible but a majority of the population should be the TM4-5 assembly form. A hypothesis was derived from the increased binding of linkers of the appropriate length that such ligands could be applied as probes specific for CXCR4 on the cell surface as the receptors are overexpressed in several kinds of malignant cells and that the dimer formation of the receptor should depend on the expression level. Accordingly, compound **7**, labeled with tetramethylrhodamine (TAMRA-labeled **7**) (**19**), was synthesized and tested for CXCR4 imaging. To obtain merge images of CXCR4 and ligands, the EGFP gene was fused to C-terminal of the CXCR4 gene and the plasmid containing the gene was transiently transfected. The increase in binding affinity of the bivalent ligand was clearly reflected in the imaging of CXCR4 receptors on the cell surface. When TAMRA-labeled **17** (**20**) was utilized as a monomer ligand, only a trace of bindig was observed. Additionally, binding to mock HeLa cells was not observed for either ligand. To assess further the binding specificity of bivalent ligands to CXCR4 expressed on the cell surface, FACS analysis utilizing Jurkat cells was performed. In the bivalent ligand binding, the MFI changes from 12.34 to 18.86. It is of interest that bivalent ligand showed clear difference from monomer binding, in which the MFI was 13.29 at 25 nM (Figure 2) [6].

Our approach has the advantages that the ligand can directly capture dimeric forms of GPCRs and the linkers can be applied to virtually any known GPCR receptors. Information from such analysis could offer a consensus to the controversial currently unsolved mechanisms.

Fig. 2. Flow cytometric analysis for CXCR4 binding of **19** and **20** to Jurkat cells. Each panel shows binding of **19** (a) and **20** (b). control MFI: 12.34, Dimer (**19**) MFI: 18.86, Monomer (**20**) MFI: 13.29.

Acknowledgments

References

1. George, S.R., O'Dowd, B.F., Lee, S.P. *Nature Rev. Drug Discov.* **1**, 808-820 (2002).
2. Tamamura, H., et al. *Biochem. Biophys. Res. Commun.* **253**, 877-882 (1998).
3. Fujii, N., et al. *Angew. Chem., Int. Ed.* **42**, 3251-3253 (2003).
4. Kuemin, M., et al. *J. Am. Chem. Soc.* **131**, 15474-15482 (2009).
5. Handl, H.L., et al. *Bioconjugate Chem.* **18**, 1101-1109 (2007).
6. Tanaka, T., et al. *J. Am. Chem. Soc.* **130**, 15899-15901 (2010).

Mimicry of Amyloid β-Sheets

Pin-Nan Cheng and James S. Nowick

Department of Chemistry, University of California, Irvine, CA, 92697-2025, U.S.A.

Introduction

Amyloids are peptide or protein aggregates with characteristic cross-β structures that are associated with a variety of neurodegenerative and other diseases [1]. Simpler compounds that mimic these complex aggregates can provide insights into their structures and interactions and may ultimately lead to new therapies for amyloid-related diseases. Developing β-sheet mimics that can display a variety of amyloidogenic amino acid sequences and still fold into β-sheets is difficult, because folding of β-sheet mimics largely depends on the amino acid sequence and a large number of variations exist among the amino acid sequences in amyloid proteins [2,3]. To achieve good folding of β-sheet mimics containing various amino acid sequences from amyloid proteins, we introduce a new class of macrocycles, **1**. Macrocycle **1** (Figure 1) is a 54-membered ring and consists of an amyloidogenic heptapeptide β-strand in the "upper" strand and a Hao β-strand mimic flanked by two dipeptides in the "lower" strand [4]. The "upper" and "lower" strands are linked by two δ-linked ornithine (δOrn) turns [5,6]. The cyclicity, Hao, and δOrn turns are designed to achieve robust folding of the β-sheet mimics that is largely independent of the amino acid sequence [7].
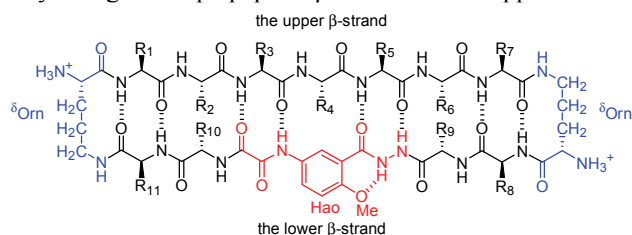
*Fig. 1. Macrocycle **1**.*

Results and Discussion

To examine the folding of macrocycles **1**, we incorporated into the "upper" strand at positions 1–7 a variety of key amyloidogenic heptapeptide sequences from amyloid proteins, including amyloid β-peptide (Aβ), tau protein (Tau), yeast Sup35 prion protein (Sup35), human prion protein (hPrP), β_2-microglobulin (β_2M), α-synuclein (α-Syn), and human islet amyloid polypeptide (hIAPP). We chose hydrophilic and hydrophobic residues at positions 8–11 in the "lower" strands to promote solubility in water and to increase side-chain interactions (Table 1).

Table 1. Amino Acid Sequences of Macrocycles **1**

	sequence	R_1-R_7	R_8-R_{11}		sequence	R_1-R_7	R_8-R_{11}
1a	Aβ$_{16-22}$	KLVFFAE	KLIE	**1i**	hPrP$_{116-122}$	AAAGAVV	KFYK
1b	Aβ$_{17-23}$	LVFFAED	KLIE	**1j**	Tau$_{305-311}$	SVQIVYK	EFYK
1c	Aβ$_{29-35}$	GAIIGLM	KFYK	**1k**	β_2M$_{62-68}$	FYLLYYT	KNSA
1d	Aβ$_{30-36}$	AIIGLMV	KFYK	**1l**	β_2M$_{63-69}$	YLLYYTE	FKVS
1e	Aβ$_{30-36}$ G33F	AIIFLMV	KFYK	**1m**	α-Syn$_{69-75}$	AVVTGVT	KFYV
1f	Aβ$_{34-40}$	LMVGGVV	KFYK	**1n**	α-Syn$_{75-81}$	TAVANKT	VFYK
1g	Aβ$_{34-40}$ G37F	LMVFGVV	KFYK	**1o**	hIAPP$_{11-17}$	RLANFLV	KFYV
1h	Sup 35$_{7-13}$	GQQNNQY	KFYK	**1p**	hIAPP$_{26-32}$	ILSSTNV	KFYK

Macrocycles **1** were easily synthesized by standard Fmoc-based solid-phase peptide synthesis, followed by solution-phase cyclization, deprotection, and purification. Figure 2 summarizes the synthesis of a representative macrocycle, **1a**. Initially, Boc-Orn(Fmoc)-OH was loaded onto 2-chlorotrityl chloride resin and the linear peptide was elongated by standard automated Fmoc solid-phase peptide synthesis. The protected linear peptide was then cleaved from the resin under mildly acidic conditions and cyclized to the corresponding protected cyclic peptide with HCTU and *N,N*-diisopropylethyl-amine in dilute (ca. 0.5 mM) DMF solution. Deprotection with TFA followed by

RP-HPLC purification yielded **1a** in 29% overall yield, based on the loading of Boc-Orn(Fmoc)-OH
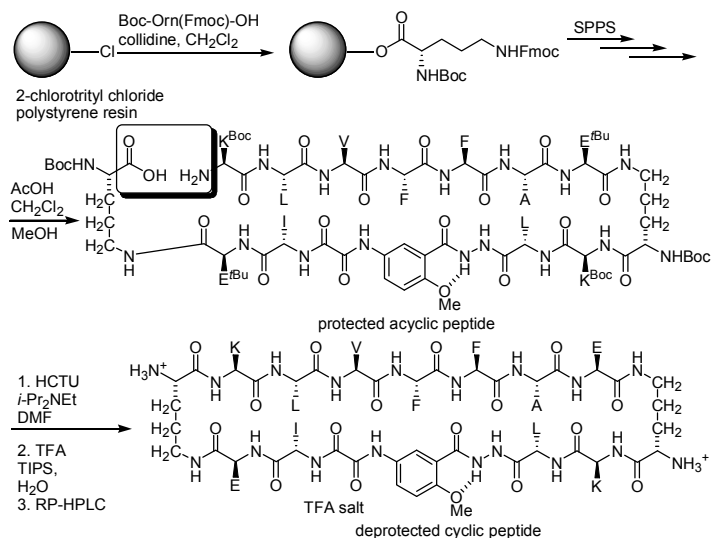
*Fig. 2. Synthesis of macrocycle **1a**.*

onto the resin.
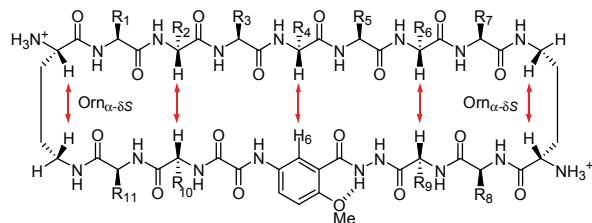
*Fig. 3. Key NOEs in macrocycle **1** in D₂O solution.*

^{1}H NMR studies show that macrocycles **1** fold into β-sheet structures in aqueous solution and do not aggregate significantly at millimolar or submillimolar concentrations. Most of the macrocycles exhibit five characteristic interstrand NOE cross peaks in ROESY studies in D₂O solution that indicate β-sheet folding (Figure 3). Only macrocycles **1h**, **1i**, and **1l** do not appear to fold completely, giving only NOEs associated with the $^\delta$Orn turn structures.

In summary, macrocycles **1** constitute a new family of water-soluble non-aggregating β-sheet mimics that are easy to prepare and well-behaved and can incorporate a variety of amyloidogenic heptapeptide sequences and fold into β-sheet structures.

References

1. Chiti, F., Dobson, C.M. *Annu. Rev. Biochem.* **75**, 333-366 (2006).
2. Gellman, S.H. *Curr. Opin. Chem. Biol.* **2**, 717-725 (1998).
3. Lopez de la Paz, M., Serrano, L. *Proc. Natl. Acad. Sci. U. S. A.* **101**, 87-92 (2004).
4. Nowick, J.S., Chung, D.M., Maitra, K., Maitra, S., Stigers, K.D., Sun, Y. *J. Am. Chem. Soc.* **122**, 7654-7661 (2000).
5. Nowick, J.S., Brower, J.O. *J. Am. Chem. Soc.* **125**, 876-877 (2003).
6. Woods, R.J., Brower, J.O., Castellanos, E., Hashemzadeh, M., Khakshoor, O., Russu, W.A., Nowick, J.S. *J. Am. Chem. Soc.* **129**, 2548-2558 (2007).
7. Cheng, P.-N., Nowick, J.S. *J. Org. Chem.* **76**, 3166-3173 (2011).

Stimulus-Responsive β-Sheet Peptide Self-Assembly

Charles J. Bowerman and Bradley L. Nilsson

Department of Chemistry, University of Rochester, Rochester, NY, 14627-0216, U.S.A.

Introduction

Stimulus-responsive self-assembly of β-sheet peptides into amyloid-like nanofibrils has facilitated the development of amyloid-inspired biomaterials for biomedical applications including tissue engineering and wound healing [1]. Peptides that self-assemble only upon exposure to specific environmental and chemical stimuli, including changes in ionic strength, light, temperature, and pH or upon enzymatic manipulation have been reported. We have previously shown that chemical reductants can also be exploited as a trigger for peptide self-assembly in β-sheet fibrils [2]. When the $(FKFE)_n$ assembly motif was flanked with Cys residues, the resulting $Ac-C(FKFE)_2CG-NH_2$ peptide could be prevented from undergoing self-assembly by oxidizing the Cys thiol groups to provide a cyclic peptide. The cyclic peptide was unable to adopt the β-sheet orientation that is required to self-assemble into higher order fibrillar structures. Self-assembly of this peptide could be triggered by addition of chemical reductants, which cleave the disulfide bond and allow relaxation of the peptide into its native β-strand secondary structure [2]. To further test the viability of this stimulus-response trigger we synthesized and studied the self-assembly of $Ac-C(VKVE)_2CG-NH_2$ (Scheme 1). The purpose of these further studies was to establish, in part, the generality of reduction-triggered self-assembly as a function of the hydrophobic side chain groups (X) of the general $(XKXE)_2$ assembly motif.

Results and Discussion

The $Ac-C(VKVE)_2CG-NH_2$ peptide was prepared and cyclized in order to characterize its reduction-dependent self-assembly properties. The peptide was synthesized by standard solid phase peptide synthesis (Fmoc protection, HBTU/HOBt activation). The peptide was cleaved from the solid support using a TFA/ethanedithiol/water cleavage cocktail. Excess ethanedithiol was removed by evaporation of the cleavage cocktail, dissolution of the peptide in water/acetonitrile (0.1% TFA), and filtration through a short column of reverse phase silica. Peptide macrocyclization was accomplished by dilution of the crude peptide into acetonitrile and water followed by the addition of 4,4′-pyridyldisulfide [2]. The cyclization reaction was monitored by reverse phase HPLC; once cyclization was complete, the cyclic peptide (Scheme 1) was purified by reverse phase HPLC. Peptide identity was confirmed by MALDI-TOF mass spectrometry. An HPLC concentration curve was constructed by correlating a linear plot of serial dilutions of cyclic peptide against peak area (determined by integration of peaks in the HPLC trace) to amino acid analysis of the injected solutions [2]; HPLC concentration curves facilitate precise and convenient determination of peptide concentration.
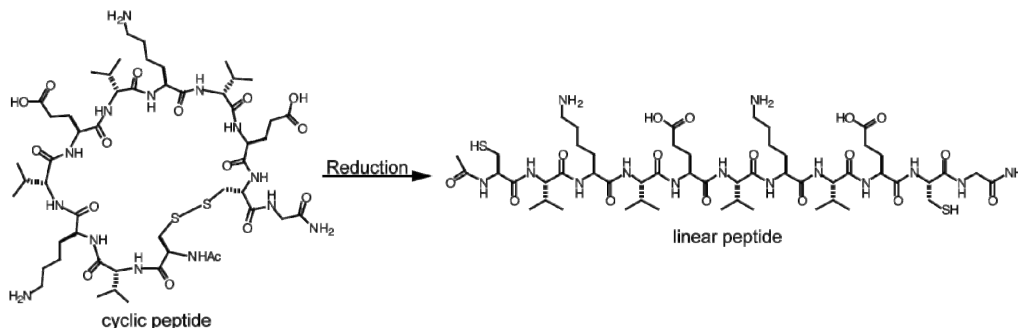
Scheme 1. Conversion of cyclic to linear peptide upon chemical reduction.

It was found that, consistent with our previous report, the cyclic $Ac-C(VKVE)_2CG-NH_2$ peptide did not undergo self-assembly into fibril structures [2]. The cyclic peptide was dissolved

in deionized water (18 Ω) followed by three cycles of agitation (1 minute) and sonication (5 minutes) to give homogenous solutions (1 mM peptide). These peptide solutions were analyzed by CD spectroscopy; CD spectra displayed a single minimum at 201 nm (Figure 1A). This CD spectrum is consistent with a random coil structure. TEM analysis of the cyclic peptide solution confirms that no higher order fibril aggregates were formed while the peptide is in a cyclic form.
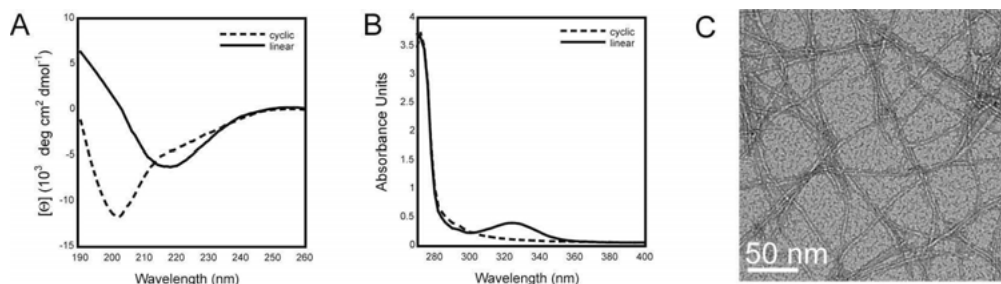
Fig. 1. A. CD spectra of cyclic and linear Ac-C(VKVE)$_2$CG-NH$_2$ ([peptide]=1 mM); B. UV spectra of cyclic and linear peptide; C. TEM micrograph of fibrils formed by the linear peptide upon reduction of the cyclic peptide.

The self-assembly behavior of the cyclic peptide was then characterized as a function of linearization by addition of chemical reducing agents. Addition of TCEP, a water-soluble phosphine that effectively reduces disulfide bonds, resulted in rapid reduction of the disulfide bond (< 2 min) and relaxation to the linear peptide as indicated by CD spectroscopy. Analysis of the linear peptide solution by CD indicated a significant and immediate change in the CD spectrum; the minimum at 201 nm shifted to 218 nm, consistent with formation of a β-sheet conformation (Figure 1A). The UV spectrum showed development of strong absorbance at 324 nm upon addition of TCEP (Figure 1B). TEM analysis of this solution confirmed that self-assembly and formation of a dense network of fibrils (~4 nm in diameter, Figure 1C) occurred immediately addition of TCEP. These results confirm that redox-triggered self-assembly of the Ac-C(VKVE)$_2$CG-NH$_2$ peptide occur in a manner that is identical to that of the (FKFE)$_2$ counterpart.

Moderate changes in the identity of the assembly motif (Phe to Val mutations) do not reduce the efficiency of reduction-triggered self-assembly. The generality of the principle of disulfide-mediated peptide cyclization to prevent self-assembly of β-sheet peptides requires additional study. The influence of Coulombic effects on reduction triggered self-assembly is of interest [3,4]. In addition, the effect of more dramatic changes to the identity of the assembly motif, including peptide sequence and length, is of interest in the context of cyclization of the assembly motif as a strategy to inhibit self-assembly. It is possible that as the macrocycle increases in size, the formation of β-hairpin structures that are competent to self-assembly in the cyclic form may be observed. It will also be of interest to explore the behavior of reduction-triggered self-assembling peptides in biological systems, in which differences in reduction potential define significant subcellular microenvironments.

Acknowledgments

References

1. Cavalli, S., Albericio, F., Kros, A. *Chem. Soc. Rev.* **39**, 241-263 (2010).
2. Bowerman, C.J., Nilsson, B.L. *J. Am. Chem. Soc.* **132**, 9526-9527, (2010).
3. Bowerman, C.J., Ryan, D.M., Nissan, D., Nilsson, B.L. *Mol. Biosyst.* **5**, 1058-1069, (2009).
4. Bowerman, C.J., Liyanage, W., Federation, A.J., Nilsson, B.L. *Biomacromolecules* 12, 2735-2745, (2011).

Global Versus Regional Stability in Tropomyosin: Propagation of Single-Mutation Effects through a Rod-Like Protein

J. Paul Kirwan and Robert S. Hodges

Program in Structural Biology and Biophysics, Department of Biochemistry and Molecular Genetics, University of Colorado School of Medicine, Aurora, CO, 80045, U.S.A.

Introduction

Deciphering the relationship between amino acid sequence and protein stability, structure and function remains an unmet challenge despite decades of protein research. The two-stranded α-helical coiled-coil is a perennial model protein-folding motif for the study of these relationships. Tropomyosin (TM) is an actin-binding, thin filament protein critical to muscle contraction (in skeletal, smooth and cardiac muscle) and is useful as a model coiled-coil to gain a detailed understanding of stability. In TM (residues 97-119), we made the first identification of a stability control region that controls final protein stability but is not required for folding
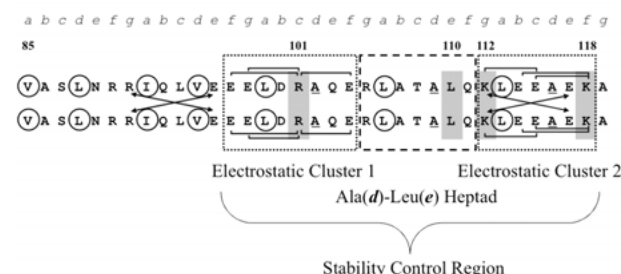
*Fig. 1. TM sequence including the stability control region (97-118). This region was identified from an observed thermal stability (T_m) increase of 15 ℃ between TM fragments 1-99 and 1-119 [1]. Electrostatic clusters are shown in dotted boxes with potential intrachain and interchain salt bridges indicated by lines and arrows respectively. The dashed box shows the critical Leu110e residue (shaded) that contributes 2.7 kcal/mol to the stability of each strand [2]. Additional stabilizing residues R101, K112, and K118 are also shaded. Position **a** and **d** hydrophobes are circled. Alanine residues in three consecutive hydrophobic core **d** positions 102, 109 and 116 are underlined.*

(Figure 1) [1]. We also used a synthetic peptide approach to characterize the critical interactions in this region and found that a Leu (110) residue in heptad position *e* remarkably contributes 2.7 kcal/mol to the stability of the monomeric α-helices [2]. We believe that the stability control region maintains the structural integrity of the helical strands in the presence of three consecutive destabilizing *d*-position alanine residues, allowing the dynamic coiled-coil motion required for proper function. New questions arise. Is the effect of a single mutation (L110A) in the stability control region of TM a global effect that is transmitted throughout the entire rod-like molecule? If not, to what extent (how many residues) is regional stability affected? What functional aspect of TM is modulated by the stability control region through its stabilization of the monomeric helices via Leu110*e*? Does the stability control region have any regulatory role? How might the effects of one or more of the thirteen known cardiomyopathy mutations in TM compare to the effects that result from changes in the stability control region? We begin to address these questions with an investigation of the distance-dependence of single mutations on protein stability in the rod-like protein tropomyosin.

Results and Discussion

We prepared recombinant TM fragment constructs of length 1-119, 1-131 and 1-260. Additional constructs of each fragment were designed to include the native TM sequence and two mutants for a total of 9 constructs. Thermal stability of the purified expression products was evaluated by circular dichroism. The native TM fragments 1-119 and 1-131 show two-state behavior, whereas, the stability of the 1-260 fragment is non-two-state (Figure 2, Panel A). This establishes the presence of a stable N-terminal domain, clearly observed in all three fragments, and a less-stable C-terminal domain observed in TM 1-260. Furthermore, destabilizing (L110A)
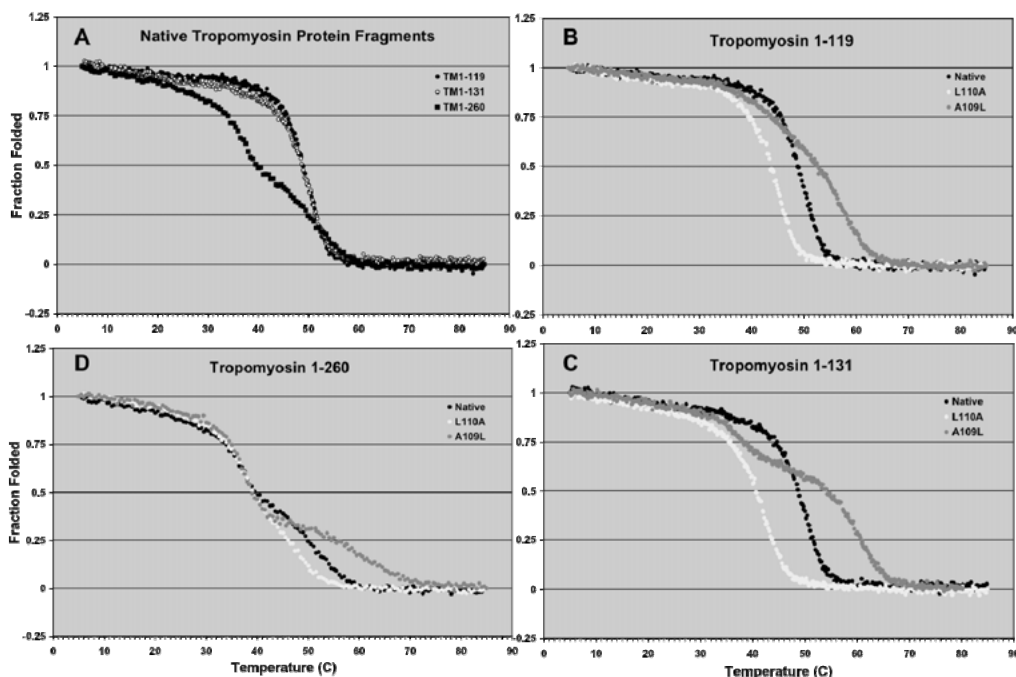
Fig. 2. Thermal denaturation profiles of native and analog TM fragments. Native TM sequences of (A) lengths 1-119 (black circles), 1-131 (white circles) and 1-260 (black squares). TM sequences Native (black circles), L110A (white circles) and A109L (grey circles) of length (B) 1-119, (C) 1-131 and (D) 1-260.

and stabilizing (A109L) single mutations in the stability control region of TM fragments 1-119 and 1-131, cause significant effects (Figure 2, Panels B and C). The effect of the L110A mutation completely destabilizes the first 131 residues of TM (see single transitions, Figure 2, Panels B and C). In contrast, the A109L mutation provides a more localized stabilizing effect, inducing two transitions (non-two-state behavior) in TM 1-131 (Figure 2, Panel C). The less stable C-terminal domain observed in TM 1-260 is unaffected by single mutations in the stability control region (Figure 2, Panel D, upper half). However, a more stable N-terminal domain is also present in TM 1-260 and is clearly affected by our mutations in the stability control region, with effects similar to those observed in the smaller TM fragments (Figure 2, Panel D, lower half).

We have evidence that a single mutation (L110A) in the stability control region completely affects the first 131 residues of TM (the N-terminal domain). This effect is still clearly measurable in TM 1-260. As a result, we believe the effect of the stability control region will also be measurable in full length TM 1-284. The total number of residues in the N-terminal domain governed by the stability control region is still unknown, but most likely extends well beyond the first 131 residues of TM to some region between residues 131 and 260.

Acknowledgments

References

1. Hodges, R.S., Mills, J., McReynolds, S., Kirwan, J.P., Tripet, B., Osguthorpe, D. *J. Mol. Biol.* **392,** 747-762 (2009).
2. Kirwan, J.P., Hodges R.S. *J. Struct. Biol.* **170**, 294-306 (2010).

Solid-Phase Synthesis of a Branched Peptide to Form a Homo-Two-Stranded Coiled-Coil for the Development of a Universal Flu Vaccine

Wendy J. Hartsock, Zhe Yan, and Robert S. Hodges

Biochemistry and Molecular Genetics, University of Colorado, School of Medicine, Aurora, CO, 80045, U.S.A.

Introduction

Millions of people worldwide are infected with influenza virus, resulting in 250,000-500,000 deaths annually [1]. Efforts to combat the virus through vaccination are repeatedly thwarted by mutations of the antigenic viral proteins hemagglutinin (HA) and/or neuraminidase (NA) [2]. Our goal is to develop a "**Universal Flu Vaccine**" that will provide long-lasting protection against heterotypic strains of influenza A virus. We have developed synthetic peptide immunogens based on helical regions of the HA protein that are conserved across a diverse range of influenza A virus strains. Our immunogens are 2-stranded α-helical coiled-coils, which form stabilized helical epitopes for the generation of protective antibodies *in vivo*. Helical segments of the HA protein in its pre-fusion state were inserted into our 2-stranded coiled-coil template. Our previously reported strategy of immunogen formation [3,4] required 18 distinct steps to assemble the peptide immunogen conjugated to a carrier protein. Product yield was decreased due to the number of steps and low yields of specific steps required to form the carrier conjugated peptide immunogen. The branched peptide immunogen was designed to overcome synthetic and purification challenges and to increase the efficiency of product formation by significantly decreasing the number of steps required to form the final conjugated immunogen.

Results and Discussion

Assembly of the branched peptide immunogen (immunogen B, Figure 1) requires 9 steps, including conjugation to the carrier protein. Rather than synthesizing each strand as separate peptides followed by derivatization and oxidation to join the strands, a diamine bridge, diaminopropionic acid (Dap), was used to combine both strands into a single peptide (Figure 1). Immunogen B was assembled by Fmoc solid-phase peptide synthesis on the CEM Liberty microwave peptide synthesizer. Following complete assembly of epitope 1, the N terminus was acetylated and the N^β of the Dap residue was selectively deprotected. Epitope 2 was then assembled on the free beta-amine of Dap using the Liberty synthesizer. The peptide was cleaved from the resin and purified by reversed-phase chromatography.

Disulfide Bridged Immunogen:

```
             a   d   a   d   a   d   a   d
Epitope 1  Linker-IRTLDFHISNLKNLIEKLKSQIKNLAKECRR-amide
Epitope 2      Ac-IRTLDFHISNLKNLIEKLKSQIKNLAKECRR-amide
                        Immunogen A
```

Branched Immunogen:

```
Epitope 1  Linker-IRTLDFHISNLKNLIEKLKSQIKNLAKEG-Nᵝ-CH₂
Epitope 2      Ac-IRTLDFHISNLKNLIEKLKSQIKNLAKEG-Nᵅ-CH₂-amide
                        Immunogen B
```
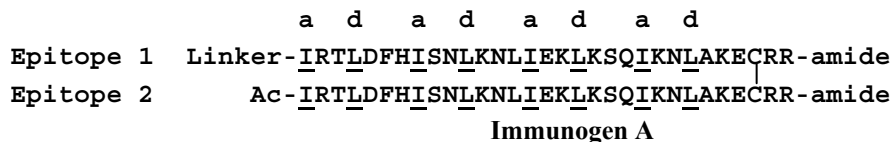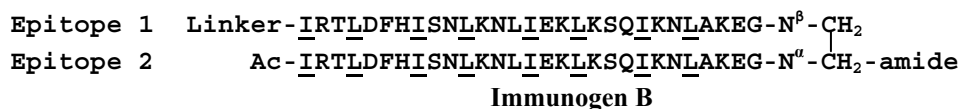
*Fig. 1. Templated peptide immunogens. Once a helical epitope is selected, it is inserted into our coiled-coil template and amino acids at positions **a** and **d** (underlined in all of the sequences) in the native sequence are converted to isoleucine and leucine, respectively, to form the hydrophobic core of the coiled-coil. Identical peptide epitopes are bridged via a disulfide linkage in immunogen A to form the homo-2-stranded coiled-coil peptide immunogen. Epitopes in the branched peptide, immunogen B, are bridged by a diamine linker.*

Circular dichroism (CD, Figure 2) of both immunogen A and immunogen B produced double minima at 208 nm and 222 nm in benign (100 mM KCl, 50 mM phosphate, pH 7.0) media, typical of peptides with α-helical secondary structure. In the helix-inducing environment of 50% TFE, an increase in the 208 nm minima was observed for both peptides although, more so for immunogen B compared to immunogen A. The ratio of 222/208 nm in benign media was 1.10 for immunogen A and 1.04 for immunogen B, indicative of interacting helices of the coiled-coil structure. This ratio decreased to 0.933 for immunogen A and 0.90 for immunogen B in 50% TFE, a solvent that induces secondary structure but disrupts tertiary and quaternary structures. Both peptides retained structure during thermal denaturation in benign media and exhibited similar $\Theta_{222}(T)/\Theta_{222}$ (5°C) (i.e. fraction folded) ratios of 0.75 and 0.70 at 85°C for immunogen A and immunogen B, respectively.

Fig. 2. CD spectra. In benign media, both immunogen A (left spectrum, closed diamonds) and immunogen B (right spectrum, open circles) exhibited double minima at 208 nm and 222 nm. In 50% TFE, the elipticity is greater at 208 nm compared to 222 nm for both immunogen A (left spectrum, closed squares) and immunogen B (right spectrum, open squares).

Fig. 3. ELISA. Purified antibody bound with similar affinity to immunogen A (closed diamonds) compared to immunogen B (open circles).

An ELISA of immunogen A and immunogen B demonstrated similar affinities of these peptides for a polyclonal antibody that was raised against immunogen A (Figure 3), indicating that the presentation of the epitope is similar in both peptides. These peptide immunogens did not bind to the pre-immune serum, indicating a specific interaction with the immunogen A antibody.

The synthesis of a branched peptide immunogen, immunogen B, derived from the HA protein of influenza A was successfully completed and demonstrated similar characteristics to the parent disulfide-bridged peptide, immunogen A, in CD and ELISA experiments.

Although the synthetic yield of our initial analog was low, the data obtained from CD experiments and ELISA demonstrated that our new strategy is a viable alternative to previous techniques employed for immunogen formation. Once optimized, our strategy of forming branched peptide immunogens will dramatically increase the efficiency of product generation. Following the acquisition of appropriate CD and ELISA data, the branched peptide immunogens will be used to raise polyclonal antibodies for passive immunization. Finally, these branched immunogens will be investigated in active immunization studies *in vivo*.

Acknowledgments

References

1. http://www.who.int/topics/influenza/en/.
2. Compans, R.W., Orenstein, W.A. (Eds.), *Vaccines for Pandemic Influenza*. Springer Verlag, Berlin Heidelberg, 2009.
3. Lu, S.M., Hodges, R.S. *J. Biol. Chem.* **277**, 23515-23524 (2002).
4. Tripet, B., Kao, D., Jeffers, S., Holmes, K., Hodges, R.S. *J. Struct. Biol.* **155**, 176-194 (2006).

Evaluation of an α-Helical Antimicrobial Peptide Targeting Gram-Negative Pathogens in a Systemic Animal Model

Wendy J. Hartsock[1], Ziqing Jiang[1], Lajos Gera[1], Colin T. Mant[1], Adriana I. Vasil[2], Michael Vasil[2], and Robert S. Hodges[1]

[1]*Department of Biochemistry and Molecular Genetics;* [2]*Department of Microbiology, University of Colorado, School of Medicine, Aurora, CO, 80045, U.S.A.*

Introduction

Microbial resistance to antibiotics is a major and growing threat. By targeting the bacterial membrane, we believe the ability of microbes to develop resistance is low since substantial reorganization of the cellular membrane would be required to limit interaction with our antimicrobial peptides (AMPs). We recently described how substituting a lysine residue into the center of the non-polar face (a "specificity determinant") of a *de novo* designed amphipathic α-helical AMP (Figure 1) targeting Gram-negative pathogens produced a dramatic increase in specificity (therapeutic index (TI)) for prokaryotic cells [1]. The equivalent activities of the L- and D-enantiomers showed that interaction with a non-chiral target, the cell membrane, was the mechanism of action [2]. Addition of a single specificity determinant (SD) to peptide **D-V13** yielded peptide **D1** (Table 1) and resulted in a significant increase in the TI. An unprecedented increase in the TI resulted from the substitution into the non-polar face of **D1** with a second SD, a change in location of hydrophobes, the substitution of all hydrophobic residues with Leu and the addition of basic residues to the polar face (increasing charge from +6 for **D-V13** to +11 for **D16**). Placement of Lys residues in the center of the non-polar face breaks the continuous hydrophobic surface of **D-V13**,

Fig. 1. Helical nets of peptides D-V13 and D16 with the non-polar face displayed down the center of the helical net. Peptide D16 contains two "specificity determinants" (lysine residues 13 and 16 in the center of the non-polar face (triangles). Hydrophobic residues circled and black bars indicate the i→i+3 and i→i+4 interactions. Lys residues (boxed) and other polar residues (unboxed) are shown along the polar face.

producing two distinct hydrophobic patches, eliminates α-helical structure in aqueous conditions and prevents peptide self-association. These features allow for inducible helical structure in the membrane environment of bacteria. In our mechanistic perspective of microbial specificity, the AMPs **D1** and **D16** interact with the bacterial membrane in a detergent-like fashion as described by the carpet model [3]. Hemolytic activity via transmembrane insertion into human red blood cells can be designed out of our AMPs while retaining parallel interaction with bacterial membranes. The remarkable microbial specificity of peptide **D16** results from the manipulation of key features such as peptide self-association, environmental induction of helical structure, hydrophobicity, amphipathicity, net positive charge, the number and continuity of hydrophobic interactions and the ability to target the cell membrane.

Results and Discussion

Peptide **D16** was investigated for antimicrobial activity against *A. baumannii* in an animal model of infection. Following intraperitoneal injection of *A. baumannii*, rats were administered

with antibiotic, peptide or vehicle. Bacteria were cleared from the blood and the peritoneal cavity (Table 2) 12 hours after infection as determined by culture of lavage and blood samples from rats treated with 0.5 mg/rat of peptide or 3 mg/rat of antibiotic. Furthermore, cytokine levels in peptide/antibiotic treated animals were substantially reduced compared to vehicle treated rats. The *in vivo* experimental results clearly demonstrate that peptide **D16** is a highly efficacious compound for the treatment of Gram-negative infections.

Table 1. Hemolytic and antimicrobial activity of antimicrobial peptides

Peptide Name	Hemolytic activity	Antimicrobial activity			
		Acinetobacter baumannii		*Pseudomonas aeruginosa*	
	HC_{50} $(\mu M)^a$	MIC_{GM} $(\mu M)^b$	*Therapeutic Index^c*	MIC_{GM} $(\mu M)^b$	*Therapeutic Index^c*
D-V13	1.8	0.7	2.57	1.8	1.0
D1	140.9	1.1	128.1	4.1	34.4
D16	**1342.0**	**0.4**	**3355.0**	**1.5**	**894.7**

^{a}*HC_{50} is the concentration of peptide that results in 50% hemolysis after 18 h at 37°C; ^{b}MIC_{GM} is the geometric mean (GM) for 11 and 6 different strains of A. baumannii and P. aeruginosa, respectively, of the minimum inhibitory concentration (MIC) of peptide required to inhibit bacterial growth after 24 h at 37°C; ^{c}Therapeutic index is the ratio of the HC_{50} value to the MIC_{GM} value. A larger number indicates greater antimicrobial specificity.*

Table 2. Effects of a single dose of antibiotic/peptide in rats infected with A. baumannii

Group	IP bacterial dose (CFU/rat)	IV drug treatment	Lavage count	Blood count	Cytokines (pg/ml)				
	0 hour	2 hours	cfu/mL	cfu/mL	MCP-1	IL-1β	IL-6	IL-10	GRO/KC
Control	**None**	**None**	—	—	394	< 97.7	< 97.7	< 1562.5	536
A (no treatment)	**4.5×10⁹**	**None (vehicle)**	7×10⁸	2.3×10⁶	6,436	809	31,596	26,102	> 100,000
			3×10⁸	2.1×10⁶	2,488	214	13,948	12,226	> 100,000
			5×10⁸	5×10⁶	13,430	1,473	> 100,000	34,087	> 100,000
			4.2×10⁸	1.2×10⁷	4,551	364	47,871	14,272	> 100,000
B (antibiotic treated)	**4.5×10⁹**	**3 mg/rat (imipenem)**	0	0	3,077	< 97.7	833	< 1562.5	2,791
			0	0	757	< 97.7	361	< 1562.5	346
			0	0	1,014	< 97.7	< 97.7	< 1562.5	495
			0	0	1,384	< 97.7	118	< 1562.5	1,204
			0	0	1,161	< 97.7	< 97.7	< 1562.5	414
C (peptide treated)	**4.5×10⁹**	**0.5 mg/rat (peptide)**	0	0	1,218	< 97.7	133	< 1562.5	455
			0	0	1,505	< 97.7	< 97.7	< 1562.5	773
			0	0	1,356	< 97.7	178	< 1562.5	3,288
			2.7×10²	0	1,730	< 97.7	222	< 1562.5	1,019

References

1. Ziqing, J., et al. *Chem. Biol. Drug Des.* **77**, 225-240 (2011).
2. Chen, Y., et al. *Chem. Biol. Drug Des.* **67**, 162-173 (2006).
3. Pouny, Y., et al. *Biochemistry* **34**, 6521-6526 (1992).

Antigenic Determinants of Cross-Reactivity in the Development of a *Pseudomonas aeruginosa* Peptide Vaccine Targeting the Receptor Binding Domain of the Type IV Pilus

Clifton L. Hackbarth and Robert S. Hodges

Program in Structural Biology and Biophysics, Department of Biochemistry and Molecular Genetics, University of Colorado, School of Medicine Anschutz Medical Campus, Aurora, CO, 80045, U.S.A.

Introduction

Pseudomonas aeruginosa (*Pa*) is an ubiquitous opportunistic pathogen that is one of the leading causes of nosocomial infections. *Pa* infections are typically treated with antimicrobials which are ineffective against chronic infections. Thus, we believe it is important to target the initial stages of infection with a vaccine. Furthermore, *Pa* has several mechanisms to initiate an infection and one particular way uses a type IV pilus, specifically the Receptor Binding Domain (RBD) that is part of the pilin protein. The RBD binds to a disaccharide that is part of various epithelial cell surface receptors. Moreover, the RBD of *Pa* consists of a disulfide loop, at the C-terminus of the protein, composed of 14 residues for most strains. Two strains, PAK and PAO, have nine homologous residues and five variable residues among the RBD disulfide loop region, residues 129-144.

In this study, we wanted to determine which amino acid structural features of a peptide immunogen generate cross-reactive antibodies to the pilin RBDs of *Pa* native strains PAO and PAK. To accomplish this, we have developed four 17-residue synthetic peptide immunogens that contain RBD residue insertions from strain PAK into strain PAO (Figure 1).

Fig. 1. Peptide immunogens synthesized, using the PAO receptor binding domain (RBD) sequence as a template. Boxed residues indicate substitutions from the native strain PAK RBD sequence into the native strain PAO RBD sequence of the peptides. The circled residues indicate native strain PAO specific residues.

The five peptide immunogens were synthesized and conjugated to carrier protein KLH and then used to immunize New Zealand White Rabbits. The sera were collected and purified for IgG, which was then used in direct and competitive ELISAs with native strain monomeric pilins PAK and PAO, residues 129-144.

Results and Discussion

The direct ELISAs showed that each of the peptide immunogens generated antibodies to both native strain PAK and PAO pilins. This indicated that only P135E and M136Q substitutions were needed in the PAO peptide immunogen sequence to generate antibodies to PAK pilin. It should also be noted that immunogen A, the native strain PAO RBD sequence, generated PAO specific antibodies. However, when the Abs were used in competitive ELISAs, PAO pilin could not compete off PAK pilin and PAK pilin could not compete off PAO pilin. This was unexpected considering that the Abs bound to both PAK and PAO pilins by direct ELISA. This led us to hypothesize that there were at least two strain specific Ab populations in the IgG, one PAO specific and the other PAK specific. Furthermore, we hypothesized that perhaps PAO residues A128, D143, and N144 were an important part of the PAO specific Abs epitope, since these residues were present in each peptide immunogen. To prove or disprove this hypothesis, site-directed mutagenesis was used to interchange residues 128, 143, and 144 between native

strain PAK and PAO pilins (Figure 2) and then the mutant pilins were used in direct and competitive ELISAs.

Strain	128	129	130	131	132	133	134	135	136	137	137	139	140	141	142	143	144
PAO Pilin (29-144)	A	C	K	S	T	Q	D	P	M	F	T	P	K	G	C	D	N
PAO Pilin (29-144) mutant	K	C	K	S	T	Q	D	P	M	F	T	P	K	G	C	S	K
PAK Pilin (29-144)	K	C	T	S	D	Q	D	E	Q	F	I	P	K	G	C	S	K
PAK (ADN) (29-144) mutant	A	C	T	S	D	Q	D	E	Q	F	I	P	K	G	C	D	N

Fig. 2. Shown are the native strain PAO and PAK pilin sequences of the receptor binding domain, residues 128-144, and two mutants. The mutated residues in PAO and PAK pilins (29-144) are boxed.

The results supported our hypothesis: PAK (ADN) could now compete off native strain PAO pilin since it has PAO specific residues A128, D143, and N144 which comprise part of the epitope for PAO specific Abs. Thus, each rabbit produced at least two strain specific Abs, one specific for PAO pilin and one specific for PAK pilin [1]. The important residues for Ab specificity are shown in Figure 3.

Key residues for Antibody specificity for PAO Pilin

Peptide Immunogen
PAO (128-144)
D135E/M136Q

128   135 136   143 144

A C K S T Q D E Q F T P K G C D N - OH

Key residues for Antibody specificity for PAK Pilin
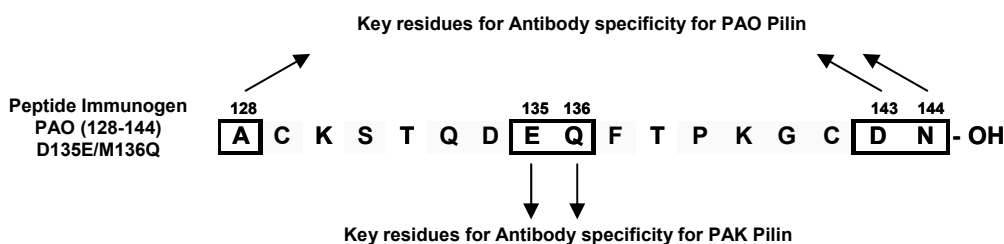
Fig. 3. Shown is the amino acid sequence for one peptide immunogen, PAO (128-144) (D135E/M136Q). The boxed residues are the suggested key residues, (A128, D143, N144) and (E135, Q136), responsible for generating antibodies that are PAO or PAK specific.

To elucidate the specific structural features of the RBD that control the immunogenicity of the peptide immunogens, X-ray crystallography studies were undertaken. Native strain PAK pilin has already been crystallized [2]; thus, we used site directed mutagenesis to change the RBD of the native strain PAK pilin into that of PAO pilin. The PAK PAO RBD chimera crystallized and diffracted to 1.65 Å. Molecular replacement was used to solve the structure. The PAK PAO RBD chimera structure is very similar to that of native strain PAK pilin with only 0.24 Å r.m.s.d. between the full length structures and an r.m.s.d. of only 0.36 Å between residues 129-144 which comprise the RBD. In both structures, residues 135,136, 128, 143, and 144 are all exposed on the surface of the pilin proteins and residues 128, 143, and 144 are clustered together. Thus, it is easy to see how these surface residues could comprise part of an epitope and that any change in side-chains could affect the epitope and thus specificity of Ab binding.

The Hodges' laboratory has previously crystallized and solved by X-ray crystallography a consensus sequence (Cs1) peptide vaccine [3]. We can now engineer RBDs from other native strains, which will not crystallize, into that of native strain PAK pilin and subsequently crystallize them as PAK chimeras. The structural information gained can then be used in the design of the next generation consensus sequence peptide vaccine.

Acknowledgments

References

1. Hackbarth, C.L., Hodges, R.S. *Chem. Biol. Drug Des.* **76**, 293-304 (2010).
2. Hazes, B., Sastry, P.A., Hayakawa, K., Read, R.J., Irvin, R.T. *J. Mol. Biol*. **299**, 1005-1017 (2000).
3. Kao, D.K., Churchill, M.E.A., Irvin, R.T., Hodges, R.S. *J. Mol. Biol.* **374**, 426-442 (2007).

Cold Denaturation and Protein Stability

Miquel Adrover[1,2], Veronica Esposito[2], Gabriel Martorell[3], Annalisa Pastore[1], and Piero Andrea Temussi[1,4*]

[1]National Institute for Medical Research, The Ridgeway, London, NW7 1AA, UK; [2]Department de Química, Universitat de les Illes Balears, Palma de Mallorca, E07122, Spain; [3]Serveis Científico-Tècnics, Universitat de les Illes Balears, Palma de Mallorca, E07122, Spain; [4]Department of Chemistry, Università di Napoli Federico II, via Cinthia, 80126, Napoli, Italy

Introduction

We have recently identified a protein, Yfh1, whose cold denaturation occurs at accessible temperatures close to 0°C and under physiological conditions at pH 7; that is, without the need of adding denaturants [1]. The structural characterization of the unfolded state at low temperature validates the current theoretical interpretation of the mechanism of cold denaturation [2].

Results and Discussion

Yfh1 is apparently the first example of a wild type protein undergoing cold denaturation at temperatures accessible by normal NMR spectrometers, in the absence of destabilizing agents. We exploited these properties to characterize the cold denatured state and to address difficult problems in protein stability. Characterization of the cold unfolded state was based on a nearly full assignment of the NMR spectrum of Yfh1 at 272 K. We did not observe a marked similarity between the cold denatured state and the native one. In addition, the difference in chemical shifts does not support the possible co-presence of the native and denatured state. However, the low temperature state of Yfh1 has chemical shifts distinctly different from the literature random coil values at room temperature. The main difference is an overall downfield shift as compared to the expected unfolded spectrum, hinting at strong solvation effects. This observation is consistent with the currently accepted mechanism of cold denaturation [1]. Privalov has hypothesized that cold denaturation is caused by the temperature-dependent interaction of nonpolar groups of the protein with water [1].
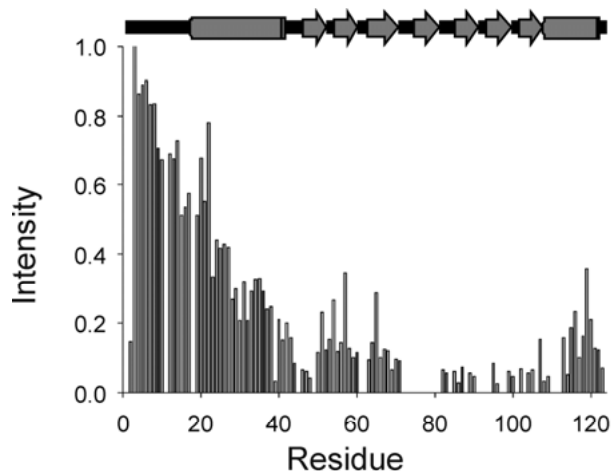
Fig. 1. Plot of the intensities of HSQC peaks of Yfh1 at 0°C as a function of residue numbers. The secondary structure of the folded protein is reported above for reference.

This counterintuitive hydration forces the polypeptide chain to unfold at a sufficiently low temperature, exposing internal nonpolar groups to water. Secondary chemical shifts and NOE effects suggest that regions adopting helical and β-structures in the folded protein in the cold denatured state have a nascent helix character. As shown in Figure 1, we observed, in the cold denatured state of Yfh1, a different dynamic behavior along the sequence: the N-terminus seems to be the most flexible part, suggesting a more cooperative collapse of this region upon unfolding. On the other hand, resonances from the C-terminus are overall less intense, possibly because of conformational exchange. Altogether these results represent an interesting *caveat* concerning the relationship between flexibility and structure: at first sight, they seem to imply that the N terminal residues are very flexible and therefore less structured than other parts of the sequence, as one would automatically assume in the case of several intrinsically unfolded proteins. However, the analysis of all secondary structure indicators showed convincingly that the same region retains more secondary structure than the remaining regions of the sequence. The low intensity of the resonances from the central part of the sequence can be attributed to conformational exchange among several unstructured species, dominated by cis-trans proline isomerism. Thus, it seems fair to conclude that although helix 1 is the first secondary structure element to collapse, it is also the most persistent one in retaining a secondary structure in the cold denatured species. Our data provide both new insights into the early events that cause protein folding and give us a glimpse into the effects that low temperature forces have onto protein structure.

Yfh1 proved a good system to investigate protein stability in difficult cases. The first instance in which it was used in a general sense to study the stability of proteins was a study on the influence of alcohols at low concentrations. We determined the stability curve on the basis of both high and low temperature unfolding in the presence of three commonly used alcohols: trifluoroethanol, ethanol and methanol [3]. We suggest that alcohols, at low concentration and physiological pH, *stabilize* proteins by greatly widening the range of temperatures over which the protein is stable. Another important instance for which measuring both transitions, and thus determining the full stability curve, could be decisive is when the high temperature transition point might be difficult or impossible to determine, e.g. for the interference of aggregation. A domain module of the multi-domain muscle protein titin (I28) looked as a promising candidate, because of the strong interference between thermal unfolding and aggregation. An NMR study of the thermal stability of titin I28 in the temperature range from -5°C to 65°C showed that it can undergo cold denaturation at physiological conditions [4]. Our study confirmed that the possibility of direct observation of cold denaturation, and the consequent reliable determination of the whole stability curve, may be the only way to assess thermal stability of proteins that have a high tendency to aggregate at high temperatures.

Acknowledgements

References

1. Pastore, A., et al. *J. Am. Chem. Soc.* **129**, 5374-5375 (2007).
2. Privalov, P.L. *Crit. Rev. Biochem. Mol. Biol.* **25**, 281-305 (1990).
3. Martin, S.R., et al. *J. Am. Chem. Soc.* **130**, 9963-9970 (2008).
4. Sanfelice, D., et al. *J. Am. Chem. Soc.* **131**, 11662-11663 (2009).

Biophysical Features and Folding Stability of a Multi-Membrane-Spanning Domain Fragment of a G Protein-Coupled Receptor (GPCR)

Zhanna Potetinova[1], Boris Arshava[1], Jeffrey M. Becker[2], and Fred Naider[1]

[1]*Department of Chemistry, College of Staten Island, The City University of New York, Staten Island, NY, 10314, U.S.A.;* [2]*Department of Microbiology, University of Tennessee, Knoxville, TN, 37996, U.S.A.*

Introduction

GPCRs constitute one third of the known therapeutic targets [1]. Therefore, a better understanding of GPCR structure, function and mechanism of action would play a key role in drug development. However, some aspects of GPCR biology remain underdescribed. The thermal instability, heterogeneity, and the short lifetime of such polypeptides in aqueous-organic and detergent solutions often limit biophysical studies. We biosynthesized multi-milligram quantities of the unlabeled and [^{15}N]-labeled five-transmembrane fragment Ste2p(I_{120}-L_{340}) [5TMC] of a yeast GPCR, and investigated its properties in membrane mimetic environments by CD, NMR, and fluorescence spectroscopy.

Results and Discussion

The 5TMC construct contains some mutations (M165I, M180I, M189I, M218L, M250I, C252S, M294I, A299V) and has a truncation of the N-terminal and the first two transmembrane (TM) domains. It has a N-terminal His8-Tag, the five C-terminal TM segments of the receptor [TM3-TM4-TM5-TM6-TM7], and 40 residues of the cytoplasmic tail (Figure 1). This polypeptide was directly expressed using a pET21a vector in *E.coli* BL21(DE3) cells at 30ºC, accumulated in inclusion bodies and was purified by RP-HPLC to yield 18-20 mg/L (by weight).

The secondary structure of the 5TMC fragment was analyzed in organic-aqueous (TFE/H_2O and HFIP/H_2O) and micellar environments by CD. This study indicated the expected highly α-helical content for 5TMC and suggested that this receptor fragment existed as an isolated α-helix ($[\theta_{222}]/[\theta_{208}]$=0.90-0.92) at high concentrations of the organic solvents (50-95%) but may assume a coiled-coil ($[\theta_{222}]/[\theta_{208}]$=1.36) at a low content of HFIP (25%). CD screening uncovered suitable conditions for detergent reconstitution of the large highly-hydrophobic fragment and showed that pre-lyophilization from HFIP increases incorporation of the construct into micelles. 5TMC demonstrated the best CD helical parameters in 1-stearoyl-2-hydroxy-*sn*-glycero-3-phospho-(1'-*rac*-glycerol) (LSPG) micelles with the longest hydrophobic tail (Figure 2A). Fluorescence spectroscopy, which provides information about the local environment of the single Trp295 in the TM7 domain, was used to study the effect of urea on the 5TMC structure. In LSPG, the Ste2p fragment, fully buried in the hydrophobic micellar core, exhibited a pronounced blue shift of the fluorescence emission maximum (Figure 2B). The addition of urea
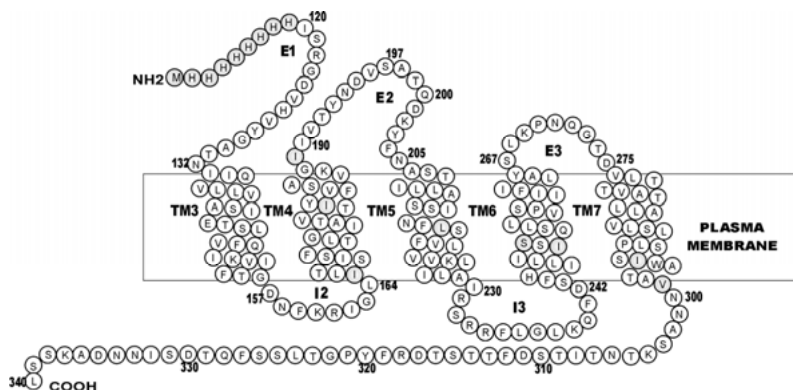
Fig. 1. Cartoon drawing of the five-transmembrane construct. TM - transmembrane domain; E – extracellular loop; I – intracellular loop.
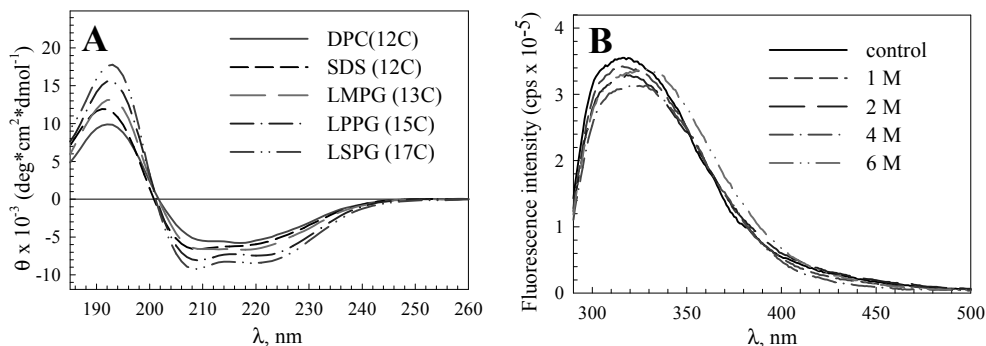
Fig. 2. CD and fluorescence studies of 5TMC in micelles. A) CD spectra of 5TMC ([c]=10 μM) in 20 mM phosphate buffer, pH 5.6 containing 20 mM of the indicated detergent. B) Fluorescence emission spectra of 5TMC ([c]=2.5 μM) in 20 mM phosphate buffer, pH 5.6 containing 10 mM LSPG after a 1 h incubation at different concentrations of urea (1-6 M).

to 5TMC in micelles leads to a moderate red-shift in the emission maximum with minor reduction in fluorescence intensity consistent with changes in the Trp polarity and in the structure of the micellar system. In contrast, in organic solvents, a remarkable 60% increase in fluorescence intensity without changes in the emission maximum wavelength (λ_{max}=343 nm) was detected at 6 M urea. CD indicated only a 15% decrease in helicity at 6M urea.

2D-NMR experiments were performed in organic-aqueous media (TFE-d2/H_2O or HFIP-d2/H_2O) and LSPG or LPPG-containing HEPES or phosphate buffer with and without sodium chloride. The [^{15}N,^{1}H]-HSQC-TROSY spectrum in TFE/water at 45°C showed better resolution and sensitivity than the [^{15}N,^{1}H]-HSQC spectrum as judged by the observed number of peaks and the line width. To evaluate stability, we compared 5TMC spectra acquired for the freshly prepared sample and after incubation for one and two weeks at 45°C. Overall the integrated intensities of the amide and aromatic proton region in the ^{1}H NMR spectrum retained about 70% of the initial value after one week sample incubation and about 55% of the intensity after two weeks. MALDI analysis indicated slight degradation had occurred after two weeks. The observed 5TMC lifetime for one to two weeks indicates that sample stability should be sufficient for the recording of the set of 3-dimensional NMR spectra, necessary for assignments and structure determination. In comparison to the TFE solution, the NMR spectra in HFIP had a slightly broader dispersion of NH chemical shifts and better peak resolution. In micelles, the best resolution of NMR signals was observed in the LSPG/HEPES solution without salt. In attempts to reassemble the entire Ste2p GPCR, the first two [2] and last five or first three [3] and last four transmembrane domain segments were reconstituted into SDS micelles and analyzed by Western Blot and MALDI demonstrating weak interactions between these fragments. The extent of heterodimer formation observed in MALDI spectra was comparable to that of homodimers. Nevertheless the predominant species was the monomer as judged by MALDI and SDS-PAGE.

To conclude conditions have been optimized for biophysical characterization of a large predominantly hydrophobic segment of Ste2p. Fluorescence spectroscopy revealed high resistance of the recombinant 5TM Ste2p fragment to urea. The NMR results show promise for further structural studies that should provide insights into the 3D-structure and mechanism of action of the receptor domains.

Acknowledgments

References

1. Overington, J.P., AI-Lazikani B., Hopkins, A.L. *Nat. Rev. Drug Discov.* **5**, 993-996 (2006).
2. Cohen, L.S., Becker, J.M., Naider, F. *J. Pept. Sci.* **16**, 213-218 (2010).
3. Caroccia, K.E., et al. *Biopolymers (Peptide Science)* in press (2011).

A PNA Peptide Inducing DNAs to Form G-Quadruplex Structures Depending on a Protease Activity

Kenji Usui[1,2], Keita Kobayashi[1], and Naoki Sugimoto[1,2]

[1]*Faculty of Frontiers of Innovative Research in Science and Technology (FIRST), Konan University;*
[2]*Frontier Institute for Biomolecular Engineering Research (FIBER), Konan University,*
Kobe, 6500047, Japan

Introduction

Research over the last few decades has elucidated that some DNA and RNA secondary structures modulate a variety of cellular events. One secondary structure in particular, the G-quadruplex, regulates cellular events such as transcription, translation, pre-RNA splicing, and telomerase elongation, and these events are related to serious diseases and aging [1,2]. Thus, systems capable of controlling DNA and RNA G-quadruplex structures would be useful to modulate various cellular events for the purpose of producing biological effects. Because of their biological importance, many G-quadruplex–targeting ligands have been developed, including phthalocyanine derivatives [3], porphyrin derivatives, and others. The next generation of binders should have more G-quadruplex sequence specificity, higher inducing or collapsing ability of the structure and a greater degree of functionality including binding-on-off-switching, cellular penetration, and the ability to target organelles. From this point of view, we attempted to construct a system using alternative small molecules to regulate G-quadruplex structures with an on-off switching module depending on cellular environments.

Results and Discussion

First of all, a peptide conjugated with peptide nucleic acids (PNAs), Lmyc, was designed (Figure 1). The molecules consisted of two parts. One part was composed of guanine PNA-rich sequences to induce G-rich DNA/RNA sequences to form G-quadruplex structures with the PNAs. PNAs have some advantages not only that PNAs have enzyme resistance but also that functions such as cell-penetrating or switching can be introduced. In this study, a switching module from "on" to "off" depending on a particular cellular environment was adopted into the other part and we selected a particular protease concentration

Fig. 1. Sequences of the PNA peptide and the target DNA.

as the cellular environment. Therefore, this system would induce DNA/RNA to form G-quadruplex structure when the protease would not be expressed in cells, and once expressing the protease, these conjugates would be digested and simultaneously loose the induction ability resulting in collapse of a DNA-PNA quadruplex structure (Figure 2). Calpain I, which is related with serious diseases such as Dystrophia and Alzheimer's disease, was chosen as a model particular protease. Thus a calpain I substrate sequence was put into the center of the small molecule as the switching module.

After synthesis of the peptides by Fmoc chemistry [4], we checked the G-quadruplex structure induction by far-UV CD spectroscopy using a model DNA sequence myc19 (Figure 1), which was a part of *human* c-Myc proto-oncogene promoter. We performed CD experiments to investigate induction of structural and conformational changes in the myc19 G-quadruplex upon interaction with Lmyc. The myc19 G-quadruplex yielded spectra that were characteristic of parallel quadruplexes, with a maximum at 260 nm and a minimum at 240 nm, a result that is consistent with a prior study [5]. Interestingly, addition of Lmyc led to an increase in the parallel G-quadruplex signature. UV melting curves of the target DNA with/without the conjugate showed that T_m of the PNA-DNA structure at 260 nm was ca. 10°C higher than that

of the DNA alone. This implied that a G-rich DNA could be induced to form PNA-DNA G-quadruplex by the PNA peptide.

Also we attempted to demonstrate the switch function depending on the protease concentration. We at first checked by HPLC and MS whether calpain I could digest the Lmyc smoothly. Then digestion experiments using the DNA-PNA quadruplex were conducted. It was found that the behavior of peptides digested by calpain I was almost similar to that of DNA alone. This implied that quadruplex structure of myc19 and Lmyc is destabilized by calpain I.

With more improvement of binding-specificity and adding other functions such as cellular penetrating, this system may lead to controls of the DNA and/or RNA events including RNA expression. Throughout this study, these PNA-peptide conjugates would be one of the promising tools for regulation of important cellular events toward cell engineering and tissue engineering.
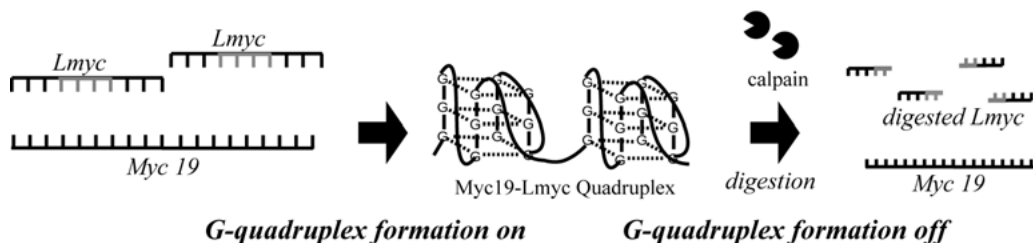
Fig. 2. Outline drawing of the switching system for regulation of G-quadruplex structure using Lmyc.

Acknowledgments

References

1. Miyoshi, D., Matsumura, S., Nakano, S., Sugimoto, N. *J. Am. Chem. Soc.* **126**, 165-169 (2003).
2. Yu, H.Q., Miyoshi, D., Sugimoto, N. *J. Am. Chem. Soc.* **128**, 15461-15468 (2006).
3. Yaku, H., Murashima, T., Miyoshi, D., Sugimoto, N. *Chem. Commun.* **46**, 5740-5742 (2010).
4. Sano, S., Tomizaki, K.-Y., Usui, K., Mihara, H. *Bioorg. Med. Chem. Lett.* **16**, 503-506 (2006).
5. Roy, S., Tanious, F.A., Wilson, W.D., Ly, D.H., Armitage, B.A. *Biochemistry* **46**, 10433-10443 (2007).

All Peptide Membranes and Membrane Chimeras

Anil K. Mehta, Rong Ni, W. Seth Childers, and David G. Lynn

NSF/NASA Center for Chemical Evolution, Center for Fundamental and Applied Molecular Evolution and Department of Chemistry and Biology, Emory University, Atlanta, GA, U.S.A.

Introduction

The Aβ peptide associated with Alzheimer's disease is generated via cleavage of the amyloid precursor protein (APP) within the plasma membrane. Several prions also originate within and traverse lipid membranes and increasingly other cellular components, including phospholipids, have been implicated in disease etiology [1]. These realizations have refocused attention on the micron-long, unbranched, 10nm diameter amyloid fibers formed with residues 16 to 22 of the Aβ peptide, [16]KLVFFA[22]E, the nucleating core of the Aβ peptide [2], and its ability to assemble into 52nm diameter nanotubes (Figure 1A) containing a wall thickness most consistent with a bilayer architecture that approximates biological membranes [3].

A combination of isotope-edited IR, solid-state NMR and oriented diffraction experiments demonstrated that these nanotubes have identical tertiary cross-β structure as the amyloid fibers with H-bonded peptides spaced at 4.7Å in β-sheets and the sheets laminated with a spacing of 9.9Å. Fitting of the small-angle x-ray scattering data to a tube form factor was consistent with a 52nm diameter tube with a 4.3nm thick wall (Figure 1B) [3]. As the length of the KLVFFAE peptide is only 2.2nm, two peptides were assigned to form the tube wall, much like lipid membranes, but the peptides are anti-parallel and out of register by one residue [4]. This peptide bilayer model places the lysine residues at both the solvent exposed nanotube surface and at the bilayer leaflet interface (Figure 1C), creating significant buried positive charge density.

Results and Discussion

The homogeneity and robustness of these assemblies made them accessible to high-resolution solid-state NMR analyses. Of the several tests of the bilayer model, spin-counting $^{13}C\{^{19}F\}$REDOR experiments using the N-acetyl ^{13}CO carbons dephased by tri-fluoroacetic acid (TFA) proved particularly informative. N-Acetyl $CH_3{}^{13}CO$-KLVFFAE-NH_2 peptides were prepared and assembled into nanotubes in the presence of TFA. $^{13}C\{^{19}F\}$REDOR dephasing indicated that all of the acetate ^{13}CO carbons were close to ^{19}F, consistent with TFA serving as the counter-ion for the Lys16 sidechain amine [5]. Washing the nanotubes with Na_2SO_4 removed only half of the TFA ions, as determined by ^{13}CO's dephasing, suggesting that TFA associated with the solvent exposed lysine sidechains were replaced by $SO_4{}^{2-}$. These results identify two distinct and equal populations of TFA ions, and are consistent with the slower exchanging ions being buried at the leaflet interface of a bilayer to passivate the positively charged lysine residues (Figure 1C).

Struck by the similarity of the peptide and lipid bilayer dimensions, taken together with the data that the parent Aβ peptide is generated within a biological membrane, we wondered how this nucleating core might assemble at a lipid/H_2O interface. To simplify the analysis, alkyl chains ranging from two to 16 carbons were covalently attached at the N-terminus of the
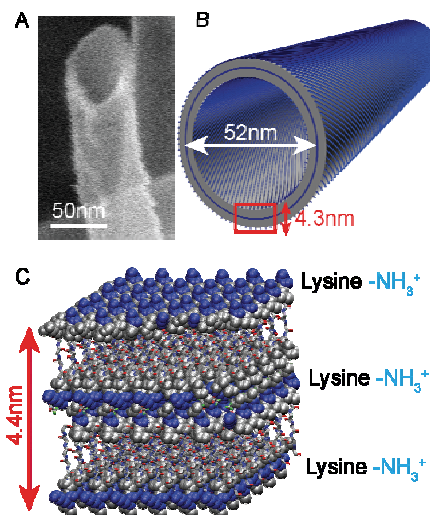
Fig. 1. (A) HR-cryo SEM of cross-β nanotubes assembled from KLVFFAE peptide [4]. (B) Cartoon of nanotube with dimensions from SAXS. (C) Model of peptide bilayer corresponding to red box in (B).

KLVFFAE-NH$_2$ peptide. All these lipid/peptide chimeras self-assembled, but surprisingly, the N-acetyl (C-2) and N-lauryl (C-12) constructs assembled with virtually identical tube morphology visualized by TEM and SEM. Closer examination found that not only were the tube diameters and wall thicknesses of these assemblies indistinguishable, but the characteristic β-sheet CD and IR signatures of both cross-β assemblies were also equivalent. However, the diffraction data indicated that the laminate sheet spacing increased from 9.8Å for the N-acetyl to 11.5Å for the N-lauryl assemblies, and indeed, the laminate sheet spacing increased systematically from 9.8 Å to 13.5Å as a function of the alkyl chain length. Taken together, these data were most consistent with the alkyl chain length specifically modulating cross-β sheet-stacking.

To better understand how sheet stacking could be impacted by the lipid, ^{13}C–^{13}C and ^{13}C–^{15}N distances were measured in nanotubes assembled from the N-[1-^{13}C]lauryl K[^{15}N]LVFFAE-NH$_2$ peptide with ^{13}C DQF-DRAWS and ^{13}C{^{15}N} REDOR solid-state NMR experiments. These distance measurements established that the N-carbonyl of the lauryl fatty acid was bent closer to the peptide backbone in its assembly relative to the acetyl. Similarly, ^{13}C enrichment of the ω-methyl of the C-12 lipid chimera positioned it closer to Val18 than to Leu17 amide nitrogens via ^{13}C–^{15}N distance measurements. These distances triangulated the alkyl chain (Figure 2A) and positioned it buried within the hydrophobic cross-β laminate. While at this point we expect the lipid to remain somewhat mobile within the laminate cavity, constraining both ends of the chain has allowed global structural models to be developed (Figure 2B).

The ability of the nucleating core of the Aβ peptide of Alzheimer's disease to organize as bilayer architectures with dimensions similar to biological membranes may be important to disease etiology. While the dynamics of the H-bonded peptides are certainly different from the flexible

Fig. 2. *(A) Triangulated solutions of ^{13}C-^{15}N distance measurements (green and red spheres) positions ω-^{13}CH$_3$ within the cross-β laminate. The blue spheres represent the amine nitrogens that were ^{15}N enriched. (B) Low resolution structural model positions the alkyl chain buried homogeneously within the cross-β fold.*

alkanes of the lipid membranes, the "accordion like" expansion of the laminate packing to accommodate lipid chains suggests that similar intermolecular assemblies, ones not resolvable by TEM analyses alone, may well form *in vivo*. Indeed, peptide amphiphiles can in principle exhibit behaviors dominated by either the alkane or peptide blocks, and with more finely matched components, respond dynamically to environmental fluctuations. Further analyses of such structures and the evaluation of their physiological and material relevance are now in progress.

Acknowledgments

References

1. Williams, T.L., Serpell, L.C. *FEBS J.*, "Accepted Article"; doi: 10.1111/j.1742 (2011).
2. Williams, A.D., et al. *J. Mol. Biol.* **335**, 833 (2004).
3. Lu, K., Jacob, J., Thiyagarajan, P., Conticello, V.P., Lynn, D.G. *J. Am. Chem. Soc.* **125**, 6391 (2003).
4. Mehta, A.K., et al. *J. Am. Chem. Soc.* **130**, 9829 (2008).
5. Childers, W.S., Mehta, A.K., Ni, R., Taylor, J.V., Lynn, D.G. *Angew. Chem.* **49**, 4104 (2010).

Significance of Intermolecular Hydrogen-Bonding to Form Ion Channel by the Cyclic Tetrapeptide cyclo(D-Ala-Dap)$_2$

Torao Suga, Satoshi Osada, and Hiroaki Kodama

Department of Chemistry, Graduate School of Science and Engineering, Saga University,
Saga, 840-8502, Japan

Introduction

Ion channel peptides allow ions to influx into a lipid membrane through interaction with a lipid bilayer. It has been reported that the cyclic octapeptide cyclo(Trp-D-Leu-Trp-D-Leu-Trp-D-Leu-Gln-D-Leu) results in the ion channel formation [1]. The study has shown cyclic octapeptides stack in the membrane, followed by forming a hollow "nanotube". As a result, ions pass through this intra-molecular pore of the nanotube. According to the nanotube model, a ring-size of cyclic tetrapeptide is too small to cause an appropriate intra-molecular pore for ions passing. However, we previously reported that the use of some cyclic tetetrapeptides induces the ion channel formation [2]. It was suggested that the formation of inter-molecular nanotube aggregates allows for ions passing [3]. However, the specific mechanism is unknown.

In the present study, we evaluated the ion channel formation and the CD spectra for the cyclic tetrapeptide cyclo(D-Ala-Dap)$_2$ (Dap; L-2,3-diaminopropionic acid) under 8 M urea condition to denature intra- or inter-molecular hydrogen-bonding. The purpose of our research was to clarify the mechanism of the ion channel formation by cyclic tetrapeptides.

Results and Discussion

Peptide synthesis was carried out using Fmoc chemistry. The specific experimental procedure had been reported previously [2]. Homology and structure of synthetic peptide was confirmed by analytical RP-HPLC and MALDI-TOF MS. MALDI-TOF MS for cyclo(D-Ala-Dap)$_2$ was 315.03 [expected for (M+H)$^+$ 315.18].

Single ion channel recording for the cyclic tetrapeptide was evaluated with the tip-dipping method in diphytanoylphosphatidylcholine (DPhPC) bilayer [2]. Electrolyte solution was 500 mM KCl solution buffered with 5 mM N-(2-hydroxethyl)piperazine-N'-2-ethanesulfonic acid (HEPES) at pH 7.4. To examine ion selectivity for cyclo(D-Ala-Dap)$_2$, 500 mM CsCl solution buffered with 5 mM HEPES at pH 7.4 was also employed for the sample preparation. Similarly, 500 mM potassium L-Aspartate (KAsp) solution buffered with 5 mM HEPES at pH 7.4 was used for the measurement. The electrolyte composition was symmetrical for both sides of the lipid bilayer. The peptide concentration was 10 nM. To disrupt hydrogen-bonding involved with the peptide, urea was used as a denaturant and 8 M urea solution was prepared at 10 nM peptide concentration, 500 mM KCl solution buffered with 5 mM HEPES at pH 7.4. Data acquisition and analysis were performed using the pClamp software package. Data was filtered at 5 kHz.
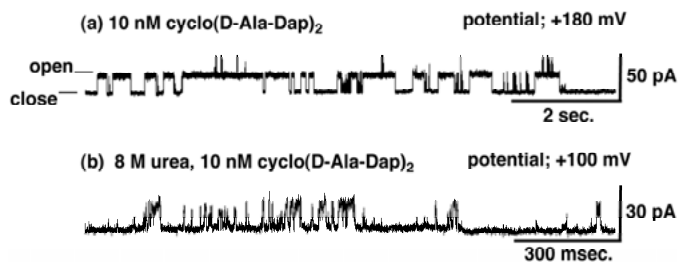
Fig. 1. The single ion channel recording of cyclo(D-Ala-Dap)$_2$ with 500 mM KCl.

As shown in Figure 1(a), the specific open-close transition of pore that reflected ion channel formation was observed at KCl measurement. Ion channel formation was also observed

at CsCl but it was not observed at KAsp measurement (data not shown). Given the common ion species such as KCl and CsCl that were used when ion channel formation was observed, the use of the cationic cyclic tetrapeptide cyclo(D-Ala-Dap)$_2$ resulted in Cl$^-$ anion-selective ion channel formation. This ion selectivity may be attributed to the charge state of peptides, which means a cationic cyclic peptide attract an anion by electrostatic attraction. From the recording under urea condition (Figure 1(b)), clear ion channel formation was not observed at KCl measurement compared to no-urea condition (Figure 1(a)). Instead, fluctuated and discrete current value change was observed. These ion channel recordings suggest the importance of intermolecular hydrogen-bonding between cyclic tetrapeptides to achieve stable ion channel formation. It has been suggested that hydrogen-bonding is important for nanotube formation because one of the most critical driving forces for nanotube formation is stacking cyclic peptides by intermolecular hydrogen-bonding between amide-skeletons of each peptide [1]. If these hydrogen-bondings are disrupted by the denaturant, the nanotube formation may be inhibited. That means it is difficult to form the inter-molecular pores by aggregating nanotubes for ions passing.

CD measurements were carried out with 2 mM DPPC (dipalmitoyl phosphatidylcholine) liposome at 50 mM phosphate buffer. The specific CD spectra change was observed under 8 M urea condition (Figure 2, gray line) compared to no-urea condition (Figure 2, black line). This result shows specific urea effect on conformation change of cyclo(D-Ala-Dap)$_2$ through disrupting hydrogen-bonding.

From the results of urea addition experiments, the destabilization of ion channel formation and conformation change for cyclic tetrapetide cyclo(D-Ala-Dap)$_2$ was suggested. This suggestion indicates a significance of intermolecular hydrogen-bonding for ion channel formation. It may be related to the nanotube formation by hydrogen-bonding between stacking cyclic peptides and aggregation of nanotubes which is necessary for the inter-molecular pore formation to pass through ions.
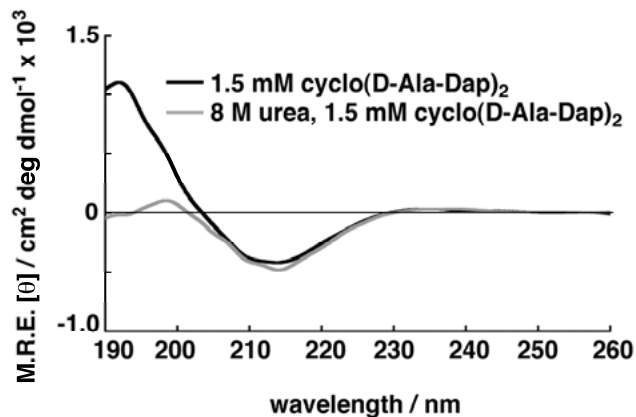
Fig. 2. The CD spectra of cyclo(D-Ala-Dap)$_2$ under 8 M urea condition.

References

1. Ghadiri, M.R., Granja, J.R., Buehler, L.K. *Nature* **369**, 301-304 (1994).
2. Suga, T., Taira, J., Osada, S., Kodama, H. (2010) *Peptide Science* 195-198 (2009).
3. Fernandez-Lopez, S., Kim, H.S., Choi, E.C., Delgado, M., Granja, J.R., Khasanov, A., Kraehenbuehl, K., Long, G., Weinberger, D.A., Wilcoxen, K.M., Ghadiri, M.R. *Nature* **412**, 452-455 (2001).

Crystal Structure of Collagen Model Peptide Containing 4*S*-Hydroxyproline at the X-Position

Daisuke Motooka[1], Kazuki Kawahara[1], Shota Nakamura[2], Masamitsu Doi[3], Yuji Nishiuchi[4], Takashi Nakazawa[5], Takuya Yoshida[1], Yoshinori Nishi[6], Tadayasu Ohkubo[1], and Yuji Kobayashi[6]

[1]*Graduate School of Pharmaceutical Sciences, Osaka University, Osaka , 565-0871, Japan;* [2]*Research Institute for Microbial Diseases, Osaka University, Osaka, 565-0871, Japan;* [3]*Department of Material Science, Wakayama National Collage of Technology, Wakayama, 644-0023, Japan;* [4]*Peptide Institute Inc., Osaka, 562-8686, Japan,* [5]*Department Chemistry, Nara Women's University, Nara, 630-8506, Japan,* [6]*Osaka University of Pharmaceutical Sciences, Osaka, 569-1094, Japan*

Introduction

The collagen molecule consists of three left handed helical polypeptides which twist together to form a loose right handed helix. This unique higher order structure has been shown to due to its characteristic amino acid sequence with repetitions of X-Y-Gly tripeptides where X and Y positions are often occupied by imino acids (Pro or Hyp).

Substituting hydroxyproline derivatives for Pro residues of $(Pro-Pro-Gly)_{10}$ which was first shown to undergo a conformation transition from triple helical structure to single random coil with the temperature change [1], we have investigated the effect of hydroxylation of Pro on collagen which is an interesting post-translational modification during protein synthesis [2]. The results of substitution are summarized in Table 1. We once thought that only substitution by $(2S,4R)$-hydroxyproline (Hyp^R) at the X-position stabilizes the triple helix. Zagari et al. proposed an empirical rule to explain the effects of the substitution on stability of the triple helix depending on the position and the stereochemistry of the proline derivatives [3]. Based on the results of X-ray analyses which revealed that $(2S,4R)$ derivatives have a propensity to take up pucker and $(2S,4S)$ derivatives to take down pucker while Pro itself can take both puckers, the rule insists that the helix can be stabilized, when a residue with down pucker exists in X position and one with up pucker in Y position. This rule applies well for the cases listed in Table 1 except for $(Hyp^S-Pro-Gly)_{10}$ where Hyp^S is $(2S,4S)$-hydroxyproline. Zagari et al. [3] explained this exception by hypothesizing that hydroxyl group of Hyp^S with down pucker might come into collision with the pyrrolidine ring in the adjacent chain. Later we found that $(Hyp^S-Pro-Gly)_{15}$ forms triple helix though it is less stable even than $(Pro-Pro-Gly)_{15}$ [4]. Here we tried to clarify this controversial problem by X-ray analysis. Although we failed to crystallize $(Hyp^S-Pro-Gly)_{15}$, we succeeded in crystal analysis of the host-guest copolypeptide $(Pro-Hyp^R-Gly)_4$-$(Hyp^S-Pro-Gly)_2-(Pro-Hyp^R-Gly)_4$ named as $(PH^RG)_4(H^SPG)_2(PH^RG)_4$.

Table 1. Summary of the structures of collagen model peptides

peptides	*structure[a]*	$T_{1/2}/{}^oC$	*peptides*	*structure[a]*	$T_{1/2}/{}^oC$
$(Pro-Pro-Gly)_{10}$	t	31			
$(Pro-Hyp^R-Gly)_{10}$	t	62	$(Pro-Hyp^S-Gly)_{10}$	s	< 4
$(Hyp^R-Pro-Gly)_{10}$	s	< 4	$(Hyp^S-Pro-Gly)_{10}$	s	< 4

[a]*at 4°C, t = triple helix, s = single chain*

Material and Method

$(PH^RG)_4(H^SPG)_2(PH^RG)_4$ was synthesized by polycondensation of the tripeptides with the Fmoc method as previously described. CD spectra were measured on a JASCO J-720W spectropolarimeter. The crystals of $(PH^RG)_4(H^SPG)_2(PH^RG)_4$ were obtained by the sitting drop vapor diffusion method. X-ray diffraction data were collected with a RIGAKU Jupiter 210 CCD detector at beamline BL38B1 of SPring-8 (Hyogo, Japan) at 100 K. Phase determination was

performed by molecular replacement method with the whole structure of $(Pro-Pro-Gly)_{10}$ (PDB entry 1K6F) as a search model.

Results and Discussion

The CD spectra of $(PH^RG)_4(H^SPG)_2(PH^RG)_4$ were characteristic of a triple helix and showed the transition to a single coil state with the transition temperature of 49^oC which is lower than that at 62^oC observed for $(Pro-Hyp^R-Gly)_{10}$. Therefore the substitution of two central triplets of $(Pro-Hyp^R-Gly)_{10}$ with $(Hyp^S-Pro-Gly)_2$ resulted in the marked decrease of the thermal stability of the triple helix.

On the contrary, the resulting structure after the structural refinements shows that the main chain conformation of $(PH^RG)_4(H^SPG)_2(PH^RG)_4$ was very similar to that of $(Pro-Hyp^R-Gly)_{10}$ [5]. There was almost no difference of the averaged values of the unit height and the unit twist between those in the host and the guest peptide units and, furthermore, these values are almost same to those of $(Pro-Hyp^R-Gly)_{10}$. This means that the main chain of $(PH^RG)_4(H^SPG)_2(PH^RG)_4$ takes the triple helical structure without any disturbance due to the incorporation of Hyp^S unit. It is noteworthy that 30% of Hyp^S residues which exist in X position take up pucker while 70% of them are in down pucker and that the averaged χ^1 value of Hyp^S in down pucker was far less than that typically observed for Pro analogs with down puckering at the X position of collagen model peptides (Figure 1). Thus we concluded that this shallow puckering of Hyp^S should allow the peptide to form a triple helix by avoiding the steric clash which Zagari et al. expected and that the stress to deform the pyrorridine ring of Hyp^S should decrease its stability. Also the existence of Hyp^S with up pucker in violation of its propensity might reduce the stability.
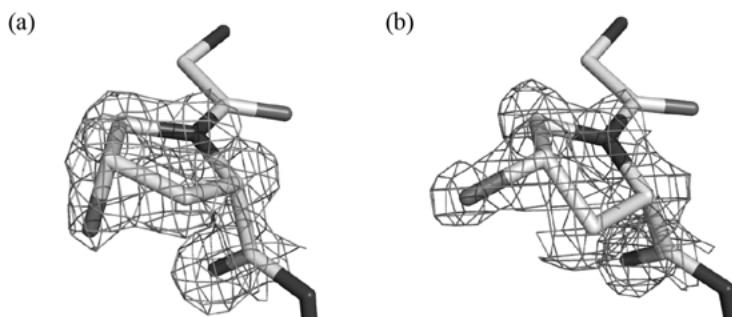
Fig. 1. $2F_o$-F_c ($\sigma = 1.5$) maps of Hyp^S, (a) Hyp^S with down pucker, (b) Hyp^S with up pucker.

Acknowledgments

References

1. Kobayashi, Y., Sakai, R., Kakiuchi, K., Isemura, T. *Biopolymers* **9**, 415-425 (1970).
2. Nishi, Y., Uchiyama, S., Doi, M., Nishiuchi, Y., Nakazawa, T., Ohkubo, T., Kobayashi, Y. *Biochemistry* **44**, 6034-6042 (2005).
3. Vitagliano, L., Berisio, R., Mazzarella, L., Zagari, A. *Biopolymers* **58**, 459-464 (2001).
4. Motooka, D., Kawahara, K., Sato, N., Nakamura, S., Uchiyama, S., Doi, M., Nishiuchi, Y., Nakazawa, T., Yoshida, T., Ohkubo, T., Nishi, Y., Kobayashi, Y. *Peptides 2008* **30**, 612-613 (2008)
5. Okuyama, K., Hongo, C., Fukushima, R., Wu, G., Narita, H., Noguchi, K., Tanaka, Y., Nishino, N. *Biopolymers* **76**, 367-377 (2004).

A Nanometric Platform for Synthesis and Biological Evaluation of Peptides

Victoria Machtey[1,2], Raz Khandadash[1], Adva Aizer[3], Rakefet Ben-Yishai[3], Yaron Shav-Tal[3], Aryeh Weiss[2], and Gerardo Byk[1]

[1]*Laboratory of Nano-Biotechnology, Department of Chemistry;* [2]*School of Engineering;* [3]*Center for Advanced Materials and Nanotechnology, Mina and Everard Goodman Faculty of Life Sciences, Bar Ilan University, Ramat Gan-52900, Israel*

Introduction

There is a keen research interest in developing nano-sized particles useful for varied applications such as biomedicine and drug delivery, biophotonics, sensors and catalysis. One important class of nanoparticles are stimuli-responsive hydrogel nanoparticles such as thermo-sensitive Poly (N-isopropylacrylamide) (PNIPAAm) nanoparticles (NP's). These NP's have recently become widely studied for biomedical applications because of their reversible thermo-sensitive property. However, while their potential applications are diverse, the high toxicity measured for PNIPAAm particles prevents their eventual future use in clinical trials. Cross-linked Polyethylene glycol (PEG) based hydrogel materials are especially interesting for biological and medicinal applications because of their biocompatibility without being degraded by the host and low protein adsorption in comparison to non-PEG containing particles, however many of the available nano particles hydrogels (NPHG's) contain highly degradable functional groups [1], thus they lack chemical stability. Synthesis of NPHG's with both chemical and biological compatibility remains a challenging task. Herein, we designed and synthesized cross-linked NPHG's with well-controlled size and size distributions. The toxicity of these new NPHG's was evaluated in appropriate cell models using XTT viability assay at different concentrations. For nuclear transport, direct synthesis of FITC-Nuclear Localizing Signal (NLS) on NPHG's was performed using a unique methodology disclosed in a separate presentation in this proceedings book [2], and their bio-functionality was assessed in live cells.

Results and Discussion

Cross-linked PEG NPHG's were directly synthesized by free radical dispersion polymerization reaction to obtain 20, 50, 100 and 160 nm, using mixtures containing low molecular weight PEG-mono and diacrylamide, N,N-methylenebisacrylamide (BIS) and N-isopropylacrylamide (NIPA) that plays as nucleation growth for the polymerization and formation of the nanoparticles thanks to its low lower critical solution temperature (LCST) of 32°C. The monoacrylamide-PEG possesses free amino groups necessary for the further synthesis of the biomolecules or their conjugation. The PEG-diacrylamide and BIS play the role of cross linkers necessary for obtaining non soluble/stable NP's. Figure 1 shows the TEM micrograph and Dynamic light scattering (DLS) profiles of three representative batches of NPHG's of 20, 100 and 150 nm prepared at different polymerization conditions.
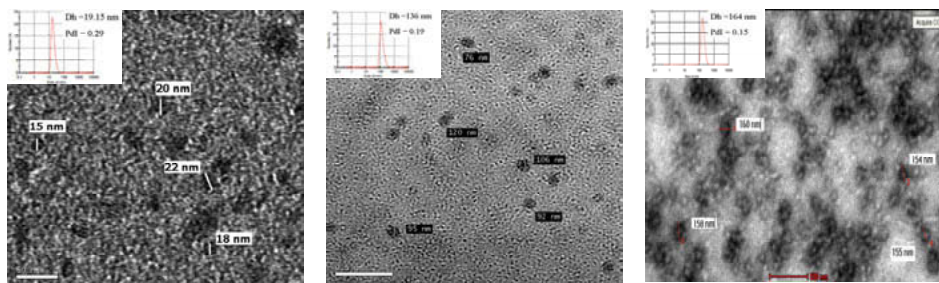
Fig. 1. TEM micrographs DLS analysis of dry NPHG's produced by the reaction of NIPAAm/(Acr)$_{1.1}$PEG$_{1900}$/BIS at different ratios (stained with uranyl acetate).
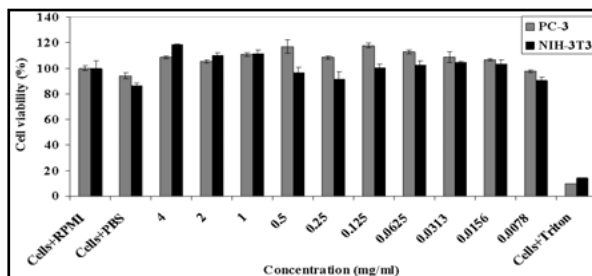
Fig. 2. Cell viability (%) of NPHG's at increasing concentrations after 24 h incubation (XTT assay). Each point represents the mean value±SD (n=2). PC-3 (grey); NIH-3T3 (black).

Dose dependent cytotoxicity studies of 150 nm NPHG's were carried out on PC-3 and NIH-3T3 cell lines. Results demonstrate a complete lack of toxicity even at a high dose of 4 mg/ml on both cell lines making this material suitable for live cells assays (see Figure 2).

Understanding the interaction of NPHG's with the cell membrane and their trafficking through cells is imperative to properly explore the use of NP's for efficient intracellular delivery of therapeutics agents such as peptides or nucleic acids. Thus, in this study, we carried out assays to test the ability of NPHG's (150 nm) to enter the cell and nucleus by incorporating NLS peptide (PKKKRKV) which has been shown to facilitate nuclear targeting. The resulting NLS-modified NPHG's were tested for PC-3 cells uptake in culture. FITC-NLS-NPHG's were incubated with cells for 4 hours and visualized by confocal microscopy. The FITC-NLS-NPHG's were taken up into the cytoplasm as observed in the different Z-cuts, but couldn't be observed in the nucleus (see Figure 3). FITC-labeled NPHG's (150 nm) with no NLS signal, disclosed lower entrance to the cells when incubated in the same conditions (data not shown). We suggest that NPHG's of 150 nm are too-big for crossing the nuclear pore even in the presence of the NLS signal. In the future, we will test the ability of smaller nanoparticles to enter the nucleus using the same NLS signal peptide. Other cell signaling/trafficking modifications are being investigated for their application to drug targeting, imaging and live cell screening and will be reported elsewhere.
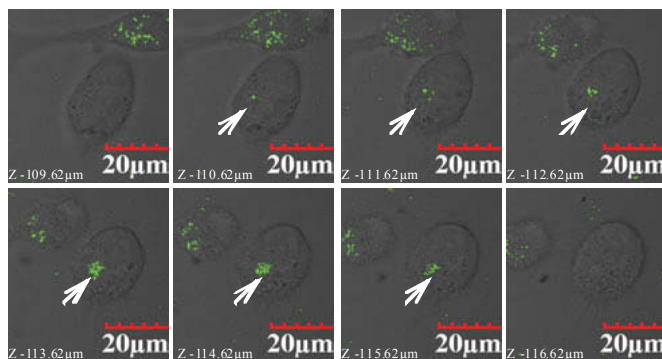
Fig. 3. Confocal images showing the cellular localization and distribution of FITC-labeled NLS-NPHG's (150 nm) in PC-3 cell lines. Each stack is 1 μm. Arrows point on the NPHG's accumulation in the cells.

Acknowledgments

References

1. Leobandung, W., Ichikawa, H., Fukumori, Y., Peppas, N.A. *J. Appl. Polym. Sci.* **87**, 1678-1684 (2003).
2. Khandadash, R., et al. *in this Proceedings Book*.

Versatile Nanoplatform for Cancer Imaging and Therapy

Yuanpei Li, Juntao Luo, Kai Xiao, Joyce Lee, Wenwu Xiao, and Kit S. Lam*

Department of Biochemistry and Molecular Medicine, University of California Davis, 2700 Stockton Blvd., Sacramento, CA, 95817, U.S.A., E-mail: Kit.Lam@ucdmc.ucdavis.edu

Introduction

We recently developed a versatile nanocarrier drug-delivery system based on micelles formed by a novel class of well-defined polymers of linear PEG and oligo-cholic acids (telodendrimers) in aqueous solution [1-5]. Various poorly water-soluble anticancer drugs, such as paclitaxel (PTX), doxorubicin, vincristine, SN-38, BCNU, temsirolimus, bortezomib, lapatinib, sorafenib and dexamethasone can be effectively incorporated inside these polymeric micelles. The novel micelle preparations of paclitaxel were demonstrated to be not only more efficacious in nude mice bearing ovarian cancer xenografts but also less toxic than the clinical paclitaxel formulations, such as Taxol® and Abraxane® [1-3]. Furthermore, the modular design enables us to assemble the different components in a step-wise fashion with high flexibility via standard peptide synthesis method (Fmoc-chemistry). For example, building blocks, such as hydrophilic spacers and amino acids, can be easily introduced into the telodendrimer at the desired position with the optimal density. In the present study, we synthesized a series of thiolated telodendrimers and developed a self-assembling disulfide-crosslinking system so that micelles can be further stabilized to avoid premature release of the loaded drugs during circulation. After reaching the tumor sites, the intra-micellar disulfide bonds will be cleaved under reductive conditions inside the tumor cells (~10 mM concentration of glutathione) or at the tumor site on-demand after intravenous administration of N-acetylcysteine (NAC), a FDA approved reducing agent, leading to drug release.
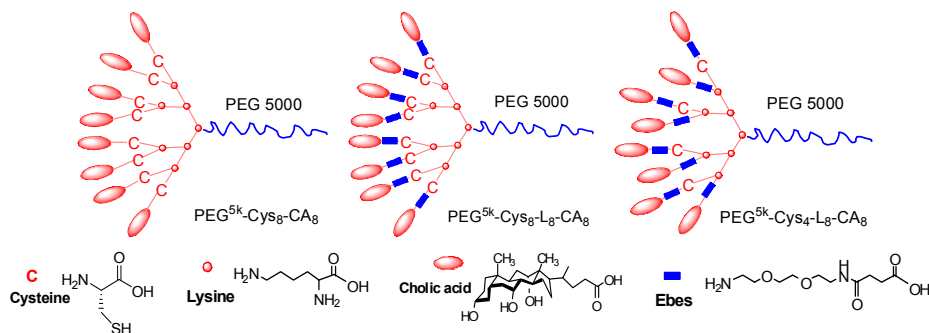
Fig. 1. The schematic representation the thiolated telodendrimers.

Results and Discussion

In order to develop a reversible stable nanocarrier system, we designed and synthesized a series of thiol containing telodendrimers by introducing different number of cysteines and hydrophilic spacers (Ebes) to the dendritic lysine cluster (Figure 1) via step-wise peptide chemistry [1-3]. Telodendrimer is designated as PEG^{5k}-Cys_8-CA_8, PEG^{5k}-Cys_8-L_8-CA_8 and PEG^{5k}-Cys_4-L_8-CA_8 corresponding to length of PEG, and the number of cysteines, hydrophilic spacers and cholic acids in the dendritic structure (Figure 1). The thiol-free telodendrimer, PEG^{5k}-CA_8 was also synthesized for comparison as described previously [1]. Quantitative Ellman's test indicated that the number of covalently attached cysteines in these thiolated telodendrimers was consistent with the molecular formula of the target telodendrimers (Table 1).

Reversibly cross-linked micelles were prepared by oxidization of free thiols to form disulfide bonds in the core. After the instant formation of micelles upon dispersion in aqueous solution, the free thiols of PEG^{5k}-Cys_8-CA_8, PEG^{5k}-Cys_8-L_8-CA_8 and PEG^{5k}-Cys_4-L_8-CA_8 were gradually

Table 1. Physico-chemical properties of thiolated telodendrimers and the corresponding disulfide cross-linked micelles

	N_{thiol} In structure [a]	N_{thiol} By Ellman's test [b]	Size before crosslink (nm) [c]	Size after crosslink (nm) [c]	PTX Loading (mg/mL) [d]
PEG^{5k}-Cys$_8$-CA$_8$	8	7.96	35 ±12	34 ±11	0.6
PEG^{5k}-Cys$_8$-L$_8$-CA$_8$	8	7.93	32 ± 8	32 ± 8	1.5
PEG^{5k}-Cys$_4$-L$_8$-CA$_8$	4	3.97	30 ± 7	28 ± 4	4.6

[a]*Number of cysteines in the structure of the thiolated telodendrimers.* [b]*Number of cysteines, obtained via Ellman's test.* [c]*Measured by dynamic light scattering particle sizer.* [d]*PTX loading capacity of disulfide cross-linked micelles, in the presence of 20 mg/mL of telodendrimers and 5 mg/ mL PTX initial loading, measured by HPLC.*

oxidized by oxygen to form disulfide linkages. Interestingly, these micelles retained similar particle sizes of around 30 nm with the narrow distribution before and after disulfide cross-linking (Table 1). This result suggests that disulfide bond formation occurred within micelles. We believe the disulfide crosslinking reaction was confined to within each micelle by the PEG corona, thus preventing any inter-micellar crosslink that could lead to aggregates. We have demonstrated that PTX, a wide-spectrum anti-tumor agent, can be conveniently encapsulated into these disulfide cross-linked micelles via solvent evaporation method [1]. PTX loading capacity for PEG^{5k}-Cys$_8$-CA$_8$, PEG^{5k}-Cys$_8$-L$_8$-CA$_8$ and PEG^{5k}-Cys$_4$-L$_8$-CA$_8$ micelles was determined to be 0.6, 1.5 and 4.6 mg/mL, respectively (Table 1).

Cross-linking of the micelles reduced their apparent critical micelle concentration and greatly enhanced their stability in non-reductive physiological conditions (e.g. human plasma, 50% v/v) as well as under severe micelle-disrupting condition (sodium dodecyl sulfate, 2.5 mg/mL). The release of PTX from these disulfide cross-linked micelles was significantly slower than that from non-cross-linked micelles, but drug release can be facilitated by increasing the concentration of reducing agent (glutathione) to an intracellular reductive level (10 mM). We further prepared micelles with different levels of disulfide crosslinking (0%, 10%, 20%, 30%, 50%, 75% and 100%) by using different ratios of PEG^{5k}-CA$_8$ and PEG^{5k}-Cys$_4$-L$_8$-CA$_8$. As expected, the higher the crosslinking level, the more stable the micelles, the slower the release of drugs from the micelles, and the longer it took for the micelles to dissociate in the presence of SDS and glutathione.

In summary, we have developed a reversible disulfide cross-linked micellar drug-delivery system that can minimize premature drug release during circulation but can be triggered to release drug inside the tumor cells with high glutathione level or at the tumor site with exogenously added reducing agents on demand. This new class of nanotherapeutics shows great promise in future cancer therapy and imaging.

Acknowledgments

References

1. Xiao, K., et al. *Biomaterials* **30**, 6006-6016 (2009).
2. Li, Y., Xiao, K., Luo. J., Lee, J., Pan, S., Lam, K.S. *J. Control Release* **144**, 314-323 (2010).
3. Luo, J., et al. *Bioconjug. Chem.* **21**, 1216-1224 (2010).
4. Xiao, K., et al. *Biomaterials* **32**, 3435-3446 (2011).
5. Li, Y., et al. *Biomaterials* **32**, 6633-6645 (2011).

Au$_{25}$ Nanoclusters Capped by Photoactive Aib-based Peptide Ligands

Ivan Guryanov, Sabrina Antonello, Mahdi Hesari, Martina Zamuner, and Flavio Maran

Department of Chemistry, University of Padova, via Marzolo 1, Padova, 35131, Italy

Introduction

Nanostructured materials are essential elements of new technologies and biomedical research. Monolayer-protected gold nanoclusters (MPC) with a core diameter <1.5 nm are of particular interest because electronic-band energetics leads to quantum confinement effects, thereby causing these MPCs to display molecule-like properties, such as a well defined HOMO-LUMO gap [1,2]. The monolayer not only protects the core from particle aggregation but also furnishes a way to control the electrochemical, optical, and chemical properties of the MPC itself. Peptides based on the α-aminoisobutyric (Aib) acid unit are very interesting molecules because they form stiff 3$_{10}$-helices and also they are short [3]. Thiolated Aib peptides can be used to stabilize particularly small MPCs [4] and we showed that, due to their strong dipole moment, these peptides affect the MPC energy levels and thus its electrochemical behavior [5]. Here we report the synthesis and properties of gold MPCs modified by ligand exchange with a thiolated azobenzene peptide,

HS-CH$_2$CH$_2$-Ph-N=N-Ph-CO-Aib$_3$-NHtBu. We speculated that *trans-cis* isomerization of the N=N bond would have changed the orientation of the peptide dipole moment with respect to the nanoparticle core and, consequently, modified the MPC properties.

Fig. 1. Structure and MALDI-TOF spectrum of Au$_{25}$(SCH$_2$CH$_2$Ph)$_{18}$ (A), ligands used for MPC modification (B) and scheme of the ligand exchange reaction with subsequent photoisomerization (C).
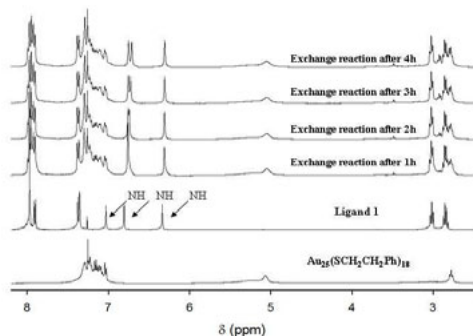
*Fig. 2. NMR spectra of Au$_{25}$(SCH$_2$CH$_2$Ph)$_{18}$, ligand **1** and the ligand exchange reaction mixture of MPC with 0.7 eq of **1** (CDCl$_3$).*

Results and Discussion

The ligand exchange method was used to introduce different amounts of thiolated azo-derivatives **1** and **2** into the capping monolayer of preformed Au$_{25}$(SCH$_2$CH$_2$Ph)$_{18}$ clusters. We started from monodisperse clusters, as shown by matrix-assisted laser desorption ionization time-of-flight (MALDI-TOF) mass spectrometry experiments (Figure 1). The exchange percentage was determined by destruction of the MPCs with iodine, followed by ^{1}H NMR determination of the ratio between the resulting oxidized phenylethanethiol and exogenous ligand (Table 1).

The exchange reaction was monitored by NMR spectroscopy. Figure 2 shows that while the characteristic NMR pattern of Au$_{25}$(SCH$_2$CH$_2$Ph)$_{18}$ does not change [6], noticeable changes in the NMR spectrum of the thiolated ligand take place. This is attributed to the insertion of the new ligand into the MPC monolayer.

A *B* *C*

Fig. 3. FT-IR analysis of the substituted MPC (A), UV spectra of trans→cis isomerization of Trt-protected **1** (B) and of the MPC containing 20% of **1**(C) at 366 nm.

Table 1. Gold nanoparticles obtained by ligand-exchange

Ligand	Exogenous Ligand to Ph(CH$_2$)$_2$SH Molar Ratio	Extent of Exchange	Percentage of Exchange
1	1.72	16-17	~90%
1	0.7	5-6	~30%
1	0.2	3-4	~20%
2	0.7	7-8	~40%

FT-IR analysis (Figure 3, *A*) indicates that the peptide part of the ligand adopts a helical conformation. The IR bands of free NH-groups as well as interchain and intrachain H-bonds could be identified. The red shift of the intrachain H-bond frequency can be attributed to the enhancement of the stiffness of the peptide helix in the monolayer. A further shift takes place upon irradiation at 366 nm causing *trans→cis* isomerization, but the effect vanishes when the nanoparticle is heavily substituted (90%), in keeping with sterical hindrance hampering isomerization. This is in line with the optical behavior of the MPCs: the decrease of the intensity of the main band due to the *trans→cis* transition upon irradiation at 366 nm is much less pronounced than for the free ligand (Figure 3, *B* and *C*), and this decrease is less marked for more substituted MPCs (data not shown). Furthermore, the reverse *cis→trans* isomerization (thermal decay) is about 3 times faster than in the case of the free ligand.

The MALDI-TOF spectra of the exchanged products revealed the presence of a mixture of clusters with a main stoichiometry Au$_{21}$L$_x$L'$_{14-x}$S (L = SCH$_2$CH$_2$Ph, L' = **1** or **2**, x = 8-14), together with smaller clusters derived from successive losses of AuL. Differential pulse voltammetry (DPV) showed that the ligand exchange causes a shift of the two main oxidation peaks toward more positive potentials; the same result was observed for exchange with ligand **2** (Figure 4, *B*). While the current of the two peaks progressively decreases, a new peak appears at about 0.7 V. In 8h all the peculiar signals of Au$_{25}$ cluster disappeared. Both MALDI-TOF and DPV experiments thus highlight a delicate balance between extent of exchange and etching of the cluster core.

A *B*

Fig. 4. DPV of Au$_{25}$(SCH$_2$CH$_2$Ph)$_{18}$ (A), ligand exchange reaction with 0.7 eq of **2** (B), 0.1M TBAPF$_6$/CH$_2$Cl$_2$.

References

1. Murray, R.W. *Chem. Rev.* **108**, 2688-2720 (2008).
2. Antonello, S., et al. *J. Am. Chem. Soc.* **129**, 9836-9837 (2007).
3. Toniolo, C., et al. *Biopolymers* **60**, 396-419 (2001).
4. Fabris, L., et al. *J. Am. Chem. Soc.* **128**, 326-336 (2006).
5. Holm, A.H., et al. *Langmuir*. **22**, 10584-10589 (2007).
6. Venzo, A., et al. *Anal. Chem.* DOI: 10.1021/ac2012653.

Effects of Peptide-Amphiphile α1(IV)1263-1277 on Liposome Stability

Margaret W. Ndinguri[1,2] and Gregg B. Fields[1,2]

[1]*Department of Biochemistry, University of Texas Health Science Center, 7703 Floyd Curl Drive, San Antonio, TX, 78229, U.S.A.; [2]Torrey Pines Institute for Molecular Studies, 11350 SW Village Parkway, Port St. Lucie, FL, 34987, U.S.A.*

Introduction

One of the major goals in drug delivery is the creation of new modifications to established drugs with the aim of steering them to their objective target in the most effective way. Encapsulation of drugs into liposomes can effectively enhance drug delivery to its intended biological target. Liposomes in particular have attracted much attention as site-specific drug delivery vehicles because of their biocompatibility [1,2], and the ease with which they can be manipulated to accommodate targeting ligands to further increase the specificity and therefore potency of encapsulated chemotherapeutics. The sequence to which CD44 binds within the type IV collagen triple-helix has been identified as α1(IV)1263-1277 [3]. Peptide-amphiphiles (PAs) can be used as targeting ligands with high specificity and low degradation and can conveniently be incorporated into various drug delivery vehicles such as liposomes [4]. Our group has previously reported an efficient synthetic method for preparation of targeted liposomes using various formulations. In the present study, we prepared targeted liposomes with 5% and 10% α1(IV)1263-1277 PA and examined the physical stability of the liposomes.

Results and Discussion

Preparation of liposomes containing peptide-amphiphiles have been described previously by Rezler et al. [4] The present study used an α1(IV)1263-1277 PA construct with a C_{16} tail which maximizes the potential hydrophobic interactions with the C_{18} phospholipid tails of DSPG and DSPC in the lipid bilayer. To confirm the incorporation of α1(IV)1263-1277 PA within the lipid bilayer, liposomes were treated with ethanol. MALDI-TOF mass spectral analysis of the resulting solution produced a peak corresponding to the mass of the α1(IV)1263-1277 PA ($[M+H]^+$ = 3813.3 Da, theoretical $[M+H]^+$ = 3813.3 Da).

To determine the effect that α1(IV)1263-1277 PA has on liposomal stability, DOX-loaded liposomes were prepared with and without the α1(IV)1263-1277 PA. Fluorescence intensity for each vesicle sample at 4, 25, or 37°C was then measured at selected time points over a 1 month period. The fluorescence intensity was measured using a Spectra Max Gemini EM Fluorescent Plate Reader (Molecular Devices) at $\lambda_{excitation}$ = 480 nm and $\lambda_{emission}$ = 590 nm. Complete release of DOX from the vesicles at each time point yields 100% dequenching, and was obtained from control ethanol-treated liposome samples. The percentage release of DOX from the vesicles was determined from the fluorescence intensity of each sample relative to 100% dequenching, which can then be expressed in terms of percentage of DOX release.

The presence of α1(IV)1263-1277 PA did not serve to destabilize the liposomes used in this study. The targeted and non-targeted liposomes exhibited similar stability profiles over a 1 month period, with ~30% DOX release at 4°C (Table 1) and 36-49% DOX release at 25 and 37°C (Tables 2 and 3). Within the first few hours following preparation, the liposomes again demonstrated similar and minimal DOX release. At 4°C, only <6% release was observed for both targeted and non-targeted liposomes, and <10 or ~12% release when incubated at either 25 or 37°C, respectively.

Table 2. DOX release from liposomes^a at 25°C

Time (h)	% Leakage	
	Targeted	*Non- targeted*
0	0	0
1	7	10
500	25	23
1000	49	43

Table 3. DOX release from liposomes^a at 37°C

Time (h)	% Leakage	
	Targeted	*Non- targeted*
0	0	0
1	12	11
500	27	34
1000	37	45

^{a}The ratio of distearoyl phosphatidylglycerol (DSPG), distearoyl phosphatidylcholine (DSPC), cholesterol and distearoyl phosphatidylethanolamine poly(ethyleneglycol) 2000 (DSPE-PEG-2000) in non-targeted liposomes is (1:4:5:0.5) and the ratio of DSPG, DSPC, cholesterol, α1(IV)1263-1277 PA and DSPE-PEG-2000 in targeted liposomes is (1:4:5:0.5-1:0.5)

Data presented here is for the targeted liposomes possessing 10% PA, but similar results were observed for liposomes incorporating 5% PA. Thus, the presence of the α1(IV)1263-1277 PA did not serve to destabilize the liposomes used in this study.

Acknowledgments

References

1. New, R.R.C. *Characterization of liposomes. In Liposomes: A Practical Approach*, New, R.R.C., Ed. IRL Press: Oxford, 1990; pp 105-161.
2. Tarahovsky, Y.S. *Biochemistry (Moscow) 75*, 811-824 (2010).
3. Lauer-Fields, J.L., Malkar, N.B., Richet, G., Drauz, K., Fields, G.B. *J. Biol. Chem.* **278**, 14321-14330 (2003).
4. Rezler, E.M., Khan, D.R., Lauer-Fields, J.L., Cudic, M., Baronas-Lowell, D., Fields, G.B. *J. Am. Chem. Soc.* **129**, 4961-4972 (2007).

Peptide/Agarose Matrices as a New Biomaterial

Yuji Yamada and Motoyoshi Nomizu

Laboratory of Clinical Biochemistry, Tokyo University of Pharmacy and Life Sciences, Hachioji, Tokyo, 192-0392, Japan

Introduction

Tissue engineering consists of cells, scaffold materials, and suitable signals to maintain or improve tissue functions. In native tissues, cells are held within three-dimensional extracellular matrices (ECM) and mimicking ECM as a scaffold is a common goal in biomaterial studies for tissue engineering. Matrigel is a commercially-available, soluble extract of basement membrane, a thin layer of ECM, which has been widely used as a substrate for three-dimensional cell culture *in vitro*. However, Matrigel is from mouse tumor and not applicable for clinical use as a basement membrane material. Our goal is development of a chemically synthetic Matrigel as a biomaterial for tissue engineering. We have identified a number of bioactive peptides from laminin, a major component of the basement membrane, using a systematic screening with synthetic peptides [1]. Previously, we conjugated the peptides to polysaccharides, including chitosan and alginate, and demonstrated that the peptide-chitosan and -alginate matrices have various biological activities. We also found that chitosan and alginate behave in a different manner as a cell scaffold [2]. Here, we focused on agarose, a common polysaccharide, as a scaffold material. Laminin bioactive peptide AG73 (RKRLQVQLSIRT, binds to syndecan receptors) [3] was mixed with agarose matrices and biological activities of the AG73/agarose matrices were examined using several types of cells.

Results and Discussion

In this study, AG73 was mixed with three different agarose matrices, 0.1% agarose hydrogel, 0.5% agarose hydrogel, and agarose membrane. The agarose membrane was prepared by drying up of the 0.5% agarose hydrogel for 24 hr. First, human dermal fibroblast (HDF) attachment was evaluated. HDFs (2 x 10^4 cells/well) were added on the AG73/agarose matrices in 96-well plate and incubated for 1 hr. As a result, the AG73/agarose matrices promoted cell attachment and cell behavior depended on the amount of AG73 and hardness of the matrices (Figure 1). The AG73/agarose membrane showed the strongest cell attachement activity and the AG73/0.1% agarose hydrogel showed the weakest activity, suggesting that the hard agarose matrices promoted strong cell attachment than soft matrices.
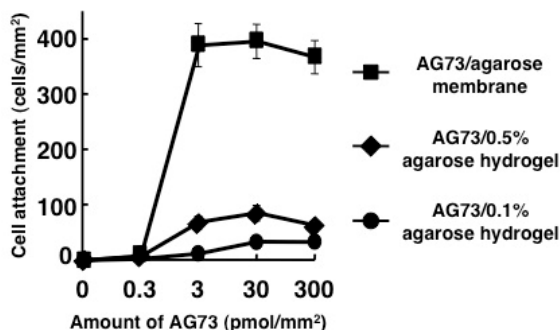
Fig. 1. Cell attachment activity of the AG73/agarose matrices.

We cultured human submandibular gland (HSG) cells on the AG73/agarose matrices and examined acinar formation assay. HSG cells (3 x 10^4 cells/well) were added on the AG73/agarose matrices and double diluted Matrigel, and incubated for 48 hr. As a result, HSG cells cultured on the AG73/0.1% agarose hydrogel formed multicellular structures (Figure 2B) that are similar to the acinar formation structures on the Matrigel (Figure 2A). On the other hand, AG73/0.5% agarose hydrogel and AG73/agarose membrane did not induce multicellular structures (Figure 2C,D). These data suggest that the soft matrices are suitable for acinar structure formation. However, the structures that formed with AG73 do not have cell nuclei polarized to the basal surface (Figure 2F) as well as those that formed with the double diluted Matrigel (Figure 2E). As Hoffman et al. reported [4], AG73 may be providing some but not all of the signals for the morphological changes in the process of acinar differentiation.
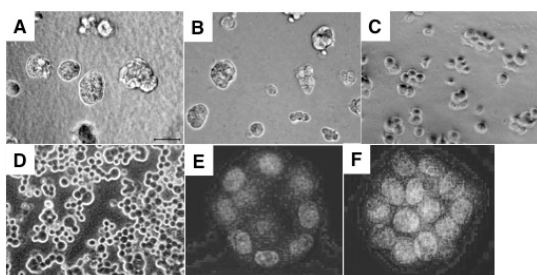
Fig. 2. Multicellular structures of HSG cells on double diluted Matrigel (A), AG73/0.1% agarose hydrogel (B), AG73/0.5% agarose hydrogel (C), and AG73/agarose membrane (D). The cell nuclei were stained with DAPI (on the double diluted Matrigel (E) and AG73/0.1% agarose hydrogel (F)).

Next, we examined endothelial capillary formation assay using the AG73/agarose matrices. SVEC4-10 cells (6×10^4 cells/well) were added on the matrices and Matrigel, and incubated for 4 hr. As a result, SVEC4-10 cells formed cellular network structures on the AG73/agarose membrane (Figure 3D). This structure was similar to the capillary-like structures on Matrigel (Figure 3A). The cells did not form the network on the AG73/agarose hydrogels (Figure 3B,C), suggesting that the soft matrices are difficult to promote the capillary-like network structures. We also examined effect of EDTA and heparin to the capillary network formation on the AG73/agarose membrane. EDTA inhibits cation-dependent cell adhesion and heparin inhibits glycosaminoglycan (GAG), including syndecan, -dependent cell adhesion. As a result, heparin strongly inhibited cell-matrix adhesion, on the other hand, EDTA inhibited cell-cell adhesion, respectively. These results suggested that the capillary-like structure formation with the AG73/agarose membrane was induced by syndecan-dependent cell-matrix adhesion and cation-dependent cell-cell adhesion, such as cadherin and integrin.

In summary, the AG73/agarose matrices promoted various biological activities, including cell attachment, acini-like structure formation, and capillary-like network structure formation, as well as Matrigel. It was found that cell behavior on the AG73/agarose matrices depended on hardness of the matrices. The HSG cells formed acini-like structures on the soft matrices but not on the hard matrices. On the other hand, SVEC4-10 cells formed capillary-like network structures on the hard matrices but not on the soft matrices. That is, as with Matrigel, biological functions of the AG73/agarose matrices can be controlled by their hardness. These results suggest that the peptide/agarose matrices have a potential to be used as an artificial basement membrane, replacing

Fig. 3. Endothelial cells (SVEC4-10 cells) were cultured on Matrigel (A), AG73/0.1% agarose hydrogel (B), AG73/0.5% agarose hydrogel (C), and AG73/agarose membrane (D). The cells were also cultured on the AG73/agarose membrane in the presence of heparin (E) and EDTA (F).

Matrigel. Further, from this study, we found that the peptide/agarose matrices can be applied to both two- and three-dimensional cell culture systems because agarose hydrogels are easy to regulate their hardness and forms. Finally, the peptide/agarose matrices will be a powerful tool for tissue engineering and clinical applications as a multifunctional biomaterial.

Acknowledgments

References

1. Suzuki, N., et al. *Connect. Tissue Res.* **46**, 142-152 (2005).
2. Yamada, Y., et al. *Biopolymers* **94**, 711-720 (2010).
3. Yamada, Y., et al. *Biomaterials* **32**, 4327-4335 (2011).
4. Hoffman, M.P., et al. *J. Biol. Chem.* **273**, 28633-28641 (1998).

Hydrazone-Tethered Drug Release from Peptide Amphiphile Gels

John B. Matson[1] and Samuel I. Stupp[1,2]

[1]Institute for BioNanotechnology in Medicine; [2]Departments of Chemistry, Materials Science and Medicine, Northwestern University, Chicago, IL, 60611, U.S.A.

Introduction

Increased control of drug release rate from biomaterials remains a significant goal in the field of regenerative medicine [1]. In many injectable systems, hydrolytically labile hydrazones are used to bind and release drugs at the desired site of action [2]. The release rate is usually governed by the pH of the surrounding media, with faster release observed in acidic (pH 5-6) environments compared with physiological media (pH 7.4). Hydrazone bonds are convenient hydrolytically labile bonds due to the usually facile incorporation of hydrazides into delivery materials; however, site-specific incorporation of hydrazides into peptides via solid phase peptide synthesis (SPPS) is still synthetically challenging. Here we discuss a new building block that can be site-specifically incorporated onto peptide side chains to reveal a hydrazide upon cleavage from the resin. We then study the self-assembly properties of peptide amphiphiles (PAs) that contain the hydrazide functionality.

Results and Discussion

Inspired by work from Melnyk on hydrazines in SPPS [3], we synthesized triply-protected hydrazide **4** as shown in Scheme 1. First, *tert*-butylcarbazate was coupled to adipic acid monobenzyl ester (**1**) using EDC and DPTS, affording monoprotected hydrazide **2**. Addition of Boc$_2$O to **2** yielded the triprotected derivative, **3**. Hydrogenolysis of the benzyl ester with Pd/C furnished triprotected hydrazido acid **4**.

Utilizing building block **4** in the synthesis of potentially bioactive materials, PA **5** was synthesized using standard Fmoc-based SPPS conditions. A lysine ε-amine was generated on-resin by addition of a Lys(Mtt) residue, removing the Mtt protecting group on resin using 5% TFA in CH$_2$Cl$_2$. Hydrazino acid **4** was activated using HBTU and DIEA and added on-resin to the exposed amine. An N-terminal palmitic acid tail was added to form a PA. The PA was cleaved from the resin using 95% TFA and purified by HPLC, affording hydrazide-containing PA **5**.

Peptide amphiphiles (PAs) are a broad class of biocompatible small molecules that have recently received great attention due to their promise as bioactive materials in regenerative applications [4]. PAs are synthesized by attaching a hydrophobic tail to a short peptide sequence, which typically includes a β-sheet forming region to induce cylindrical micelle formation and one or more charged residues to promote solubility and control gelation through charge screening [5]. PAs can self-assemble into long, filamentous aggregates in aqueous solution, with dimensions of approximately 10 nm in width and up to several microns in length.

To study the potential capability of PA **5** to bind and deliver drugs via hydrazone formation and hydrolysis, we reacted PA **5** with the drug nabumetone (4-(6-methoxy-2-naphthyl)-2-butanone) (**Nb**). Condensation of **Nb** with PA **5** (Scheme 2) was performed in DMSO at room temperature, forming hydrazone-containing PA **6** in high conversion, followed by HPLC purification. Structural characterization of PAs **5** and **6** was then carried out by transmission electron microscopy (TEM) to assess the self-assembly of the PAs.

PAs **5** and **6** were characterized in aqueous solution by conventional TEM, as shown in Figure 1. PA **5** showed long, cylindrical nanofibers with high persistence lengths, typical of many PAs synthesized in our laboratory. Some bundling of fibers can be observed in the TEM image. TEM of PA **6** showed
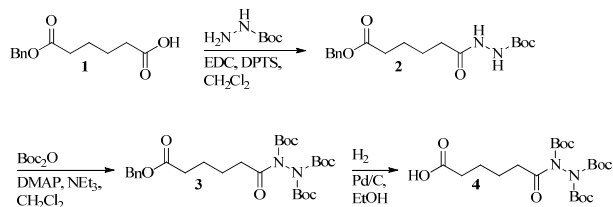
Scheme 1. Synthesis of hydrazide building block from previously reported monobenzyl protected adipic acid. All products were recovered in good to excellent yields with no chromatography.
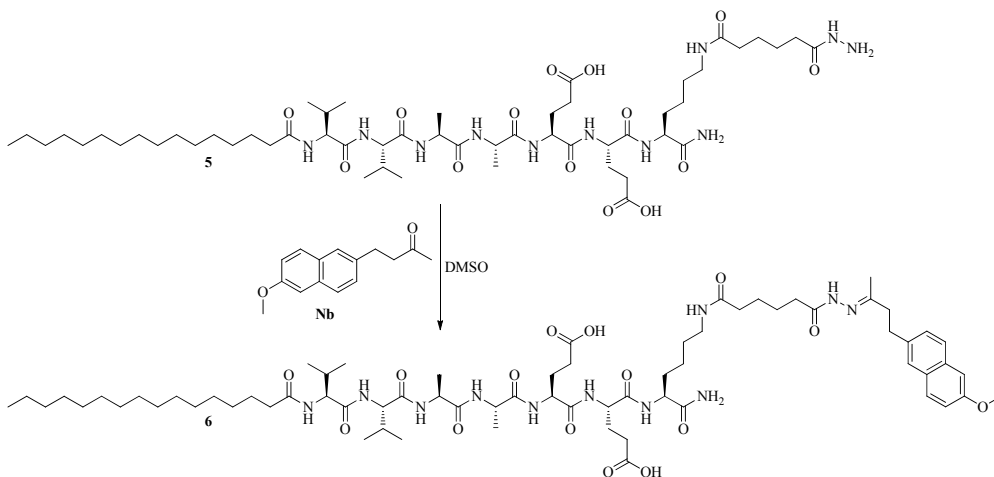
*Scheme 2. Hydrazone formation by reaction of **Nb** with PA **5** to form drug-tethered PA **6**.*

similar cylindrical nanofibers, though they appeared shorter and less bundled than those of PA **5**. We attribute the bundling observed in PA **5** to interfiber hydrogen bonding between surface hydrazide groups. Addition of **Nb** yields a hydrazone that is less capable of hydrogen bonding, which may explain the reduced number of higher-order aggregates observed in PA **6**. These data
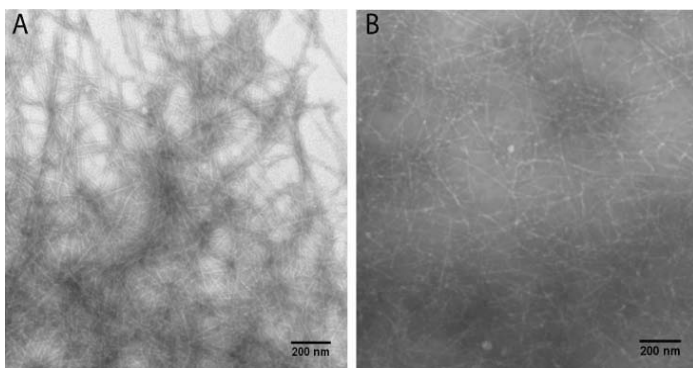
*Fig. 1. Conventional TEM images of PAs **5** and **6**, stained with uranyl acetate.*

indicate that neither addition of the hydrazide functionality nor the **Nb**-hydrazone group affect the ability of the PAs to self-assemble into nanofibers. We anticipate that sustained drug release from PAs such as PA **6** will be achievable through hydrazone hydrolysis. We also expect that building block **4** may be useful in several areas of peptide and polymer-based medicine, including peptide-based biomaterials, peptide labeling and polymeric drug conjugation.

References

1. Goldberg, M., Langer, R., Jia, X.Q., *J. Biomater. Sci.-Polym. Ed*. **18**, 241-268 (2007).
2. Sawant, R.M., Hurley, J.P., Salmaso, S., Kale, A., Tolcheva, E., Levchenko, T.S., Torchilin, V.P. *Bioconjugate Chem*. **17**, 943-949 (2006).
3. Bonnet, D., Grandjean, C., Rousselot-Pailley, P., Joly, P., Bourel-Bonnet, L., Santraine, V., Gras-Masse, H., Melnyk, O. *J. Org. Chem*. **68**, 7033-7040 (2003).
4. Webber, M.J., Kessler, J.A., Stupp, S.I. *J. Intern. Med*. **267**, 71-88 (2010).
5. Hartgerink, J.D., Beniash, E., Stupp, S.I. *Science* **294**, 1684-1688 (2001).

A Collagen Peptide-Based Hydrogel with Rehydrating Properties

Charles M. Rubert Pérez[1], Alyssa Panitch[2], and Jean Chmielewski[1,2]

[1]*Department of Chemistry, Purdue University, West Lafayette, IN, 47906, U.S.A.;* [2]*Weldon School of Biomedical Engineering, Purdue University, West Lafayette, IN, 47906, U.S.A.*

Introduction

Collagen is one of most abundant protein of the extracellular matrix in mammals [1]. Its primary chemical structure is composed of the Xaa-Yaa-Gly amino acid triad, where Xaa and Yaa are mostly occupied by L-proline (Pro or P) and 4(R)-hydroxy-L-proline (Hyp or O) amino acids, respectively [2]. The unique characteristic of collagen is the ability of single peptide strands to acquire a polyproline type II (PPII) helical conformation, in which three of those strands can come together and form a stable triple helix [3]. The triple helical structural motif is critical for the subsequent self-assembly into high order fibers and fibrous networks in nature.
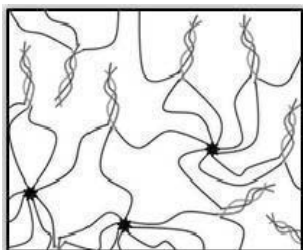
Fig. 1. Schematic of the three-dimensional network within the PSP-POG8 hydrogels.

This last feature has been the inspiration of many research groups to try and construct new biomaterials based on small synthetic collagen peptides and try to mimic nature's assembly [4]. The ability to synthesize collagen peptides and build new biomaterials by rational design is advantageous since working with natural collagen is disfavored for its heterogeneity, its potential transfer of toxic agents and difficulties with further chemical modification [5].

With the purpose of developing a synthetic scaffold based on collagen peptides, we have focused our efforts in designing a collagen-based hydrogel, for the use in three-dimensional cell culture. Our hydrogel design consists of conjugating a collagen peptide comprised of 8 repeating units of Pro-Hyp-Gly, with an N-terminal Gly-Gly-Cys tripeptide **(CGG-(POG)₈)** via Michael addition to an 8-arm 40kDa polyethylene glycol star polymer **(PSP)** with terminal maleimide functionality **(8-arm PEG-MAL)** to yield **PSP-POG8** hydrogels. The PEG polymer will provide three-dimensionality due to the multiple and lengthy arms and the collagen triple helices will provide the physical crosslinks to form a highly ordered structure (Figure 1).

Results and Discussion

In order to form hydrogels, we first determined the minimal concentration of **PEG-MAL** precursor needed. First, 3 different stock solutions of **PEG-MAL** were made and reacted with varying concentrations of the collagen peptide. The procedure consisted of adding the polymer stock solution to a solution of peptide and incubating the mixture until an elastic-solid formed. Specifically, 50 µL of the stock polymer **PEG-MAL** solution (2.0, 5.0 and 10.0 w/v %) was added to a 50 µL solution of the **CGG-(POG)₈** peptide (4, 10, 20 mM, respectively), both in PBS buffer pH 7.4. A 1:8 and 1:16 ratio of polymer to peptide was used to assure that the 8 maleimide functionalized arms of the star polymer were conjugated to the collagen peptides efficiently. For the solution containing 2% of polymer precursor, hydrogel formation was not seen, rather a viscous liquid formed. However,

Fig. 2. Evidence for hydrogel formation using 5% or 10% PEG-MAL polymer precursor.

increasing the polymer concentration to 5% and 10% yielded the desired **PSP-POG8** hydrogels (Figure 2). Both of these materials formed in less than one minute and were 4% and 8% in **PSP-POG8**, respectively, when final polymer-peptide conjugate concentration is taken into consideration.

An interesting characteristic of the hydrogel was its ability to be reformed if the hydrogel is dehydrated and turned into a dry solid. This in part is expected since the peptide remains

covalently bonded to the star polymer, and once the collagen peptide is in aqueous solution it is able to reform a stable triple helix. As proof of principle, a 4% **PSP-POG8** hydrogel sample was frozen and lyophilized to remove all the water. After obtaining a dry solid, water was mixed with the dry solid and the hydrogel was reformed. To visualize the morphology of both dry and wet species, we performed electron microscopy experiments. The dry **PSP-POG8** material was found to consist mostly of bundles of small fibrous constructs aggregated all throughout the sample (Figure 3a). Once the material is hydrated, the dry fibers seems to swell or 'inflate' into a highly crosslink network of micron-sized pores (Figure 3b).
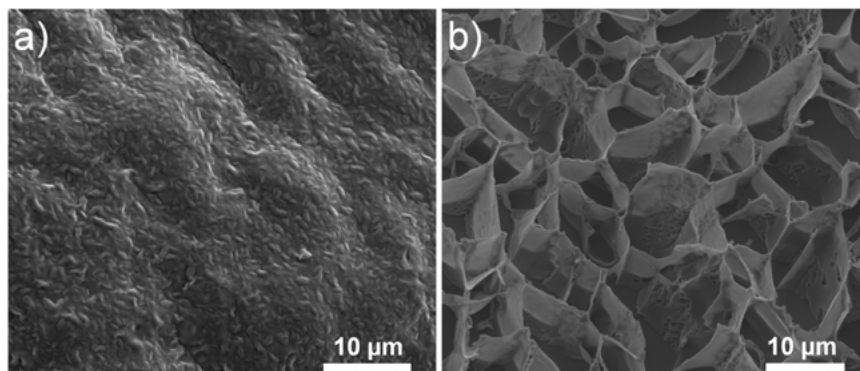
*Fig. 3. a) SEM image of the dehydrated 4% **PSP-POG8** hydrogel b) Cryo-SEM image of the 4% **PSP-POG8** hydrogel.*

Overall, we have evaluated a physical PEG-based hydrogel using collagen peptides. Apart from being able to form this rehydratable material with varying concentrations of polymer precursor, the **PSP-POG8** hydrogels have recently been found to exhibit thermoresponsive properties as well as being a promising biomaterial for three-dimensional cell culture [6].

Acknowledgments

References

1. a) Brinckmann, J. *Top. Curr. Chem.* **247**, 1-16 (2005); b) Koide, T., Nagata, K. *Top. Curr. Chem.* **247**, 85-114 (2005); c) Gordon, M.K., Hahn, R.A. *Cell Tissue Res.* **339**, 247-257 (2010).
2. a) Fietzek, P.P., Kühn, K. *Mol. Cell. Biochem.* **8**, 141-157 (1975); b) Ramshaw, J.A., Shah, N.K., Brodsky, B. *J. Struct. Biol.* **122**, 86-91 (1998).
3. a) Josse, J., Harrington, W.F. *J. Mol. Biol.* **9**, 10262-10268 (1964); b) Jenkins, C.L., Raines, R.T. *Nat. Prod. Rep.* **19**, 49-59 (2002); c) Engel, J., Bachinger, H.P. *Top. Curr. Chem.* **247**, 7-33 (2005).
4. a) Przybyla, D.E., Chmielewski, J. *Biochem.* **21**, 4411-4419 (2010); b) Shoulders, M.D., Raines, R.T. *Annu. Rev. Biochem.* **78**, 929-958 (2009); c) Koide, T. *Phil. Trans. R. Soc. B* **362**, 1281-1291 (2007); d) Yu, S.M., Li, Y., Kim, D. *Soft Matter.* **ASAP** (2011).
5. Lynn, A.K., Yanmas, I.V., Bonfield, W. *J. Biomed. Mater. Res. Part* **71**, 343-354 (2004).
6. Rubert Pérez, C.M., Panitch, A., Chmielewski, J. *Macromol. Biosci.* **ASAP** (2011).

Protein Mimicry with Bioinspired Peptoid Polymers

Ronald N. Zuckermann

Biological Nanostructures Facility, The Molecular Foundry, Lawrence Berkeley National Laboratory, 1 Cyclotron Rd., Berkeley, CA, 94720, U.S.A.; rnzuckermann@lbl.gov

Introduction

Despite the fact that proteins and bulk polymers share a common linear polymeric architecture, the fields of Structural Biology and Polymer Science are presently separated by a great divide [1]. In fact, there are relatively few non-natural polymer systems that include even the most fundamental of biopolymer attributes: chemical diversity and sequence specificity. The chemical information encoded within the polypeptide chain, by virtue of its linear sequence of chemical functional groups, is sufficient to "instruct" it to fold into a precise 3D architecture, and to exhibit advanced properties, such as molecular recognition and catalysis [2]. We are exploring the concept of building analogous protein-mimetic materials from "information rich" synthetic polymers [3]. The solid-phase submonomer synthesis of *N*-substituted glycine peptoid oligomers has emerged as one of the most efficient ways to synthesize sequence-specific polymers from a highly chemically diverse monomer set [4-6]. We are applying fundamental rules that govern protein folding to the world of polypeptoids, with the aim of folding peptoid polymers into artificial protein-like structures to yield a new generation of robust protein-mimetic materials [7-11].

The *de novo* design of proteins remains a challenging problem despite the availability of a large database of protein structures and sophisticated computational tools. So where do we start when approaching the problem of folding non-natural polymers into atomically-defined architectures? We have simplified the problem by first focusing on mimicry of the two fundamental secondary structural units found in protein structure: alpha helices and beta sheets.

We have shown that despite a lack of H-bond donors in the peptoid backbone, peptoids bearing alpha-chiral sidechains can fold into helices [12,13]. This effect was first predicted in 1997, and then demonstrated experimentally in 1998. But the peptoid beta-sheet mimetic was not discovered until over a decade later [10,11]. This is because a helix involves only the local folding of a single chain, whereas folding into a sheet involves chain-chain interactions, a higher level of complexity [14]. Here, we explore the sequence requirements to fold a peptoid chain into an achiral, supramolecular nanosheet (Figure 1).
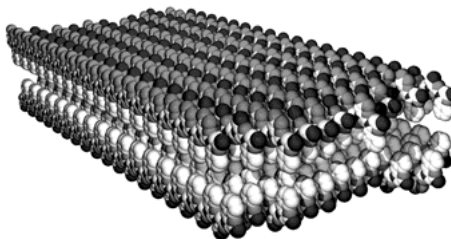
Fig. 1. Polypeptoid nanosheets are a mimetic of peptidic beta sheets, despite a lack of chirality and backbone H-bond donors.

Results and Discussion

We reasoned that the most fundamental rules that govern protein folding should also apply to peptoid polymers. We therefore began our search for peptoid beta-sheet mimetics by considering the visionary ideas of Ken Dill, Michael Hecht and others, who noted the overwhelming importance of the patterning of hydrophilic and hydrophobic groups within the polypeptide chain [15,16]. It was demonstrated that the exact identity of an amino acid was not as important as whether it was polar or non-polar. It was also shown that helices and sheets also exhibit distinct sequence periodicities of polar and non-polar residues.

These observations inspired us to explore the impact of sequence periodicity on peptoid structure. We set out to synthesize repeating patterns of hydrophilic and hydrophobic peptoid sequences using our robotic parallel synthesizers. To enable such a study, we used a minimalist monomer set that included one hydrophobic monomer (*N*-2-phenylethylglycine), and a pair of polar monomers (*N*-2-aminoethylglycine and *N*-2-carboxyethylglycine). This way the number of possible sequence variants could be kept manageable. A systematic set of 36mer peptoids was synthesized consisting of different repeating patterns of these monomers (the two-fold
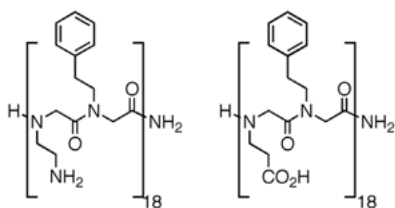
Fig. 2. A 1:1 mixture of oppositely charged two-fold periodic peptoid 36mer amphiphiles forms nanosheets in dilute aqueous conditions at room temperature.

periodic sequences are shown in Figure 2). The purified peptoids were then dissolved in dilute physiological buffers and examined by optical and electron microscopy.

Peptoids containing an alternating two-fold repeating pattern of hydrophilic and hydrophobic sidechains assembled into micron-sized nanosheets in high yield (Figure 3) [10,11]. The nanosheets were further characterized by atomic force microscopy, X-ray powder diffraction, and transmission electron microscopy, and found to be uniformly ~3 nm thick and highly ordered. The data are consistent with a bilayer model (Figure 1), where the hydrophobic groups are buried in the core, and the ionic groups are exposed to water. The nanosheets often have very straight edges, are stable over a broad pH range (3-11) and can survive in hot water and even drying under vacuum. They spontaneously dissolve in the presence of >50% acetonitrile. Because the nanosheets are comprised of achiral peptoid polymers, the resulting planar structure shows no surface curvature, in contrast to peptidic beta sheets [17].

The peptoid nanosheets demonstrate that a non-natural polymer can be folded into a defined structure based on the monomer sequence pattern. The nanosheet structure itself is an excellent two-dimensional platform upon which to display functionality, which may find utility as membrane mimetics, sensors for chem/bio detection, templates for the growth on inorganic materials, and substrates for electron microscopy. More broadly, the ability to introduce chemical sequence information into polymer chains promises to yield a new family of protein-mimetic polymers.

Fig. 3. Scanning electron micrograph of a peptoid nanosheet.

Acknowledgments

References

1. Jones, R.A.L. *J. Polym. Sci. B* **43**, 3367 (2005).
2. Anfinsen, C.B. *Science* **181**, 223 (1973).
3. Goodman, C.M., Choi, S., Shandler, S., DeGrado, W.F. *Nat. Chem. Biol.* **3**, 252 (2007).
4. Culf, A.S., Ouellette, R.J. *Molecules* **15**, 5282 (2010).
5. Fowler, S.A., Blackwell, H.E. *Org. Biomol. Chem.* **7**, 1508 (2009).
6. Yoo, B., Kirshenbaum, K. *Curr. Op. Chem. Biol.* **12**, 714 (2008).
7. Burkoth, T.S., et al. *Chem. Biol.* **9**, 647 (2002).
8. Lee, B.C., Chu, T.K., Dill, K.A., Zuckermann, R.N. *J. Am. Chem. Soc.* **130**, 8847 (2008).
9. Lee, B.C., Zuckermann, R.N., Dill, K.A. *J. Am. Chem. Soc.* **127**, 10999 (2005).
10. Nam, K.T., et al. *Nat. Mater.* **9**, 454 (2010).
11. Kudirka, R., et al. *Biopolymers,* Early view online (2011). doi:10.1002/bip.21590.
12. Armand, P., et al. *Fold. Design* **2**, 369 (1997).
13. Kirshenbaum, K., et al. *Proc. Natl. Acad. Sci. U.S.A.* **95**, 4303 (1998).
14. Minor, D.L., Kim, P.S. *Nature* **371**, 264 (1994).
15. Dill, K.A. *Biochemistry* **29**, 7133 (1990).
16. Xiong, H. Buckwalter, B.L., Shieh, H.M., Hecht, M.H. *Proc. Natl. Acad. Sci. U.S.A.* **92**, 6349 (1995).
17. Zhang, S. *Nat. Biotech.* **21**, 1171 (2003).

Design and Application of Bioactive Materials Derived from Simple Self-Assembling Peptides

Bradley L. Nilsson, Charles J. Bowerman, John T. M. DiMaio, and Todd M. Doran

Department of Chemistry, University of Rochester, Rochester, NY, 14627-0216, U.S.A.

Introduction

The self-assembly of peptides and proteins into cross-β amyloid structures is a defining characteristic of amyloid pathologies including Alzheimer's disease, Parkinson's disease, type 2 diabetes, and prion encephalopathies. Amyloid protein assemblies are not limited to pathological conditions, but also exist as evolutionarily conserved motifs with defined biological function. There is growing interest in exploiting peptide self-assembly phenomena for the development of novel functional structures with applications in biomedicine, energy, and materials. The use of amyloid-derived materials for applications in biomedicine requires understanding of the noncovalent interactions that drive peptide self-assembly in order to facilitate novel approaches to exploit these interactions for the noncovalent synthesis of functional and dynamic self-assembled materials. We have conducted studies to probe the influence of the hydrophobic and aromatic character of peptides on the self-assembly of simple sequences with alternating hydrophobic and hydrophilic amino acids. The outcome of these studies and the utility of the resulting materials to problems of biological significance are discussed herein.

Results and Discussion
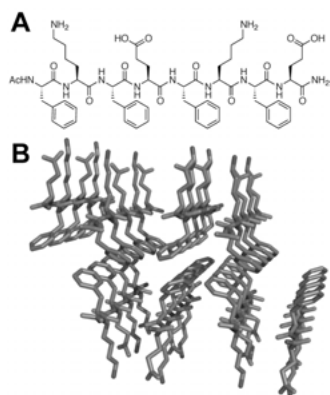
Fig. 1. A) Chemical structure of Ac-(FKFE)₂-NH₂. B) Model of self-assembled bilayer fibrils derived from Ac-(FKFE)₂-NH₂.

Amphipathic peptides of general sequence (XKXE)ₙ have a strong propensity to assemble into cross-β bilayer fibrils that maintain high solubility in aqueous solutions (Figure 1) [1]. We have discovered that the aromatic and hydrophobic character of amino acid X influences the self-assembly propensity, fibril morphology, and hydrogel viscoelastic behavior of fibrils derived from Ac-(XKXE)₂-NH₂ peptides [1]. Peptides in which X = Ala fail to self-assemble, while sequences in which X = Val or Leu readily assemble into morphologically similar fibrils. In contrast, when X = Phe, fibrils of distinct helical tape morphologies are observed; when X = cyclohexylalanine (Cha), smaller and more abundant fibrils are formed, consistent with more rapid nucleation of this significantly more hydrophobic sequence.

Self-assembly of amphipathic β-sheet peptides can be frustrated by simple modification of the cationic character of the parent sequence. For example, we have found that Glu to Lys mutation of the parent sequence provides Ac-(XKXK)₂-NH₂ peptides that fail to undergo self-assembly in unbuffered aqueous solvents. Failure to self-assemble into amyloid-like fibrils can be attributed to cationic charge repulsion. Self-assembly can be promoted by increasing the ionic strength of the solvent by addition of NaCl; at sufficient ionic strength the repulsive charges can be effectively screened and self-assembly becomes favorable. We have found that the required ionic strength to induce self-assembly can be tuned as a function of the hydrophobicity of the amino acid residues in position X [2,3]. As the hydrophobicity of X increases, the required [NaCl] needed to promote self-assembly decreases (Table 1) [2,3].

Table 1. Salt-dependent self-assembly of cationic peptides

Entry	Peptide	Π^a	[NaCl] required to induce self-assembly
1	Ac-K$_2$(FKFE)$_2$-NH$_2$	Phe 1.79	100 mM
2	Ac-K$_4$(FKFE)$_2$-NH$_2$	Phe 1.79	300 mM
3	Ac-K$_2$(ChaKChaE)$_2$-NH$_2$	Cha 2.72	0 mM
4	Ac-K$_4$(ChaKChaE)$_2$-NH$_2$	Cha 2.72	40 mM
5	Ac-(FKFK)$_2$-NH$_2$	Phe 1.79	700 mM
6	Ac-(ChaKChaK)$_2$-NH$_2$	Cha 2.72	60 mM

[a]*Hydrophobicity of amino acid in position X* [4]

Placement of the cationic groups has a strong influence on the effects of molecular frustration on peptide self-assembly. When cationic residues are placed at the *N*-terminus (Ac-K$_n$(XKXE)$_2$-NH$_2$) instead of evenly dispersed throughout the peptide sequence (Ac-(XKXK)$_2$-NH$_2$), the effects of charge-mediated frustration of self-assembly are partially abrogated (Table 1). For example, peptides in which X = Phe that contain an overall charge of +4 vary significantly in the amount of NaCl that is needed to initiate self-assembly (entries 2 and 5, Table 1); Ac-K$_n$(FKFE)$_2$-NH$_2$ assembles at 300 mM NaCl while Ac-(FKFK)$_2$-NH$_2$ requires 700 mM NaCl before self-assembly is observed. The Cha-containing peptides (entries 4 and 6, Table 1) show similar trends; clustering of the charged residues at the *N*-terminus has a weaker effect on the inhibition of self-assembly than does placement of the charged residues throughout the *β*-sheet assembly motif. These effects are consistent with an antiparallel fibril packing structure as shown in Figure 1B. Placement of charge at the *N*-terminus minimizes the direct interaction between charged residues, thus reducing the burden for initiation of self-assembly.

Understanding of the relationship between peptide hydrophobicity, charge, and self-assembly propensity is critical for the design and application of self-assembling peptides to biological problems. We recently reported the use of cationic Ac-K$_n$(XKXE)$_2$-NH$_2$ peptides to probe the effects of amyloid structures on HIV-1 infectivity [3]. It was hypothesized that cationic amyloid materials would enhance HIV infectivity. In order to test this hypothesis it was critical to design amyloid-inspired materials that would be highly assembled under the assay conditions and Ac-K$_n$(XKXE)$_2$-NH$_2$ peptides proved to be ideal for this application. These results illustrate the importance of detailed understanding of peptide self-assembly processes and indicate the great potential for amyloid-inspired biomaterials.

Acknowledgments

References

1. Bowerman, C.J., Ryan, D.M., Nissan, D.A., Nilsson, B.L. *Mol. BioSyst.* **5**, 1058-1069 (2009).
2. Bowerman, C.J., Liyanage, W., Federation, A.J., Nilsson, B.L. *Biomacromolecules* **12**, 2735-2745 (2011).
3. Easterhoff, D., DiMaio, J.T.M., Dewhurst, S., Nilsson, B.L. *Biophys. J.* **100**, 1325-1334 (2011).
4. Fauchère, J.L., Charton, M., Kier, L.B., Verloop, A., Pliska, V. *Pept. Protein Res.* **32**, 269-278 (1988).

Oligo-Benzamides: Versatile Scaffolds to Mimic Protein Helical Surfaces

Jung-Mo Ahn

Department of Chemistry, University of Texas at Dallas, Richardson, TX, 75080, U.S.A.

Introduction

Protein-protein interactions are one of the fundamental themes in biological systems and regulate diverse cellular functions. Since α-helical structures are often found to strongly contribute to protein complex formations, short helical peptides have been developed as a valuable research tool as well as potential therapeutic candidates. However, peptides in general have drawbacks that severely compromise their effective *in vivo* use, such as rapid enzymatic degradation, poor bioavailability, and lack of membrane penetration. Whereas several strategies have been developed to stabilize helical peptides (e.g., lactam bridge formation, hydrocarbon stapling), small molecules that mimic functions of helical peptides would be of high interest. To this end, many rigid and pre-organized scaffolds have been developed to place side chain functional groups of helical peptides. These include terphenyl, trispyridylamide, fused polycyclic ether, oligo-benzamide, pyridazine, and oligooxopiperazine structures [1].

Results and Discussion

Tris-Benzamide Scaffold:
Inspired by Hamilton's trispyridylamide structure [2], we have designed a tris-benzamide scaffold [3]. This template comprises of three 3-alkoxy-4-aminobenzoic acids and places three alkyl substituents corresponding to the side chains of amino acid residues located at the i, $i+4$, and $i+7$ positions in a helix (Figure 1). Despite its structural similarity to the trispyridylamide, the tris-benzamide scaffold has higher torsional flexibility owing to the absence of extensive hydrogen bond network in the trispyridylamide. This facilitates superior α-helix mimicry by arranging its substituents in a more staggered fashion. With this scaffold, we have designed and synthesized peptidomimetics of long peptide hormones [4], BH3 domains of pro-apoptotic Bcl-2 proteins [5], and androgen receptor-targeting LXXLL motifs. The effectiveness of the tris-benzamide scaffold has been also demonstrated by other investigators [6-8].

Fig. 1. (A) Tris-benzamide scaffold. (B) Lowest energy conformation superimposed on a helix.

Amphiphilic Bis-Benzamide Scaffold:
Whereas most of α-helices in peptides and proteins are amphiphilic, possessing a hydrophilic surface on the opposite side of a hydrophobic one, many α-helix mimetics reported to date focus on reproducing only one side of helices, not suitable for emulating amphiphilic α-helices. The lack of functional groups on the opposite side may result in not only weak interaction with target proteins but also lower specificity that may potentially limit utility due to potential promiscuity. In order to simultaneously represent two opposing helical faces, we have designed amphiphilic bis-benzamide scaffold [9]. As shown in Figure 2, the amphiphilic scaffold is made up of two bi-directional monomers and places four substituents corresponding to the side chains at the i, $i+2$, $i+5$, and $i+7$ positions which form two opposing helical faces simultaneously. It is interesting that the amphiphilic structure is secured by two hydrogen bonds as evidenced in a X-ray crystal structure [9].
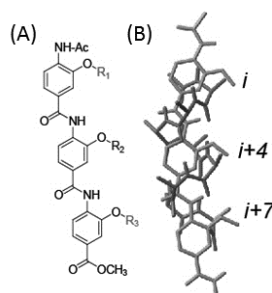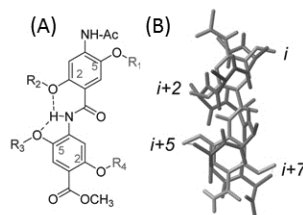
Fig. 2. (A) Amphiphilic bis-benzamide scaffold. (B) Lowest energy conformation superimposed on a helix.
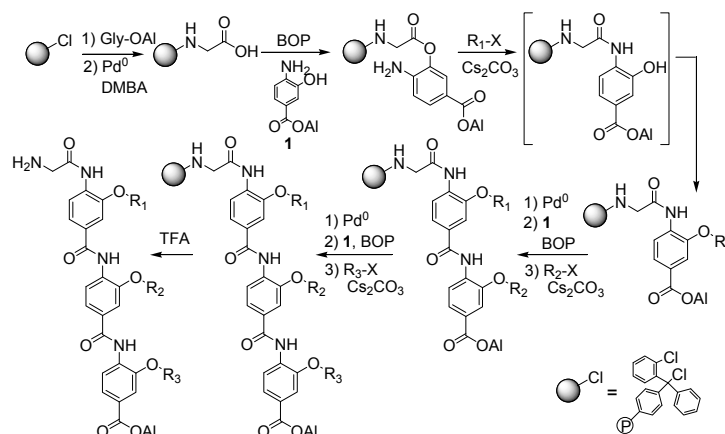
Scheme 1. Solid-phase synthesis of oligo-benzamides.

Solid-Phase Synthesis of Oligo-Benzamides:

In addition to outstanding α-helix mimicry, synthetic convenience is a key advantage of the oligo-benzamide scaffolds compared to other α-helix mimetics. Although primary sequences of α-helical segments can guide initial design of suitable α-helix mimetics, generating a number of α-helix mimetics has been frequently practiced to rapidly identify potent leads by exploring diverse functional groups as substituents for improving target recognition. Thus, synthetic efficiency, such as higher yields, easy derivatization, readily available starting materials, and synthetic chemistry suitable for automation, may need to be considered. Since solution-phase synthesis of tris-benzamides can be achieved by straightforward reactions that are compatible to solid-phase strategy, we have developed a parallel solid-phase synthetic method for efficient and rapid construction of oligo-benzamides as α-helix mimetics [10]. As illustrated in Scheme 1, the solid-phase synthetic route involves iterative steps of amide bond formation, O→N acyl migration, and O-alkylation reactions. This methodology allowed facile and rapid construction of α-helix mimetics that we have used to target various proteins.

Taken all of these together, the oligo-benzamide structure is a versatile scaffold for mimicking helical peptides and has a high potential in modulating protein functions for studying biochemical pathways and developing therapeutic interventions.

Acknowledgments

References

1. Cummings, C.G, Hamilton, A.D. *Curr. Opin. Chem. Biol.* **14**, 341-346 (2010).
2. Ernst, J.T., et al. *Angew. Chem. Int. Ed.* **42**, 535-539 (2003).
3. Ahn, J.-M, Han, S.-Y. *Tetrahedron Lett.* **48**, 3543-3547 (2007).
4. Ahn, J.-M., et al. In Escher, E., Lubell, W.D., Del Valle, S. (Eds.) *Peptides: Chemistry, Structure and Biology (Proceedings of the 20th American Peptide Symposium)*, Springer, New York, 2009, p. 125-126.
5. Bhimani, K., et al. In Lebl, M. (Ed.) *Peptides: Chemistry, Structure and Biology (Proceedings of the 21st American Peptide Symposium)*, American Peptide Society, San Diego, 2009, p. 72-73.
6. Saraogi, I., Incarvito, C.D., Hamilton, A.D. *Angew. Chem. Int. Ed.* **47**, 9691-9694 (2008).
7. Shaginian, A., et al. *J. Am. Chem. Soc.* **131**, 5564-5572 (2009).
8. Plante, J.P., et al. *Chem. Commun.* 5091-5093 (2009).
9. Marimganti, S., Cheemala, M.N., Ahn, J.-M. *Org. Lett.* **11**, 4418-4421 (2009).
10. Lee, T.-K., Ahn, J.-M. *ACS Comb. Sci.* **13**, 107-111 (2011).

Solution- and Solid-Phase Synthesis of Bis-Benzamide Libraries as α-Helix Mimetics and Their Evaluation on Inhibitory Activity to Prostate Cancer

Tae-Kyung Lee[1], Preethi Ravindranathan[2], Ganesh V. Raj[2], and Jung-Mo Ahn[1,*]

[1]Department of Chemistry, University of Texas at Dallas, Richardson, TX, 75080, U.S.A.; [2]Department of Urology, University of Texas Southwestern Medical Center, Dallas, TX, 75390, U.S.A.

Introduction

Mimicking α-helices is a promising approach for the treatment of human diseases since they are often involved in protein-protein interactions and modulate various disease pathways. Toward this goal, non-peptidic frameworks that have pre-organized conformations have been developed for reproducing side chain functional groups in an α-helix. They have served as an effective tool to target α-helical structures offering advantages, such as proteolytic stability and cell permeability [1]. While α-helix mimetics are typically designed based on the structure of an ideal α-helix, helical segments in many proteins frequently differ from the flawless one because the locations of side chains subtly deviate from the perfect helical geometry. Thus, fine-tuning of substituents' structures and positions and constructing libraries of α-helix mimetics would facilitate rapid achievement of optimal interactions with target proteins [2].

We describe herein the preparation of combinatorial libraries of bis-benzamides as α-helix mimetics, which present two functional groups corresponding to the side chains of the *i*th and *i+4*th residues in an α-helix [3]. To demonstrate proof of principle, a bis-benzamide library was examined on inhibitory activities against a prostate cancer cell line.

Results and Discussion

For rapid and efficient construction of bis-benzamide libraries, we exploited 3-alkoxy-4-nitrobenzoic acid as a monomer since enhanced electrophilicity by the 4-nitro group allowed facile amide bond formation between 3-alkoxy-4-nitrobenzoyl chloride and 3-alkoxy-4-aminobenozate in high yield. This approach also facilitates modular synthesis of bis-benzamides. A variety of alkyl chains were introduced as substituents of bis-benzamides, such as *n*-propyl, isopropyl, *n*-butyl, isobutyl, *s*-butyl, *n*-pentyl, and isopentyl groups (Scheme 1a). The libraries of bis-benzamides were constructed in both solution- and solid-phase. In solution-phase synthesis, a 49-membered library L1 containing a methyl ester at the C-terminus was prepared
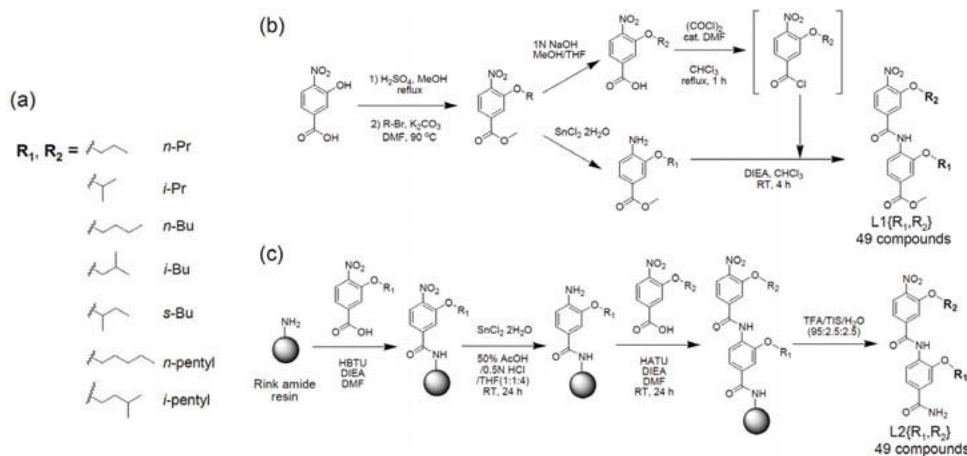
Scheme 1. (a) Functional groups introduced as substituents of bis-benzamides; (b) Solution-; (c) solid-phase syntheses of bis-benzamide libraries.
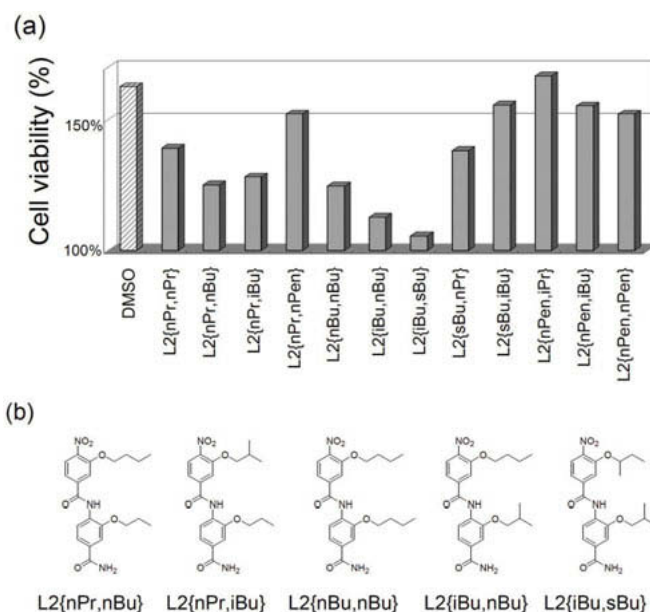
Fig. 1. Bis-benzamide library screening against a prostate cancer line (LNCaP); (a) cell viability measured by MTT assay (100 nM); (b) identified leading compounds.

by an amide bond formation reaction of methyl 3-alkoxy-4-aminobenzoates with 3-alkoxy-4-nitrobenzoyl chlorides (Scheme 1b). A library L2 of 49 bis-benzamides containing a carboxamide at the C-terminus was synthesized by following a solid-phase route of iterative coupling of a 3-alkoxy-4-nitrobenzoic acid and subsequent reduction of the nitro group (Scheme 1c). Unlike the solution phase synthesis, oxalyl chloride was not effective for amide-bond formation reactions on solid supports, however HATU offered successful conversions.

The bis-benzamide library L2 was screened to examine inhibitory activities on LNCaP, a prostate cancer cell line, and several leads were identified with their IC_{50} values of lower than 50 nM (Figure 1). *n*-Propyl, *n*-butyl, isobutyl, and *s*-butyl groups as substituents of bis-benzamides were found to be effective for suppressing proliferation of the tumor cell line, whereas *n*-pentyl and isopentyl group were much less active.

In this study, we synthesized libraries of bis-benzamides for rapid screening in order to compensate subtle differences in spatial arrangement of side chains in naturally occurring helices from an ideal α-helix. Their evaluation of anti-proliferative activities on a prostate cancer cell line identified several potent inhibitors. This study exemplifies rapid lead discovery by combining a rational design approach and combinatorial synthesis.

Acknowledgments

References

1. Davis, J.M., Tsou, L.K., Hamilton, A.D. *Chem. Soc. Rev.* **36**, 326-334 (2007).
2. Lee, T.-K., Ahn, J.-M. *ACS Comb. Sci.* **13**, 107-111 (2011).
3. Ahn, J.-M., Han, S.-Y. *Tetrahedron Lett.* **48**, 3543-3547 (2007).

Solution Structure of a GLP-1 Receptor Peptidomimetic Agonist, Ac-SH3-GLP-1(22-36)-NH$_2$

Isuru R. Kumarasinghe, Eunice Murage, and Jung-Mo Ahn*

Department of Chemistry, University of Texas at Dallas, Richardson, TX, 75080, U.S.A.

Introduction

Glucagon-like peptide-1 (GLP-1) is an incretin involving in glucose homeostasis and demonstrated to be an effective therapeutic option for diabetes mellitus. Compared to other present anti-diabetic agents, such as sulfonylureas and glinides, the GLP-1 therapy does not result in side effects like hypoglycemia and weight gain. However, proteolytic degradation by enzymes like dipeptidyl peptidase-IV limits GLP-1 to have a short plasma half-life *in vivo*. In order to overcome this issue, we have previously designed and synthesized a novel GLP-1 peptidomimetic, Ac-SH3-GLP-1(22-36)-NH$_2$ (Figure 1) that can activate the GLP-1 receptor [1]. This GLP-1 peptidomimetic was designed by substituting a helical segment of GLP-1 for an α-helix mimetic based on a tris-benzamide scaffold that can reproduce one side of a helix by presenting side chain groups found at the *i*, *i+4* and *i+7* positions [2].

Results and Discussion

GLP-1 predominantly adopted an amphiphilic helical conformation (residues 7-29) with a short distortion (residues 21-23) when it was associated with micelles [3]. It also upheld the helical structure (residues 7-28) in 35% aqueous trifluoroethanol [4]. In addition, the structure of GLP-1 when co-crystalized with an N-terminal domain of the GLP-1 receptor was found to be helical (residues 13-33) [5]. Recently, we confirmed the presence and locations of the helical segments in a receptor-bound conformation of GLP-1 by strategically placing lactam bridges [6,7]. These NMR analysis and conformational studies indicate the significance of the N-terminal helix for receptor interaction, and tris-benzamide SH3 was synthesized to mimic Phe[12], Val[16], and Tyr[19] [8].
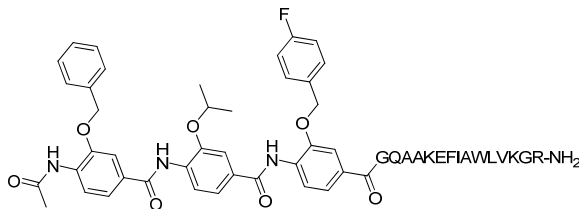
Fig. 1. Structure of Ac-SH3-GLP-1(22-36)-NH$_2$.

To determine the structure of the GLP-1 peptidomimetic and confirm the α-helix mimicry of the tris-benzamide, it was studied by NMR. TOCSY, DQF-COSY, and NOESY spectra were acquired in the presence of perdeuterated dodecylphosphocholine micelles with a 600 MHz Varian NMR spectrometer. A number of medium- and long-range NOE cross-peaks were identified and allowed us to determine the structure of the peptidomimetic by restrained simulated annealing. As shown in Figure 2, we found that the C-terminal peptide segment of the GLP-1 peptidomimetic had a well-defined α-helical structure. This helix appeared to be less organized at the N-terminal end of the peptide segment. As previously demonstrated for the native GLP-1, we have seen hydrophobic and hydrophilic surfaces of the NMR structure. The hydrophobic face comprises of Ala, Ile, Phe, Trp, Leu, and Val, whereas the hydrophilic one contains polar residues like Gln, Lys, Glu, and Arg. Furthermore, the tris-benzamide SH3 was found to have three substituents (benzyl, isopropyl, and 4-fluorobenzyl groups) on the same side, confirming the α-helix mimicry of the scaffold.
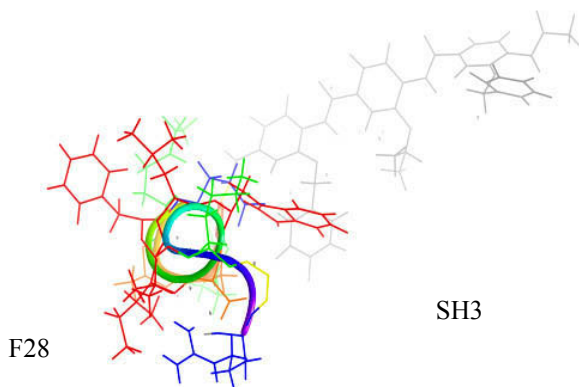
Fig. 2. Conformation of Ac-SH3-GLP-1(22-36)-NH$_2$ determined by 2D-NMR.

    The NMR structure of the GLP-1 peptidomimetic revealed a folded conformation while the structures of GLP-1 previously determined by NMR and X-ray showed helical conformations substantially extended from the N- to C-termini. This NMR study suggests a possibility of a sharp turn between the two helical elements, which may need to be considered for developing non-peptide GLP-1 receptor agonists.

Acknowledgments

References

1. Ahn, J.-M., et al. In Escher, E., Lubell, W.D., Del Valle, S. (Eds.) *Peptides: Chemistry, Structure and Biology (Proceedings of the 20th American Peptide Symposium)*, Springer, New York, 2009, p. 125-126.
2. Ahn, J.-M., Han, S.-Y. *Tetrahedron Lett.* **48**, 3543-3547 (2007).
3. Thornton, K., Gorenstein, D.V. *Biochemistry* **33**, 3532-3539 (1994).
4. Chang, X., et al. *Magn. Reson. Chem.* **39**, 477-483 (2001).
5. Underwood, C.R., et al. *J. Biol. Chem.* **285**, 723-730 (2010).
6. Murage, E.N., Schroeder, J.C., Beinborn, M., Ahn, J.-M. *Bioorg. Med. Chem.* **16**, 10106-10112 (2008).
7. Murage, E.N., Gao, G., Bisello, A., Ahn, J.-M. *J. Med. Chem.* **33**, 6412-6420 (2010).
8. Han, S.-Y., Beinborn, M., Ahn, J.-M., In Escher, E., Lubell, W.D., Del Valle, S. (Eds.) *Peptides: Chemistry, Structure and Biology (Proceedings of the 20th American Peptide Symposium)*, Springer, New York, 2009, p. 119-120.

Inhibition of Anti-Apoptotic Bcl-2 Family Proteins by Tris-Benzamides-Based α-Helix Mimetics

Kajal A. Bhimani[1], Dang Tran[2], Myoung H. Kim[2], Rey-Chen Pong[3], Jer-Tsong Hsieh[3], and Jung-Mo Ahn[1,*]

[1]Department of Chemistry, University of Texas at Dallas, Richardson, TX, 75080, U.S.A; [2]Department of Molecular Biology and Immunology, University of North Texas Health Science Center, Forth Worth, TX, 76107, U.S.A; [3]Department of Urology, University of Texas Southwestern Medical Center, Dallas, TX, 75390, U.S.A.

Introduction

Apoptosis is critical for numerous physiological processes and any impairment may lead to diseases like cancer. Commitment of cells to programmed death is governed largely by protein-protein interactions between members of Bcl-2 protein family, which comprise of three groups. Anti-apoptotic proteins (e.g., Bcl-2, Bcl-xL, Bcl-w, Mcl-1, A1) are responsible for cell survival and have four conserved domains (BH1-4). Pro-apoptotic members promote cell death and are further classified to multi-domain proteins possessing BH1-3 (e.g., Bak, Bax) and BH3-only proteins (e.g., Bim, Bik, Bid, Puma, Noxa). Mechanistically, the process of apoptosis is initiated by BH3-only proteins either activating multi-domain pro-apoptotic proteins or inhibiting anti-apoptotic members (direct or indirect activation model, respectively) [1], resulting in release of cytochrome c through increasing mitochondrial outer membrane permeability. This in turn begins caspase cascade that ultimately leads to cell death. Thus, small molecules that inhibit anti-apoptotic Bcl-2 proteins or activate pro-apoptotic ones would be a potential candidate for treating cancer.

Results and Discussion

Interaction of BH3-only proteins with multi-domain Bcl-2 members involves α-helical BH3 domains fitting into a groove that is organized by BH1-3 domains of anti- or pro-apoptotic proteins. It appears that side chains of the amino acid residues at the *i*, *i+3/i+4* and *i+7* positions of helical BH3 domains strongly contribute to the binding, which constitute one face of the helices [2,3]. These findings gave us a rationale for developing α-helix mimetics of BH3 domains. Recently, we have developed a rigid and pre-organized tris-benzamide scaffold that can place three functional groups to mimic key residues of a helix in the same distance and angular relationship shown by an α-helix [4]. Based on the sequences of BH3-only proteins Bim, Bik and Puma, a series of tris-benzamide analogs were designed and synthesized, in which *s*-Bu, *i*-Bu, *n*-Bu and Bn substituents represent side chain groups of Ile, Leu, Met and Phe, respectively (Figure 1). In order to cover three helical turns of the BH3 domains, two analogs were prepared to present the side chains at the *i*, *i+4*, *i+7* positions (N analog) and the *i+4*, *i+7*, *i+11* positions (C analog) of each BH3 domain, resulting in six tris-benzamides in total.

Synthesis of tris-benzamides is summarized in Scheme 1, starting from 4-nitro-3-alkoxy-benzoate **1**. The nitro group was reduced with $SnCl_2$ and the resulting 4-amino-3-alkoxy-benzoate **2** was reacted with the acid chloride of benzoic acid **3.** These reaction steps were repeated to prepare tris-benzamide **7**. The monomers bearing 3-alkoxy groups (**1**, **3**, and **5**) were synthesized from 4-nitro-3-hydroxy benzoate with various alkyl halide and K_2CO_3.

BIM:	EIW**L**	AQE**L**R	R**I**GDE	**F**NAYY	ARR	BIM-N (1)	*s*-Bu	*i*-Bu	*s*-Bu
						BIM-C (2)	*i*-Bu	*s*-Bu	Bn
BIK:	SDA**L**	ALR**L**A	C**I**GDE	**M**DVSL	RAP	BIK-N (3)	*i*-Bu	*i*-Bu	*s*-Bu
						BIK-C (4)	*i*-Bu	*s*-Bu	*n*-Bu
PUMA:	ARE**I**	GAQ**L**R	R**M**ADD	**L**NAQY	ERR	PUMA-N (5)	*s*-Bu	*i*-Bu	*n*-Bu
	i	i+4	i+7	i+11		PUMA-C (6)	*i*-Bu	*n*-Bu	*i*-Bu

Fig. 1. Conserved BH3 domains of BH3-only pro-apoptotic proteins and tris-benzamides mimicking those.
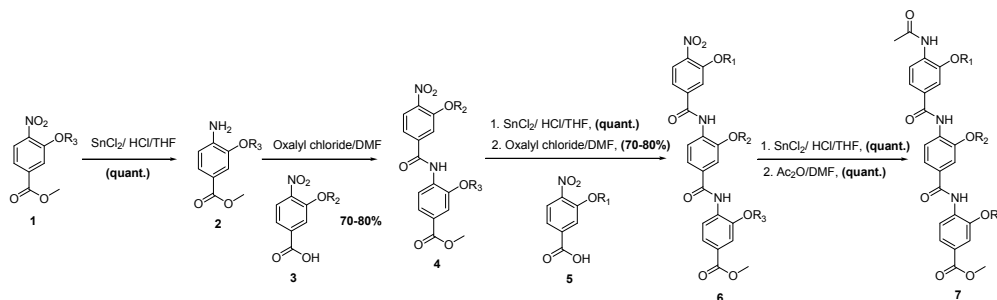
Scheme 1. Synthesis of tris-benzamide-based BH3 mimetics.

Inhibitory activities of the six tris-benzamides were examined by various cell-based assays. Cell viability was assessed by MTT assays in a dose dependent manner on DU-145 cancer cell line (Figure 2A). Strong growth inhibition was demonstrated by helix mimetics **2**, **4**, **5** and **6** with EC_{50} values of lower than 500 nM. These BH3 mimetics were also found to induce apoptosis evidenced by caspase activation (Figure 2B), and the BH3 mimetic **6** effectively triggered apoptosis on DU-145 as Paclitaxel.

Taken together, the tris-benzamide **6** derived from the BH3 domain of PUMA strongly inhibited cell growth and induced apoptosis through mitochondrial pathway, demonstrating the potential of tris-benzamide-based α-helix mimetics for disrupting protein-protein interactions and modulating protein functions.
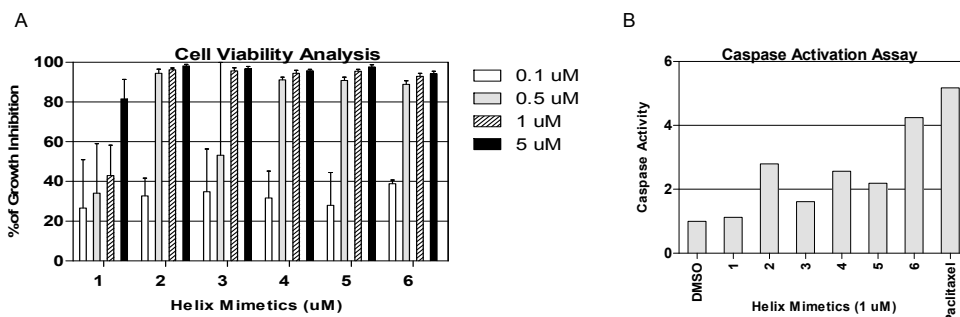
Fig. 2. Biological evaluation of BH3 mimetics. (A) MTT assay and (B) caspase activity analysis.

Acknowledgments

References

1. Kuwana, T., et al. *Mol. Cell.* **17**, 525-535 (2005).
2. Kelekar, A., et al. *Mol. Cell Biol.* **17**, 7040-7046 (1997).
3. Lessene, G., Czabotar, P.E., Colman. P.M. *Nat. Rev. Drug Discov.* **7**, 989-1000 (2008).
4. Ahn, J.-M., Han, S.-Y. *Tetrahedron Lett.* **48**, 3543-3547 (2007).

Mechanisms of Cancer Cell Death Induced by Two Novel Cationic β-Peptidomimetics

Dominik Ausbacher[1], Terkel Hansen[1], Gunbjørg Svineng[2], and Morten B. Strøm[1]

[1]*Natural Products and Medicinal Chemistry Research Group, Department of Pharmacy; [2]Tumorbiology Research Group, Department of Medical Biology, University of Tromsø, Tromsø, 9037, Norway*

Introduction

We have developed and synthesized a series of small β-peptidomimetics with a molecular mass below 500 Da that display high antimicrobial activity and have the potential for oral drug administration [1]. Recently we discovered that some of these compounds also possess anticancer activity (unpublished results). Additionally, the compounds display no or very low toxicity against human erythrocytes and a non-malignant cell line. In the current project we have studied the mechanisms of action of our two lead β-peptidomimetics, THAP131 and THAP164, by combining different biochemical assays, flow cytometry and electron microscopy. The results have provided important insight into details regarding induction of cancer cell death and revealed two distinct mechanisms of action of the structurally related compounds THAP131 and THAP164.

Results and Discussion

The two β-peptidomimetics THAP131 and THAP164 have been shown to be very potent against the human Burkitt's lymphoma cell line Ramos when assessed with a resazurin based cytotoxicity assay. The IC_{50} values measured after 8 h was 8.1 µg/ml for THAP131, and 3.8 µg/mL for THAP164. Furthermore, no significant changes in IC_{50} values occurred after prolonged incubation up to 24 h (Figure 1). By using an annexin-V-FITC/PI apoptosis assay and staining with tetramethylrhodamine ethyl ester perchlorate (TMRE), a dye able to accumulate in the inner membrane of unaffected mitochondria [3], flow cytometry results indicated that the two compounds had different cell killing properties. THAP164 induced apoptosis while THAP131 worked differently (data not shown). The results were confirmed by running a caspase activity assay, in which THAP164 was shown to be an inducer of apoptosis involving activation of caspases while THAP131 did not influence these cellular mechanisms (data not shown). Transmission electron microscopy (TEM) (Figure 2) revealed that THAP131 killed Ramos cells via necrosis indicated by massive vacuolization and an early loss of cell integrity [2]. THAP164 treated cells featured the same degree of vacuolization, however, cell integrity was maintained much longer and the cells displayed chromatin condensation typical of apoptosis (Figure 2) [2].

Fig. 1. IC_{50} values of THAP131 and THAP164 after 8 and 24 h incubation (four parallels).
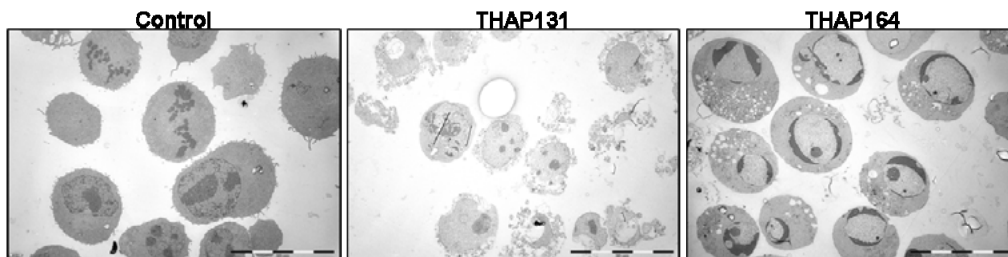
Fig. 2. Transmission electron microscopy pictures of Ramos cells. Untreated control cells and cells treated with IC$_{50}$ of THAP131 and THAP164 for 3h are shown. Characteristic differences in morphology are displayed by the three populations. Scale bar = 20 μm.

The data collected using different assays and analytical methods suggest two different mechanisms of action for the two structurally related β-peptidomimetics THAP131 and THAP164. No signs of caspase activity or apoptotic mechanisms were observed for cells treated with THAP131 but TEM revealed necrotic morphology during a multi time point study. THAP164 in contrast induced apoptosis, involving caspase activation and collapse of the mitochondrial membrane potential with TEM confirming the findings. We therefore conclude that these structurally related β-peptidomimetics possess two distinctly different mechanisms of action where THAP131 kills cells by necrosis while THAP164 induces apoptosis indicating a possible direct interaction of THAP164 with mitochondria.

Acknowledgments

References

1. Hansen, T., Ausbacher, D., Flaten, G.E., Havelkova, M., Strøm, M.B. *J. Med. Chem*. **54**, 858-68 (2011).
2. Kerr, J.F., Gobe, G.C., Winterford, C.M., Harmon, B.V. *Methods Cell Biol.* **46**, 1-27 (1995).
3. Ehrenberg, B., Montana, V., Wei, M.D., Wuskel, J.P, Loew, L.W. *Biophys. J.* **53**, 785-94 (1988).

Development of CXCR4 Specific Peptidomimetic Agonists

**Christine Mona[1], Marilou Lefrançois[1], Marie-Reine Lefebvre[1],
Jérôme Cabana[1], Simon Lamothe[2], Richard Leduc[1], Eric Marsault[1],
Nikolaus Heveker[2], and Emanuel Escher[1]**

[1]*Département de Pharmacologie FMSS Université de Sherbrooke, Sherbrooke, J1H 5N4, Canada;*
[2]*Centre de Recherche, Hôpital Sainte-Justine, Montréal, H3T 1C5, Canada*

Introduction

The interaction of the chemokine receptor CXCR4 with its ligand SDF-1 [1] is involved in many biological processes such as hematopoiesis, migration of immune cells, as well as in cancer metastasis. CXCR4 also mediates the infection of T-cells with X4-tropic HIV functioning as a co-receptor for the viral envelope protein gp120. CXCR4, as a pharmaceutical target, is of utmost importance but the lack of synthetic agonists has seriously slowed down drug development. A very large library of antagonist compounds has been developed but most of them present a high toxicity. Studying this receptor and developing agonists could provide more information about the functionality of CXCR4 by stimulating it. Moreover, agonists are highly important for stem cells therapies and to direct them to the bone narrow.

It has been recently described by some of us [2] that grafting the SDF-1 N-terminus onto a side-chain of the inverse agonist T140 [3] provided high affinity synthetic agonists as well as partial agonists for the chemokine receptor $CXCR_4$ (Scheme 1).
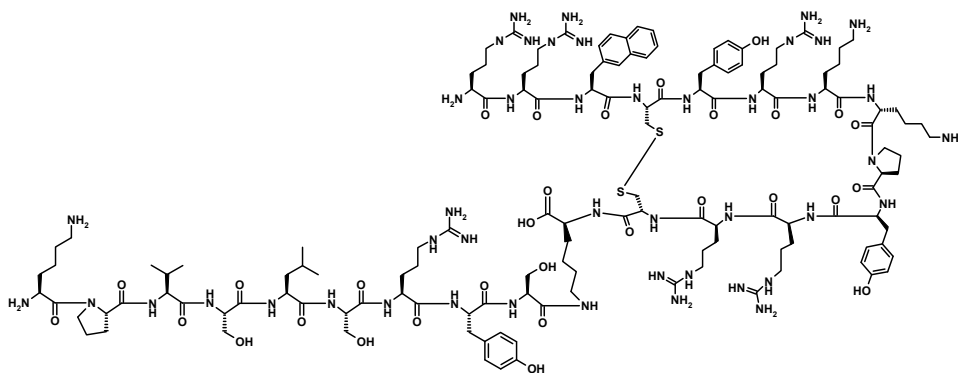
Scheme 1. Compound 1280: T140-Lys^{14}-ε [SDF-Ser^9-(1-9)], partial agonist of CXCR$_4$.

For these agonists to become useful pharmaceutical tools the PK-ADME properties need to be improved with a transition to peptidomimetic structures. Medicinal chemistry witnessed major advances with the discovery of natural peptide ligand-mimetic small synthetic molecules, insensitive to proteolytic degradation and of good PK-ADME properties. Poly-(ethylene glycol) (PEG) is a linear polyether; it is water soluble, biocompatible, non-toxic, metabolically stable, clinically approved and non-immunogenic. In addition, PEG retains the 3-carbon building block of amino acids and confers high flexibility. T140 cyclopeptide is relatively stable towards proteolysis but the linear SDF-1 terminal part remains a fragile part of the molecule. In order to improve proteolytic stability of the latter, the SDF-1 chain was replaced partially (PEG_4) or completely (PEG_8) and the influence of these replacements on affinity and intrinsic activity was studied.

Results and discussion

Peptides were synthesized using the conventional Fmoc-based solid-phase strategy in a manual reaction vessel; as a first step the synthesis of the (Lys^{14}[ε-DDE])T140 was done and the resin divided. This side chain protection was selectively removed with hydrazine, the sequences completed, then cleaved from the resin (TFA/water/TIPS/EDT = 92.5/2.5/2.5/ 2.5) and finally

cyclized to **1311-1313** (Scheme 2). Purification was achieved using preparative RP-HPLC. Analytical HPLC indicated purity greater than 97%, and correct molecular weights were confirmed by LC/MS.
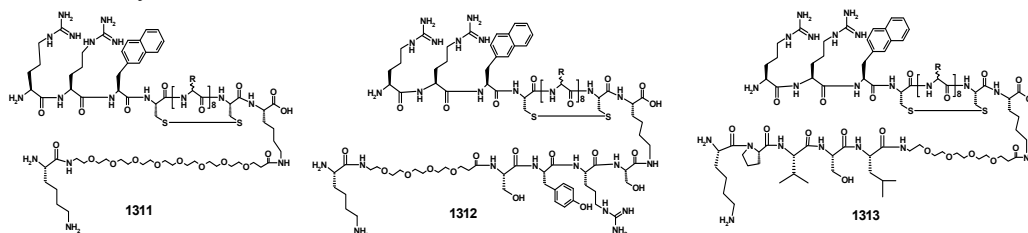
Scheme 2. T140 Chimeras.

Competition binding assays were performed on these peptides confirming that they displayed high affinity for $CXCR_4$ (Table 1).

Table 1. Structure and affinities of T140 chimeras

Compound	IC50 (nM)	Efficacy at 10nM
SDF-1 *H*-KPVSLSYRCPCRFFESHVARANVKHLKILNTPNCA LQIVARLKNNNRQVCIDPKLKWIQEYLEKALNK-*OH*	0.08	1
T140-Lys[14]	1.56	0
1280	5.67	0.115
1311	**2.14**	**0**
1312	9.55	0
1313	**30.7**	**0.070**

To test our hypothesis, transwell migration assays where performed on these three compounds and it appears that compound 1313 induces a small chemotaxis of REH cells (Figure 1), behaving as a partial agonist of CXCR4. Compounds **1311** and **1312** were devoided of any chemotactic activity, indicating that at least some amino acids are required in the N-terminal SDF-1 part of the molecule for agonistic activity.
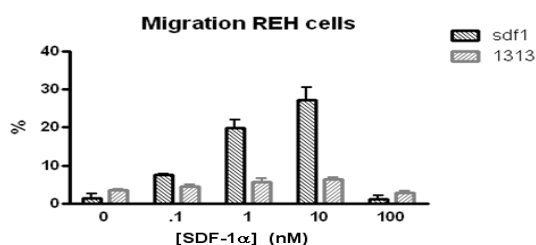
Fig. 1. Transwell migration assays of chimera 1313.

Acknowledgements

References

1. The CXC chemokine sdf-1 is the ligand for lestr/ fusin and prevents infection Tcell line adapted HIV-1 *Nature* **382**, 833-835 (1996).
2. Agonists for the Chemokine Receptor CXCR4, doi10.1021/ml200084n |*ACS Med. Chem.* (in press).
3. Tamamura, et al. *Biochem. Biophys. Res. Commun.* **253** (3), 877-882 (1998).

In vitro Assessment of the Cytotoxic Effects of Novel RGD-Mimetics

Tamara Pajpanova[1], Kaloyan Georgiev[2], Tatyana Dzimbova[1], Milena Georgieva[1], Desislava Staneva[1], and George Miloshev[1]

[1]*Institute of Molecular Biology "Acad. R. Tsanev", Bulgarian Academy of Sciences, 1113, Sofia, Bulgaria, [2]Medical University of Varna, Varna, Bulgaria*

Introduction
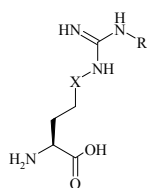
Xaa:
1. Arg (X = CH_2, R = H);
2. Arg (X = CH_2, R = NO_2)
3. Cav (X = O, R = H)
4. Cav (X = O, R = NO_2)
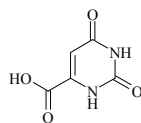
5. Orotic acid

Fig. 1. Structures of unnatural building blocks.

Peptides display a variety of important biological activities and most of their physiological functions are regulated by interactions with specific receptors, through relatively small regions of their surfaces. For instance, the integrin αvβ3, vitronectin receptor, is expressed in a number of cell types and has been shown to mediate adhesion of osteoclasts to bone matrix, vascular smooth muscle cell migration, and angiogenesis. Integrin αvβ3 also play a significant role in tumor growth, invasion and metastasis, and is a receptor for the extracellular matrix proteins with the exposed arginine-glycine-aspartic (RGD) tripeptide sequence. RGD has been shown to be potent antagonist of the integrin αvβ3, and has excellent anti-angiogenic properties including its suppression of tumor growth in animal models [1,2]. Therefore drug design based on the RGD structure may provide new treatments for diseases such as thrombosis, osteoporosis, and cancer.

Herein we describe the SPPS and the biological evaluation of a series of short RGD-mimetics containing the sequence **Xaa-GD**, where Xaa is Arg-mimetics, and differ by presence or absence of orotic acid moiety (Figure 1). Their cytotoxic potential on **3T3** (standard mouse embryonic fibroblast cell line) and **HepG2** (human liver hepatocellular carcinoma cell line) cells were examined as well.

Results and Discussion

Use of both natural and artificial modifications of bioactive peptides provides opportunities to better understand the basis for bioactivities of the parent structures and to find novel functionality that may be applied for new purposes.

As a promising candidate we have chosen L-canavanine (**Cav**) instead of the basic residue Arg. Several studies have demonstrated that L-canavanine possesses growth retardation activity toward tumor cells in culture and experimental tumors *in vivo* [3,4].

Synergic antitumor effects upon combination of L-canavanine with 5-fluorouracil, or γ-irradiation have been reported, indicating that L-canavanine may modulate the chemo- or radiosensitivity of tumors [5].

The second surrogate that we choose was orotic acid (OA). OA exhibits anti-angiogenic and anti-tumor activities *in vitro* and *in vivo* [6], and we applied for N-terminal modification, in order to improve antitumor activity of the parent molecule.

Considering these data we synthesized six RGD mimetics (Figure 2):

- **OA**-Arg-Gly-Asp (**1**)**;**
- Arg(NO_2)-Gly-Asp (**2**);
- Arg(NO_2)-Gly-Asp-ester (**3**);
- **Cav**-Gly-Asp (**4**);
- **Cav(NO_2)**-Gly-Asp (**5**);
- **OA-Cav**-Gly-Asp (**6**).
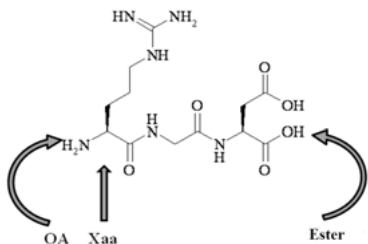
Fig. 2. Design of RGD Mimetics.

Peptides **1-3** were prepared by classical solution procedure. For the synthesis of peptides **4-6** standard Fmoc-SPPS was applied using HBTU as a coupling reagent. Peptide deprotection and cleavage from the resin were carried out in a mixture of TFA and scavengers.

We are able to obtain the RGD mimetics with satisfactory purities (typically > 95%), as assessed by analytical HPLC (Figure 3).

The cytotoxic potential of the peptides is under investigation. The cytotoxic activities of peptide **4** on 3T3 and HepG2 cells were examined (results not shown) but only the highest concentration used (2 mM) revealed cell growth inhibitory effect (85%).
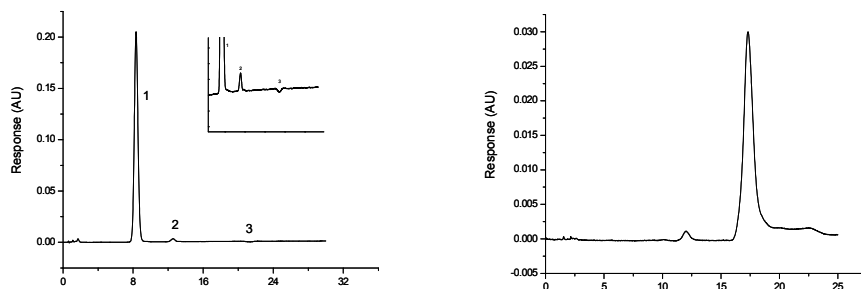
Fig. 3. HPLC-chromatograms of crude peptides **3** and **4**. Chromatographic conditions: column: Atlantis^{TM}dC$_{18}$, 4.6×150 mm, particle size 5µm, mobile phase: acetonitrile/deionised water 40/60 (v/v), column and sample temperature: 25°C, flow rate: 1ml/min, UV detection - 206 nm.

Acknowledgments

References

1. Risau, W. *Nature* **386**, 671-674 (1997).
2. Gottschalk, K.-E., Kessler, H. *Angew. Chem. Int. Ed.* **41,** 3007-3011 (2002).
3. Bence, A.K., Worthen, D.R., Adams, V.R., Crooks, P.A. *Anticancer Drugs* **13**, 313-320 (2002).
4. Miersh, J., Grancharov, K., Pajpanova, T., Neumann, D., Tabakova, S., Stoev, S., Krauss, G.-J., Golovinsky, E. *Amino Acids* **18**, 41-59 (2000).
5. Swaffar, D.S., Ang, C.Y., Desai, P.B., Rosenthal, G.A., Thomas, D.A., Crooks, P.A., John, W.J. *Anticancer Drugs* **6**, 586-593 (1995).
6. Lu, H., Klein, R.S., Schwartza, E.L. *Clinical Cancer Research* **15**, 5138-5144 (2009).

Novel Cyclic β-Hairpin-like Peptidomimetics Modulating Cell Adhesion in Multiple Myeloma

Priyesh Jain*[1,2], David Badger[1], Philip Murray[1], Yi Liang[1], Anthony W. Gebhard[3], Michael F. Emmons[4], Rajesh R. Nair[5], Lori A. Hazlehurst[3,4,5], and Mark L. McLaughlin[1,2]

[1]*Department of Chemistry, University of South Florida, 4202 E. Fowler Avenue, CHE 205, Tampa, FL, 33620, U.S.A.;* [3]*Department of Molecular Pharmacology and Physiology, University of South Florida, 4202 E. Fowler Avenue Tampa, FL, 33620, U.S.A.;* [4]*Cancer Biology Program, University of South Florida, 4202 E. Fowler Avenue, Tampa, FL, 33620, U.S.A.;* [2]*Drug Discovery and* [5]*Molecular Oncology Departments, H. Lee Moffitt Cancer Center & Research Institute, 12902 Magnolia Drive, Tampa, FL, 33612, U.S.A.*

Introduction

Multiple Myeloma (MM) patients often exhibit symptoms of relapse due to unsuccessful elimination of minimal residual disease (MRD). The existing standard chemotherapeutic treatments that target apoptotic cell death pathways in treating multiple myeloma are encountering multi-drug resistance (MDR) by tumor cells [1,2]. MRD is observed in the bone marrow which suggests that the bone marrow microenvironment is essential for tumor cell survival [3]. Previous studies have shown that adhesion of leukemia and multiple myeloma cells to the extracellular matrix (ECM) components promotes cell survival and inhibits drug induced apoptotic cell death [4,5]. Hence, development of ligands that block bone marrow microenvironment interactions would be an effective strategy for encountering strong multi-drug resistance by tumor cells. Herein, we describe the synthesis of a cyclized peptidomimetic analog of a linear all D-amino acid peptide that inhibits MM–ECM interactions and kills cells by programmed cell necrosis [6].

Results and Discussion

Using a combinatorial peptide library and a functional binding assay, Lam et. al. have identified a synthetic all D-amino acid peptide HYD1 (KIKMVISWKG) that blocks binding of epithelial prostate carcinoma cells to extracellular matrix components [7]. Hazlehurst and co-workers identified MVISW as the core residues of HYD1 required for biological activity. Replacement of Val for Ile gave a more active HYD1 analog. Based on these results, we designed and synthesized cyclic D-HYD1 that displays the core residues (MVVSW) in the recognition strand whereas residues (KLKLK) constituted the non-recognition strand.
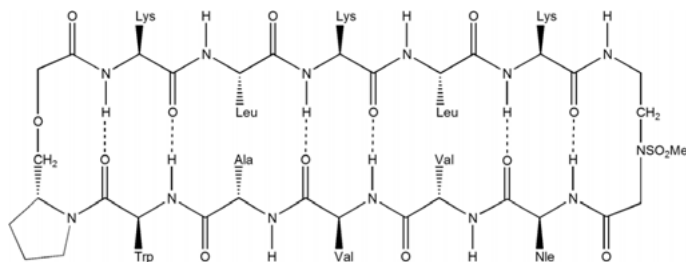
Fig. 1. Lead cyclic HYD1 peptide for inhibiting integrin mediated cell adhesion.

A sequential alanine substitution analysis on the recognition strand helped us to determine the key residues of cyclic HYD1 peptide responsible for biological activity. Replacement of Ser by Ala gave us cyclic HYD1 with ten fold greater potency (MVVAW). Another substitution of Norleucine for methionine increased potency by 15 fold. Hence NleVVAW was adopted as the lead recognition strand of cyclic HYD1 peptide. The IC$_{50}$ value of the lead cyclic HYD1 peptide in H929 cells was 1 μM whereas the linear HYD1 peptide was 33 μM. We have used both off-resin and on-resin cyclization strategies. For off-resin cyclization, the cyclic HYD1 peptides were synthesized on 2-chlorotrityl chloride resin as solid support using Fmoc solid phase peptide synthesis methods. The linear peptide was selectively cleaved from the resin without

cleaving side chain Boc-groups using trifluoroethanol. The linear peptide was cyclized in solution using HCTU followed by treatment with TFA to give cyclic peptides in low to modest yields. For the on-resin cyclization, the N^ε-amino group of a Fmoc-lysine allyl ester was attached to carbonate Wang resin. The linear peptide was synthesized followed by allyl ester deprotection, cyclization on resin using HCTU and subsequently released from the resin using TFA treatment of the peptide.

All cyclic HYD1 peptides were characterized for their secondary structures using CD and NMR spectroscopy. The CD and NMR data of these cyclic peptides were consistent with a cyclic beta-hairpin peptide-like conformation. The α-proton chemical shifts of amino acid residues and cross strand NOE peaks indicated that these peptides adopted β-hairpin conformation. These cyclic peptides have also found to be exhibiting promising in vivo activity in SCID mice model with no toxicity.

Acknowledgments

References

1. Hazlehurst, L.A., Enkemann, S.A., Beam, C.A., Argilagos, R.F., Painter, J., Shain, K.H., Saporta, S., Boulware, D., Moscinski, L., Alsina, M., Dalton, W.S. *Cancer Res.* **63** (22), 7900-7906 (2003).
2. Damiano, J.S., Cress, A.E., Hazlehurst, L.A., Shtil, A.A., Dalton, W.S. *Blood* **93**(5), 1658-1667 (1999).
3. Meads, M.B., Hazlehurst, L.A., Dalton, W.S. *Clin. Cancer Res.* **14** (9), 2519-2526 (2008).
4. Hazlehurst, L.A., Damiano, J.S., Buyuksal, I., Pledger, W.J., Dalton, W.S. *Oncogene* **19** (38), 4319-4327 (2000).
5. Hazlehurst, L.A., Argilagos, R.F., Emmons, M.F., Boulware, D., Beam, C.A., Sullivan, D.M., Dalton, W.S. *Cancer Res.* **66** (4), 2338-2345 (2006).
6. Nair, R.R., Emmons, M.F., Cress, A.E., Argilagos, R.F., Lam, K., Kerr, W.T., Wang, H.-G., Dalton, W.S., Hazlehurst, L.A. *Mol. Cancer Ther.* **8** (8), 2441-2451 (2009).
7. Pennington, M.E., Lam, K.S., Cress, A.E. *Mol. Diversity* **2**, 19-28 (1996).

Cyclic β-Hairpin Peptides as Inhibitors of p53-MDM2 Interactions

Priyesh Jain*[1,2], Yi Liang[1], Xiaolong Li[3], David Badger[1], Jiandong Chen[3], and Mark L. McLaughlin[1,2]

[1]*Department of Chemistry, University of South Florida, 4202 E. Fowler Avenue, Tampa, FL, 33620, U.S.A.;* [2]*Drug Discovery;* [3]*Molecular Oncology Departments, H. Lee Moffitt Cancer Center & Research Institute, 12902 Magnolia Drive, Tampa, FL, 33612, U.S.A.*

Introduction

The tumor suppressor p53 plays a pivotal part in protection from tumor development that arises due to various forms of cellular stress. p53 is a potent transcription factor that regulates multiple downstream genes implicated in cell cycle control, apoptosis, antiangiogenesis and senescence. Approximately half of all human tumors express p53 that is disabled by mutations in its DNA-binding domain. Growth suppressive and proapoptotic activity of p53 could harm proliferating cells that are not under stress [1]. The level of p53 in cells is controlled by its negative regulator MDM2 through a feedback loop mechanism. The NH_2 terminal transactivation domain of p53 displays an α-helix that binds MDM2. The MDM2 blocks p53 transcriptional activity directly and also directs the destruction of the p53 through its E3 ligase activity. The p53 α-helix surface formed by amino acids phenylalanine, tryptophan and leucine fit deeply into the hydrophobic cleft of MDM2 [2]. Disruption of p53/MDM2 interaction is a well-validated therapeutic target for the treatment of cancer. Various novel proteomimetic scaffold-based strategies to mimic the recognition surface have been proposed as inhibitors of p53/MDM2 interaction. Cyclic β-hairpins have been explored as inhibitors of p53-MDM2 interactions [3]. Herein we present the design and synthesis of cyclic β-hairpin peptidomimetics mimicking the α-helix of p53 using our novel β-turn promoters and show that structurally diverse hexameric, decameric, and 14-mer-like cyclic beta-hairpin scaffolds can disrupt p53-MDM2 interactions.

Results and Discussion

Based upon the crystal structure of p53-derived peptide in complex with its MDM2 domain as reported by Pavelitch and Robinson's studies, we designed cyclic beta-hairpin peptides that display the critical residues of Phe, Trp and Leu along a face of the recognition strand including beta-turn positions of the cyclic peptide for hexameric and decameric-like scaffolds and this gave ELISA assays that showed 5 and 2 µM IC50 in vitro activity (Figure 1a and Figure 1b, respectively) [3,4]. A 14-mer-like scaffold (Figure 1c) also showed activities as low as 600 nM IC50 in the ELISA assay.
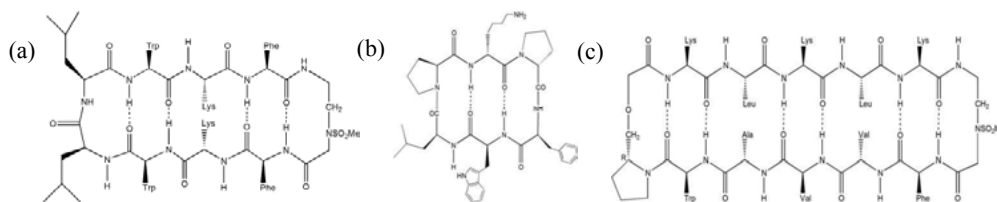
Fig. 1. a) Cyclic β-hairpin analogue with IC$_{50}$ of 2µM; b) Cyclic hexamer with IC$_{50}$ of 5µM; c) Lead cyclic β-hairpin peptide for inhibiting p53-MDM2 interactions.

These peptides were synthesized using Fmoc solid phase synthesis strategy. Linear peptides were synthesized first by using side-chain attachment strategy i.e. the N^{ε}-amino group of lysine was attached to 4-nitrophenyl-carbonate Wang resin. The linear peptide was then cyclized on resin followed by treatment with TFA to give cyclic peptide in excellent yields. The peptides obtained using this strategy usually require little or no purification. Circular Dichroism and NMR studies were carried out on selected peptides to determine their secondary structure. The

CD and NMR data revealed that these cyclic peptides adopted cyclic beta-hairpin-like conformation.

Acknowledgments

References

1. Bond, G.L., Hu, W., Levine, A.J. *Curr. Cancer Drug Targets* **5** (1), 3-8 (2005).
2. Fischer, P.M., Lane, D.P. *Trends Pharmacol. Sci.* **25** (7), 343-6 (2004).
3. Fasan, R., Dias, R.L.A., Moehle, K., Zerbe, O., Vrijbloed, J.W., Obrecht, D., Robinson, J.A. *Angew. Chem., Int. Ed.* **43** (16), 2109-2112 (2004).
4. Kussie, P.H., Gorina, S., Marechal, V., Elenbaas, B., Moreau, J., Levine, A.J., Pavletich, N.P. *Science* **274** (5289), 948-953 (1996).

Cyclic Raf-1 Peptide as Modulator of Rb-Raf1 Interactions

Priyesh Jain*[1], Philip Murray[1], Monika Verma[2], Srikumar P. Chellappan[2], and Mark L. McLaughlin[1,2]

[1]*Department of Chemistry, University of South Florida, 4202 E. Fowler Avenue, Tampa, FL, 33620, U.S.A.* [2]*Drug Discovery Department, H. Lee Moffitt Cancer Center & Research Institute, 12902 Magnolia Drive, Tampa, FL, U.S.A.*

Introduction

Retinoblastoma tumor suppressor protein, Rb, plays a vital role in regulating cell cycle progression. Rb prevents cell cycle progression from G1 phase into S-phase unless the cell receives a mitogenic signal and inactivation of Rb is necessary for normal mammalian cells to replicate. Rb is inactivated in most tumors by phosphorylation mediated by cyclin D and cyclic E dependent kinases (CDK) [1,2]. Previous studies have shown that the kinase Raf-1 binds and phosphorylates Rb in early G1 phase [3]. Overexpression of Raf-1 inactivates Rb and triggers activation of transcription factors of the E2F family thus facilitating S-phase entry. Disruption of Rb-Raf1 interaction inhibits cell proliferation and arrests tumor growth. Chellappan and co-workers have shown that Rb-Raf1 interaction is mediated by amino acid residues 10-18 of Raf-1 [4]. A linear Raf-1 peptide ISNGFGFK corresponding to residues 10-18 was shown to disrupt Rb-Raf1 interaction by preventing Rb phosphorylation and an alanine scan had shown the GFGFK portion of the 8-mer to be critical to the Rb-Raf1 disruption activity [5].

Results and Discussion

Herein we report the synthesis of cyclic Raf-1 peptidomimetics, which inhibit Rb-Raf-1 protein-protein interaction (PPI) in the low μM range. The cyclic β-hairpin peptide-like scaffold displays the GFGFK sequence on opposite strands and it is cyclized using our novel β-turn promoter in Figure 1a Chellappan, et al. have previously reported that Rb-Raf-1 PPI inhibitors function only in cells that have functional Rb gene and does not inhibit cells that do not express the Rb gene. The Raf-1 cyclic beta-hairpin (Figure 1a) showed Rb-Raf-1 PPI inhibition activity in vitro with an IC50 of 4 μM. Cyclic Raf-1 peptide inhibits Rb-Raf-1 intracellularly based on inhibition of BrdU incorporation in cells that depend on Rb-Raf-1 for proliferation. This peptide is our best current lead inhibitor for disrupting Rb-Raf1 PPI. In an effort to determine the minimum structure for this PPI inhibitory activity we shortened the β-hairpin loop and incorporating lysine as part of turn (Figure 1b), but that was less active.

(a)   (b)
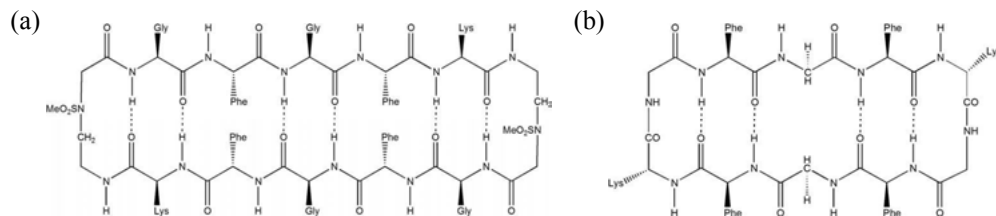
Fig. 1. a) Lead cyclic Raf-1 peptidomimetic; b) cyclic Raf-1 peptides with shorter loop and lysine residue at the β-turn.

    All cyclic Raf1 peptides were synthesized by Fmoc solid phase synthesis using side-chain attachment strategy. Linear peptides were first prepared by attaching the Nε-amino group of a lysine to the 4-nitrophenyl-carbonate Wang resin. The two antiparallel strands are linked using our novel methyl sulfonamide aminoethyl glycine linker. Cyclization of linear peptides was performed on resin to obtain cyclic peptides with better yields. On contrary to solution phase cyclization, the cyclic peptides obtained by on resin cyclization were usually clean and required little or no purification.

Acknowledgments

References

1. Sherr, C.J. *Harvey Lect.* **96**, 73-92 (2000).
2. Harbour, J.W., Luo, R.X., Dei Santi, A., Positgo, A.A., Dean, D.D. *Cell* **98**, 859-869 (1999).
3. Reddy, G.P.V. *Journal of Cellular Biochemistry* **54** (4), 379-86 (1994).
4. Wang, S., Ghosh, R., Chellappan, S. *Mol. Cell. Biol.* **18**, 7487-7498 (1988).
5. Dasgupta, P., Sun, J., Wang, S., Fusaro, G., Betts, V., Padmanabhan, J., Sebti, S.M., Chellappan, S.P. *Mol. Cell. Biol.* **24**, 9527-9541 (2004).

Designer Binding Proteins as Peptide and Antibody Mimics

Shohei Koide

Department of Biochemistry and Molecular Biology, the University of Chicago,
Chicago, IL, 60637, U.S.A.

Introduction

Peptides, small molecules and antibodies have served as common modalities for generating target-binding agents. Designer binding proteins are those molecules constructed from the so-called molecular scaffolds, typically small, single-domain proteins [1]. Combinatorial libraries are constructed using molecular display technologies such as phage display, from which variants that bind to a target of interest are identified. Designer binding proteins bridge the size gap present between peptides and antibodies. The binding surface of designer binding proteins are usually constructed from discontiguous segments within a molecular scaffold, and thus, although they are much smaller than antibodies and their fragments, designer binding proteins mimic the architecture of antigen-binding sites of antibodies. This paper focuses on the "monobody" system that my group has developed.

Results and Discussion

The monobodies are constructed using the tenth fibronectin type III domain (FN3) of human fibronectin [2]. The FN3 scaffold is a small (~10 kDa) beta-sandwich domain that is ubiquitous in mammalian proteomes. The FN3 architecture is similar to that of the immunoglobulin fold, with three loops that are structurally similar to the antigen-binding loops of the immunoglobulin domains. Notably, the tenth FN3 of human fibronectin is highly stable, although, unlike immunoglobulin domains, it lacks a disulfide bond. The high stability and the disulfide independent folding make the FN3 domain an ideal scaffold for generating target-binding molecules to be used under both reducing and oxidizing environments.

Many combinatorial libraries of monobodies have been developed [3]. Whereas early library designs introduced the 20 genetically encoded amino acids using the standard degenerate DNA base mixtures, recent advances in our understanding of protein-protein interaction energetics have resulted in major changes in how we design combinatorial libraries. Because the amino acid Tyr is particularly capable of creating productive molecular interactions [4], recent library designs enrich Tyr content. Conformational diversity is indirectly encoded by the length diversity of loops and high contents of Gly. Monobody libraries with highly biased amino acid compositions were highly effective in generating high-affinity monobodies [5,6]. Quite surprisingly, these monobodies also exhibited high specificity. Therefore, the use of biased amino acid compositions enables us to overcome the combinatorial challenge of encoding sufficient numbers of functional molecules within the size limitation of phage-display libraries, typically 10^{11}.

Monobodies that bind to the SH2 domain of the BCR-Abl oncoprotein was generated [7]. The motivations behind this work were two folds. First, we wished to determine how specific a monobody could be. Because there are 121 SH2 domains in the human proteome [8] and there is high structural homology among them, it is a formidable challenge to discriminate one SH2 domain from the others. Second, we wished to determine whether inhibiting the SH2 domain would represent a viable approach to inhibiting BCR-Abl. Although tyrosine kinase inhibitors such as Imatinib are highly effective against BCR-Abl, the emergence of drug resistant mutations pose a major challenge against chronic myeloid leukemia (CML) that BCR-Abl causes.

The monobody, termed HA4, had the Kd value of 7 nM, significantly higher affinity than phospho-Tyr peptides and nonphosphorylated peptides that bind to SH2 domains. Protein microarray assays showed that the HA4 monobodies were highly selective to Abl SH2. To define its specificity in the cellular context, the HA4 monobody was expressed in human cell lines as a fusion protein with tandem affinity purification tag. Cellular proteins that bind to HA4 were captured and analyzed using mass spectroscopy-based proteomics. The results indicated that HA4 was highly specific to Abl SH2 even in the presence of high concentrations of cellular proteins [7].

Structural analysis revealed that the HA4 monobody uses one of the diversified loops to closely mimic the binding mode of the canonical phospho-Tyr peptides to SH2 domains (Figure 1B). However, the monobody also created large interaction surfaces that recognize regions of the Abl SH2 domain that are not conserved among the SH2 domains (Figure 1A). These observations rationalize the high affinity and high selectivity of the HA4 monobody. Furthermore, they illustrate the ability of the monobody system to produce peptide-like interactions as well as antibody-like interactions. A similar binding mode has recently been observed in a monobody that bind to yeast small ubiquitin-like modifier (SUMO) [9].
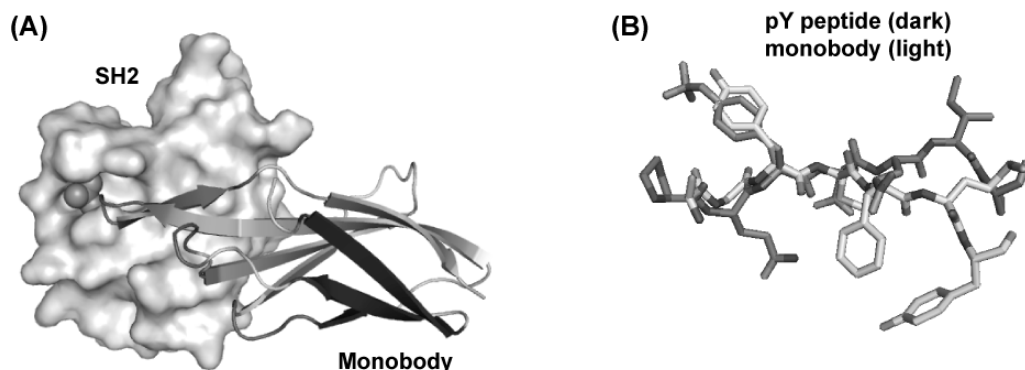
Fig. 1. (A) The crystal structure of a monobody bound to the Abl SH2 domain [7]. (B) Superposition of a phospho-Tyr peptide bound to an SH2 domain, taken from the PDB entry 1LCJ, and an equivalent segment of the monobody showing close mimicry by the monobody of the natural peptide.

Acknowledgments

References

1. Skerra, A. *Curr. Opin. Biotechnol.* **18**, 295-304 (2007).
2. Koide, A., Bailey, C.W., Huang, X., Koide, S. *J. Mol. Biol.* **284**, 1141-1151 (1998).
3. Bloom, L., Calabro, V. *Drug Discovery Today* **14**, 949-955 (2009).
4. Koide, S., Sidhu, S.S. *ACS Chem. Biol.* **4**, 325-334 (2009).
5. Gilbreth, R.N., Esaki, K., Koide, A., Sidhu, S.S., Koide, S. *J. Mol. Biol.* **381**, 407-418 (2008).
6. Koide, A., Gilbreth, R.N., Esaki, K., Tereshko, V., Koide, S. *Proc. Natl. Acad. Sci. U.S.A.* **104**, 6632-6637 (2007).
7. Wojcik, J., Hantschel, O., Grebien, F., Kaupe, I., Bennett, K. L., Barkinge, J., Jones, R. B., Koide, A., Superti-Furga, G., Koide, S. *Nat. Struct. Mol. Biol.* **17**, 519-527 (2010).
8. Liu, B.A., Jablonowski, K., Raina, M., Arce, M., Pawson, T., Nash, P.D. *Molecular Cell* **22**, 851-868 (2006).
9. Gilbreth, R.N., Truong, K., Madu, I., Koide, A., Wojcik, J.B., Li, N.S., Piccirilli, J.A., Chen, Y., Koide, S. *Proc. Natl. Acad. Sci. U.S.A.* **108**, 7751-7756 (2011).

Synthesis and SAR around the R6 Position of 2(1H)-Pyrazinone Based Hepatitis C (HCV) NS3 Protease Inhibitors

Anna Karin Belfrage[1], Johan Gising[1], Hiba Alogheli[1], Angelica Ehrenberg[2], Sofia Svahn Gustafsson[2], Mats Larhed[1], U. Helena Danielson[2], and Anja Sandström[1]

[1]Department of Medicinal Chemistry, Organic Pharmaceutical Chemistry, BMC, Uppsala University, Box 574, SE-751 23, Uppsala, Sweden; [2]Department of Biochemistry and Organic Chemistry, BMC, Uppsala University, Box 596, SE-751 24, Uppsala, Sweden

Introduction

Hepatitis C virus (HCV) infects nearly 180 million of the worldwide population, with an estimated 3 million new infections every year. A chronic HCV infection potentially leads to cirrhosis and hepatocellular carcinoma. The current standard treatment, pegylated interferon-α and ribavirin (pegIFNα/ RBV), is associated with severe adverse effects and inconvenient dosing regimens. Moreover, the efficacy is highly dependent on the genotype of the virus [1]. Victrelis, a covalent peptidomimetic NS3 protease inhibitor, was recently approved for the treatment of chronic HCV in combination with pegIFNα/RBV [2]. Viral resistance might be one of the major issues. Thus, there is a need for novel structural motifs in the development of the next generation HCV NS3 protease inhibitors. The substituted pyrazinone is a heterocyclic system useful in peptidomimetic compounds. It can act as a β-strand inducer in protease inhibitors, with retained H-bonding pattern of the peptide backbone. We have previously
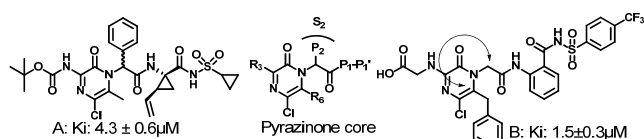
Fig. 1. Lead compounds A, B and the pyrazinone core structure.

presented the discovery and synthesis of achiral pyrazinone based HCV NS3 protease inhibitors indicating that the S2 pocket could be reached from the R6 position of the pyrazinone (**A, B**) [3,4]. We herein present further optimization of this unique type of inhibitors.
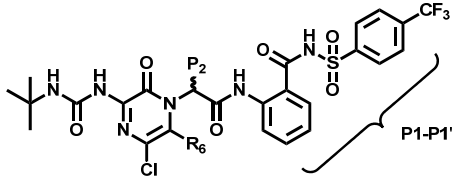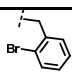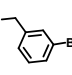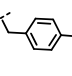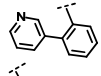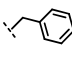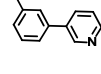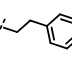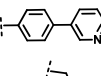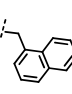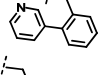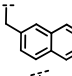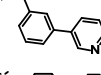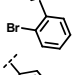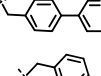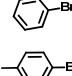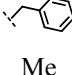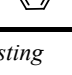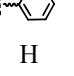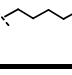
Results and Discussion

According to molecular modeling the R6 substituent has the ability to reach the S2 pocket with maintained backbone interactions of the inhibitor as well as crucial interactions with the oxy-anion cavity. In our attempt to further explore this new type of inhibitors we introduced different R6 groups, in particular while keeping P2 unsubstituted, during the synthesis of those compounds (Scheme 1, Table 1). In order to synthesize more stable compounds, the urea functionality was introduced at the R3 position. Via Suzuki coupling conditions, compounds **N-S** were successfully prepared from compounds **H-M**. Compound **D** showed retained inhibitory potency compared to the reference compound **B**.
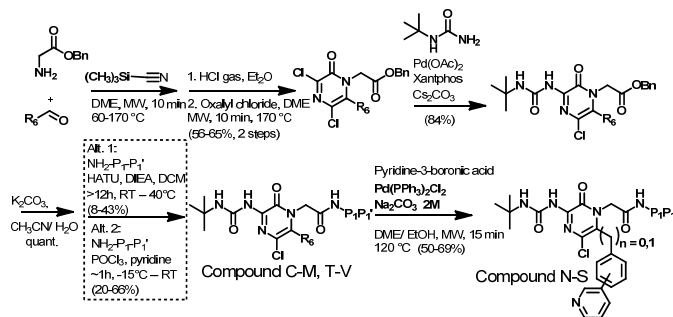
Scheme 1. Synthesis of the pyrazinone based inhibitors.

Table 1. Synthesized compounds assessed in an in vitro biochemical assay using the full length NS3 protein

Compd	R6	P2	K_i (µM)
K		H	0.25
L		H	0.29
M		H	0.44
N		H	#
O		H	#
P		H	#
Q		H	#
R		H	#
S		H	0.66
T			#
U	Me		#
V		H	#

Compd	R6	P2	K_i (µM)
C	H	H	1.9
D		H	3.4
E		H	0.12
F		H	0.29
G		H	0.33
H		H	0.40
I		H	0.60
J		H	0.38

[#]*Submitted for testing*

Prolongation of the R6 substituent with one carbon spacer (**E**) resulted in a significant improvement in inhibitory potency, indicating that extension of the R6 group is tolerated and preferred in order to reach more interactions with the S2 pocket. Moreover, introduction of bromo-substituents was positive in general (compounds **H**-**M**). Deeper understanding of the SAR around the R6 position should be obtained when the entire set of synthesized inhibitors has been evaluated in the biochemical assay.

Acknowledgments

References

1. Soriano, V., et al. *J. Antimicrob. Chemoth.* **65,** 2063-2069 (2011).
2. http://www.fda.gov/NewsEvents/Newsroom/PressAnnouncements/ucm255390.htm.
3. Örtqvist, P., et al. *Bioorg. Med. Chem.* **18**, 6512-6525 (2010).
4. Gising, J., et al. O*rg. Biomol. Chem.* **7**, 2809-2815 (2009).

Design and Synthesis of Linear Natriuretic Peptide Clearance Receptor (NPR-C) Antagonists: Series I

Elaref Ratemi[1*], Denis Gravel[1], T.J. Reddy[1], Gaoqiang Yang[1], Cedric Rieux[1], Ali Haddadine[1], Philippe Crine[2], Thomas Loisel[2], Isabelle Lemire[2], and Leng Hong Pheng[2]

[1]*Departments of Medicinal Chemistry and* [2]*Pharmacology, Enobia Pharma Inc., 2901 Rachel Street East, Montreal, Quebec, H1W 4A4, Canada; *Corresponding author (ratemi_e@jic.edu.sa)*

Introduction

The natriuretic peptides ANP, BNP and CNP bind two classes of cell surface receptors: the guanyl cyclase-linked A and B receptors (NPR-A and NPR-B) and the C receptor (NPR-C) which serves as a clearance receptor for the three peptides [1]. Achondroplasia (Ach), the most common form of short-limbed dwarfism, is an autosomal dominant disorder that interferes with the synthesis of the cartilage growth plate of long bones. Yasoda reported that CNP can rescue growth defect in achondroplastic mice [2]. Therefore, we envisioned that small molecules that potentiate endogenous CNP by antagonizing the CNP clearance receptor (NPR-C) would constitute a potential therapy for achondroplasia.

Results and Discussion

We recently cloned the bone peptide osteocrin and discovered that it specifically binds NPR-C with low nanomolar affinity (Figure 1A) and potentiates CNP action on cGMP (Figure 1B).
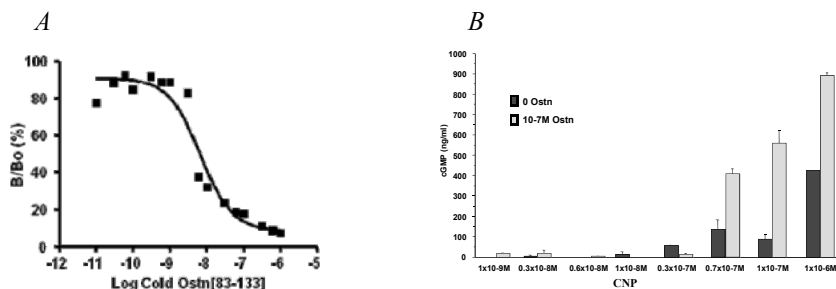
Fig. 1. A) Binding of osteocrin to NPR-C; B) Potentiation of cGMP by osteocrin.

Osteocrin and CNP are not drug candidates for obvious reasons and thus we looked at smaller molecules that augment CNP action in bone by blocking the NPR-C mediated clearance. Compound **ENB-0150** (Figure 2) is

Fig. 2. Compound ENB-0150.

Fig. 3. Effect of ENB-0150 on Ach bone explants.
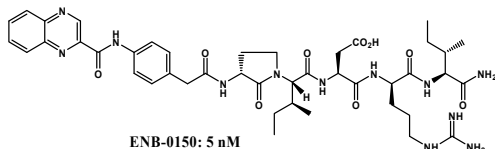
a known ANP-CR antagonist [3] and we initially chose it for a *proof-of-concept* (POC). ENB-0150 potently binds NPR-C (5nM). It significantly increased femur growth in Ach bone explants experiment (Figure 3) which constituted an *ex-vivo* POC.

Table 1. SAR on the aromatic tether moiety and its effect on potency

Cpd	Aromatic Tether	IC_{50} (nM)	Cpd	Aromatic Tether	IC_{50} (nM)	Cpd	Aromatic Tether	IC_{50} (nM)
1	(structure)	1400	5	(structure, MeO-indole)	11	9	(structure, HO-naphthalene)	11
2	(structure, Ph)	1000	6	(structure, benzofuran)	5	10	(structure, quinoline)	31
3	(structure)	210	7	(structure)	25	11	(structure, quinoline)	15
4	(structure, naphthalene urea)	11000	8	(structure, sulfonamide)	11	12	(structure, quinoline)	12

ENB-0150 showed no degradation after 2 hrs (at 4°C or 37°C) during an *in vitro* stability study. However, the *in vivo* half life was only 10 minutes which prompted us to undertake an SAR study on this compound in search for molecules with better PK profiles. Table 1 shows the effect of the aromatic tether on activity. In order to access novelty in the design, we investigated the replacement of the Freidinger Lactam (FL) in **ENB-0150** with readily available amino acids. We envisioned that Pro may induce a similar β-turn that the FL is known to induce. Successfully, this replacement led to an equally potent compound **13** (Table 2). The peptide sequence in **13** was then investigated and as Table 2 shows Asp at position 3 is very critical for activity (cpds **18-20**). We made few hundred compounds and among the 100 tested for PK, the longest $t_{1/2}$ was 1 h.

Table 2. Representative SAR study on the peptide sequence in compound 13

P^1-AA^2-AA^3-AA^4-AA^5-NH$_2$

Cpd	Pep. Seq.	IC_{50} (nM)	Cpd	Pep. Seq.	IC_{50} (nM)	Cpd	Pep. Seq.	IC_{50} (nM)
13	L^2-D^3-dR^4-I^5	7	18	I^2-A^3-dR^4-I^5	>1000	23	I^2-D^3-N-MeG^4-I^5	3
14	Chg^2-D^3-dR^4-I^5	18	19	I^2-βD^3-dR^4-I^5	330	24	I^2-D^3-Cpg^4-I^5	7
15	Y^2-D^3-dR^4-I^5	550	20	I^2-N-MeD^3-dR^4-I^5	>1000	25	I^2-D^3-dR^4-N-MeI^5	739
16	N-MeI^2-D^3-dR^4-I^5	>1000	21	I^2-D^3-P^4-I^5	1	26	I^2-D^3-dR^4-F^5	>1000
17	Bip^2-D^3-dR^4-I^5	>1000	22	I^2-D^3-Aib^4-I^5	7	27	I^2-D^3-dR^4-A^5	>1000

dR = D-Arg, Chg = Cyclohexylglycine, Bip = L-Biphenylalanine, Aib = Aminoisobutyric acid, Cpg = Cyclopropylglycine

Acknowledgments

References

1. Rose, R.A., Giles, W.R. *J. Physiol.* **586**, 353-366 (2008).
2. Yasoda, et al. *Nature Medicine* **10**, 80-86 (2004).
3. Veale, C.A., et al. *Bioorg. Med. Chem. Lett.* **10**, 1449-1952 (2000).

Cyclic Peptidomimetics as Natriuretic Peptide Clearance Receptor (NPR-C) Antagonists: Series II

Elaref Ratemi[1*], Denis Gravel[1], T.J. Reddy[1], Gaoqiang Yang[1], Ali Haddadine[1], Philippe Crine[2], and Isabelle Lemire[2]

*[1]Departments of Medicinal Chemistry; [2]Pharmacology, Enobia Pharma Inc., 2901 Rachel Street East, Montreal, Quebec, H1W 4A4, Canada; *Corresponding author (ratemi_e@jic.edu.sa)*

Introduction

We have recently established that osteocrin (a 133-amino acid bone peptide discovered by Enobia) raises the endogenous levels of CNP by antagonizing NPR-C and restoring normal bone synthesis. CNP and osteocrin bind NPR-C by an almost identical sequence and they cannot be useful drugs for obvious reasons. In series I, we reported on how much smaller linear peptidomimetics can act as osteocrin mimics and effectively block NPR-C. This investigation was aimed at developing cyclic peptidomimetics that would act as NPR-C antagonists and hopefully resolve the PK issues that we encountered with the linear series. We here report on the design, synthesis and *in vitro* biological testing of stable cyclic NPR-C antagonists.

Results and Discussion

The X-ray crystal structure of the extracellular domain of NPR-C complexed with CNP has been published [1]. Figure 1 shows the structure and the modeled bound conformation of CNP.

Based on the SAR study with linear NPR-C antagonists (series I), we learned that mimics of the LDRI region and the FGL region of CNP are important for binding. We first focused on the D and R residues and linked them through different tethers. After many attempts comprising similar

Fig. 1. Structure and bound conformation of CNP.

structures to the aminomethyl benzoic acid (AMB) tethered derivative **1**, the carbocyclic **2** and several cyclic disulfides incorporating D and R residues, we were pleased to identify the lead compound **3** (Figure 2). Modeling **3** with NPR-C receptor indicated that extension to the Phe-7' pocket may increase potency. In this regard, we first looked at substituting the AMB tether. Unfortunately, none of these attempts led to any appreciable activity.

Fig. 2. Peptidomimetics designed after the LDRI region.

Table 1. Optimization at the β-Ala residue
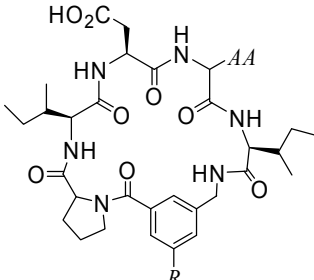
Cpd	β-Ala Sub. (R)	IC_{50} (μM)	Cpd	β-Ala replacement	IC_{50} (μM)	Cpd	β-Ala replacement	IC_{50} (μM)
4	4-OH-Ph	inactive	**8**	Arg	inactive	**12**		inactive
5	Benzyl	15	**9**	Tyr	inactive			
6	2-*n*-Butyl	inactive	**10**	AMB	inactive	**13**		40
7	*p*-NO$_2$-Benzyl	inactive	**11**	Ile	40			
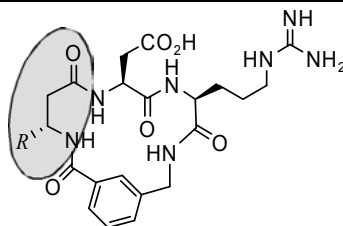
In the light of the above rather disappointing results, we next attempted the optimization of the β-alanine residue in **3**. Table 1 shows that β-substitution did not lead to any activity with the exception of compound **5** which gave modest potency. Replacing β-alanine with other amino acids was not very fruitful. Ile and the Ile-containing Freidinger Lactam replacement gave only modest activity, compounds **11** and **13**, respectively.

Compounds **11** and **13** prompted us to launch another series since Ile is, in fact, in this position in CNP. Here, as we did in the linear series of NPR-C antagonists, we sought the replacement of the lactam with proline. We also envisioned that this strategy will increase the ring size and hence allow for the extension to the Phe-7' pocket. After synthesizing few small libraries and testing them, we were pleased to discover that compound **14** had a relatively much better binding with an IC_{50} of 145 nM (Table 2). Equally potent, was compound **15** where Arg was replaced with Gly. Substitution at the position 5 on the AMB tether also led to increased potency although this contact seemed sensitive to the length and polarity of substituent (Table 2). Compound **19** represents thus far the most potent cyclic peptidomimetic that is acting as an NPR-C antagonist.

Table 2. Optimization at the AMB tether

Cpd	AA	R	IC_{50} (nM)
14	Arg	H	145
15	Gly	H	140
16	Arg	PhCONH-	124
17	Arg	PhCH$_2$CONH-	322
18	Arg	PhCH$_2$CH$_2$CONH-	398
19	Arg	*p*-MeO-PhCH$_2$CONH-	82

Acknowledgments

References

1. Garcia, K.C. *Science* **293**, 1200-1209 (2001).

Exploring Species Selectivity in Protein-Protein Interactions using Synthetic Binding Site Mimetics

Julia Meier[1], Kristin Kassler[2], Heinrich Sticht[2], and Jutta Eichler[1]

[1]*Department Medicinal Chemistry, University of Erlangen-Nurnberg, Erlangen, 91052, Germany;* [2]*Institute of Biochemistry, University of Erlangen-Nurnberg, Erlangen, 91054, Germany*

Introduction

Apart from their biomedical significance as inhibitors of protein-protein interactions, synthetic mimetics of protein binding sites are also valuable tools for the exploration of these interactions at the molecular level. HIV entry into human cells is initiated by the interaction of gp120 with the cellular receptor CD4 [1]. The molecular basis of the fact that mice cannot be infected with HIV [2] lies in the lack of affinity of HIV gp120 to murine CD4 [3], in spite of a fairly high sequence homology between the first extracellular domain (D1) of murine and human CD4 (mCD4 and hCD4), which contains its binding site for gp120. Furthermore, affinity to gp120 could be restored in mCD4 by exchanging the residues critical for binding to gp120 by the respective amino acids in hCD4 [2,4]. In an attempt to reproduce that transfer of affinity to gp120 from human to murine CD4, in binding site mimetics, we have designed and synthesized peptides (Table 1) that present the gp120 binding site of human and murine CD4, respectively, as well as a "humanized" mCD4 mimetic peptide containing the hot spot residues F43 and R59.

Table 1. Sequences of CD4 mimetic peptides

	Peptide	Sequence
1	hCD4-M wt	Ac-KSIQFHWKNSNQIKILGNQGS**F**LTKGPSKLNDRADS**RR**SLWDQ-NH₂
2	hCD4-M Ala	Ac-KSIQFHWKNSNQIKILGNQGS**A**LTKGPSKLNDRADS**AA**SLWDQ-NH₂
3	mCD4-M wt	Ac-KITVFTWKFSDQRKILGQHGKG**V**LIRGGSPSQFDRFDS**KK**GAWEK-NH₂
4	mCD4-M Ala	Ac-KITVFTWKFSDQRKILGQHGKG**A**LIRGGSPSQFDRFDS**AA**GAWEK-NH₂
5	mCD4-M hum.	Ac-KITVFTWKFSDQRKILGQHGKG**F**LIRGGSPSQFDRFDS**RR**GAWEK-NH₂

Results and Discussion

The lack of affinity of HIV gp120 to murine CD4 could be confirmed in our ELISA binding assay using recombinant proteins (Figure 1, left). This effect was reproduced when using, instead of gp120, a synthetic peptide that mimics the CD4 binding site of gp120 [5], re-confirming the functional mimicry of CD4-binding by this gp120 mimetic peptide (Figure 1, center). Surprisingly, the differences in affinity to gp120 between hCD4 and mCD4 could not be seen in CD4 mimetic
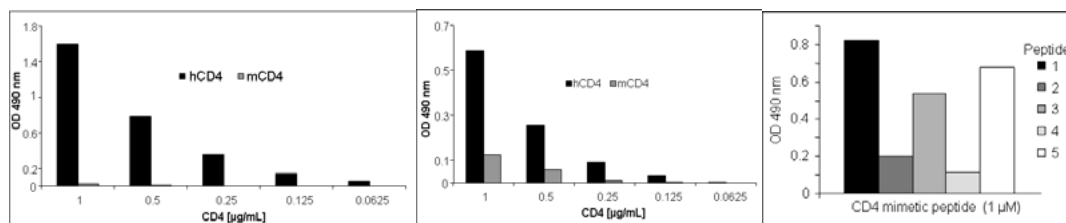
Fig. 1. Binding of HIV gp120 IIIB (0.5 μg/mL) (left) and a peptide mimicking the CD4 binding site of gp120 (4 μM) (center), respectively, to human and murine CD4. Right: Binding of HIV gp120 IIIB (0.5 μg/mL) to CD4 mimetic peptides (see Table 1).

peptides, i.e. the human and murine *wt* peptides (1 and 3) had comparable affinities to gp120 (Figure 1, right).

Consequently, the gain in affinity in the humanized mCD4 mimetic peptide 5 is marginal. Furthermore, replacement of the hot spot residues F43 and R59 in hCD4-M and their analogues residues V44 and K61 in mCD4-M (peptides 2 and 4) respectively, with alanine, largely reduced affinity to gp120, indicating specific binding to gp120.

In order to address the structural basis of this unexpected behaviour, molecular models for mCD4, as well as the mCD4 mimetic peptide, in complex with gp120 were generated and compared to the hCD4-gp120 complex structure [6]. Consistent with the experimental data, the dynamic simulations show that the hCD4-gp120 interaction, but not the mCD4-gp120 interaction, remains stable. The poor interaction of mCD4 with gp120 results from clashes of inserted CD4 residues, which have no structural equivalent in hCD4, preventing hydrophobic interactions of V44 (mCD4 residue equivalent to F43 of hCD4) with D368 and E370 of the CD4 binding loop of gp120 (Figure 2, left). These clashes are prevented in mCD4-M, where C''-flanking loops are flexible, and the inserted residues even contribute to the stabilization of the interface by establishing contacts other than those in the hCD4-gp120 interaction (Figure 2, right).

In conclusion, the lack of affinity of mCD4 to HIV gp120 appears to not be based on its amino acid sequence, but most likely on protein structure. This affinity can be partly restored in less structured binding site mimetic peptides.

Fig. 2. Unlike F43 of hCD4, V44 of mCD4 cannot contact D368 and E370 of the CD4 binding loop of gp120 (left). Unlike mCD4 (center), the more flexible mimetic peptide mCD4-M (right) is able to contact the CD4 binding site of gp120.

Acknowledgments

References

1. Kowalski, M., et al. *Science* **237**, 1351-1355 (1987).
2. Clayton, L., et al. *Nature* **335**, 363-366 (1988).
3. McClure, M.A., et al. *Nature* **330**, 487-489 (1987).
4. Wieder, K.J., et al. *AIDS Res. Hum. Retroviruses* **12**, 867-876 (1996).
5. Franke, R., Hirsch, T., Overwin, H., Eichler, J. *Angew. Chem. Int. Ed.* **46**, 1253-1255 (2007).
6. Kwong, P.D., et al. *Nature* **393**, 648-659 (1998).

The Wild Bee Venom – Rich Source of Antimicrobial Peptides

Lenka Monincová, Sabína Čujová, Jiřina Slaninová, Vladimír Fučík, Lenka Borovičková, Zdeněk Voburka, Oldřich Hovorka, Josef Cvačka, Lucie Bednárová, and Václav Čeřovský

Institute of Organic Chemistry and Biochemistry, Academy of Sciences of the Czech Republic, Flemingovo nam 2, 16610, Prague, Czech Republic

Introduction

Antimicrobial peptides (AMPs) which kill bacteria with fundamentally different mode of action than do traditional antibiotics represent new trend in the fight against resistant pathogens. In our laboratory we have focused on the search of novel AMPs identified in the venom of hymenopterans. We have found that the venom of wild bees offers promising source of AMPs showing potent antimicrobial activity and low or moderate toxicity to eukaryotic cells [1-6]. After identifying their primary structure we synthesized these AMPs for biological assays and structural studies. In addition, we prepared several analogs attempting to improve their biologically properties.

Results and Discussion

In our laboratory we have discovered 18 novel antimicrobial peptides isolated from 9 species of wild bee. None of the peptides displays any homology to apamin or melittin - the peptides, which have already been identified in the venom of honey bee. Fifteen of them belong to the category of linear α-helical amphipathic peptides (Table 1). They consist of 12 to 19 amino acid residues and are rich in hydrophobic (50% and more) and cationic amino acid residues (2-5 Lys or Arg). CD study showed that these peptides have disordered structure in aqueous solution, whereas they form highly amphipathic α-helical conformations in the presence of membrane-mimicking environment such as SDS or organic solvents like trifluoroethanol. One subgroup represents peptides having Pro at position 11 that causes a kink in peptide helical structure. This conformational element plays a key role in the selectivity of those peptides towards bacterial cells. The replacement of Pro 11 by Lys, Ala or Gly in MEP resulted in a negligible change in antimicrobial activity, but a remarkable increase in hemolytic activity. In the peptide sequence there is a positional conservation of individual residues: Ser at positions 4, Leu at positions 6, Arg or Lys at positions 7, 8, His at positions 16. AMPs of the second subgroup do not contain Pro in their sequence, but another helix breaker Gly is often present in the central part of their sequences. Obvious positional conservation in terms of residue types can be also observed: Trp at position 3, Leu or Ile at positions 6, 7, 10, 11, basic amino acid residues (Arg or Lys) at position 12 and the C-terminal amidation. All peptide possess antimicrobial activity against both Gram-positive and Gram-negative bacteria (especially peptides MAC-1 and LL-III against *Staphylococcus aureus*, LL-I - IV against *Pseudomonas aeruginosa*) and activity against *Candida albicans* (especially LL-IV).

We have also identified unique 25 to 27 residues long AMPs containing two intramolecular disulfide bridges (Table 1). PNG-R and PNG-K isolated from the venom of *Panurgus calcaratus* differ only in amino acid residue at position 14. However, LAS isolated from *Lasioglossum laticeps* showed no significant homology with PNG-R and PNG-K. PNG-R had only weak antimicrobial activity, whereas LAS showed potent antimicrobial activity against both Gram-positive and Gram-negative bacteria, especially against pathogenic *Pseudomonas aeruginosa* and also activity against *Candida albicans* and no hemolytic activity. CD spectra of LAS were measured in water and in presence of increasing proportion of SDS and TFE. Unlike linear α-helical peptides synthetic PNG-R and LAS exhibited some content of α-helical conformation already in water and α-helix content changed very little in the presence of TFE or SDS.

We prepared analogs (Table 1) with increased killing potencies against some bacteria and decreased hemolytic activity in comparison to their parent peptides. Some of these peptides exhibit a potency to kill various cancer cells in vitro and they have also antifungal activity. Comparison to other AMPs of similar size shows, that most of wild bee venom peptides exhibit better antimicrobial properties than peptides previously described by others.

Table 1. Antimicrobial and hemolytic activities of AMPs identified in the venom of wild bees vs. antibiotic tetracycline, antifungal drug Clotrimazol and two peptides described in literature – indolicidine [7] and anoplin [8]

	Species	Peptide	Sequence[a]	Antimicrobial activity MIC [μM][b]					MIC [μM]	Hemolytic activity LC$_{50}$[μM]
				B.s.	E.c.	S.a.	P.a.	C.a.		
with Pro kink	Melecta albifrons	MEP	GFLSILKKVLPKVMAHMK-NH$_2$	0.8	2.0	6.8	18.5	8.7		>100
	Coelioxys quadridentata	Coe	GVWSTLKKLVPAIMQHA-NH$_2$	4.7	6.3	>100	100	40.0		>100
	Nomada	Nom	LFGSMLKKLLPLIKSHLK-NH$_2$	1.7	2.5	35.0	57.5	9.5		137
	Anthophora plamipes	Antp-8	GLLSALRKMIPHILSHIK	2.0	1.8	8.0	38.8	6.4		127
		Antp-7	GLLSALRKMIPHILSHIKK	1.8	3.3	36.7	46.7	10.0		>100
without Pro kink	Halictus sexcinctus	HAL-1	GMWSKILGHLIR-NH$_2$	0.8	3.8	7.7	45.0	6.3		82
		HAL-2	GKWMSLLKHILK-NH$_2$	1.0	2.5	8.1	42.1	6.6		78
	Macropis fulvipes	MAC	GFGMALKLLKKVL-NH$_2$	1.3	3.0	3.7	35.0	6.3		97
	Lasioglossum laticeps	LL-I	VNWKKVLGKIIKVAK-NH$_2$	0.8	1.7	14.3	15.8	9.1		>200
		LL-II	VNWKKILGKIIKVAK-NH$_2$	0.7	1.4	9.0	14.4	10.0		>200
		LL-III	VNWKKILGKIIKVVK-NH$_2$	0.8	1.4	3.9	18.7	11.7		>200
		LL-IV	IKWGKILKKIIK-NH$_2$	0.9	3.8	30.8	11.5	4.4		>200
		LL-V	INVGKILKKILRR-NH$_2$	1.5	15.0	>100	21.7	90.0		>200
	Trachusa byssinum	Tra	GILSVLKNLLKKHMAS-NH$_2$	2.0	7.2	41.7	46.7	11.3		>200
	Panurgus calcaratus	PNG-1	LNWGAILKHIIK-NH$_2$	1.3	3.7	10.6	51.7	7.3		120
S-S bridges	Lasioglossum laticeps	LAS	GLPRKILCAIAKKKGKCKGPLKLVCKC	0.3	5.5	90	15	4.5		>200
	Panurgus calcaratus	PNG-R	LDVKKIICVACKIRPNPACKKICPK	1.5	33	>100	>100	25.0		>>100
		PNG-K	LDVKKIICVACKIKPNPACKKICPK	n.d.	n.d.	n.d.	n.d.	n.d.		n.d.
Analogs		HAL-1/10	GMW**K**KILG**K**LIR-NH$_2$	0.8	2.3	15	13	4.7		>200
		HAL-2/2	GKWM**K**LLKHILK-NH$_2$	0.8	2.5	4.5	11	4.5		87.4
		MAC-10	GF**K**MALKLLKKVL-NH$_2$	0.8	1.8	6.7	12.8	5.5		>200
		LL-III/12	*VNWKKILGKIIKVVK*-NH$_2$	0.4	0.7	2.5	24.2	5.0		111
		LL-III/A	KNWKK-**Aib**-LGK-**Aib**-IK**Aib**-VK-NH$_2$	0.5	1.1	10.0	20.0	3.7		>200
		Anoplin	GLLKRIKTLL-NH$_2$	5.0	20.0	>100	40.0	n.d.		>200
		Indolicidin	ILPWKWPWWPWRR-NH$_2$	1.0	>100	13.0	>100	n.d.		>200
		Clotrimazol	-	n.d.	n.d.	n.d.	n.d.	20-60		n.d.
		Tetracycline	-	12.5	0.4	1.5	75.7	6		>200

[a] Amino acid replacements are bold; D-amino acids are in italic; Aib, aminoisobutyric acid, [b] B.s., Bacillus subtilis; S.a., Staphylococcus aureus; E.c., Escherichia coli; P.a., Pseudomonas aeruginosa; C.a., candida albicans; n.d., not determined

Acknowledgments

References

1. Čeřovský, V., et al. *ChemBioChem* **9**, 2815-2821(2008).
2. Čeřovský, V., et al. *ChemBioChem* **12**, 2089-2099 (2009).
3. Monincová, L., et al. *Amino Acids* **39**, 763-775 (2010).
4. Monincová, L., et al. *Collection Symposium Series* **11**, ÚOCHB AV ČR 2009, p. 77.
5. Monincová L., Slaninová J., Fučík V., et al. In M. Lebl, M. Meldal, K.J. Jensen, T. Hoeg-Jensen, Eds. *Peptides: Tales of Peptides (Proceedings of the 31st European Peptide Symposium)* 2010, p. 406.
6. Čujová, S., et al. *Biologically Active Peptides XII, Book of Abstracts* 2011, p. 27.
7. Selsted, M.E., et al. *J. Biol. Chem.* **267**, 4292-4429 (1992).
8. Konno, K., et al. *Biochm. Biophys. Acta* **1550**, 70-80 (2001).

Comparative Study on the Antimicrobial Effect of Small Cationic Homopeptides

Fanny Guzmán[1], Felipe León[1,4], Sergio Marshall[1,5], Claudia Ojeda[1], Fernando Albericio[2], and Patricio Carvajal-Rondanelli[3,5]

[1]*Biotechnology Nucleus, Pontificia Universidad Católica de Valparaíso, Chile (PUCV);* [2]*Department of Organic Chemistry, Universitat de Barcelona, Spain;* [3]*School of Food Engineering, PUCV;* [4]*Department of Biochemistry, Universidad de Santiago de Chile, Chile;* [5]*Regional Centre for the Study of Healthy Foods (CREAS), Valparaíso, Chile*

Introduction

Cationic antimicrobial peptides (CAMPs) have a broad spectrum of activity, not only against Gram-negative and Gram-positive bacteria, but also against antibiotic-resistant bacterial strains [1]. CAMPs often contain proline and the cationic amino acids arginine and lysine. The latter amino acids are thought to mediate peptide interactions with negatively charged cell walls of bacteria and it has been proposed as a primary mechanism of action for CAMPs; however, it is not clear which are the main factors driving the interaction. To gain an improved understanding of peptide bacteria interaction we conducted a fundamental study on the effect of side-chain hydrophobicity, backbone length and secondary structure of model homopeptides on bacterial inhibitory activity using a series of chemically synthesized cationic homopeptides (lysine, and arginine) and proline.

Results and Discussion

CD spectra for two homopeptides, $[Lys]_{11}$ (K11) and $[Arg]_{11}$ (R11) collected at pH 7.0 and a temperature of 37ºC, are given in Figure 1. These series display characteristic polyproline II helix (PPII) signature, with a weak positive band maximum at ~228 nm and strong minima at ~200 nm [1]. Proline homopeptides previously has been shown to be a PPII helix via a combination of CD and NMR spectroscopy [2]. K11 and R11 possess a CD spectrum similar to that of $[Pro]_{11}$ (P11).
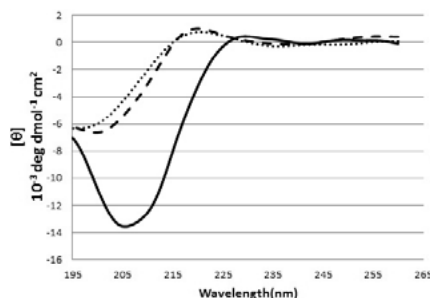
Fig. 1. CD spectra of lysine, arginine and proline homopeptides of 11 residues in aqueous solution.

The per residue molar ellipticities for the three characteristics bands are somewhat weaker for R11 and K11 than for proline polymers, indicating a lower per residue PPII helical content. Nonetheless, it is clear that K11 and even R11 possess significant PPII helical content. Indeed, we observed the same structure propensity for all synthesized Arg and Lys homopeptides, ranging from 7 to 14 residues (data not shown).

Figure 2 shows the percentage of bacterial growth inhibition for Gram-positive (A) and Gram-negative bacteria (B) as a function of chain length (or number of residues) for homopeptides of lysine and arginine. The experiments were conducted at 37°C and a peptide concentration level of 100 μM.

Homoproline peptides did not exhibit antimicrobial activity, which is an indicative that the PPII-like secondary structure is not the sole determinant of antibacterial action. Lysine homopeptides produced stronger antibacterial peptides as compared to arginine homopeptides of the same size. Among the chain lengths studied, the 11 or 13-residue peptides seem to offer the best anchoring capacity to the bacterial membrane surface, since they inhibited the growth of 73% of the strains tested. This suggests that the hydrophobic content of the cationic side chain strongly modulates the antibacterial action of small cationic peptides.

The effects of size, composition, and structure have not been easy to deconvolute. In essence, the study of CAMPs mechanism using heterogeneous peptides is limited since every
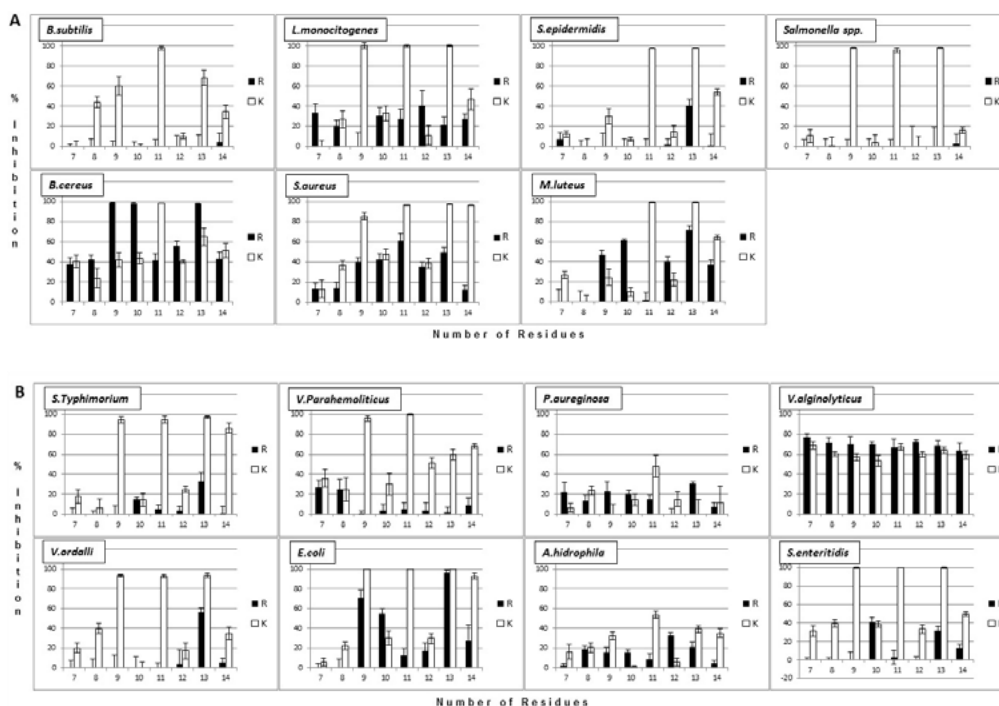
Fig. 2. Percentage of bacterial inhibition for Lysine and Arginine homopeptides on (A) Gram-positive bacteria and (B) Gram-negative bacteria.

amino acid in the peptide sequence could influence in a different manner the antimicrobial action. One simplification of the problem to investigate the effect of the length, composition and structure of peptides is using simple repeat sequences of difference length as we have done.

Our study suggests that antimicrobial activity of short peptides containing K is higher than those of peptides containing R. The single amine of K has a less dispersed positive charge than the guanidinium group of R. Moreover, the stem of the side-chain lysine is more hydrophobic than the arginine one, possible enhancing a more efficient interaction with bacterial membrane surfaces, allowing peptides to partition in the bilayer interface and destroying it.

Recent studies suggest that arginine-rich peptides function as cell penetrating peptides that are able to penetrate very quickly almost any cell with little or no membrane disruption. Therefore, arginine rich peptide can exert an antimicrobial action not at the membrane surface but targeting intracellular components [3].

This research is a fundamental study that will help to interpret and design more efficient novel antibacterial peptides.

Acknowledgments

References

1. Woody, R. *J. Am. Chem. Soc.* **131**, 8232-8245 (2009).
2. Kelly, M., et.al. *Biochemistry* **40**, 14376-14383 (2001).
3. Herce, H., Garcia, A. *J. Biol. Phys.* **33**, 345-356 (2007).

Exploring the Spectrum of Biological Activities of Fusaricidins and Their Analogs

Nina Bionda[1,2], Mare Cudic[1], and Predrag Cudic[1]

[1]Torrey Pines Institute for Molecular Studies, 11350 SW Village Parkway, Port St. Lucie, FL, 34987, U.S.A. [2]Florida Atlantic University, 777 Glades Road, Boca Raton, FL, 33431, U.S.A.

Introduction

Cyclic lipodepsipeptides are natural products with broad spectrum of biological activities. Fusaricidin/LI-F, a family of cyclic lipodepsipeptides isolated from *Paenibacillus polymyxa* strains, exhibits strong activity against an array of Gram-positive bacteria, including multiple-drug resistant strains [1]. Potent antimicrobial activities combined with relatively simple structure make these natural products particularly interesting lead structures for the development of new drugs. As part of our efforts to assess the spectrum of biological activities of these natural products, we have synthesized several fusaricidin/LI-F analogs. These analogs include modifications in the amino acid sequence as well as replacement of an ester bond with an amide bond. Fusaricidin/LI-F synthetic analogs were tested for antimicrobial activity, hemolytic activity, and serum stability.

Results and Discussion

Using synthetic strategy previously described by our group for Fmoc solid-phase synthesis of fusaricidin/LI-F class of cyclic lipodepsipeptides [2], a total of 16 analogs have been prepared. The sequences of synthesized analogs are shown in Figure 1. Antimicrobial activities of prepared peptides were assessed against several Gram-positive bacteria using standard microdilution broth method [3,4], and obtained results are listed in Table 1.
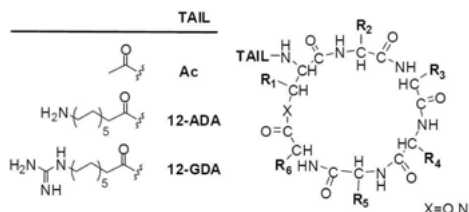
Analog	Tail	R^1	R^2	R^3	R^4	R^5	R^6
1	Ac	L-Thr^1	D-Val^2	L-Val^3	D-Thr^4	D-Asn^5	D-Ala^6
2	Ac	L-Thr^1	D-Val^2	L-Val^3	D-*a*Thr^4	D-Asn^5	D-Ala^6
3	12-ADA	L-Thr^1	D-Val^2	L-Val^3	D-Thr^4	D-Asn^5	D-Ala^6
4	12-ADA	L-Thr^1	D-Val^2	L-Val^3	D-*a*Thr^4	D-Asn^5	D-Ala^6
5	12-GDA	L-Thr^1	D-Val^2	L-Val^3	D-Thr^4	D-Asn^5	D-Ala^6
6	12-GDA	L-Thr^1	D-Val^2	L-Val^3	D-*a*Thr^4	D-Asn^5	D-Ala^6
7	12-GDA	L-Thr^1	D-Val^2	L-Val^3	D-Ala^4	D-Asn^5	D-Ala^6
8	12-GDA	L-Thr^1	D-Val^2	L-Ala^3	D-*a*Thr^4	D-Asn^5	D-Ala^6
9	12-GDA	L-Thr^1	D-Ala^2	L-Val^3	D-*a*Thr^4	D-Asn^5	D-Ala^6
10	12-GDA	L-Thr^1	D-Val^2	L-Val^3	D-*a*Thr^4	D-Asn^5	Gly^6
11	12-GDA	L-Thr^1	D-Val^2	L-Phe^3	D-*a*Thr^4	D-Asn^5	D-Ala^6
12	12-GDA	L-Lys^1	D-Val^2	L-Val^3	D-*a*Thr^4	D-Asn^5	-
13	12-GDA	L-Dap^1	D-Val^2	L-Val^3	D-*a*Thr^4	D-Asn^5	D-Ala^6
14	12-GDA	L-Dap^1	D-Val^2	L-Ala^3	D-*a*Thr^4	D-Asn^5	D-Ala^6
15	12-GDA	L-Dap^1	D-Val^2	L-Phe^3	D-*a*Thr^4	D-Asn^5	D-Ala^6
16	12-GDA	L-Dap^1	D-Val^2	L-Tyr^3	D-*a*Thr^4	D-Asn^5	D-Ala^6

Fig. 1. Sequences of synthesized fusaricidin /LI-F analogs.

We have shown previously that depsipeptide analogs containing 12-guanidino dodecanoic acid exhibited the most potent activity (MIC 8 µg/mL) against Gram-positive bacteria, Table 1. However, they were most hemolytic and an ester bond undergoes hydrolysis in 50% human serum after incubation for 24 h at 37°C. Replacement of an ester by amide bond, analogs **12-16**, resulted in dramatic increase in cyclic peptide stability. In the case of analog **6** hydrolysis of the ester bond was confirmed by RP-HPLC and MALDI TOF mass spectrometry (**6**, R_t=15.7 min, [M+H$^+$], m/z=825.4956; hydrolysis product R_t=15.6 min, [M+H$^+$], m/z=845.1799). On the other hand, no decomposition was observed for amide counterpart, analog **13**, under the same experimental conditions. Quite interestingly, amide analogs parallel antibacterial activity of the parent depsipeptides, Table 1. Besides greater serum stability, hemolytic activity of the most active amide analogs **13** and **15** was undetectable at concentrations 8 x MIC, whereas parent depsipeptides **6** and **11** at the same concentrations showed 43% and 72% of hemolysis, respectively, compared to 1% Triton X-100 detergent. In time-kill studies performed on *S. aureus* ATCC 29213 bacterial strain ester and amide analogs showed different behavior. Cyclic lipodepsipeptide **6** showed bactericidal activity, whereas its amide counterpart, analog **13**, showed bacteriostatic activity. Membrane depolarization studies using DiSC$_3$(5) and the same *S. aureus* strain showed that all tested analogs, **6**, **11**, **13** and **15**, exhibit relatively rapid, concentration-dependent membrane depolarization. However, in all cases this effect on the bacterial membrane is not paralleled by bacterial killing, thus eliminating membrane depolarization as main mode of action for these peptides. Further investigations are currently underway to determine bacterial target and exact mode of action of these peptides.

Table 1. *Minimum inhibitory concentrations (MIC) determined by the broth microdilution method [3,4]*

	MIC (µg/mL)				
Analog	*S. aureus* ATCC-29213	*S. aureus* (MRSA) ATCC-33591	*S. aureus* (VRSA) ATCC-700699	*S. epidermidis* (MRSE) ATCC-27626	*S. pyogenes* ATCC-19615
2	-	>64	>64	-	-
4	-	>64	>64	-	-
5	32	16	16	16-32	32-64
6	8	16	16	16	16
7	-	>64	>64	32	64
8	32	16	16	8	16
9	-	32	64	16	64
10	-	>64	>64	>64	>64
11	8	8	16	8	8
12	-	64	>64	>64	>64
13	8	16	16	16	16
14	-	64	-	64	128
15	8	8	-	16	16
16	-	32	-	64	64

Acknowledgments

References

1. a) Kurusu, K., Ohba, K. *J. Antibiot.* **40**, 1506-1514 (1987); b) Kajimura, Y., Kaneda, M. *J. Antibiot.* **50**, 220-228 (1997); c) Kuroda, J., Fukai, T., Konishi, M., Uno, J., Kurusu, K., Nomura, T. *Heterocycles* **53**, 1533-1549 (2000).
2. Cudic, P., Stawikowski, M. *Tetrahedron Lett.* **47**, 8587-8590 (2006).
3. Otvos, L., Cudic, M. In G.B. Fields (Ed.) *Peptide Characterization and Application Protocols, Methods in Mol. Biol.* Humana press, Totowa, 2007.
4. CLSI *Methods for dilution antimicrobial susceptibility tests for bacteria that grow aerobically* **29**, M7-A8. CLSI, Wayne, 2011.

Isolation, Identification, and Distribution of Phoenixin

Rong-Ming Lyu[1], Xiang-Qun Chen[1], Qing Tian[1], Oliver Jahraus[2], Nae J. Dun[3], and Jaw-Kang Chang[1]

[1]Phoenix Pharmaceuticals Inc., Burlingame, CA, 94010, U.S.A.; [2]Phoenix Europe GMBH, Viktoriastrasse 3-5, D-76133 Karlsruhe, Germany; [3]Department Pharmacology, Temple University, Philadelphia, PA, 19140, U.S.A.

Introduction

There is considerable interest in the discovery of new endogenous ligands such as peptides that modulate the homeostasis of multicellular organisms. Based on bioinformatic analysis of signal peptides and proteolytic processing sites, we predicted the existence of several peptides in the uncharacterized proteins LOC389203 and LOC501923. As a first step towards realizing the function of these peptides, we first isolated the peptides and generated antibodies against the putative peptides. The identified peptides, named Phoenixin-20 amide, Phoenixin-15 (Phoenixin-14-Gly), and Phoenixin-14 amide have been found in the heart, and certain regions in the brain.
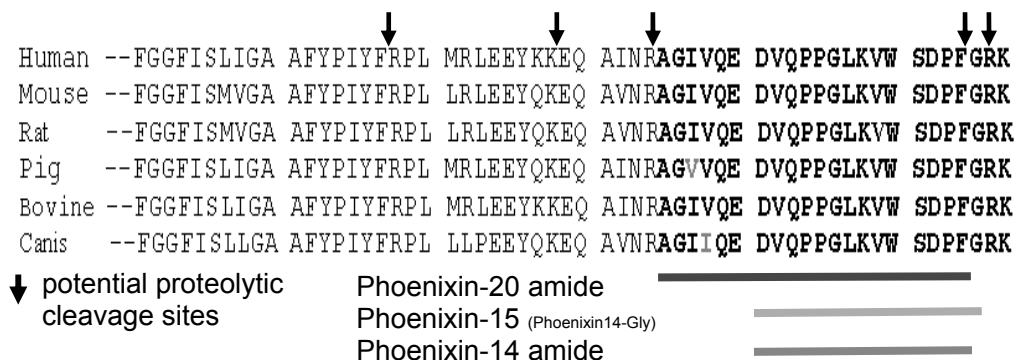
Fig. 1. Based on potential proteolytic cleavage sites, three C-terminal hypothetical peptides were predicted: Phoenixin-20 amide, Phoenixin15 (Phoenixin-14-Gly), and Phoenixin-14 amide.
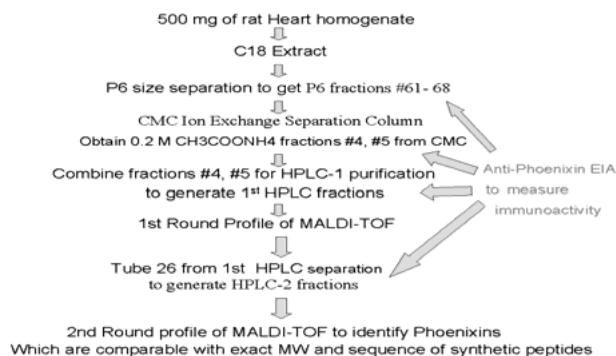
Fig. 2. Flow chart for peptides isolation and identification.

Results and discussion

Using a bioinformatics approach, we selected the high homology regions in the preproprotein and the possible pro-hormone cleavage sites to design several peptides (Figure 1).

After the peptides were synthesized and purified by RP-HPLC, several rabbit polyclonal antisera against the synthetic peptides were generated. Radioimmunoassay (RIA) and Enzyme immunoassay (EIA) were established and the specificity of antibody in the both assays was
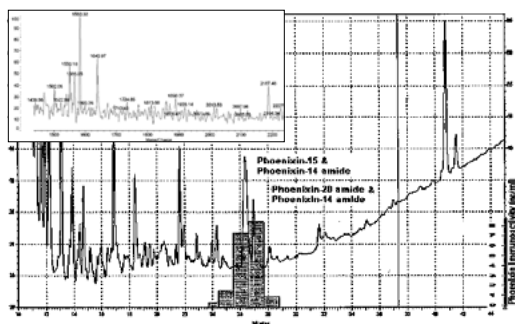
Fig. 3. HPLC profile and immunoreactivity of isolated peptides from the heart homogenate extracts. The eluate at 27 min of the 1st HPLC column has the highest activity of peptides which have been identified as native phoenixins.

verified. With the quantitative measurements of the immunoactivity to different extracts of tissue homogenates, we found rat hypothalamus and heart homogenates contained the highest levels of immunoreactive peptides. Using 500 mg of heart tissue homogenates, we have analyzed the immunoreactivity of HPLC eluents to corresponding to the native phoenixins peptides in the eluents (Figure 2). From the MALDI-TOF analysis of HPLC eluents, we found the eluted fraction at 27 min contains peptide ions at MW 1583, 1641 and 2187 which were corresponding to the theoretical molecular weight of the peptides, Phoenixin-14 amide, Phoenixin-15 and Phoenixin-20 amide. In addition, the synthetic peptides, Phoenixin-14 amide, Phoenixin 15 and Phoenixin-20 amide eluted from the HPLC at 27 min and showed the same peak positions (Figure 3).
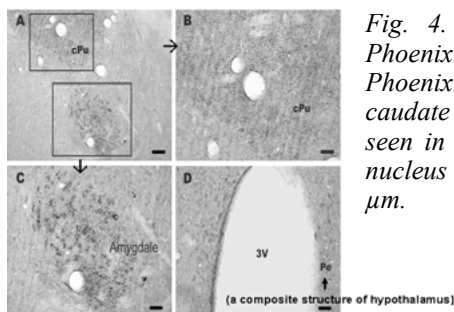
Fig. 4. (A) through (D), the immunoreactivity of native Phoenixin peptides in tissue samples of the rat forebrain. Phoenixin-immunoreactive cell bodies are detected in the caudate putamen (CPu) in (A); fine cell processes can also be seen in the CPu in (B); amaygdala (C), and periventricular nucleus (Pe) in D. Scale bar: (A), 100 µm; (B), (C) and (D), 50 µm.

In the immunohistochemistry analysis, we observed the presence of immunoreactive peptides from the rat forebrain and hypothalamus. In particular, Phoenixin-immunoreactive cell bodies are detected in the periventricular nucleus of the hypothalamus and amygdala (Figure 4). Also, rat pituitary adenoma cells, RC-4B/C cells, were used in the assay of radioligand binding. For the binding displacement, cells were incubated for 30 min with 50 pM ^{125}I-Y0-Phoenixin-20 amide in the absence or presence of increasing concentrations of unlabeled Phoenixin-20 amide or Phoenixin-14 amide. Nonspecific binding was defined as total binding in the presence of 1 µM unlabeled Phoenixin-20 amide or Phoenixin-14 amide. After termination of the binding reaction by washing the cells with 1 ml of cold PBS, cells were solubilized with 0.5 ml of 1% SDS, and radioactivity was detected in a gamma counter. From non-linear curve fitting, the IC50 for Phoenixin-20 amide is 21.5 nM and for Phoenixin-14 amide is 17.9 nM.

In conclusion, we have identified Phoenixin-20 amide, Phoenixin-15, and Phoenixin-14 amide in brain and heart tissue extracts. The amounts of Phoenixin-20 amide and Phoenixin-14 amide are about 150 pg/mg protein both in the rat heart and bovine hypothalamus. Phoenixin-14 amide appears to be able to compete with Phoenixin-20 amide for the binding to pituitary cells.

Acknowledgments

References

1. Strausberg, R.L., et al. *Proc. Natl. Acad. Sci. U.S.A.* **99**(26), 16899-16903 (2002).

Targeted Non-Invasive Optical Imaging Agent for Fluorescence Optical Tomography Studies

Richard S. Agnes[1], Ann-Marie Broome[1,2], and James P. Basilion[1,2,3]

[1]*Department of Radiology;* [2]*Department of Biomedical Engineering;* [3]*National Foundation of Cancer Research, Case Western Reserve University, Cleveland, OH, 44106, U.S.A.*

Introduction

The development of non-invasive optical imaging technologies for the diagnosis and monitoring therapeutic response has garnered tremendous interest. As optical instrumentation continues to advance (e.g. tomographic imaging), imaging molecules that are both selective and sensitive in *in vivo* imaging studies are fast becoming important for cancer research [1]. Molecules labeled with near infrared fluorescence are one such type of imaging agent that can be used to target cell surface receptors that are prevalent in multiple cancer types. The epidermal growth factor receptor (EGFR) is overexpressed in various human cancers, such as tumors found in breast, prostate, bladder, digestive system, pancreas and ovaries. Thus, EGFR is often utilized as a tumor-specific target. A short peptide (YHWYGYTPQNVI) ligand (K_d = ca. 22 nM) for EGFR, discovered through phage display screening, has been used in the development of targeted drug delivery [2]. Using this EGFR peptide ligand, we are developing fluorescently-labeled, tumor-selective agents that can be used for *in vivo* imaging of tumors using fluorescence molecular tomography (FMT) which allows for a three-dimensional rendering of tumor and quantification of injected imaging dose in live animals. These agents could prove to be an invaluable tool for cancer research, particularly when performing longitudinal studies in small animal models.

Results and Discussion

For preparation of the imaging agent (Figure 1), standard Fmoc-based solid phase strategy was employed to synthesize a peptide mini-PEG linker. The EGFR targeting peptide was labeled with Cy5 NHS-ester in solution. The labeled peptide was purified by HPLC and confirmed by mass spectrometry. For the *in vivo* orthotopic brain tumor imaging, athymic nude mice were intracranially injected with various tumor-generating cancer cell lines (i.e. U87G with low levels of EGFR expression or Gli36Δ5 with high levels of EGFR expression). After nine days, the brain tumor-bearing mice were intravenously injected through the tail vein with the fluorescent EGFR-targeting agent and the agent was allowed to circulate for 4 hours. Tumor targeting specificity of the imaging agent was monitored via FMT. The uptake of the agent by the tumor was validated with histological staining to the human intermediate filament vimentin and human EGFR. The instrument used for FMT was FMT2500 (VisEnd Medical, now Perkin Elmer) and Maestro (CRi, now Caliper Life Sciences).
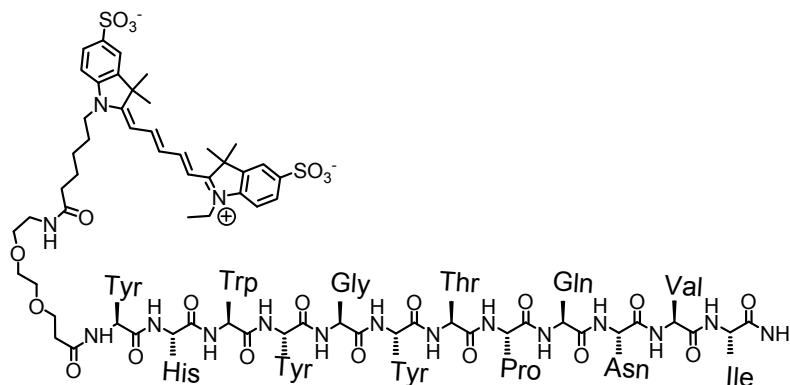
Fig. 1. Representative Cy5-labeled EGF peptide with a monodiscrete PEG linker.

As shown in Figure 2, Cy5-labeled EGF-binding peptides are specifically localized within the brain tumor following an injection. The fluorescence signal identifies the position of the tumor with a high signal to noise ratio (SNR). The signal is validated by the tumor location which can be estimated by the depth of the injection. For example, tumor cells were injected 4 mm from the top of the brain which corresponds to the Z-plane of the tomographic image of the brain tumor. Approximately, 10 pM of the agent accumulates in the tumor. The targeting of the probe was further validated by immunohistochemical staining. In Figure 3, a brain, containing an EGFR-overexpressing tumor, was cryosected, and stained with anti-EGFR antibodies. The image on the left shows the Cy5 signal (EGFR-targeted agent) localized in the tumor mass and the image on the right reveals the cells overexpressing EGFR. Overlay of the two signals demonstrates that the probe specifically accumulates in cells overexpressing EGFR in the tumor.

Fig. 2. Representative 3D-image of ex vivo whole brain highlighting the location of tumor.
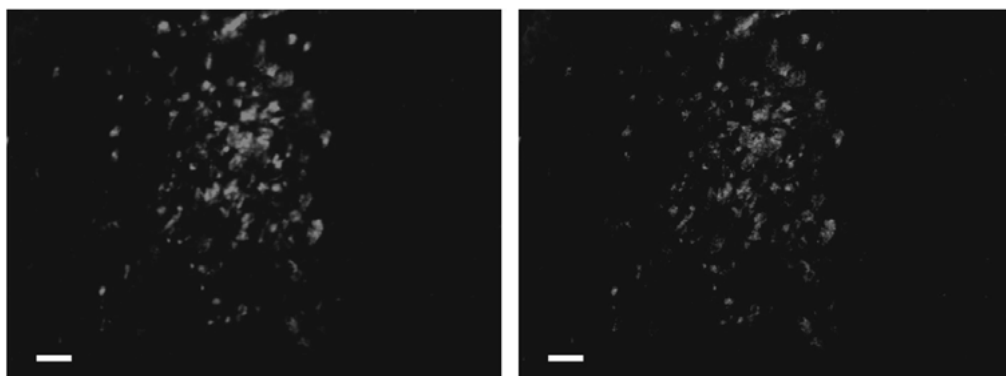
Fig. 3. Co-localization of imaging agent and EGFr in brain tumors. The panel shows the probe (Cy5, right) targeting accumulating in cells overexpressing EGF receptor (anti-EGFr, left). Scale bar = 100 μm.

In conclusion, FMT is a powerful optical imaging tool for cancer research. We have developed a near infrared fluorescence probe using overexpressed EGFR as a biomarker for tumor location. The probe was then used to detect the brain tumor *in vivo* within a relatively short time period. The tumor detection was validated using *ex vivo* and immunohistochemical experiments. With these promising preliminary results, we are currently making analogues of the probe and expanding the utility in cancer and translational studies.

Acknowledgments

References

1. Weissleder, R., Pittet, M.J. *Nature* **452**(7187), 580-589 (2008).
2. Li, Z., Zhao, R., Wu, X., Sun, Y., Yao, M., Li, J., Xu, Y., Gu, J. *FASEB J.* **19**(14), 1978-1985 (2005).

Probing the Effect of Gomesin and Its Analogues on Tumoral Cells via Confocal Microscopy

Marcus V. Buri[1], Edgar J. Paredes-Gamero[1], Elaine G. Rodrigues[2], and Antonio Miranda[1]

[1]Departamento de Biofísica; [2]Unidade de Oncologia Experimental, Universidade Federal de São Paulo, São Paulo, SP, 04044-020, Brazil

Introduction

Gomesin (Gm) is an antimicrobial peptide, isolated from *Ancathoscurria gomesiana* tarantula hemocytes. Its cationic charge provided by some of its amino acids residues (5 Arginines and 1 Lysine) binds strongly with the negative charge of the phospholipid membrane [1]. Gm (pGlu-CRRLCYKQRCVTYCRGR-NH$_2$) has two disulfide bridges (2/15 and 6/11), and adopts a β-hairpin-like structure [2]. In order to evaluate their antitumoral effect we employed Gm and some of its analogues (Table 1). Peptides were synthesized by the solid-phase methodology, purified by HPLC and characterized by LC/ESI-MS and Amino Acid Analysis. Peptides were evaluated by their ability to reduce cell viability (MTT assay) and to penetrate (Confocal microscopy) in B16-F10 and its progeny (8H and 10C) murine melanoma cells.

Results and Discussion

3-(4.5-Dimethylthiazol-2-yl)-2.5-diphenyltetrazolium bromide (MTT) is a yellow tetrazole which can be reduced to purple formazan by living cells mitochondria [3]. Using this colorimetric propriety was possible to analyze the cytotoxicity of Gm and its analogues. Cells were seeded in a 96 well plate using RPMI medium with 10% of Fetal Bovine Serum and Antibiotics. Peptides were added in different concentrations (range from 1.38 to 440 µM) and after a period of 24 hours of incubation, the plate was read in an Elisa Plate Reader in the wavelength of 540 nm. From these experiments we observed that Gm and its analogues caused a significant decrease in the cell viability with their increasing concentration, but with some notable differences, as shown in Figure 1.

Table 1. Sequence of Gm and its analogues

Name	Sequence
Gm	Z-C-R-R-L-C-Y-K-Q-R-C-V-T-Y-C-R-G-R-NH$_2$
[Trp^7]-Gm	Z-C-R-R-L-C-W-K-Q-R-C-V-T-Y-C-R-G-R-NH$_2$
[Rh-Lys^8]-Gm	Rh Z-C-R-R-L-C-Y-K-Q-R-C-V-T-Y-C-R-G-R-NH$_2$
[Ser^{2,6,11,15}]-Gm	Z-S-R-R-L-S-Y-K-Q-R-S-V-T-Y-S-R-G-R-NH$_2$
[Ser^{2,6,11,15}; Rh-Lys^8]-Gm	Rh Z-S-R-R-L-S-Y-K-Q-R-S-V-T-Y-S-R-G-R-NH$_2$
[Thr^{2,6,11,15}, D-Pro^9]-Gm	Z-T-R-R-L-T-Y-K-p-R-T-V-T-Y-T-R-G-R-NH$_2$
[D-Thr^{2,6,11,15}, Pro^9]-D-Gm	z-t-r-r-l-t-y-k-P-r-t-v-t-y-t-r-g-r-NH$_2$

Z = pyroglutamic acid; Rh = rhodamine and small letters correspond to D-amino acids
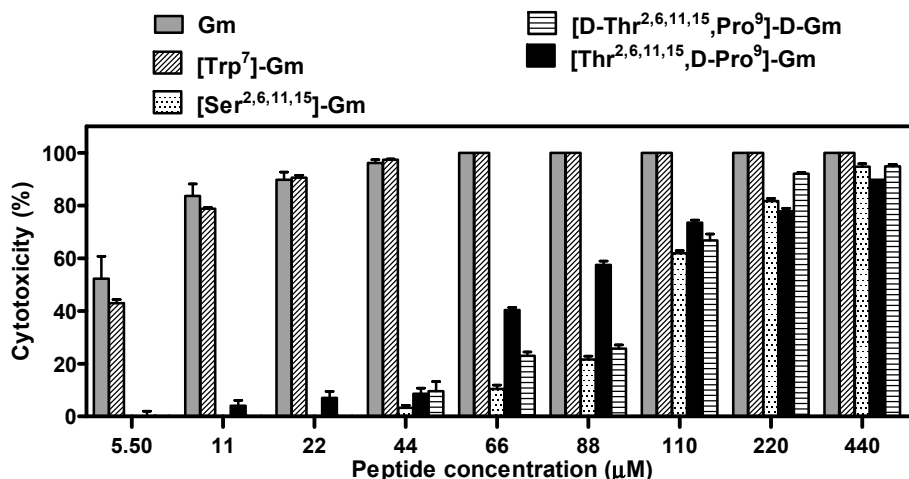
Fig. 1. Comparison in the cytotoxicity of Gm and its analogues.

From this assay was possible to observe that 44 μM of *Gm* and [Trp[7]]-*Gm* were able to decrease around 95% of the cell viability. On the other hand, to achieve the same effect, 440 μM of the other analogues, [Ser^{2,6,11,15}]-Gm, [D-Thr^{2,6,11,15}, Pro^9]-D-Gm and [Thr^{2,6,11,15}, D-Pro^9]-Gm, were needed. The replacement of the Tyr residue by Trp at position *7* does not change the molecule structure, the antimicrobial [4] and the cytotoxicity activities. Although when the disulfide bonds were removed by exchanging the cysteine by serine or threonine residues, the concentration of the corresponding linear analogues had to be increased ten times to reach the Gm cytotoxicity.

With the aim of understanding their different potency, *Gm* and [Ser^{2,6,11,15}]-*Gm* were labeled with rhodamine incorporated in the lysine side chain. Peptides permeation in the B16 tumor cell was observed by confocal microscopy, which allows detecting the peptide position inside the cell (data not shown). The cell penetration behavior of the two peptides was distinctly different. In fact, *Gm* (44 μM) penetrates more intensively and faster than [Ser^{2,6,11,15}]-*Gm* (300 μM) demonstrating that the killing mechanism of the two compounds were completely different. From our results we could conclude that the beta-hairpin conformation is important for the cytotoxicity and in the ability of the gomesin molecule to permeate and destabilize tumor cells.

Acknowledgments

References

1. Moraes, L.G.M., et al. *B.B. Acta - Biomembranes* **1768**, 52-58 (2007).
2. Mandard, N., et al. *Eur. J. Biochem*. **269**, 1190-1198 (2002).
3. Mosmann, T. *J. Immun. Meth.* **65**, 55-63 (1983).
4. Fázio, M.A., et al. *Biopolymers* **88,** 386-400 (2007).

Highly Constrained GLP-1 Analogues as Non-Invasive PET Imaging Agents for the Assessment of Pancreatic Beta-Cell Mass

Jung-Mo Ahn[1],*, Eunice N. Murage[1], Su-Tang Lo[2], Mai Lin[2], and Xiankai Sun[2]

[1]Department of Chemistry, University of Texas at Dallas, Richardson, TX, 75080, U.S.A.; [2]Department of Radiology, University of Texas Southwestern Medical Center, TX, 75390, U.S.A.

Introduction

Non-invasive assessment of functional pancreatic beta-cells has attracted significant attention since it would be a tremendous help for diagnosis and prognosis of diabetes as well as prevention of the diseases and evaluation of effectiveness of therapeutic interventions. However, no reliable methods have been established yet to measure human pancreatic beta-cell mass *in vivo*. Among molecules that interact with the beta-cells, glucagon-like peptide-1 (GLP-1) is found to be highly relevant to beta-cell functions. Secreted from intestinal L-cells upon food intake, it binds to the GLP-1 receptor on the beta-cells and stimulates insulin release [1]. In addition, this incretin promotes beta-cell proliferation and regeneration. Thus, it is a potential candidate for monitoring beta-cell mass.

However, GLP-1 is highly susceptible to proteolytic degradation, especially dipeptidyl peptidase-IV (DPP-IV) and neutral endopeptidase 24.11 (NEP 24.11), and has an extremely short plasma half life *in vivo* [2]. To address this issue, we have designed highly constrained GLP-1 analogues containing two lactam bridges. In prior studies, we and others have demonstrated that a strategically positioned lactam bridge can enhance receptor interaction by stabilizing a binding determinant in the peptide [3,4]. These studies confirmed that GLP-1 have two α-helical segments in the N- and C-terminal regions which are connected with a short non-helical segment when it binds to the receptor, as evidenced by NMR and X-ray studies [5,6].

Results and Discussion

Based on these findings, we have introduced two lactam bridges between Glu^i/Lys^{i+4} to simultaneously stabilize the two α-helical segments in the N- and C-terminal regions [7]. A series of bicyclic GLP-1 analogues were synthesized in solid-phase by using standard Fmoc/tBu peptide chemistry and examined for their receptor interaction by cAMP accumulation assays on HEK293 cells stably expressing human GLP-1 receptors. As shown in Table 1, the resulting bicyclic peptides showed stronger receptor activation compared to the native GLP-1. In particular, two lactam bridges between residues 18-22 and 30-34 in peptide **4** led to 4-fold increase in potency.

In addition to the enhancement of receptor interaction, the lactam bridges also shielded the cyclic peptides from enzyme degradation. Whereas the DPP-IV degradation can be avoided by replacing Ala^8 with other amino acids like D-Ala, the cleavage by NEP 24.11 is difficult to be prevented by the same approach because NEP 24.11 cleaves at multiple sites in the GLP-1 sequence [8]. The two lactam bridges installed in the bicyclic peptide **4** were found to provide outstanding protection against the enzyme, resulting in the half-life of greater than 96 hours when incubated with the enzyme.

The most potent and enzymatically stable bicyclic peptide **4** was modified with an Ahx-Cys spacer at the C-terminus to attach a metal chelator DOTA via conventional maleimide-thiol
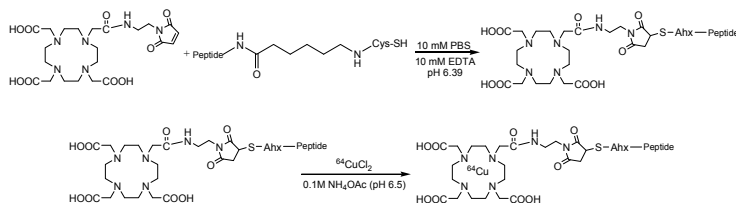
*Fig. 1. Synthesis of a PET imaging agent by using bicyclic GLP-1 analogue **4**.*

Table 1. Receptor activation by bicyclic GLP-1 analogues

	Peptide	Sequence	EC50 (nM)
	GLP-1	HAEGTFTSDVSSYLEGQAAKEFIAWLVKGR	4.7
1	c[E^{16},K^{20}]GLP-1(7-36)- NH$_2$	- - - - - - - - - E - - - K - - - - - - - - - - - - - - - -	4.0
2	c[E^{30},K^{34}]GLP-1(7-36)-NH$_2$	- E - - - K - -	5.8
3	c[E^{16},K^{20}]-c[E^{30},K^{34}] GLP-1 (7-36)- NH$_2$	- - - - - - - - - E - - - K - - - - - - - - - E - - - K - -	3.3
4	c[E^{18},K^{22}]-c[E^{30},K^{34}] GLP-1 (7-36)- NH$_2$	- - - - - - - - - - - E - - - K - - - - - - - E - - K - -	1.2
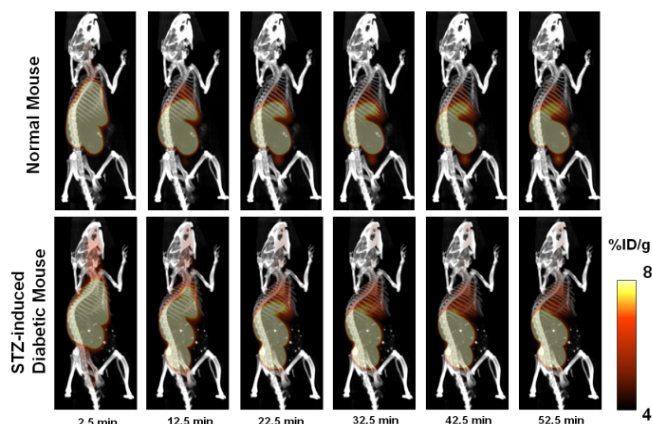
Fig. 2. In vivo dynamic PET scan of normal and STZ-induced diabetic mice by using ^{64}Cu-labeled bicyclic GLP-1 analogue 4.

conjugation chemistry as illustrated in Figure 1. The peptide conjugates were characterized by HPLC and MALDI-MS. After labeling with ^{64}Cu, DOTA-conjugated bicyclic peptide **4** was evaluated in normal healthy and streptozocin (STZ)-induced diabetic mice by dynamic PET scan on a Siemens Inveon PET/CT multimodality system over 60 min after injection.

As shown in Figure 2, the peptide showed rapid and preferential uptake by pancreas despite high renal accumulation. The uptake of the peptide in pancreas was confirmed by the absence of the PET signal in the STZ-induced diabetic mice. *Ex vivo* scans and histology were also carried out to further confirm the PET imaging findings. Taken together, this study demonstrates a high potential of the bicyclic GLP-1 analogue **4** in pancreatic beta-cell imaging through the GLP-1 receptor.

Acknowledgments

References

1. Drucker, D.J. *Endocrinology* **142**, 521-527 (2001).
2. Kreymann, B., et al. *Lancet* **2**, 1300-1304 (1987).
3. Murage, E.N., Schroeder, J.C., Beinborn, M., Ahn, J.-M. *Bioorg. Med. Chem*. **16**, 10106-10112 (2008).
4. Miranda, L.P., et al. *J. Med. Chem*. **51**, 2758-2765 (2008).
5. Thornton, K., Gorenstein, D.G. *Biochemistry* **33**, 3532-3539 (1994).
6. Underwood, C.R., et al. *J. Biol. Chem*. **285**, 723-730 (2010).
7. Murage, E.N., Gao, G., Bisello, A., Ahn, J.-M. *J. Med. Chem*. **33**, 6412-6420 (2010).
8. Hupe-Sodmann, K., et al. *Peptides* **18**, 625-632 (1997).

Rare Earth Endo-Nitrite-Cluster-Fullerenes Functionalized with the BioShuttle Carrier – Candidates for MR-Contrast Agents?

Ruediger Pipkorn[1], Lothar Dunsch[2], Manfred Wiessler[1], Waldemar Waldeck[1], and Klaus Braun[1]

[1]German Cancer Research Center, INF 280, D-69120, Heidelberg, Germany; [2]Leibniz-Institute for Solid State & Materials Research, Helmholtzstr. 20, D-01069, Dresden, Germany

Introduction

Carbon's multi-facetted character is given [1-3]. Other than the diamond and the graphite, the fullerene is considered as the third carbon variant. Its typical structure was named in honor of the architect Buckminster Fuller, whose constructions feature geometrical structures similar to the spatial structure of this carbon variant. The electronic and magnetic properties of these fullerenes are well documented. A further variant, the endofullerenes can trap atoms, cluster or ions like Gd^{3+} inside their inner sphere [4] resulting in a polar molecule by an electron charge transfer [5-10]. Their use as a contrast agent in MRT demands characteristics like water solubility which was realized by functionalizations of the fullerene's surface [11,12]. To use fullerenes as tools for Molecular Imaging (MI) studies, further modifications are mandatory, like the improvement of the passage across biologic membranes, necessary to obtain local concentrations sufficient for imaging of metabolic processes [13]. Here, in a condensed form, the synthesis of a Gd-cluster@-BioShuttle using the DAR_{inv} based click chemistry and the SPPS technology is shown.

Results and Discussion

The synthesis of the Rare Earth endo-nitrite-cluster-fullerene **1** was performed by a modified Kraetschmer-Huffmann DC arc-discharge method with the addition of NH_3 [14]. Their detailed design procedure routes and quality characteristics are documented by the Dunsch group [8,15,16]. The product **5**, ready for DAR_{inv} was obtained by functionalization of **1** (shown schematically in Figure 1).
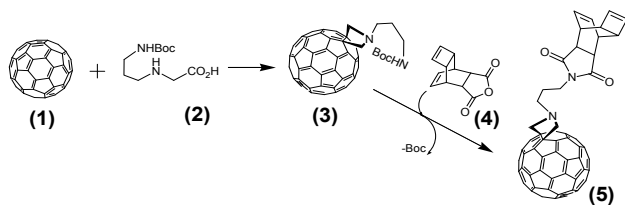
Fig. 1. Schematic representation of the functionalization of the fullerene 1 with the Reppe anhydride 4. The resulting product 5 acts as a dienophile component.

The peptide-based module (CPP) **9**, facilitating the transport across the cell membranes and NLS module **7** consisting of the diene component **6** (the synthesis is documented by Wiessler [17]) were ligated to a peptide sequence. This peptide is a substrate for proteins enabling an active transport of molecules through the nuclear envelope into the cell nucleus. The peptides were prepared by the solid phase peptide synthesis (SPPS) and Fmoc-protection group methodologies as first documented by the Merriefield's [18] and Carpino's [19] groups, modified by Pipkorn [20]. The coupling between the NLS and the CPP module was realized by disulfide bridge formation. The reaction product **10** is shown in (Figure 2).

Fig. 2. Scheme of the synthesis and the disulfide bridge formation to form 10 as a diene reaction partner.
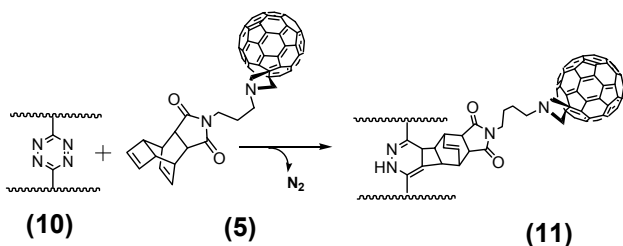
Fig. 3. The DAR$_{inv}$ as the terminal ligation step of 10 and 5 to form the Gd-cluster@-BioShuttle 11 as a final product ready for use in MR imaging studies.

The final step of the Gd-cluster@-BioShuttle synthesis was carried out by DAR$_{inv}$ Click-Chemistry (Figure 3). The physico-chemical properties of this compound can contribute to the development of high field MR contrast agents suitable for MI in the increasingly important scientific and clinical fields of theranostics.

Acknowledgments

References

1. Kraetschmer, W., Thumm, M. Fullerene und Fullerite - neue Formen des Kohlenstoffs /Gyrotrons - Moderne Quellen für Millimeterwellen höchster Leistung, pp. 1-88. Schoeningh Verlag, Paderborn, 1996.
2. Curl, R.F., Smalley, R.E., Kroto, H.W., O'Brien, S., Heath, J.R. *J. Mol. Graph. Model.* **19**, 185-186 (2001).
3. Smalley, R.E. *Rev. Mod. Phys.* **69**, 723-730 (1997).
4. Bartl, A., Dunsch, L., Frohner, J., Kirbach, U. *Chemical Physics Letters* **229**, 115-121 (1994).
5. Mattoussi, H., Rubner, M.F., Zhou, F., Kumar, J., Tripathy, S.K., Chiang, L.Y. *Applied Physics Letters* **77**, 1540-1542 (2000).
6. Funasaka, H., Sakurai, K., Oda, Y., Yamamoto, K., Takahashi,T. *Chemical Physics Letters* **232**, 273-277 (1995).
7. Chen, C.,Lieber, C.M. *Science* **259**, 655-658 (1993).
8. Dunsch, L., Bartl, A., Kirbach, U., Froehner, J. Fullerenes. In: Ruoff, R.S. and Kadish, K.M. (eds). *Recent Advances in Chemistry and Physics of Fullerenes and related Materials*, pp. 182-190. Electrochem. Soc., Pennington N.Y., 1995.
9. Lee, K.W., Lee, C.E. *Phys. Rev. Lett.* **106**, 166402 (2011).
10. Bartl, A., Dunsch, L., Kirbach, U. *Applied Magnetic Resonance* **11**, 301-314 (1996).
11. Anderson, S.A., Lee, K.K., Frank, J.A. *Invest Radiol.* **41**, 332-338 (2006).
12. Chiang, L.Y., Swirczewski, J.W., Hsu, C.S., Chowdhury, S.K., Cameron, S., Creegan, K. *J. Chem. Soc., Chem. Comm.* 1791-1793 (1992).
13. Braun, K., Dunsch, L., Pipkorn, R., Bock, M., Baeuerle, T., Yang, S., Waldeck, W., Wiessler, M. *Int. J. Med. Sci.* **7**, 136-146 (2010).
14. Dunsch, L. Yang, S. *Phys. Chem. Chem. Phys.* **9**, 3067-3081 (2007).
15. Dunsch, L., Georgi, P., Ziegs, F., Zöller, H. Deutsches Patent, Verfahren zur Herstellung endohedraler Fullerene. In: 2002.
16. Krause, M., Dunsch, L. *Angew. Chem. Int. Ed Engl.* **44**, 1557-1560 (2005).
17. Waldeck, W., Wiessler, M., Ehemann, V., Pipkorn, R., Spring, H., Debus, J., Didinger, B., Mueller, G., Langowski, J., Braun, K. *Int. J. Med. Sci.* **5**, 273-284 (2008).
18. Merriefield, R.B., *J. Amer. Chem. Soc.* **85**, 2149-2154 (1963).
19. Carpino, L.A., Han, G.Y. *J. Org. Chem.* **37**, 3404-3409 (1972).
20. Braun, K., Peschke, P., Pipkorn, R., Lampel, S., Wachsmuth, M., Waldeck, W., Friedrich, E., Debus, J. *J. Mol. Biol.* **318**, 237-243 (2002).

A Novel Nitric Oxide Sensor Using Fluorescent Peptides Attached to Iron Complexes

Hiroshi Miyazaki[1], Kenji Usui[1,2], and Satoshi Fujii[1,2]

[1]*Faculty of Frontiers of Innovative Research in Science and Technology (FIRST), Konan University; *[2]*Frontier Institute for Biomolecular Engineering Research (FIBER), Konan University, Kobe, 650-0047, Japan*

Introduction

Iron complexes with dithiocarbamate (Fe-DTC) have been used for trapping agents for endogenous nitric oxide (NO), which is produced by nitric oxide synthases, in conjunction with electron paramagnetic resonance (EPR) spectroscopy [1]. These complexes changed their structure from octahedron to square-pyramid upon NO binding (Figure 1) [2]. Such structural changes upon diatomic molecules binding to metal centers are found in gas sensor proteins like CooA and soluble guanylate cyclase. In the gas sensor proteins, the structural change is a key step to exert their physiological roles [3].

Inspired by the gas sensor proteins, we have been developing novel functional materials mimicking the structural change induced by diatomic molecule binding. Recently, much progress has been made in a research field of artificial proteins under the concepts of template-assisted synthetic proteins (TASPs) [4] and/or metal-directed protein self-assembly (MDPSA) [5]. Under these concepts, a lot of *de novo* proteins have been developed from small peptides and metal ions and helix bundle structure is one of the most successful structures ever made. In this study, taking one step further, we attempt to disrupt the MDPSA structure by a diatomic molecule binding to the metal center. Thus we designed a FRET (Förster Resonance Energy Transfer)-based NO sensor consisting of the Fe-DTC-peptide conjugate that has a fluorescent moiety on C-termini of the peptides. The formation of iron complexes with DTC-peptide conjugate resulted in the formation of three-helix bundle structure. We now report the FRET detection of NO-dependent conformational changes that indicate the collapse of the three-helix bundle structure (Figure 2).
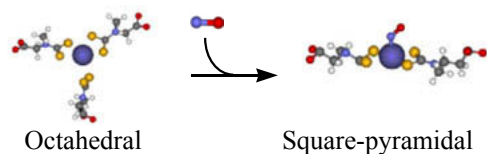
Fig. 1. Conformational change of Fe-DTC complex upon NO binding.

Results and Discussion

A water-soluble, α-helical amphipathic peptide (AEQLLQEAEQLL) was adopted from the literature [6] and slightly modified. At the N-termini of the peptide, sarcosine (Sar) was attached and the addition of carbon disulfide under basic condition resulted in the formation of *N*-dithiocarboxyl group at the new terminal N of sarcosine (Table 1) [2]. At the C-termini of the peptide, two
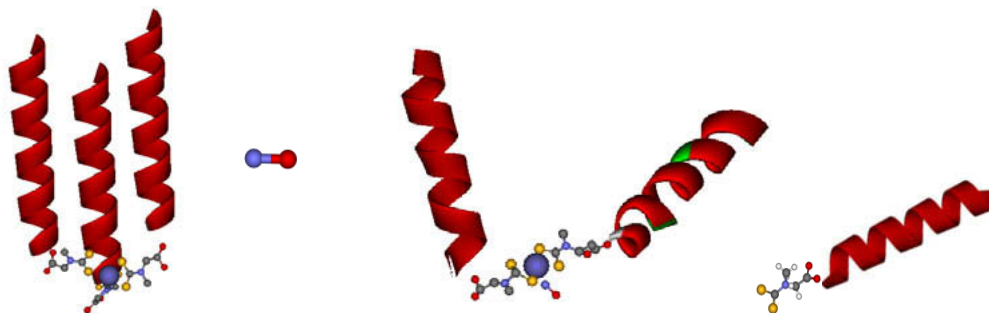
Fig. 2. Schematic illustration of the collapse of three-helix bundle constructed above the Fe-DTC complex upon NO binding.

Table 1. Sequences of fluorescent peptides, S_2C-N-Sar-AEQLLQEAEQLL-$X^a(Z^b)$-NH$_2$

Name	X	Z
p-DTCS	Gln	—
p-F-DTCS	Lys	fluorescein
p-D-DTCS	Lys	DABCYL
p-E-DTCS	Cys	EDANS

[a]*Amino acid;* [b]*Chromophore*

fluorescent probes, fluorescein (5(6)-carboxyfluorescein) and EDANS (5-[(2-aminoethyl)amino]-naphthalene-1-sulfonic acid), and a quencher, DABCYL (4-(4-dimethyl-aminophenyl)diazenyl-benzoic acid) were attached via side chain of Lys, Lys, Cys, respectively (Table 1). The peptides were synthesized by using the standard solid phase Fmoc chemistry, and characterized by HPLC analysis and MALDI-TOF mass spectrometry. The formation of dithiocarboxyl group at the N-termini was checked by UV-vis spectroscopy (characteristic double λ_{max} between 250-300 nm [2]) and MALDI-TOF mass spectrometry.

CD spectra of peptides alone (50 μM) indicated that the peptides were random coil in 20 mM Tris/HCl, 60% EtOH, 20°C at pH 7.2. In the presence of Fe(III) ion, UV-vis spectra showed the typical pattern of Fe(III)-DTC$_3$ complex [2]. The formation of Fe-DTC$_3$ complex changed the CD spectra from typical of random coil to that of α-helix structure. Similar CD spectral changes were reported in the literatures [6,7], suggesting that the formation of the helix bundle structure was accompanied by the metal complex formation. Dynamic light scattering measurements also supported the formation of three-helix bundle structure.

The reaction of Fe(p-DTCS)$_3$ complex with NO was first investigated by EPR spectroscopy. When NOC5 (Dojindo, Japan), a kind of NONOate, was added to the solution, typical three-line EPR signal of NO-Fe-DTC$_2$ complex was observed [1], indicating that NO certainly reacts with Fe(p-DTCS)$_3$ complex to form NO-Fe(p-DTCS)$_2$ complex. Then under the same experimental condition, fluorescent spectra measurements were carried out. Fe(p-E-DTCS)$_3$ and Fe(p-F-DTCS)$_3$ having no FRET pairs showed moderate fluorescent intensity. Reaction of NO with these two complexes resulted in a slight increase of fluorescent intensity. This is probably due to a decrease of self-quenching of the fluorescent probe since the three-helix bundle structure collapses upon NO binding (Figure 2). In contrast, iron complexes with p-E-DTCS/p-D-DTCS and p-E-DTCS/p-F-DTCS showed only a weak fluorescent intensity, indicating that EDANS quenched fluorescence effectively. Reaction of NO with these complexes having FRET pairs showed drastic increase in fluorescent intensity. These results clearly demonstrate that the three-helix bundle structure once formed collapses upon NO binding.

In conclusion, we succeeded in developing a FRET-based NO sensor. Further systematic studies are now under way to improve sensitivity toward NO.

Acknowledgment

References

1. Fujii, S., Yoshimura, T. *Coord. Chem. Rev.* **198**, 89-99 (2000).
2. Fujii, S., Kobayashi, K., Tagawa, S., Yoshimura, T. *J. Chem. Soc. Dalton Trans*. 3310-3315 (2000).
3. Aono, S. *Dalton Trans*. 3137-3146 (2008).
4. Mutter, M. In Marshall, G.R. (Ed.) *Peptides: Chemistry and Biology* (*Proceedings of the 10th American Peptide Symposium*), Eacom, Leiden, 1988, pp.349-353.
5. Salgado, E.N., Radford, R.J., Tezcan, F.A. *Acc. Chem. Res*. **43**, 661-672 (2010).
6. Lieberman, M., Sasaki, T. *J. Am. Chem. Soc*. **113**, 1470-1471 (1991).
7. Ghadiri, M.R., Soares, C., Choi, C. *J. Am. Chem. Soc*. **114**, 825-831 (1992).

Iron Complexes of Peptide Conjugates: Theoretical and Raman Spectroscopic Study

Jaroslav Šebestík, Martin Šafařík, and Petr Bouř

Institute of Organic Chemistry and Biochemistry, Academy of Sciences of the Czech Republic, Flemingovo nam. 2, 16610, Prague, Czech Republic

Introduction

Iron-specific chelators (ISC) are efficient drugs for clinical treatment of a pathological iron overload [1]. They could be used for a cure of neurodegenerative problems such as Alzheimer's and prion diseases [2]. Bi-, tri-, and hexadentate ligands provide a stable octahedral arrangement for iron(III). Bidentate conjugates of peptides with 3-hydroxy-4-pyridinones (3,4-HPs) were used as artificial siderophores [3].

Previously, we have shown that hexadentate conjugate of 2-methyl-3,4-HPs with Kemp's acid and diamine linkers are powerful ISCs [4]. In modeling, geometries obtained from density functional theory (DFT) were different from those obtained from molecular mechanics (MM) simulation. This was attributed to high energetics restrains imposed on iron and its surrounding in MM due to lack of good force field parameters for ferric complexes. The iron complex in MM simulation is more rigid, whereas it is more flexible in DFT. To validate the theoretical predictions of the structure, we compare the calculated and experimental Raman scattering [5].

For a model chelator, a deferiprone, the geometry, complex stability, conformations, and Raman spectra were modeled by DFT. The importance of basis set size, pseudo potential, functional and solvent environment for the computational design of peptide-based ISCs is discussed.

Results and Discussion

Two possible complexes of deferiprone with iron(III) were found (Figure 1) on the basis of DFT methods implemented in Gaussian09 [6]. The complex A was previously identified by X-ray crystallography [7]. In vacuum, the A:B conformer ratio was predicted to be 1:9, whereas the COSMO model of the water solvent gave approximately equal populations of A and B. Supposedly, the crystal packing forces not included in the calculations cause the preference of A form in the crystal.
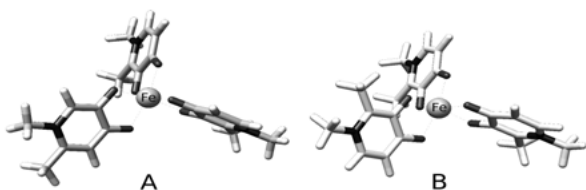
Fig. 1. Two possible isomers of deferiprone ferric complex forming propellers. A symmetrical one (A) and unsymmetrical one (B) with the left blade rotated upside down.

Calculated Raman spectra were compared to experiment. Two most intense peaks were examined (experiment in water: 1511 and 573 cm^{-1}). Computed 573 cm^{-1} band is almost insensitive to the solvent model, basis set, and the pseudo potential on iron. The CAM-B3LYP functional predicted this vibration within 1 cm^{-1} of the experimental position, whereas larger error of 40-90 cm^{-1} was observed for the B97D functional.

Calculated normal mode frequencies involving the conjugated system were less accurate. Among them, the vibration at 1511 cm^{-1} was also very sensitive to the solvent model; the error could be significantly reduced by COSMO. The pseudo potential provided the same results as the full basis set on iron, only with slightly longer computation times. The best frequencies were obtained with the B3LYP functional (ca 13 cm^{-1} error), the worst were again B97D results (deviations of 160-200 cm^{-1}).

An important criterion is also the ratio of intensities (Figure 2b). The B97D spectrum did not resemble the experiment very well, but the other functionals gave realistic intensity ratios of vibrations 2 and 3, about 1:1.

The spectrum in Figure 2b was obtained as a weighted sum of spectra of isomers A and B (Figure 1), using Boltzmann weights based on the cam-B3LYP energies. The cam-B3LYP spectrum was scaled for $\nu > 1218$ cm^{-1} (Figure 2, see the dp point) to enhance the comparison to experiment.

Based on the calculations, the marker peaks were assigned to normal mode vibrations (Figure 2a, peaks 1-3). The vibration 1 at 300 cm^{-1} involves motion of the iron. It is blue shifted for the solvated ferric ion to 327 cm^{-1}. A bending of chelating oxygens contributes to the bend 2 at 573 cm^{-1}. The most intense signal 3 at 1511 cm^{-1} is caused by an aromatic C=C stretching. It is slightly red shifted from the free deferiprone (1516 cm^{-1}).
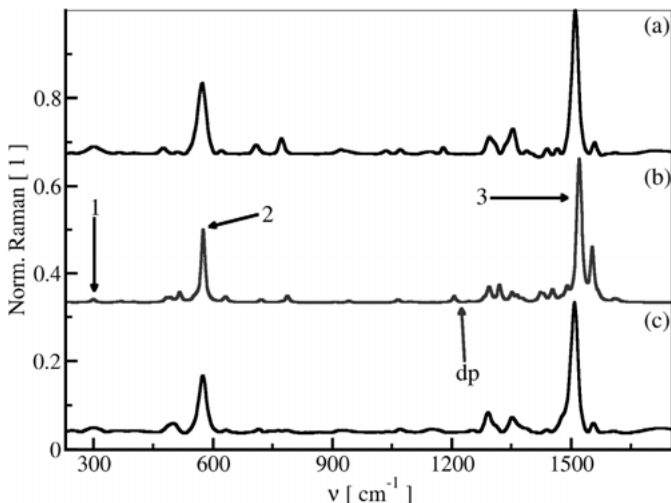
Fig. 2. Raman spectra of ferric complexes: (a) experiment and (b) calculation for deferiprone and (c) experiment for Lys conjugate with 3-hydroxy-4-pyridinone. Numbers 1, 2, and 3, indicate vibrations involving the iron, chelating oxygens, and aromatic carbons, respectively. A "dp" indicates the scaling limit at 1218 cm^{-1}.

The spectra of deferiprone complex differ from the Lys(2-methyl-3-hydroxy-4-pyridinone) one (cf Figure 2a, c). Nevertheless, the three characteristic vibrations are similar. They are localized close to ferric ion binding site in the 3-hydroxy-4-pyridinone ring. The simpler deferiprone is a realistic model of the iron binding in peptide conjugates for the purpose of Raman spectroscopy. In the future, we plan to use these results to parameterize Amber force field and simulate peptide-iron interactions by molecular dynamics.

References

1. Liu, Z.D., Hider, R.C. *Med. Res. Rev.* **22**, 26-64 (2002).
2. Hider, R.C., Ma, Y., Molina-Holgado, F., Gaeta. A., Roy, S. *Biochem. Soc. Trans.* **36**, 1304-1308 (2008).
3. Katoh, A., Hikita, Y., Harata, M., Ohkanada, J., Tsubomura, T., Higuchi, A., Saito, R., Harada, K. *Heterocycles* **55**, 2171-2187 (2001).
4. Grazina, R., Gano, L., Šebestík, J., Santos, M.A. *J. Inorg. Biochem.* **103**, 262-273 (2009).
5. Barron, L.D., Buckingham, A.D. *Chem. Phys. Lett.* **492**, 199-213 (2010).
6. Frisch, M.J., et al. (2009) Gaussian 09, Revision A.1, Gaussian, Inc., Wallingford CT.
7. Charalambous, J., Dodd, A., McPartlin, M., Matondo, S.O.C., Pathirana, N.D., Powell, H.R. *Polyhedron* **7**, 2235-2237 (1988).

Use of Environmentally Sensitive Fluorophores to Assess Peptoid Structures

Amelia A. Fuller[*], Stanley C. Hiew, Frederick J. Seidl, and Marisa A. Plescia
Department of Chemistry & Biochemistry, Santa Clara University, Santa Clara, CA, 95053, U.S.A.

Introduction

Peptoids, oligomers of *N*-substituted glycine (Figure 1), are peptidomimetics that have found broad application owing to the ease of synthesis of diverse, sequence-specific molecules, their biostability properties, and the propensity of certain sequences to recapitulate peptide structural features (e.g., helices) [1-3]. However, the conformational heterogeneity of peptoids has made high resolution

Fig. 1. Peptoid synthesis.

structural studies of these molecules challenging; our understanding of peptoid sequence-structure relationships remains incomplete. There is a need for new, complementary methods to assess peptoid structures. To address this need, we hypothesize that environmentally sensitive fluorophores 4-DMN and 4-DMAP [4] will be efficient probes of secondary structure when installed site-selectively as side chains in an amphiphilic helical peptoid.

Results and Discussion

Peptoid variants based on reported amphiphilic helix template **1** [5,6] that include either 4-DMN or 4-DMAP as side chain moieties were prepared (Figure 2). The fluorophore side chain was substituted for residues 1 or 8 in peptoid **1** (4DMN1, 4DMAP1, 4DMN8, and 4DMAP8) or for residues 1 and 8 of an achiral variant of **1** (a4DMN1, a4DMAP1, a4DMN8, and a4DMAP8). The achiral variants lack *N*-α-chiral side chains and are predicted to be less helical. Lastly, the 4-DMN fluorophore was introduced at position 8 of a "scrambled" variant of **1** which maintains all of the same side chains but eliminates helix amphiphilicity (Figure 2E, sc4DMN8). To install 4-DMN side chains, a 4-DMN-functionalized primary amine was prepared [6] and included in the standard sub-monomer synthesis methods. The 4-DMAP-moiety was introduced by site-selective on-resin derivatization of an orthogonally protected ethylamine peptoid side chain using a procedure analogous to that described by the Imperiali laboratory [7].
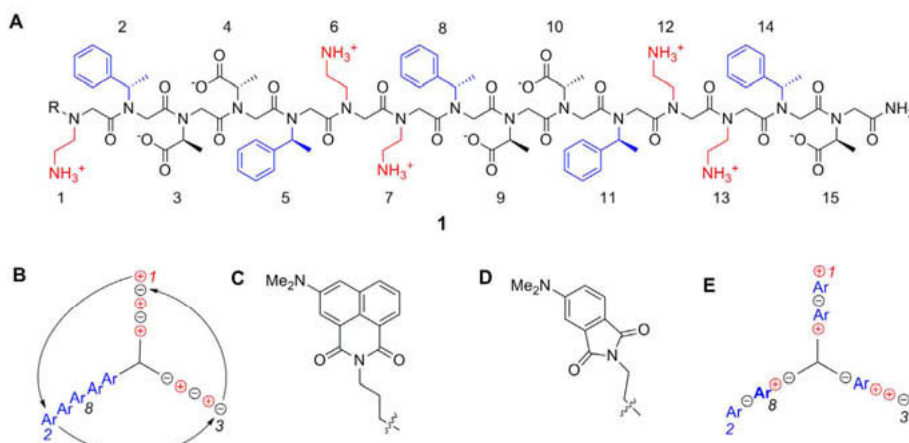
*Fig. 2. Peptoid designs used in these studies. (A) template peptoid **1**; (B) Schematic of the amphiphilic helix of **1** viewing down the helix axis; (C) 4-DMN peptoid side chain; (D) 4-DMAP peptoid side chain; (E) Schematic of the helix adopted by the "scrambled" analog of **1** that lacks amphiphilicity.*
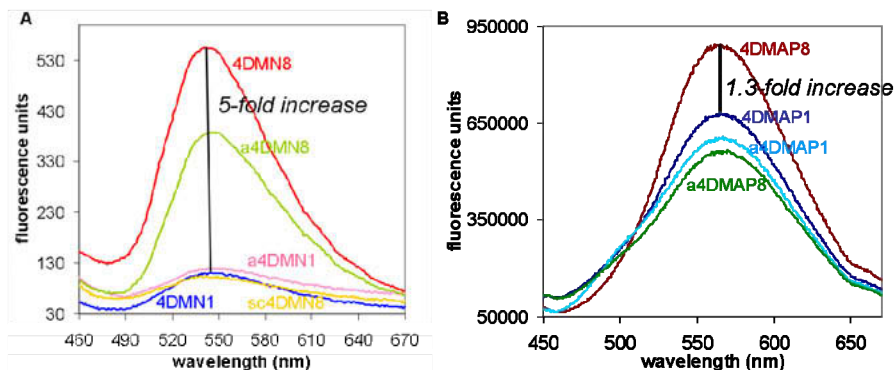
Fig. 3. Fluorescence spectra of peptoids studied (25 μM peptoid in TBS buffer, pH 7.4). (A) 4-DMN-modified peptoids (λ_{ex} = 408 nm); (B) 4-DMAP-modified peptoids (λ_{ex} = 390 nm).

Fluorescence emission spectra of all 4-DMN- and 4-DMAP-modified peptoids were compared (Figure 3). When the *N*-terminal residue of the peptoid contains the dye (4DMN1 or 4DMAP1), fluorescence intensity is low, reflecting the solvent exposed, conformationally mobile local environment of this moiety. In contrast, when the fluorophore is in position 8, it is in the middle of the helix on the aromatic face and emission is higher. This correlates well with the expected increase in hydrophobicity and rigidity of the dye environment for 4DMN8 and 4DMAP8 peptoids relative to 4DMN1 and 4DMAP1. Changes that decrease helicity (achiral peptoids) or amphiphilicity (scrambled peptoids) likewise result in lower fluorescence relative to inclusion of the dyes in position 8. This result correlates well with expected enhanced mobility and reduced hydrophobicity of the dye environment in these peptoids. Overall, 4-DMN is more sensitive than 4-DMAP to local environment changes as a result of secondary structure and is a better probe of peptoid secondary structural features.

Circular dichroism (CD) spectroscopy was used to validate that the dye incorporation did not substantially alter peptoid secondary structure. The CD spectra of all peptoids exhibited minima at approximately 200 nm and 218 nm that are found for **1** and are characteristic of the peptoid helix (peptoids ~30-40 μM in 5 mM Tris with 30% acetonitrile by volume, pH 7.5). Although intensities of the minima at these wavelengths vary moderately between peptoids, the helix likely remains a major contributor to the conformational ensemble of these molecules.

Because the peptoids synthesized are amphiphilic, we wished to confirm that aggregation or other self-association is minimal at the low concentrations at which fluorescence data were collected. Peptoid CD spectra were recorded in 5 mM Tris, pH 7.5 at a range of concentrations up to 172 μM, and CD signal intensity was found to be linear with peptoid concentration. Additionally, peptoids eluted from a Superdex Peptide 10/300 GL size exclusion chromatography column as a single peak, suggesting that they do not readily aggregate (100 μM peptoid injected, eluted with TBS buffer). The retention times of these peaks correlate well with the expected molecular weights of the peptoids when compared to standards. Both of these methods suggest that peptoids do not aggregate.

Acknowledgments

References

1. Zuckermann, R.N., et al. *J. Am. Chem. Soc.* **114**, 10646-10647 (1992).
2. Czyzewski, A.M., Barron, A.E. *AIChE J.* **54**, 2-8 (2008).
3. Yoo, B., Kirshenbaum, K. *Curr. Opin. Chem. Biol.* **12**, 714-721 (2008).
4. Loving, G., Imperiali, B. *J. Am. Chem. Soc.* **130**, 13630-13638 (2008).
5. Lee, B.-C., Chu, T.K., Dill, K.A., Zuckermann, R.N. *J. Am. Chem. Soc.* **130**, 8847-8855 (2008).
6. Fuller, A.A., Seidl, F.J., Bruno, P.A., Plescia, M.A., Palla, K.S. *Peptide Science* (2011), in press.
7. Sainlos, M., Imperiali, B. *Nat. Protocol.* **2**, 3201-3209 (2007).

Synthesis and Application of Fluorescent SDF-1 Derivatives

Ryo Masuda, Shinya Oishi, Noriko Tanahara, Hiroaki Ohno, Akira Hirasawa, Gozoh Tsujimoto, Yoshiaki Yano, Katsumi Matsuzaki, and Nobutaka Fujii

Graduate School of Pharmaceutical Sciences, Kyoto University, Sakyo-ku, Kyoto, 606-8501, Japan

Introduction

Stromal cell derived factor-1 (SDF-1)/CXCL12 belongs to the CXC chemokine family. By interaction with the cognate receptor CXCR4, SDF-1 is implicated in the proliferation and differentiation of B cell progenitors and immune activation of T cells. SDF-1 works as an inhibitory peptide against infection of human immunodeficiency virus type 1 (HIV-1) into T cells, disturbing the interaction of the envelope glycoprotein gp120 with host CXCR4. In addition, CXCR4-overexpressing malignant tumor cells metastasize toward specific organs such as lymph nodes, lung, liver, and bone marrow, which secrete high concentration of SDF-1. Thus CXCR4 is a promising target for anti-HIV and anti-metastatic agents as well as imaging probes to detect malignant tumors.

We recently developed a fluorescent CXCR4 antagonist, TY14015, by structure-activity relation study of polyphemusin II-derived T140 [1]. Using TY14015, CXCR4-positive malignant bladder tumor cells were clearly detected [2]. In contrast, there are few reports regarding SDF-1-based probes to visualize localization and/or internalization process of CXCR4 by induction of agonist signals. Herein, we report the design, synthesis and biological evaluation of fluorescent SDF-1 derivatives.

Results and Discussion

SDF-1 comprises three major structural regions such as N-terminal region, central core region with β-sheet structure, and C-terminal α-helical region. The N-terminal region of SDF-1 plays critical roles in initial binding to and activation of CXCR4. The C-terminal region also contributes to CXCR4 activation. To evaluate structure-activity relationship for fluorescent labeling quantitatively, several SDF-1 derivatives with modification at the N-terminus, Lys^{27} (central region) or Asn^{67} (C-terminal region) were designed [3].

Protected peptide chain for SDF-1 was constructed by Fmoc-based solid-phase synthesis. For fluorescent labeling of SDF-1, the residue at the labeled position was substituted with propargylglycine (Pra). Final deprotection and cleavage from the resin followed by air oxidation provided the expected Pra-substituted SDF-1. Subsequently, fluorochrome-azide was conjugated to SDF-1 by azide-alkyne cycloaddition.

Binding affinity of SDF-1 derivatives to CXCR4 was evaluated as inhibitory potency for [^{125}I]-SDF-1 binding (Table 1). As expected, N-terminal modification of SDF-1 decreased binding affinity to CXCR4. By contrast, modification at the middle and C-terminal residues with AlexaFluor® 488 and tetramethylrhodamine (TAMRA) restored the strong binding affinity.

Next, a labeling system of CXCR4 on cellular membrane was established to trace the internalization process of CXCR4 induced by SDF-1. To distinguish the cellular membrane CXCR4 from that in intracellular compartment, E3-tag/K4-peptide pair was employed [4]. CHO cells stably expressing E3-tagged CXCR4 (E3-CXCR4-CHO) were constructed by transfection of pcDNA5/FRT/TO encoding E3-CXCR4 gene into Flp-In CHO cells by the manufacturer's protocol. Using synthetic TAMRA-labeled K4-peptide (TAMRA-K4), specific staining of CXCR4 receptor on cell membrane was observed by confocal microscopy and flow cytometry analyses. The staining of E3-CXCR4 by TAMRA-K4 in the presence of SDF-1 suggested that SDF-1 binding did not affect the interaction between E3-tag and K4-peptide. SDF-1 binding with E3-CXCR4 was also not disturbed by K4-peptide, as verified by competitive inhibition assay using [^{125}I]-SDF-1.

This system was applied to monitoring the localization process of SDF-1/CXCR4 pair after receptor activation. When SDF-1(67-Alexa488) was appended to TAMRA-K4/E3-CXCR4-CHO cells, both fluorescent signals were merged, indicating that internalized CXCR4 co-existed with SDF-1(67-Alexa488) in the intracellular compartment. Intracellular colocalization

Table 1. Biological activity of SDF-1 analogs for CXCR4

Peptide	Substituted residue	IC_{50} (nM)[a]
SDF-1	-	2.3
SDF-1(N-fluorescein)[b]	-	580
SDF-1(27-TAMRA)	Lys^{27}	8.3
SDF-1(67-Alexa488)	Asn^{67}	5.6
SDF-1(67-TAMRA)	Asn^{67}	1.6

[a]*IC50 values were derived from dose-response curves generated from triplicate data points;* [b] *Fluorescein conjugated at the Lys1 ε-amino group*

of SDF-1(67-TAMRA) with GFP-conjugated CXCR4 was also observed, which is consistent with the result of E3-tag/K4-peptide staining.

The process was also verified using SDF-1(67-Alexa488) and CXCR4-CHO cells without E3 tag. SDF-1(67-Alexa488) was moved into the intracellular compartment. Live cell imaging studies revealed that SDF-1(67-Alexa488) merged with the transferrin fluorescence, suggesting that fluorescent SDF-1 derivatives induced internalization of CXCR4 towards endosome.

In conclusion, we developed fluorescent SDF-1 derivatives with potent binding activity for CXCR4. In addition, a receptor labeling system for cellular membrane CXCR4 was established using coiled-coil tag-probe pairing. The analysis of receptor localization demonstrated that fluorescent SDF-1 derivatives work well as the probes to trace the internalization process of CXCR4, and that CXCR4 was delivered to endosomal compartment when stimulated by SDF-1.

Acknowledgments

References

1. Oishi, S., Masuda, R., Evans, B., Ueda, S., Goto, Y., Ohno, H., Hirasawa, A., Tsujimoto, G., Wang, Z., Peiper, S. C., Naito, T., Kodama, E., Matsuoka, M., Fujii, N. *Chembiochem* **9**, 1154-1158 (2008).
2. Nishizawa, K., Nishiyama, H., Oishi, S., Tanahara, N., Kotani, H., Mikami, Y., Toda, Y., Evans, B. J., Peiper, S. C., Saito, R., Watanabe, J., Fujii, N., Ogawa, O. *Int. J. Cancer* **127**, 1180-1187 (2010).
3. Hatse, S., Princen, K., Liekens, S., Vermeire, K., De Clercq, E., Schols, D. *Cytometry A* **61**, 178-188 (2004).
4. Yano, Y., Yano, A., Oishi, S., Sugimoto, Y., Tsujimoto, G., Fujii, N., Matsuzaki, K. *ACS Chem. Biol.* **3**, 341-345 (2008).

Novel ^{99m}Tc(CO)$_3$-Labeled Cyclic α-MSH Analogs

Maurício Morais, Paula D. Raposinho, Maria Cristina Oliveira, João D.G. Correia, and I. Santos

Unit of Chemical and Radiopharmaceutical Sciences, Instituto Tecnológico e Nuclear,
Estrada Nacional 10, 2686-953, Sacavém, Portugal

Introduction

Improvement in the survival rate of patients with malignant melanoma, which is known by its high metastatic potential and resistance to cytotoxic agents, relies mostly on an early diagnosis and accurate staging of the disease. Since most human and murine melanoma cells overexpress melanocortin type 1 receptor (MC1R), radiolabeled α-melanocyte stimulating hormone (α-MSH) analogs have been explored for melanoma imaging or therapy [1,2]. Among α-MSH analogs, the cyclic peptides display improved metabolic stability and potency, which arise from a less flexible conformation, stable secondary structure, and most likely a better fit into the receptor pocket [2,3]. Aiming to target the MC1R *in vivo*, we are exploring the MC1R targeting properties of new cyclic peptides containing thioether or amine bridges within the main ring [4]. Herein, we report on the synthesis and characterization of those peptides and their labeling with the ^{99m}Tc(CO)$_3$ moiety. *In vitro* studies and biological evaluation in B16F1 melanoma cells are also reported.

Results and Discussion

The macrocyclic peptides c[S-NO$_2$-C$_6$H$_3$-CO-His-D-Phe-Arg-Trp-Cys]-Lys-NH$_2$ (**I**) and c[NH-NO$_2$-C$_6$H$_3$-CO-His-D-Phe-Arg-Trp-Lys]-Lys-NH$_2$ (**II**) were prepared by a three step procedure described by Grieco et al. [4]. The first step comprised the capping of linear chain peptides with 2-fluoro-5-nitrobenzoic acid, after assembling the peptide intermediates to Rink amide resin in a Microwave-assisted Solid Phase Peptide Synthesizer (CEM Liberty) using the Fmoc strategy. Before cyclization through an aromatic nucleophilic substitution, the Trt or Mtt protecting groups of Cys or Lys, respectively, were removed with a diluted TFA solution. Peptide cyclization was done by treating the supported peptides on the resin with potassium carbonate in DMF for 36h at 25ºC. The resulting macrocyclic peptides were cleaved from the resin under standard conditions, precipitated with diethyl ether, purified by semi-preparative RP-HPLC and characterized by ESI-MS. The final peptide conjugates c[S-NO$_2$-C$_6$H$_3$-CO-His-D-Phe-Arg-Trp-
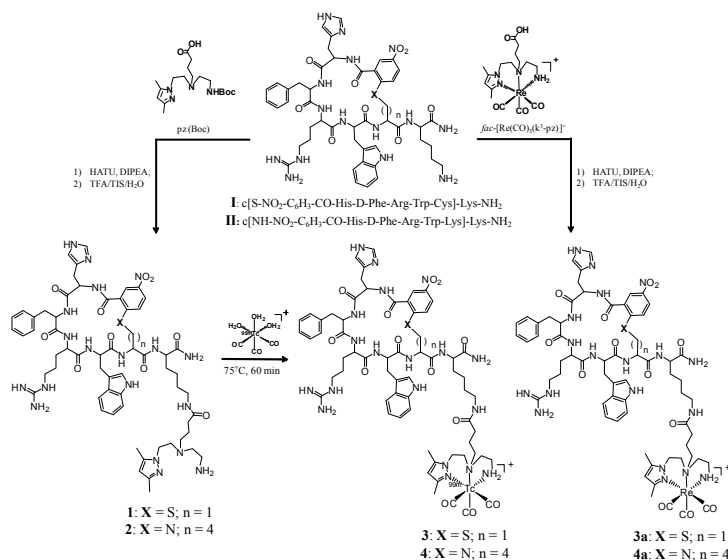
Scheme 1. Synthesis of cyclic peptide derivatives.

Table 1. Analytical data for cyclic peptide derivatives

Compounds	formula	calculated mass [ion]	mass found	t_R (purity)
1	$C_{61}H_{81}N_{19}O_{10}S$	1272.5 $[M+H]^+$	1272.5	10.2 min (98%)
2	$C_{64}H_{88}N_{20}O_{10}$	1297.7 $[M+H]^+$	1297.7	10.4 min (98%)

Cys]-Lys(Pz)-NH$_2$ (**1**) and c[NH-NO$_2$-C$_6$H$_3$-CO-His-D-Phe-Arg-Trp-Lys]-Lys(Pz)-NH$_2$ (**2**) were synthesized by conjugation of the Boc-protected pyrazolyl-diamine (pz) ligand to the respective peptides **I** and **II** through the free ε-amino group of the Lys in solution using standard coupling conditions (HATU/DIPEA in DMF) (Scheme 1). After full deprotection, **1** and **2** were purified by semi-preparative RP-HPLC and characterized by ESI-MS (Table 1).

The radioactive complex **3** and **4** were prepared in high yield and radiochemical purity (98%) by direct reaction of **1** and **2** with $[^{99m}Tc(CO)_3(H_2O)_3]^+$ (Scheme 1). The hydrophilic radiocomplexes (**3**: log P$_{o/w}$= - 0.34 ± 0.03; **4**: log P$_{o/w}$= - 0.80 ± 0.05) were characterized/identified by comparing their RP-HPLC chromatograms with the ones obtained for **3a** and **4a** (Scheme 1), synthesized as surrogates (Figure 1).

In vitro studies have shown that **3** and **4** are stable in human serum (6h, 37°C). Internalization studies for both radioactive compounds in B16F1 murine melanoma cells revealed that over 10% of the total activity was internalized after 2h, at 37°C.
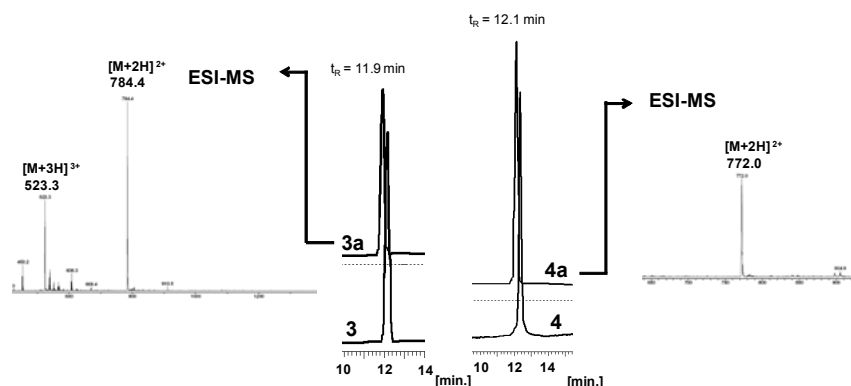
Fig. 1. RP-HPLC chromatographic profiles for 3 and 4 (γ - detection) and respective cold surrogates 3a and 4a (UV-vis detection).

In conclusion, we have synthesized and characterized two novel metallated cyclic α-MSH analogs containing thioether or amine bridges within the main ring. Preliminary studies have shown that both radioactive complexes are enzymatically stable and presented high cellular uptake in MC1R-expressing murine melanoma. Further studies are underway to evaluate the *in vivo* MC1R targeting properties of **3** and **4**.

Acknowledgments

References

1. Miao, Y., Quinn, T. *Crit. Rev. Oncol/Hematol.* **67**, 213 (2008).
2. Raposinho, P.D., Correia, J.D.G., Cristina, M.C., Santos, I. *Biopolymers: Peptides Science* (2010).
3. Raposinho, P.D., Xavier, C., Correia, J.D.G., Falcão, S., Gomes, P., Santos, I. *J. Biol. Inorg. Chem.* **13**, 449, (2008).
4. Grieco, P., Cai, M., Mayorov, A., Chandler, K., Trivedi, D., Lin, G., Campiglia, C., Novellino, E., Hruby, V. *J. Bioorg. J. Med. Chem.* **51**, 2701-2707 (2008).

Synthesis and Characterization of Tetra-Amine Chelator Conjugated Peptide for Melanoma Imaging

F. Gallazzi[1], X. Zhang[2], and T.P. Quinn[2]

[1]*Research Cores and* [2]*Department of Biochemistry, University of Missouri, Columbia, MO, 65211, U.S.A.*

Introduction

Radiolabeled cyclic CCMSH peptides have shown great promise for melanoma diagnostic imaging [1]. Direct radiolabeling approaches of peptides and proteins with [99mTc] often result in poor synthetic yields and multiple labeled species. An alternative approach employs a bifunctional chelator, which utilizes a radiometal chelator tethered to the targeting molecule.

The chelator contains the radiometal coordination atoms in the optimal geometry for efficient and stable radiometal incorporation. Recently, the synthesis and application of a new tetraamine chelator (N4) was reported [2]. The N4 chelator was shown to be effective in radiolabeling gastrin-releasing peptide with [99mTc]. However, the solution synthesis of the N4 tertaamine chelator was laborious. In this report an efficient solid-phase synthetic scheme for the N4 chelator is reported. The N4 chelator was conjugated to a cyclic peptide Re-CCMSH that targets the melanocortin 1 receptor (MC1-R) up regulated on melanoma tumor cells. N4 chelator and peptide synthesis as well as the bioactivity and radiolabeling efficiency of the N4 chelator conjugated ReCCMSH peptide was examined *in vitro*.

Results and Discussion

Three consecutive reactions with commercially available reagents were employed to rapidly prepare the protected 'N4' bifunctional chelate on 2-ClTrt Chloride resin (Figure 1). First, 3-bromo-2-(bromomethyl) propionic acid was first loaded on the resin after deprotonation with diisopropylethylamine. Nucleophilic substitution of the bromine atoms with the free amino group of ethylene diamine in presence of diisopropylethylamine yield the unprotected tetraamine ligand. The reaction was performed with a very large excess of ethylene diamine, in order to minimize the competitive formation of cyclic mono ethylene diamine substituted derivate. Finally, the reaction of the unprotected primary and secondary amino groups with BOC anhydride yielded the final BOC protected ligand. The protected chelator was cleaved
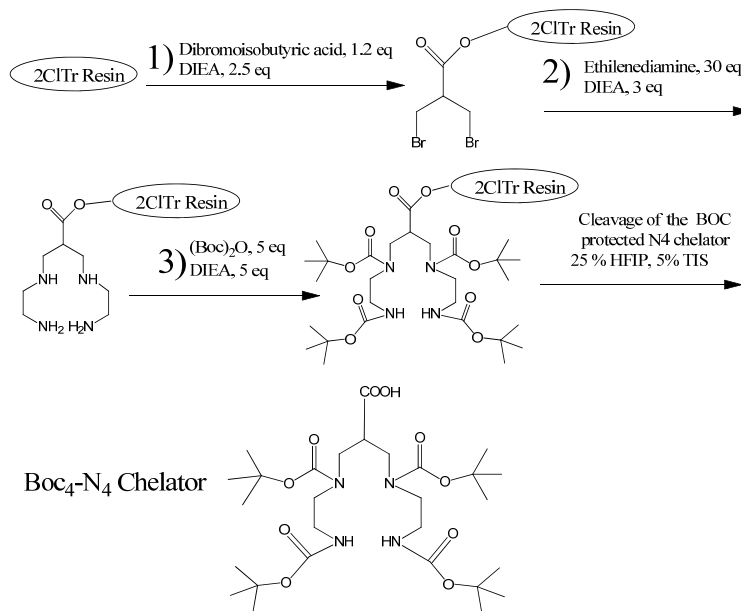
Fig. 1. Solid Phase Synthesis of the 'N4' chelator.
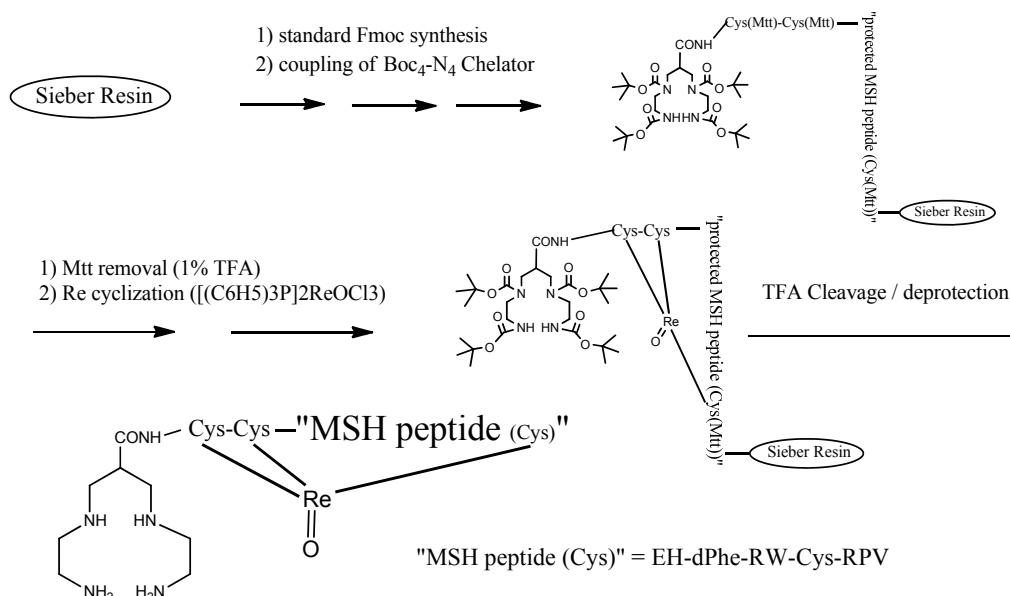
Fig. 2. Synthesis of N4-Re-CCMSH.

from the resin with 25% hexafluoroisopropanol and characterized by liquid chromatography–mass spectrometry (LC-MS).

CCMSH peptide was prepared separately in solid phase by standard Fmoc strategy and the Boc-protected chelator was added without intermediate purification as terminal step of the solid phase elongation process. Mmt orthogonal protecting groups were removed from the cysteine thiols of N4-CCMSH by 1% TFA and the peptide conjugate was cyclized via site-specific coordination of rhenium while attached to the resin by reaction with $[(C_6H_5)_3P]_2ReOCl_3$. The final crude N4 chelator conjugated cyclic peptide product (Figure 2) was deprotected and cleaved from the resin, in a single reaction with TFA and scavengers, purified by preparative high performance liquid chromatography (HPLC) and finally characterized by LC-MS.

The final purified target molecule N4-Re-CCMSH' was radiolabeled with ^{99m}Tc with an efficiency of >90%, yielding a single radiolabeled species. ^{99m}TcO$_2$-N4-Re-CCMSH was stable over a 4 hr period in mouse serum as determined by HPLC analyses. Cell binding studies demonstrated that the N4-Re-CCMSH molecule had high specificity and low nanomolar affinity for the MC1-R expressed on B16-F1 cells. *In vivo*, biodistribution and SPECT imaging studies in melanoma bearing mice showed good tumor uptake and favorable whole body clearance properties making ^{99m}TcO$_2$-N4-Re-CCMSH a potential candidate for melanoma imaging.

References

1. Miao, Y, Quinn, T.P. *Front Biosci.* **12**, 4514-4524 (2007).
2. Abiraj, K., Mansi, R., Tamma, M.L., Forrer, F., Cescato, R., Reubi, J.C., Akyel, K.G., Maecke, H.R. *Chemistry* **16**, 2115-2124 (2010).

Synthesis and Characterization of DOTA-Coupled Dimeric Y1 Receptors Antagonists for Breast Cancer Targeting

David Chatenet[1], Renzo Cescato[2], Beatrice Waser[2], Judit Erchegyi[1], Jean Rivier[1], and Jean Claude Reubi[2]

[1]The Clayton Foundation Laboratories for Peptide Biology, The Salk Institute for Biological Studies, 10010 N. Torrey Pines Rd., La Jolla, CA, U.S.A.; [2]Division of Cell Biology and Experimental Cancer Research, Institute of Pathology, University of Berne, Berne, Switzerland

Introduction

Peptide hormone receptors play an increasing role in cancer medicine. This role is based primarily on the peptide receptor over-expression on tumor cells which allows a specific receptor-targeted scintigraphic tumor imaging and tumor therapy with radiolabeled peptide analogs [1]. The last decade has seen the development of numerous novel somatostatin agonists suitable for tumor targeting [2,3]. Interestingly, it was recently shown that potent somatostatin receptor antagonists, known to poorly internalize into tumor cells, can visualize tumors *in vivo* as well, or even better than the corresponding agonists [4]. Prompted by the success of somatostatin receptor targeting, the over-expression of other peptide receptor families was evaluated in tumors *in vivo* [1]. Promising new candidates for such an *in vivo* peptide receptor targeting of tumors are neuropeptide Y (NPY) receptors, based on their high expression in specific cancers, in particular breast carcinomas [5]. The aim of the present study was to design and develop dimeric DOTA-coupled NPY analogs (Figure 1) suitable for radiolabeling that could be used for imaging and for radiotherapy of Y_1-expressing tumors.

Results and Discussion

The DOTA-free and DOTA-coupled analogs listed in Table 1 were analyzed in receptor autoradiography experiments for NPY Y_1 and Y_2 receptor binding affinities using SK-N-MC cells endogenously expressing Y_1 and SH-SY5Y cells endogenously expressing Y_2, respectively. The IC_{50} values for all tested compounds are listed in Table 1.

Ile^{28}-**Xa^{29}**-Pro^{30}-Cys^{31}-**Xc^{32}**-Arg^{33}-**Xd^{34}**-Arg^{35}-Tyr^{36}-amide

Ile$^{28'}$-**Xa$^{29'}$**-Pro$^{30'}$-Cys$^{31'}$-**Xc$^{32'}$**-Arg$^{33'}$-**Xd$^{34'}$**-Arg$^{35'}$-Tyr$^{36'}$-amide

Fig. 1. General structure of the dimeric NPY analogs.

The addition of two DOTA moieties at the N-terminus (analogs 2 and 4) or at position 29 (analogs 6 and 10) of the homodimeric analogs decreases the Y_1 binding affinity up to 2-30 fold. However, the addition of only one DOTA to the heterodimeric scaffold dimer (7) did markedly improve the binding affinity, from 1 µM for 6 to 29 nM for 8. Finally, increasing the distance between the chelator and the peptide backbone, *i.e.* analog 11, enhanced the binding affinity (IC_{50} = 13 ± 3 nM; Table 1) of this asymmetric peptide dimer for the Y_1 receptor. None of the tested compounds showed Y_2 binding affinity.
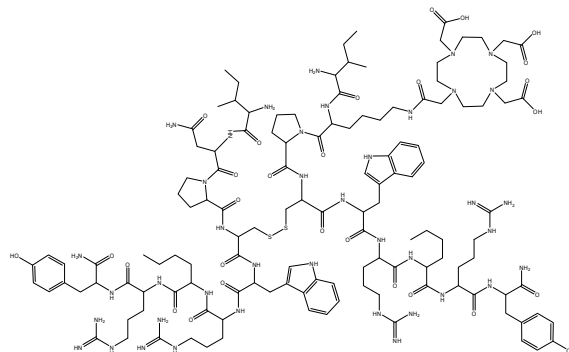
Fig. 2. Structure of the most promising DOTA-conjugated NPY dimeric antagonist.

Table 1. Binding affinities at NPY Y_1 and Y_2 receptors and Y_1-related functional characteristics for NPY analogs

	Amino acid residues				*N-term DOTA*	*Binding affinity*[a]		*Functional assay cAMP for Y_1*
	Xa^{29}	*$Xa^{29'}$*	*Xc*	*Xd*		*Y_1*	*Y_2*	
DOTA-Free Analogs								
1	Asn	Asn	Tyr	Leu	No	11 ± 7	>1000	Antagonist
3	Asn	Asn	Trp	Nle	No	9.0 ± 3	>1000	Antagonist
5	Dpr	Dpr	Trp	Nle	No	143 ± 20	>1000	ND
7	Dpr	Asn	Trp	Nle	No	19 ± 5	>1000	Antagonist
9	Lys	Lys	Trp	Nle	No	127 ± 50	>1000	Antagonist
DOTA-Coupled Analogs								
2	Asn	Asn	Tyr	Leu	Yes	143 ± 37	>1000	Antagonist
4	Asn	Asn	Trp	Nle	Yes	294 ± 33	>1000	Antagonist
6	Dpr(DOTA)	Dpr(DOTA)	Trp	Nle	No	>1000	>1000	ND
8	Dpr(DOTA)	Asn	Trp	Nle	No	29 ± 7	>1000	Antagonist
10	Lys(DOTA)	Lys(DOTA)	Trp	Nle	No	283 ± 52	>1000	Antagonist
11	Lys (DOTA)	Asn	Trp	Nle	No	13 ± 3	>1000	Antagonist

[a]*IC_{50} values in nM; mean $\pm$ SEM; n $\geq$3. ND = not determined*

Since the addition of a DOTA moiety can change the functional characteristics of a compound as recently shown in the somatostatin receptor field for sst_3 [6], compounds having a high or moderate Y_1 affinity were analyzed in an adenylate cyclase activity assay for their agonistic or antagonistic properties. All tested compounds, DOTA-free and DOTA-coupled, behaved like full antagonists (Table 1). Given alone at a high concentration of 20 µM, they were not able to inhibit forskolin-stimulated cAMP accumulation but efficiently antagonized the agonistic effect of 100 nM [Leu[31], Pro[34]]-hPYY. Moreover, analog **11** (20 µM), the best compound of this series, given together with an increasing concentration of [Leu[31], Pro[34]]-hPYY in the range from 10 nM up to 20 µM is able to shift by at least 3 orders of magnitude the dose response curve of [Leu[31], Pro[34]]-hPYY to the right, indicating that **11** efficiently antagonizes the agonist effect of [Leu[31], Pro[34]]-hPYY. Thus, this dimeric DOTA-conjugated compound, *i.e.* analog **11**, with its high binding affinity for Y_1 over Y_2 and its antagonist property represents a potential candidate for *in vivo* tumor targeting.

References

1. Reubi, J.C. *Endocr. Rev.* **24**, 389-427 (2003).
2. Ginj, M., et al. *Clin. Cancer Res.* **14**, 2019-2027 (2008).
3. Wild, D., et al. *Eur. J. Nucl. Med. Mol. Imaging* **30**, 1338-1347 (2003).
4. Ginj, M., et al. *Proc. Natl. Acad. Sci. U.S.A.* **103**, 16436-16441 (2006).
5. Korner, M., Reubi, J.C. *Peptides* **28**, 419-425 (2007).
6. Reubi, J.C., et al. *Eur. J. Nucl. Med. Mol. Imaging.* **37**, 1551-1558 (2010).

^{99m}Tc(I)-Labeled Homobivalent α-MSH Analogs for Melanoma Detection

João D. G. Correia, Maurício Morais, Paula D. Raposinho, Maria Cristina Oliveira, and I. Santos

Unit of Chemical and Radiopharmaceutical Sciences, Instituto Tecnológico e Nuclear,
Estrada Nacional 10, 2686-953, Sacavém, Portugal

Introduction

Unless primary melanoma is detected early enough to be surgically removed, the disease prognosis is poor due to the ineffective treatments available to fight a tumor with high metastasizing potential. Therefore, the design of melanoma-specific radiopharmaceuticals for Single Photon Emission Computed Tomography (SPECT), Positron Emission Tomography (PET) or internal radiotherapy is a field of great interest and intense research [1,2]. Several radiolabelled α-melanocyte stimulating hormone (α-MSH) analogs have been proposed for probing melanocortin type 1 receptor (MC1R), which is considered a specific molecular target for melanoma detection, being overexpressed in most murine and human melanoma cells [3,4]. Aimed at targeting MC1R *in vivo*, and based on the affinity enhancement expected when using a multivalent approach, we report on the synthesis and characterization of novel homobivalent NAPamide (Ac-Nle-Asp-His-*D*Phe-Arg-Trp-Gly-Lys) conjugates based on pyrazolyl-diamine containing chelators. We will also describe their (radio)metallation with the organometallic fragment *fac*-[M(CO)$_3$]$^+$ (M = ^{99m}Tc, Re) and the preliminary biological evaluation of the radiometallated peptides.

Results and Discussion

The fully protected α-MSH analog NAPamide was synthesized by Fmoc-based Solid Phase Peptide Synthesis on a CEM Liberty automated peptide synthesizer, using the methyltrityl (Mtt) protecting group for Lys^{11} side chain and a Sieber Amide resin. The partially protected α-MSH analog **Pp-NAPamide** was obtained after selective removal of the Mtt group and resin cleavage under mild acidic conditions (Scheme 1).
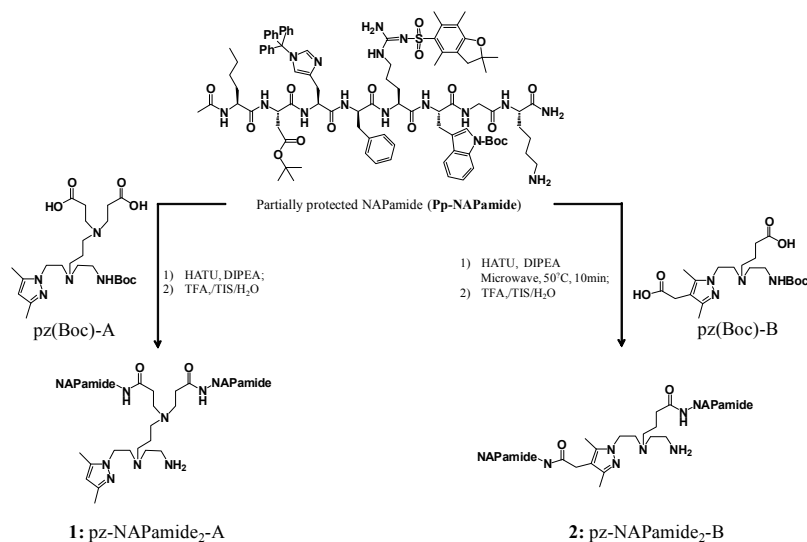
*Scheme 1. Synthesis of the homobivalent NAPamide derivatives **1** and **2**.*

Table 1. Analytical data for NAPamide homodimeric derivatives

Compounds	formula	calculated mass [ion]	mass found (ESI-MS)	t_R (purity)
1	$C_{122}H_{177}N_{37}O_{24}$	849.5 $[M+3H]^{3+}$	849.5	15.3 min. (98%)
2	$C_{119}H_{170}N_{36}O_{24}$	1244.6 $[M+2H]^{2+}$	1244.6	15 min. (98%)
3a	$C_{68}H_{96}N_{20}O_{15}Re$	810.8 $[M+2H]^{2+}$	810.4	15.9 min. (98%)
4a	$C_{125}H_{177}N_{37}O_{27}Re$	705.0 $[M+3H]^{3+}$	705.0	15.4 min. (98%)

Pp-NAPamide was conjugated to the pyrazolyl-diamine based chelators pz(Boc)-A and pz(Boc)-B through the free ε-amino group of Lys[11] in solution, yielding the homobivalent conjugates **1** and **2** after full deprotection (Scheme 1). **1** and **2** were purified by semi-preparative RP-HPLC and characterized by ESI-MS (Table 1).

The hydrophilic radiopeptides **3** (log $P_{o/w}$= - 1.34 ± 0.04) and **4** (log $P_{o/w}$= - 1.82 ± 0.02) were prepared in high yield and radiochemical purity (98%) by direct reaction of the precursor $[^{99m}Tc(CO)_3(H_2O)_3]^+$ with **1** and **2**, respectively (Scheme 2). Both radioactive compounds were identified by comparing their RP-HPLC chromatograms with the ones obtained for **3a** and **4a** (Scheme 2), synthesized as surrogates and characterized by ESI-MS (Table 1).
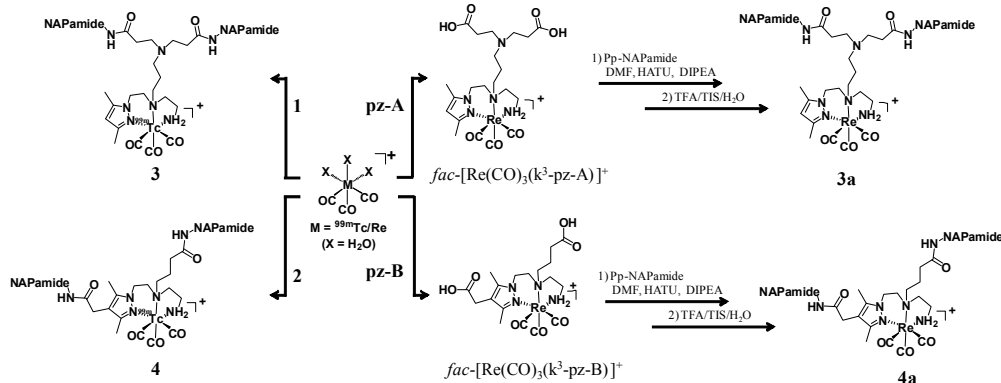
Scheme 2. Synthesis of (radio)metallated homobivalent NAPamide derivatives.

In vitro studies have shown that **3** and **4** are stable in concentrated solutions of amino acids (e.g. cysteine and histidine) and in human serum (6h, 37°C). Internalization studies for both radiopeptides in B16F1 murine melanoma cells have shown that over 45% of the cell-associated activity was internalized after 4 h, at 37°C.

In conclusion, we have synthesized and characterized novel *fac*-$[M(CO)_3]^+$ (M = Re/^{99m}Tc) complexes bearing homobivalent NAPamide conjugates (**3**/**3a** and **4**/**4a**). Preliminary biological studies have shown that **3** and **4** are enzymatically stable and presented high cellular uptake in MC1R-expressing murine melanoma cells. The biological evaluation of both radioactive compounds in tumour-bearing mice is currently underway

Acknowledgments

References

1. Miao, Y., Quinn, T. *Crit. Rev. Oncol/Hematol.* **67**, 213-228 (2008).
2. Raposinho, P.D., Correia, J.D.G., Cristina, M.C., Santos, I. *Biopolymers: Peptide Science* (2010).
3. Vagner, J., Handl, H.L., Gillies, R.J., Hruby, V. *J. Bioorg. Med. Chem. Lett.* **14**, 211-215 (2004).
4. Raposinho, P.D., Correia, J.D.G., Alves, S., Botelho, M.F., Santos, A.C., Santos, I. *Nucl. Med. Biol.* **35**, 91-99 (2008).

Design, Synthesis and Study of New Multimeric Ligands - Application as Vectors for Cancer Diagnosis and Therapy

Nabila Brabez[1,2], Liping Xu[3], Robert J. Gillies[3], Ronald M. Lynch[4], Gerard Chassaing[1], Solange Lavielle[1], and Victor J. Hruby[2]

[1]University Pierre et Marie Curie, Laboratoire des Biomolecules, UMR 7203 UPMC-CNRS-ENS, Paris, 75005, France; [3]Lee Moffitt Cancer Center, Tampa, FL, 33612, U.S.A.; [4]University of Arizona, Department of Physiology, Tucson, AZ, 85721, U.S.A.; [2]University of Arizona, Department of Chemistry and Biochemistry, Tucson, AZ, 85721, U.S.A.

Introduction

Cancer cells can be differentiated from normal cells by their over-expressed or mutated proteins. Our research strategy consists of using multimers [1], comprised of multiple ligands attached to the same template, to selectively bind to cancer cells thanks to a cooperative effect [2]. Here we describe new dendrimer-based multimeric ligands, which have been synthesized using a tetravalent scaffold leading to multimers that could possess up to three ligands and a tag.

Results and Discussion

Multimeric constructs were assembled using the Boc strategy on MBHA resin. Our scaffold

Fig. 1. Scaffold.

(Figure 1) is first synthesized in solution following a procedure described by Chassaing *et al*. [3], which was optimized for our application (up to 40% yield in 10 steps). Using standard solid-supported synthesis, the scaffold is first coupled to the resin followed by synthesis of the desired peptide spacer to the linker arms. The azide moiety is then added by coupling of azido acetic acid to the resin to afford the base of the template ready to receive the peptide by click reaction.

The other moiety to be prepared for click chemistry is the peptide containing the triple bond. MSH(4) ligand is modified on its N-terminus, where modifications don't affect its properties, by acylation using pentynoic acid or with an additional lysine bearing pentynoic acid on its side chain. To obtain a high yield for the click chemistry it was necessary to use protected peptides, which were synthesized on a Sieber amide resin following a standard Fmoc strategy.

The click reaction between the protected peptide bearing a triple bond and the template containing the azide moiety is done using a 5 fold excess per arm of copper iodide and ascorbic acid as well a 7 fold excess per arm of DIEA in a DMF/ 2,6-lutidine mixture [4]. After completion of the cycloaddition, the construct is cleaved from the resin using HF to afford the desired multivalent construct (Figure 2), which is purified by HPLC and characterized by ESI-MS or Maldi-TOF. Binding of the multimeric ligands is evaluated by competitive binding assay using time resolved fluorescence on HEK293 cells overexpressing hMC4R.

Peptide = MSH(4) : H-f-R-W-CONH$_2$
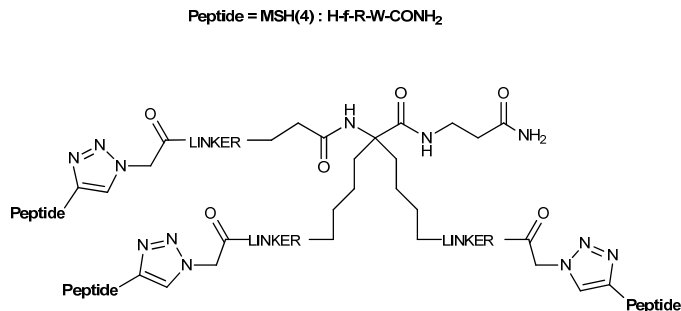
Fig. 2. Homomultivalent ligand of melanocortin receptor(hMC4R).

Table 1. Valency effect on potency

Compound	IC50 (nM)	Relative potency to A
Monovalent on scaffold A	4900 ± 760	-
Bivalent on scaffold	310 ± 73	16
Trivalent	14 ± 1.5	350

The linker length was investigated using either a semi-rigid glycine-proline sequence [5], a flexible β-Ala or no linker. We found that in our case using no linker or a flexible linker led to better results with a 7 to 350 fold increase compared to Ac-MSH(4) (Table 1).

From the optimal construct, which turned out to be the one with the shortest length between peptides (about 25Å), the effect of valency on the scaffold was tested and showed a fold increase for bivalent of 16 and for trivalent of 350 times better than the monovalent version (Table 1), which proves the efficacy and strong avidity of the trivalent construct. These constructs and their unique properties are being utilized to develop sensitive diagnostic and therapeutic agents for targeting cancer.

Acknowledgments

References

1. Whitesides, G.M., et al. *Angew. Chem.* **37**, 2754-2796 (1998).
2. Hruby, V.J., Gillies, R.J., et al. *Expert Opin. Ther. Targets* **8**(6), 565-586 (2004).
3. Chassaing, G., et al. *Tetrahedron Letters* **47**, 3723-3726 (2006).
4. Zhang, Z., et al. *Tetrahedron Letters* **47**, 665-669 (2006).
5. Vagner, J., Hruby, V.J., et al. *Angew. Chem. Int. Ed.* **47**, 1685-1688 (2008).

Spectroscopic Studies of Conformational Properties of Bradykinin and its TOAC-Labeled Derivatives in Solution and in the Presence of Model Membranes

Nélida Marín[1], Renata F.F. Vieira[2], Clóvis R. Nakaie[2], and Shirley Schreier[1]

[1]*Department of Biochemistry, Institute of Chemistry, University of São Paulo, São Paulo, SP, C.P. 26077, 05513-970, Brazil;* [2]*Department of Biophysics, Federal University of São Paulo, São Paulo, SP, 04023-062, Brazil*

Introduction

The peptide hormone bradykinin (RPPGFSPFR, BK) is a very potent vasodilator [1]. Making use of spectroscopic techniques, we have investigated the conformational properties of BK and its TOAC-containing derivatives (TOAC[0]-BK and TOAC[3]-BK) in solution and in the presence of model membranes - micelles of 1-palmitoyl-2-hydroxy-phosphatidylcholine (LPC) and 1:1 mol:mol LPC:1-palmitoyl-2-hydroxy-phosphatidylglycerol (LPG), and large unilamellar vesicles (LUV) of 1-palmitoyl-2-oleoyl phosphatidylcholine (POPC) and 1:1 mol:mol POPC:1-palmitoyl-2-oleoyl phosphatidylglycerol (POPG).

The paramagnetic amino acid TOAC (2,2,6,6–tetramethylpiperidine-1-oxyl-4-amino-4-carboxylic acid) was initially incorporated by Nakaie, et al. [2,3] at the N-terminus of another peptide hormone, angiotensin II (AII) through a peptide bond, making use of the Boc (tert-butyloxycarbonyl) methodology [4,5]. Following the introduction of the Fmoc (9-fluorenylmethyloxycarbonyl) methodology [6,7], the Boc/Fmoc combined strategy allowed the insertion of TOAC at any position of the peptide backbone [8].

Results and Discussion

In solution, BK and TOAC[0]-BK displayed similar CD spectra, characteristic of a flexible structure resulting from the equilibria between different conformations (Figure 1). In the case of TOAC[3]-BK, TOAC imposes a bend different from that caused by native P[3]. Binding to the model membranes favored the acquisition of secondary structure. In the presence of zwitterionic LPC micelles conformational changes were observed only for the internally-labeled peptide (not shown). All three peptides bound to 1:1 LPC:LPG anionic micelles. The conformation acquired by TOAC[3]-BK was different from those achieved by BK and TOAC[0]-BK (Figure 1). Changes in the CD spectra of the peptides were observed in the presence of 1:1 POPC:POPG LUV at pHs 4.0 and

Fig. 1. CD spectra of peptides (100 μM) in solution: BK (■), TOAC[0]-BK (▲), and TOAC[3]-BK (●), and in the presence of 40 mM of LPC:LPG micelles: BK (□), TOAC[0]-BK (△), and TOAC[3]-BK (○). pH 4.0.

7.0, except for TOAC[0]-BK at pH 7.0. No significant conformational changes were observed at pH 10.0 or in the presence of POPC LUV at all three pHs.

EPR spectra of the labeled peptides in solution gave rise to narrow lines (Figure 2), indicating fast tumbling in the time scale of the experiment; TOAC[0]-BK displayed a greater freedom of motion than TOAC[3]-BK, as indicated by the calculated values of rotational correlation times, τ_C (Table 1).

Table 1. Rotational correlation time of peptides (40 μM) in solution

	τ_C (x 10^{-10} s)	
	TOAC^0-BK	TOAC^3-BK
pH 4.0	1.94	4.73
pH 7.0	1.37	4.54
pH 10.0	1.40	4.76

Line broadening occurred as a result of peptide binding to model membranes (Figure 2). As expected, the motion was more restricted for the internally-labeled peptide. Partition Coefficients (P) were calculated from EPR data according to ref. 9 (Table 2).

Although the intrinsic fluorescence of peptides is low, data could be obtained for the binding of the peptides to micelles, but not to vesicles, due to light scattering.

In conclusion, the results showed that the peptides bound to a much lesser extent to zwitterionic than to negatively charged model membranes. The more pronounced binding at lower pH (when the peptides carry higher positive charge) points to the role of electrostatic interactions for peptide-membrane interaction. The conformations in the presence of model membranes could be related to the bioactive conformation adopted by the peptides upon binding to the receptor, according to the Membrane Compartment Theory [10].
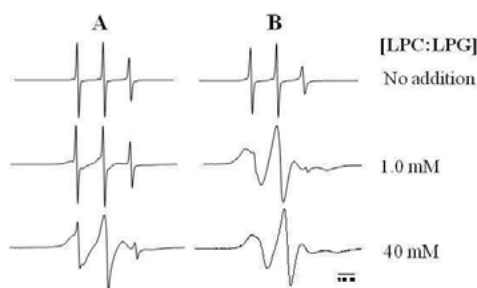
Fig. 2. EPR spectra of (A) TOAC^0-BK and (B) TOAC^3-BK (40 μM) in the presence of increasing concentrations of LPC:LPG micelles, pH 4.0.

Table 2. Partition coefficients of the peptides in model membranes

	P (x 10^3)	
	TOAC^0-BK	TOAC^3-BK
LPC:LPG, pH 4.0	5.0	41
LPC:LPG, pH 7.0	n.b.	19
LPC:LPG, pH 10.0	n.b.	1.6
POPC:POPG, pH 4.0	1.2	4.6

n.b.: no binding

Acknowledgments

References

1. Golias, Ch., Charalabopoulos, A., Stagikas, D., Charalabopoulos, K., Batistatou, A. *Hippokratia* **11**, 124-128 (2007).
2. Nakaie, C.R., Goissis, G., Schreier, S., Paiva, A.C.M. *Braz. J. Med. Biol. Res.* **14**, 173-180 (1981).
3. Nakaie, C.R., Schreier, S., Paiva, A.C.M. *Biochim. Biophys. Acta* **742**, 63-71 (1983).
4. Barany, G., Merrifield, R.B. *The Peptides* Vol. 2. Academic Press, New York, 1980.
5. Stewart, J.M., Young, J.D. *Solid Phase Peptide Synthesis* Pierce Chemical Co., Rockford, 1984.
6. Atherton, E., Sheppard, R.C. *Solid Phase Peptide Synthesis: A Practical Approach* I.L.R. Press, Oxford, 1989.
7. Fields, G.B., Noble, R.L. *Int. J. Peptide Protein Res.* **35**, 161-214 (1990).
8. Marchetto, R., Schreier, S., Nakaie, C.R *J. Am. Chem. Soc.* **115**, 11042-11043 (1993).
9. Bianconi, M.L., Schreier, S. *J. Phys. Chem.* **95**, 2483-2486 (1991).
10. Schwyzer, R. *Biopolymers* **37**, 5-16 (1995).

Structural Characterization of a Three Transmembrane Domain Fragment of a GPCR in Membrane Mimetic Environments

Katrina E. Caroccia[1,2], Martin Poms[3], Racha Estephan[1], Leah S. Cohen[1], Boris Arshava[1], Oliver Zerbe[3], Jeffrey M. Becker[4], and Fred Naider[1,2]

[1]*Department of Chemistry, The College of Staten Island, City University of New York (CUNY), Staten Island, NY, 10314, U.S.A.;* [2]*Department of Biochemistry, The Graduate Center, CUNY, New York, NY, 10016, U.S.A.;* [3]*Institute of Organic Chemistry, University of Zurich, Zurich, Switzerland;* [4]*Department of Microbiology, University of Tennessee, Knoxville, TN, 37996, U.S.A.*

Introduction

G protein-coupled receptors (GPCRs) are a class of proteins, involved in cellular signaling cascades, which are composed of seven transmembrane (TM) domains connected by intra- and extracellular loops (IL and EL, respectively). Structural information regarding these proteins is extremely valuable, but characterization of these proteins is difficult due to their hydrophobicity, flexibility and large size. Smaller fragments of GPCRs are useful for studying membrane protein folding and NMR structural analysis.

Our group has been focusing on NMR analysis of fragments of the yeast α-factor receptor, Ste2p. We have published an NMR structure for a fragment containing the first two TMs of the receptor in LPPG micelles [1] and have submitted a paper describing the structure in trifluoroethanol:water (TFE:water). We are currently working on the NMR characterization of a 3TM fragment containing 130 residues of Ste2p, G31-R161, including 19 residues from the N-terminal domain, the first TM through the third TM with connecting loops and five residues of the second IL. Complete backbone assignments for this fragment have been made in both TFE:water [2] and lysopalmitoylphosphatidylglycerol:dodecylphosphatidylcholine (LPPG: DPC) micelles. Three-dimensional heteronuclear NMR experiments performed on [^{15}N,^{13}C,^{2}H(^{1}H(methyl)-ILV)]-labeled TM1-TM3 in TFE:water allowed for the assignment of the methyl groups of isoleucine, leucine, and valine residues. Potential interhelical connections were identified using a NOESY experiment performed on [^{15}N,^{13}C,^{2}H(^{1}H(methyl)-ILV)]-peptide. Additional constraints are currently being obtained for structure calculation.

Results and Discussion

The TM1-TM3 peptide has been expressed with a number of isotopic labeling patterns. We have previously reported complete backbone assignment of the fragment using [^{15}N, ^{13}C, ^{2}H]-TM1-TM3 (50% ^{2}H incorporation) for HNCA, HNCO, HN(CA)CO, HNCACB, and TOCSY experiments in TFE:water [2]. Backbone assignments have also been completed in detergent micelles. To date, 128 of 131 and 125 of 131 assignments have been completed in TFE:water and LPPG:DPC micelles, respectively.

Secondary structural analysis has been completed using backbone chemical shifts in both membrane mimetics [2]. The Cα shifts are consistent with the presence of three transmembrane helices with additional helicity in the N-terminal tail and the first extracellular loop. This additional helicity is believed to be biologically relevant since the N-terminal helix was previously observed in the TM1-TM2 structure [1] and biochemical data suggests that the beginning of EL1 contains a 3_{10} helix and a short β-sheet [3]. Hydrogen-deuterium exchange experiments performed in TFE:water also support the presence of three TM helices, with additional helicity in the loop regions.

Expression of [^{15}N,^{13}C,^{2}H(^{1}H(methyl)-ILV)]-labeled TM1-TM3 was conducted in order to identify tertiary contacts between the methyl groups of I, L, V residues [4]. This was accomplished using 2-keto-3 methyl-d,3-d$_1$-1,2,3,4-^{13}C butyrate as the metabolic precursor for V and L and 2-keto-3-d$_2$-1,2,3,4-^{13}C butyrate as the metabolic precursors for I. (HM)CM(CGCBCA)NH, (HM)CM(CBCA)NH an [^{13}C]-HSQC experiments performed on this peptide allowed for the assignment of the 43 I, L, V methyl groups present in this peptide. Two potential long-range connections between L66 and I83 and V57 and I91 were identified in a NOESY experiment. In order to probe for interhelical contacts using paramagnetic relaxation

enhancements (PRE) we have constructed and expressed analogs of TM1-TM3 with strategically placed cysteine residues. The thiol groups of these Cys residues in EL1 were coupled with a spin label. The release of spin-labeled TM1-TM3 from the fusion protein is currently being optimized. The positioning of the spin-labels in the first EL should allow us to determine whether TM1 and TM3 associate with TM2. PRE experiments using [^{15}N]-TM1-TM3 peptide containing the nitroxide spin label are currently being performed in order to identify additional tertiary contacts for structure determination.

Acknowledgments

References

1. Neumoin, A., Cohen, L.S., Arshava, B., Tantry, S., Becker, J.M., Zerbe, O., Naider, F. *Biophys. J.* **96**, 3187-3196 (2009).
2. Caroccia, K.E., Estephan, R., Cohen, L.S., Arshava, B., Hauser, M., Zerbe, O., Becker, J.M., Naider, F. *Peptide Science* 2011 DOI: 10.1002/bip.21614.
3. Hauser, M., Kauffman, S., Lee, B.K., Naider, F., Becker, J. M. *J. Biol. Chem.* **282**, 10387-10397 (2007).
4. Tugarinov, V., Kay, L.E. *J. Am. Chem. Soc.* **125**, 13868 (2003).

Studies on Large Fragments of a G Protein-Coupled Receptor in Membrane Mimetic Media

L.S.Cohen[1,2], A. Neumoin[3], B. Arshava[1], K. Caroccia[1,2], Z. Potetinova[1], M. Hauser[4], J.M. Becker[4], O. Zerbe[3], and F. Naider[1,2]

[1]*Department of Chemistry, The College of Staten Island, City University of New York (CUNY), Staten Island, NY, 10314, U.S.A.;* [2]*Department of Biochemistry, The Graduate Center, CUNY, New York, NY, 10016, U.S.A.;* [3]*Institute of Organic Chemistry, University of Zurich, Switzerland,* [4]*Department of Microbiology, University of Tennessee, Knoxville, TN, 37996, U.S.A.*

Introduction

Advances in structure determination methodology in the last 50 years resulted in an exponential increase in the number of structures in the Protein Data Bank [1]. Advances are being made with membrane proteins as well [2,3], although structural studies by both X-ray crystallography and nuclear magnetic resonance (NMR) are hampered by the size and membrane environment of integral membrane proteins (IMPs). The inherent flexibility required for signaling by G protein-coupled receptors (GPCRs) make these membrane protein structures among the more difficult to ascertain. In the last five years, systems that introduce stabilizing mutations into this class of proteins have increased the number of crystal structures for class A GPCRs to seven [4-10] out of 800 coded by the human genome. Though these structures represent important steps in the field of protein structure, more information is needed on non-class A GPCRs that bind peptide hormones that control many physiological processes.

Our lab has been focusing on determining the structure of the GPCR Ste2p, the *Saccharomyces cerevisiae* alpha-mating factor receptor, one fragment at a time. Support for this approach comes from the fact that co-expressed fragments in eukaryotic cells can find each other to form reconstituted, functional receptors. Furthermore, fragments of GPCRs have been shown to fold into correct secondary structure in membrane mimetic media. However, it remains to be proven that the tertiary fold of a fragment is the same as the corresponding segment in the context of the full receptor. The use of segmentally labeled receptor in which one portion is NMR visible and the remaining protein is NMR invisible is expected to provide a convenient tool to address this important aspect of working with fragments.

Results and Discussion

Spontaneous reconstitution in SDS micelles. Solubilization of fragments in micellar environments could lead to the spontaneous formation of heterodimer products that could be used in NMR analysis. Other products of this *in vitro* mixing reaction include homodimers of each fragment and/or heterodimers of incorrect orientation. In order to check the hypothesis that these fragments could correctly reconstitute in the micelle environment, fragments of Ste2p that encompassed the first two transmembrane (TM) domains, Ste2p(G31-T110), and the last five TM domains, Ste2p(I120-L340) were each expressed and purified in bacterial expression cells [11, Potetinova, unpublished]. Detailed polyacrylamide gel electrophoresis and MALDI analysis in SDS micelles indicated that the efficiency of the spontaneous assembly of these fragments into a reconstituted receptor was low [Potetinova, unpublished].

Guided reconstitution of Ste2p. Protocols that will be useful for the efficient reconstitution of GPCRs must direct the formation of heterodimers as the dominant species and must ensure that dimerization correctly orients the fragments of the heterodimer that is formed. Disulfide bond formation would result in the correct orientation of the TM domains, but, unguided it may increase the yield of homodimeric byproducts. To favor the predominance of heterodimer, we added oppositely charged residues near the Cys residues on each fragment and have used Ellman's reagent to activate the Cys residue of one fragment. We tried this method with test peptides, corresponding to residues K100 to N132, that mimic the first extracellular loop 1 (EL1) of Ste2p, with a cross-link point between I120C and S121C. The N-terminal peptide (NT-EL1) included residues 100-120 (NH_3^+-K^{100}YLLSNYSSVTYALTGFPQFC^{120}-GMGDDD-COO$^-$) and the C-terminal peptide (CT-EL1) included residues 121-132 (NH_3^+-KKKMGC^{121}RGDVHVYGATN^{132}-COO$^-$) with an engineered crosslink point at I120C and

S121C. The Cys residue in the NT-EL1 peptide was activated with Ellman's reagent, purified and mixed with a slight molar excess of the CT-EL1 peptide. The reaction in 6M Guanidium HCl buffer at pH 8.5 resulted in NT-CT heterodimer formation with very little homodimer (Figure 1). The resulting peptide was cleaved with CNBr to remove the charged tails generating the desired disulfide linked peptide as judged by ESI-MS. These results demonstrate the feasibility of guided reconstitution to generate predominantly heterodimer that could be further manipulated.

Discussion and Future Goals. We have developed an efficient method to assemble an NT-CT heterodimer of a GPCR using a guided reconstitution method. A Ste2p construct containing Cys residues at I120 and S121 has been shown to be biologically active using gene induction and growth arrest assays. Fragments of Ste2p linked by disulfide formation between Cys120 and Cys121 are expected, therefore to exhibit biological function. Our protocol will be applied to fragments of Ste2p containing the first two and last five TM domains. The resulting heterodimer will be segmentally labeled and used in high-resolution NMR analyses to investigate whether the structure previously determined for TM1-TM2 in micelles is consistent with the structure of the same segment in the context of the full reconstituted receptor.

Fig. 1. Top - HPLC chromatogram of NT-EL1 peptide. Middle –Activation of NT-EL1 peptide. Bottom - Results of dimerization reaction after 4 hours.

Acknowledgments

References

1. Berman, H.M., et al. *Nucleic Acids Research* **28**, 235-242 (2000).
2. White, S. (Stephen White Laboratory, 2011).
3. Topiol, S., Sabio, M. *Biochem. Pharmacol.* **78**, 11-20, (2009).
4. Cherezov, V., et al. *Science* **318**, 1258-1265 (2007).
5. Park, J.H., et al. *Nature* 454, 183-187 (2008).
6. Jaakola, V.P., et al. *Science* **322**, 1211-1217 (2008).
7. Warne, T., et al. *Nature* **454**, 486-491 (2008).
8. Wang, T., Duan, Y. *Infect. Disord. Drug Targets* **9**, 279-288 (2009).
9. Wu, B., et al. *Science* **330**, 1066-1071, (2010).
10. Chien, E.Y., et al. *Science* **330**, 1091-1095, (2010).
11. Cohen, L.S., et al. *Biopolymers* **90**, 117-130 (2008).

Tat-Mediated Delivery and Visualization of Antiparasitic Drugs into *Leishmania*

B.G. de la Torre[1], J.R. Luque[2], V. Hornillos[3], A.U. Acuña[3], F. Amat-Guerri[4], L. Rivas[2], and D. Andreu[1]

[1]*Department of Experimental and Health Sciences, Pompeu Fabra University, Dr Aiguader 88, 08003, Barcelona, Spain;* [2]*Centro de Investigaciones Biológicas-CSIC, Ramiro de Maeztu 9, 28040, Madrid, Spain;* [3]*Instituto Química Física Rocasolano-CSIC, Serrano 119, 28006, Madrid, Spain;* [4]*Instituto Química Orgánica General-CSIC, Juan de la Cierva 3, 28006, Madrid, Spain*

Introduction

Among parasitic diseases, leishmaniasis ranks only second to malaria in clinical and social impact. The repertoire of leishmanicidal drugs is brief and further hampered by poor uptake into parasites. This opens opportunities for cell-penetrating peptides, as ideal vectors for delivering drugs otherwise impassable through the plasma membrane. Using miltefosine (MT, hexadecylphosphocholine) as a model leishmanicidal, we have studied its Tat-mediated delivery to *Leishmania*, including as proof-of-concept the reversion into susceptible of MT-resistant *L. donovani* R40 strain.

Results and Discussion
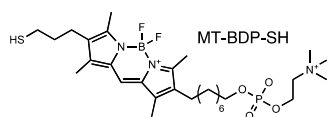
Fig. 1. Thiol-functionalized miltefosine analog.

A fluorescent MT analog (Figure 1) with a Bodipy (BDP) moiety well separated from the essential phosphocholine polar head-group and a short three-carbon spacer between the BDP moiety and the thiol group, to facilitate disulfide bonding, was prepared based on previous experience [1,2]. In parallel, a Tat(48-60) sequence was assembled with its N-terminus extended by an Fmoc-Lys(Mmt) residue (Figure 2). The orthogonality of the protecting groups allowed the introduction of a Quasar 670 fluorophore at the α-amino, and of a Boc-Cys (Npys) at the ε-amino side chain. Deprotection, cleavage and RP-HPLC purification led to a Quasar 670-Tat-Cys(Npys) intermediate (Figure 2) that chemoselectively reacted with MT-BDP-SH to give the desired Quasar 670-Tat-SS-MT-BDP heterodisulfide conjugate, with double emission at 538 and 670 nm (BDP and Quasar, respectively).

The uptake and antiparasitic efficacy of the conjugate were tested by incubating it with promastigotes of *L. donovani* R40, a strain resistant to MT due to a mutation of the LdMT3 aminophospholipid translocase that impairs uptake of the drug. The Tat conjugate successfully ferried MT into *Leishmania* cells, inhibiting promastigote proliferation by 82% at 7.5 µM, whereas MT alone, or simultaneous addition of non-conjugated MT plus Tat showed scarce penetration or killing activity (Figure 3). Intracellular MT concentration was estimated at a
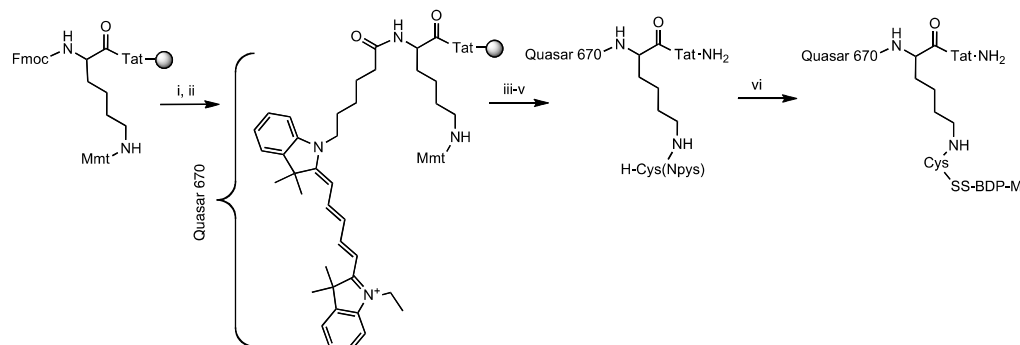
Fig. 2. Synthesis of doubly labeled Tat-miltefosine conjugate. i: piperidine; ii. Quasar 670, DIPCDI; iii. 1% TFA; iv. Boc-Cys(Npys)-OH; v. TFA cleavage; vi. MT-BDP-SH.
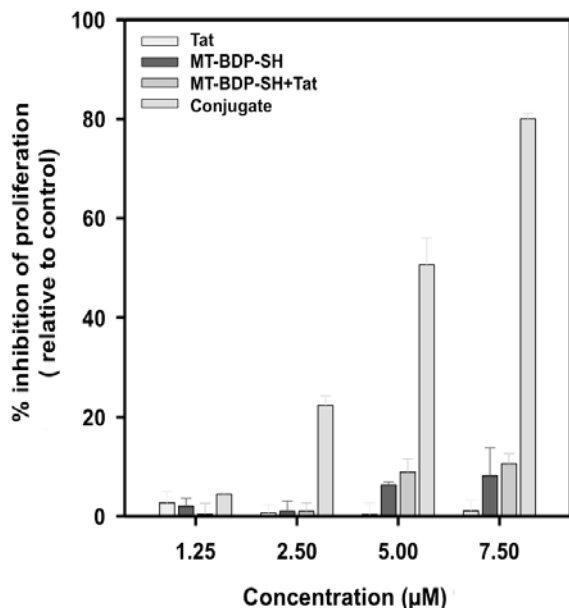
Fig. 3. Leishmanicidal activity of the Quasar 670-Tat-BDP-MT conjugate.

sizable 3 mM value by fluorescence measurement, demonstrating the good potential of this strategy for delivering the otherwise impermeable MT molecule into the parasite Furthermore, as the emission wavelengths of BDP-MT and Quasar 670 (538 and 670 nm, respectively) do not overlap, one can expect that intracellular cleavage, by *Leishmania*'s own redox system, of the disulphide linking the BDP-MT cargo with the Quasar 670-Tat vector will allow to visualize these moieties at independent locations within the parasite. Alternatively, if the conjugate is cleaved otherwise/ elsewhere, the intracellular fate of Quasar 670-Tat and BDP-MT should be identical and a homogenous fluorescence expected. In practice, after pulsing the parasite for 4h with the conjugate, confocal microscopy showed clearly differentiated staining areas, confirming that intracellular disulfide cleavage had taken place, hence corroborating the ability of Tat to deliver antiparasitic MT into *Leishmania* in the absence of a dedicated transporter.

Acknowledgments

References

1. Saugar, J.M., et al. *J. Med. Chem.* **50**, 5994-6003 (2007).
2. Hornillos, V., et al. *Bioorg. Med. Chem. Lett.* **18**, 6336-6339 (2008).

Pulsed ESR Study of the Topology and Dynamics of a Spin-Labeled Lipopeptaibol Antibiotic in a Lipid Membrane

Victoria N. Syryamina[1], Nicolay P. Isaev[1], Marta De Zotti[2], Cristina Peggion[2], Fernando Formaggio[2], Claudio Toniolo[2], Jan Raap[3], and Sergei A. Dzuba[1]

[1]*Institute of Chemical Kinetics and Combustion, 630090, Novosibirsk, Russia;* [2]*Department of Chemistry, University of Padova, 35131 Padova, Italy;* [3]*Leiden Institute of Chemistry, University of Leiden, 2300RA, Leiden, The Netherlands*

Introduction

To elucidate the mechanism by which antibiotic peptides change the permeability of microbial membranes, detailed information is needed on the membrane-peptide topology. Trichogin GA IV, isolated from the mold *Trichoderma longibrachiatum*, belongs to the class of peptaibols characterized by a high percentage of α-aminoisobutyric acid (Aib) residues and an 1,2-amino alcohol at the C-terminus. The primary structure of this peptaibol is unique due to its lipophilic *n*-octanoyl group at the N-terminus instead of the acetyl group present in most of the other members of this class. Despite the short length of its main chain (10 amino acid residues), trichogin GA IV exhibits remarkable membrane modifying properties. The orientation of the peptide in the membrane was studied by fluorescence and by applying the electron spin echo envelope modulation (ESEEM) (PELDOR) technique [1,2]. It was found that at low molar peptide to lipid (P/L) ratio individual peptide molecules are randomly distributed at the membrane surface, while at a high P/L ratio aggregates of these molecules are inserted more deeply into the membrane. In the present communication we report about the topology and dynamics of the membrane-associated peptide molecules from electron spin echo (ESE), ESEEM and continuous wave (CW)-ESR experiments. In this work, one of the Aib residues is replaced by the electron spin label TOAC (2,2,6,6-tetramethylpiperidine-1-oxyl-4-amino-4-carboxylic acid; Figure 1), whereas the native C-terminal 1,2-amino alcohol leucinol (Lol) is replaced by its synthetic precursor leucine methyl ester (Leu-OMe). The N-terminal *n*-octanoyl (*n*Oct) group is substituted by the equally hydrophobic, but fluorescent, fluorenyl-9-methyloxycarbonyl (Fmoc) group.

*n*Oct - Aib - Gly-Leu-Aib-Gly-Gly-Leu - Aib - Gly-Ile-Lol   (trichogin GA IV)
Fmoc-**TOAC**-Gly-Leu-Aib-Gly-Gly-Leu - Aib - Gly-Ile-Leu-OMe   (FTOAC-1)
Fmoc - Aib - Gly-Leu-Aib-Gly-Gly-Leu-**TOAC**-Gly-Ile-Leu-OMe   (FTOAC-8)

Results and Discussion

The three-pulse stimulated electron spin echo (ESE) technique is sensitive to orientation-dependent types of motions of spin labels at temperatures low enough to observe an echo signal [3]. Since the TOAC-spin label is rigidly attached to the peptide molecule, it reports directly on the backbone dynamics. Two types of motions are found above 100 K: (1) at P/L 1:200, fast stochastic librations, with a correlation time in the nanosecond scale, and (2) at P/L 1:20, slow millisecond rotations, which are observed by small-angle reorientations in the accessible microsecond time scale. The latter effect may be safely attributed to the dynamics of peptides which are elongated along the lipid molecules of the membrane. At room temperature, broadening of the continuous wave ESR spectrum of FTOAC-1 (compared to FTOAC-8) gives strong evidence that the N-terminal spin labels of the transmembrane peptides are mutually in close contact. From ESEEM spectroscopy the water accessibilities of the spin labels were investigated. The effects observed are in line with membrane surface (P/L 1:200) and deeply buried (P/L 1:20) spin labels, respectively. It is worth noting, however, that the water accessibility of the N-terminal spin label is low, but not zero. A possible explanation could be that the rotational mobility of the peptide helices promotes the transfer of water molecules from the outer to the interior of the membrane.

   The N-to-N dimerization of this lipopeptide is similar to the manner of association shown by the channel-former gramicidin A. In the case of trichogin GA IV, however, the helical peptide molecule does not have enough space inside to allow ion transport compared with the

much wider pore of the β-helices of gramicidin A. Thus, trichogin might act as a hole-drilling device, influencing the packing of the lipids of the membrane and creating micro-water channels. It is not clear yet why the trichogin helices would associate in a head-to-head manner. Possibly, the transmembrane dimers are optimizing packing of the bilayer lipids.

Formation of water channels at the outside of the N-to-N transmembrane dimers may explain why trichogin GA IV is able to induce membrane leakage, which explains its antibiotic activity. A room temperature study of membrane leakage induced by fluorescent labeled trichogin analogs showed a strong correlation between leakage and concentration of membrane bound aggregates [4]. However, the kinetics of membrane leakage was found much slower compared to that found for the barrel-stave type of ion channels typical of zervamicin and alamethicin [5,6]. Thus, the antibiotic activity of trichogin GA IV might be better explained by a disturbance induced in the membrane by transiently formed N-to-N dimers.
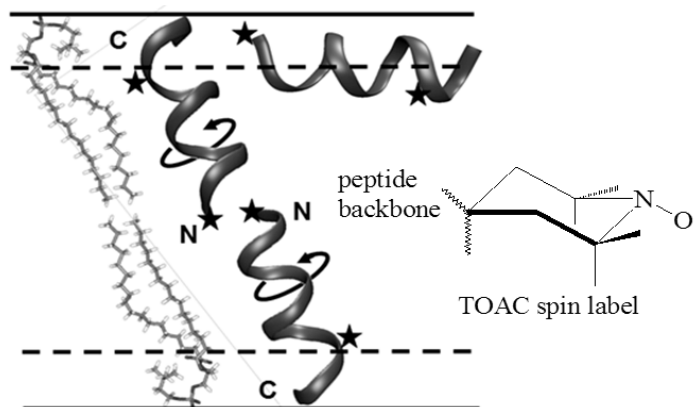
Fig. 1. Topologies of the TOAC labeled peptide molecules at the surface of the membrane at low peptide concentration and the head-to-head associated transmembrane dimer at high concentration. The circular arrows show molecular rotation of the peptide helices. The stars indicate the positions of spin labels at the peptide backbone, which were taken from an X-ray crystal structure. This simple model suggests a transport mechanism through water channels located at the interface between the peptide and the membrane interior to overcome the membrane barrier.

References

1. Mazzuca, C., Stella, L., Venanzi, M., Formaggio, F., Toniolo, C., Pispisa, B. *Biophys. J.* **88**, 3411-3421 (2005).
2. Salnikov, E.S., Erilov, D.A., Milov, A.D., Tsvetkov, Y.D., Peggion, C., Formaggio, F., Toniolo, C., Raap, J., Dzuba, S. A. *Biophys. J.* **91**, 1532-1540 (2006).
3. Syryamina, V.N., Isaev, N.P., Peggion, C., Formaggio, F., Toniolo, C., Raap, J., Dzuba, S. A. *J. Phys. Chem. B* **114**, 12277-12283 (2010).
4. Stella, L., Mazzuca, C., Venanzi, M., Palleschi, A., Didoné, M., Formaggio, F., Toniolo, C., Pispisa, B. *Biophys. J.* **86**, 936-945 (2004).
5. Kropacheva, T.N., Raap, J. *Biochim. Biophys. Acta* **1567**, 193-203 (2002).
6. Mazzuca, C., Orioni, B., Coletta, M., Formaggio, F., Toniolo, C., Maulucci, G., De Spirito, M., Pispisa, B., Venanzi, M., Stella, L. *Biophys. J.* **99**, 1791-1800 (2010).

Cationic Antimicrobial Peptide-Induced Bacterial Membrane Disruption Monitored by Atomic Force Microscopy

Lois M. Yin[1,2], Soyoung Lee[1], Michelle A. Edwards[3], Christopher M. Yip[2,3], and Charles M. Deber[1,2]

[1]*Division of Molecular Structure & Function, Research Institute, Hospital for Sick Children, Toronto, M5G 1X8, Canada;* [2]*Department of Biochemistry, University of Toronto, Toronto, M5S 1A8, Canada;* [3]*Institute of Biomaterials and Biomedical Engineering, University of Toronto, Toronto, M5S 3G9, Ontario, Canada*

Introduction

Resistance to small molecule antibiotics is on the rise and as a consequence novel approaches to the treatment of microbial infections are urgently required. Cationic antimicrobial peptides (CAPs) have become increasingly recognized in current research as prospective antibiotics. In nature, these peptides occur as important innate immunity agents that are found in a wide range of organisms, ranging from plants to insect to mammals – including humans [2]. The positively charged CAPs often bind to anionic bacterial membranes via electrostatic attractions, then insert into the lipid bilayers, leading to membrane destabilization or lysis and eventually cell death [4].

Our laboratory has designed the 6K-F17 series of CAPs in the sequence KKKKKKAXF-AXWXAFXA-NH$_2$, where X is either Ala or Leu [3]. These CAPs show significant antimicrobial activity against *Pseudomonas aeruginosa* [3], which is the major cause of chronic bacterial infection in cystic fibrosis patients, and of bacteremia in burn and cancer victims [5]. Using these CAPs as models, we have found that their core segment hydrophobicity plays an important role in their antimicrobial activity [3,6]. In the current study, we have focused on two CAPs distinctly varying in core hydrophobicity (Table 1), and directly visualized their modes of action within bacterial membrane lipids using atomic force microscopy to further understand how they exert their action at the bacterial membrane.

Table 1. Sequences, hydrophobicity levels, and antimicrobial activities of CAPs used in this work

Peptide	Sequence	CSH[a]	MIC[b] (µM)
6k-f17	kkkkkkaafaawaafaa-NH$_2$	1.48	2
6K-F17-4L	KKKKKKALFALWLAFLA-NH$_2$	3.14	64

[a]*CSH is the core segment hydrophobicity values of the peptides, derived from the Liu-Deber scale [1]. Amino acids in lowercase are D-enantiomers.* [b]*MIC is the minimum inhibitory concentration, defined here as the lowest peptide concentration required to fully inhibit the bacterial growth. Values adapted from [3]*

Results and Discussion

In situ atomic force microscopy (AFM) is a powerful means of directly imaging the impact of peptide-membrane interactions on membrane stability and structure [7]. The CAPs 6k-f17 and 6K-F17-4L, with the same number of positive charges but different core hydrophobicity, were each added to solid-supported lipid bilayers comprised of 3:1 POPE/DOPG (DO = di-oleoyl), typifying bacterial membranes. Real-time AFM imaging revealed the immediate formation of defects in the membrane bilayers upon CAP addition at concentrations lower than or equal to the MIC values (Figure 1). When peptides were added to the bacterial membrane lipid bilayers, a 1-2 nm height difference resolved by AFM indicated that the peptides were binding to the membrane surface initially (Figure 1b,e). As additional peptide was added, concave regions greater in number and size appeared in the membrane (Figure 1c,f), suggestive of peptide-induced membrane defects spanning the entire height of the bilayer. Both CAPs induced defects in the model membrane bilayer in a concentration-dependent manner. These experiments support the observation that the CAP with lower hydrophobicity is more effective in its antimicrobial activity [3] – a result that may be
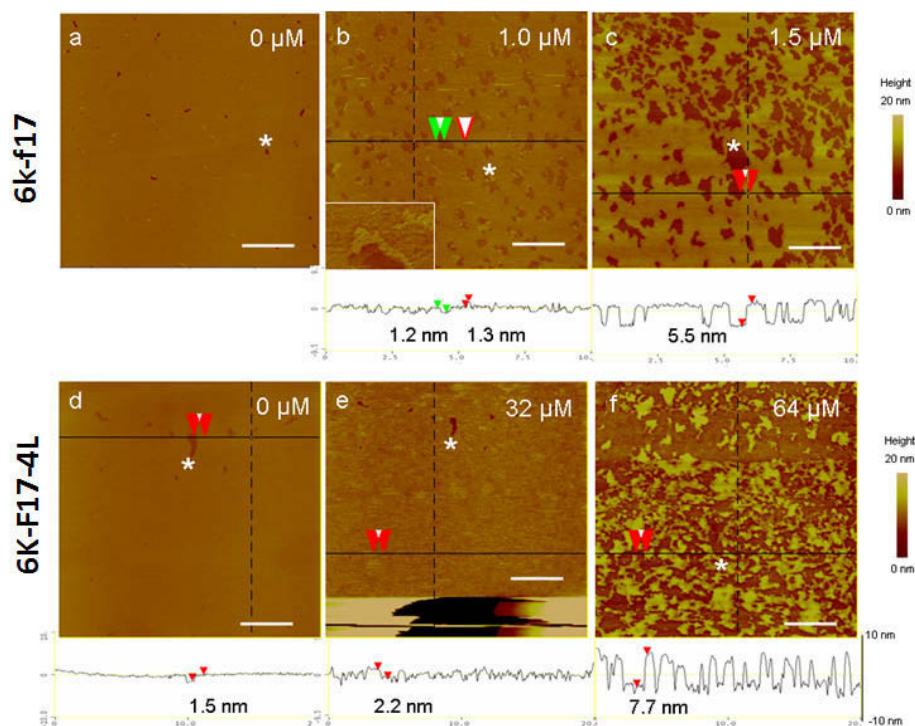
Fig. 1. AFM topography images of 6k-f17 (a-c) and 6K-F17-4L$_{8,11,13,16}$ (d-f) at various concentrations in bacterial membrane lipid mimics. Images were recorded immediately after CAP additions. The color indicates the local height of the lipid sample, ranging from 0 (lightest brown) to 20 nm (darkest brown). The white asterisk indicates the same point in each of the experiments (a-c) and (d-f). Red and green arrows indicate the difference in heights, as shown on the line spectra below the images.

attributable, in part, to the reduced availability of the 4L peptide to the membrane due to its tendency toward pre-aggregation in aqueous media.

These topographical images demonstrate not only how peptide concentration affects membrane lysis, and how rapidly these defects occur in the membranes, but also provide a valuable tool for correlating CAP MICs with their membrane disruptive power.

Acknowledgments

References

1. Liu, L.P., Deber, C.M. *Biopolymers* **47**, 41-62 (1998).
2. Zasloff, M. *Nature* **415**, 389-395 (2002).
3. Glukhov, E., Burrows, L.L., Deber, C.M. *Biopolymers* **89**, 360-371 (2008).
4. Yeaman, M.R., Yount, N.Y. *Pharmacol. Rev.* **55**, 27-55 (2003).
5. Govan, J.R., Deretic, V. *Microbiol. Rev.* **60**, 539-574 (1996).
6. Glukhov, E., Stark, M., Burrows, L.L. Deber, C.M. *J. Biol. Chem.* **280**, 33960-33967 (2005).
7. Shaw, J.E., Epand, R.F., Hsu, J.C.Y., Mo, G.C.H., Epand, R.M., Yip, C.M. *J. Struct. Biol.* **162**, 121-138 (2008).

An Unusual Spectroscopic Approach for Assessing the Binding Site of the Bradykinin B2 Receptor

Douglas L. Duarte[1], Luciana Malavolta[1], Renata F.F. Vieira[1], Laerte Oliveira[1], Shirley Schreier[2], and Clovis R. Nakaie[1]

[1]*Department of Biophysics, Federal University of Sao Paulo, Sao Paulo, 04044020, Brazil;* [2]*Department of Chemistry, Institute of Chemistry, University of Sao Paulo, Sao Paulo, 05513870, Brazil*

Introduction

The vasoactive peptide bradykinin (BK) and its transmembrane B2 receptor [1] were selected in order to test an innovative strategy that might allow the assessment of the BK binding site in its receptor structure. With the use of the 2,2,6,6-tetramethylpiperidine-1-oxyl-4-amino-4-carboxylic acid (TOAC) paramagnetic probe [2,3], a biologically active agonist (TOAC[0]-BK), as well as an inactive control (TOAC[3]-BK) analogs [4] were used comparatively for monitoring a possible binding with B2 receptor fragments. In respect to this receptor segments to be evaluated, we decided to test the hypothesis [5,6] which proposes as the binding site, a fragment composed of the N-terminal and the third extracellular loop regions maintained by a Cys-Cys linkage between them. Thus the B2 N-terminal P15 (47-61, FSEVNCPDTEWWSWL) and P13 (301-313, LRLGLSGCWNER) fragments were synthesized and tested separately or linked (in parallel or cyclic) as shown in Table 1. These B2 fragments were thus evaluated in terms of intermolecular interaction capacity towards the active BK analogue (TOAC[3]-BK) with the use of EPR methodology. CD spectra of B2 fragments were also examined in terms of conformational properties aiming at searching for some structural features that might help understand the mechanism of agonist-receptor interaction.

Results and Discussion

Table 1 presents the general structures of B2 receptor fragments synthesized and tested in the present investigation. As expected, the results indicated pronounced difficulties in the synthesis procedure or even in the HPLC purification step, due to low solubility mainly of most of S-S bearing cyclic peptide and attaching a $(CH_2)_6$ or C_6-spacer between P15 and P13 segments.

Table 1. Fragments of B2 receptor examined

Fragment	Sequence
P13 (301-313)	LRLGLSGCWNER – amide
P15 (47-61)	FSEVNCPDTEWWSWL – amide
(P15-P13)p	FSEVNCPDTEWWSWL | LRLGLSGCWNER
P15-C6-13	IQLGVIHDCKISD-C6-RIQDDCPKAGRHSYI – amide

Peptide conformation study was initiated with CD experiments examining the P15, P13, P15-P13p (in parallel) and P15-C6-P13 (cyclic) B2 fragments varying the pH of solution and the amount of secondary structure inducing TFE. All compounds depicted extended and flexible conformations but of note, only the cyclic and larger receptor fragment depicted a different random coiled profile in the CD curves. In terms of EPR experiments, Figure 1 shows the rotational correlation time (τ) of each solution containing a mixture either of the active or inactive (TOAC[0]-BK and TOAC[3]-BK) with B2 fragments above described. It was possible to detect intermolecular interaction only with TOAC[0]-BK and the cyclic sequence formed by P15 and P13 segments linked by a disulfide bond (P15-C_6-P13) (Figure 1A). This result suggested

that the B2 binding site for BK contains this cyclic structure. To reinforce this assertion, no intermolecular interaction was observed when the inactive TOAC^3-BK was used.
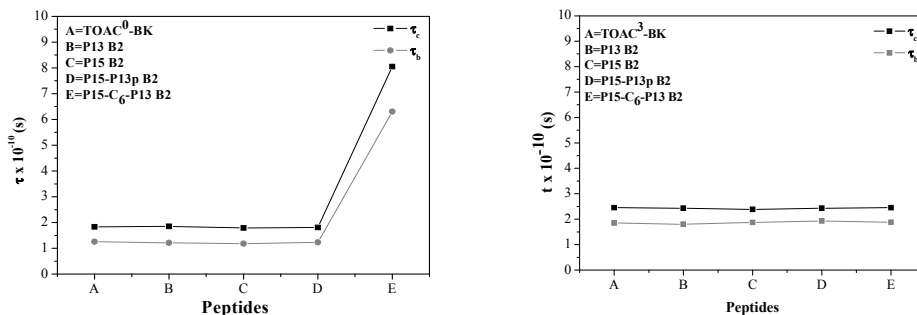
Fig. 1. τ_C and τ_B values of solutions containing B2 fragments and TOAC^0-BK (A) and TOAC^3-BK (B).

These findings allowed to stress that the herein applied EPR-TOAC strategy seems to be of value not only for help monitoring the position of the binding site of the receptor, but also, this procedure might be considered a relevant experimental approach in terms of evaluating intermolecular associations of many types of macromolecules.

Acknowledgments

References

1. McEarchan, A.E., Shelton, E.R., Bhakta, S., Obernolte, R., Back, C., Zuppan, P., Fujisaki, J., Aldrich, R.W., Jargainin, K. *Proc. Natl. Acad. Sci. U.S.A.* **88**, 7724 (1991).
2. Nakaie, C.R., Goissis, G., Schreier, S., Paiva, A.C.M. *Braz. J. Med. Biol. Res.* **14**, 173-180 (1981).
3. Marchetto, R., Schreier, S., Nakaie, C.R. *J. Am. Chem. Soc.* **115**, 11042-11043 (1993).
4. Nakaie, C.R., Silva, E.G., Cilli, E.M., Marchetto, R., Schreier, S., Paiva, T.B., Paiva, A.C.M. *Peptides* **23**, 65-70 (2002).
5. Oliveira, L., Costa-Neto, C.M., Nakaie, C.R., Schreier, S., Shimuta, S., Paiva, A.C.M. *Physiol. Rev.* **87**, 565-592 (2007).
6. Correa, S.A.A., Pignatiari, G.C., Ferro, E.S., Pacheco, N.A.S., Costa-Neto, C.M., Pesquero, J.B., Oliveira, L., Paiva, A.C.M., Shimuta, S.I. *Regul. Pept.* **134**, 132-140 (2006).

Structure, Dynamics, and Bioactivity of Synthetic Analogues of the Antimicrobial Peptide Trichodecenin I

Emanuela Gatto[1], Gianfranco Bocchinfuso[1], Antonio Palleschi[1], Lorenzo Stella[1], Mariano Venanzi[1], Simona Oancea[2], Marta De Zotti[3], Fernando Formaggio,[3] and Claudio Toniolo[3]

[1]Department of Chemical Sciences and Technologies, University of Rome "Tor Vergata", 00133, Rome, Italy; [2]Department of Food Chemistry and Engineering, University of Sibiu "Lucian Blaga", 550012, Sibiu, Romania; [3]ICB, Padova Unit, CNR, Department of Chemistry, University of Padova, 35131, Padova, Italy

Introduction

Lipopeptaibols are members of a family of antimicrobial peptides characterized by the presence of the helix inducer Aib (α-aminoisobutyric acid) residue, an N-terminal fatty acyl group, and a C-terminal 1,2 amino alcohol. In spite of their relevant pharmacological interest as potential, new antibiotic agents, the 3D-structural motifs determining their biological activities are still fiercely debated. The primary structure of trichodecenin I (**TDI**), one of the shortest member of the peptaibol family, is (Z)-4-decenoyl-Gly-Gly-Leu-Aib-Gly-Ile-Lol (Lol, leucinol). NMR in CDCl$_3$ solution and crystal structure analyses showed that **TDI** adopts a non-helical, multiple β-turn (U-shaped) conformation [1,2]. To study the **TDI** dynamic and conformational properties in solution by means of steady-state and time-resolved optical spectroscopy methods, we synthesized and fully characterized the following analogues:

n-Decanoyl-Gly-Gly-Leu-Aib-Gly-Ile-Leu-OMe   (**TD**)
n-Decanoyl-Gly-Gly-Leu-Aib-Gly-Trp-Leu-OMe   (**TDW6**)
n-Decanoyl-Gly-Gly-Leu-TOAC-Gly-Trp-Leu-OMe (**TDT4W6**)

where *n*-decanoyl replaces the (Z)-4-decenoyl group at the N-terminus and TOAC is 2,2,6,6-tetramethylpiperidine-1-oxyl-4-amino-4-carboxylic acid. In **TDW6** and **TDT4W6** the Ile[6] residue is substituted by Trp. In **TDT4W6** a TOAC residue, a conformationally-constrained α-amino acid characterized by a stable nitroxide radical, replaces Aib[4] for our photophysical studies based on the Trp/TOAC donor-acceptor pair. Molecular dynamics (MD) simulations were also carried out to analyze the conformational properties of the **TDI** analogues investigated. Surprisingly, the X-ray diffraction structure of **TDT4W6** shows that the peptide is largely (3$_{10}$-/α-)helical with the TOAC[4] and Trp[6] side chains located on opposite faces [3].

Results and Discussion

The UV absorption spectra of the **TDW6** and **TDT4W6** peptides in methanol (MeOH) solution are dominated by the typical π → π* transitions of the Trp indole chromophore [λ$_{max}$ = 222, 283, 295 nm; ε(280 nm) = 5840 M^{-1} cm^{-1}]. In **TDT4W6** the π → π* transition of the TOAC nitroxyl chromophore [λ$_{max}$ = 238 nm; ε (238 nm) ≅ 2260 M^{-1} cm^{-1}] is overlapped by that of the Trp absorption. The UV absorption spectrum of the latter peptide corresponds to the sum spectra of the Trp and TOAC isolated chromophores, suggesting that electronic coupling between the two probes is absent in the ground state.

Steady-state fluorescence spectra (λ$_{exc}$= 280 nm) in MeOH show a substantial quenching of Trp singlet emission by TOAC, the fluorescence quantum yield of **TDW6** (φ$_0$) being 0.291 ± 0.008 and that of **TDT4W6** (φ) 0.034 ± 0.007. From the above results, it turns out that the estimated quenching efficiency, E$_{ss}$, is 0.88 [E$_{ss}$=1-(φ/φ$_0$)]. Fluorescence time-decays (λ$_{exc}$ = 280 nm, λ$_{em}$=350 nm) can be described by a sum of exponential lifetimes τ$_i$.

$$I(t) = \sum_{i}^{n} \alpha_i \cdot e^{-\frac{t}{\tau_i}}$$

Table 1. Time-decay parameters for the peptides investigated in MeOH[a]

Peptide	α_1	$\tau_1(ns)$	α_2	$\tau_2(ns)$	$<\tau>(ns)$
TDW6	0.44	1.9	0.56	4.8	3.52
TDT4W6	0.67	0.2	0.33	1.1	0.50

[a]$\lambda_{exc}=280$ nm; $\lambda_{em}=350$ nm.

The pre-exponential factor α_i, in case of slow conformational dynamics, is proportional to the conformational population in the excited state. The parameters obtained from the experimental decays of the two Trp-containing analogues are listed in Table 1. From these data, an average quenching efficiency can be obtained, *i.e.* $E_{dyn}= 0.86$ [$E_{dyn}=1-(<\tau>/<\tau>_0)$]. The agreement between the quenching efficiencies calculated from steady-state and time-resolved fluorescence experiments indicate that the Trp/TOAC ground-state interactions can be neglected.

MD simulations on **TDW6**, starting from an extended peptide conformation, showed that, in agreement with the NMR results, a U-shaped conformation is attained in a time shorter than 1 ns. However, in the case of **TDT4W6**, this tendency is much less evident, and a stable U-shaped conformation is not reached during the simulation time (20 ns). In any case, these data suggest that the insertion of the Trp residue at position 6 in the **TDI** sequence does not perturb the general conformational property of the peptaibol.

Similar results were obtained for **TDW6** by starting the simulation from a helical conformation. This secondary structure was lost in about 2 ns. In Figure 1, the RMSD of the **TDW6** backbone (residues 2-6), calculated from MD simulations, with respect to the backbone structure of **TDI**, obtained from its NMR experiments, is reported. In the insets, suitably sampled MD conformations are depicted in blue, while the NMR structures are reported in red.
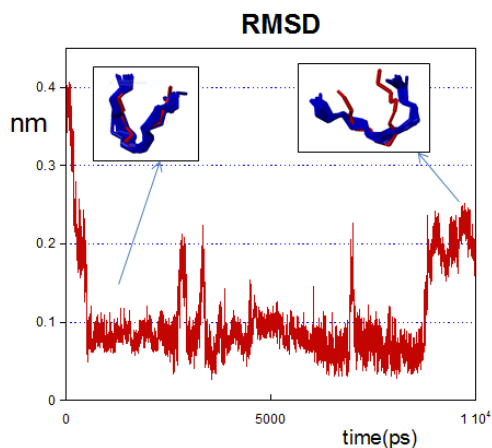
*Fig. 1. RMSD values of the **TDW6** (MD) vs. **TD1** (NMR) structures. Left inset: RMSD lower than 0.1 nm. Right inset: RMSD roughly equal to 0.2.*

Membrane leakage experiments were carried out on 100-nm liposomes formed by egg phosphatidylcholine entrapping a carboxyfluorescein dye. The membrane activity of **TDW6** and **TDT4W6** were found to be comparable, but slightly lower than that of the parent peptide (**TDI**).

In conclusion, the results of our studies suggest that in solution **TDT4W6** adopts only a few conformations, not interconverting on the nanosecond time scale. Conversely, **TDW6** maintains the same U-shaped conformation shown by NMR and crystal-state investigations on **TDI**. Liposome leakage experiments show that the membrane perturbing properties of **TDI** are essentially preserved in its **TDW6** and **TDT4W6** analogues.

References

1. Gurunath, R., Balaram, P. *Biopolymers* **35**, 21-29 (1995).
2. Monaco, V., Formaggio, F., Crisma, M., Toniolo, C., Shui, X., Eggleston, D.S. *Biopolymers* **39**, 31-42 (1996).
3. Crisma, M., Deschamps, J.A., George, C., Flippen-Anderson, J.L., Kaptein, B., Broxterman, Q.B., Moretto, A., Oancea, S., Jost, M., Formaggio, F., Toniolo, C. *J. Pept. Res.* **65**, 564-579 (2005).

Single-Channel Properties of Peptides Inserted in Natural and Artificial Membranes

Mascia Benedusi[1], Anna Fasoli[1], Sara Bobone[2], Barbara Orioni[2], Marta De Zotti[3], Fernando Formaggio[3], Claudio Toniolo[3], Lorenzo Stella[2], and Giorgio Rispoli[1]

[1]CNISM, Department of Biology, University of Ferrara, Ferrara, 44100, Italy; [2]Department of Chemical Sciences and Technologies, University of Rome "Tor Vergata", Rome, 00133, Italy; [3]ICB, Padova Unit, CNR, Department of Chemistry, University of Padova, Padova, 35131, Italy

Introduction

Any investigation on pore-forming peptides has the long-term goal to understand how the interactions between peptides and lipids influence the conformation and the orientation of both, leading eventually to membrane permeabilization. Here, we studied the lipid environment dependence of the single channel properties generated by alamethicin (Alm) F50/5 and its [L-Glu(OMe)[7,18,19]] analog (having the Gln residues at positions 7, 18 and 19 substituted by Glu, characterized by a methyl ester group in the γ-position). Both peptides were inserted in a cell plasma membrane (recorded in whole-cell) and in membrane patches excised from giant unilamellar vesicles (GUVs). The possibility to compare the channel activity in the precisely controlled lipid environment of GUVs, with the channel activity recorded in a natural membrane with the same ionic electrochemical gradients, will open new possibilities in the biophysical characterization of the pores.

Results and Discussion

F50/5 Alm and [L-Glu(OMe)[7,18,19]] Alm were inserted in the plasma membrane of a cell (recorded in whole-cell configuration), and in patches excised from GUVs. The peptides were applied to the membranes at concentrations low enough to give single-channel events. The cell system consisted in an isolated rod outer segment of vertebrate photoreceptor (OS), that has been proven to be an ideal preparation to study pore-forming peptides under strict physiological conditions [1,2].
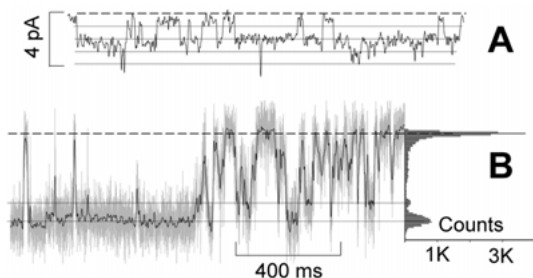
Fig. 1. Single channel properties of Alm inserted in an OS (A). Current produced by F50/5 Alm (B). Left: channel activity produced by [L-Glu(OMe)[7,18,19]] Alm, low-pass filtered at 2 KHz (gray trace) and at 100 Hz (superimposed black trace). Right: cumulative current amplitude distribution. Both recordings have the same scales and V_h=-20 mV; continuous and dotted lines indicate the most probable single channel amplitudes and 0 pA, respectively.

GUVs (diameter >10 μm) were prepared by electroformation [3], using different lipid compositions, which include fluorescent-labeled lipids, in order to optimize their mechanical properties, stability, and visualization. The best composition found was: 40% phosphatidylcholine, 20% phosphatidylglycerol, 30% cholesterol, and 10% 7-nitro-2,1,3-benzoxadiazol-4-yl-labeled phosphatidylethanolamine. GUVs were viewed by exploiting a contrast-intensified camera that was used to check also their unilamellarity in fluorescence. To perform patch-clamp recordings, the GUVs should lie on the bottom of the recording chamber. This situation was achieved by having a 0.3 M sucrose internal solution and a solution containing 120-180 mM KCl and 1-5 mM $CaCl_2$ in the bath. The latter solution filled the patch pipette as well, so that the ionic current through the peptide channels was driven by the holding potential (V_h) only. Peptides were applied to, and removed from, the membranes in ~50 ms by using a fast perfusion system [1].

F50/5 Alm produced single channel events of repetitive amplitude in an OS (Figure 1A) and GUVs (Figure 2A). The larger events were usually an integer multiple of a fixed size. Since the events recorded in the OS were smaller than in GUVs, in the former case the traces were low-pass filtered at 100 Hz (Figure 1A) t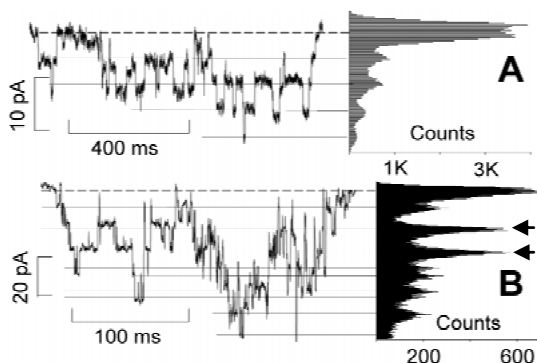o cut the high-frequency noise, which would otherwise cover most of these events. In the OS, single channel events produced by F50/5 Alm at concentrations in the range 0.25-0.5 μM manifested within 5 s from peptide application. Their amplitude resulted of ~50±8 pS at -20 mV (3500 events averaged in 3 cells). In Figure 1A we show up to 4 such events. In GUVs, under the same ionic and voltage conditions, it was necessary to raise the peptide concentration to 1-2.5 μM to obtain single channel events, that again manifested within 5 s from peptide application. Since the single channel events were about 5-fold larger than the OS, the recordings were filtered at 2 KHz, instead of 100 Hz.

Fig. 2. Single channel properties of Alm inserted in GUVs. (**A**) Left: F50/5 Alm (V_h=-20 mV). Right: cumulative distribution of the current amplitudes. (**B**) Left: [L-Glu(OMe)^{7,18,19}] Alm (V_h=-56 mV). Right: cumulative distribution of the current amplitudes.

Although large events were occasionally recorded not being an integer multiple of a fixed size, the cumulative distribution of current amplitudes in 3 GUVs (6500 events) gave at least 5 peaks equally separated by about 5 pA, corresponding to a single channel amplitude of 250±20 pS. Since it was not possible to obtain long, stable recordings of just one channel opening and closing, we could not measure kinetic parameters, such as the distribution of the mean open and closed times. However, a rough inspection of the traces indicates that F50/5 Alm tends to form channels that remain open and closed longer in GUVs than in the OS.

[L-Glu(OMe)^{7,18,19}] Alm produced larger events than F50/5 Alm in both OS and GUVs. Many different amplitudes were observed. Some were so fast that they were cut by the patch-clamp amplifier, even when filtering as high as 2 KHz (Figure 1B, left, gray trace). Since the majority of the events were anyway much slower, in order to compare the single channel amplitude for [L-Glu(OMe)^{7,18,19}] Alm in the two lipid environments, these very fast events were usually cancelled out upon low-pass filtering the traces at 100 Hz (Figure 1B, left, black trace; Figure 2B, left). In the OS, current activated ~20 s after peptide application at V_h=-20 mV, due to the very low probability of pore formation by this peptide [2]. The distribution of current amplitudes (Figure 1B, right) showed that the most probable amplitude was 310±30 pS (820 events, n=3), but events of smaller sizes (as 260 pS) were recorded as well. In GUVs, the events at V_h=-20 mV were very scarce, due to the low probability of pore formation. Therefore, V_h was raised to more negative voltages (Figure 2B) to obtain a sustained channel activity. Many different channel amplitudes were recorded (Figure 2B): the two major peaks of their cumulative distribution gave the most frequent conductances of ~250 and ~470 pS (arrows; 1400 events, n=3), although many events of larger size (up to 1 nS) were recorded. In conclusion, [L-Glu(OMe)^{7,18,19}] Alm has a lower probability of channel formation and produces larger events with respect to F50/5 Alm in both GUVs and OS, but both peptides generate larger events in GUVs than in OS.

Acknowledgments

References

1. Vedovato, N., Rispoli, G. *Eur. Biophys. J.* **36**, 771-778 (2007).
2. Vedovato, N., Baldini, C., Toniolo, C., Rispoli, G. *Chem. Biodivers.* **4**, 1338-1346 (2007).
3. Orioni, B., Bocchinfuso, G., Kim, J.Y., Palleschi, A., Grande, G., Bobone, S., Park, Y., Kim J.I., Hahm, K.-S., Stella, L. *Biochim. Biophys. Acta* **1788**, 1523-1533 (2009).

A Nondestructive Methodology for the Configurational Assignment of Iva Residues in Peptaibiotics

Marta De Zotti[1], Barbara Biondi[1], Marco Crisma[1], Claudia U. Hjørringgaard[2], Albrecht Berg[3], Hans Brückner[4,5], and Claudio Toniolo[1]

[1]ICB, Padova Unit, CNR, Department of Chemistry, University of Padova, 35131, Padova, Italy; [2]Department of Chemistry, Åarhus University, 8000 Åarhus C, Denmark; [3]Innovent e.V., Department of Biomaterials, 07745, Jena, Germany; [4]Research Center for BioSystems, Land Use and Nutrition, University of Giessen, 35392, Giessen, Germany; [5]Department of Food Sciences and Nutrition, College of Food Sciences and Agriculture, King Saud University, Riyadh, 11451, Saudi Arabia
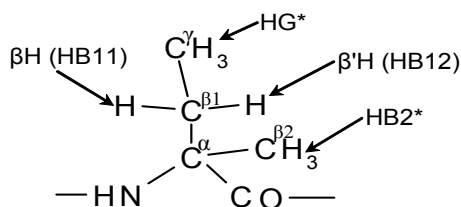
Introduction

Fig. 1. Chemical formula of the Iva residue where the β-CH$_2$, and the β - and γ-CH$_3$ side-chain notations are highlighted with arrows.

The non-coded, C^α-tetrasubstituted, helicogenic, chiral α-amino acid isovaline (Iva) (Figure 1) is remarkably spread in the biosphere [1] and in particular it is a characteristic marker of a class of naturally occurring, fungal peptide antibiotics, termed peptaibiotics [2], where it occurs as the *S*- or the *R*-enantiomer. It is clear that the unequivocal determination of the configuration of the Iva residues in peptides is imperative before one could correctly attempt their total chemical syntheses.

Results and Discussion

In this work, we applied and expanded our recently developed NMR method [3] to a large set of peptaibiotics (Figure 2), which enabled the nondestructive assignment of the configuration of each Iva residue if the helical screw sense of these compounds is known (by CD). In one of the peptaibiotics studied (bergofungin A), the Iva configuration, as reported in the literature, was found (and independently confirmed) to be incorrect.

(1) **ANTIAMOEBIN I** Ac-Phe-Aib-Aib-Aib-**(R)-Iva**[5]-Gly-Leu-Aib-Aib-Hyp-Gln-**(R)-Iva**[12]-Hyp-Aib-Pro-Phol

(2) **BERGOFUNGIN A** Ac-Val-Aib-Aib-Aib-Val-Gly-Leu-Aib-Aib-Hyp-Gln-**(R)-Iva**[12]-Hyp-Aib-Phol

(3) **NEOEFRAPEPTIN A** Ac-Pip-Aib-Pip-**(R)-Iva**[4]-Aib-Leu-βAla-Gly-Ac₃c-Aib-Pip-Aib-Gly-Leu-**(S)-Iva**[15]-PIHPPE

(4) **TRICHOTOXIN A40/5** Ac-Aib-Gly-Aib-Leu-Aib-Gln-Aib-Aib-Aib-Ala-Aib-Aib-Pro-Leu-Aib-**(R)-Iva**[16]-Glu-Vol

(5) **TRICHOTOXIN A50/G** Ac-Aib-Gly-Aib-Leu-Aib-Gln-Aib-Aib-Aib-Ala-Ala-Aib-Pro-Leu-Aib-**(R)-Iva**[16]-Gln-Vol

(6) **TYLOPEPTIN A** Ac-Trp-Val-Aib-**(S)-Iva**[4]-Ala-Gln-Ala-Aib-Ser-Aib-Ala-Leu-Aib-Gln-Lol

(7) **TYLOPEPTIN A'** Ac-Trp-Val-Aib-**(R)-Iva**[4]-Ala-Gln-Ala-Aib-Ser-Aib-Ala-Leu-Aib-Gln-Lol

Fig. 2. Amino acid sequences of the peptaibiotics studied in this work (Ac, acetyl; Aib, α-aminoisobutyric acid; Phol, phenylalaninol; Vol, valinol; PIHPPE, 2,3,4,6,7,8-hexahydro-1-pyrrole [1,2-α] pyrimidine; Hyp, (2S,4R)-hydroxyproline; Pip, pipecolic acid; Ac₃c, 1-aminocyclopropane-1-carboxylic acid; β-Ala, β-alanine or 3-aminopropionic acid).

A statistical analysis of the preferred main- and side-chain conformations of the Iva residues in peptides, performed on the basis of their published X-ray diffraction structures, allowed us to provide sound bases to the rationalization of the NMR criteria (Table 1) exploited to establish the configuration of this amino acid [4].

Table 1. Summary of the NMR parameters used to assess the absolute configuration of Iva residues in a right-handed helical peptide[a]

Criteria	NMR parameter	Value for (R)-Iva	Value for (S)-Iva
1	^{1}H-NMR Chemical shift of the γ-CH$_3$ protons	$\delta < 0.89$ ppm	$\delta > 0.91$ ppm
2	Difference between the chemical shifts ($\Delta\delta$) of the two β-CH$_2$ protons	$\Delta\delta > 0.28$ ppm	$\Delta\delta < 0.20$ ppm
3	^{13}C-NMR Chemical shift of the β-CH$_2$ carbon	$\delta < 29$ ppm	$\delta > 33$ ppm

[a]*For a left-handed helical peptide, the parameters should be reversed*

References

1. Brückner, H., Becker, D., Gams, W., Degenkolb, T. *Chem. Biodivers.* **6**, 38-56 (2009).
2. Toniolo, C., Brückner, H. *Peptaibiotics: Fungal Peptides Containing α-Dialkyl α-Amino Acids*, Wiley-VCH, Weinheim, Germany, 2009.
3. De Zotti, M., Schievano, E., Mammi, S., Kaptein, B., Broxterman, Q.B., Singh, S.B., Brückner, H., Toniolo, C. *Chem. Biodivers.* **7**, 1612-1624 (2010).
4. De Zotti, M., Biondi, B., Crisma, M., Hjørringgaard, C.U., Berg, A., Brückner, H., Toniolo, C. *Biopolymers (Pept. Sci.)* (2011), in press.

Inhibition of P-Glycoprotein Using "Clicked" Bivalent Inhibitors

Jerrin Kuriakose, Christine A. Hrycyna, and Jean Chmielewski

Department of Chemistry, Purdue University, 560 Oval Drive, West Lafayette, IN, 47909-2084, U.S.A.

Introduction

P-Glycoprotein (P-gp), an ATP-Binding Cassette (ABC) transporter, is widely recognized as the primary protein responsible for conferring multi drug resistance (MDR) across a diverse range of therapeutics [1,2]. It is highly expressed at therapeutic target sites such as the blood brain barrier (BBB) and cancer cells. P-gp effluxes a diverse set of drug substrates, from the anti-cancer taxol to the anti-HIV agent saquinavir, limiting their effective accumulation and therapeutic action. Using substrates of P-gp, we have designed unique cross-linked bivalent agents that have been shown to inhibit P-gp mediated efflux in cultured cells. Emetine [3] and quinine [4] are two such substrates that upon dimerization were proven to inhibit P-gp. Furthermore, these dimers were able to reverse the MDR phenotype of cells when co-administered with drugs such as taxol and doxorubicin. It was also observed that the tether design played a crucial role in determining inhibitory performance of these dimers.

With the aim of exploring the P-gp substrate binding region and discovering potent inhibitors, we used the copper catalyzed azide-alkyne cycloaddition ("Click") reaction to dimerize emetine and quinine. Emetine homodimers and emetine-quinine heterodimers were cross linked using click chemistry to form bivalent agents and their ability to inhibit P-gp investigated by a rhodamine-123 (R-123) substrate accumulation assay in MCF7/DX1 cells.

Results and Discussion

We initially focused on the development of crosslinked emetine homodimers. The azide and alkyne functionalities were tethered to emetine individually via amide bonds utilizing the pendant emetine secondary amine (Scheme 1). The relevant alkyne/azide functionalized carboxylic acids were either commercially available or synthesized by reported procedures [5]. The HATU coupling of 4-azidobutanoic acid and 5-hexynoic acid was carried out with emetine to give the **E3Z** and **E3A** monomers respectively. The click reaction was performed using Cu(I) and the standard 1:1 *tert*-butanol/water solvent system. **E3** was purified using semi-prep reverse phase HPLC to >95%purity (Scheme 1). Characterization was carried out using electrospray ionization mass spectrometry (ESI).
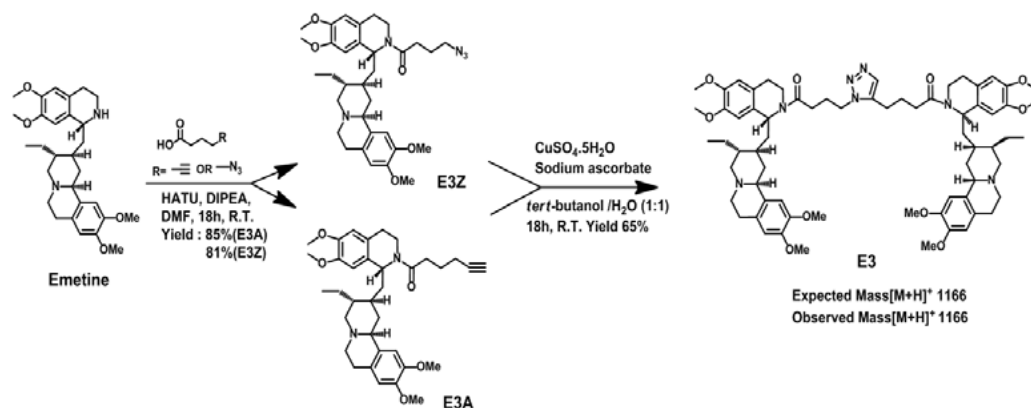
*Scheme 1. Synthesis of **E3**.*

In order to make the emetine-quinine heterodimer, we reacted quinine with 4-azidobutanoic acid to form **Q3Z** (Scheme 2). The pendant secondary alcohol of quinine was used to form **Q3Z** under standard EDC coupling conditions. The click reaction between **E3A** and **Q3Z** was carried out and characterized as before to give **E3Q3**.
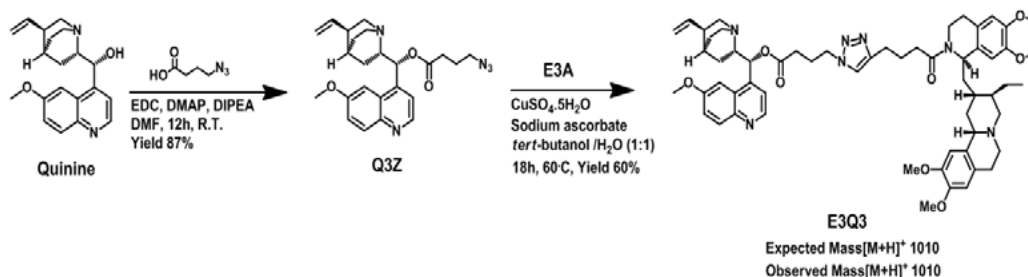
*Scheme 2. Synthesis of **E3Q3**.*

Inhibitory activity of the dimers was investigated by the R-123 substrate accumulation assay. This assay follows the accumulation of R-123, a fluorescent substrate of P-gp, within MDR cells as a consequence of P-gp inhibition by the dimeric agents. The MCF7/DX1 cancer cell line, known to over express P-gp, was employed. Flow cytometry was used to quantify the resulting fluorescence accumulation within MCF7/DX1 cells. The known P-gp inhibitor GF120918 (GF) was used as the positive control. The emetine homodimer **E3** displayed low inhibitory potency against P-gp (Figure 1a).This is in line with our previous observations with emetine homodimers where we observed hydrophilic moieties to be detrimental to activity [3]. However, the emetine-quinine heterodimer **E3Q3** showed highly potent inhibition of P-gp mediated efflux, with an IC_{50} of approximately $2.5\pm0.1\mu M$ (Figure 1b). Multi-valency of these agents is demonstrated to be responsible for their inhibitory activity as the monomers, emetine and quinine, have IC_{50} values of approximately 33 µM and 103µM respectively [3,4].
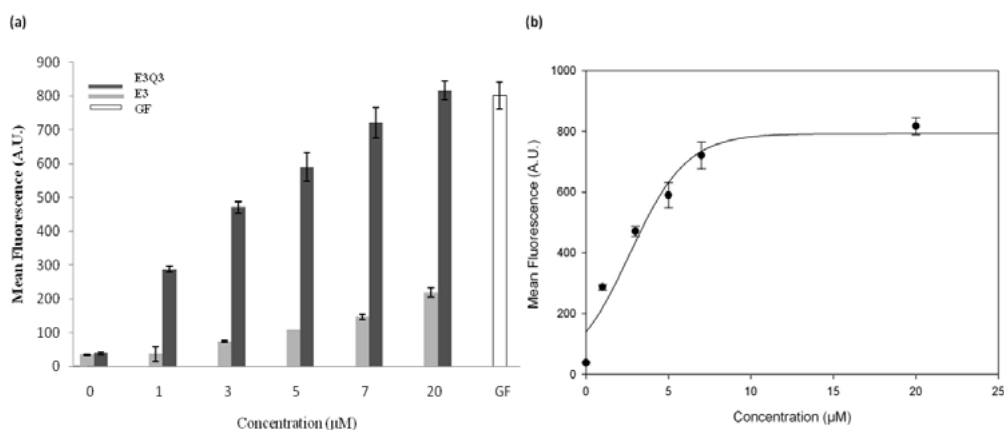
*Fig. 1. (a) Flow cytometry data for MCF-7/DX1 cells treated with R-123 and bivalent agents **E3** and **E3Q3** (b) IC_{50} curve generated for **E3Q3**.*

In summary, we have applied click chemistry in the design and synthesis of bivalent P-gp substrates, based on emetine and quinine, to probe the binding region of P-gp. While the emetine homodimers showed poor inhibitory activity, we discovered a potent heterodimeric inhibitor **E3Q3**. Dimer activity is a balance between the nature of the tether as well as the substrate monomer. Investigation of "clicked" quinine homodimers and optimum tether modifications will be investigated.

References

1. Ambudkar, V.S., Dey, S., Hrycyna, C.A., Ramachandra, M., Pastan, I., Gottesman, M.M. *Annu. Rev. Pharmacol. Toxicol.* **39**, 361-398 (1999).
2. Gottesman, M.M., Hrycyna, C.A., Schoenlein, P.V., Germann, U.A., Pastan, I. *Annu. Rev. Genet.* **29**, 607-649 (1995).
3. Pires, M.M., Hrycyna, C.A., Chmielewski, J. *Biochemistry* **45**, 11695-11702 (2006).
4. Pires, M.M., Emmert, D., Hrycyna, C.A., Chmielewski, J. *Mol. Pharmacol.* **75**, 92-100 (2009).
5. Khoukhi, N., Vaultier, V., Carrié, V. *Tetrahedron* **43**, 1811-1822 (1987).

Synthesis of Fmoc-Gly-Ile Phosphinic Pseudodipeptide: An Essential Building Block for Construction of Matrix Metalloproteinase Inhibitors (MMPIs)

Manishabrata Bhowmick and Gregg B. Fields

Torrey Pines Institute for Molecular Studies, 11350 SW Village Parkway, Port St. Lucie, FL, 34987, U.S.A.

Introduction

Our growing interest is to develop effective matrix metalloproteinase (MMP) inhibitors as activation of these enzymes have been associated with primary and metastatic tumor growth, angiogenesis, and pathological degradation of extracellular matrix (ECM) components, such as collagen and laminin [1,2]. A well-established strategy to develop a protease inhibitor is the backbone modification of the bioactive peptide with replacement of the hydrolytically susceptible peptide bond in enzymatic hydrolysis. The use of phosphinic pseudodipeptides (PPDs) is a very effective approach to develop highly s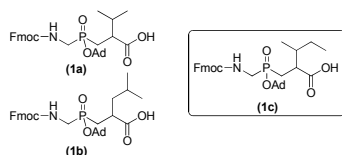elective and potent inhibitors of a variety of Zn metalloproteases [3-8], as phosphinic dipeptides contain hydrolytically stable tetrahedral phosphinic moieties which mimic the tetrahedral intermediate formed during enzymatic hydrolysis. PPDs are of growing interest as a building block in medicinal chemistry but their practical application in peptide modification is limited due to their lack of accessibility. Currently we are working to develop efficient and scalable synthetic methods for the preparation of various phosphinic pseudodipeptide building blocks which will allow us to prepare different MMPIs in large scale. Very recently we have reported an efficient synthetic method by developing a one pot reaction procedure involving a single step bis-deprotection followed by Fmoc-protection leading to the phosphinate dipeptide **1a** and its Gly-Leu analog **1b** (Figure 1) [9]. Herein we report the synthesis of phosphinic dipeptide Gly-Ile analog **1c** (Figure 1) via α'-substitution dependent adamantyl protection followed by our previously reported bis-deprotection strategy.

Fig. 1. Structures of Phosphinic Pseudodipeptides.

Results and Discussion

As we described previously, our general strategy for the synthesis of **1c** involved the formation of a new phosphorous-carbon bond followed by adamantyl protection and finally $Pd(C)/H_2$ reduction (Figure 2). We have successfully synthesized Cbz-protected aminomethyl phosphinic acid **2** starting from commercially available ammonium hypophosphite using previously described literature procedures [9-12]. Michael-type addition of **2** with acrylate **3** which in turn was prepared [13] from commercially available benzyl acetoacetate ester afforded Cbz-protected phosphinic pseudodipeptide benzyl ester **4** in 80% yield. However, esterification of **4** by applying our previously reported procedure [9] using in situ generated phosphinic acid chloride with the sodium salt of adamantanol failed to provide protected dipeptide **5**. The
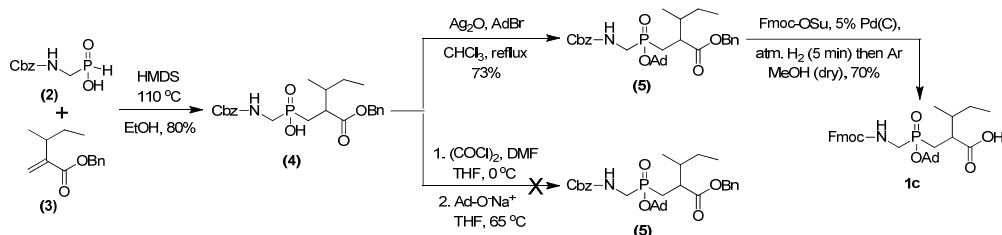

Fig. 2. Synthetic scheme of pseudodipeptide 1c.

adamantyl protection was achieved by treating **4** with Ag$_2$O and AdBr under refluxing condition in chloroform solvent under inert atmosphere [14]. This alternate esterification method provided fully protected phosphinic pseudodipeptide **5** in 73% yield. Finally catalytic hydrogenation of **5** with 5% Pd/C under hydrogen (atm. pressure) in the presence of Fmoc-OSu afforded desired pseudo-dipeptide **1c** in 70% yield (Figure 2).

Conclusion

We have successfully developed an easy and scalable method for the synthesis of Fmoc-protected Gly-Ile phosphinic pseudodipeptide. Large scale preparation of this building block will allow us to synthesize transition state analog triple helical matrix metalloproteinase inhibitors and evaluate their MMP inhibition potency.

Acknowledgments

References

1. Egeblad, M., Werb, Z. *Nat. Rev. Cancer* **2**, 161-174 (2002).
2. Fingleton, B. *Curr. Pharm. Design* **13**, 333-346 (2007).
3. Vassiliou, S., Mucha, A., Cuniasse, P., Georgiadis, D., Lucet-Levannier, K., Beau, F., Kannan, R., Murphy, G., Knauper, V., Rio, M.C., Basset, P., Yiotakis, A., Dive, V. *J. Med. Chem.* **42**, 2610-2620 (1999).
4. Buchardt, J., Schiodt, C.B., Krog-Jensen, C., Delaissé, J.-M., Foged, N.T., Meldal, M. *J. Comb. Chem.* **2**, 624-638 (2000).
5. Yiotakis, A., Vassiliou, S., Jiráček, J., Dive, V. *J. Org. Chem.* **61**, 6601-6605 (1996).
6. Buchardt, J., Ferreras, M., Krog-Jenson, C., Delaissé, J-M., Foged, N.T., Meldal, M. *Chem. Eur. J.* **5**, 2877-2884 (1999).
7. Lauer-Fields, J., Brew, K., Whitehead, J.K., Li, S., Hammer, R.P., Fields, G.B. *J. Am. Chem. Soc.* **129**, 10408-10417 (2007) and references cited therein.
8. Lauer-Fields, J., Whitehead, J.K., Li, S., Hammer, R.P., Brew, K., Fields, G.B. *J. Biol. Chem.* **283**, 20087-20095 (2008).
9. Bhowmick, M., Sappidi, R.R., Fields, G.B., Lepore, S.D. *Peptide Science* **96**, 1-3 (2011).
10. Li, S., Whitehead, J.K., Hammer, R.P. *J. Org. Chem.* **72**, 3116-3118 (2007).
11. Maligres, P.E., Houpis, I., Rossen, K., Molina, A., Sager, J., Upadhyay, V., Wells, K.M., Reamer, R.A., Lynch, J.E., Askin, D., Volante, R.P., Reider, P.J. *Tetrahedron* **53**, 10983-10992 (1997).
12. Lauer-Fields, J., Whitehead, J.K., Li, S., Hammer, R.P., Brew, K., Fields, G.B. *J. Biol. Chem.* 283, 20087-20095 (2008).
13. Lee, H-S., Park, J-S., Kim, B.M., Gellman, S.H. *J. Org. Chem.* **68**, 1575-1578 (2003).
14. Buchardt, J., Ferreras, M., Krog-Jenson, C., Delaissé, J-M., Foged, N.T., Meldal, M. *Chem. Eur. J.* **5**, 2877-2884 (1999).

Synthesis of Small Peptides to Probe Oligomeric Enzyme Structure in Pyrimidine Biosynthesis

Betsy Huang, Allesha Cutlip, Raneem AlKhatib, Mahalakshmi Kotichukkala, Hedeel Evans, and Deborah L. Heyl

Department of Chemistry, Eastern Michigan University, Ypsilanti, MI, 48197, U.S.A.

Introduction

The early steps of pyrimidine biosynthesis are catalyzed by the enzymes carbamoyl phosphate synthetase (CPSase), aspartate transcarbamoylase (ATCase), and dihydroorotase (DHOase), which are commonly expressed separately and either function independently or associate into multifunctional complexes (Figure 1). In mammals, the enzymes are expressed as a single polypeptide chain (CAD) in the order CPS-DHO-ATC and associate into a hexamer [1,2]. The three-dimensional structure of the noncovalent oligomer of DHOase and ATCase from the *Aquifex aeolicus* organism shows three active site loops that are disordered in the free, inactive form, and are ordered in the complex [3]. In this project, a peptide was designed and synthesized to mimic the contact interface between the *Aquifex aeolicus* DHOase and ATCase domains, aimed at disrupting their physical association and/or functional interaction. A decrease in activity of this enzyme complex would result in a reduction in the rate of de novo pyrimidine biosynthesis, diminishing the precursors for DNA in proliferating cells.
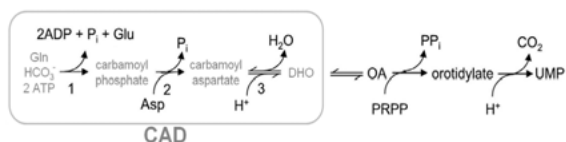
Results and Discussion

Fig. 1. De novo pyrimidine biosynthetic pathway.

NEGEVSALLGLS is a sequence within the DHOase that interacts with ATCase. The peptide was synthesized using solid phase techniques (Fmoc protection strategy) and cleaved from the resin with trifluoroacetic acid (TFA)/scavenger solution followed by precipitation with cold diethyl ether. After lyophilization, it was then purified by reverse-phase high performance liquid chromatography (RP-HPLC) with a gradient of water and acetonitrile (0.1% TFA). Peptide NEGEVSALLGLS (MW: 1187 g/mol) purity and identity were confirmed by RP-HPLC and mass spectrometry. DHOase and ATCase purity and identity were confirmed by SDS-PAGE, and the peptide was assayed using DHOase alone, ATCase alone, and DHOase-ATCase Complex (DAC) to study its effect on enzymatic activity in a colorimetric assay based on product formation. Results are provided in Figure 2.
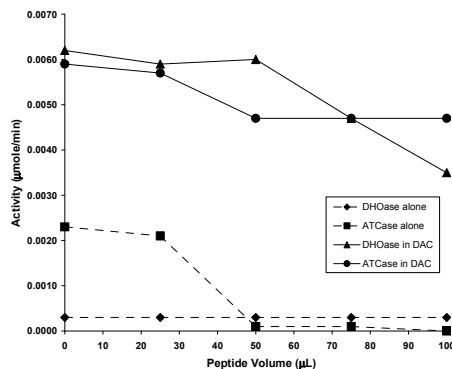

Fig. 2. Aquifex aeolicus ATCase, DHOase, and DAC (ATCase in complex, lower line and DHOase in complex, top) enzyme assay with peptide NEGEVSALLGLS.
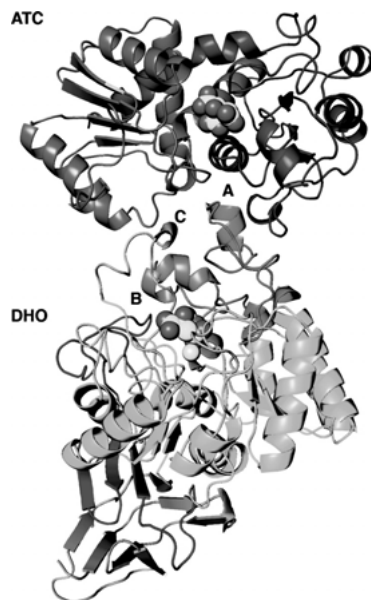
Fig. 3. Quaternary protein structure of ATCase and DHase heterodimer.

The peptide solution (1mg/mL in DMSO, 8.42 x 10^{-4} M) was added in final concentrations of 25 μL (2.1×10^{-5} M), 50 μL (4.2×10^{-5} M), 75 μL (6.3×10^{-5} M), and 100 μL (8.4×10^{-5} M) to a 1 mL assay reaction. Peptide NEGEVSALLGLS greatly decreased the activity of ATCase by itself in a concentration dependent manner; the enzyme completely lost function at high peptide concentration. DHOase was not expected to be active alone since it requires the ATCase for activity, and results confirmed that assumption.

In the DAC complex, the peptide NEGEVSALLGLS reduced the activity of both DHOase and ATCase to a similar extent (a reduction of about 20% for ATCase and 40% for DHOase at the highest peptide concentration tested, compared to the activity without the peptide). This may indicate an interruption of the functional and/or physical oligomeric interaction between the DHOase and the ATCase components (Figure 3). Since the peptide mimics the loop on DHOase where it interacts with ATCase, it may compete for interaction with the ATCase enzyme and disrupt formation of the complex. Interestingly, the extent of inhibition of ATCase by the peptide was lower in the DAC complex than alone, indicating that the DHOase is somewhat protective from the peptide's effect and suggesting that complex formation between ATCase and DHOase shields ATCase from inhibition by the peptide.

Future work will include the synthesis and testing of other peptides of four to twelve amino acids to further probe the oligomeric structure in this enzyme as well as cross-linking studies to determine if the loss of functional interaction/activity is indeed linked to changes in oligomeric enzyme structure. Understanding this process has potential application in several pharmaceutical areas, including antibacterial therapeutics and cancer chemotherapy.

Acknowledgments

References

1. Ahuja, A., Purcarea, C., Ebert, R., Sadecki, S., Guy, H.I., Evans, D.R. *J. Biol. Chem.* **279**(51), 53136-53144 (2004).
2. Evans, D.R., Guy, H.I. *J. Biol. Chem.* **279**(32), 33035-33038 (2004).
3. Zhang, P., Martin, P.D., Purcarea, C., Vaishnav, A., Brunzelle, J.S., Fernando, R., Guy-Evans, H.I., Evans, D.R., Edwards, B.F. *Biochemistry* **48**(4), 766-778 (2009).

Design and Application of Bpa-Containing Peptides for Studying Ras-Converting Enzyme

Kelly Kyro[1], Walter K. Schmidt[2], and Mark D. Distefano[1]

[1]*Departments of Chemistry and Medicinal Chemistry, University of Minnesota, Minneapolis, MN, 55455, U.S.A.;* [2]*Department of Biochemistry and Molecular Biology, University of Georgia, Athens, GA, 30602, U.S.A.*

Introduction

The post-translational modification steps of protein prenylation are key processes in the Ras pathway of oncogenic signal transduction. Ras membrane localization and subsequent downstream signaling is dependent upon enzymatic processing of a tetrapeptide "CAAX box" sequence possessing a prenylcysteine moiety. One such processing enzyme, the membrane associated prenyl protease Rce1, is responsible for endoproteolytic removal of the *C*-terminal "AAX" tripeptide from prenylated Ras proteins. However, due to its membrane-bound nature, purification has been challenging and its mechanism of proteolysis and active site sequence have yet to be fully defined [1,2].

Results and Discussion

Site-directed mutagenesis has been a useful approach to identify residues involved in Rce1 substrate binding [2]. Here, we describe an additional tool for mapping the binding pocket of Rce1. Employing an activity-based, chemical profiling approach a series of four, 9-aa K-Ras-derived farnesylated "CAAX" peptides that serve as substrate analogues for Rce1 were developed. These photoactive peptides were designed to crosslink to and label residues in or near the Rce1 active site due to incorporation of an unnatural amino acid residue, *p*-benzoyl-*L*-phenylalanine (Bpa), proximal to the naturally recognized farnesyl cysteine moiety. Bpa residues are useful in photoaffinity labeling experiments due to their ability to form a covalent adduct with the target protein upon UV irradiation [3]. By alternately substituting Bpa into the P9 (K) (Peptide **1**) through P6 (T) (Peptide **4**) positions of the *C*-terminal K-Ras sequence KSKTKC(farnesyl)VIM [4], substrate activity and photolabeling efficiency of the Bpa-containing peptides was examined. Incorporation of biotin on the *N*-terminus of the peptides allowed photolabeled Rce1 to be isolated via a pull-down and the labeling was characterized by Western blotting.
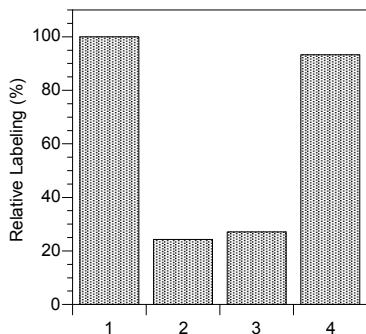
Yeast membranes over-expressing Rce1 [2] were photolyzed in the presence of the Bpa-containing peptides for 30 min prior to precipitation of the protein and subsequent streptavidin pull-down. Following SDS-PAGE electrophoresis, the protein was transferred to a PVDF membrane and cross-linking was visualized using antibodies against HA-tagged Rce1. The labeling efficiency of **1** and **4** was approximately the same, with **1** labeling the enzyme slightly better than **4** (Figure 1). Peptides **2** and **3** labeled Rce1 25-30% less than **4**, so were not used further. Due to its superior solubility, **4** was used in subsequent experiments.

*Fig. 1. Densitometric quantification of labeling efficiency of Bpa Peptides **1-4**.*

Additional evaluation of the substrate activity of Rce1 on **4** involved performing proteolysis assays to characterize the product of Rce1-catalyzed cleavage, **4'** (Figure 2). Following 4 h of incubation of peptide **4** with Rce1 at rt, reactions were separated by RP-HPLC. A 79% conversion of **4** to **4'** representing a 4:1 ratio of product to starting material was determined by integrating the full-length and product peaks in the chromatogram. MS/MS sequencing of **4'** established its structure and confirmed the site of proteolysis.

A known Rce1 substrate, Abz-KSKTKC(farnesyl)K(Dnp)IM [5], was used in competition experiments with **4**. Increasing amounts of the known substrate were added in a photolysis experiment with **4** to test its substrate specificity. Western blotting of the labeling showed that as increasing amounts of competitor were added, the extent of labeling by **4** decreased indicating that the two compounds were competing for the same binding site in Rce1.
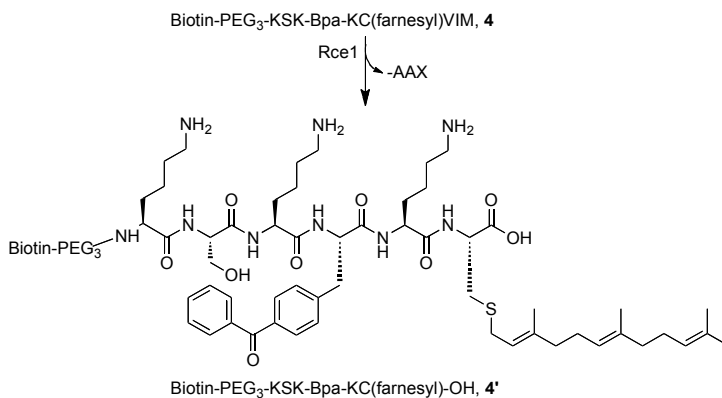

Fig. 2. *Rce1-catalyzed –AAX cleavage of Peptide 4.*

We have demonstrated that Bpa-containing peptides have potential use for further investigation into the mechanism and active site sequencing of Rce1. By increasing the labeling efficiency of substrate photoprobes, further structural information on Rce1 may be obtained via isolation and characterization of the covalent photoadduct formed by peptide probe and the enzyme.

Acknowledgments

References

1. Dolence, E., Dolence, J., Poulter, C. *Bioconjugate Chem.* **12**, 35-43 (2001).
2. Plummer, L., Hildebrandt, E., Porter, S., Rogers, V., McCracken, J., Schmidt, W. *J. Biol. Chem.* **281**, 4596-4605 (2006).
3. Dorman, G., Prestwich, G.D. *Biochemistry* **33**, 5661-5673 (1994).
4. Hollander, I., Frommer, E., Mallon, R. *Anal. Biochem.* **289**, 129-137 (2000).
5. Hollander, I., Frommer, E., Aulabaugh, A., Mallon, R. *Biochim. Biophys. Acta* **1649** (1), 24-29 (2003).

Light Activatable, Fluorescence Reporting cAMP Dependent Protein Kinase

Hsien-Ming Lee[1], Weichen Xu[2], and David S. Lawrence[2]

[1]Institute of Chemistry, Academia Sinica, Taipei, 115, Taiwan; [2]Department of Chemistry, University of North Carolina at Chapel Hill, Chapel Hill, NC, 27599, U.S.A.

Introduction

Light-activatable (also known as "caged") protein is a useful chemical biology tool. It provides a means to control the timing and the location of the protein activation, and potentially allow us to further control the cellular behavior. Fluorescence, on the other hand, is an important readout that is widely used in cellular biology to report the concentration, activity, and location of the protein of interest. In 2004, Muir and his colleagues, using an engineered protein prepared via the expressed protein ligation method, produced a photo-activatable protein with a fluorescent response [1]. In this manuscript, we report a strategy that utilizes active site recognition for propinquity labeling of a non-active site residue. This approach is a more general, and potentially more widely applicable, method for preparing caged and profluorescent proteins. cAMP-dependent protein kinase (PKA), an important signal transduction kinase, was chosen to demonstrate this methodology. The catalytic subunit (C) of PKA contains two readily modifiable Cys residues, one at the base of the active site (Cys-199) and the other approximately 20 Å away in the c-term tail region (Cys-343). In the past, PKA catalytic subunit was caged by installing a thiol-reactive caging group directly at Cys 199 in the active site region [2] or at the thiophosphorylated Thr 197 in the activating loop region [3]. Our approach is to selectively conjugate the caging peptide at Cys 343, which has no significant role in structure and activity. After conjugation, this caging peptide can non-covalently block the active site to temporally cease the enzyme activity. The designed caging peptide contains a (i) active site-directed peptide inhibitor to non-covalently block enzyme activity site, (ii) a polyethylene glycol (PEG) spacer to optimally position an appended electrophilic maleimide near Cys-343, and (iii) a tripeptide profluorescent cassette composed of a photolabile (PL) moiety inserted between a fluorophore and a fluorescent quencher to report fluorescence after a successful uncaging [4].

Results and Discussion

The caging peptide (Figure 1) is prepared in a stepwise solid phase synthesis with three subsequent side chain modifications. The peptide backbone was synthesized on the TGR resin with the side chains of the C-terminal Lys orthogonally protected by ivDde to ensure site selective attachment of the fluorophore (TAMRA) and electrophilic (maleimide) components. The hydrazine sensitive
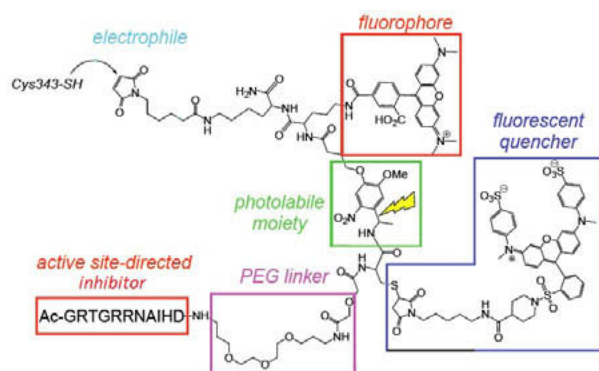
Fig. 1. Structure of PKA caging peptide.

ivDde protecting group was removed first, allowing the TAMRA fluorophore to be positioned at the C-terminal of the photolabile linker. Subsequent global deprotection and cleavage of the peptide from the resin exposed both the Cys and remaining Lys side chain functionalites. The Cys sidechain was modified by the thiol reactive QSY-maleimide first, and the remaining Lys sidechain is modified by the activated N-hydroxysuccinimide (NHS) ester of 6-maleimido-haxanoic acid, which provided the desired caging peptide (Figure 1).

The caged enzyme (<3% residual activity) was acquired by exposing the native C subunit to the caging peptide. The conjugation between PKA catalytic subunits and the caging peptide can be evaluated by SDS-PAGE. The gel migratory and photophysical behavior of the caged and photolyzed enzymes are consistent with light-induced loss of the PKI-PEG-Cys(QSY7) fragment (Figure 2). Specifically, the light exposed C subunit displays enhanced migratory aptitude relative to its higher molecular weight caged counterpart (Figure 2a). In addition, the photolyzed enzyme displays enhanced fluorescence relative to the non-photolyzed species (Figure 2b).
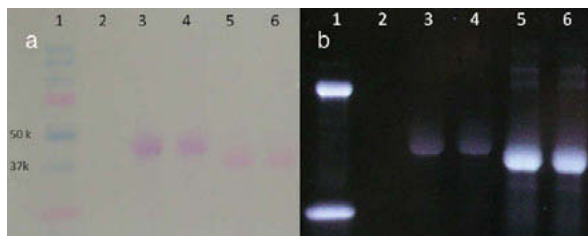

Fig. 2. (a) SDS-PAGE under white light. Lane 1: molecular weight standards; Lane 2: native PKA (not observable without staining); Lanes 3 and 4: caged PKA; Lanes 5 and 6: photolyzed PKA. (b) Under UV light.
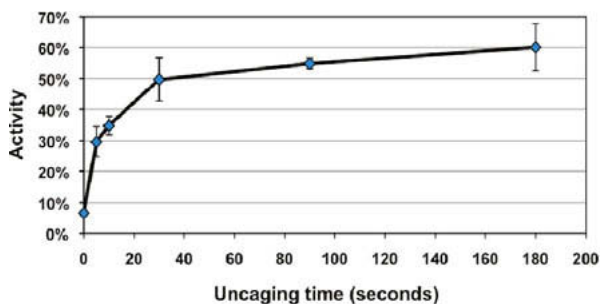
As expected for a light-dependent process, both catalytic activity and fluorescence are enhanced in response to photolysis (Figure 3). In the presence of Prionex (porcine collagen with protein stabilizing properties) maximal restoration of catalytic activity is 80% and the fluorescence enhancement is 10-fold. In the absence of Prionex, 60% of native catalytic activity is recovered, but a 20-fold fluorescence yield is achieved.

We have demonstrated a new enzyme caging methodology using a modifiable Cys moiety that lies outside the active site as a covalent anchoring residue. A fluorescence reporting design have also been incorporated in the photo-uncaging mechanism. This strategy furnishes chemically engineered enzymes that can be remotely controlled in time, space and activity. The fluorescence readout generated from the photolysis can also report the location and the concentration of the photoactivated enzyme. This profluorescent caged enzyme can be an important biological tool in the future.

Fig. 3. Percent protein kinase activity as a function of irradiation time.

Acknowledgments

References

1. Pellois, J.P., Hahn, M.E., Muir, T.W. *J. Am. Chem. Soc.* **126**, 7170-7171 (2004).
2. Chang, C., Fernandez, T., Panchal, R., Bayley, H. *J. Am. Chem. Soc.* **120**, 7661-7662 (1998).
3. Zou, K.Y., Cheley, S., Givens, R.S., Bayley, H. *J. Am. Chem. Soc.* **124**, 8220-8229 (2002).
4. Lee, H.M., Priestman, M.A., Lawrence, D.S. *J. Am. Chem. Soc.* **132**, 1446-1447 (2010).

Rational Design of a Novel Allosteric Peptide that Selectively Inhibits One of δPKC Function

Nir Qvit, Marie-Helene Disatnik, and Daria Mochly-Rosen

Department of Chemical and Systems Biology, Stanford University School of Medicine, Stanford, CA, 94305, U.S.A.

Introduction

Protein kinase C (PKC) is a family of 11 lipid-dependent isozymes that plays a critical role in signal transduction and in a variety of diseases. Upon activation each isozyme can phosphorylate different substrates by localizing to various sub-cellular sites.

Here, we describe a rational design of peptide inhibitors that will regulate just one substrate, Separation-of-Function (SOF) regulators. The first such SOF peptide is an allosteric inhibitor of δPKC phosphorylation of one substrate, the mitochondrial enzyme pyruvate dehydrogenase kinase (PDK). We previously reported that δPKC activation increases cardiac damage after heart attack (cardiac ischemia) through the phosphorylation and activation of PDK, which in turn, phosphorylates and inactivates pyruvate dehydrogenase (PDH) [1]. This δPKC effect results in a decline in ATP regeneration at the period after the ischemic event [2]. We previously reported that the C2 domain of δPKC is critical for protein-protein interactions and therefore focus our study on that domain [3]. Since there are over 60 proteins with a C2 domain, our approach is likely relevant to a number of normal and disease-associated signaling events.

Results and Discussion

We hypothesized that there may be a PDK-like sequence in δPKC that is involved in intra-molecular inhibitory interactions in the enzyme. A sequence homology search identified a five amino acid stretch in δPKC (A_{35}LST$\underline{E}$) that is almost identical to a sequence in PDK (A_{390}LST$\underline{D}$). A number of features of this sequence homology are of interest: i. The homologous sequences are located in an exposed region in the two proteins, available for protein-protein interaction. ii. The homologous sequences are conserved in all the species that express δPKC. iii. ALSTE is found within δPKC C2 domain, the domain that we have already found to be critical in protein-protein interactions [3]. iv. ALSTE is not found in other PKC isozymes. We synthesized ALSTER and named it ψPDK, as a control we also synthesized δV1-5, which completes the β hairpin in δPKC C2 domain. The peptides were conjugated to TAT_{47-57} for intracellular delivery [2,3].

We first demonstrated that ψPDK peptide inhibited δPKC phosphorylation of PDK by ~30% in an *in vitro* kinase assay, but did not affect Drp1 phosphorylation, another δPKC substrate. These data suggest that ψPDK peptide is a specific inhibitor of PDK phosphorylation by δPKC.

As discussed, δPKC phosphorylation of PDK following myocardial infarction (MI) leads to the phosphorylation of PDH. However, after treatment with ψPDK peptide, MI-induced increased phosphorylation of PDK and the subsequent phosphorylation of PDH were inhibited. Moreover, under the same MI conditions, ψPDK peptide did not affect the phosphoryaltion of other δPKC substrates, MARCKS and Drp1, indicating that ψPDK peptide is a specific inhibitor of PDK phosphorylation.

If PDK phosphorylation is critical for δPKC-mediated function, we expected that ψPDK peptide, which selectively inhibits only PDK phosphorylation, should protect the myocardium from MI-induced injury. Using three criteria: MI-induced infarct size, levels of released creatine phosphokinase (CPK), as a marker of myocardial infarction, and the levels of JNK protein phosphorylation, a known marker of cellular stresses and apoptosis, we confirmed that treatment with the ψPDK peptide was sufficient to induced cardiac protection following MI injury.

We also synthesized ψPDK as a single polypeptide connected to TAT_{47-57} through an amide bond with a spacer of 3 amino acids (GSG); ψPDK-GSG-TAT peptide. Interestingly, we found that ψPDK-GSG-TAT was a better δPKC regulator and more cardioprotective as compared with ψPDK-Cs-sC-TAT peptide (Cargo and TAT connected by disulfide bond). Since δPKC phosphorylation of PDK occurs inside the mitochondria, this improved activity of the second

peptide may be due to improved delivery of ψPDK-GSG-TAT into this organelle, although this remains to be determined.

To determining the contribution of each amino acid on the effect of the ψPDK peptide, we used Ala-scan. The ψPDK peptide analogs were then used in the same MI model, but none exerted cardioprotection. These data are consistent with a role for each of the side groups of these amino acids in the interaction with δPKC.

Fig. 1. Scheme representing the mode of action of the SOF ψPDK peptide. ψPDK peptide inhibits PDK phosphorylation (S2), without affecting the phosphorylation of other substrates (e.g., S1; left lower panel). The inhibitory effect of ψPDK differs from δV1-1 peptide [3], which inhibits of δPKC phosphorylation of all substrates in any subcellular compartment (right).
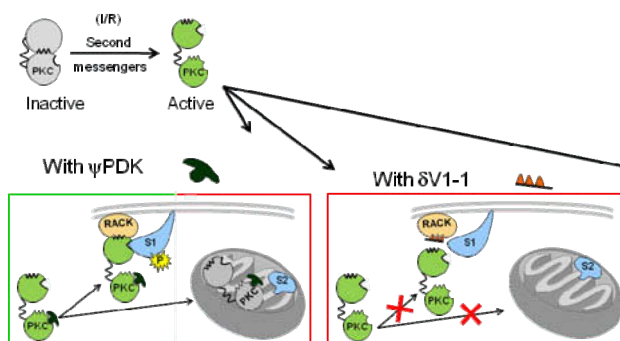
Together, we described a rational approach to identify a peptide inhibitor of just one phosphorylation event of δPKC, a separation-of-function (SOF) inhibitor. This peptide, also called ψPDK SOF, inhibits only δPKC-mediated phosphorylation of PDK and the resulting functions; it does not affect any other δPKC-mediated function. Importantly, ψPDK peptide demonstrates that δPKC-mediated phosphorylation of PDK is likely the main phosphorylation event that is required for δPKC-dependent cardiac injury following an ischemic event.

Inhibitors of signaling enzyme are useful tools for basic research and are important also as therapeutics. To our knowledge, ψPDK is the first SOF inhibitor to be described. Our work demonstrates that SOF peptide inhibitors can be rationally designed and that these peptides provide missing tools to determine the role of one of several cellular functions of, for example, a given PKC isozyme. This approach is likely applicable for other signaling enzymes, enabling the generation of SOF regulators of protein-protein interactions.

Acknowledgments

References

1. Churchill, et al. *Circ. Re.* **97**, 78-85 (2005).
2. Inagaki, et al. *Circulation* **108**, 2304-2307 (2003).
3. Chen, et al. *PNAS* **98**, 11114-11119 (2001).

Synthesis of Novel Dipeptidyl Oxymethyl Ketones as Caspase Inhibitors

Hinyu N. Nedev[1] and H. Uri Saragovi[1,2]

[1]*Lady Davis Institute - Jewish General Hospital, 3999 Cote St. Catherine, Montreal, H3T 1E2, Canada;*
[2]*McGill University, Montreal, H3A 2T5, Canada*

Introduction

Programmed cell death, or apoptosis, is executed by a series of proteases (caspases) [1] that carry out or activate a proteolytic cascade. Increased levels of apoptosis and caspase activity are frequently observed at sites of cellular damage in both acute (e.g. stroke) and chronic (e.g. Alzheimer's, Parkinson's disease) pathological conditions. Thus, inhibition of caspase activity with the aim of reducing cell death, and hence tissue damage, could be beneficial.

Caspase inhibitors could be of therapeutic value [2] in the treatment of inflammatory and degenerative diseases as they might be able to halt or reduce the disease progression. The development of small molecule inhibitors of caspases has been a target of intensive research [3]. However caspase inhibition *in vivo* has proven elusive as an effective and safe approach; bringing into question whether targeting caspases is a sound approach.

Clearly better and more selective reagents are needed to target caspases, especially if they can be delivered specifically to the intended target tissue.
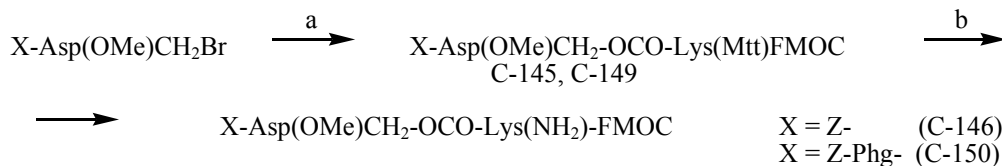
In a previous publication [4], we described phenylglycine derivatives as potent and rather selective caspase inhibitors. One of the oxymethyl ketones synthesized by us (HU44) containing N-terminal phenylglycine and benzoic ring on the C-termini of the scaffold, has very pronounced activity against caspase-3.

Results and Discussion

Herein we describe further optimization of this structural class of caspase inhibitors in order to obtain novel analogues with potent, broad spectrum activity. In addition we coupled the inhibitors to monoclonal antibodies (mAbs) to deliver the inhibitors to the target. MAbs that bind to the extracellular domain of TrkA or TrkC receptors expressed in neurons, were used to deliver caspase inhibitors to neurons.

Novel caspase inhibitors were prepared that can be conjugated to mAb 5C3 (anti-TrkA) or 2B7 (anti-TrkC) [5] for selective delivery. The binding and selectivity of the conjugated mAbs was verified.

The strategy for preparation of bromomethyl ketone peptide derivatives, comprised incorporating Lys as a warhead. The synthesis was performed using N-α-FMOC-N-ε-4-methyltrityl-L-lysine (FMOC-Lys(Mtt)-OH) as a main scaffold. It was attached to the N,O-protected bromomethyl ketone of the respective amino acid prepared *in situ* [4], followed by Mtt deprotection by TFA in dichloromethane, using Scheme 1. The intermediate and final compounds were purified and the structures were confirmed by MS.

X-Asp(OMe)CH$_2$Br $\xrightarrow{\text{a}}$ X-Asp(OMe)CH$_2$-OCO-Lys(Mtt)FMOC $\xrightarrow{\text{b}}$
C-145, C-149

$\longrightarrow$ X-Asp(OMe)CH$_2$-OCO-Lys(NH$_2$)-FMOC

X = Z-   (C-146)
X = Z-Phg- (C-150)

Scheme 1. Synthesis of C-146 [Z-Asp(OMe)CH$_2$-OCO-Lys(ε-NH$_2$)-α-FMOC] and C-150 [Z-Phg-Asp(OMe)CH$_2$-OCO-Lys(ε-NH$_2$)-α-FMOC]; (a). FMOC-Lys(Mtt)-OH, KF, 4h RT; (b). 1% TFA/DCM.

The next part of our work was directed towards the attachment of these drug molecules to the carrier SPDP (N-succinimidyl 3-(2-pyridyldithio)-propionate) and conjugation with two monoclonal antibodies: 5C3 (for TrkA) and 2B7 (for TrkC). The reactions of conjugation were carried out at 4°C, followed by three dialyses against PBS. The coupling reaction between dipeptide C-146 and mAb 2B7 is illustrated on the Scheme 2.

Data from the FACS (Figure 1) shows similarity in the binding activity for the free 5C3 mAb and the respective conjugate with C-146. In contrast, the conjugate of C-150 with 5C3 has lost some of its binding activity. Thus, each conjugate requires a certain degree of optimization so that the targeting moiety remains active.
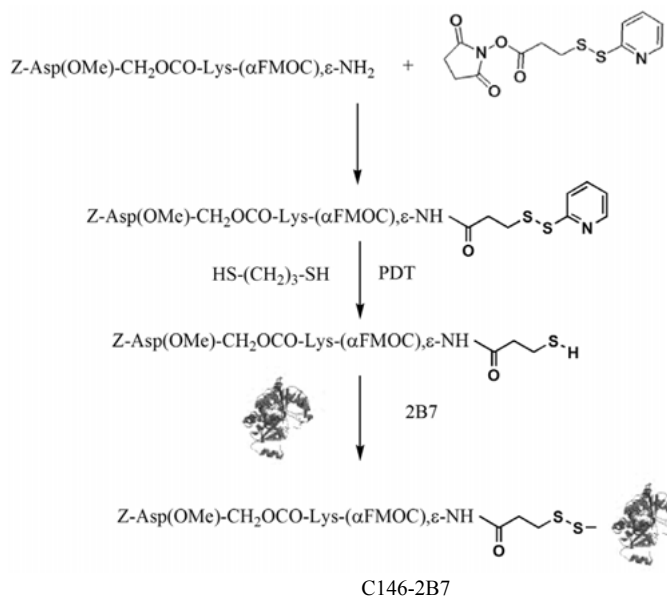
Scheme 2. Preparation of the conjugate C-146-2B7. (C-146-5C3 and C-150-5C3 conjugates were synthesized following the same reaction scheme).
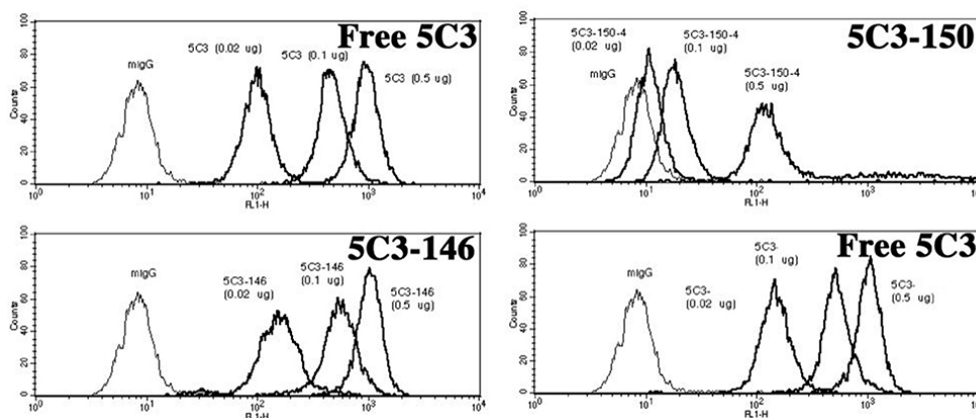

Fig. 1. Binding activity of the conjugates compared to free mAbs.

Conclusion

Novel caspase inhibitors were designed, prepared and conjugated to receptor-targeting mAbs. This approach will allow testing the hypothesis that targeted delivery of caspase inhibitors may be beneficial, with reduced side effects and improved efficacy.

References

1. Otto, H.H., Schirmeister, T. *Chem. Rev.* **97**, 133-171 (1997).
2. Talanian, R.V., Brady, K.D., Cryns, V.L. *J. Med. Chem.* **43**, 3351-3371 (2000).
3. Cai, S.X., Drewe, J., Wang, Y., Weber, E. *US Patent* 1999, WO99/47154.
4. Nedev, H., Klaiman, G., LeBlanc, A., Saragovi, H.U. *BBRC* **336**, 397-400 (2005).
5. Guillemard, V., Ivanisevic, L., Saragovi, H.U., et al. *Dev. Neurobiol.* **15**, 70(3), 150-164 (2010).

Preparation and Analysis of One-Bead One-Compound Libraries for Studying Protein Prenylation Specificity

Yen-Chih Wang and Mark Distefano

Department of Chemistry, University of Minnesota, Minneapolis, MN, 55455, U.S.A.

Introduction

Protein prenylation is a common post-translational modification of specific protein-derived cysteine residues in eukaryotic cells. Previous experiments with tetrapeptide sequences identified the so-called C-terminal CaaX box motif as the key structural element recognized by protein farnesyltransferase (PFTase) and geranylgeranyltransferase (GGTase) [1]. However, the sequence specificities of these enzymes remain unclear [2]. Here we describe the synthesis of peptides containing free C-termini on solid supports and their reactions with PFTase.

Results and Discussion

We applied a general method [3] to synthesize peptides containing free C-termini. In order to analyze peptides with free C-termini on beads, a linker should be installed so that the peptides can be cleaved from the beads and sequenced by MS/MS. A photocleavable linker was chosen because it is orthogonal to other functional groups and the cleavage conditions need no other reagents except light. The photocleavable linker we chose has the advantage that the by products of photolysis remain on the beads so that they do not interfere with the subsequent assays (Figure 1).
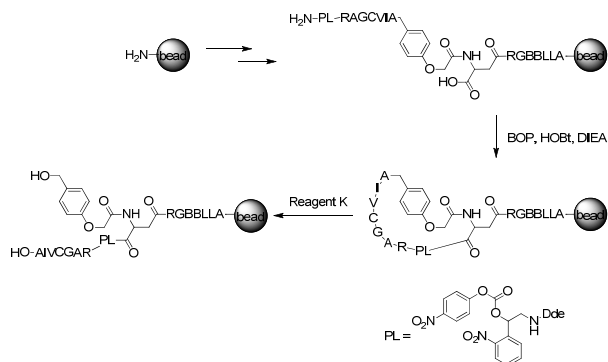

Fig. 1. Synthesis of inverted peptides.

To perform enzymatic reactions on beads, we employed three types of solid supports (TentaGel, PEGA, CPG) [4]. We found that only when we used controlled pore glass as the solid phase, can we detect prenylated peptides by MS. This implies that only CPG is sufficiently porous to permit access to PFTase and GGTase which are large 90 kDa heterodimeric proteins.

We then synthesized four different sequences (RAGCVIA, RAGCVLL, RAGCVIL, RAGSVIA) and subjected them to yeast PFTase-mediated prenylation followed by photochemical release (Figure 2). Because RAGCVIA is an optimized substrate for PFTase, most of the released peptides are prenylated with only a small amount of starting peptides remaining. RAGCVLL and RAGCVIL are poor substrates for PFTase hence we still detected predominantly starting peptides after the reaction. It was reported that cysteine is required for prenylation to occur so when we substituted cysteine with serine, we did not detect any prenylated products. These results are in agreement with previous reports using peptides in solution. This strategy opens the door to generating a one-bead one-compound peptide library. Screening of that library and sequencing of the hits should allow us to completely define the substrate specificity of PFTase and GGTase. Such information should also be useful for identifying all possible substrates for prenylation.
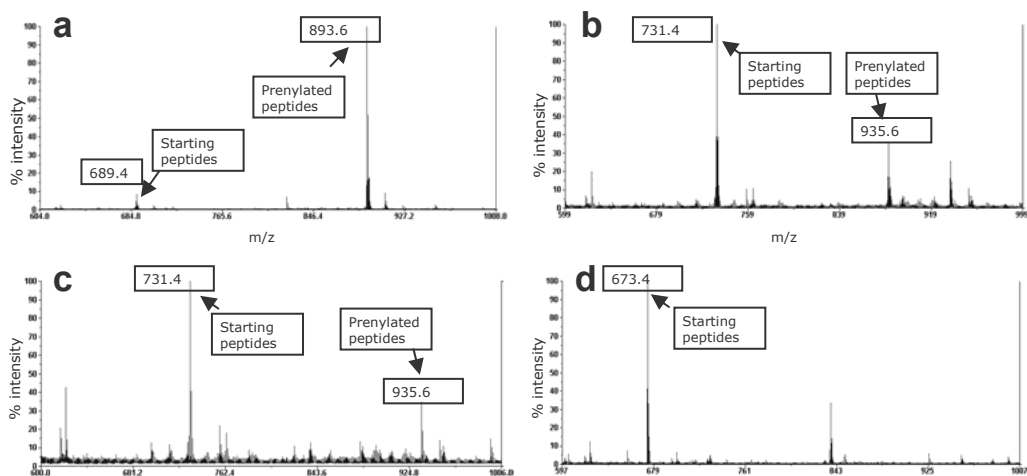
Fig. 2. MALDI-MS analysis of a) RAGCVIA beads prenylated with FPP by FTase for 3h; b) RAGCVIL beads prenylated with FPP by FTase for 3h; c) RAGCVLL beads prenylated with FPP by FTase for 3h; d) RAGSVIA beads prenylated with FPP by FTase for 3h.

Acknowledgments

References

1. Reid, S.T., et al. *J. Mol. Bio.* **343**, 417 (2004).
2. Hougland, J.S., et al. *Biochemistry* **48**, 1691 (2009).
3. Pei, D., Joo, S.H. *Biochemistry* **47**, 3061 (2008).
4. Bradley, M., et al. *Chem. Eur. J.* **8**, 3769 (2002).

The Role of Protein Kinase C Epsilon in the Regulation of Endothelial Nitric Oxide Synthase (eNOS) During Oxidative Stress Caused by Extracorporeal Shock Wave Lithotripsy (ESWL)

Edward S. Iames, Kerry-Anne Perkins, Qian Chen, and Lindon Young

Department of Pathology, Microbiology, Immunology, and Forensic Medicine, Philadelphia College of Osteopathic Medicine, Philadelphia, PA, 19131, U.S.A

Introduction

ESWL is an effective, non-invasive therapy utilized to fragment stones in the kidney and urinary tract. A lithotripter generates high-energy acoustic pulses and propagates those shock waves through a lens towards focal point at the location of the stone. After treatment, fragmentation of the stone allows debris to be cleared by flow of the urinary tract. Although lithotripsy provides a safer alternative to invasive treatments, ESWL may cause prolonged vasoconstriction after ESWL treatment, reducing renal blood flow and resulting in subsequent endothelial dysfunction, which may cause kidney damage leading to acute to chronic hypertension clinically [1]. ESWL-induced vascular oxidative stress and further endothelial dysfunction may be mediated by reduced levels of endothelial-derived nitric oxide (NO) and/or increased reactive oxygen species. Previously we have shown that ESWL increases hydrogen peroxide (H_2O_2) release and decreases NO release, resulting in decreased NO bioavailability and increased oxidative stress [2]. When the dihydrobiopterin to tetrahydrobiopterin ratio is increased, eNOS becomes uncoupled and produces superoxide (SO) instead of NO [3]. SO is converted to H_2O_2 by superoxide dismutase. Protein kinase C epsilon (PKC-ε) positively regulates eNOS activity by phosphorylation at Ser-1177 and is expressed in endothelial cells, but not in leukocytes. Previously it was shown that cell-permeable myristoylated (Myr) PKC-ε activator (PKC-ε+) and inhibitor (PKC-ε-) peptides dose-dependently increased and decreased NO release, respectively, in aortic tissue [4]. By using PKC-ε activator and inhibitor peptides, we can determine the role of PKC-ε in ESWL-induced oxidative stress through regulating eNOS.

Results and Discussion

We hypothesized that ESWL can increase H_2O_2 and decrease NO in the blood of rat renal veins compared to those with no ESWL exposure, both with saline infusion. We predict that the PKC-ε peptide inhibitor (N-Myr-EAVSLKPT, MW=1054, Genemed Synthesis, San Antonio, TX) would decrease ESWL-induced H_2O_2 release and increase NO bioavailability compared to ESWL-saline control rats. By constrast, we predict the PKC-ε activator (N-Myr-HDAPIGYD, MW=1097, Genemed Synthesis) will show a similar increase/decrease in H_2O_2/NO release, respectively, in the blood of rat renal veins in comparison to ESWL-saline control rats. The PKC-ε activator and inhibitor peptides work by facilitating or inhibiting PKC ε translocation to the cell membrane, respectively, thereby promoting or inhibiting PKC ε phosphorylation of cell membrane substrates such as eNOS.

Upon catheterization of the left renal vein with a 22-gauge catheter, a selective H_2O_2 or NO microsensor (100μm) was inserted through the catheter and connected to a free radical analyzer, TBR-4100 (World Precision Instruments, Sarasota, FL). After establishment of a stable baseline, ESWL treatment was induced by a Dornier Epos Ultra HE (high-energy) lithotripter (Multimed Technical Services, Inc., Beltsville, MD). A total of 1000 shocks, 13 minutes of shockwave treatment, at 16kV intensity were transmitted; 500 shocks at 60 beats per minute followed by 500 shocks at 120 beats per minute. Immediately post-ESWL treatment, 0.5mL saline or drug bolus was infused through the jugular vein followed by 0.5mL of saline as a flush. Real-time measurements of H_2O_2 or NO were made throughout the duration of the experiment and recorded every five minutes for 30 minutes post-treatment. The recorded electrical signal in picoamps was converted to molar concentration using the standard curve from each calibration. Multiple groups were compared using ANOVA with Bonferroni-Dunn post-hoc tests.

Experimental Groups: (NO or H_2O_2) Group 1: No-ESWL, Saline infusion (Control) (n=5), Group 2: ESWL, Saline infusion (Control) (n=6), Group 3: ESWL, 0.8mg/kg (10μM) PKC-ε inhibitor (-) (n=5), Group 4: ESWL, 0.9mg/kg (10μM) PKC-ε activator (+) (n=5).
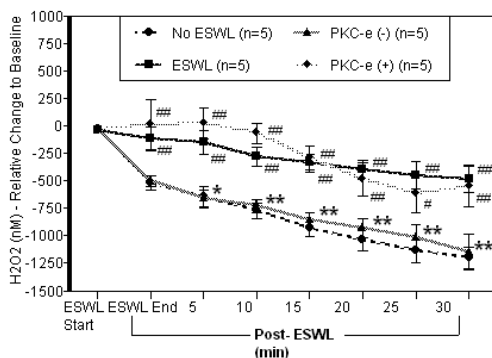

Fig. 1. Real-time H_2O_2 changes relative to baseline. This graph shows change in H_2O_2 renal vein blood values post-ESWL. ESWL significantly induced a 700nM increase in H_2O_2 release compared to no-ESWL ($^\#p \leq 0.05$, $^{\#\#}p \leq 0.01$) and this effect was significantly attenuated by PKC-ε inhibitor, lowering levels similar to no-ESWL (*$p \leq 0.05$, **$p \leq 0.01$, compared to ESWL). PKC-ε activator H_2O_2 levels significantly increased by 650nM compared to no-ESWL controls ($^\#p \leq 0.05$, $^{\#\#}p \leq 0.01$) and was similar to ESWL-saline.
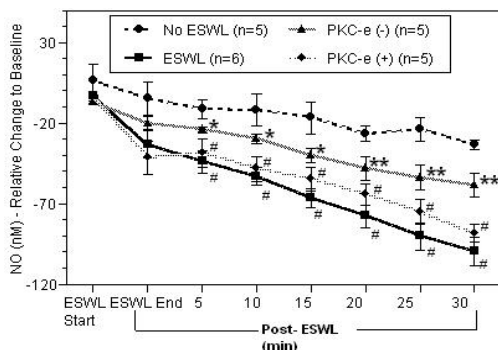

Fig. 2. Real-time NO changes relative to baseline. This graph shows change in NO renal vein blood values post-ESWL. ESWL significantly induced a 66nM decrease in NO release compared to no-ESWL ($^\#p \leq 0.01$) and this effect was significantly attenuated by PKC-ε inhibitor (*$p \leq 0.05$, **$p \leq 0.01$, compared to ESWL). By contrast, PKC-ε activator was similar to control ESWL and significantly decreased NO release by 53nM compared to no-ESWL controls ($^\#p \leq 0.01$).

In ESWL-treated rats, blood H_2O_2/NO significantly increases/decreases post-ESWL compared to no-ESWL controls (Figures 1 and 2). This supports our hypothesis that oxidative stress is induced by ESWL treatments and NO bioavailability is reduced. PKC-ε activator was similar to ESWL-saline controls, which may be principally due to increased uncoupled eNOS activity. PKC-ε inhibitor significantly attenuated ESWL-induced effects on H_2O_2 increase and NO decrease. The data suggests beneficial effects of PKC-ε inhibitor may be due to inhibition of uncoupled eNOS activity which may be the primary source of oxidative stress post-ESWL since PKC-ε inhibitor reduces H_2O_2 levels to near no-ESWL levels. By using PKC-ε inhibitor after ESWL, the decreased oxidative stress can attenuate vascular endothelial dysfunction to the renal vasculature. The data suggests that PKC-ε inhibitor may be applied clinically post-ESWL to reduce vascular complications that can lead to development of hypertension.

Acknowledgments

References

1. McAteer, J.A., Evan, A.P. *Semin. Nephrol.* **28**(2), 200-213 (2008).
2. Chen, Q., et al. *Curr. Topics in Pharmacol.* **14,** 11-24 (2010).
3. Vasquez-Vivar, J., et al. *Biochem. J.* **362**, 733-739 (2002).
4. Teng, J.C., et al. *Naunyn-Schiemedeberg's Arch. Pharmacol.* **378,** 1-15 (2008).

Effects of Protein Kinase C Selective Beta II Peptide Inhibitor on Real-Time Blood Nitric Oxide and Hydrogen Peroxide Release Under Acute Hyperglycemia

Michael Minni, Qian Chen, Kyle Bartol, Edward Iames, Maria Kern, Kerry-Anne Perkins, Brian Rueter, and Lindon Howard Young

Department of Pathology, Microbiology, Immunology & Forensic Medicine, Philadelphia College of Osteopathic Medicine (PCOM), Philadelphia, PA, 19131, U.S.A.

Introduction

Vascular endothelial dysfunction is one of the earliest recognizable events under hyperglycemic conditions. It is characterized by decreased endothelium-derived nitric oxide (NO) from endothelial NO synthase (eNOS) and increased oxidative stress, such as superoxide and hydrogen peroxide (H_2O_2). In a state of hyperglycemia, the enzyme protein kinase C (PKC), especially PKC beta II, becomes stimulated, which activates NADPH oxidase generating superoxide and also inhibits eNOS attenuating NO production. Moreover, superoxide can either directly quench NO to form peroxynitrite (ONOO-) or be converted to H_2O_2 by superoxide dismutase. Both ONOO- and H_2O_2 can promote eNOS uncoupling to produce superoxide instead of NO. Therefore, more superoxide is generated and less NO is remained available. Thereby, a vicious cycle can propagate causing vascular endothelial damage and if prolonged can ultimately cause organ failure.

Recently, we have developed a novel acute hyperglycemia-induced oxidative stress rat model by measuring blood NO and H_2O_2 in real-time. Moreover, a selective cell permeable myristoylated (Myr) PKC beta II peptide inhibitor exhibited the anti-oxidant and anti-inflammatory effects under ischemia/reperfusion conditions [1,2]. Therefore, it is intriguing to test if this selective PKC beta II peptide inhibitor (N-Myr-SLNPEWNET, mol.wt.= 1300, Genemed Synthesis, San Antonio, TX) would attenuate the oxidative stress and/or enhance NO bioavailability to stop the vicious cycle triggered by hyperglycemia. The mechanism of action of PKC beta II inhibitor is that it binds to its receptor-activated C kinase region. This binding can serve to inhibit PKC translocation and ultimately attenuate the formation of superoxide [3].

From these previous findings we hypothesized that the administration of the selective PKC beta II peptide inhibitor will cause a significant decrease in superoxide and subsequent H_2O_2 production and increase in endothelial-derived NO in blood under acute hyperglycemic conditions.

Results and Discussion

Rats were anesthetized and the carotid artery was catheterized to monitor mean arterial blood pressure (MABP). The MABP ranged from 90-130mm Hg throughout the entire experiment. Moreover, the jugular vein was also catheterized for intravenous infusion of saline, 20% or 30% D-glucose, or 30% D-glucose with PKC beta II inhibitor (1.08 mg/kg, ~ 10 µM in blood) for 3 hrs, respectively. The blood glucose in saline group was maintained around 80-100 mg/dl (i.e. euglycemia) throughout the whole experiment. By contrast, hyperglycemic conditions were induced and maintained at about 200 mg/dl after 20 min infusion of 20% D-glucose. Moreover, 30% D-glucose or 30% D-glucose with PKC beta II inhibitor treated rats reached about 400 mg/dl hyperglycemia after 20-40 min infusion. All the hyperglycemic rats urinated between 20-40 min after glucose infusion.

Blood NO and H_2O_2 were measured in real-time with the calibrated NO and H_2O_2 sensors (100 µm, WPI, Sarasota, FL), one in each femoral vein, respectively. The changes of blood H_2O_2 levels in different experimental groups relative to saline group were illustrated in the left panel of Figure 1. The 200 mg/dl and 400 mg/dl hyperglycemic groups exhibited a dose-dependent increase in blood H_2O_2 levels throughout the experiment compared to the saline group (*$p<0.05$ compared to saline). By contrast, 400 mg/dl with PKC beta II peptide inhibitor group demonstrated significantly reduced blood H_2O_2 levels at 20 min, 60 min, 80 min, 100 min and 180 min compared to the 400 mg/dl group (#$p<0.05$).

The changes of blood NO levels in different experimental groups relative to saline group were shown in Figure 1 right panel. The 200 mg/dl and 400 mg/dl hyperglycemic groups

showed a dose-dependent decrease in blood NO levels compared to the saline group (*p<0.05 compared to saline). By contrast, 400 mg/dl with PKC beta II peptide inhibitor group exhibited significantly higher blood NO levels throughout the experimental period compared to the 400 mg/dl group (#p<0.05) and were similar to the saline group.
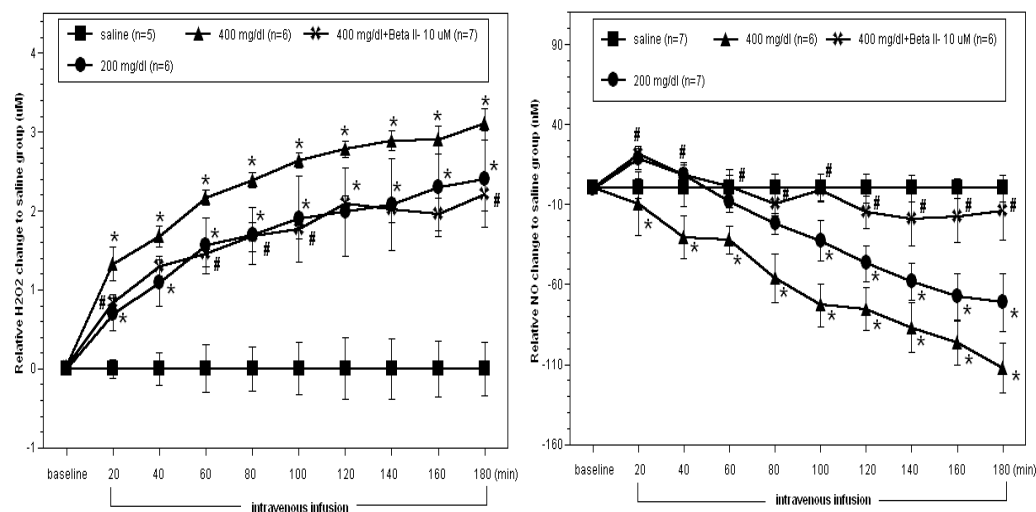

Fig. 1. The changes of blood H_2O_2 (left panel) and NO levels (right panel) in different experimental groups relative to saline group. *p<0.05 compared to saline; #p<0.05 compared to 400 mg/dl hyperglycemic group by ANOVA using Fisher's test.

These results demonstrate that the use of PKC beta II peptide inhibitor attenuated oxidative stress and the decreased levels of NO in blood caused by hyperglycemia. The effects of PKC beta II inhibitor may be due to inhibiting leukocyte/endothelial NADPH oxidase and enhancing eNOS activity. Thereby, the vicious cycle under an acute hyperglycemic state can be attenuated by PKC beta II inhibitor to enhance NO bioavailability. This study provides the novel evidence for the potential use of PKC beta II inhibitor to preserve normal endothelial function in diabetic patients.

Acknowledgments

References

1. Omiyi, D., et al. *J. Pharmacol. Exp. Ther.* **314**(2), 542-551 (2005).
2. Chen, Q., et al. *Current Topics in Pharmacology* **14**, 11-24 (2010).
3. Korchak, H.M., Kilpatrick, L.E. *J. Biol. Chem.* **276**(12), p. 8910-8917 (2001).

The Effects of Gö 6983 and a Selective Protein Kinase C beta II Peptide Inhibitor on Local Hyperglycemia-Induced Leukocyte-Endothelial Interactions

Qian Chen, Edward Iames, Daniel Torino, Kerry-Anne Perkins, Brian Rueter, Catherine Prince, and Lindon Howard Young

Department of Pathology, Microbiology, Immunology & Forensic Medicine, Philadelphia College of Osteopathic Medicine (PCOM), Philadelphia, PA, 19131, U.S.A.

Introduction

The cascades involved in hyperglycemia-induced vascular and organ damage are complex and partially understood. Studies suggest that endothelial dysfunction and subsequent inflamation may initialize the cascade resulting in vascular complications in diabetic patients. Currently, there is not a diabetic medication that is specifically designed to attenuate the vascular dysfunction and inflammatory responses associated with diabetes. Therefore, there is a great need to test the potential vascular protective and anti-inflammatory effects of novel compounds. Protein kinase C (PKC), especially PKC beta II isoform, is upregulated under hyperglycemic conditions. Activation of PKC may decrease nitric oxide bioavailability and increase superoxide production, which can lead to vascular dysfunction and tissue/organ damage. By contrast, inhibition of PKC beta, such as ruboxistaurin, has exhibited beneficial effects for diabetic retinopathy and nephropathy. However, the regulatory mechanisms of PKC, especially PKC beta II, on inflammatory responses induced by hyperglycemia are still unclear. Our previous studies suggest that a broad-spectrum PKC inhibitor (Gö 6983, MW=442) or a cell permeable myristoylated (Myr) PKC beta II peptide inhibitor (PKC beta II-, *N-Myr*-SLNPEWNET, MW = 1300, Genemed Synthesis, San Antonio, TX) decreases leukocyte-endothelial interactions and attenuates endothelial dysfunction induced by N^G nitro L-arginine methyl ester [1]. In this study, the anti-inflammatory effects of Gö 6983 or the selective PKC beta II- were tested on hyperglycemia induced leukocyte-endothelial interactions in postcapillary venules of rat mesentery via intravital microscopy [2].

Results and Discussion

Mean arterial blood pressure (MABP) was monitored via a catheter in the carotid artery to indicate the hemodynamic status of rats during the experiment. We found that MABP was maintained between 90-110 mmHg throughout the experiment in all groups. Microcirculation of postcapillary venules was observed by intravital microscopy during baseline and 30 min, 60 min, 90 min, 120 min of superfusion of Krebs' buffer, Gö 6983, or the selective PKC beta II-. Recorded postcapillary venule diameter ranged from 15-25 µm. The intraperitoneal glucose level in D-glucose pretreated groups (2.5 ml of 25 mM D-glucose intraperitoneally (i.p.) injected 12 hrs earlier) were significantly higher (238 ± 8 mg/dl, n=26) compared to that in saline pretreated group (2.5 ml saline i.p. 12 hrs. earlier; 186 ± 11 mg/dl, n=6, p<0.01).

D-glucose pretreated group (n=6) exhibited significantly higher leukocyte rolling, adherence and transmigration during baseline and throughout the 2 hrs superfusion of Krebs' buffer compared to saline pretreated group (n=6). By contrast, superfusion of Gö 6983 (200 nM, n=8) or PKC beta II- (5 µM, n=6; 10 µM, n=6) to D-glucose pretreated rats significantly attenuated hyperglycemia-induced leukocyte-endothelial interactions (see Table 1).

The superfused mesenteric tissues in different experimental groups were harvested after intravital microscopy for hematoxylin-eosin (H and E) staining of leukocytes to further confirm the findings obtained from intravital microscopy. We found that D-glucose pretreated rats (n=4) showed significantly higher leukocyte vascular adherence and transmigration compared to saline pretreatment (n=3). By contrast, superfusion of 10 µM PKC beta II- (n=3) or 200 nM Gö 6983 (n=4) for 2 hours significantly reduced hyperglycemia-induced leukocyte vascular adherence and tissue infiltration (see Figure 1).

Table 1. The comparision of leukocyte rolling, adherence and transmigration among different experimental groups

Leukocyte-endothelial interactions		baseline	30 min	60 min	90 min	120 min
Rolling	Saline	31±3[**]	35±4[**]	35±4[**]	37±5[**]	33±8[**]
	D-glucose	64±8	61±4	78±12	96±13	107±7
	D-glucose+5 μM PKC beta II-	55±7	46±11	37±11[**]	55±17	74±23
	D-glucose+10 μM PKC beta II-	53±8	36±4	37±5[**]	59±10	52±9[**]
	D-glucose+200 nM Gö 6983	49±4	40±4	34±4[**]	49±6[**]	46±7[**]
Adherence	Saline	3±1[**]	4±1[**]	5±1[**]	6±2[**]	8±2[**]
	D-glucose	11±1	16±1	18±1	23±3	25±4
	D-glucose+5 μM PKC beta II-	9±1	7±1[**]	10±2[**]	11±1[**]	14±2[**]
	D-glucose+10 μM PKC beta II-	10±1	9±1[**]	10±1[**]	12±1[**]	13±1[**]
	D-glucose+200 nM Gö 6983	10±1	9±1[**]	9±2[**]	9±1[**]	12±1[**]
Transmigration	Saline	2±1[**]	2±1[**]	3±1[**]	4±1[**]	6±1[**]
	D-glucose	6±1	8±1	10±1	11±1	13±1
	D-glucose+5 μM PKC beta II-	6±1	6±1	7±1	7±1[**]	9±1[**]
	D-glucose+10 μM PKC beta II-	6±1	7±1	8±1	8±1[**]	9±1[**]
	D-glucose+200 nM Gö 6983	6±1	6±1	6±1[**]	7±1[**]	8±1[**]

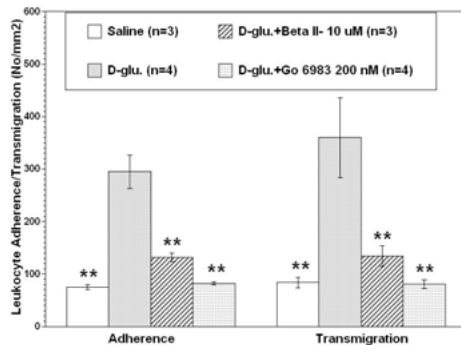**p<0.05, **P<0.01 compared to D-glucose by ANOVA using Bonferroni/Dunn test*

Fig. 1. Leukocyte vascular adherence and infiltration by H&E staining the mesenteric tissue (**P<0.01 compared to D-glucose).

This study provides the novel evidence to support the contributory role of PKC, especially PKC beta II isoform, in inflammatory responses under hyperglycemic conditions. It also suggests that the anti-inflammatory effects of Gö 6983 and the PKC beta II- may be potentially beneficial for diabetic patients to reduce the vascular or organ damage.

Acknowledgments

References

1. Chen, Q., et al. *Current Topics in Pharmacology* **14**, 11-24 (2010).
2. Booth, G., et al. *Am. J. Physiol. Endocrinol. Metab*. **280**(6), E848-856 (2001).

Effects of a Selective Protein Kinase C beta II Peptide Inhibitor on Real-Time Blood Nitric Oxide and Hydrogen Peroxide Release in Femoral Artery/Vein Ischemia and Reperfusion

Kyle D. Bartol, Kerry-Anne Perkins, Qian Chen, and Lindon Young

Department of Pathology, Microbiology, Immunology, and Forensic Medicine, Philadelphia College of Osteopathic Medicine, Philadelphia, PA, 19131, U.S.A.

Introduction

Vascular endothelial dysfunction is a key component initiating oxidative stress in ischemia/reperfusion (I/R). Endothelial dysfunction is characterized by an increase in hydrogen peroxide (H_2O_2) and a decrease in the bioavailability of endothelial-derived nitric oxide (NO).
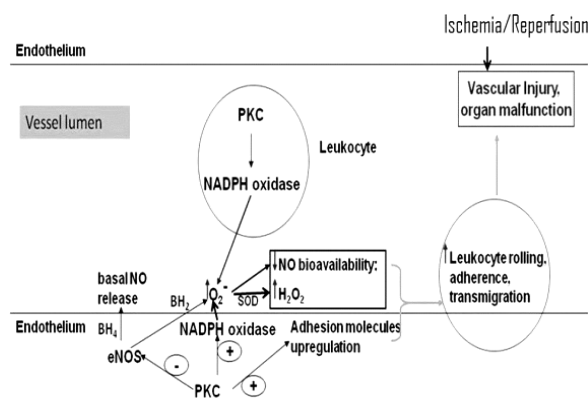
Fig. 1. PKC regulation of eNOS and NADPH oxidase in leukocytes and endothelial cells. (BH_4 tetrahydrobiopterin; BH_2 dihydrobiopterin).

When activated, protein kinase C (PKC) stimulates superoxide (SO) and subsequent H_2O_2 release from NADPH oxidase in both leukocytes/endothelial cells and inhibits endothelial nitric oxide synthase (eNOS) causing an increase in oxidative stress (Figure 1). Previous studies using a broad-spectrum PKC inhibitor Gö 6983 (mol. wt. 442) or selective PKC Beta (β) II peptide inhibitor (N-Myr-SLNPEWNET mol. wt. 1300) improved cardiac function in myocardial I/R (*ex vivo*), decreased leukocyte-endothelial interactions (*in vivo*)/leukocyte superoxide (SO) release (*in vitro*) and increased endothelial-derived NO release (*in vitro*) [1,2]. PKC βII peptide inhibitor works by binding to the receptor for activated kinase (RACK-1) and attenuates the translocation of PKC βII to the cell membrane. By contrast, Gö 6983 inhibits the ATP binding site of PKC. The attenuation of PKC activity by these mechanisms in turn decreases PKC phosphorylation of substrates (i.e. NADPH oxidase and eNOS). Collectively, this results in attenuating SO thereby inhibiting SO release from NADPH oxidase and increasing eNOS activity to enhance NO release, both of which reduces oxidative stress in I/R injury.

Results and Discussion

H_2O_2 or NO was measured in real-time in femoral veins: one subjected to I/R and the other served as a sham control. The H_2O_2 or NO microsensors (100μm, World Precision Instruments, Sarasota, FL) were connected to a free radical analyzer and were inserted into a catheter placed inside the femoral vein. Once baseline is established for each sensor, a 20 min ischemic period is introduced in one limb by clamping the femoral artery and vein. Upon removal of the clamp, we record picoamp (pA) values every 5 min for a total of 45 min reperfusion. pA was converted to molar concentration via a calibration curve for each sensor. Multiple groups were compared using ANOVA with Fisher's PLSD post-hoc tests. Relative difference in I/R to sham femoral veins in saline controls increased blood H_2O_2 levels by 2.8 μM and decreased NO levels by 20 nM relative to baseline. By contrast, Gö 6983 (7.4 μg/kg I.V.) or PKC βII inhibitor (0.55 mg/kg I.V.) given at reperfusion significantly decreased blood H_2O_2 levels to baseline and increased NO levels between 50-150 nM relative to baseline (Figure 2 and Figure 3). This may be due to inhibiting the phosphorylation of NADPH oxidase via PKC βII in leukocytes/vascular tissue.

The decrease in H_2O_2 levels with PKC βII inhibitor is similar to Gö 6983. This finding is consistent with previous studies that show that PKC βII isoform is essential in the phosphorylation of NADPH oxidase [3]. The PKC βII inhibitor also significantly increased NO; however, this response was less robust than Gö 6983. This may be due to additional isoform inhibition exerted by Gö 6983 in endothelial cells resulting in enhanced eNOS activation.
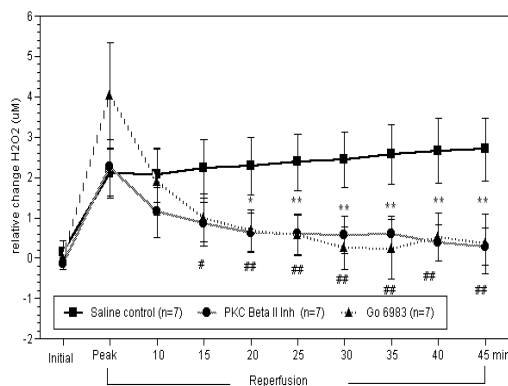

Fig. 2. Relative difference in H_2O_2 release between I/R and sham femoral veins during reperfusion. Anesthetized rats were given saline or Gö 6983 or PKC βII inhibitor I.V. at the beginning of reperfusion. There was a significant decrease in H_2O_2 release in drug-treated groups compared to saline (* $p<0.05$, **$p<0.01$ from saline for Gö 6983; # $p<0.05$, ## $p<0.01$ from saline for PKC βII inhibitor).
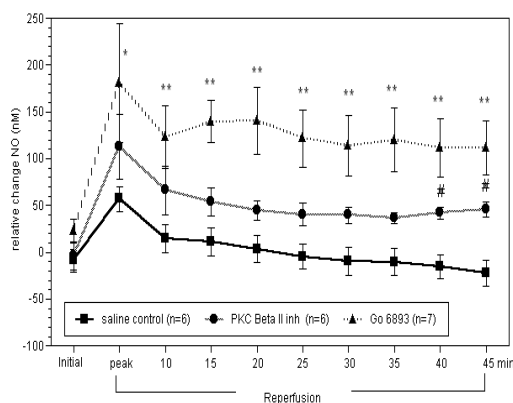

Fig. 3. Relative difference in NO release between I/R and sham femoral veins during reperfusion. Anesthetized rats were given saline or Gö 6983 or PKC βII inhibitor I.V. at the beginning of reperfusion. There was a significant increase in NO release in drug-treated groups compared to saline (* $p<0.05$, **$p<0.01$ from saline for Gö 6983; # $p<0.05$, from saline for PKC βII inhibitor).

Acknowledgments

References

1. Chen, Q., et al. *Curr. Topics in Pharmacol.* **14**, 11-24 (2010).
2. Young, L.H., Balin, B.J., et al. *Cardiovasc. Drug Rev.* **23**, 255-272 (2005).
3. Korchak, H.M., Kilpatrick, L.E. *J. Biol. Chem.* **276**, 8910-8917 (2001).

The Effects of Protein Kinase C (PKC) Epsilon Peptide Regulation on Endothelial Nitric Oxide Synthase (eNOS) Uncoupling on Leukocyte-Endothelial Interactions in Rat Mesenteric Postcapillary Venules

Maria A. Kern, Lindon H. Young, Edward S. Iames, and Qian Chen

Department of Pathology, Microbiology, Immunology, and Forensic Medicine, Philadelphia College of Osteopathic Medicine, Philadelphia, PA, 19131,U.S.A.

Introduction

Endothelial-derived nitric oxide (NO) is essential in the regulation of blood pressure and promotes an antithrombotic surface which attenuates leukocyte-endothelial interactions associated with vascular injury. eNOS produces NO from L-arginine in the presence of essential cofactor tetrahydrobiopterin (BH_4). When BH_4 is oxidized to dihydrobiopterin (BH_2), the ratio of BH_2/BH_4 is increased during vascular injury and promotes eNOS uncoupling, causing eNOS to produce superoxide (SO) instead of NO [1]. However, the role of BH_2 to induce eNOS uncoupling and promote leukocyte-endothelial interactions in mesenteric circulation has not been characterized *in vivo*. Moreover, the role of compounds that can increase or decrease eNOS activity in the presence of an increased BH_2/BH_4 ratio has yet to be determined. PKC epsilon (PKC ε) positively regulates eNOS activity via phosphorylation of serine 1177. Cell-permeable myristoylated (Myr) PKC ε peptide activator (PKC ε+) or inhibitor (PKC ε-) are known to increase or decrease NO release in vitro, respectively [2]. The effect of PKC ε+ is known to be inhibited with classical NOS inhibitors, such as N^G-nitro-L-arginine methyl ester (L-NAME). However, the effect of PKC ε+ or PKC ε- to exacerbate or attenuate BH_2-induced leukocyte-endothelial interactions has not yet been determined.

Results and Discussion

We predict that increased BH_2/BH_4 ratio will promote eNOS uncoupling and induce leukocyte-endothelial interactions similar to L-NAME. When eNOS activator PKC ε+ (N-Myr-HDAPIGYD, MW=1097, Genemed Synthesis, San Antonio, TX) is co-administered with BH_2, it will augment and/or sustain BH_2-induced leukocyte-endothelial interactions. By contrast, eNOS inhibitor PKC ε- (N-Myr-EAVSLKPT, MW=1054, Genemed Synthesis) co-administered with BH_2 will attenuate BH_2-induced leukocyte-endothelial interactions via inhibition of uncoupled eNOS. We examined leukocyte-endothelial interactions in rat mesenteric venules on leukocyte rolling, adherence, and transmigration by using intravital microscopy. Multiple groups were compared using ANOVA with Fisher's PLSD post-hoc tests. **Experimental Groups:** Control Group: Krebs' buffer (n=5), BH_2 group: 100 μM BH_2 (n=6), BH_2 + PKC ε+ group: 100 μM BH_2 + 10 μM PKC ε+ (n=3), BH_2 + PKC ε- group: 100 μM BH_2 + 10 μM PKC ε- (n=3), L-NAME group: 50 μM L-NAME (n=3).
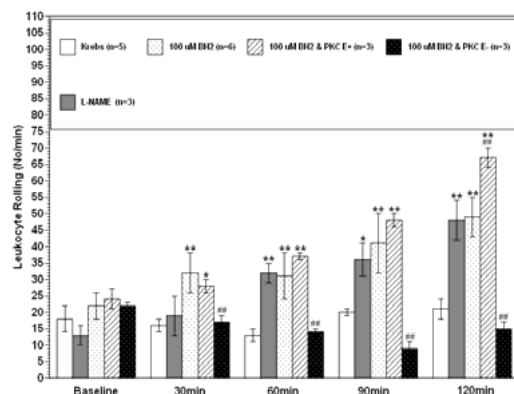

Fig. 1. Leukocyte rolling among different experimental groups. L-NAME and 100 μM BH_2 significantly increased leukocyte rolling (*P<0.05, **P<0.01 from Krebs'). The effect of BH_2 was significantly enhanced by PKC ε+ ($^{\#\#}$P<0.01 from 100 μM BH_2). This effect was significantly attenuated by PKC ε- ($^{\#\#}$P<0.01 from 100 μM BH_2) suggesting that uncoupled eNOS was inhibited.
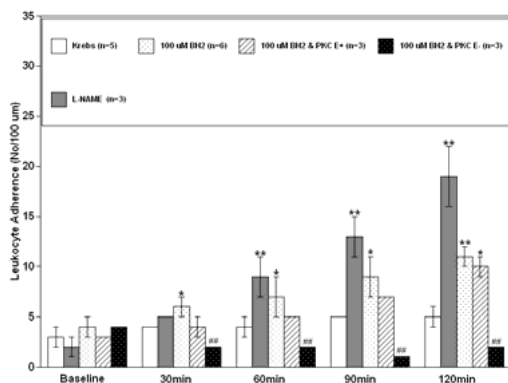
Fig. 2. Leukocyte adherence among different experimental groups. L-NAME and 100 μM BH₂ significantly increased adherence (*P<0.05, **P<0.01 from Krebs'). The effect of BH₂ was sustained, but delayed by PKC ε+ (*P<0.05 from Krebs'). The effect of BH₂ was significantly attenuated by PKC ε- ($^{##}P<0.01$ from 100 μM BH₂) suggesting uncoupled eNOS was inhibited.
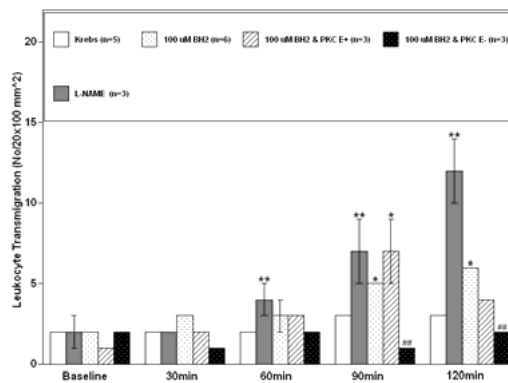

Fig. 3. Leukocyte transmigration among different experimental groups. L-NAME and 100 μM BH₂ (*P<0.05, **P<0.01 from Krebs') significantly increased leukocyte transmigration and this effect was sustained by PKC ε+ (*P<0.05 from Krebs'). The effect of BH₂ was significantly attenuated by PKC ε- ($^{##}P<0.01$ from 100 μM BH₂) suggesting that uncoupled eNOS was inhibited.

Intravital microscopy was performed on a loop of mesentery of male Sprague-Dawley rats (275-325 g, Ace Animals, Boyertown, PA) and microcirculation of mesenteric venules was observed under light microscopy [3]. Additionally, right carotid artery cannulation was performed to monitor mean arterial blood pressure. During the experiment, test solutions were superfused over mesentery and number of rolling (number per minute), adhered (number adhered for >30 sec), and transmigrated (number emigrated within 10 μm of venule) leukocytes were recorded [3].

We found that superfusion of BH₂ (100 μM n=6, P<0.05) significantly increased leukocyte rolling, adherence, and transmigration, similar to L-NAME (n=3, P<0.05), when compared to Krebs' control rats (n=5). The effect of BH₂ was further potentiated with eNOS activator PKC ε+, on leukocyte rolling (n=3, P<0.05 compared to BH₂) and sustained on leukocyte adherence and transmigration. The data suggest that eNOS uncoupling may be an important mechanism mediating inflammation-induced vascular injury. This study outlines the importance that stimulating eNOS activity may not always be advantageous and can induce cell injury under conditions where the BH₂/BH₄ ratio is increased, such as vascular injury. Our data demonstrates that administration of PKC ε+ enhanced or sustained BH₂-induced leukocyte-endothelial interactions. PKC ε- significantly attenuated all three types of leukocyte-endothelial interactions. The data suggest that inhibiting uncoupled eNOS activity with PKC ε- may attenuate oxidative stress and restore vascular endothelial function. This provides indirect evidence to support that inhibiting uncoupled eNOS may be a potential strategy to attenuate endothelial dysfunction-induced inflammatory responses in various vascular diseases.

Acknowledgments

References

1. Schmidt, T.S., Alp, N.J. *Clinical Science* **113,** 47-63 (2007).
2. Teng, J.C., et al. *Naunyn-Schmiedeberg's Arch. Pharmacol.* **378**, 1-15 (2008).
3. Chen, Q., et al. *Curr. Topics in Pharmacol.* **14**, 11-24 (2010).

Myristoylation of Protein Kinase C Beta II/Zeta Peptide Inhibitors, or Caveolin-1 Peptide Facilitates Rapid Attenuation of Phorbol 12-Myristate 13-Acetate (PMA) or N-Formyl-L-Methionyl-L-Leucyl-L-Phenylalanine (fMLP) Activated Leukocyte Superoxide Release

Kerry-Anne A. Perkins, Kyle Bartol, Qian Chen, Erin Feinstein, and Lindon Young

Department of Pathology, Microbiology, Immunology & Forensic Medicine, Philadelphia College of Osteopathic Medicine (PCOM), Philadelphia, PA, U.S.A.

Introduction

Protein kinase C (PKC) beta II (βII, a classical isoform) and zeta (ζ, an atypical isoform) activation of polymorphonuclear leukocyte (PMN) NADPH oxidase is essential to generate superoxide (SO) release. Inhibition of PMN SO release attenuates inflammation mediated vascular injury (e.g. ischemia-reperfusion). fMLP peptide activates PMN chemotactic receptor to stimulate NADPH oxidase via PKC. PMA is a lipid soluble broad-spectrum PKC agonist that directly activates PKC. Myristoylation of peptides is known to be an effective strategy to enable simple diffusion through cell membranes to affect PKC function [1]. Myristoylated (Myr) PKC βII and ζ peptide inhibitors are known to inhibit PMN SO release with doses that correlated with restoration of post-reperfused cardiac function [2,3]. Myr-PKC βII peptide inhibitor (10 μM) (N-myr-SLNPEWNET), attenuates PKC βII translocation to the cell membrane. By contrast, Myr-PKC ζ peptide inhibitor (5 μM) (N-myr-SIYRRGARRWRKL), inhibits the pseudo-substrate domain of PKC ζ. Whereas, caveolin-1 peptide (10 μM) (DGIWKASFTTFTVTKY-WFYR), an inhibitor of classical and atypical PKC isoforms in cell homogenates via sequestration to the scaffolding region in cell membrane caveolae [4] has not been previously evaluated in PMN SO release. Moreover, the efficiency of the myr-peptides has not been studied by comparison to their non-myr peptides on PMA or fMLP-induced PMN SO release. We hypothesized that myr-peptides would attenuate both PMA and fMLP induced PMN SO release compared to their non-myr-peptide counterpart.

Results and Discussion

PMNs were harvested from 0.5% glycogen induction in male Sprague-Dawley rats (350–400 g) with >90% pure and >95% viable. The SO release from PMNs was measured spectrophotometrically by the reduction of ferricytochrome c as previously described [2,3]. The PMNs (5×10^6) were incubated in the presence or absence of myr or non-myr PKC βII inhibitor (10 μM), ζ inhibitor (5 μM) or caveolin-1 peptide (10 μM) for 15 min at 37°C in spectrophotometric cells. Thereafter, PMNs were stimulated with 100 nM PMA or 1 μM fMLP. Positive control samples were given SO dismutase (SOD; 10 μg/ml). Absorbance (Abs.) at 550 nm was measured every 30 sec for up to 360 sec for PMA and 60-90 sec for fMLP (peak response), and the change in abs. (SO release) from PMNs was determined relative to time 0. Multiple groups were compared using ANOVA with Fisher's PLSD post-hoc analysis. SOD inhibited fMLP (n=9; abs = 0.010 ± 0.004) or PMA (n=8; abs. = 0.045 ± 0.005) induced PMN SO release by >90%.
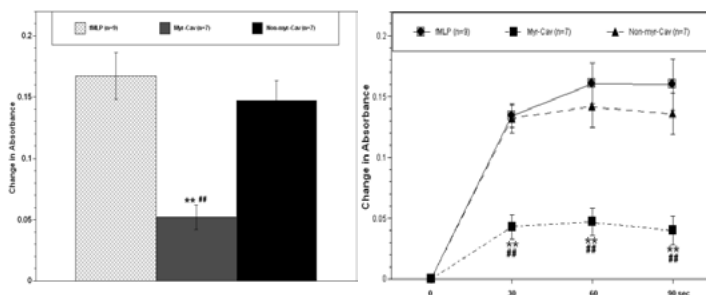

Fig. 1. Peak response (left) and time course (right) of fMLP-induced SO release in PMNs. Myr-Caveolin-1 (Cav) significantly attenuated fMLP-induced SO release by 69% compared to fMLP (**P<0.01) and by 65% compared to non-myr-Cav (\#\#P<0.01).

Myr-caveolin-1, myr-PKC βII and myr-PKC ζ peptide inhibitors significantly attenuated PMA and fMLP-induced leukocyte SO release, whereas their non-myr peptide counterparts were similar to PMA or fMLP alone and did not significantly inhibit leukocyte SO release (see Figures 1-2 and Table 1). These results suggest that myristoylation of these peptides is essential for rapid diffusion into cells to significantly exert biochemical effects on PMN SO release. Moreover, myr-caveolin-1 exerted the highest inhibitory effects on fMLP-induced SO release suggesting that classical and atypical PKC isoforms may be attenuated.
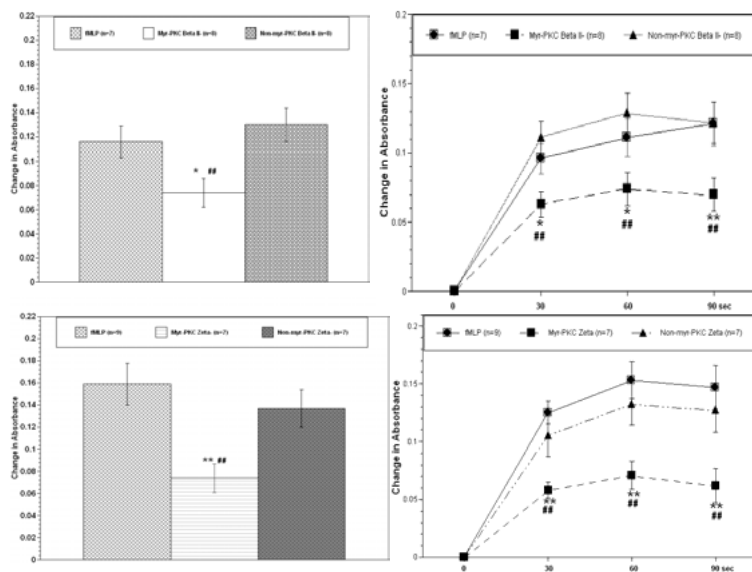
Fig. 2. Peak response (left) and time course (right) of fMLP-induced SO release in PMNs. Myr-PKC βII inhibitor (-) and myr-ζ inhibitor (-) significantly attenuated fMLP-induced SO release by 36% and 53%, respectively, compared to fMLP (*P<0.05, **P<0.01) and by 43% and 47%, respectively, compared to their non-myr-PKC peptides (##P<0.01).

Table 1. PMA induced PMN SO release

Change in Absorbance (from baseline)	1 min	3 min	6 min
PKC Beta II Peptide Inhibitor			
PMA (n=9)	0.14±0.03	0.5±0.07	0.69±0.06
Myristoylated (n=6)	0.04±0.03**	0.34±0.06#	0.52±0.06*##
Non-myristoylated (n=8)	0.12±0.03	0.54±0.08	0.80±0.06
PKC Zeta Peptide Inhibitor			
PMA (n=9)	0.08±0.02	0.43±0.04	0.71±0.02
Myristoylated (n=7)	0.04±0.01*##	0.24±0.02**##	0.38±0.02**##
Non-myristoylated (n=8)	0.10±0.01	0.50±0.02	0.72±0.03
Caveolin-1 Peptide			
PMA (n=8)	0.20±0.03	0.51±0.03	0.68±0.03
Myristoylated (n=7)	0.10±0.02*##	0.32±0.03**##	0.45±0.03**##
Non-myristoylated (n=7)	0.18±0.03	0.51±0.03	0.68±0.03

*P<0.05, **P<0.01compared to PMA; #P<0.05, ##P<0.01 compared to non-myr-peptide.

References

1. Eichholtz, T., et al. *J. Biol. Chem*. **268**(3), 1982-1986 (1993).
2. Omiyi, D., et al. *J. Pharmacol. Exp. Ther*. **314**(2), 542-551 (2005).
3. Phillipson, A., et al. *Am. J. Physiol. Heart Circ. Physiol*. **289**(2), H898-907 (2005).
4. Oka, N., et al. *J. Biol. Chem*. **272**(52), 33416-33421 (1997).

SNARE Based Peptide Linking as an Efficient Strategy to Retarget Botulinum Neurotoxin's Enzymatic Domain to Specific Neurons Using Diverse Neuropeptides as Targeting Domains

Jason Arsenault, Enrico Ferrari, John O'Brien, Chungjing Gu, Dhevahi Niranjan, Violeta Ruipérez, and Bazbek Davletov

Medical Research Council – Laboratory of Molecular Biology, Neurobiology Division, Cambridge, CB2 0QH, United Kingdom

Introduction

Many disease states are caused by miss-regulated neurotransmission. A small fraction of these diseases can currently be treated with botulinum neurotoxin type A (BoNT/A). BoNT/A is composed of three functional domains – the light chain (Lc) is a zinc metalloprotease that cleaves intracellular SNAP25 which inhibits exocytosis, the translocation domain (Td) that enables the export of the light chain from the endosome to the cytosol, and the receptor binding domain (Rbd) that binds to extracellular gangliosides and synaptic vesicle glycoproteins while awaiting internalisation [1]. Current endeavours are directed towards retargeting Bont/A as well as finding safer methods of preparation and administration. Recently, our laboratory has developed a SNARE based linking strategy to recombine non-toxic BoNT/A fragments into a functional protein by simple mixing [2]. This SNARE based linking strategy permits the step-wise assembly of highly stable macromolecular complexes [2,3]. Onto these three SNARE peptides, diverse functional groups can be attached to the N- or C- terminus by direct synthesis and/or by genetic design. To enhance the therapeutic potential of BoNT/A, this method enables the rapid assembly of a large array of neuropeptide-SNAREs to their cognate LcTd-SNARE. A substitution of the Rbd with various neuropeptide sequences permits a large throughput combinatorial assay of LcTd to target new cell types. In this study, we have fused LcTd to 3 different Synaptobrevin sequences; we also use a small protein staple, and 26 different Syntaxin-neuropeptide fusions (permitting the assay of 78 new chimeric LcTd proteins with modified targeting domains). These neuropeptides such as, but not exclusively, somatostatin (SS), vasoactive intestinal peptide, substance P, opioid peptide analogues, Gonadotropin releasing hormone, and Arginine Vasopressin, which natively function through G protein coupled receptors (GPCR) can undergo agonist induced internalisation upon activation. The ability of our new constructs, once endocytosed, to inhibit neurotransmitter release was tested on different neuronal cell lines with immunoblotting of endogenous SNAP25. This cleavage by Lc reflects the ultimate readout of the enzyme's efficacy, which incorporates the cell surface
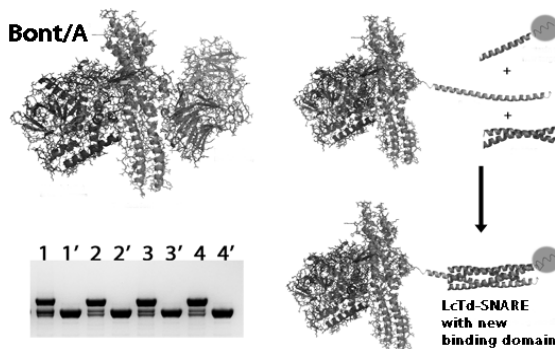

Fig. 1. SNARE-linked botulinum neurotoxins used for the retargeting of Bont/A.

binding, internalisation kinetics, translocation of the Lc to the cytosol, and finally the enzymatic cleavage of SNAP25. Internalisation of the toxins can also be monitored with confocal microscopy and FACS by the substitution of the staple peptide for a fluorescent homologue. Figure 1 shows that whole boNT/A (upper left) can have its Rbd replaced with SNARE peptides, which will fuse together to form highly stable chimeric proteins with an altered targeting domain (right). Figure 1 also shows 4 different neuropeptide synthaxins in complex, resolved on SDS-PAGE gel (bottom left lanes 1-4, boiled 1'-4').

Results and Discussion

The reassembled toxins were tested on mouse neuroblastoma 2A (N2A), rat pheocytochroma (PC-12), human neuroblastoma (SH-5YSY) cells as well as rat hippocampus, cortex and dorsal root ganglion neurons at nM concentrations from 18 to 42h. The resulting cleavage bands, as revealed by western immunoblotting, were quantified as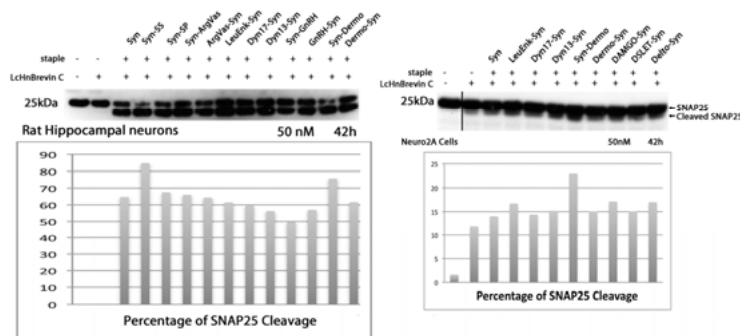 previously described [4]. Figure 2 shows a typical example of a SNAP25 cleavage assay. The same concentration of LcHn-BrevinC can have variable efficacy once pre-complexed with various neuropeptide targeting domains. As a noted example, we can see that the LcHn/Dermorphin complex has higher efficacy on N2A cells as well as on hippocampus neurons compared to the use of other Syntaxins, while LcHn-SS has a higher

Fig. 2. SNAP25 cleavage assay on rat hippocampal neurons (left) and N2A cells (right) with corresponding densitometric analysis.

efficacy on Hippocampus neurons. These results could reflect the cell surface expression of opioid and somatostatin receptors respectively, as well as the permissive structure activity of each neuropeptide in complex.

To this end, further structural refinement of the peptides implicated in these complexes could capitulate a higher potency and more selective medicinal enzyme. SNARE peptide stapling facilitates these structural refinements. Modifications in the SNARE motifs could enhance the versatility of the staple peptide, while modifications of the new targeting domains and its cross-linkers could enhance the structure activity (i.e. binding affinities, internalization activity). The SNARE based protein stapling is thus a versatile avenue for the efficient and high throughput subunit rearrangement of diverse protein that can exploit the advantages of both direct synthesis and recombinant expression to yield interesting *de novo* protein assemblies.

Assembled LcTd-SNARE complexes have also demonstrated to be important cell penetrating moieties (as well as BoNT/A fragments individually; data not shown), this ability can be advantageous to enhance the cell penetration of chimeric proteins of diverse interest that have been assembled using SNARE protein stapling. Our results have also shown that the internalized BoNT/A-SNARE complexes (with fluorescent staple) co-localize with acidic organelles inside cells (data not shown); a necessary step in the intracellular activation of the light chain. Current endeavors are also directed towards minimizing the cell penetrating properties of SNARE peptides to lead to exclusive endocytosis via GPCR internalization and minimizing any potential off target side effects.

Acknowledgments

References

1. Mahrhold, S., et al. *FEBS Lett.* **580**(8), 2011-2014 (2006).
2. Darios, F., et al. *Proc. Natl. Acad. Sci.* **107**(42), 18197-18201 (2010).
3. Ferrari, E., et al. *J. Nanobiotechnology* **8**, 9 (2010).
4. Arsenault, J., et al. *Biochem. Pharmacol*. **80**(7), 990-999 (2010).

Conjugates of β-Lactams and Host Defense Peptides as Antibiotic Prodrug Candidates

Stéphane Desgranges[1], Liam P. Burke[2], Carol C. Ruddle[1], Tara M. Mc Fadden[1,2], Deirdre Fitzgerald-Hughes[2], Hilary Humphreys[2,3], Timothy P. Smyth[4], and Marc Devocelle[1]

[1]*Centre for Synthesis and Chemical Biology, Department of Pharmaceutical & Medicinal Chemistry, Royal College of Surgeons in Ireland, 123, St. Stephen's Green, Dublin 2, Ireland.;* [2]*Department of Clinical Microbiology, Royal College of Surgeons in Ireland, Dublin 9, Ireland;* [3]*Department of Microbiology, Beaumont Hospital, Dublin 9, Ireland;* [4]*Department of Chemical & Environmental Sciences, University of Limerick, Ireland*

Introduction

Host defense peptides (HDPs) have been recognized as promising candidates for the generation of novel antibacterial agents harnessing the effector mechanisms of innate immunity [1]. The development of systemic therapies based on antimicrobial peptides requires, however, solutions addressing the question of possible toxicity. A prodrug approach can overcome a barrier due to toxicity problems and has been proposed as a promising strategy to achieve clinical success with HDPs [2]. The conjugation of a classical antibiotic to a HDP through a cleavable linker is described here as potential method to generate HDP prodrugs. β-Lactam agents such as cephalosporins can be used as promoieties [3] to transiently mask essential determinants of a peptide's antimicrobial activity. N-terminal conjugation of the sequence at the 3'-position of the cephem core exploits the activity of bacterial enzymes of antibiotic resistance (β-lactamases) to selectively activate the peptide at sites of infection (Figure 1).

Results and Discussion

Conjugation of a peptide to a cephalosporin involves the development of a synthetic approach which meets the requirements of both the β-lactam and peptide chemistries.
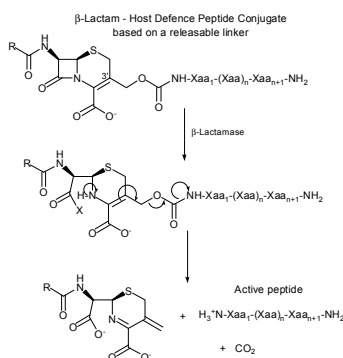

Fig. 1. β-Lactamase-dependent prodrugs.

Different synthetic strategies and protection schemes were evaluated, but were found to be associated with a lack of reliability and/or with degradation of the cephalosporin's β-lactam ring. Alternatively, the copper (I)-catalysed azide-triazole cyclo-addition reaction, applied to an azido-peptide and an alkyne-functionalised cephalosporin, allowed the versatile and reliable conjugation of these 2 agents. This reaction offers the additional advantage of producing a peptide bond isostere, the triazole ring, between these two ligated moieties. A candidate based on cephalothin, a first generation cephalosporin, and an 8-mer sequence derived from the bactenecin peptide (Bac8c) [4] was prepared by this method (Figure 2). The peptide sequence is proteolytically stable (all-D peptide) and short (close to the minimal length of a continuous epitope for an antigen sequence).

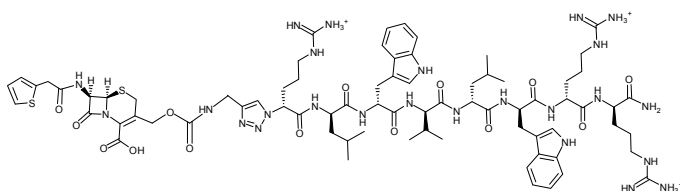Chemical and enzymatic hydrolysis assays performed with a purified β-lactamase indicated that the cephalothin-

Fig. 2. Cephalothin-bactenecin conjugate.

Table 1. Minimum Inhibitory Concentrations (µM)

Bacterial strains	β-Lactam Cephalothin	Peptide D-Bac8c	Prodrug candidate	Triazole peptide	Controls	
					C-7 conjugate	Oxime conjugate
MRSA ATCC 44330	2.0	1.0	1.5	2.0-4.0	12.8	>20
E. coli ATCC 25922	31.6	2.1	12.0	5.0	>25.6	>20

bactenecin conjugate can release its peptide component upon cleavage of the β-lactam ring, while no background hydrolysis is observed in buffer alone.

Representative strains of Gram-positive (MRSA) and Gram-negative (*Escherichia coli*) organisms were used to assess the antimicrobial activities of the cephalothin-bactenecin conjugate (Table 1). They were compared to those of its parent cephalosporin and peptide and to those of the triazole-modified peptide which can be released from the conjugate upon β-lactamase-mediated hydrolysis of the cephalosporin (Figures 1 and 2).

The antimicrobial activities of the conjugate were found to be distinct from those of its parent components. Minimum Inhibitory Concentrations (MICs) against the Gram-negative organisms were higher than those against the Gram-positive strains, although the conjugate can have MICs as low as 3 µM against clinical isolates of *E. coli* expressing extended-spectrum β-lactamases (ESBLs).

Two control molecules of the cephalothin-bactenecin prodrug candidate, based on non-cleavable linkers, were prepared and tested to assess the specificity of its activity. The first one consists of the bactenecin sequence conjugated at the C-7 position of the cephem nucleus (C-7 control) and the second one of a C-3' conjugate identical to the prodrug candidate but where the self-immolative carbamate linker was replaced by a stable oxime bond (oxime control). Both controls had reduced antimicrobial activities against MRSA and *E. coli* indicating that the release of the peptide component from the cephalosporin may contribute to the mechanism of action of the conjugate.

Furthermore, testing of the cephalothin-bactenecin prodrug candidate against a same strain of *E. coli* expressing or not an ESBL showed a MIC differential consistent with a β-lactamase-dependent prodrug activity (3 µM and 6 µM against ESBL-positive and ESBL-negative *E. coli*, respectively). The MIC of the C-7 control against this strain was of 26 µM, regardless of its β-lactamase status.

The results of these studies indicate that the conjugation of a host defense peptide to a β-lactam agent can be exploited to generate peptide prodrug candidates targeting resistant bacteria. The method developed to generate these candidates will be applied to different cephalosporin promoieties and peptide sequences to optimize the activity differentials between the conjugated and free forms of the HDP.

Acknowledgments

References

1. Zasloff, M. *Nature* **415**, 389-395 (2002).
2. Hancock, R.E.W. *Lancet Infect. Dis.* **1**, 156-164 (2001).
3. Rautio, J., Kumpulainen, H., Heimbach, T., Oliyai, R., Oh, D., Järvinen, T., Savolainen, J. *Nat. Rev. Drug Discov.* **7**, 255-270 (2008).
4. Hilpert, K., Volkmer-Engert, R., Walter, T., Hancock R.E.W. *Nat. Biotechnol.* **23**, 1008-1012 (2005).

Peptide-Membrane Interaction Analysis of an Improved Antimicrobial Peptide Derived from the 107-115 hLz Fragment

Nancy B. Iannucci[1,2], Axel Hollmann[3], María R. Diaz[3], Osvaldo Cascone[1], Fernando Albericio[4,5,6], and Aníbal E. Disalvo[3]

[1]*School of Pharmacy and Biochemistry, University of Buenos Aires, Buenos Aires, 1113, Argentina;* [2]*Therapeutic Peptides Research and Development Laboratory, Chemo-Romikin, Buenos Aires, 1605, Argentina;* [3]*Laboratory of Physicochemistry of Lipidic Membranes and Liposomes, School of Pharmacy and Biochemistry, University of Buenos Aires, Buenos Aires, 1113, Argentina;* [4]*Institute for Research in Biomedicine, Barcelona Science Park, Barcelona, 08028, Spain;* [5]*CIBER-BBN, Networking Centre on Bioengineering, Biomaterials and Nanomedicine, Barcelona Science Park, Barcelona, 08028, Spain;* [6]*Department of Organic Chemistry, University of Barcelona, Barcelona, 08028, Spain.*

Introduction

Antimicrobial peptides (AMPs) are produced by almost all species of living beings as a component of their innate non-specific defense against infections [1]. AMPs are typically short peptides with consensus amphiphilic attributes represented by positively charged and hydrophobic amino acids. The lethal step in most cationic AMPs is the disruption of the microbial plasma membrane; this process is accomplished in two steps: membrane binding, predominantly governed by electrostatic interactions, and membrane insertion/permeation, related to the hydrophobicity of the peptide and its capacity of partitioning into the plasma membrane [2]. AMPs are very important resources for human therapeutics as lead compounds to counteract the drug resistance development.

An improved analog derived from the 107-115 human lysozyme (107-115 hLz) fragment was developed by sequential substitutions of both alanine residues (108 and 111). The sequence of 107-115 hLz peptide is: RAWVAWRNR-NH$_2$. The novel peptide [K^{108}W^{111}]107-115 hLz resulted in a 20-fold increase in the anti-staphylococcal activity and its hemolytic activity remained significant at 10-fold its MIC [3]. This analog displays an additional positive charge near the N-terminus and an extra Trp residue at the center of the molecule, thus suggesting that this constellation improves its interaction with the bacterial membrane. In order to understand the role of this arrangement in the membrane interaction, studies with model bacterial membranes composed by staphylococcal-isolated lipids and synthetic saturated phosphatidyl-cholines and phosphatidylethanolamines (DMPC and DMPE) were carried out.

Results and Discussion

As shown in Figure 1, the differential behavior of [K^{108}W^{111}]107-115 hLz in DMPC and DMPE monolayers highlights the importance of the head group in the interaction, considering that both lipids have the same hydrocarbon chain length. As revealed in Figure 2, peptide [K^{108}W^{111}]107-115 hLz shows higher ΔΠs than 107-115 hLz in DMPC monolayers, thus meaning that at similar pressures than those found in cells, the interfacial effect of this analog is stronger than that of 107-115 hLz. In bacterial lipid monolayers both peptides cause higher changes in the surface pressure than in synthetic lipid monolayers (Figure 3). Interestingly, in bacterial lipid monolayers at initial pressures between 20-25 mN/m, peptide [K^{108}W^{111}]107-115 hLz induces higher changes in the surface pressure than 107-115 hLz (Figure 3).

Both peptides were able to interact with bacteria-extracted and synthetic lipid monolayers, inducing in the former higher surface pressure variations even at high initial pressures. This result may be due to the electrostatic nature of the interaction, between the cationic peptides and the negatively charged bacterial membrane phospholipids. Table 1 shows the kinetic parameters of the interaction of peptides with DMCP
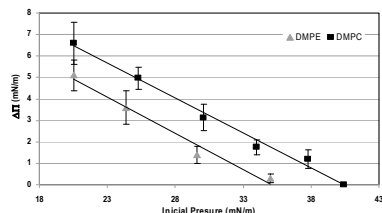

Fig. 1. Variation of the surface pressure after the injection of peptide [K^{108}W^{111}]107-115 hLz in synthetic lipid monolayers as a function of the initial surface pressure.

Table 1. Kinetic parameters of the interactions between peptides and DMPC monolayers

Equation	107-115 hLz	$[K^{108}W^{111}]$107-115 hLz
$\Delta\Pi \approx k.t^n$	n=0.556	n=0.699
$\theta = \Delta\Pi/\Delta\Pi max = [peptide]^n/Kd + [peptide]^n$	Kd= 3.3×10^{-3} M^{-1}	Kd= 1.0×10^{-3} M^{-1}

monolayers and the equations applied for their calculation. The dissociation constant of peptide 107-115 hLz results threefold higher than that of peptide $[K^{108}W^{111}]$107-115 hLz. The kinetic analysis of peptides reveals that 107-115 hLz attach to the membrane following a *fickean* pattern (n=0.5), while $[K^{108}W^{111}]$107-115 hLz do it following a *non fickean* pattern (Figures 4 and 5 respectively). Altogether, the higher affinity and the *non fickean* process suggest a stronger interaction of peptide $[K^{108}W^{111}]$107-115 hLz with lipid monolayers. These interactions may affect the packing and structure of the lipid bilayer, probably causing changes in its permeability barrier property. The specific peptide-lipid interaction affects the thermodynamic stability of the membrane and the kinetic process of association, driving to different biological answers. In order to clarify the pore forming consequence of this interaction, leakage assays will be performed.
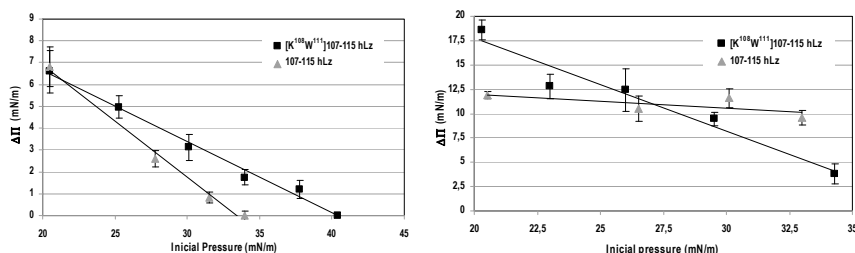
Fig. 2. and Fig. 3. Variation of the surface pressure after the injection of peptides in DMPC monolayers, and in Staphylococcus lipid-extracted monolayers, respectively as a function of the initial surface pressure.
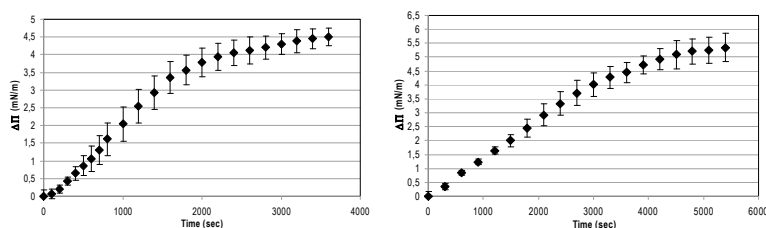
Fig. 4. and Fig. 5. Variation of the surface pressure after the injection of 107-115 hLz, and $[K^{108}W^{111}]$107-115 hLz, respectively in DMPC monolayers as a function of time.

Acknowledgments

References

1. Menendez, A, Ferreira, R.B.R., Brett, F.B. *Nat. Immunol.* **11**, 49-50 (2010).
2. Papo, N., Shai, Y. *Peptides* **24**, 1693-1703 (2003).
3. González, R., Albericio, F., Cascone, O., Iannucci, N.B. *J. Pept. Sci.* **16**, 424-429 (2010).

Characterization of LPS-Targeting Peptides Binding to Live *Pseudomonas*

Timothy Paradis, Wen Lin[*], Ron Gladue, and Jeffrey Culp

Pfizer Global Research & Development, Groton Laboratories, Pfizer Inc, Groton, CT, 06340, U.S.A.

Introduction

Antibiotic resistant Gram negative bacteria represent a major obstacle for successful bacterial clearance. Therefore, alternative therapeutic approaches are needed. The focus of our research involves the development of a broadly reactive bio-conjugate opsonin antibody that would direct Fc-mediated complement deposition and/or phagocytotic bacterial cell destruction. Lipopolysaccharide (LPS) is the major constituent of the outer membrane of Gram negative bacteria. Anti-microbial binding peptides (AMPs) bind to conserved regions on LPS with high affinity, which makes AMPs broadly cross-reactive across strains. Therefore, AMPs may be good candidates to function as the bio-conjugate bacterial binding moiety. As a first step in designing such a molecule, we selected 10 AMPs with diverse physical properties [1-15] in an attempt to identify those with the highest binding affinity to live bacteria via flow cytometry (FACS). Each peptide was labeled with fluorescein 5-maleimide (at the C-terminal Cysteine) and then tested for cell surface binding via flow cytometry. The 10 peptides examined all showed certain levels of binding to live bacteria, with the CAP-18 peptide demonstrating the highest activity at 0.16 µM (Table 1). Thus, once attached to an effector antibody, the CAP-18 bio-conjugate can be tested for broad cross-reactive binding to multiple strains and its ability to act as an opsonin agent for Gram negative bacteria.

Table1. FACS Analysis of Fluorescein-5-Maleimide Labeled LPS Binding Peptides

Peptide name	Peptide sequence	MW	½ Max [a]
CAP-18 [1,12]	LRKRLRKFRNKIKEKLKKIC-NH$_2$	2598.3	0.16
SAP-14 [2,3]	QALNYEIRGYVIIKPC-NH$_2$	1879.2	3.7
LF-11 [4,7,8,9]	FQWQRNIRKVRC-NH$_2$	1632.9	1.9
LBP-18 [5,6]	WKVRKSFFKLQGSFDVSVC-NH$_2$	2260.7	20
LALF-10 [10,11]	VTFRRLKWKYC-NH$_2$	1498.8	5.9
JP-1 [13]	kYSSSISSIRAC-NH$_2$	1300.5	31
JP-2 [13]	kNYSSSISSIHAC-NH$_2$	1395.5	40
NRC-16 [14]	GWKKWLRKGAKHLGQAAIKC-NH$_2$	2278.8	0.47
MMP-12 Elastase [15]	NQLFLFKDEKYWLINC-NH$_2$	2073.4	1.3
MMP-12 Elastase [15]	NQVFLFKDDKYWLISNC-NH$_2$	2132.5	7.2

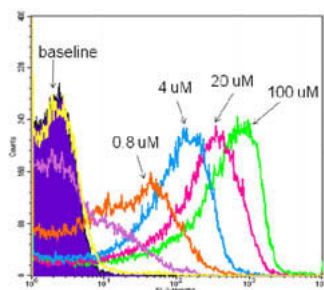[a] *½ Max (µM) of Fc-5-peptide*

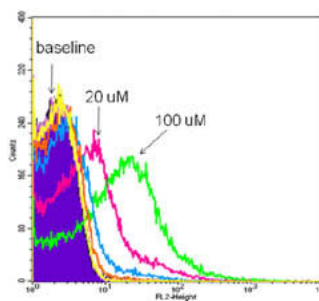*Fig. 1. Fc-CAP-18 FACS titration.*
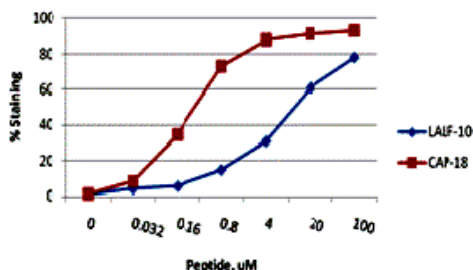

Fig. 2. Fc-LALF FACS titration.

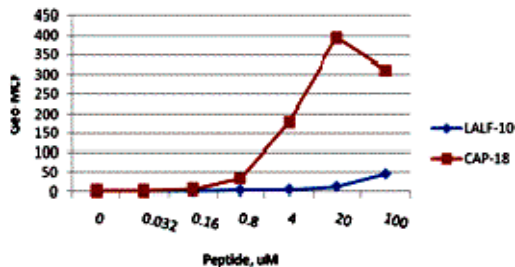Fig. 3. Percent staining of Fc-peptide to PA01 via FACS analysis.

Fig. 4. Geo MCF staining of Fc-peptide to PA01 via FACS analysis.

Results and Discussion

Flow cytometry is a technique that allows one to analyze biological material (i.e. cells) by the detection of the light-absorbing and fluorescing properties by passing cells through a laser beam and measuring the emitted light using electronic detectors (Figures 1 and 2). We utilized Fluorescein labeled LPS binding peptides in FACS assay to study the binding activity of each peptide to bacterial cell wall. We compared the binding affinities of 10 AMPs labeled with Fluorescein-5-maleimide to live *Pseudomonas aeruginosa* using this technique. CAP-18 and NRC-16 demonstrated the highest binding affinities, at 0.16 and 0.47 µM, respectively (Figure 3, 4, and Table 1). The AMPs were rank-ordered for binding strength, with CAP-18 demonstrating the highest binding affinity followed by NRC-16 >, MMP-12 (1) > LF-11 > SAP-14 >LALF-10 > MMP-12 (2) > LBP-18 > JP-1 > JP-2. FACS analysis is proven helpful in studying direct binding of cationic peptides to Gram negative bacteria.

Future Direction

Covalently link CAP-18 and NRC-16 to an antibody effector scaffold (human IgG1). Determine the bio-conjugate for anti-microbial activity (complement deposition and opsonization/ phagocytosis of target cells). The future lies in establishing an appropriate combination of therapeutic approaches, and it appears likely that direct neutralization of LPS using a cationic peptide will be part of this cocktail therapy approach. The use of antibiotics will kill bacteria, and yet this treatment itself leads to the release of LPS endotoxin. Using a structure-based approach to understand how agents bind to and neutralize LPS will aid in the design and optimization of LPS-neutralizing compounds. The successful antisepsis agents depend both on the production of agents that can neutralize LPS at the very early preseptic stage (i.e., a prophylactic agent) and combination with other approaches to "mop up" LPS once liberated from bacterial membranes.

References

1. Larrick, J.W., et al. *J. Immunol.* **152**, 231-240 (1994).
2. Thomson, D., Pepys, M.B., Tickel, I., Wood, S., *JMB* **320**, 1081-1086 (2002).
3. de Haas, C.J.C., et al. *Infect. Immun.* **67**, 2790-2796 (1999).
4. Japelj, B., Pristovšek, P., Majerle, A., Jerala, R. *JBC* **280**, 16955-16961 (2005).
5. Beamer, L.J., Carroll, S.F., Eisenberg, D. *Prot. Sci.* **7**, 906-914 (1998).
6. Taylor, A.H., et al. *JBC* **270**, 17934-17938 (1995).
7. Applemelk, B.J. An, Y.Q., Geerts, M. *Infect. and Immun.* **62**, 2628-2632 (1994).
8. Ellisson, R.T., Giehl, T.J. *J. Clinic. Invest.* **88**, 1080-1091 (1991).
9. Majerle, A., Kidric, J., Jerala, R. *J. Antimicro. Chemo.* **51**, 1159-1165 (2003).
10. Battafarano, R.J., Dahlberg, P.S., Ratz, C.A. *Surgery* **118**, 318-324 (1995).
11. Hoess, A., Watson, S., Siber, G. R., Liddington, R. *EMBO J.* **12**, 3351-3356 (1993).
12. Wang, G. *JBC* **283**, 32637-32643 (2008).
13. Matsumoto, M., Suzuki, M., Patent US 2009/0048178.
14. Douglas, S., Gallant, J., Patrzykat, A., Patent US 2006/0093596.
15. Houghton, A.M., et al. *Nature* **460**, 637-641 (2009).

Bioassays of Analogs of Pleurocidin-Amide Indicate that Change at *N*-Terminus is Key to Improved Efficacy

Roxanne LaCroix, Krishna Tamminedi, David E. Ryder, Jay F. Sperry, and Lenore M. Martin[*]

Department of Cell & Molecular Biology, University of Rhode Island, Kingston, RI, 02881, U.S.A.

Introduction

We have a problem. Many microbial pathogens are becoming resistant to conventional therapeutics, and are no longer affected by them. We need to develop the next generation of antimicrobials or return to times when a minor bacterial infection could be fatal. Antimicrobial peptides (AMPs) typically have broad-spectrum specificity, which makes them ideal for critical treatment situations when the identity of the pathogen is unknown. Pleurocidin, an AMP found in secretions from winter flounder (*Pleuronectes americanus*), adopts an amphipathic α-helical structure crucial for activity, and this conformation is induced or stabilized by peptide-membrane interactions [1]. We evaluated the impacts of novel pleurocidin analogs on the exponential growth curves of two Gram (+) and two Gram (-) human pathogens using high-throughput broth bioassays capable of simultaneous monitoring the growth of multiple bacterial species on a single 96-well plate [2]. Our hypothesis holds that specific additions to the *N*-terminus of our "base peptide" pleurocidin-amide, (**LM4-12**), which were designed to enhance initiation of peptide-cell membrane interactions, will increase antimicrobial efficacy and selectivity [3]. We have tested the effects of grafting combinations of **R**, **G**, & **W** onto the *N*-terminus of base peptide **LM4-12**, synthesized using Boc-SPPS methods on an MBHA resin [4]. Comparison of the effects of adding each of these three amino acids to the *N*-terminus of **LM4-12** generated the lead peptide **LM4-15**, with an *N*-terminal arginine, that yielded dramatically improved broad-spectrum efficacy against *Enterococcus faecalis* (EF), *Staphylococcus aureus* (SA), *Pseudomonas aeruginosa* (PA) and *Escherichia coli* (EC).

LM4-15 (*N*-Ter) H-$\underline{R}$GWGSFFKKAAHVGKHVGKAALTHYL-NH$_2$ (*C*-Ter)

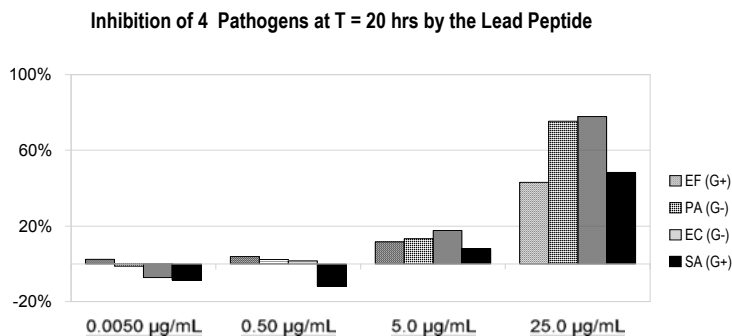**Inhibition of 4 Pathogens at T = 20 hrs by the Lead Peptide**

Fig. 1. Lead Peptide ***LM4-15***.

Results and Discussion

Lead peptide **LM4-15** (Figure 1) showed a significant efficacy against all four human pathogens, with ≥48% growth inhibition relative to untreated bacterial cultures at the maximum tested dose (25 µg/mL, 8.72 µM). Base peptide **LM4-12** (Figure 2) showed a similar inhibitory effect, but only on two of the four pathogens (both Gram +), and some species selectivity, with the highest efficacy against SA. Growth inhibition was calculated as the OD$_{630}$ of peptide-treated bacteria, divided by the OD$_{630}$ of identical untreated cells grown in broth cultures, under the same conditions, measured 20 hours after a single treatment with the test peptide at the indicated dose.
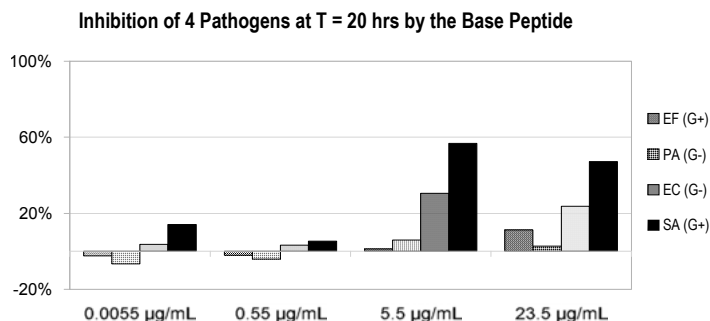
Inhibition of 4 Pathogens at T = 20 hrs by the Base Peptide

*Fig. 2. Base Peptide **LM4-12**.*

MIC assays typically test the effectiveness of potential antibiotics using a fairly low (10^4 CFU) inoculum of bacteria. Our data, obtained at a higher starting concentration of bacteria (OD_{630} = 0.12 at t = 0), shows that **LM4-12** reached a maximum efficacy for SA, and EC at the second highest dose of the base peptide tested (5.5 µg/mL, 1.85 µM), but was not effective against either PA or EF, even at the highest tested dose (23.5 µg/mL, 8.64 µM). **LM4-15** however, was found to reach a much higher efficacy against all 4 target species at the maximum tested dose of the lead peptide (25.0 µg/mL, 8.72 µM), attaining an efficacy of greater than 48% growth inhibition when tested on gram positive microorganisms SA and EF. What is more, **LM4-15,** at the highest tested dose, showed greater than 73% growth inhibition when tested on the gram negatives, EC and PA, which were not inhibited by **LM4-12** to any great extent (Figures 3-6).
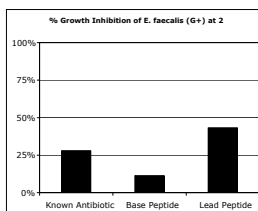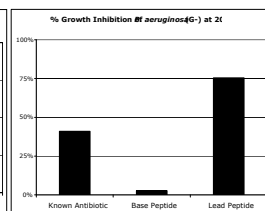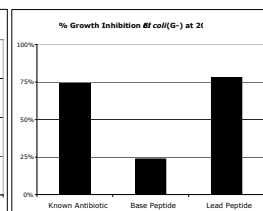
Fig. 3. EF (G+).   *Fig. 4.PA (G-).*   *Fig. 5. EC (G-).*   *Fig. 6. SA (G+).*
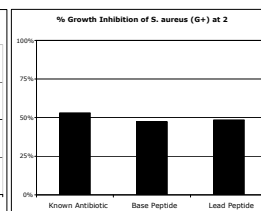
In conclusion, modifying the *N*-terminus of the base antimicrobial peptide by adding arginine dramatically enhanced antimicrobial efficacy in the lead peptide **LM4-15** over that of the base peptide **LM4-12**. As the assay data in Figures 1 and 2 demonstrates, peptide doses as low as 5 µg/mL slightly retard bacterial growth, with a significant level of inhibition reached at only 25 µg/mL, the maximum dose assayed in these experiments. Comparing the efficacies of the lead and base peptides with those of a known antibiotic, oligomycin, confirmed that the lead peptide inhibited bacterial growth of three of the four pathogenic microbial species tested (EF, PA, and EC) as well as (or better than) the known antibiotic in our assays. This lead peptide shows great promise as a therapeutic agent, especially now that more bacteria are becoming increasingly resistant to conventional antibiotics. The dramatic increase in antibiotic efficacy observed with a single arginine addition onto the *N*-terminus of pleurocidin in **LM4-15**, versus the low efficacy of similar synthetic peptide analogs prepared with tryptophan, lysine, and glycine at that position, suggests that *N*-terminal arginine addition onto existing AMPs may prove to be a general strategy for increasing AMP effectiveness in targeting diverse bacterial membranes.

References

1. Cole, A.M., Weis, P., Diamond, G. *JBC* **272**, 12008-12013 (1997).
2. Tamminedi, K., (2009), Synthesis and study of Pleurocidin amide and an analog, *URI, Masters Thesis. Presented at 21st APS in Indianapolis*. http://www.americanpeptidesociety.org/symposiums/
3. LaCroix, R., Martin, L. US Patent Pending, June 2011.
4. Merrifield, R.B. *J. Am. Chem. Soc.* **85**, 2149-2154 (1963).

Effect of Membrane Negative Charge on the Interaction of the Bioactive Peptide Gomesin and Its Linear Analogue with Lipid Bilayers

Tatiana M. Domingues, Katia R. Perez, Karin A. Riske, and Antonio Miranda

Department of Biophysics, Federal University of São Paulo, São Paulo, 04044-020, Brazil

Introduction

Antimicrobial peptides play a key role in the innate immune defense system of animal and plants against microorganisms. Here we focus the antimicrobial peptide Gomesin (Gm) isolated from the Brazilian spider *Acanthoscurria gomesiana* [1,2]. Gm is very effective against a wide range of bacteria, fungi and parasites. Gm has six positive charges, adopts a β-hairpin structure due to two disulfide bridges and exhibits an amphipathic character. Its positive charges play an important role in its interaction with negatively charged membranes. Here, we evaluate the binding of Gm and its linear analogue (Ser[2,6,11,15]-Gm, named GmL) to model membranes composed of mixtures of neutral (palmitoyl oleoyl phosphatidylcholine, POPC) and anionic (palmitoyl oleoyl phosphatidylglycerol, POPG) lipids. Different approaches are used, such as isothermal titration calorimetry (ITC); fluorescence measurements of leakage of carboxyfluorescein (CF) entrapped in large unilamellar vesicles (LUVs); and zeta potential measurements.

Results and Discussion

Different experimental setups were used to study the interaction between the antimicrobial peptides and the vesicles (LUVs). First we tested the interaction between Gm and GmL, and LUVs by using ITC. With this technique the heat released or absorbed is measured when a dispersion of LUVs is titrated into a solution of peptide. With a proper model, the thermodynamics of peptide-lipid interaction can be assessed. Titration of LUVs composed of POPC with 15, 25, 50 mol% POPG and pure POPG were done into both Gm and GmL at 25°C (data not shown). The magnitude of the enthalpy variation, ΔH, increased with the mol% of POPG. Besides that, the interaction of Gm with the same bilayer composition was always stronger than the interaction of its linear analogue [3,4]. The sigmoidal curves of ΔH (per mol of injected lipid) as function of lipid-to-peptide molar ratio obtained at high mol% POPG fall close to a master curve when the data is shown relative to the mol% POPG only.

In another setup, we studied the effect of both peptides in the leakage of CF. LUVs were prepared by extrusion (hydrodynamic diameter, D_h = 100 nm) and loaded with 50 mM CF, at several POPC and POPG molar ratios (10 mM Phosphate buffer, pH 7.4). Non-entrapped CF was removed after elution of LUVs in a Sephadex-G25 column. At high concentrations, CF is self-quenched. When CF contained in the internal liposome compartment is released to the external media by peptide or surfactant addition, the fluorescence of the diluted CF increases. Aliquots of LUVs were added to a fluorescence cuvette containing the same buffer used for the Sephadex-G25 column elution (10 mM Phosphate buffer, 300 mM NaCl, pH 7.4). The increase in CF fluorescence as a function of time at 25°C was recorded continuously in a Hitachi F-2500 Fluorescence Spectrophotometer (λ_{ex} = 490 nm and λ_{em} = 520 nm). At the end of each experiment, total CF fluorescence was determined by the addition of 10 µL of 10% (w/v) Triton X-100. The percentage of CF leakage, % leakage, was determined by using Equation 1, as previously described in literature [5]:

$$\text{Leakage (\%)} = \frac{I_{(t)} - I_0}{I_T - I_0} \times 100$$

Eq. 1. The percentage of CF leakage, % leakage, where $I_{(t)}$ is the fluorescence intensity on time (t), I_0 is the fluorescence intensity before peptide addition and I_T is the fluorescence intensity after Triton X-100 addition.
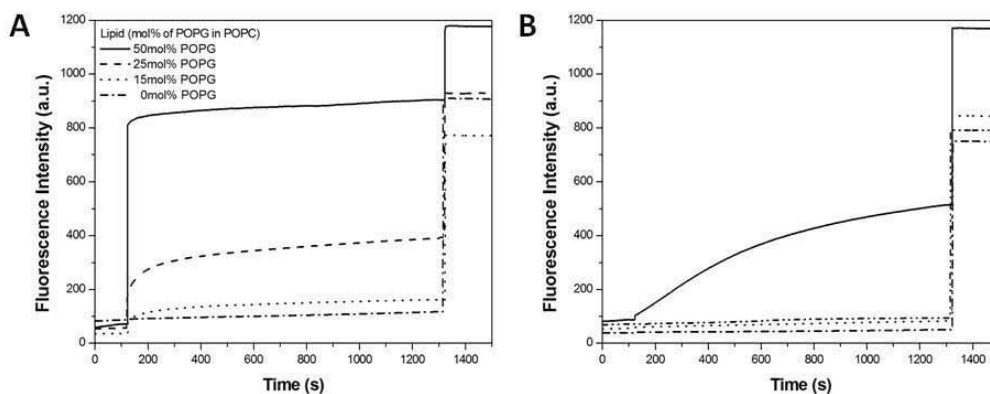
Fig. 1. Fluorescence release vs. time measured with fluorimeter. In the quartz cuvette (1 cm path length) was transferred LUVs suspensions of different content of POPG following 50 μM of Gm (A) and GmL (B) was added. T = 25°C, 10 mM Phosphate buffer, 300 mM NaCl, pH 7.4.

The experiments (Figure 1) show an increase in the fluorescence intensity (a.u.) as function of the time after addition of 50 μM peptide. For Gm (1A), CF leakage is more pronounced the higher the mol% POPG (75.4% of CF release for 50 mol% POPG). On the other hand, GmL (1B) induced significant leakage only from LUVs composed of 50 mol% POPG (39.1%).

We also investigated the binding of these peptides to the membrane surface by using zeta potential analysis (data not shown). Eletrophoretic mobility of LUVs composed of 50 mol% POPG was recorded as a function of increasing concentrations of Gm or GmL (25 °C; 10 mM Phosphate buffer, pH 7.4). Zeta potential (ζ) was calculated from electrophoretic mobility using the Helmholtz-Smoluchowski relation. As the cationic peptides bind to the negative membrane surface, the zeta potential becomes less negative and can even become positive. Electrical neutrality for Gm ($\zeta = 0$) is observed at a peptide-to-lipid ratio of 0.125, implying that the peptide charge (z_p) must be at least $0.50/0.125 = 4$ to achieve charge neutralization. This number defines a lower limit for z_p if indeed all Gm were bound to PG lipids. However, some Gm molecules remain always in solution in thermodynamic equilibrium, and the true peptide charge must be larger than 4. In the case of GmL, neutralization of the membrane surface was not observed, indicating a lower binding affinity of GmL to the bilayer.

According to data above, we can assume that the interaction of both Gm and GmL with POPC/POPG membranes is due to two main factors: the electrostatic attraction between peptide and lipid, and also the presence of β-hairpin structure. Therefore, using these settings we could differentiate the action of Gm from that of its linear analogue.

Acknowledgments

References

1. Silva Jr., P.I., et al. *J. Biol. Chem.* **275**, 33464-33470 (2000).
2. Fazio, M.A., et al. *Biopolymers* **84**, 205-218 (2006).
3. Domingues, T.M., et al. *Langmuir.* **26**, 11077-11084 (2010).
4. Seelig, J. *Biochim. Biophys. Acta.* **1331**, 103-116 (1997).
5. Alvarez, C., et al. *Chem. Phys. Lipids.* **122**, 97-105 (2003).

Pharmacokinetic Profile of FE 203799: A Novel Long Acting Peptide Agonist of Glucagon-Like Peptide-2 (GLP-2)

Karthik Srinivasan, Steve Qi, Diane M. Hargrove, Jennifer Hartwig, Nicky Ferdyan, Sudarkodi Alagarsamy, Glenn Croston, Régent Laporte, Javier Sueiras-Diaz, Kazimierz Wiśniewski, Halina Wiśniewska, Mark Lu, Alexander P. Posch, Claudio D. Schteingart, and Pierre J-M. Rivière

Ferring Research Institute Inc., 4245 Sorrento Valley Boulevard, San Diego, CA, 92121, U.S.A.

Introduction

GLP-2 is a 33-amino acid peptide secreted by the intestinal L-cells in response to nutrition ingestion. It is known to stimulate intestinal growth, nutrient absorption and mesenteric blood-flow [1,2]. Native GLP-2 has a short elimination half-life (6.4 & 7.2 min in rats and humans, respectively) and high clearance (24.6 and 6.8 ml/kg/min in rats and humans, respectively), in part due to its susceptibility for the dipeptidyl peptidase-IV (DPP4) enzyme [3]. A DPP4 resistant analog of GLP2, teduglutide, has marginally lower clearance (9.9 and 2 ml/kg/min in rats and humans, respectively) than GLP-2 [4]. Herein, we describe the pharmacokinetics (PK) and in vivo efficacy of a novel GLP-2 agonist, FE 203799, which retains potency and selectivity at the hGLP-2 receptor but has a superior pharmacokinetic (PK) and pharmacological profile.

Methods

Peptide synthesis: Conducted using Fmoc solid phase method. The compounds were purified using reverse phase-HPLC.

Rat, Monkey and Minipig PK: In the *in vivo* PK experiments, the jugular vein was used for compound administration intravenously (IV) and the carotid artery was used for blood sampling. The dosing vehicle was 25 mM phosphate buffer, pH 7.4. The PK parameters were determined by non-compartmental analysis using PK Solutions software. (a) Rat: Drugs were administered subcutaneously (SC) or IV by bolus injection to catheterized male Sprague Dawley rats (~0.3 kg). Blood was collected at multiple time points post-injection up to 5 h (IV) and 103 h (SC). (b) Monkey: Drugs were administered SC or IV by bolus injection to male cynomologous monkeys (~5.4 kg). Blood was collected at multiple time points post-injection up to 6 h (IV) and 80 h (SC). (c) Minipig: Drugs were administered SC or IV by bolus injection to catheterized male Yucatan pigs (~67 kg). Blood was collected at multiple time points post-injection up to 10 h (IV) and 169 h (SC).
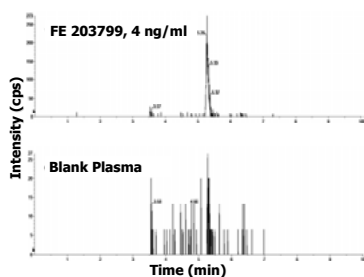

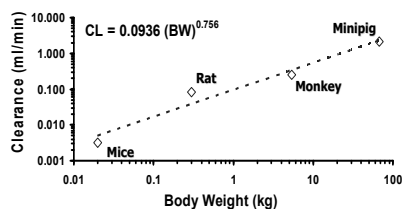*Fig. 1. LC/MS/MS chromatogram of FE 203799 and control in rat plasma.*

Fig. 2. Allometric scaling of clearance in multiple species.

Bioanalysis: Plasma was isolated from blood samples, flash frozen and stored at -20ºC. The method involved protein precipitation extraction electrospray ionization LC/MS/MS (AB Sciex API4000 MS, Shimadzu Prominence HPLC (CBM-20A, SIL-20ACHT). The gradient HPLC method involved reverse-phase column (Phenomenex Jupiter 00B-4053-B0, C_{18}, 50x2.0mm, 5µm, 300Å) and mobile phase (A: 0.01% TFA, 1.0% Formic acid in water, B: 0.01% TFA, 1.0% Formic acid in 70% ACN) at a flow rate of 0.5 ml/min.

Rat PD (Small Intestine Growth): Compounds or vehicle were administered (dose-range 0.3-1000 nmol/kg) by SC injection to male Sprague Dawley rats. Compounds were dosed daily for five days, the rats euthanized, and small intestines were carefully dissected, cleaned, and weighed.
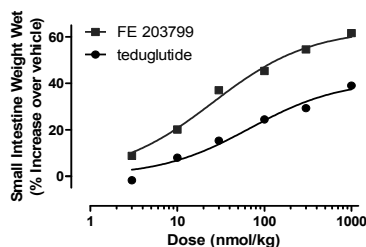
Results and Discussion

Fig. 3. Dose response curve of FE 203799 and teduglutide (QD, 5 d).

The bioanalytical method was precise, sensitive (Figure 1) and reliable. Multispecies PK experiments showed that FE 203799 possesses a favorable PK profile with long terminal half-lives and low systemic clearance (Table 1, Figure 2,4), possibly due to high plasma protein binding (>99%, data not shown). The unique properties of FE 203799 include: (1) Potency and selectivity at the hGLP-2 receptor comparable to native hGLP-2 (2) unique PK profile with low clearance and unprecedented SC half-life (flip-flop PK, possibly due to solubility limiting SC absorption) (3) a greater *in vivo* potency for stimulation of intestinal growth in rats compared to teduglutide. The above properties may confer to FE 203799 a superior therapeutic profile in the treatment of GI diseases.

Table 1. PK parameters of GLP2 analogs in rat, monkey and minipig

Peptide	Rat				Monkey				Minipig			
	IV Dose		SC Dose		IV Dose		SC Dose		IV Dose		SC Dose	
	Elim. half-life	CL	Terminal half-life	F	Elim. half-life	CL	Terminal half-life	F	Elim. half-life	CL	Terminal half-life	F
	min	ml/kg/min	min	%	min	ml/kg/min	min	%	min	ml/kg/min	min	%
Dose (mg/kg)	0.2	0.2	5	5	0.1	0.1	0.25	0.25	0.025	0.025	0.15	0.15
FE 203799	159	0.27	1349	54	474	0.046	1941	32	782	0.032	1808	43
teduglutide	18.7	9.9	31.3	74	43	2.4	56	77	88*	0.99*	164	53
hGLP-2	6.4*	24.6*	21.4*	27.5*	Not Determined							

* hGLP-2 dose: IV 1 mg/kg, SC 2 mg/kg; tedulgutide IV dose: 0.1 mg/kg
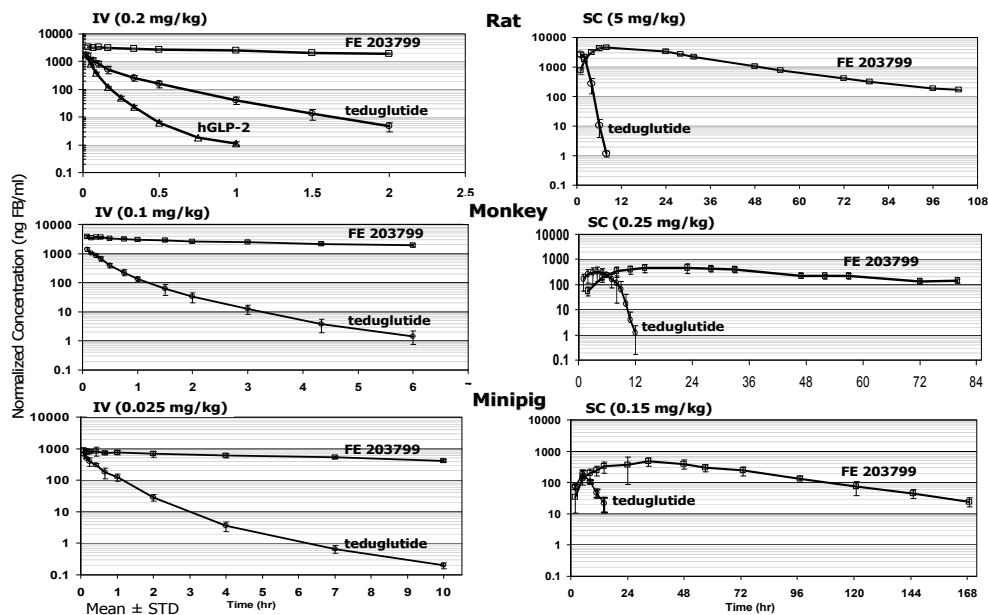
Fig. 4. PK profiles of GLP2 analogs in rat, monkey, and minipig (IV and SC dose).

References

1. Estall. J.L., Drucker. D. *J. Annu. Rev. Nutr.* **26**, 391-411 (2006).
2. Rowland, K.J., Brubaker, P.L. *Mol. Cell Endocrinol.* **288**(1-2), 63-70, (2008).
3. Drucker, D.J., et al. *Nat. Biotechnol.* **15**(7), 673-7 (1997).
4. Marier, J.F., et al. *J. Clin. Pharmacol.* **48**(11), 1289-99 (2008).

Synthesis and Pharmacological Characterization of Novel, Potent and Low Clearance GLP-2 Analogues

Kazimierz Wiśniewski, Javier Sueiras-Diaz, Guangcheng Jiang, Robert Galyean, Mark Lu, Glenn Croston, Diane M. Hargrove, Steve Qi, Karthik Srinivasan, Jennifer Hartwig, Nicky Ferdyan, Halina Wiśniewska, Régent Laporte, Sudar Alagarsamy, Claudio D. Schteingart, and Pierre J-M. Rivière

Ferring Research Institute Inc., San Diego, CA, 92121, U.S.A.

Introduction

GLP-2, **1**, is a 33 amino acid peptide released from intestinal L-cells following food ingestion and acts at G protein coupled GLP-2 receptors in the small intestine and colon to promote intestinal growth and increase nutrient absorption. Native hGLP-2 has a high systemic clearance (CL) due in part to proteolytic cleavage of its N-terminus by dipeptidyl peptidase IV (DPP4), limiting its potential clinical use. A DPP4 resistant analogue, teduglutide, $[Gly^2]hGLP-2$ (**2**), displays similar intestinotrophic properties with an improved pharmacokinetic profile [1]. **2** is in clinical trials in patients with short bowel syndrome [2] and Crohn's disease [3]. Two other analogues with C-terminal hexalysine extensions, ZP1846 and ZP1848 are also in clinical trials for the treatment of chemotherapy-induced diarrhea and for the treatment of Crohn's disease, respectively [4].

In search of GLP-2 agonists pharmacologically superior to compounds currently in clinical development, we synthesized and biologically evaluated (*in vitro* receptor potency and selectivity, *in vivo* rat pharmacokinetics), a series of analogues based on $[Gly^2]hGLP-2$ (1-30) peptide amides where the Met^{10} residue was replaced by the more stable isosteric norleucine. Based on our internal data and literature [5], positions 11 and 16 were selected for modifications. The most promising modifications were then incorporated in full length 1-33 peptides. Here we report on the discovery of potent, low-clearance and clinically relevant GLP-2 analogues.

Results and Discussion

Based on our preliminary C-terminal truncation study (results not shown here) the 1-30 peptide amide was selected for initial SAR studies. To prevent side reactions associated with aspartimide formation [5] due to the presence of the Asp^3-Gly^4 motif, peptides were synthesized by Fmoc SPPS up to position 5 and coupling the protected 1-4 fragment prepared separately on trityl resin. The introduction of single hydrophobic residues in positions 11 or 16 resulted in analogues nearly as potent *in vitro* as the natural hormone, **1**. Compounds with D-aromatic amino acids in position 11 (**3-5**) or aromatic/aliphatic L-amino acids in position 16 (**6-9**) were the most potent in the series. When combined, these modifications resulted in compounds equipotent in vitro with **1** (i.e. **14**). Some analogues modified in position 11 (e.g. **3**, **4**) showed decreased selectivity vs. hGLP-1 receptor. The selectivity was considerably improved when the L-amino acid residues in this position were replaced with their D-enantiomers (**11**, **12**, respectively). The introduction of aromatic D-amino acid residues in position 11 yielded compounds with greatly improved pharmacokinetic profiles in rat as illustrated by their low systemic clearance (CL) values after iv administration (e.g. the D-3-Cpa^{11}, compound **4**). Combination of hydrophobic modifications in positions 11 and 16 led to compounds **13-15** with

	1	2	3	4	5	6	7	8	9	10	11	12	13	14	15	16	17	18	19	20	21	22	23	24	25	26	27	28	29	30	31	32	33	34	
hGLP-2, **1**	H	A	D	G	S	F	S	D	E	M		N	T	I	L	D	N	L	A	A	R	D	F	I	N	W	L	I	Q	T	K	I	T	D	OH
teduglutide, **2**	H	**G**	D	G	S	F	S	D	E	M		N	T	I	L	D	N	L	A	A	R	D	F	I	N	W	L	I	Q	T	K	I	T	D	OH
Compounds **3-15**	H	**G**	D	G	S	F	S	D	E	**Nle**	**Xaa**	T	I	L	D	**Yaa**	L	A	A	R	D	F	I	N	W	L	I	Q	T	K					**NH₂**
Compounds **16-19**	H	**G**	D	G	S	F	S	D	E	**Nle**	**Xaa**	T	I	L	D	**Yaa**	L	A	A	R	D	F	I	N	W	L	I	Q	T	K	I	T	D		**R**

Fig. 1. Sequences of GLP-2 analogues synthesized in this study.

Table 1. Pharmacological profile of GLP-2 analogues

| Analogue | Structure[a] | | In vitro profile[b] | | | Rat PK |
	Xaa^{11}	Yaa^{16}	hGLP-2 EC_{50} (nM)	hGLP-1 EC_{50} (nM)	Selectivity	CL (ml/kg/min)
1	Asn	Asn	0.07	>1000[c]	>14000	25
2	Asn	Asn	0.09	520	5700	9.9
3	D-Phe	Asn	0.09	120[d]	1300	3.3
4	D-Cpa	Asn	0.09	60	660	0.51
5	D-Thi	Asn	0.10	80[d]	800	1.1
6	Asn	Leu	0.10	>1000[c]	>10000	0.84
7	Asn	Cha	0.10	>1000[c]	>10000	0.41
8	Asn	Tyr	0.11	>1000[c]	>9000	1.2
9	Asn	Phe	0.14	>1000[c]	>7100	NT[e]
10	Phe	Asn	0.15	16	100	NT[e]
11	Cpa	Asn	0.16	8.9	55	NT[e]
12	D-3-Cpa	Asn	0.11	45	400	0.32
13	D-Phe	Phe	0.09	>1000[c]	>11000	0.30
14	D-Phe	Tyr	0.07	90[d]	120	0.48
15	D-Phe	Leu	0.08	>1000[c]	>11000	0.30
16	D-Phe	Leu	0.03	>1000[c]	>33000	0.27
17	D-Phe	Leu	0.03	>1000[c]	>33000	0.22
18	D-Phe	Phe	0.06	>1000[c]	>16000	0.24
19	D-Phe	Phe	0.06	>1000[c]	>16000	0.15

[a]*1 has Ala and 2-19 have Gly in pos. 2. 1, 2 have Met and 3-19 have Nle in pos. 10. R is OH for 1, 2, 17 and 19 and NH_2 for all other compounds;* [b]*cell based functional assays of receptor activation;* [c]*No agonism up to the highest concentration tested, 1000 nM;* [d] *Partial agonist;* [e]*Not tested*

further reduced CL values in rat. The full length peptides **16-19** were equipotent or more potent *in vitro* than the parent hormone (analogues **16**, **17** were 2-fold more potent than **1**). CL values were additionally decreased in peptides **16-19** as compared to shortened analogues **13-15**. The C-terminal acid peptides **17** and **19** had pharmacological profiles similar to their corresponding primary amide compounds **16** and **18**.

A series of potent and selective GLP-2 analogues modified in position 11 and/or 16 with pharmacokinetic characteristics superior to that of native hormone and/or teduglutide have been discovered. A member of this series, compound **16** (FE 203799), is a potent, selective and low CL analogue that has been selected for clinical development as a potential treatment of gastrointestinal diseases and disorders. More comprehensive accounts on the pharmacological profile of FE 203799 and related compounds will be presented elsewhere.

References

1. Drucker, D.J., DeForest, L., Brubaker, P.L. *Am. J. Physiol.* **273**, G1252-G1262 (1997).
2. Jeppesen, P.B., et al. *Gut.* **60**, 902-914 (2011).
3. Buchman, A.L., et al. *Inflamm. Bowel. Dis.* **16**, 962-973 (2010).
4. http://www.zealandpharma.com.
5. DaCambra, M.P., et al. *Biochemistry* **39**, 8888-8894 (2000).

Theoretical Studies of Angiotensin II Analogues Against *Plasmodium gallinaceum*

Adriana F. Silva, Marcelo D. T. Torres, Mayra Chamlian, Erick L. Bastos, and Vani X. Oliveira Jr.

Centro de Ciências Naturais e Humanas (CCNH), Universidade Federal do ABC, Santo André, 09210-170, Brazil

Introduction

Malaria is a disease that affects about 2 million people, and kills about 300,000 people per year. Angiotensin II (AGT-II) is a natural peptide with pressor activity which, according to previous researches from our group, also features anti-plasmodium activity against *Plasmodium gallinaceum* responsible for avian malaria [1].

Results and Discussion

Our group designed conformationally constrained analogues, scanning the whole AII sequence with i-(i+2) and i-(i+3) lactam bridge consisting of the Asp-(Xaa)$_n$-Lys scaffold, and investigating its anti-plasmodium and pressor activity. These analogues reduced the proliferation of *P. gallinaceum* in the vertebrate host, inactivating up to 75% of the sporozoites.

Then, structures were generated in the extended conformation, in the protonation state equivalent to pH 7, and the side chain dihedral angles were defined in accordance with the highest probability of occurrence in the rotamer library of Lovell, Word and Richardson. The structures were subjected to two steps of energy minimization followed by molecular dynamics simulations (NVT, 1 ns, 298.15K) using the CHARMm force field and GBSW implicit solvation model (Figure 1).
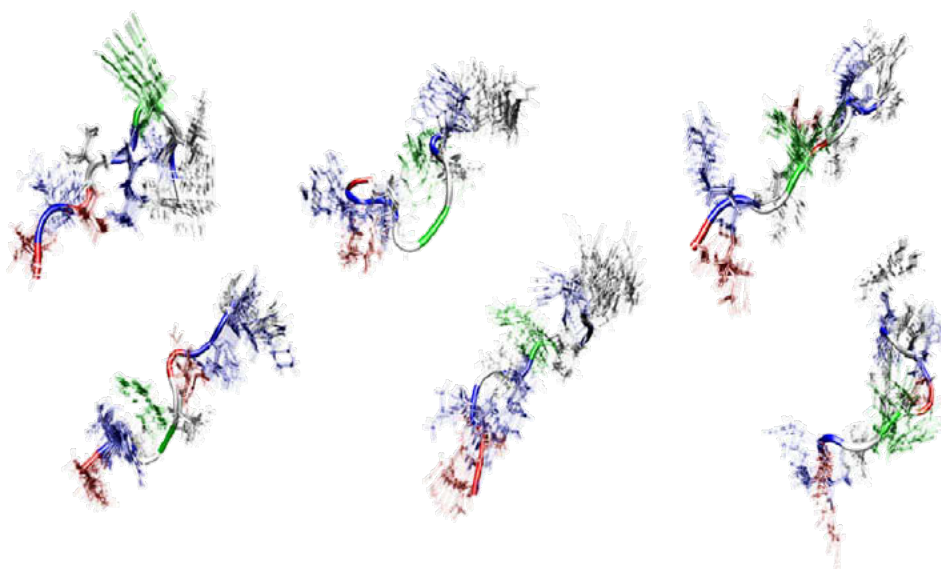
Fig.1. The most active peptides.

Next, thermodynamic and electronic properties of the most relevant and statistically uncorrelated (N = 100) structures for each peptide were determined by quantum mechanics calculations (COSMO/PM6, s-QM/MM approach). These parameters (Table 1) were used in the development of a quantitative structure-activity relationship model for the prediction of anti-

plasmodial activity of AGT-II peptide analogues. Models were designed using a genetic algorithm and were classified according to the Friedman's lack-of-fit parameter.

Table 1. Main analogues chosen and their physicochemical properties

Analogue	D_Z	Q_{YY}	E_{mag}^{IC}	IpE
VC-4	59,757	-321,917	116,138	62
VC-5	86,949	318,719	116,062	76
VC-12	47,828	445,727	116,096	87
VC-16	101,405	-540,107	116,109	53
VC-17	20,417	-376,811	116,161	67
VC-19	27,802	606,966	116,138	74
VC-20	107,241	139,967	116,171	53
VC-25	59,802	-546,379	116,146	56
VC-26	83,974	314,930	116,096	73
VC-28	62,263	-675,416	116,077	67
VC-29	59,757	-321,917	116,174	62

The anti-plasmodial activity of the 11 more efficient analogues was modeled through a genetic algorithm (three parameters binary interactions) and the spores of *P. gallinaceum* percentage of inhibition (IpE) was defined as a dependent variable. The models obtained were classified according to the Friedman`s Lack-of-Fit (LOF). The chosen model to represent this class of peptides is:

$$IpE = 21842 - 0,187E_{mag}^{IC} - 0,271D_Z + 0,012Q_{YY}$$
$$(adj\text{-}R^2 = 0.9479, R^2\text{-pred} = 0.8889, LOF = 27.21, N = 11),$$

in which E_{mag}^{IC} is the magnetic topological descriptor of Bonchev, D_Z is the Z component of de dipole moment and Q_{YY} is the YY component of the quadrupole moment. This study demonstrates the importance of these three parameters in the structure of the peptides of this class and enables future design of new analogues with anti-plasmodial activity.

Acknowledgments

References

1. Maciel, C., Oliveira, V.X., Fázio, M.A., Nacif-Pimenta, R., Miranda, A., Pimenta, P.F., Capurro, M.L. *PLoS ONE* **3**, e3296 (2008).
2. Chamlian, M. *Estudos da ação de análogos cíclicos da angiotensina II nos esporozoítas da malária*. Dissertação de Mestrado; Orientador: Oliveira, V.X., UFABC (2010).
3. Coutinho, K., Canuto, S. *Adv. Quantum Chem.* **28,** 89 (1997).

The Role of the Amino Acid Side Chain Residues in the Biological Action of Angiotensin II, Against the Malaria Sporozoites

Adriana F. Silva[1], Ceres C. Maciel[2], Margareth de L. Capurro[2], Antonio Miranda[3], and Vani X. Oliveira Jr.[1]

[1]*Universidade Federal do ABC (UFABC), Santo André, 09210-170, Brazil;* [2]*Department of Parasitology, Universidade de São Paulo (USP), São Paulo, 05508-000, Brazil;* [3]*Department of Biophysics, Universidade Federal de São Paulo (UNIFESP), São Paulo, 04023-062, Brazil*

Introduction

Malaria is an acute and febrile infectious disease caused by protozoa of the *Plasmodium* genus. It is transmitted by mosquitoes of the *Anopheles* genus. The World Health Organization has reported that 250-500 million people get malaria annually, resulting in around one million deaths [1]. However, efforts to control this disease are hampered by drug resistance in parasites, insecticide resistance in mosquitoes, and the lack of an effective vaccine [2]. Recently, we have reported a research, which showed the angiotensin II (AII) action in mature sporozoites of *Plasmodium gallinaceum* [3]. In an attempt to establish the importance of the amino acids side-chains on the biological activity, we synthesized a series of Ala-scan AII analogues, analyzing all regions of the molecule (Table 1).

Results and Discussion

AII analogues were synthesized using solid phase method on a chloromethylated resin. The peptides were cleaved from the resin using TFMSA/TFA mixture, purified by RP-HPLC and characterized by LC/ESI-MS (Table 1). Conformational studies were performed by circular dichroism (CD) (data not shown). Lytic activity assays were performed using mature sporozoites, collected from salivary glands of *A. aegypti* infected. The sporozoites were incubated with each peptide for 1 hour at 37°C, and the cell membrane integrity was monitored by fluorescence microscopy. The results are shown in Figure 1.
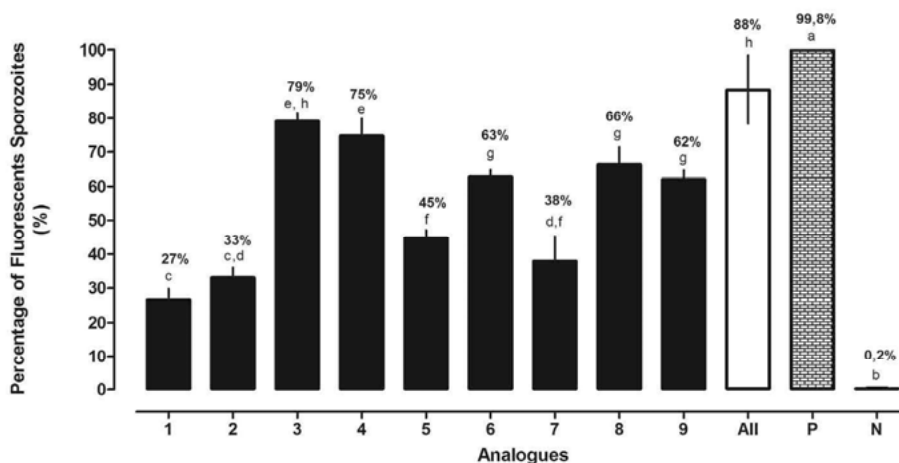
Fig. 1. Effects of the AII analogues on membrane permeability of the mature sporozoites. Data are presented as mean ± standard deviation of fluorescent sporozoites percentage/blade (n=6). Different letters indicate significant difference between the groups treated with AII, peptide analogues and positive control group (P, treated with digitonin and PBS) and negative (N, treated with PBS), respectively (ANOVA followed by Tuckey test, p<0,05).

Table 1. Percent purity of the AII analogues determined by HPLC and Mass Spectrometry

Nº	Name	Sequence	HPLC Purity[a] (%)	Calc mass[b] (Da)	Obsd mass[b] (Da)
1	[Ala^8]-AII	H$_3$N$^+$-D-R-V-Y-I-H-P-**A**-COO$^-$	99	969.5	972
2	[Ala^7]-AII	H$_3$N$^+$-D-R-V-Y-I-H-**A**-F-COO$^-$	100	1019.5	1021
3	[Ala^6]-AII	H$_3$N$^+$-D-R-V-Y-I-**A**-P-F-COO$^-$	100	979.5	980
4	[Ala^5]-AII	H$_3$N$^+$-D-R-V-Y-**A**-H-P-F-COO$^-$	100	1003.5	1006
5	[Ala^4]-AII	H$_3$N$^+$-D-R-V-**A**-I-H-P-F-COO$^-$	99	953.5	954
6	[Ala^3]-AII	H$_3$N$^+$-D-R-**A**-Y-I-H-P-F-COO$^-$	99	1017.5	1018
7	[Ala^2]-AII	H$_3$N$^+$-D-**A**-V-Y-I-H-P-F-COO$^-$	100	960.5	961
8	[Ala^1]-AII	H$_3$N$^+$-**A**-R-V-Y-I-H-P-F-COO$^-$	100	1001.5	1004
9	AII-NH$_2$	H$_3$N$^+$-D-R-V-Y-I-H-P-F-**CONH$_2$**	99	1045.4	1047

[a]*HPLC profiles were obtained in the following conditions: Column Supelcosil C$_{18}$ (4.6 x 150 mm), 60 Å, 5 µm; Solvent System: A (0.1% TFA/H$_2$O) and B (0.1% TFA in 60% ACN/H$_2$O); Gradient: 5-95% B in 30 minutes, Flow: 1.0 mL/min; λ=220 nm; Injection Volume: 50µL and Sample Concentration: 1.0 mg/mL.*

[b]*The mass observed were determined by LC/ESI-MS using a Micromass instrument, model ZMD coupled on a Waters Alliance, model 2690 system. Mass measurements were performed in a positive mode in the following conditions: mass range between 500 to 2000 m/z; nitrogen gas flow: 4.1 L/h; capillary: 2.3 kV; cone voltage: 32 V; extractor: 8 V; source heater: 100ºC; solvent heater: 400ºC; ion energy: 1.0 V and multiplier: 800V.*

We observed that some analogues presented an equipotent anti-plasmodium activity, when compared to AII (Figure 1): [Ala^6]-AII and [Ala^5]-AII with 79% and 74%, respectively. Analogues [Ala^3]-AII, [Ala^1]-AII and AII-NH$_2$ also showed significant biological effects (62 to 66% of activity). Moreover, the analogues, [Ala^8]-AII, [Ala^7]-AII, [Ala^4]-AII and [Ala^2]-AII, presented low lytic activity on the parasite membrane (27 to 45% of activity) indicating the importance of these amino acid side chains. CD studies obtained suggest that the active analogues adopt a β-fold conformation similar to the one obtained for the angiotensin II achieved by several techniques such as NMR and X-Ray diffraction [4,5]. We could conclude that the amino acid residues His and Ile have not an important role in the AII action; however, the residues Phe, Pro, Tyr and Asp are quite important in the antimalarial activity.

This approach is helpful to understand the contribution of each amino acid residue in bioactivity and can provide new perspectives in the design of new chemotherapeutic agents.

Acknowledgments

References

1. Lundqvist, J., Larsson, C., Nelson, M., Andersson, M., Bergstrom, S., Persson, C. *Concomitant Infect. Immun.* **78,** 1924-1930 (2010).

2. Ito, J., Ghosh, A., Moreira, L.A., Wimmer, E.A., Jacobs-Lorena, M. *Nature* **417,** 452-455 (2002).

3. Maciel, C., Oliveira, V.X., Fázio, M.A., Nacif-Pimenta, R., Miranda, A., Pimenta, P.F., Capurro, M.L. *PLoS ONE* **3,** e3296 (2008).

4. Carpenter, K.A., Wilkes, B.C., Scheller, P.W. *Eur. J. Biochem.* **251,** 448-453 (1998).

5. Tzakos, A.G., Bonvin, A.M.J.J., Troganis, A., Cordopatis, P., Amzel, M.L., Gerothanassis, I.P., van Nuland, N.A.J. *European Journal of Biochemistry/FEBS* **270,** 849-860 (2003).

Synthesis and Biological Evaluation of Novel CXCR4 Antagonists Containing Amidine-Type Peptide Bond Isosteres

Eriko Inokuchi[1], Shinya Oishi[1], Tatsuhiko Kubo[1], Hiroaki Ohno[1], Kazuya Shimura[2], Masao Matsuoka[2], and Nobutaka Fujii[1]

[1]Graduate School of Pharmaceutical Sciences; [2]Institute for Virus Research, Kyoto University, Kyoto, 606-8501, Japan

Introduction

FC131 [*cyclo*(-D-Tyr-Arg-Arg-Nal-Gly-)] is a chemokine receptor CXCR4 antagonist that exhibits potent anti-HIV activity [1]. We have investigated the structure-activity relationship of FC131 through optimization of the component amino acids as well as modification using several types of peptidomimetics [2-4]. For the design of FC131 analogs to improve bioactivity, we focused on the common basic functional groups among highly potent CXCR4 antagonists reported so far. For example, the small-molecule antagonist AMD3100 contains eight secondary and tertiary amino groups; the peptide-based antagonist T140 possesses seven basic amino acid residues. In this study for lead optimization of FC131, amidine-type peptide bond isosteres **2** were employed to increase the number of basic groups (Figure 1) [5]. This isostere was originated by substitution of the peptide bond carbonyl (C=O) group with the basic imino (C=N) surrogate to provide an additional cationic moiety with maintenance of the planar sp^2-carbon. For the structure-activity relationship study of FC131, each peptide bond was replaced with the amidine substructure.
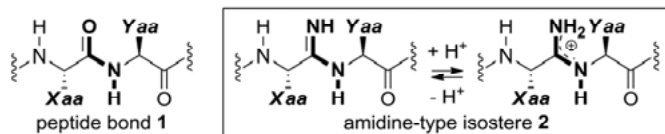
Fig. 1. Structures of peptide bond and the amidine-type isostere.

Results and Discussion

Recently, we established a novel synthetic methodology for amidine-type peptide bond isostere via nitrile oxide-mediated *N*-hydroxyamidine bond formation [5]. Because the key nitrile oxides for the upward component can be prepared from amino acid-derived aldoximes, coupling with the α-amino group of the downward component affords a variety of dipeptide isosteres. Figure 2 shows the synthesis of the D-Nal-Gly-substituted FC131 analog. Briefly, the protected peptide was prepared by standard Fmoc-based solid-phase synthesis using *N,N'*-diisopropyl-carbodiimide/*N*-hydroxybenzotriazole in DMF on aminooxy-2-chlorotrityl resin **3**. The first D-Nal residue was loaded by treatment with Fmoc-D-3-(2-naphthyl)alaninal **4** under acid-free conditions. The linear peptide aldoxime **7** was obtained by cleavage of peptide aldoxime resin **6**. Macrocyclization using *N*-chlorosuccinimide and triethylamine afforded the cyclic amidoxime (*N*-hydroxyamidine) **8**. Raney Ni-mediated reduction to the amidine **9** followed by final deprotection provided the amidine-containing FC131 analog **10c**. The other analogs were synthesized by the same procedure.

Biological activities of the resulting FC131 mimetics **10a-g** were evaluated for inhibition against [^{125}I]-SDF-1 binding to CXCR4 and HIV infection (Table 1). More potent inhibitory activities than the parent FC131 were observed in peptides **10a-e**, indicating that the basic amidine motifs improved affinity with CXCR4 as expected. By contrast, modification of the Tyr-Arg dipeptide decreased the CXCR4 antagonistic activity (**10f,g**). Similar antagonistic activities between two stereoisomers of Nal-Gly- (**10b,c**) and Tyr-Arg-modified peptides (**10f,g**) may suggest more flexible local conformation around the amidine moiety in cyclic peptides compared with the standard peptide bond. Anti-HIV activity of **10a-g** was similar to their inhibitory effects against SDF-1-CXCR4 binding. Of note, none of the peptides **10a-g** showed binding to CXCR7.
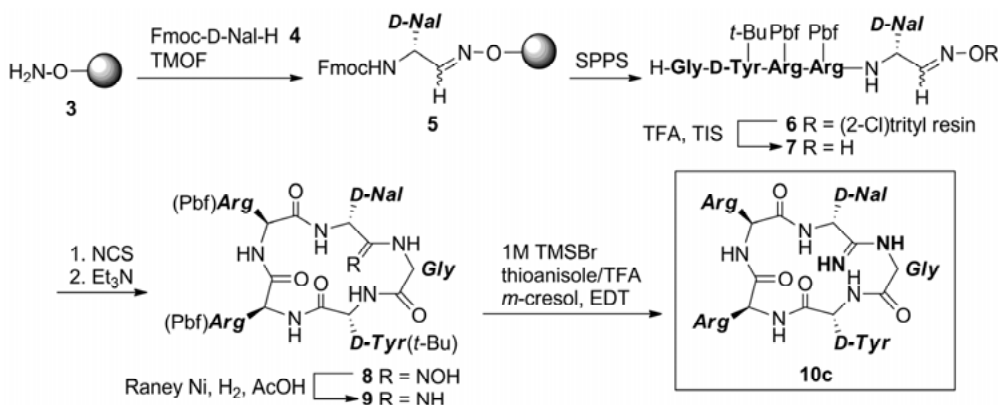
Fig. 2. Synthesis of amidine-containing FC131 mimetics.

Table 1. Biological activity of FC131 and the analog peptides

Peptide	Sequence[a]	IC_{50} (nM)[b]	EC_{50} (nM)[c]
FC131	cyclo(-D-Tyr-Arg-Arg-Nal-Gly-)	126 ± 68	21 ± 4.3
10a	cyclo(-D-Tyr-Arg-Arg-Nal-Gly-ψ[-C(=NH)-NH-]	9.4 ± 3.0	1.3 ± 0.43
10b	cyclo(-D-Tyr-Arg-Arg-Nal-ψ[-C(=NH)-NH-]-Gly-)	4.2 ± 0.31	1.4 ± 0.44
10c	cyclo(-D-Tyr-Arg-Arg-D-Nal-ψ[-C(=NH)-NH-]-Gly-)	4.9 ± 1.1	2.2 ± 0.04
10d	cyclo(-D-Tyr-Arg-Arg-ψ[-C(=NH)-NH-]-Nal-Gly-)	12 ± 2.9	4.4 ± 1.0
10e	cyclo(-D-Tyr-Arg-ψ[-C(=NH)-NH-]-Arg-Nal-Gly-)	16 ± 7.2	1.9 ± 0.47
10f	cyclo(-D-Tyr-ψ[-C(=NH)-NH-]-Arg-Arg-Nal-Gly-)	678 ± 132	300 ± 57
10g	cyclo(-Tyr-ψ[-C(=NH)-NH-]-Arg-Arg-Nal-Gly-)	334 ± 6.2	248 ± 55

[a]*Nal: 3-(2-naphthyl)alanine.* [b]IC_{50} *values are the concentrations for 50% inhibition of the $[^{125}I]$-SDF-1α binding to CXCR4 transfectant of HEK293 cells.* [c]EC_{50} *is the concentration that blocks HIV-1(NL4-3) infection by 50%.*

In summary, we developed novel potent CXCR4 antagonists containing amidine-type peptide bond isosteres. Modification of the peptide bonds in FC131, except for the D-Tyr-Arg position, with an amidine motif led to improved inhibitory potency against SDF-1 binding to CXCR4.

Acknowledgments

References

1. Fujii, N., et al. *Angew. Chem. Int. Ed.* **42**, 3251-3253 (2003).
2. Ueda, S., Oishi, S., Wang, Z.X., Araki, T., Tamamura, H., Cluzeau, J., Ohno, H., Kusano, S., Nakashima, H., Trent, J.O., Peiper, S.C., Fujii, N. *J. Med. Chem.* **50**, 192-198 (2007).
3. Narumi, T., Tomita, K., Inokuchi, E., Kobayashi, K., Oishi, S., Ohno, H., Fujii, N. *Tetrahedron* **64**, 4332-4346 (2008).
4. Narumi, T., Hayashi, R., Tomita, K., Kobayashi, K., Tanahara, N., Ohno, H., Naito, T., Kodama, E., Matsuoka, M., Oishi, S., Fujii, N. *Org. Biomol. Chem.* **8**, 616-621 (2010).
5. Inokuchi, E., Yamada, A., Hozumi, K., Tomita, K., Oishi, S., Ohno, H., Nomizu, M., Fujii, N. *Org. Biomol. Chem.* **9**, 3421-3427 (2011).
6. Inokuchi, E., Oishi, S., Kubo, T., Ohno, H., Shimura, K., Matsuoka, M., Fujii, N. *ACS Med. Chem. Lett.* **2**, 477-480 (2011).

Synthetic Agonists for the CXCR4 Chemokine Receptor

Marilou Lefrançois[1], Marie-Reine Lefebvre[1], Geneviève Saint-Onge[2], Philip Boulais[1], Jérôme Cabana[1], Simon Lamothe[2], Richard Leduc[1], Pierre Lavigne[1], Nikolaus Heveker[2], and Emanuel Escher[1]

[1]*Département de Pharmacologie FMSS Université de Sherbrooke, Sherbrooke, J1H 5N4, Canada;*
[2]*Centre de Recherche, Hôpital Sainte-Justine, and Département de Biochimie, Université de Montréal, Montréal, Canada*

Introduction

SDF-1, the sole endogenous ligand of CXCR4, has its pharmacophore on the very tip of its N-terminus chain: removing the two amino-terminal residues of SDF-1 renders it antagonistic. It is hypothesized that the N-terminal chain of this ligand enters a binding pocket, allowing it to activate the receptor. The free N-terminal octapeptide possesses agonist efficacy [1], but very low affinity for the receptor. T140, a cyclic peptide derived from polyphemusin, is an inverse agonist of CXCR4 of nanomolar affinity. We hypothesized that grafting the N-terminus of SDF-1 on an appropriate residue of T140 could create a CXCR4 agonist with low nano-molar affinity by mimicking the endogenous ligand of CXCR4. Based on our in silico docking studies on CXCR4, based on ligand binding modes of a similar class A GPCR [2,3], and subsequently on the crystal structure of CXCR4 [4] we synthesized four series of SDF-1-T140 chimera: one each with the SDF-1 N-terminus chain grafted to the 2nd or 12th amino acid of T140, and two series with the chain positioned on the 14th amino acid (Arg12 series having an arginine to compensate for the charge loss suffered on residue 14), with varying chain length. We evaluated both their affinities for CXCR4 and their ability to induce chemotaxis.

Results and Discussion

After assessing the binding affinity of our compounds by competition binding assays using ^{125}I-SDF-1α, we performed *in vitro* chemotaxis assays using neuroprobe plates with 5 µm pores. Our first series, with the chain grafted on the 12th residue of the T140 scaffold, had significantly higher affinity for CXCR4 than the other series, but proved to be cell migration antagonists shown with a concentration of 1 nM of SDF-1α and of 100 nM of the compound to be tested. The second series, with the chain grafted on the 14th residue and a Citrulline on position 12 (as in the T140 molecule) were all partial agonists in the chemotaxis assay. However, compounds in which the 12th amino acid of the T140 scaffold was replaced by Arg to compensate for the charge loss suffered by the addition of the SDF-1α chain on the 14th residue produced several partial agonists, but also a full agonist at 10 nM. This compound, **5** has a 10 amino acid graft that differs from the SDF-1α sequence by swapping SDF-Pro^{10} with Ala (Figure 1), this full agonism is probably attributable to increased flexibility. For future photolabeling assays, we have synthesized a few of the chimeras, with a Benzoyl-Phenylalanine (Bpa) replacing the Val^3 on the SDF-1α chain. Compounds **3** and **8,** both position 14 grafts with 9 amino-acid-long chains, were, unexpectedly, full agonists at 10 nM (Figure 1).

As for the series with the graft positioned on the 2nd residue of T140, for all analogues a loss of affinity but partial agonism was observed.
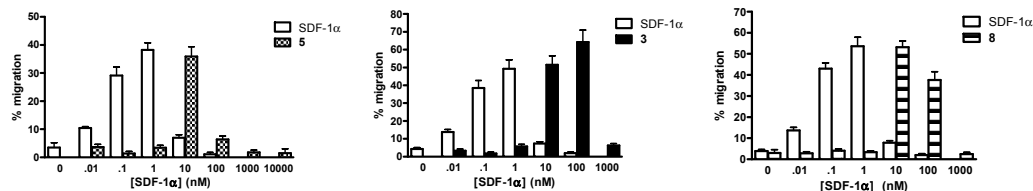
Fig. 1. Agonist chemotaxis assay.

Table 1. Structures: SDF-1α derived side chain and its site of attachment on T140

Cmp No		Affinity (IC$_{50}$) in nM
Graft Position 12	*cyclo-Arg-Arg-Nal-Cys-Tyr-Arg-Lys-DLys-Pro-Tyr-Arg-**Lys(x)**-Cys-Arg*	
1	*Lys-Pro-Val-Ser-Leu-Ser-Tyr- x*	*2.7*
2	*Lys-Pro-Val-Ser-Leu-Ser-Tyr-Arg- x*	*1.4*
Graft Position 14-Arg^{12}	*cyclo-Arg-Arg-Nal-Cys-Tyr-Arg-Lys-DLys-Pro-Tyr-Arg-Arg-Cys-**Lys(x)***	
3	*Lys-Pro-Bpa-Ser-Leu-Ser-Tyr-Arg-Ser- x*	*4.2*
4	*Lys-Pro-Val-Ser-Leu-Ser-Tyr-Arg-Ser-Pro- x*	*9.5*
5	*Lys-Pro-Val-Ser-Leu-Ser-Tyr-Arg-Ser-Ala- x*	*25*
Graft Position 14-Cit^{12}	*cyclo-Arg-Arg-Nal-Cys-Tyr-Arg-Lys-DLys-Pro-Tyr-Arg-Cit-Cys-**Lys(x)***	
6	*Lys-Pro-Val-Ser-Leu-Ser-Tyr- x*	*170*
7	*Lys-Pro-Val-Ser-Leu-Ser-Tyr-Arg-Ser- x*	*6.5*
8	*Lys-Pro-Bpa-Ser-Leu-Ser-Tyr-Arg-Ser- x*	*14.3*
Graft Position 2	*cyclo-Arg-**Lys(x)**-Nal-Cys-Tyr-Arg-Lys-DLys-Pro-Tyr-Arg-Arg-Cys-Arg*	
9	*Lys-Pro-Val-Ser-Leu- x*	*96*
10	*Lys-Pro-Val-Ser-Leu-Ser- x*	*109*
11	*Lys-Pro-Val-Ser-Leu-Ser-Tyr- x*	*62*
12	*Lys-Pro-Val-Ser-Leu-Ser-Tyr-Arg- x*	*38*
13	*Lys-Pro-Val-Ser-Leu-Ser-Tyr-Arg-Ser- x*	*132*

     To conclude, we have shown that positioning the low affinity, agonistic N-terminus chain of SDF-1 on the 14th position of T140 appears to produce full agonists (**3**, **5**, **6**, **8**) and partial agonists (**4**, **7**), whilst on the 2nd position it leads to partial agonists (**9-13**), however on the 12th residue it seems to produce antagonists of chemotaxis (**1**, **2**). Photolabeling assays will follow to identify the differences in binding sites that cause the agonistic or antagonistic efficacies.

References

1. Heveker, N., et al. *Curr. Biol.* **8**(7), 369-376 (1998).
2. Clément, M., et al. *J. Biol. Chem.* **284**(39), 26603-26612 (2009).
3. Fillion, D., et al. *J. Med. Chem.* **53**(5), 2063-2075 (2010).
4. Wu, et al. *Science* **330**(6007), 1066-1071 (2010).
5. Lefrançois, M., et al. *ACS Med. Chem. Lett.* Published online Jun 6 (2011).

Cryptides and Their Accumulative Signaling: A Novel Regulatory Mechanism by Functional Peptides Hidden in Protein Structures

Hidehito Mukai[1,2] and Yoshiaki Kiso[1,2]

[1]*Laboratory of Peptide Science, Nagahama Institute of Bio-Science and Technology, Nagahama, Shiga, 526-0829, Japan;* [2]*Department of Medicinal Chemistry, Center for Frontier Research in Medicinal Science, Kyoto Pharmaceutical University, Yamashina, Kyoto, 607-8412, Japan*

Introduction

Endogenous bioactive peptides including peptidergic hormones and neurotransmitters are firstly produced as precursor proteins, and matured by specific proteolytic cleavages of the precursors. These functional peptides are degraded by various proteases for inactivation. Although many fragmented peptides are also produced during these maturation and degradation processes, their roles have not yet been well elucidated. Recently, we discovered novel bioactive peptides derived from mitochondrial proteins which efficiently activate neutrophils at nanomolar concentrations [1-4]. At the same time, the presence of many neutrophil-activating peptides produced from various mitochondrial proteins were also found [3,4]. Therefore, we named such functional peptides hidden in protein structures as "cryptides" and those cryptides that are derived from mitochondrial proteins as "mitocryptides" [3-5]. In the present study, we attempted to identify various cryptides derived from mitochondrial proteins comprehensively utilizing bioinformatics techniques. We also discuss a novel "accumulative" signaling mechanism in which many cryptides sharing similar physicochemical properties but having different amino acid sequences cooperatively induce physiological functions.

Results and Discussion

Since many fragmented peptides of mitochondrial proteins possibly activate neutrophils [3,4], we highlighted 441 entries of human mitochondrial proteins from protein database Swiss-Prot to make a subset database of human mitochondrial proteins. Fragment peptides cleaved by various proteases such as mitochondrial processing peptidases were collected according to the information of the site of cleavages by those peptidases in each database entry. From the resultant peptide entries, a subset of the peptide database was constructed that contained fragments of 15-36 amino acid residues for subsequent functional predictions.

It is known that certain amphiphilic peptides with positive charges including mastoparan and mitocryptide-1 can induce cell functions in not only mast cells but also neutrophils by the activation of G_i-type G proteins [6-8]. Thus, neutrophil-activating peptides were sought in the above peptide database considering that the target peptides activate G_i-type G proteins. Peptides having more than two net positive charges were extracted first. Then, peptides that can form amphiphilic structures having hydrophobic core composed of aromatic or aliphatic residues were selected. Finally, peptides were extracted whose positively charged side chains are oriented on the same side when the peptide is in an α-helical conformation. These peptides were then chemically synthesized by Fmoc strategy, and their activities to stimulate HL-60 cells differentiated into neutrophilic/granulocytic cells were assessed.

Human cytochrome c (70-85) and (70-88), which are fragments of mitochondrial cytochrome c were bioinformatically identified as neutrophil-activating peptides. At the same time, cytochrome c (68-85) was purified from the porcine heart extract, indicating physiological presence of cytochrome c derived neutrophil-activating peptides. We designated these functional peptides as mitocryptide-CYC1 and mitocryptide-CYC2, respectively. Since cytochrome c is known to be involved in apoptotic processes of various cells, its fragment peptides, mitocryptide-CYC1 and -CYC2 may also have some roles in the apoptotic pathways.

Many mitochondrial transit peptides whose primary structures are not homologous were also found to induce β-hexosaminidase release from HL-60 cells differentiated into neutrophilic/granulocytic cells in a concentration dependent manner. All of these peptides promoted chemotaxis of the differentiated cells. Moreover, the mixture of these neutrophil-activating cryptides at the concentrations that did not cause the stimulation by each peptide

Additive signaling

$$\text{Effect}_{additive} = \sum_{n=1}^{n} \varepsilon_n \frac{[P_n]}{K_n + [P_n]}$$

receptor-1 peptide-1 K_1

receptors for each peptide

receptor-2 peptide-2 K_2

receptor-3 peptide-3 K_3

receptor-4 peptide-4 K_4

Accumulative signaling

$$\text{Effect}_{accumulative} = \sum_{n=1}^{n} \varepsilon_n \frac{[P_n]}{K_n'} \bigg/ \left(1 + \sum_{n=1}^{n} \frac{[P_n]}{K_n'}\right)$$

K_1' K_2' K_3' K_4'

receptor for peptides having same physicochemical features

compete with each peptide binding
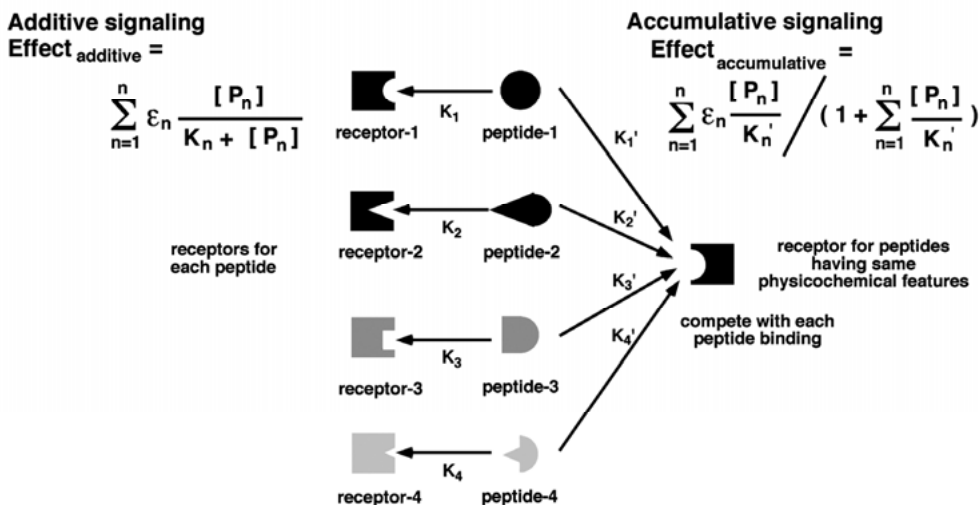
Fig. 1. Comparison of the novel accumulative signaling mechanisms and the "classical" additive signaling mechanisms. It has been considered that the bioactive peptides which have different primary structures bind to different receptors, and induce the independent signaling (additive signaling, left). In the present study, the presence of the alternative signaling mechanism, which active peptides having the common physicochemical properties bind to the "common receptors", was proposed. See text in detail.

markedly promoted β-hexosaminidase release in the differentiated HL-60 cells. These results indicate the presence of novel accumulative signaling mechanisms by these cryptides whose primary structures are not homologous but have common physicochemical properties (Figure 1). The investigation concerning cryptides and their accumulative signaling is expected to elucidate novel regulatory and pathophysiological mechanisms.

Acknowledgments

References

1. Mukai, H., Hokari, Y., Seki, T., Nakano, H., Takao, T., Shimonishi, Y., Nishi, Y., Munekata, E., In Lebl, M. Houghten, R.A. (Eds.) *Peptides: The Wave of the Future (Proceedings of the 2nd International and the 17th American Peptide Symposium)*, American Peptide Society, San Diego, 2001, p1014-p1015.
2. Mukai, H., Matsuo. Y., Kamijo, R., Wakamatsu, K., In Chorev, M. and Sawyer, T.K. (eds.) *Peptide Revolution: Genomics, Proteomics & Therapeutics (Proceedings of the 18th American Peptide Symposium)*, American Peptide Society, San Diego, 2004, p553-p555.
3. Mukai, H., Hokari, Y., Seki, T., Takao, T., Kubota, M., Matsuo, Y., Tsukagoshi, H., Kato, M., Kimura, H., Shimonishi, Y., Kiso, Y., Nishi, Y., Wakamatsu, K., Munekata, E. *J. Biol. Chem.* **283**, 30596-30605 (2008).
4. Mukai, H., Seki, T., Nakano, H., Hokari, Y., Takao, T., Kawanami, M., Tsukagoshi, H., Kimura, H., Kiso, Y., Shimonishi, Y., Nishi, Y., Munekata, E. *J. Immunol.* **182**, 5072-5080 (2009).
5. Ueki, N., Someya, K., Matsuo, Y., Wakamatsu, K., Mukai, H. *Biopolymers (Pept. Sci.)* **88**, 190-198 (2007).
6. Higashijima, T., Uzu, S., Nakajima, T., Ross, E. M. *J. Biol. Chem.* **263,** 6491-6494 (1988).
7. Higashijima, T., Burnier, J., Ross, E.M. *J. Biol. Chem.* **265**, 14176-14186 (1990).
8. Mukai, H., Munekata, E., Higashijima, T. *J. Biol. Chem.* **267,** 16237-16243 (1992).

Ala-Walk Analogs of Oxytocin – HPLC-Based Conformational Studies

Michal Lebl[1,2] and Jiřina Slaninová[2]

[1]*Spyder Institute, 3550 General Atomics Ct., San Diego, CA, 92121, U.S.A.;* [2]*Institute of Organic Chemistry and Biochemistry, Academy of Sciences of the Czech Republic, Flemingovo nam 2, 16610, Prague, Czech Republic*

Introduction

Oxytocin (OXT) is one of the first peptide hormones the structure of which was defined [1] and the importance of individual amino acid residues was studied by systematic replacements and modifications (for review see [2]). Interest in oxytocin was recently renewed after its important behavioral activities were discovered (see e.g. [3]). Conformation of oxytocin and its analogs was studied extensively (see e.g. [4,5]) utilizing various physico-chemical methods. We have shown that HPLC can be used for conformational studies as well [6,7].

Results and Discussion

We have synthesized analogs of oxytocin cycl1-6(Cys-Tyr-Ile-Gln-Asn-Cys-Pro-Leu-Gly-NH$_2$) with all but 1 and 6 positions consecutively substituted with alanines. Analogs were prepared by standard solid phase synthesis on Rink resin. After cleavage and precipitation, analogs were oxidized by diluted solution of hydrogen peroxide. For RP-HPLC studies the solution of analogs was repeatedly reduced by dithiothreitol and oxidized by hydrogen peroxide to verify the elution position of reduced and oxidized forms. Since [Ala^5]OXT did not follow the trend of the remaining analogs and showed unexpected behavior - disulfide containing cyclic form eluting later than reduced linear bis-sulfhydryl form - we confirmed these structures by mass spectroscopy.

From the previous studies of oxytocin analogues it was apparent that the asparagine residue in position 5 has a very unique behavior in NMR studies. Especially its chemical shift temperature dependence was reversed from the normal positive trend. As the HPLC retention can reflect contribution of hydrophobicity of side chains of individual amino acid residues to the

Table 1. Relationship of retention times of cyclic and linearized Ala-walk analogs of OXT

Analog	AA [a]	k' cyclic	k' linear	Ratio [b]	Pred. [c]	A/OXT (lin) [d]	A/OXT (cyc) [e]	Diff (lin) [f]	Diff (cyc) [g]	COSI CE [h]
OXT		2.891	2.982	0.970						
[Ala^2]OXT	Tyr	2.527	2.664	0.949	0.86	0.89	0.87	0.03	0.01	-0.02
[Ala^3]OXT	Ile	2.182	2.473	0.882	0.80	0.83	0.75	0.03	-0.05	**-0.08**
[Ala^4]OXT	Gln	2.964	2.982	0.994	1.09	1.00	1.03	-0.09	-0.06	0.03
[Ala^5]OXT	Asn	3.091	3.000	1.030	1.12	1.01	1.07	-0.11	-0.05	**0.06**
[Ala^7]OXT	Pro	2.773	2.782	0.997	0.96	0.93	0.96	-0.03	0.00	0.03
[Ala^8]OXT	Leu	2.336	2.345	0.996	0.74	0.79	0.81	0.05	0.07	0.02
[Ala^9]OXT	Gly	2.882	3.091	0.932	1.07	1.04	1.00	-0.03	-0.07	-0.04

[a]*Amino acid replaced by Ala;* [b]*Ratio of k' of cyclic and linear forms;* [c]*Expected ratio of retention times of analog to oxytocin (Average values from [8] and [9]);* [d]*Ratio of retention times of analog to oxytocin (linear);* [e]*Ratio of retention times of analog to oxytocin (cyclic);* [f]*Difference between observed and predicted k' ratios of linear forms of analog;* [g]*Difference between observed and predicted k' ratios of cyclic forms of analog;* [h]*Coefficient of side chain exposure.*

Table 2. Uterotonic activities of studied analogs

Analog	Uterotonic activity in vitro		Reference
	This study[a]	Literature[a]	
[Ala^2]OXT	<1% OXT	N.A.	Buku [10]
[Ala^3]OXT	<1% OXT		
[Ala^4]OXT	~2% OXT	36 I.U.	Guttmann [11]
[Ala^5]OXT	<1% OXT	<0.05 I.U.	Guttmann [11]
[Ala^7]OXT	<1% OXT	22 I.U.	Walter [12]
[Ala^8]OXT	~20% OXT	141 I.U.	Jaquenoud [13]
[Ala^9]OXT	<1% OXT	0.25 I.U.	Dutta [14]

[a]Activity of OXT is 450 I.U.

retention on the reversed phase, we speculated that contribution of asparagine to the retention time could be indicating its exposure to the molecular surroundings. We studied both cyclized and linear versions of all analogs and correlated retention times with relative hydrophobic contributions of individual side chains. As can be seen from the data in Table 1, contribution of tyrosine in position 2, glutamine in position 4, and amino acids in the carboxy terminal part of the molecule of oxytocin follow the predicted trend calculated from the literature [10,11] in both cyclic and linear form. However, the difference of predicted retention values of cyclic and linear forms of [Ala^3]OXT and [Ala^5]OXT are significantly larger. We call this value "COSICE" (coefficient of side chain exposure). A large negative value of COSICE means that the side chain being replaced (in our case isoleucine in [Ala^3]OXT) is very significantly more "buried" inside of the constrained cyclic form of the molecule than in the linear form. On the other hand, a large positive value of COSICE means that this side chain (asparagine in position 5) is being "super-exposed" in the cyclic form of the molecule.

The effect of super exposure of asparagine residue, and therefore importance for the interaction of oxytocin with its receptor, correlates with the biological activity of all analogs of oxytocin substituted in position 5 (for the list of analogs see [4]). Any attempt to replace asparagine resulted in an almost complete loss of biological activity. On the other hand, analogs replacing amino acids with small COSICE value retain some residual biological activities. Significant loss of activity of analogs with replaced C-terminal glycine is again predicted from slightly increased COSICE value explained by interaction of the tripeptide Pro-Leu-Gly-NH$_2$ with the cyclic part of the molecule which protects the glycine amide from the interaction with the environment.

Uterotonic activities *in vitro* (Table 2) of the prepared analogs were determined to confirm earlier published results - significant activity was found only in Ala^4 and Ala^8 oxytocin. Differences from published values can be attributed to the different methodologies used in different laboratories.

References

1. du Vigneaud, V. *Experientia* (Suppl 2), 9-26 (1955).
2. Lebl, M., Jošt, K., Brtník, F. In *CRC Handbook of Neurohypophyseal Hormone Analogs*, Jošt, K., Lebl, M., Brtník, F., Eds., CRC Press: Boca Raton, 1987, pp 127-268.
3. Neumann, I.D. *J. Neuroendocrinol.* **20**, 858-865 (2008).
4. Hruby, V.J., Lebl, M. In *ref. 2*, pp 105-155.
5. Lebl, M., Hruby, V. J. In *ref. 2*, pp 155-159.
6. Lebl, M. *J. Chromatogr.* **242**, 342-345 (1982).
7. Lebl, M. *J. Chromatogr. A* **644**, 285-287 (1993).
8. Meek, J.L., Rossetti, Z.L. *J. Chromatogr.* **211**, 15-28 (1981).
9. Guo, D., Mant, C.T., Taneja, A.K., Parker, J.M.R., Hodges, R.S. *J. Chromatogr.* **359**, 499-517 (1986).
10. Buku, A., Fischman, A.J., Wittbold, W.M., Wyssbrod, H.R. In *Proc. 7th Am. Pept. Symp.*, Rich, D.H., Gross, E., Eds., Pierce Chemical: Rockford, Ill., 1981; p 347.
11. Guttmann, S., Boissonnas, R.A. *Helv. Chim. Acta* **46**, 1626 (1963).
12. Walter, R., Smith, C.W., Roy, J., Formento, A. *J. Med. Chem.* **19**, 822 (1976).
13. Jaquenoud, P.A. *Helv. Chim. Acta* **48**, 1899 (1965).
14. Dutta, A.S., Anand, N., Kar, K. *Ind. J. Chem.* **7**, 3 (1969).

Enhanced Hydrophobicity at the Loop of Desmopressin Improves its Antiproliferative Activity

Nancy Iannucci[1,2], Giselle Ripoll[3], M. Belén Pastrian[1], Juan Garona[3], Osvaldo Cascone[1], Graciela Ciccia[2], Daniel Gómez[3], and Daniel Alonso[3]

[1]*School of Pharmacy and Biochemistry, University of Buenos Aires, Buenos Aires, 1113, Argentina;*
[2]*Therapeutic Peptides Research and Development Laboratory, Chemo-Romikin, Buenos Aires, 1605, Argentina;* [3]*Laboratory of Molecular Oncology, Quilmes National University, Buenos Aires, 1876, Argentina*

Introduction

Desmopressin (dDAVP), a synthetic analog of the vasopressin (AVP) hormone, shows *in vitro* antiproliferative activity when incubated with MCF-7 cells [1]. dDAVP is a safe hemostatic peptide with proved antimetastatic properties in breast cancer models in mice and veterinary clinical trials [2]. Consequently, dDAVP results in an interesting lead compound for the development of novel synthetic peptide analogs with enhanced antitumor properties. It is postulated that the antiproliferative activity is mediated by the interaction with the V2 receptor (V2R) and that enhanced hydrophobicity at the cyclic part of the peptide improves this interaction [3]. V2R are expressed in renal collecting ducts, mediating the antidiuretic action, in endothelial cells, mediating most of the non-renal effects, and also in some human tumor cells, such as breast cancer cells [4]. In order to improve this interaction, substitutions at the loop of the peptide were performed, specifically at positions 4 and 5. Antiproliferative activity of dDAVP and two analogs ([V^4]dDAVP and [V^{4}Q^5]dDAVP) was assayed on human breast cancer cells, expressing V2R (MCF-7).

Results and Discussion
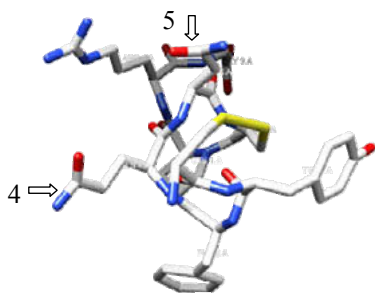
*Fig. 1. AVP molecular model, PDB: 1YF4.
(http://www.cgl.ucsf.edu/chimera/)
Positions 4 and 5 are shown by arrows.*

dDAVP substituted positions can be seen in the AVP molecular model (Figure 1). dDAVP analogs sequences are shown in Table 1. MTT assay was used to measure the ability of peptides to inhibit tumor cell proliferation. As revealed in Figure 2, [V^{4}Q^5]dDAVP analog induced a significantly greater inhibition of MCF-7 proliferation than dDAVP, at concentrations between 500-1500 nM. Almost 30% inhibition of cell proliferation was obtained with [V^{4}Q^5]dDAVP, while growth was reduced only by 10-15% with dDAVP, as reported previously [5]. Analog [V^4]dDAVP exerts a similar antiproliferative profile than dDAVP.

V2R belongs to the G protein-coupled receptors (GPCR) family; these heptahelical transmembrane receptors had a landmark feature
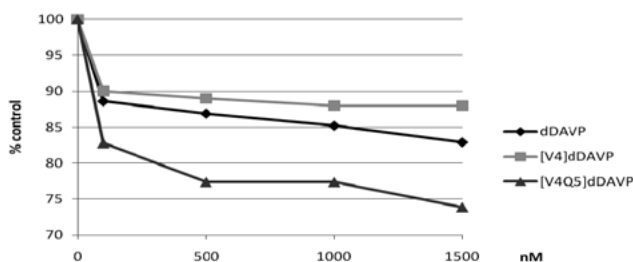
Fig. 2. 72h MCF-7 proliferation assays with dDAVP and analogs.

Table 1. Name and sequences of dDAVP analogs

Code Name	Compound	Sequence
dDAVP	[1-deamino-8-D-arginine] vasopressin (desmopressin)	Mpa-YFQNCPrG-NH$_2$
[V^4]dDAVP	[4-L-valine] desmopressin	Mpa-YFVNCPrG-NH$_2$
[V^{4}Q^5]dDAVP	[4-L-valine-5-L-glutamine] desmopressin	Mpa-YFVQCPrG-NH$_2$

Mpa: β-mercaptopropionic acid (deamino-cysteine)

which is a deep cleft on the extracellular side with a floor characterized by hydrophobic constellations. Simultaneous hydrophobicity at position 4 and a conservative substitution at position 5 improve the antiproliferative activity of analog [V^{4}Q^5]dDAVP relative to dDAVP and [V^4]dDAVP.

Molecular modeling analysis of the human V2R/agonist complex postulates the following docking: the AVP N-terminal hydrophobic triad, Cys^1-Tyr^2-Phe^3, could sit on the floor of the V2R cavity, while AVP Arg^8 could be proximal to Asp^{103} in one of the extracellular loops of the receptor [6]. Thus, hydrophobic and electrostatic forces may rule the AVP/V2R interaction. Enhancing hydrophobicity at position 4, by replacing Gln for Val, and substituting Asn for Gln at position 5 would allow a better accommodation at the bottom of the V2R cavity favored by hydrophobic interactions, thus improving the antiproliferative activity of [V^{4}Q^5]dDAVP. Further affinity binding and activity analysis of dDAVP analogs using selective antagonists for the V2R should be carried out to corroborate this hypothesis.

In order to determine the potential of [V^{4}Q^5]dDAVP as an active antitumor compound, we should evaluate its effects on several aspects of the tumor biology including apoptosis, migration, invasion and metastases. Preclinical research of the novel compound in V2R-expressing animal models is also warranted, in order to determine its potentiality as an active pharmaceutical ingredient in formulations for cancer therapy.

Acknowledgments

References

1. Alonso, D., Ripoll, G., Garona, J., Iannucci, N., Gomez, D. *Curr. Pharm. Biotech.* in press (2011).
2. Hermo, G., et al. *Vet. J.* **178**, 103-108 (2008).
3. Manning, M., et al. *Prog. Brain Res.* **170**, 473-512 (2008).
4. Petit, T., Davidson, K., Lawrence, R., von Hoff, D., Izbicka, E. *Anticancer Drugs* **12**, 133-136 (2001).
5. Keegan, B., Akerman, B., Pequeux, C., North, W. *Breast Cancer Res. Treat.* **95**, 265-277 (2006).
6. Czaplewski, C., Kázmierkiewicz, R., Ciarkowski, J. *J. Computer-Aided Molec. Desig.* **12**, 275-287 (1998).

Development and Pharmacological Characterization of a Urotensin II Derivative Exhibiting Distinctive Antagonistic Properties

David Chatenet[1,2], Quang Trinh Nguyen[3], Myriam Létourneau[1,2], Ngoc-Duc Doan[1,2], Jocelyn Dupuis[3,4], and Alain Fournier[1,2]

[1]*Institut National de la Recherche Scientifique – Institut Armand-Frappier, Université du Québec, 531 boulevard des Prairies, Ville de Laval, Qc, H7V 1B7, Canada;* [2]*Laboratoire International Associé Samuel de Champlain (INSERM – INRS-Université de Rouen);* [3]*Montreal Heart Institute, Université de Montréal, Montréal, Qc, Canada;* [4]*Department of Medicine, Université de Montréal, Montréal, Qc, Canada*

Introduction

Pharmacologically, urotensin II (UII) and urotensin II related peptide (URP) are the endogenous ligands of a G protein-coupled receptor termed UT. Both peptides are expressed with their receptor in several human tissues including brain, lung, heart, pancreas and kidney as well as the vasculature, and until recently were thought to exert redundant biological activities [1]. However, studies have reported a different action of these two peptides on cell proliferation [2] and heart contractibility [3]. Besides, distinct pathophysiological roles for UII and URP in hypertension have been suggested [4]. During the course of a structure-activity relationship on URP derivatives, we identified a new antagonist that is able to specifically block UII-associated biological activity.

Results and Discussion

In our competitive binding assay, binding of ^{125}I-hUII and ^{125}I-URP to CHO cells expressing the recombinant human UT receptors was inhibited by [Bip4]URP with an apparent IC_{50} value of 386 nM and 339 nM, respectively. In a rat isolated aorta bioassay, hUII and URP evoked a concentration-dependent contraction with a pEC_{50} of 8.88 ± 0.25 (E_{max} of $110.6 \pm 7.5\%$ response to 40 mM KCl; n = 8) and 8.13 ± 0.12 ($E_{max} = 112.2 \pm 4.6\%$; n = 8), respectively. Exposure to increasing concentrations of [Bip4]URP up to 3 μM induced only a weak vaso-constriction ($E_{max} = 8.7\%$ at $10^{-5.5}$ M). As shown in Figure 1, various concentrations of [Bip4]URP produced a significant rightward shift of the hUII concentration-response curve and the maximal response to hUII was not attainable. For instance, pre-treatment with [Bip4]URP at 10^{-6}M, produced a significant suppression ($E_{max} = 61.5 \pm 7.3\%$) of the maximum contractile response to hUII with a slight but significant shift in the concentration-response curve ($pEC_{50} = 7.79 \pm 0.31$). Interestingly, a slight but non-significant rightward shift ($pEC_{50} = 7.56 \pm 0.13$) with a non significant reduction of efficacy ($E_{max} = 102.1 \pm 5.9\%$) was observed with URP. Consistent with non-competitive antagonism, the slope of the double reciprocal plot of equiactive concentrations of agonist in the presence and absence of 1 μM [Bip4]URP was linear with a slope of 15.00 ± 0.62, equating to a pK_b of 7.15.
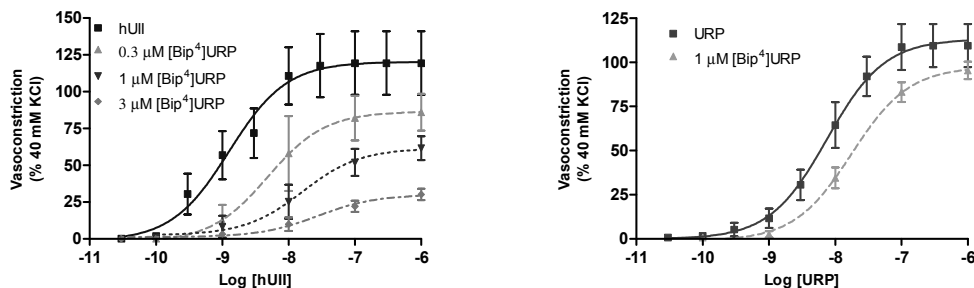
Fig. 1. Effects of [Bip4]URP on hUII- and URP-induced contraction of rat aortic rings.

We further characterized the *in vivo* pharmacological effect of systemic injection of [Bip[4]]URP in anaesthetized rats. Consistent with the vasoactive profile of [Bip[4]]URP in the rat aortic ring bioassay, at high dose (1000 nmol/kg), it produced a noticeable hypotension. Bolus *i.v.* injection of hUII (10 nmol/kg) produced a biphasic pressure response characterized by a rapid and transient pressor phase with the maximum effect occurring at ~1 min, followed by a long lasting hypotension phase reaching the maximum at ~6 min. Similar effects were observed with a bolus injection of URP but the hypotension effect was significantly less pronounced as compared to the same dose of hUII (Figure 2). Compared to control animals, bolus injection of [Bip[4]]URP (1000 nmol/kg) significantly reduced the hUII hypotensive action while keeping intact its pressor effect (Figure 2). Interestingly, [Bip[4]]URP (1000 nmol/kg) had no effect on the biphasic response induced by URP (10 nmol/kg), suggesting its specificity for hUII-mediated physiological activities (Figure 2).
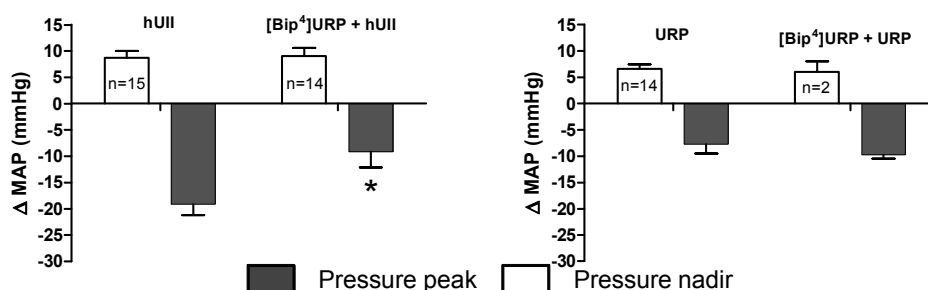
Fig. 2. Effect of [Bip[4]]URP on hUII and URP hemodynamic actions in anaesthetized rats.

In summary, we demonstrated the unique pharmacological profile of [Bip[4]]URP both *in vitro* and *in vivo*. Indeed, this compound, blocking both *in vivo* and *in vitro* hUII-associated action but not URP-mediated effect, represents the first compound of a new class of urotensinergic antagonists. Such compounds would enable a better understanding of the pathophysiological role of the urotensinergic system and would allow the discrimination of specific biological actions mediated by UII and/or URP.

Acknowledgments

References

1. Vaudry, et al. *Ann. N.Y. Acad. Sci.* **1200**, 53-66 (2010).
2. Jarry, et al. *Biochem. J.* **428**, 113-124 (2010).
3. Prosser, et al. *Peptides* **29**, 770-777 (2008).
4. Hirose, et al. *Peptides* **30**, 1124-1129 (2009).

ZP2435 Decreases Body Weight Gain in Diet-Induced Obese Wistar Rats

Lars Bo L. Hansen and Jens R. Daugaard

Zealand Pharma A/S Glostrup, 2600, Denmark

Introduction

PYY(3-36) is a hormone released post-prandially from the intestinal L-cells. PYY acts selectively via the Y2 receptor to reduce caloric intake [1]. Intraperitoneal (i.p.) injection of PYY(3-36) inhibits food intake for over 4 hours in rats and mice [1]. Similar effects have been demonstrated in obese humans [2]. Zealand Pharma A/S has generated a novel PYY(3-36) analogue (ZP2435) by attaching a Structure-Inducing Probe (SIP®) consisting of 5 lysine residues on the N-terminal of PYY(3-36).

Aim

- To evaluate and compare the dose-dependent effect of s.c. chronic administration of ZP2435 and human PYY(3-36) on body weight gain in DIO male Wistar rats.
- To study the effect of ZP2435 and PYY(3-36) on fat pad weight in DIO male Wistar rats.

Methods

50 Wistar male rats (6 weeks old), were fed high fat diet (HFD) (Research Diet # D-12492, New BrunswickUS) for 17 weeks. Rats were weighed twice a week. Osmotic mini-pumps (Alzet® Osmotic Mini-pumps, 2ML4) were filled with infusion solutions containing vehicle, PYY(3-36) or ZP2435. All animals had the osmotic mini-pumps implanted under the skin between the scapulae.

Animals were treated for 28 days and weighed daily. At the end of the study, all animals were fasted for 24 hours and then were sacrificed by exsanguination (heart puncture). Perigonadal (epididymal), retroperitoneal and intrascapular fat tissue was dissected out and weighed.

Table 1. Compounds, counter ions, purity and other data

Drug Name	ZP Number	MW (g/mol)	Salt	Peptide cont.	Purity (%)	Solvent
PYY(3-36)	ZP1740	4050	TFA	83	90	PBS
			TFA	83	96	
K5-PYY(3-36)	ZP2435	4690	Chloride	91	95	PBS
			Acetate	86	96	

Results

As can be seen from Figure 1, ZP2435 significantly decreased body weight gain and addipose tissue mass in DIO rats.
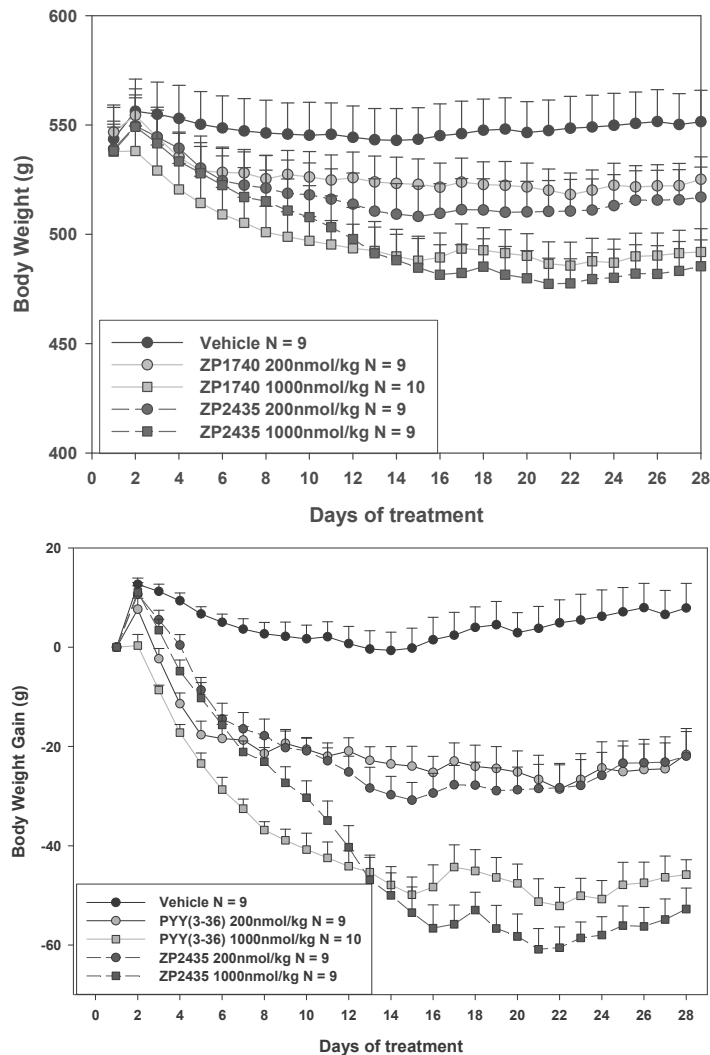
Fig. 1. Effect of 28 days treatment with equimolar concentrations 200 and 1000 nmol/kg of PYY(3-36) and ZP2435 on mean body weight a) and mean body weight gain b) in DIO rats. Values are Mean+SEM.

Conclusion

Both ZP2435 and PYY(3-36) led to marked reductions in body weight in DIO rats fed a high fat diet for 17 weeks.

The effect was dose-dependent with a rapid onset (within 3-5 days).

The decreased body weight was in part due to decreased fat depots (retroperitoneal and brown adipose tissue).

ZP2435 might induce less nausea compared to PYY(3-36).

References

1. Batterham, R.L., et al. *Nature* **418**, 650-654 (2002).
2. Batterham, R.L., et al. *N. Engl. J Med.* **349**, 941-948 (2003).

Pharmacological Characterization of Human Melanocortin-4 Receptor Polymorphisms and Targeted Functional Rescue by Ligands

Carrie Haskell-Luevano[1], Erica M. Haslach[1], Zhimin Xiang[1], Andrzej M. Wilczynski[1], Huisuo Huang[1], Richard A. Houghten[2], Jon Appel[2], Marc Guilianotti[2], Ginamarie Debevec[2], Phaedra Geer[2], and Sally A. Litherland[3]

[1]*Department of Medicinal Chemistry, University of Minnesota, Minneapolis, MN, 55455, U.S.A.;* [2]*Torrey Pines Institute for Molecular Studies, Port St. Lucie, FL, 34987 and San Diego, CA, 92121, U.S.A.;* [3]*Sandford-Burnham Institute, Orlando, FL, 32827, U.S.A.*

Introduction

Single nucleotide polymorphisms (SNPs) of the human melanocortin-4 receptor (MC4R) have been discovered in both obese and non-obese human patients [1,2]. Our research has focused upon the *in vitro* pharmacological characterization of over 60 hMC4R SNPs (Figure 1) to determine the potential molecular mechanism(s) that might associate a particular SNP with obesity [3,4,5]. These potential molecular mechanisms include; 1) not expressed at the cell surface, 2) changing endogenous ligand molecular recognition, and 3) changing endogenous ligand functional signaling (agonist and/or antagonist). These molecular deficits could manifest singly or in multiple combinations. Upon characterization of these receptor polymorphisms, we hypothesized that we could identify ligand(s) that could functionally rescue polymorphic hMC4Rs that did not respond "normally" to the endogenous melanocortin ligands. We successfully demonstrated this concept using peptide and small molecule templates [3,4]. Subsequently, we hypothesized that we could identify molecular templates that could rescue specific polymorphic receptors individually versus globally as we previously reported. Herein, we selected the L106P hMC4R polymorphic receptor [1,6] as a "proof-of-concept" target. Based upon the observation that the tetrapeptide Ac-His-DPhe-Arg-Trp-NH$_2$ possessed nM full agonist activity at the L106P hMC4R versus a lack of full endogenous agonist stimulation for
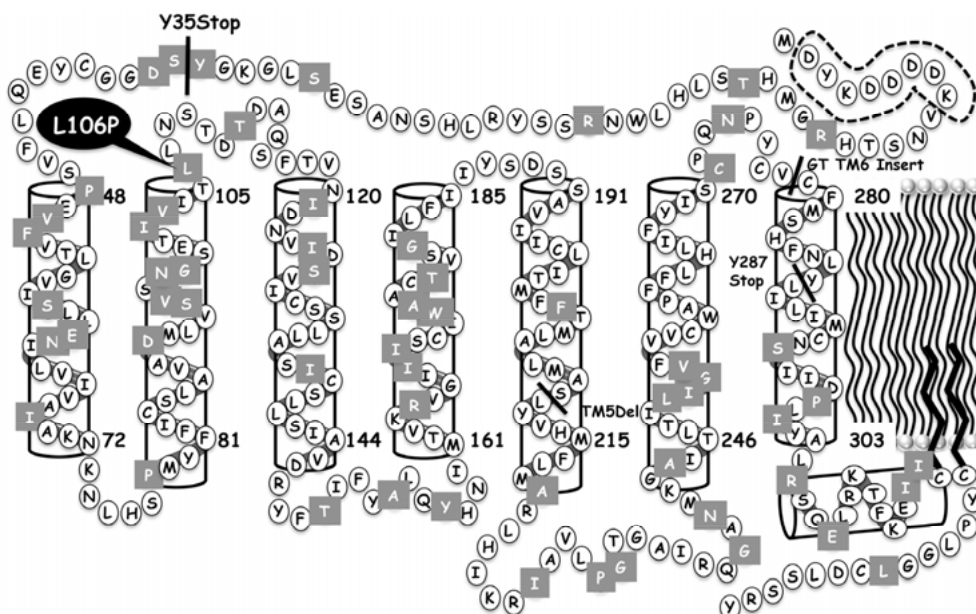
Fig. 1. Location of the hMC4R SNPs pharmacologically characterized by our group.

α-MSH and ACTH [3,4], we hypothesized that we could use a tetrapeptide template to restore this L106P polymorphic hMC4 receptor agonist functional response.

Results and Discussion

Using a mixture-based positional scanning library [7,8,9] functional screening approach, we identified multiple amino acids that could be substituted at each position. These include Arg, Trp, Tyr, DArg, Tic, DTic, (pCl)DPhe, (pI)DPhe), (3I)Tyr, (pNO$_2$)DPhe, and Nal residues. Synthesis and pharmacological characterization of 21 tetrapeptides containing single substitutions at either the His, DPhe, Arg, or Trp positions resulted in higher EC$_{50}$ agonist potencies than anticipated based upon the screening concentrations of the library mixtures. Subsequent dose-response screening of a secondary library resulted in the identification of ca 36 tetrapeptides containing multiple and unanticipated tetrapeptide amino acid combinations. A distinction between two sets of 18 at the DPhe position, with either a (pI)DPhe or (pCl)DPhe residues was evident. Based upon our previous studies identifying the presence of (pI)DPhe within the tetrapeptide Ac-His-DPhe-Arg-Trp-NH$_2$ template resulting in a nM potent mixed mouse MC3R antagonist (with partial agonist activity) and MC4R agonist [10,11], and use of this ligand in rodent feeding studies that revealed *in vivo* data supporting the hypothesis that the MC3R is involved in the regulation of food intake [12], we focused subsequent SAR studies upon this template. Further synthesis, purification, and dose-response receptor pharmacological characterization at the L106P hMC4R identified four tetrapeptide combinations that possessed nM full agonist potencies. The sequences and receptor pharmacological values are provided in this conference proceedings in the manuscript by Eric M. Haslach et al.

Acknowledgments

References

1. Farooqi, S., et al. *N. Engl. J. Med*. **348**, 1085-1095 (2003).
2. Vaisse, C., et al. *J. Clin. Invest*. **106**, 253-262 (2000).
3. Xiang, Z., et al. *Biochemistry* **45**, 7277-7288 (2006).
4. Xiang, Z., et al. *Biochemistry* **46**, 8273-8287 (2007).
5. Xiang, Z., et al. *Biochemistry* **49**, 4583-4600 (2010).
6. Yeo, G.S., et al. *Hum. Mol. Genet*. **12**, 561-574 (2003).
7. Houghten, R.A., et al. *Proc. Natl. Acad. Sci*. **82**, 5131-5135 (1985).
8. Houghten, R.A., et al. *Nature* **354**, 84-86 (1991).
9. Houghten, R.A., et al. *Drug Discovery Today* **7**, 276-285 (2000).
10. Holder, J.R., et al. *J. Med. Chem*. **45**, 3073-3081 (2002).
11. Proneth, B., et al. *J. Med. Chem*. **51**, 5585-5593 (2008).
12. Irani, B.G., et al. *Eur. J. Pharmacol*. **660**, 80-87 (2011).

Design, Synthesis and Structure Characterization of Novel Peptide Template to Probe Melanocortin Receptors Selectivity and Potency

Anamika Singh[1,3], Marvin Dirain[1], Arthur S. Edison[2], and Carrie Haskell-Luevano[1,3]

[1]*Department of Pharmacodynamics;* [2]*Department of Biochemistry & Molecular Biology, College of Pharmacy, University of Florida, Gainesville, FL, 32610, U.S.A.;* [3]*Department of Medicinal Chemistry, College of Pharmacy, University of Minnesota, Minneapolis, MN, 55455, U.S.A.*

Introduction

Melanocortin receptors (MC1-5R) are G-protein coupled receptors (GPCRs) that are regulated by endogenous agonists and antagonists. These receptors are involved in important biological pathways such as skin and hair pigmentation, erectile dysfunction, food intake, energy homeostasis and exocrine glands function [1]. The MC3R and MC4R receptors regulate weight and energy homeostasis which make them potential weight control drug targets [2]. In our ongoing efforts to identify potent and selective lead molecules on these receptors, we have developed a peptide-heterocycle hybrid template [6]. Both building blocks used in the template have non-selective melanocortin receptor agonist activity [3,4]. Previous reports have postulated the presence of a reverse turn in the bioactive conformation of endogenous and synthetic melanocortin peptides [5,8]. Recently, we have reported synthesis and characterization of six compounds based on above mentioned template and identified a potent 85 nM MC4R full agonist [6]. The structural characterization studies (2D ^{1}H-NMR and computer assisted molecular modeling) of compounds provided useful information about ligands structure and conformation. By using the knowledge gained in earlier studies, we now report the synthesis and characterization of second generation focused library.

Results and Discussion

Two libraries were synthesized based on a chimeric peptide (AMW3-130; Yc[CH-DPhe-RWNAFC]Y-NH$_2$)-thioether cyclized small molecule template. The lead compound, (mMC4R EC$_{50}$ = 85 nM) identified in the first library [6] was used to guide the design of the second library. The 18-membered second generation focused library was designed by replacing His-Phe-Arg-Trp amino acids with side chain functionality shown in Figure 1. The modified peptides were synthesized using standard Fmoc-solid phase methodology at room temperature using manual reaction vessel and was also optimized for microwave-assisted solid phase peptide synthesis. The purified compounds were at least >95% pure as determined by RP-HPLC in two diverse solvent systems and possess the correct molecular weights as determined by MS. The synthesized peptides were pharmacologically characterized by the β-galactosidase reporter gene assay at the mouse melanocortin receptor isoforms.

i) **His-** Ala, Pro, Phe, Anc, Atc
ii) **DPhe-** Ala, Pro, (pI)DPhe, DNal(1'), DNal(2'), DBip
iii) **Arg-** Ala, Pro, Lys, homoArg
iv) **Trp-** Ala, Nal(2'), DNal(2'), Bip

Fig. 1. Substitution of HFRW residues in AMW610.

This library resulted in several compounds with interesting pharmacology (Table 1) at mMC1R-mMC5Rs. Substitutions at the Phe position of lead compound by DNal(1'); AST2-38, and DNal(2'); AST2-39, resulted in mixed melanocortin receptor pharmacology. Compound AST2-39 resulted in mMC3R antagonist with some stimulatory activity, whereas,

Compound	Agonist EC_{50} (nM)		
	mMC1R	mMC3R	mMC4R
α-MSH	0.5	0.6	1.9
AMW3-130	0.4	2.0	0.3
AMW610	30	495	85
AST2-38	7	190	130
AST2-39	8.7	Partial Agonist *pA_2=7.6	190

*The antagonistic pA_2 values were determined using the Schild analysis and the agonist MTII)

AST2-38 is a full agonist at all mouse melanocortin receptors. We performed NMR and molecular modeling biophysical studies on these compounds to correlate receptor functional studies with ligand structure. It was observed in earlier studies that inserting the constraint in the peptide resulted in more flexible structures, with less populated conformational families. In present study, compounds AST2-38 and AST2-39 resulted in major families of 29% and 27% of total conformers respectively with RMSD of ~1.6 Å. The representative structure of the most
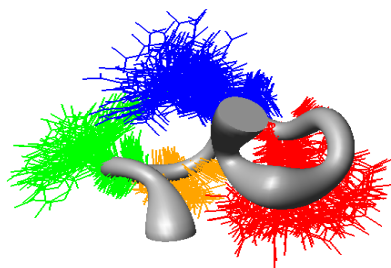
Fig. 2. Sausage representation of the backbone superposition of the major family members of AST2-38. The backbone atoms are shown in gray, side chain of His is depicted in green, DPhe in orange, Arg in blue and Trp in red.

populated conformation family of compound AST2-38 (Figure 2) possesses a reverse β-turn structure involving His and DNal(1') residues at i+1 and i+2 positions. Examination of the backbone phi and psi angles at these residues showed that this turn can be defined as type I'. These observations are consistent with earlier studies [7]. Compound AST2-39 did not show any type of classic turn structure based on dihedral angles or hydrogen bonds.

This study supported the previous hypothesis that compounds having Phe residue substituted with bulky aromatic group are responsible for MC3R antagonism vs. MC4R agonism. The substitutions at His, Arg and Trp positions also resulted in ligands with varying potency. Several of these compounds can be used as tools for *in vivo* characterization of the melanocortin receptors.

Acknowledgments

References

1. Irani, B.J., et al. *Curr. Pharma. Design* **10**, 3443-3479 (2004).
2. Huszar, D., et al. *Cell* **88**, 131-141 (1997).
3. Xiang, Z., et al. *Biochemistry* **46**, 8273-8287 (2007).
4. Bondebjerg, J., et al. *J. Am. Chem. Soc.* **124**, 11046-11055 (2002).
5. Haskell-Luevano, C., et al. *J. Med. Chem.* **42**, 4380-4387 (1999).
6. Singh, A., et al. *J. Med. Chem.* **54**, 1379-1390 (2011).
7. Wilczynski, et al. *J. Med. Chem.* **48**, 3060-3075 (2005).
8. Hruby, V.J., et al. *Pept. Protein Rev.* **3**, 1-64 (1984).

Urea Based Template for Melanocortin Receptors: Design, Synthesis, and Structure-Activity Relationship Studies

Anamika Singh[1,2], Johannes Kast[1], Marvin Dirain[1], Huisuo Huang[1,2], and Carrie Haskell-Luevano[1,2]

[1]*Department of Pharmacodynamics, College of Pharmacy, University of Florida, Gainesville, FL, 32610, U.S.A.;* [2]*Department of Medicinal Chemistry, College of Pharmacy, University of Minnesota, Minneapolis, MN, 55455, U.S.A.*

Introduction

The melanocortin receptor (MCR) family consists of five receptor subtypes (MC1R-MC5R), endogenous agonists (α, β, γ-MSH, and ACTH) and antagonists (ASIP and AGRP). This system is involved in the regulation of complex physiological functions such as pigmentation, inflammation, weight and energy homeostasis, feeding behavior, sexual function and exocrine gland function [1]. The MC4R is located in central nervous system and associated with body weight regulation and sexual function [2]. There has been extensive research in the past to identify potent and selective small molecules at the MC4R subtype based on both peptide and non-peptide templates [3]. Some of the compounds are potent and selective for the MC4R, but limited oral bioavailability and other undesirable properties prevented further development of these compounds as drugs [4]. Recently researchers from Merck have reported an orally bioavailable piperazine urea based compound which is a melanocortin-4 receptor partial agonist and showed anti-obesity efficacy in the rodent models [5]. Our laboratory has reported a small molecule linear tripeptide template (Phe-Trp-Lys-NH$_2$) that includes a urea linkage [6]. A focused library was designed and synthesized using solid phase methodology and identified ligands that possessed full agonist activity ranging from nanomolar to micromolar at the MC3R and MC4Rs.

Results and Discussion

Based upon the earlier studies [6], we designed two libraries using the indicated templates (Figure 1) and commercially available amine and diamine building blocks (Figure 2). The Fmoc-amino acids [i.e. (pCl)Phe, (pI)Phe, Phe, His, Nal(2'), Arg, Lys, Trp] are used at the R$_1$ position, R$_2$ and R$_3$ utilize amine functionality (Figure 2; Table 1). The synthesis of the urea molecules on solid support was modified from our earlier reported method [6] and was further optimized for microwave synthesis. Using microwave chemistry, the synthesis time was dramatically reduced from 5 days to 3h. The diamine, R$_2$ subunit was coupled to 4-[4-(hydroxymethyl)-3-methoxyphenoxy]butanoyl-*p*-methylbenzhydrylamine (HMPB-MBHA) resin through a carbamate linkage after activation of the resin with *p*-nitrophenylchloroformate.
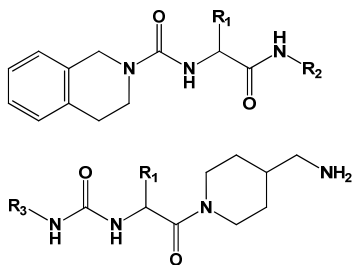
Fig. 1. Rational structure-based design approach which utilizes urea template.
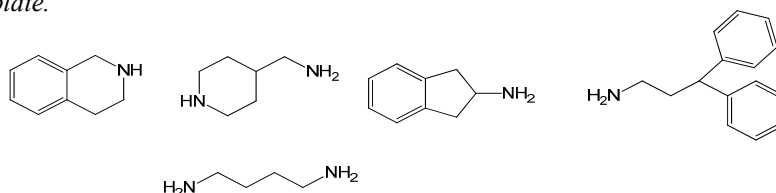
Fig. 2. Commercially available amine functionality utilized at the R$_2$ and R$_3$ positions.

Table 1. Pharmacology of the compounds at the mouse MC1, 3 and 4 Receptors

Compounds	R_2	R_3	Agonist EC_{50} (μM)		
			mMC1R	mMC3R	mMC4R
α-MSH			0.5 nM	0.6 nM	1.9 nM
AST3-115; R_1=Phe	Butyl	1,2,3,4-Tetra hydroisoquinoline	26	>100	>100
AST3-121; R_1=(pI)Phe	Butyl	1,2,3,4-Tetra hydroisoquinoline	73	75	23
AST415-5; R_1=His	4-Methyl-piperidinyl	1,2,3,4-Tetra hydroisoquinoline	29.5	>100	72
AST430-2; R_1=Phe	4-Methyl-piperidinyl	3,3-Diphenylpropyl	21	>100	10
AST455-1; R_1=Trp	*4-Methyl-piperidinyl*	*Dihydroindene*	*40*	*34*	*30*

>100 indicates that no agonist activity was observed at up to the 100 μM concentrations tested. These compounds were not tested as antagonist.

The Fmoc-protected amino acid, R_1 subunit was then added to the amine to form an amide bond with (HBTU) and diisopropyl ethylamine (DIEA) in *N,N*-dimethylformamide (DMF) as the coupling reagents. This was followed by a Fmoc deprotection with 20% piperidine. The R_3, amine subunit was subsequently attached through a urea linkage after carbonylation of the free amine of the R_2 subunit. The product was cleaved from the resin with glacial acetic acid at 45°C on an Advanced Chemtech 440MOS automated synthesizer. The crude product was purified by RP-HPLC and analyzed by mass spectrometry for the correct molecular weights and by analytical RP-HPLC in two divergent solvent systems to determine compound purities as >95%.

The urea-based libraries resulted in compounds ranging from no activity to micro molar activity at the mouse melanocortin receptor subtypes. Subtle differences in structures at R_1 seem to be detrimental in the activity vs. no activity at the mMC3R and mMC4R. The substitutions at the R_2 position with aromatic ring abolished activity at all melanocortin receptors. However aliphatic amine and cyclic amine restored activity at one or more melanocortin reeptor subtypes.

The structure-activity relationship studies based on urea scaffold presented herein provides insight into important ligand-receptor interaction for MC3R vs. MC4R activity. These results may be useful in the further design of potent and selective non-peptide ligands for the melanocortin receptors.

Acknowledgments

References

1. Irani, B.J., et al. *Curr. Pharma. Design* **10**, 3443-3479 (2004).
2. Huszar, D., et al. *Cell* **88**, 131-141 (1997).
3. Ujjainwalla, F., et al. *Curr. Top. Med. Chem.* **7**, 1068-1084 (2007).
4. Nargund, R.P., et al. *J. Med. Chem.* **49**, 4035-4043 (2006).
5. Hong, Q., et al. *Bioorg. Med. Chem. Lett.* **21**, 2330-2334 (2011).
6. Joseph, et al. *Bioorg. Med. Chem. Lett.* **13**, 2079-2082 (2003).

Use of a Tetrapeptide Library to Discover Ligands that Restore Function at a Human Melanocortin-4 Receptor Polymorphism

Erica M. Haslach[1], Huisuo Huang[1], Marc Giulianotti[2], Jon Appel[2*], Ginamarie Debevec[2], Phaedra Geer[2], Richard Houghten[2], and Carrie Haskell-Luevano[1]

[1]*Department of Pharmacodynamics, University of Florida, Gainesville, FL, 32610, U.S.A.;* [2]*Torrey Pines Institute for Molecular Studies, Port St. Lucie, FL, 34987, U.S.A., *San Diego, CA, 92121, U.S.A.*

Introduction

The melanocortin system is comprised of G-protein coupled receptors along with a series of endogenous agonists and antagonists and has been identified to be involved in weight control. The endogenous agonists all contain a core tetrapeptide sequence, His-Phe-Arg-Trp, that has been shown to be important for both molecular recognition and molecular stimulation [1]. The melanocortin-4 receptor (MC4R) has been shown to be involved in weight and energy homeostasis, as well as feeding behavior [2,3]. Obesity is a major health concern and its increasing prevalence justifies studies involving the genetic factors influencing it. Up to 6% of morbidly obese humans have a single mutation within the MC4R and studies have indicated that these mutations lead to obesity because of reduced cell surface expression and decreased affinity of the agonists for the receptor [4]. The L106P melanocortin-4 receptor single nucleotide polymorphism has been reported as a heterozygous polymorphism in an obese patient [5]. The L106P mutation is important to investigate because it is putatively located in the binding region for endogenous ligands. Also, the amino acid proline is referred to as a helix breaker and is postulated to distort the normal binding pocket. Endogenous agonists have decreased affinity and efficacy at the L106P, while tetrapeptides were shown to exhibit nM potency [6,7]. Therefore, it was hypothesized that we could screen a synthetic combinatorial tetrapeptide library, in an assay that focuses on this polymorphism in order to identify ligands that may restore functional activity [8].

Results and Discussion

The positional scanning synthetic combinatorial libraries were provided by the Torrey Pines Institute [9-12]. Screening of additional combinatorial libraries mixtures, and deconvolution has led to the identification of 2-3 specific amino acids at the four different positions that are activating the L106P polymorphism. Tetrapeptides were based on the melanocortin template, Ac-$X_1X_2X_3X_4$-NH_2. Peptides incorporating His or Arg at X_1 and either Tic-(pNO$_2$)DPhe or Arg-(pI)DPhe at X_3X_4 exhibited nM potency at the L106P hMC4R. The sequences and EC$_{50}$ values of the four most potent peptides can be seen in Table 1.

Synthetic Combinatorial Library Screening

↓

Hits/Deconvolution

↓

Synthesis/Re-assay to Confirm Hits
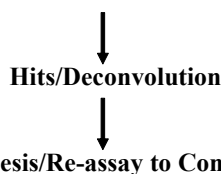
Fig. 1. Schematic of steps taken in this research to obtain results.

The library screening, synthesis of hits, and pharmacological characterization led to the identification of tetrapeptides that resulted in potent nM full agonists at the polymorphic receptor, L106P hMC4R. Tetrapeptides were chosen as the template because previously identified tetrapeptides had nM activity. In addition, it is hypothesized that the presence of proline rather than leucine is distorting the postulated binding pocket, in which this residue may be located within. Therefore, the conformational change due to the polymorphism may only be able accommodate a smaller, compact peptide for normal binding and stimulation. Ligands were not identified to specifically correct for the single L106P hMC4R polymorphism. It would be favorable to discover a ligand that both functionally restores the activity of a polymorphism that does not respond normally to the endogenous ligands and has a greater affinity for the mutation

Table 1. EC50 values for the tetrapeptides obtained

Peptide Name	Sequence	hMC4R EC_{50} (nM)	L106P hMC4R EC_{50} (nM)
1981-7	Ac-His-(pI)DPhe-Tic-(pNO$_2$)DPhe-NH$_2$	0.16	14.0
1981-11	Ac-His-(pI)DPhe-Arg-(pI)Phe-NH$_2$	0.13	2.88
1981-13	Ac-Arg-(pI)DPhe-Tic-(pNO$_2$)DPhe-NH$_2$	0.32	2.77
1981-17	Ac-Arg-(pI)DPhe-Arg-(pI)Phe-NH$_2$	0.22	3.60

over the WT hMC4R. The specific targeting of the polymorphism will ensure that the addition of the new ligand would not distort the overall homeostatic balance

Through the advancement of molecular biology, genetics, and chemistry, potential lead compounds based on a known biological target can be designed to enhance drug discovery and rational drug design efforts. This study validates the use of screening positional scanning synthetic combinatorial libraries in drug discovery and specifically, for the use in identifying molecules that can restore function at natural human polymorphisms in obese patients. Natural mutations associated with diseases are remarkable from a clinical standpoint, as they provide insights into the mechanism of pathogenicity and possible avenues for development of therapeutics. They aid us in deciphering complex relationships between protein structure and function by identifying the key actors in the molecular machinery.

Acknowledgments

References

1. Haskell-Luevano, C., Holder, J.R., Monck, E.K., et al. *J. Med. Chem.* **44**, 2247-2252 (2001).
2. Fan, W., Boston, B.A., Kesterson, R.A., Hruby, V.J., Cone, R.D. *Nature* **385**, 165-168 (1997).
3. Huszar, D., Lynch, C.A., Fairchild-Huntress, V., Dunmore, J.H., et al. *Cell* **88**, 131-141 (1997).
4. Farooqi, S., O'Rahilly, S., Monogenic Obesity in Humans. *Annu. Rev. Med.* **56**, 443-458 (2005).
5. Yeo, G.S., Farooqi, I.S., Aminian, S., Halsall, D.J., et al. *Nat. Genet.* **20**, 111-112 (1998).
6. Yeo, G.S.H., Lank, E.J., Farooqi, I.S., Keogh, J., et al. *Human Molecular Genetics* **12**, 561-574 (2003).
7. Xiang, Z., Litherland, S.A., Sorensen, N.B., Proneth, B., et al. *Biochemistry* **45**, 7277-7288 (2006).
8. Xiang, Z., Pogozheva, I.D., Sorenson, N.B., et al. *Biochemistry* **46**, 8273-8287 (2007).
9. Houghten, R.A. *Proc. Natl. Acad. Sci. U.S.A.* **82**, 5131-5135 (1985).
10. Houghten, R.A., Pinilla, C., Blondelle, S.E., Appel, J.R., et al. *Nature* **354**, 84-86 (1991).
11. Houghten, R.A., Wilson, D.B., Pinilla, C. *Drug Discovery Today* **7**, 276-285n (2000).
12. Houghten, R.A., Pinilla, C., Giulianotti, M.A., Appel, J.R., et al. *J. Comb. Chem.* **10**, 3-19 (2008).

Design Strategies to Produce Receptor Subtype Selective Peptide Agonists and Antagonists for Melanocortin Receptor System

Dhanasekaran Muthu, Robert Soto, Minying Cai, Yen Shan Lim, Dev Trivedi, and Victor J. Hruby

Department of Chemistry and Biochemistry, The University of Arizona, Tucson, AZ, 85721, U.S.A.

Introduction

The melanocortin receptor system consists of five different subtypes (MC1R, MC2R, MC3R, MC4R and MC5R) and all belong to the transmembrane G-protein coupled receptors (GPCRs) super family [1]. The peptide α-MSH is a nonselective endogenous agonist for these receptors except MC2R. The segment His-Phe-Arg-Trp of αMSH has been characterized as the essential pharmacophore for biological activity. Many different synthetic peptide analogues based on this tetrapeptide segment have been shown to be excellent agonists and antagonists for melanocortin receptors, but most of them have not shown receptor subtype selectivity. It remains a daunting challenge to produce a peptide antagonist with exclusive selectivity toward a particular subtype of melanocortin receptor [2]. A number of novel cyclic γ-MSH analogues were designed and synthesized. One of these peptides **MSG606** demonstrated potent antagonist activity and receptor selectivity for the hMC1R (IC_{50} = 17 nM). In our continued effort to produce receptor subtype selective agonist/antagonist peptides, we have designed different series of peptides targeting the MC3R receptor. The synthesis of the peptides was successfully accomplished by using the standard solid-phase synthesis method. The peptides are currently being evaluated for their biological property.

Discovery and conformational analysis of MC1R antagonist

The human melanocortine 1 receptor (hMC1R) is widely distributed both in the peripheral and central nervous systems of humans regulating skin pigmentation, immune response etc. α-Melanocyte-stimulating hormone (α-MSH: Ac-Ser-Tyr-Ser-Met-Glu-His-Phe-Arg-Trp-Lys-Pro-Val-NH₂) is the native nonselective agonist for all subtypes of melanocortin receptors except for the hMC2R. α-MSH and its analogues binding to the melanocortin MC1 receptor is of interest with regard to its potential use in targeting cytotoxic drugs or imaging melanoma. However the endogenous α-MSH lacks selectivity for the melanocortin receptors. To gain receptor selectivity with high potency we have conformationally constrained the endogenous γ-melanocyte-stimulating hormone (γ-MSH: H-Tyr-Val-Met-Gly-His-Phe-Arg-Trp-Asp-Arg-Phe-Gly-OH) by cyclization. A number of novel cyclic γ-MSH analogues were designed and synthesized, in which
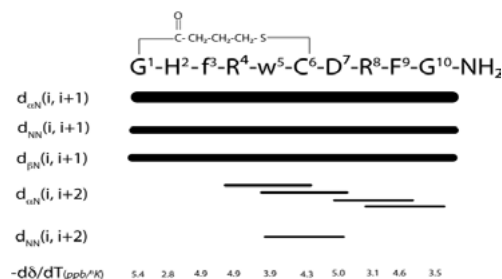
Fig. 1. Summary of observed NOEs and temperature coefficient values of amide protons for peptide MSG606 in SDS micelles.

a thioether bridge was incorporated between a cysteine side chain and an N-terminal bromoacyl group. One of these peptides **MSG606**, *cyclo*-[(CH₂)₃CO-Gly-His-D-Phe-Arg-D-Trp-Cys(S-)]-Asp-Arg-Phe-Gly-NH₂, demonstrated potent antagonist activity and receptor selectivity for the MC1R (IC_{50} = 17 nM). This novel peptide, with a 23 membered ring, is the most selective antagonist for the human hMC1R to date. The NMR analysis (Figure 1 and 2) of this peptide in membrane-like environment revealed a new binding site, specific to the hMC1R antagonist, at the C-terminal, wherein the side chain and backbone conformation of D-Trp[5] and Phe[9] of the peptide contributes to the hMC1R selectivity.
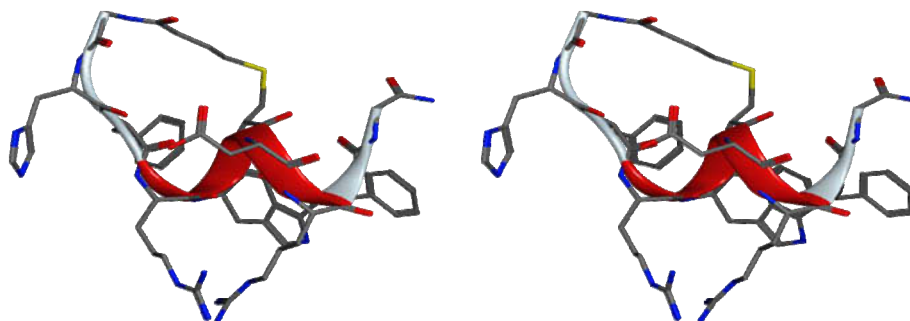
Fig. 2. Stereoview of lowest energy structure resulted from simulated annealing molecular dynamics calculations based on NMR derived distance as well as dihedral angle constraints.

Rational design of MC3R agonist and antagonist cyclic peptides

Two different cyclic peptides as shown in Figure 3 were chosen as lead molecules to design hMC3R specific agonist and antagonists. The cyclic peptide **1** was found to be a very potent and selective hMC3R agonist (EC_{50}=1.2 nM) and the cyclic peptide **2** was identified as an hMC3R/hMC5R antagonist [3]. These two peptides are excellent starting points to design conformationally constrained cyclic peptides to obtain pure hMC3R selective agonist as well as antagonist peptides. Several cyclic peptides were designed and synthesized successfully by reengineering these two lead peptides. The biological properties of the final designed peptides are being evaluated and will be reported in a separate publication.
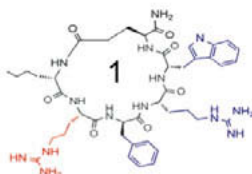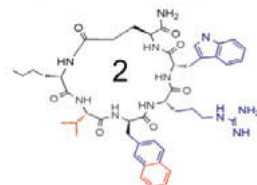
Fig. 3. Lead cyclic peptides for further modification to improve the hMC3R selectivity.

Acknowledgments

References

1. Abdel-Malik, Z.A. *Cell. Mol. Life Sci.* **58**, 434-441 (2001).
2. Hruby, V.J., Cai, M., Nyberg, J. Muthu, D. *Expert Opin. Drug Discovery* **6**, 543-557 (2011).
3. Mayorov, A.V., Cai, M. Chandler, K.B., Petrov, R.R., et al. *J. Med. Chem.* **49**, 1946-1952 (2006).

Novel Allosteric Melanotropins Lead to Selective Cell Signaling

Minying Cai, James P. Cain, Jennifer W. Bao, Dhanasekaran Muthu, Dev Trivedi, and Victor J. Hruby

Department of Chemistry and Biochemistry, University of Arizona, Tucson, AZ, 85721, U.S.A.

Introduction

The melanocortin system involves numerous physiological functions and is associated with many diseases such as skin cancer, obesity and diabetes, sexual dysfunction and neuropathic pain among others. The design of selective, potent melanotropins has great potential for novel drug discovery. Traditionally, optimizing the interaction of lead molecules with the binding site of the endogenous agonist (the orthosteric site) has been viewed as the best means of achieving selectivity of action. However, our studies have highlighted the fact that novel designed melanotropins can interact with binding sites on the receptor molecule that are distinct from the orthosteric binding sites, known as allosteric binding. Allosteric binding could offer several advantages over orthosteric melanotropins, including greater selectivity as well as selective cell signaling. Here, we introduce a series of selective allosteric antagonists of melanotropins with distinct cell signaling compared to the conventional melanotropin activation.

Results and Discussion

Allosteric modulators are compounds that bind receptors at sites which are distinct from the orthostatic (primary) ligand-binding site. They enhance or reduce the action of orthosteric agents by fine-tuning signaling responses of GPCR systems. Allosteric modulators could lower the dosage of a main drug, reduce side effects, and prevent overdose, tolerance, abuse, or dependence. Our previous studies have demonstrated that orthosteric binding sites are highly conserved for melanocortin receptors with few options for subtype selectivity. In principle, allosteric binding sites are far less conserved with many subtypes available [1]. Based on these considerations, we have designed and synthesized peptide and small molecule allosteric ligands for human melanocortin receptors. (Figure 1 and Figure 2). Their binding affinities as well as functional activities have been evaluated in Table 1.

Table 1. Competition binding assay and cAMP assays of allosteric ligands

	hMC1R		hMC3R		hMC4R		hMC5R	
	IC_{50} (nM)	EC_{50} (nM)	IC_{50} (nM)	EC_{50} (nM)	IC_{50} (nM)	EC_{50} (nM)	IC_{50} (nM)	EC_{50} (nM)
1	NB	NA	19	50	NB	NA	NB	NA
2	254	/	28	3	NB	NA	>5000	NA
3	58	6	>100	/	NB	NA	>1000	NA

IC_{50} = concentration of peptide at 50% specific binding; NB = 0% of ^{125}I-NDP-α-MSH displacement observed at 10 μM; EC_{50} = Effective concentration of peptide that was able to generate 50% maximal intracellular cAMP accumulation; NA = 0% cAMP accumulation observed at 10 μM; The peptides were tested at a range of concentration from 10^{-10} to 10^{-5} M; NB = no binding observed at 10^{-5}M.
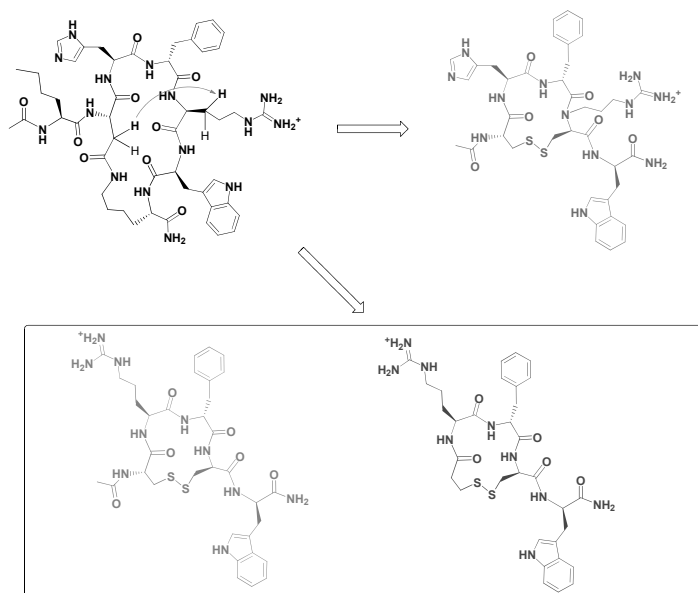
Fig. 1. Novel scaffold of allosteric peptide.

Fig. 2. Novel scaffold of allosteric small molecule.

Peptides are designed based on MSH/AGRP hybrids. A series of peptides have been made (Figure 1) [2]. Activity of one of the selective allosteric peptides (1) is shown in Table 1.

We have recently developed a new scaffold for the synthesis of small molecules and peptidomimetics [3] (Figure 2). Compounds 2 and 3 derived from this molecular template proved to bind to the melanocortin receptors, in some cases with a high degree of subtype selectivity. In continuing to explore the structure-activity relationships (SAR) of this series of compounds, we first examined the activity of analogs built from two additional diastereomers of the core structure. Two analogs were synthesized with each of the diastereomeric cores, by acylation with phenylacetyl chloride and coupling to indolepropionic acid with phosphonium reagents. Binding assay and functional selectivity from cAMP and Ca^{2+} assays (data not shown) have demonstrated that these compounds are allosteric ligands of melanocortin receptors. Functional selectivity will be exploited to learn more about existing drugs and their unique actions that can guide the development of next-generation therapeutics.

Acknowledgments

Reference

1. Hruby, V.J., Cai, M., Nyberg, J. et al. *Expert Opin. Drug Discovery* **6**, 543-557 (2011).
2. Mayorov, A.V., Cai, M., Palmer, E., Trivedi, D., Hruby, V.J. *J. Med. Chem.* **49**, 1946-1952 (2006).
3. Cain, J.P., Mayorov, A.V., Cai, M., Trivedi, D., Hruby, V.J. *Bioorganic & Med. Chem. Lett.* **16** (20), 5462-5467 (2006).

Incorporation of β-amino acids in MT-II & SHU9119

Vinod V. Kulkarni, Minying Cai, Dhanasekaran Muthu, and Victor J. Hruby

Department of Chemistry and Biochemistry, University of Arizona, Tucson, AZ, 85719, U.S.A.

Introduction

β-Amino acids are an important class of compounds especially formed as a secondary bioactive metabolite in living organisms. They play an important role contributing towards bioactivity in peptides, cyclopeptides, depsipeptides, glycopeptides, alkaloids and terpenes [1]. Synthetic β-amino acids are analogues of α-amino acids not metabolized from peptidases. Their incorporation in an endogenous peptide or a synthetic α-peptide which is biologically active gives an inherent stability by improving the half life and bioavailability. Additionally, conformational features are enhanced thus contributing overall towards the development of peptide based drugs [2].

Melanocyte Stimulating Hormone based Ac-Nle-c[Asp-His-D-Phe-Arg-Trp-Lys]-NH$_2$ (**MT-II**) and Ac-Nle-c[Asp-His-D-Nal(2′)-Arg-Trp-Lys]-NH$_2$ (**SHU9119)** are synthetically derived analogues, which have been demonstrated to be super agonists and antagonists towards melanocortin receptors (MCR 1, 3, 4 and 5). Their structure activity relationships [3] have been studied in detail to investigate their chemical and structural features to improve their selectivity thus targeting specific biological and physiological processes. The need for understanding the roles of MCR3 and MCR5 still requires the availability of specific agonists and antagonists for biological studies. Structurally within their pharmacophore, **MT-II** and **SHU9119** have exhibited subtle or drastic changes in their biological roles when substituted/replaced either with a similar/modified amino acid or a feature exhibiting a topographical shift from the side chain groups influencing the χ-orientation.

Incorporation of β^3-amino acids within the **MT-II** and **SHU9119** pharmacophore offers a novel approach to explore new structural activity relationship. Such introduction in an α-peptide can enhance the helical or turn features resulting in novel conformational analogues.

Results and Discussion

As a proof of concept we have synthesized Ac-Nle-c[Asp-β^3-hLys-D-Nal(2′)-Arg-Trp-Lys]-NH$_2$ (**KUL100**) an analogue of SHU9119. **KUL100** was synthesized manually using the standard Fmoc/*t*Bu strategy for solid phase peptide synthesis. Lactam cyclization of the peptide is achieved using microwave assisted peptide synthesis (MAPS) [4]. Competition binding experiments were performed using transfected HEK293 cells expressing human MC1, MC3, MC4 and MC5 receptors. A 120 fold greater selectivity was observed for MC3R (IC$_{50}$=14nM) over MC4R (IC$_{50}$=1700nM). No selectivity between MC3R/MC5R was observed. Molecular
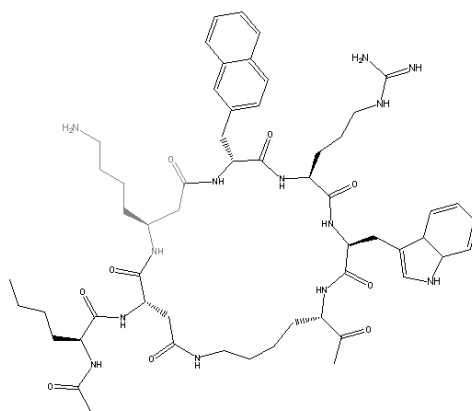
Fig. 1. Structure of KUL100: Ac-Nle-c[Asp-β^3-hLys-D-Nal(2′)-Arg-Trp-Lys]-NH$_2$.

modeling experiments using Macromodel 9.7 were performed on **KUL100**, which revealed a enhanced β-turn between β^3-hLys and D-Nal(2′) as compared to His and D-Nal(2′) of **SHU9119**. Further biological investigation of analogues of **MT-II**: Ac-Nle-c[Asp-β^3-hAaa-D-Phe-Arg-Trp-Lys]-NH$_2$ and **SHU9119**: Ac-Nle-c[Asp-β^3-hAaa-D-Nal(2′)-Arg-Trp-Lys]-NH$_2$ [β^3-hAaa = β^3-hLys, β^3-hPro, Anc (3-Amino-2-napthoic acid)] are under progress. Multiple incorporations of β^3-amino acids are also under investigation.

Acknowledgments

References

1. Spiteller, P., von Nussbaum, F. *Enantioselective Synthesis of β-Amino Acids* (Eds. Soloshonok, V. and Juaristi, E.) Wiley-VCH Verlag GmbH, Wienheim, 19-91 (2005).
2. Steer, D.L., et al. *Current Medicinal Chemistry* **9**, 811-822, (2005).
3. Hruby, V.J., et al. *Ann. N.Y. Acad. Sci.* **994**, 12-20 (2003).
4. Kulkarni, V.V., et al. "Microwave Assisted Lactam Cyclization of Peptides", *This Book,* 2011.

Synthesis of Analogue of α-MSH for Targeting of Melanocortin Receptors - Copper-Free Click Chemistry Approach

Alexander Kuzmin[1], Josef Vagner[2], Natalie Barkey[3], David Morse[3], Robert Gillies[3], and Victor J. Hruby[1]

[1]*Department of Chemistry, The University of Arizona, 1306 E University Boulevard ,Tucson, AZ ,85721, U.S.A.;* [2]*Bio5, The University of Arizona, Tucson, AZ, 85721, U.S.A.;* [4]*H. Lee Moffitt Cancer Center & Research Institute, Tampa, FL, 33612, U.S.A.*

Introduction

Melanoma is a form of cancer that starts in melanocytes cells that make pigment melanin. According to the National Cancer Institute, there were 68,130 of new cases of melanoma and 8,650 deaths in the United States in 2010. While melanoma contributes only five percent of all skin cancer, it results in more than fifty percent of deaths related to skin cancer. Also, long-term survival in patients with metastatic disease is only five percent. That is why the early diagnosis of melanoma cancer is critically important for the improvement of survival rate. Melanoma alters expression of cell surface proteins, including adhesion proteins and receptors. For example, melanocortin 1 receptor (MC1R) is one of the five G-protein coupled receptors (MC1R-MC5R) and was found to be overexpressed in more than eighty percent of melanoma tumor samples from patients with metastatic lesions. Thus, MC1R has been investigated as a target for receptor based melanoma diagnosis, as well as monitoring of therapeutic responses, resulting in a discovery of a number of highly potent ligands [1]. For example, [Nle[4], D-Phe[7]]-α-MSH labeled with [99]mTc-CGCG was shown to bind to melanomas with high avidity. However, this probe also binds to MC3R-MC5Rs, which are found in the kidney and brain. Here, we report the preparation and modification of a peptide ligand that is known to bind selectively to MC1R. We also used an azide-alkyne cycloaddition reaction using copper-free click chemistry that can allow us to modify this peptide with a range of different tag-probes for fluorescent and other types of imaging.

Results and Discussion

Analogue of α-MSH peptide **1** was synthesized using Fmoc chemistry on Tentagel Rink amide resin using solid-phase peptide synthesis approach. Following the completion of synthesis, peptide **1** was cleaved from the resin with TFA and scavengers (TFA 91%, H_2O 3%, thioanisol 3%, ethane-1,2-dithiol 3%), purified by C_{18}RP-HPLC or SEPAK, and characterized by HPLC and ESI-MS. Cyclooctyne **2** was prepared according to the procedures reported in the literature (Figure 1) [3]. Primary amine of cyclooctyne **2** was reacted with NHS-ester of compound **3** to give the desired cyclooctyne-maleimide **4**. Our strategy to introduce cyclooctyne into the peptide **1** was influenced by the fact that cyclooctynes are instable in the presence of trifluoroacetic acid and other scavengers, which are used during peptide cleavage from the resin. The conjugation of the peptide **1** to a cyclooctyne moiety **4** was achieved through a maleimide-thiol reaction in 72% yield. The ability of the strained cyclooctyne **5** to undergo azide-alkyne cyclo-
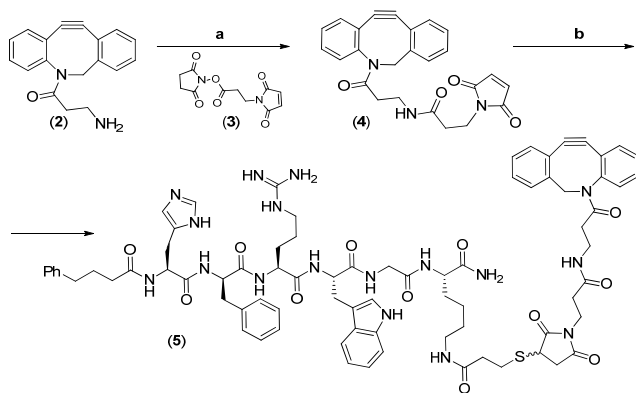
Fig. 1. Synthesis of peptide 4. (a) 3, DIEA/DMF, 60%; (b) Ph(CH₂)₃-CO-His-D-Phe-Arg-Trp-Gly-Lys(COCH₂CH₂SH)-NH₂ (1), phosphate buffer, pH 7.4, 72%.

A) Fluorescein azide

(5)   (6)   (7)

Ph(CH$_2$)$_3$CO-H-(D)F-R-W-G-K-NH$_2$ $\xrightarrow{\text{PBS}}$ Ph(CH$_2$)$_3$CO-H-(D)F-R-W-G-K-NH$_2$

B) Binding assay of peptide **5**

Ki = 1.2 nM

- Assay 1
- Assay 2

Competitive binding assays were performed using HCT116/hMC1R cells. HCT116/hMC1R cells were plated in black PerkinElmer 96-well plates, all at a density of 10,000-30,000 cells/well.
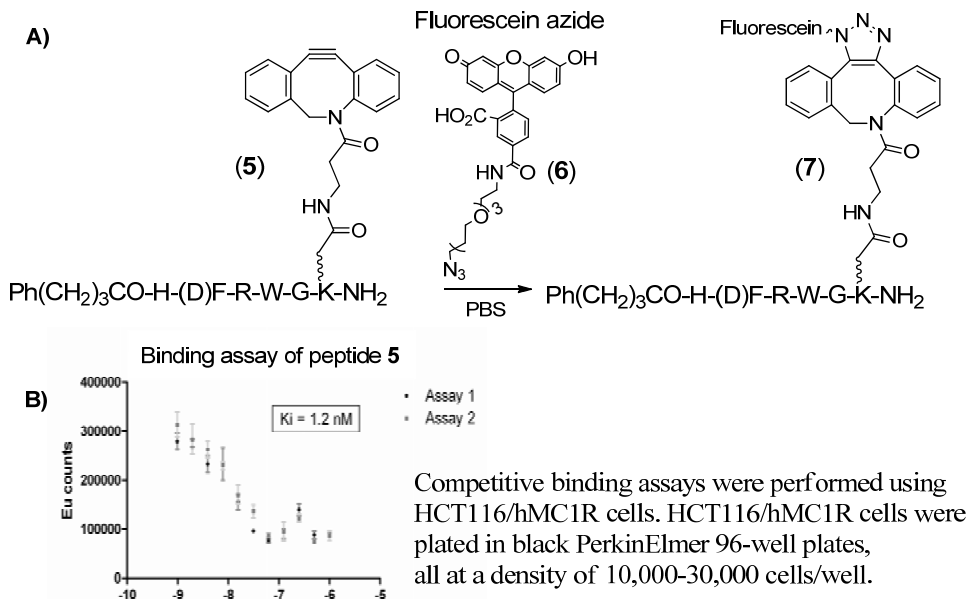
*Fig. 2. A) Conjugation of Fluorescein-PEG$_3$-N$_3$ to the peptide **5** in phosphate buffer at r.t.; B) Competitive binding assay curve of Ph(CH$_2$)$_3$-CO-His-D-Phe-Arg-Trp-Gly-Lys-(cyclooctyne)-NH$_2$ (**5**) (IC$_{50}$ = 1.2 nM). Competed against NDP-α-MSH.*

addition was tested by treating it with Fluorescein azide **6** resulting in robust trizole-conjugate **7** (Figure 2, A). Fluorescein azide **6** was prepared by reacting a commercially available Fluorescein-NHS ester with 11-Azido-3,6,9-trioxaundecan-1-amine. In this work, we screened prepared peptide-cyclooctyne **5** against cell lines that were engineered to overexpress MC1R, MC4R or MC5R, respectively. Compound **5** was tested for its ability to compete with Eu-NDP-α-MSH using a readout of time resolved fluorescence. Peptide **5** did not demonstrate a loss of affinity of MC1R following cyclooctyne functionalization (IC$_{50}$ = 1.2 nM. Figure 2, B). Competitive binding assays were performed using HCT116/hMC1R cells and HEK293/ hMC4R or hMC5R as previously described [4]. In summary, we report MC1R selective peptide **5** that was synthesized by using solid-phase strategy and solution synthesis. Strained cyclooctyne was conjugated to the obtained peptide through a thiol-maleimide reaction. Strained-promoted azide-alkyne cycloaddition allow us to modify a peptide with a range of different tags. This method is robust even under physiological conditions and does not require a metal catalyst.

Acknowledgments

References

1. Hruby, V. *J. Org. Chem.* **74**, 9245-9264 (2009).
2. Chen, J., et al. *Nucl. Med. Biol.* **26**, 687-693 (1999).
3. Kuzmin, A., et al. *Bioconjugate Chem.* **21**, 2076-2085 (2010).
4. Handl, H.L., et al. *Anal. Biochem.* **330**, 242-250 (2004).

Effects of Naloxone and JTC-801 on Analgesic Activity of Novel N/OFQ(1-13)NH$_2$ Analogues

Adriana I. Bocheva[1], Elena B. Dzhambazova[2], Petar T. Todorov[3], Nikola D. Pavlov[3], and Emilia D. Naydenova[3]

[1]*Medical University, Faculty of Medicine, Department of Pathophysiology, Sofia, 1431, Bulgaria;*
[2]*Sofia University, Faculty of Medicine, Department of Physiology, Sofia, 1407, Bulgaria;* [3]*University of Chemical Technologies and Metallurgy, Department of Organic Chemistry, Sofia, 1756, Bulgaria*

Introduction

Bioactive peptides are important starting structures for the development of potential therapeutic agents. They bind to different receptors (opioid, non-opioid or both) and are involved in the physiological control of various functions, among which nociception is particularly emphasized. Nociceptin/Orphanin FQ (N/OFQ) is a heptadecapeptide which has been found to play a direct role on pain perception. This peptide is an endogenous ligand of the nociceptin opioid peptide (NOP) receptor [1]. On the other hand, α-aminophosphonic acids and aminophosphonates have reached a position of eminence in the research works intending to discover, to understand, and to modify physiological processes in living organisms [2]. They are also a potential source of medicinal lead compounds.

Results and Discussion

N/OFQ(1-13)NH$_2$ is the minimal sequence maintaining the same activity as the natural peptide nociceptin. Structure-activity studies demonstrated that N- and C-terminal modifications of nociceptin/orphanin FQ generate highly potent NOP receptor ligands. Aiming to develop ligands for the NOP that possess stronger analgesic effects, new series of N-modified analogues of the N/OFQ(1-13)NH$_2$ with aminophosphonate moiety were prepared (Figure 1) with good yield using SPPS by Fmoc (9-fluorenylmethoxy-carbonyl) chemistry. The 1-[(dimethoxyphosphono)methyl-amino]cycloalkanecarboxylic acids were previously prepared by our group following *Kabachnik-Fields* reaction [3].

X-GGFTGARKSARK-NH$_2$ **(1, 3, 5)**

X-FGGFTGARKSARK-NH$_2$ **(2, 4, 6)**

Where **X** is:

n = 0, 2, 3
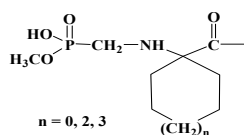
Fig. 1. N/OFQ(1-13)analogues.

Studies characterizing the role of nociceptin in pain transmission have generated conflicting results depending on the dose of N/OFQ(1-13)NH$_2$ used and the site of administration. Supraspinal administration of the peptide has been shown to produce hyperalgesia, allodynia or naloxone-reversible analgesia [1,4]. Effects of new peptide analogues with aminophosphonates moiety were assessed during acute pain in male Wistar rats by paw-pressure (PP) test.
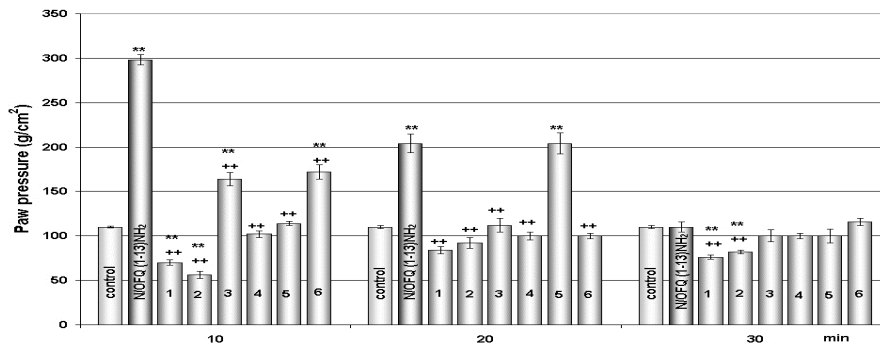
*Fig. 2. Effects of i.p. administration of nociceptin and analogues (all at a dose of 10 µg/kg) estimated by PP test. Data are presented as mean ±S.E.M.; ***P<0.01 vs. control; ++P<0.01 vs. nociceptin.*
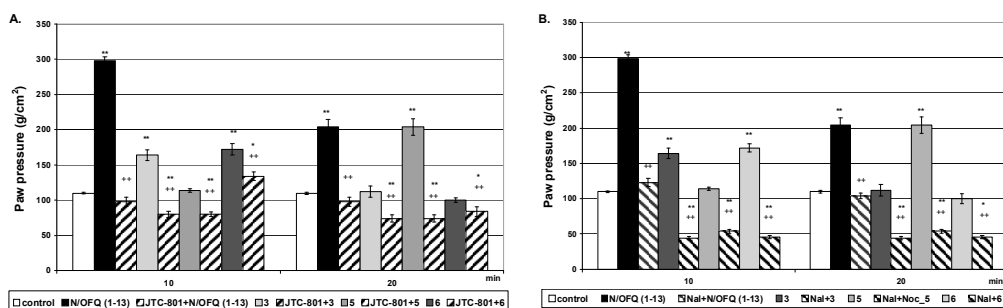
Fig. 3. Effects of N/OFQ(1-13)NH$_2$ and newly synthesized analogues 3, 5 and 6 (all in dose 10 µg/kg, i.p) pretreated with A. JTC-801 (0.5 mg/kg, i.p.) or B. Nal (1 mg/kg, i.p.) estimated by PP test in male Wistar rats. Data are presented as mean ± S.E.M.; $^*P<0.05$, $^{**}P<0.01$ vs. control; $^{++}P<0.01$ vs. respective peptide.

The biological investigations started 10 min after i.p. injection of peptides. Our previous results showed that in PP test N/OFQ(1-13)NH$_2$ (10 µg/kg, i.p.) administered alone in intact animals has significant well pronounced and time dependent analgesic effect versus control group [4]. Incorporation of 1-[(methoxyphosphono)methylamino]cycloalkanecarboxylic acid in position 1 of N/OFQ(1-13)NH$_2$ molecule decreases significantly it's analgesic effects. Only analogues 3 and 6 on the 10th min and analogue 5 on 20th min showed statistically significant (p<0.01) and short lasting analgesic effect compared to the control but these effects were lower than the N/OFQ(1-13)NH$_2$ analgesic effect (Figure 2).

Like opioid agonists, N/OFQ(1-13)NH$_2$ inhibits adenylate cyclase and calcium currents and hyperpolarizes, neurons by opening potassium channels. In contrast, the physiological and behavioral functions of N/OFQ(1-13)NH$_2$ are agreed to be quite different from those of classical opioids which exert their physiological and pharmacological effects by interacting with opioid receptors belonging to four main types: µ, δ, κ and ε [5].

To clarify involvement of nociceptin and opioidergic systems in antinociceptive effects of analogues 3, 5 and 6 we used JTC-801, N-(4-amino-2-methylquinolin-6-yl)-2-(4-ethylphenoxy-methyl) benzamide monohydrochloride, NOP receptor antagonist [6] and naloxone (Nal) as classical opioid receptor antagonist. JTC-801 (0.5 mg/kg, i.p.) applied 10 min before the injection of newly synthesized peptides significantly decreased (p < 0.01) their pain threshold during the whole investigated period. The effect was more pronounced, about 70%, for the referent compound N/OFQ(1-13)NH$_2$ (Figure 3A). Naloxone pretreatment 20 min before the investigated peptides significantly decreased (p < 0.01) their analgesic effects to hyperalgesia with exception of N/OFQ(1-13)NH$_2$ (Figure 3B).

In conclusion, the present study extended our previous findings about N/OFQ(1-13)NH$_2$. It demonstrates that incorporation of 1-[(methoxyphosphono)methylamino]cycloalkanecarboxylic acid in position 1 of N/OFQ(1-13)NH$_2$ molecule exerted lower analgesic effect compared with N/OFQ(1-13)NH$_2$. The data also suggests that in analgesic effects of N/OFQ(1-13)NH$_2$ and newly synthesized analogues with aminophosphonates moiety 3, 5 and 6 are involved nociceptin- and opioideergic systems which revealed opioid- and non-opioid mechanisms in their action.

Acknowledgments

References

1. Civelli, O. *Results and Problems in Cell Differentiation* **46**, 1-25 (2008).
2. Ambo, A., Kohara, H., Kawano, S., Sasaki, Y. *J. Pept. Sci.* **13**, 672-678 (2007).
3. Naydenova, E., Todorov, P., Troev, K. *Amino Acids* **38**, 23-30 (2010).
4. Dzhambazova, E., Nocheva, H., Bocheva, A. *Pharmacy* **55**, 30-34 (2008).
5. Bocheva, A., Dzhambazova, E. *Sci. Res. J. SWU* **2**, 33-41 (2009).
6. Habler, H., Timmermann, L., Stegmann, J., Janig, W. *Br. J. Pharmacol.* **127**, 1719-1727 (1999).

Structure-Activity Relationships of the Peptide Kappa Opioid Receptor Antagonist Zyklophin

Anand A. Joshi[1], Thomas F. Murray[2], and Jane V. Aldrich[1]

[1]*Department of Medicinal Chemistry, The University of Kansas, Lawrence, KS, 66045, U.S.A.;*
[2]*Department of Pharmacology, School of Medicine, Creighton University, Omaha, NE, 68178, U.S.A.*

Introduction

Kappa opioid receptor (KOR) antagonists have recently demonstrated potential utility in the treatment of depression, anxiety, and cocaine addiction [1,2]. Non-peptide KOR selective antagonists, however, exhibit exceptionally long durations of action (weeks after a single dose) that may complicate and potentially limit their therapeutic application [3]. Our research group has designed KOR antagonists based on the endogenous KOR peptide dynorphin (Dyn) A. We have designed and synthesized the Dyn A(1-11) amide analog zyklophin, which is a KOR selective antagonist both *in vitro* [4] and *in vivo* [2]. It exhibits a finite duration of action (12-18h) and appears to cross the blood-brain barrier after systemic administration to antagonize KOR in the CNS [2]. Hence, we are exploring the structure-activity relationships of zyklophin in order to enhance its antagonist potency and examine its potential interactions with KOR. Several linear (**1** and **2**) and cyclic analogs of zyklophin were synthesized. The cyclic analogs included analogs with amino acid substitutions (e.g. **3** and **4**), different *N*-alkyl groups and variations in the ring.

Zyklophin   NBenzyl-Tyr-Gly-Gly-Phe-D-Asp-Arg-Arg-Dap-Arg-Pro-Lys-NH$_2$

Dap = 2,3-diaminopropionic acid

Dyn A(1-11)NH$_2$ Tyr-Gly-Gly-Phe-Leu-Arg-Arg-Ile-Arg-Pro-Lys-NH$_2$
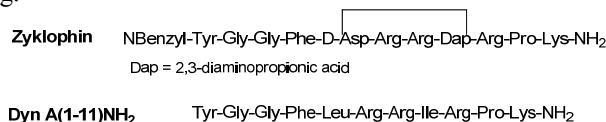
Results and Discussion

The peptides were synthesized by Fmoc solid phase synthesis. The synthesis of the cyclic peptides (Figure 1) involved selective deprotection of the 2-phenylisopropyl ester (Pip) and 4-methyltrityl (Mtt) protecting groups at positions 5 and 8, respectively, by 3% TFA and 5% triisopropylsilane (TIPS), followed by cyclization in the presence of 6-chloro-benzotriazole-1-yl-oxy-tris-pyrrolidino-phosphonium hexafluorophosphate (PyClocK), 1-hydroxy-7-azabenzo-triazole (HOAt) and *N,N*-diisopropylethylamine (DIEA). The cyclization times for the peptides ranged from 12-70h depending on the structural modification. For analogs containing amino acid substitutions within the cyclic constraint or variations in the ring, the cyclization times were longer (40-70h). This suggested that the side chains of the residues involved in and within the cyclic constraint affected the kinetics of the cyclizations.

The *N*-alkyltyrosine derivatives were prepared by reductive amination of Tyr-O*t*Bu in the presence of the appropriate aldehyde and sodium triacetoxyborohydride. The esters were
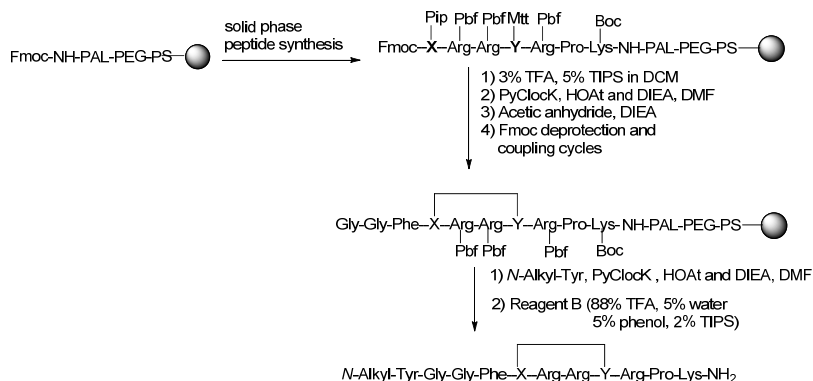
Fig. 1. Synthesis of cyclic analogs of zyklophin.

Table 1. Preliminary pharmacological data for selected zyklophin analogs

Analog	Fold decrease in affinity[a]	% Inhibition of AC $\pm$ SEM[b]
1, D-Asn[5]	2.4	14 $\pm$ 2
2, Dap (Ac)[8]	[c]	96 $\pm$ 3
3, Ala[4]	18	–
4, Ala[6]	8	–
Zyklophin		<10

[a]*Compared to zyklophin;* [b]*At 10 µM relative to Dyn A(1-13) NH₂;* [c]*Increased affinity 8-fold; – = not determined.*

purified by silica gel flash column chromatography, followed by TFA cleavage of the *t*-butyl ester. The resulting *N*-alkylTyr derivatives required heating to 80-110°C to solubilize them in DMF prior to coupling to the (2-11) fragment in the presence of PyClocK, HOAt and DIEA. The peptides were cleaved from the resin by Reagent B [5] and purified by preparative RP-HPLC. The pure peptides were analyzed by ESI-MS and analytical RP-HPLC.

The analogs are being evaluated for opioid receptor affinity in radioligand binding assays [6] and for efficacy in the adenylyl cyclase (AC) assay using Chinese hamster ovary cells stably expressing opioid receptors [7]. The pharmacological data obtained from the linear analogs (Table 1) suggested that the residue in position 5, but not residue 8, is important for zyklophin's lack of efficacy at KOR. The low KOR affinity for the initial alanine-substituted analogs (Table 1) suggested that the residues in positions 4 and 6 are important for interaction with KOR. Other modifications to the N-terminus and cyclic constraint of zyklophin resulted in less than a 2-fold change in KOR affinity compared to zyklophin, suggesting that these modifications are well tolerated by KOR.

Additional analogs of zyklophin are being prepared to determine which functionalities are important for zyklophin's interaction with KOR and to identify new analogs with enhanced antagonist potency. Ongoing studies include completing the *in vitro* pharmacological analysis of the analogs and *in vivo* analysis of selected analogs.

Acknowledgments

References

1. Aldrich, J.V., McLaughlin, J.P. *AAPS J.* **11**, 312-322 (2009).
2. Aldrich, J.V., Patkar, K.A., McLaughlin, J.P. *Proc. Natl. Acad. Sci. U.S.A.* **106**, 18396-18401 (2009).
3. Metcalf, D., Coop, A. *AAPS J.* **7**, E704-E722 (2005).
4. Patkar, K.A., Yan, X., Murray, T.F., Aldrich, J.V. *J. Med. Chem.* **48**, 4500-4503 (2005).
5. Solè, N.A., Barany, G. *J. Org. Chem.* **57**, 5399-5403 (1992).
6. Arttamangkul, S., et al. *J. Med. Chem.* **40**, 1211-1218 (1997).
7. Soderstrom, K., Choi, H., Aldrich, J.V., Murray, T.F. *Eur. J. Pharmacol.* **338**, 191-197 (1997).

Orally Active Opioid Peptides as Leads for Drug Development

Jane V. Aldrich[1], Santosh S. Kulkarni[1], Sanjeewa N. Senadheera[1],
Nicolette C. Ross[2], Kate J. Reilley[2], Shai O. Eans[2], Michelle L. Ganno[2],
and Jay P. McLaughlin[2]

[1]*Department of Medicinal Chemistry, The University of Kansas, Lawrence, KS, 66045, U.S.A.;* [2]*Torrey Pines Institute for Molecular Studies, Port St. Lucie, FL, 34987, U.S.A.*

Introduction

A major challenge in developing peptides as potential therapeutics is their delivery, which typically involves injection. We are interested in developing peptide kappa opioid receptor (KOR) ligands as potential analgesics and as treatments for drug abuse [1]. The natural product cyclic tetrapeptide CJ-15,208 (Figure 1) was reported to be a KOR antagonist with modest affinity and selectivity for KOR [2], but the chirality of the Trp residue in the natural product was not determined. We synthesized both isomers of this peptide [3,4], and characterized their pharmacological activity *in vitro* and *in vivo* after intracerebroventricular (i.c.v.) injection [5].
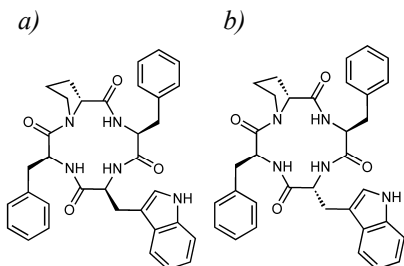
Fig. 1. The a) L- and b) D-Trp isomers of CJ-15,208.

The two peptides exhibited distinctly different pharmacological profiles *in vivo* in the 55°C warm-water tail-withdrawal antinociceptive assay in mice following i.c.v. administration [5]. The L-Trp isomer, which based upon its optical rotation appears to be the natural product [4], exhibited antinociceptive activity mediated predominately by KOR, but also by mu opioid receptors (MOR). This peptide also displayed KOR-selective antagonism in this assay after dissipation of the agonist activity. In contrast, the D-Trp isomer exhibited KOR-selective antagonism with minimal agonist activity in this assay.

Because of their cyclic structure these peptides were expected to be active after peripheral administration. Therefore we evaluated the antinociceptive and KOR-selective antagonist properties of these peptides after systemic administration, focusing on potential oral activity.

Results and Discussion

Both peptides were evaluated in the 55°C warm-water tail-withdrawal assay in mice following systemic administration. The L-Trp isomer was a potent analgesic in this assay following both
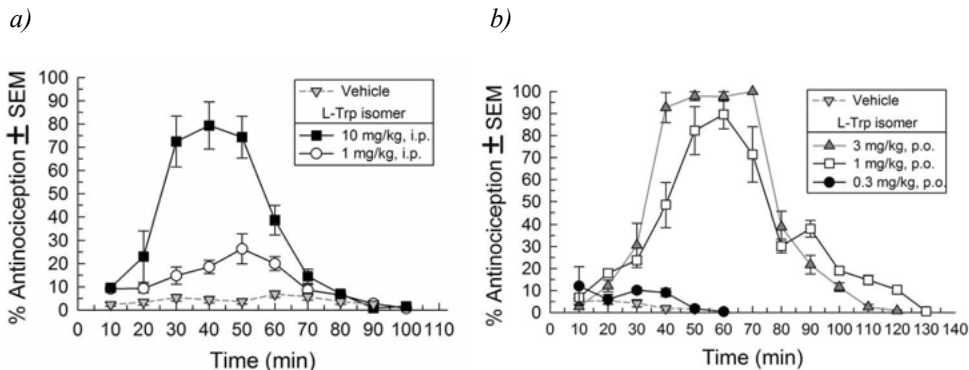
Fig. 2. Antinociceptive activity of the L-Trp isomer or vehicle (1:1:8 ethanol/Tween-80/saline) in the 55°C warm-water tail-withdrawal assay following a) i.p. or b) oral administration to mice.

intraperitoneal (i.p.) and oral administration (Figure 2), producing maximal antinociception at a dose of 3 mg/kg when administered orally (Figure 2b). Consistent with its activity following i.c.v. administration, orally administered peptide also antagonized the KOR-selective agonist U50,488. This peptide was also evaluated for potential liabilities compared to the prototypical narcotic analgesic morphine. In an acute model of tolerance [6], significant tolerance developed to morphine administered i.c.v. (9.5-fold increase in the ED_{50}), but not to the L-Trp cyclic tetrapeptide.
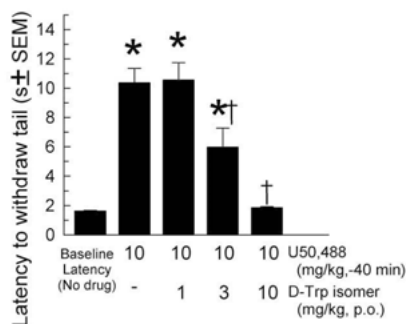
Fig. 3. Antagonism of the KOR-selective agonist U50,488 (10 mg/kg, i.p.) in the 55^oC mouse warm-water tail-withdrawal assay by pretreatment with the D-Trp isomer or vehicle by oral administration.

As expected, the D-Trp isomer exhibited KOR antagonism *in vivo* following oral administration (Figure 3) with minimal agonist activity. Like other KOR-selective antagonists [7,8] and similar to the results found following i.c.v. administration [5], in preliminary studies p.o. administration of the D-Trp peptide resulted in prevention of stress-induced reinstatement of cocaine seeking behavior in the conditioned place preference assay in mice. These positive results following oral administration in this assay strongly suggest that the D-Trp isomer crosses the blood-brain barrier to reach KOR in the CNS.

Thus both peptides are active after oral administration and are lead compounds for further development. The L-Trp peptide has potential as an orally bioavailable, low liability analgesic, while The D-Trp isomer has potential as a treatment for drug abuse. Additional *in vivo* studies are ongoing with these compounds. These orally active cyclic peptides represent significant advances in the development of potential peptide therapeutics for opioid receptors.

Acknowledgments

References

1. Aldrich, J.V., McLaughlin, J.P. *AAPS J.* **11**, 312-322 (2009).
2. Saito, T., et al. *J. Antibiot.* **55**, 847-854 (2002).
3. Kulkarni, S.S., Ross, N.C., McLaughlin, J.P., Aldrich, J.V. *Adv. Exp. Med. Biol.* **611**, 269-270 (2009).
4. Ross, N.C., Kulkarni, S.S., McLaughlin, J.P., Aldrich, J.V. *Tetrahedron Lett.* **51**, 5020-5023 (2010).
5. Ross, N.C., et al. *Br. J. Pharmacol.* in press (2011).
6. Mathews, J.L., Smrcka, A.V., Bidlack, J.M. *J. Neurosci.* **28**, 12183-12189 (2008).
7. Carey, A.N., Borozny, K., Aldrich, J.V., McLaughlin, J.P. *Eur. J. Pharmacol.* **569**, 84-89 (2007).
8. Aldrich, J.V., Patkar, K.A., McLaughlin, J.P. *Proc. Natl. Acad. Sci. U.S.A.* **106**, 18396-18401 (2009).

Improved Synthesis of CJ-15,208 Isomers and Their Pharmacological Activity at Opioid Receptors

Sanjeewa N. Senadheera[1], Santosh S. Kulkarni[1], Jay P. McLaughlin[2], and Jane V. Aldrich[1]

[1]*Department of Medicinal Chemistry, The University of Kansas, Lawrence, KS, 66045, U.S.A.;*
[2]*Torrey Pines Institute for Molecular Studies, Port St. Lucie, FL, 34987, U.S.A.*

Introduction

In recent years kappa (κ) opioid receptor (KOR) antagonists have demonstrated potential as therapeutic agents in the treatment of drug abuse, depression and anxiety [1]. Cyclic tetrapeptides are potential candidates for development because of their low molecular weight and expected metabolic stability *in vivo*. The head-to-tail cyclic tetrapeptide CJ-15,208 was isolated from the fermentation broth of a fungus, *Ctenomyces serratus*, and was reported to be a novel KOR antagonist [2]. Here we describe a modified synthetic protocol to prepare larger quantities of the cyclic tetrapeptides for detailed pharmacological evaluation *in vivo*.

In the initial report by Saito, et al. [2] the stereochemistry of the tryptophan residue in the natural product CJ-15,208 was not determined. Therefore, we synthesized both the L- and D-Trp isomers of CJ-15,208 (Figure 1) and determined their binding affinities at KOR [3,4].

Interestingly, the L- and D-Trp isomers of CJ-15,208 both exhibited similar nanomolar affinity for KOR ($K_i = 21 \pm 6$ nM and 47 ± 16 nM for the L- and D-Trp isomers, respectively, in mouse brain) [3-5]. We are synthesizing analogues of both peptides to explore the structure-activity relationships for KOR activity and to identify compounds for use *in vivo*.

The syntheses of cyclic tetrapeptides can be difficult due to the constrained 12-membered ring structure of the final products and often lead to cyclic dimers. The cyclic tetrapeptides were synthesized by a combination of solid phase synthesis of the linear peptide precursors on the 2-chlorotrityl chloride resin, followed by cyclization in solution [3,4]. We had previously identified appropriate cyclization conditions to minimize dimer formation and purified the crude peptides by reverse phase high performance liquid chromatography (RP-HPLC) in order to obtain sufficient material for initial pharmacological evaluation. We further optimized the crucial cyclization step by modifying the cyclization reaction conditions we previously reported [3,4] to increase the yield of the reaction. The crude cyclic tetrapeptides were then purified on a larger scale using normal phase column chromatography (Table 1) in order to prepare larger quantities of the peptides for detailed pharmacological evaluation *in vivo*.

Fig. 1. L- and D-Trp isomers of the natural product CJ-15,208.

Results and Discussion

Modification to the reported procedures [3,4] for the syntheses of the L- and D-Trp isomers of CJ-15,208 improved the yields of these cyclic tetrapeptides (Table 1). The major modifications were an increase in temperature in the cyclization step (from room temperature to 30°C) and reduction of the rate of addition of the linear peptide to the reaction (from 1.6 mL to 1 mL per hour). The hydrophobic nature and small molecule character of these two peptides prompted us to use normal phase column chromatography as the purification method instead of RP-HPLC. A gradient solvent system of hexane and ethyl acetate was used to elute the pure peptides from the column. The improvements in yields of the peptides using the modified protocol, especially for the less polar D-Trp isomer, is likely due in part to the high solubility of the peptides in the organic solvents used in the normal phase chromatographic purification.

Table 1. Significant changes between the reported procedure [3,4] and modified protocol in the synthesis of the cyclic tetrapeptides and their purification

Major differences between the two methods	Reported Method [3,4]	Modified Method
Reaction temperature (cyclization step)	room temperature	30°C
Amount of linear peptide cyclized	100 mg	600 mg
Amount of crude cyclic peptide purified at one time	20-50 mg	~ 580-585 mg
Yield for the cyclization step and purification:		
L-Trp isomer	61%	75%
D-Trp isomer	27%	51%

The agonist and antagonist activities of these peptides were evaluated *in vivo* using the 55°C warm-water tail-withdrawal assay in mice. The L-Trp isomer exhibits robust, dose-dependent antinociceptive (agonist) activity following intracerebroventricular administration, whereas the D-Trp isomer exhibits minimal agonist activity in this assay [6]. Pretreatment with either isomer of the cyclic tetrapeptide antagonized the antinociceptive effects of the KOR-selective agonist U50,488, but not of the mu opioid receptor-preferring agonist morphine or the delta opioid receptor-selective agonist SNC-80. Thus both the L-and D-Trp isomers exhibit antagonist activity *in vivo* that is selective for KOR. The D-Trp isomer was then shown to block stress-induced reinstatement of extinguished cocaine-seeking behavior in a cocaine-conditioned place preference assay with mice [6]. With the larger quantities of pure peptides now available, the two isomers are being further evaluated following peripheral administration, most notably by oral delivery.

In conclusion, modifications to the crucial cyclization step during synthesis and the use of normal phase column chromatographic purification of the crude cyclic peptides facilitated the preparation of larger quantities of peptides for detailed pharmacological evaluation *in vivo*. The isomers of the natural product CJ-15,208 can be used as templates to generate new compounds to explore the structure-activity relationships for opioid activity. These studies are ongoing in our laboratories. Cyclic tetrapeptides that interact with KOR have potential for clinical development as therapeutic agents as analgesics and for the treatment of drug abuse.

Acknowledgments

References

1. Aldrich, J.V., McLaughlin, J.P. *AAPS J*. **11**, 312-322 (2009).
2. Saito, T., et al. *J. Antibiot*. **55**, 847-854 (2002).
3. Kulkarni, S.S., Ross, N.C., McLaughlin, J.P., Aldrich, J.V. *Adv. Exp. Med. Biol*. **611**, 269-270 (2009).
4. Ross, N.C., Kulkarni, S.S., McLaughlin, J.P., Aldrich, J.V. *Tetrahedron Lett*. **51,** 5020-5023 (2010).
5. Dolle, R.E., et al. *Bioorg. Med. Chem. Lett*. **19**, 3647-3650 (2009).
6. Ross, N.C., et al. *Brit. J. Pharmacol.* in press (2011).

Development of Non-opioid Dynorphin A Analogs for the Modulation of Pain

Yeon Sun Lee[1], David Rankin[2], Briana Paisely[2], Sara M. Hall[1], Dhana Muthu[1], Jose J. Ortiz[1], Frank Porreca[2], Josephin Lai[2], and Victor J. Hruby[1]

[1]*Department of Chemistry and Biochemistry, The University of Arizona, Tucson, AZ, 85721, U.S.A.;*
[2]*Department of Pharmacology, The University of Arizona, Tucson, AZ, 85721, U.S.A.*

Introduction

It has been shown that after nerve injury, up-regulated dynorphin A directly interacts with bradykinin receptors (B1R and B2R) resulting in hyperalgesia, and HOE140, a bradykinin 2 receptor antagonist, affords antihyperalgesic effect by blocking the interaction between bradykinin-2 receptor and dynorphin [1,2]. This is a non-opioid effect that cannot be blocked by opioid antagonists. Since [des-Tyr[1]] Dyn A-(2-13) (Figure 1) is known to bind allosterically with the bradykinin-2 receptor in the micromolar range [1], systematic structure-activity relationships study was performed by truncating each amino acid of the C-terminal or N-terminal position of the ligand. The study was undertaken to identify the key structural features of dynorphin A for the bradykinin-2 receptor recognition.

Results and Discussion

dynorphin A: H-Tyr-Gly-Gly-Phe-Leu-Arg-Arg-Ile-Arg-Pro-Lys-Leu-Lys-Trp-Asp-Asn-Gln-OH

[des-Tyr[1]]-Dyn A-(2-13)
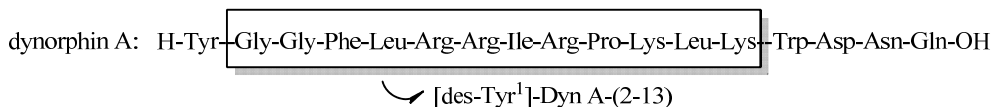
Fig. 1. Structure of Dynorphin A.
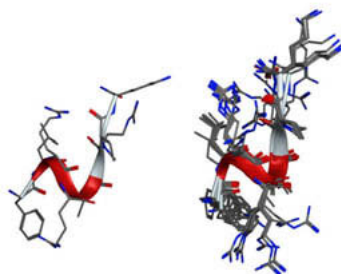
Fig. 2. Lowest energy structure and overlay of ten low energy structures of Dyn A-(4-11).

For the structure-activity relationships study, dynorphin A analogs were synthesized by solid phase synthesis using standard Fmoc-chemistry on the Wang resin, except for the analogs with a Pro residue at the C-terminus. Due to serious side reactions of Pro on the resin, Chlorotrityl resin was used as an alternative. In most cases, crude peptides could be obtained by the cleavage using 92% TFA cocktail solution containing 4% TIS, 2% water, and 2% anisole in high purity (72- 90%) and could be purified by preparative RP-HPLC in a short time (<15 min) owing to their hydrophilic characters (refer to aLOGPs in Table 1). The purified analogs were validated by analytical HPLC and Mass spectroscopy and were tested for their binding affinities by competition assay using [3H]kallidin in rat brain membranes where non-specific binding is defined by 10 µM kallidin.

As shown in Table 2, dynorphin A analogs exhibited very broad range ($K_i = 82 – 4700$ nM) of binding affinities at the bradykinin-2 receptor. These binding affinities were shown to be very dependent on the structure of the analogs and, as a result, the structure-activity relationships were very straightforward. First, Dyn A-(4-11), which showed the same range of binding affinity at the bradykinin-2 receptor ($K_i = 82$ nM) with Dyn A-(2-13) ($K_i = 98$ nM), was identified as a minimum pharmacophore for the receptor. Secondly, the SAR results revealed a significant fact that the bradykinin-2 receptor recognition predominantly depends on the basicity of the C-terminal amino acid. The analogs, Dyn A-(2-13), Dyn A-(3-13), Dyn A-(4-13), Dyn A-(4-11), and Dyn A-(4-9), which have a C-terminal basic amino acid residue such as Lys or Arg increased their binding affinities more than the analogs, Dyn A-(4-12), Dyn A-(3-10), and Dyn A-(4-8),

Dyn Analogs	Molecular Formula	HRMS[a]		HPLC t_R(min)[c]	aLOGPs[d]
		calcd	obsd		
Dyn A-(3-13)	$C_{64}H_{114}N_{22}O_{12}$	692.4566	692.4560	11.5	-1.59
Dyn A-(4-13)	$C_{62}H_{111}N_{21}O_{11}$	663.9459	663.9459	10.2	-1.54
Dyn A-(4-12)	$C_{56}H_{99}N_{19}O_{10}$	599.8984	599.8981	11.4	-1.53
Dyn A-(4-11)	$C_{50}H_{88}N_{18}O_9$	543.3564	543.3559	9.4	-1.80
Dyn A-(4-11)-NH₂	$C_{50}H_{89}N_{19}O_8$	362.2453[b]	362.2456[b]	9.6	-0.78
Dyn A-(3-10)	$C_{46}H_{79}N_{17}O_9$	507.8196	507.8200	10.6	-2.17
Dyn A-(4-9)	$C_{39}H_{69}N_{15}O_7$	430.7825	430.7829	9.5	-2.17
Dyn A-(4-8)	$C_{33}H_{57}N_{11}O_6$	352.7319	352.7321	9.2	1.08

[a]$[M+2H]^{2+}$; [b]$[M+3H]^{3+}$; [c]10-40% of acetonitrile containing 0.1% TFA in 15 min, 1mL/min; [d]http://www.vcclab.org/lab/alogps/

Table 2. Binding affinities of dynorphin A analogs at bradykinin 2 receptor

Dyn Analogs	G^2	G^3	F^4	L^5-R^6-R^7-I^8	R^9	P^{10}	K^{11}	L^{12}	K^{13}	K_i (nM)[a]
Dyn A-(2-13)										98
Dyn A-(3-13)										190
Dyn A-(4-13)										230
Dyn A-(4-12)										3200
Dyn A-(4-11)										82
Dyn A-(4-11)-NH₂								-NH₂		4700
Dyn A-(3-10)										820
Dyn A-(4-9)										970
Dyn A-(4-8)										2800

[a]$[^3H]$kallidin, rat brain membrane

with a C-terminal hydrophobic amino acid such as Ile, Pro, or Leu. In addition, the modification of C-terminal acid in Dyn A-(4-11) to amide in Dyn A-(4-11)-NH₂ decreased the binding affinity dramatically from 82 nM to 4700 nM. We also observed that Dyn A-(4-12) did not conserve such good binding affinity as Dyn A-(4-11) even with the same net positive charges (+4). On the basis of these results, it is considered that the positive charge at the C-terminus of the analogs is more critical for the bradykinin-2 receptor recognition, which can be through the electrostatic interactions, than total net charge.

The dynorphin analog discovered here as a minimum pharmacophore is an octapeptide containing four basic amino acid residues (three Arg and one Lys). To study the topographical structure of the minimum pharmacophore, an NMR study in SDS micells (5.8 nM, pH=5.5 at 25°C) was performed. The study identified that the analog possesses a 3_{10}-helical segment (or two consecutive type III β-turn) at the N-terminus and a distorted type I β-turn at the C-terminus (Figure 2), which might play a role in retaining good binding affinity.

Acknowledgments

References

1. Lai, J., Luo, M., Chen, Q., Ma, S., Gardell, l.R., Ossipov, M.H., Porreca, F. *Nature Neuroscience* **9**, 1534-1540 (2006).
2. Altier, C., Zamponi, G.W. *Nature Neuroscience* **9**, 1465-1467 (2006).

Design and Synthesis of Novel Bifunctional Ligands (Opioid Agonist and Bradykinin Antagonist) for Treatment of Chronic and Neuropathic Pain

Srinivas Deekonda[1], David Rankin[2], Peg Davis[2], Josephine Lai[2], Frank Porreca[2], and Victor J. Hruby[1]

[1]*Department of Chemistry and Biochemistry, University of Arizona, Tucson, AZ, 85719, U.S.A.;*
[2]*Department of Pharmacology, University of Arizona, Tucson, AZ, 85721, U.S.A.*

Introduction

Pain is a perception based on the signal received from the environment and transmitted and interrupted by the nervous system. More than two million people in the United States alone are debilitated by chronic pain. Unfortunately, the current treatments of pain are partially effective, and many cause life style altering, debilitating or cause dangerous side effects. The major goal of our research is to develop a multidisciplinary approach to discover novel peptide and peptidomimetic ligands which have potent antinociceptive activities in both acute and neuropathic pain states.

Kinins are naturally occurring vasoactive peptides which are known to be important mediators of a variety of biological effects, including cardiovascular homeostasis, inflammation and nociception [1,2]. The kinin family includes Bradykinin and Kallidin, and their active metabolites des-Arg-bradykinin and des-Arg-kallidin. The biological actions of these kinins are mediated by two major G-protein coupled Bradykinin receptors: B1 and B2 [3]. Opioid receptors are another important class of GPCRs which deal with the antinociceptive effects in humans. Opioids have been used throughout the history for their antinociceptive activities. Our approach is to design bifunctional ligands which can synergistically trigger both Bradykinin and Opioid activity.

Results and Discussion

Many potent Opioid receptor agonists and Bradykinin receptor antagonists are already discovered [4]. Here we designed and synthesized novel bifunctional ligands based on the most well known second generation Bradykinin B2 receptor antagonist **HOE 140** (DArg-Arg-Pro-Hyp-Gly-Thi-Ser-DTic-Oic-Arg) and B1 Receptor antagonist **B-9858** (Lys-Lys-Arg-Pro-Hyp-Gly-Igl-Ser-DIgl-Oic), where in the Opioid pharmacophore (Opioid μ/δ agonist Tyr-DAla-Phe, Tyr-DAla-Gly-Phe and Tyr-Pro-Phe) is maintained towards the N-terminal.

Design Approach

Opioid mu/delta Agonists	B2 receptor Antagonist
Tyr-DAla-Phe	DArg-Arg-Pro-Hyp-Gly-Thi-Ser-DTic-Oic-Arg(HOE 140)
Tyr-DAla-Gly-Phe	B1 receptor Antagonist
Tyr-Pro-Phe	Lys-Lys-Arg-Pro-Hyp-Gly-Igl-Ser-DIgl-Oic (B-9858)

Opioid mu/delta agonist	Bradykinin antagonist
Tyr-Pro-Phe	DArg-Arg-Pro-Hyp-Gly-Thi-Ser-DTic-Oic-Arg

Tyr-Pro-Phe-DArg-Arg-Pro-Hyp-Gly-Thi-Ser-DTic-Oic-Arg

All peptides are synthesized by solid phase peptide synthesis using the Fmoc/*t*Bu strategy on Wang and Chlorotrityl chloride resin, and cleaved by 92% Trifluoroacetic acid cocktail solution containing 4% TIS, 2% water, and 2% anisole. Final purification is performed by

semi-preparative RP-HPLC with 10-40% acetonitrile gradient in water containing 0.1% TFA in 15 min, 3mL/min).

The following are the designed and synthesized novel bifunctional ligands containing Bradykinin antagonist and Opioid agonist pharmacophore.

Designed and synthesized peptides for Opioid and Bradykinin 2 receptor antagonists

DS-009   H-Tyr-Pro-Phe-DArg-Arg-Pro-Hyp-Gly-Thi-Ser-DTic-Oic-Arg

DS-010   H-Tyr-DAla-Phe-Met-DArg-Arg-Pro-Hyp-Gly-Thi-Ser-DTic-Oic-Arg

DS-011   H-Tyr-Pro-Phe-Phe-DArg-Arg-Pro-Hyp-Gly-Thi-Ser-DTic-Oic-Arg

DS-012   H-Tyr-DAla-Gly-Phe-DArg-Arg-Pro-Hyp-Gly-Thi-Ser-DTic-Oic-Arg

Designed and synthesized peptides for Opioid and Bradykinin 1 receptor antagonists

DS-014   H-Tyr-Pro-Phe-Lys-Lys-Arg-Pro-Hyp-Gly-Igl-Ser-DIgl-Oic

DS-015   H-Tyr-DAla-Gly-Phe-Lys-Lys-Arg-Pro-Hyp-Gly-Igl-Ser-DIgl-Oic

DS-016   H-Tyr-DAla-Phe-Met-Lys-Lys-Arg-Pro-Hyp-Gly-Igl-Ser-DIgl-Oic

DS-017   H-Tyr-DAla-Phe-Lys-Lys-Arg-Pro-Hyp-Gly-Igl-Ser-DIgl-Oic

Table 1. In vitro binding assay of Bifunctional Ligands

Compound	*rMOR ^{3}H-DAMGO Ki (nM) (n=2)*	*Bradykinin activity guinea pig ileum LMMP (nM) Ke ± sem (n=2)*
DS-009	2300	1.8 ± 0.2
DS-010	70	1.9 ± 0.3
DS-011	480	1.7 ± 0.2
DS-012	10	1.7 ± 0.2

Here we conclude that a series of bifunctional peptides with Bradykinin and Opioid activities have been synthesized. Bifunctional ligands showed good affinity towards both Opioid and Bradykinin receptors. Functional assays and *in vivo* assays are in progress.

Acknowledgments

References

1. Leeb-Lundberg, L.M.F., Marceau, F., Muller-Esterl, W., Pettibone, D.J., Zuraw, B.L. *Pharmacol. Rev.* **57**, (2005).
2. Dziadulewicz, E. *Ann. Reports in Med. Chem.* **39**,113-121 (2004).
3. Marceau, F., Regoli, D. *Nat. Rev.* 845-852 (2004).
4. Kyle, D.J. *Current Pharmaceutical Design* **1**, 233-254 (1995).

Kappa Opioid Tetrapeptides from Expanded Deconvolution of a Positional Scanning Library

Jaime A. Misler, Margaret E. Cazares, Travis LaVoi, Tina Gibbins, Laura Maida, Angela Morales, Marc A. Giulianotti, and Colette T. Dooley

Torrey Pines Institute for Molecular Studies, Port Saint Lucie, FL, 34952, U.S.A.

Introduction

We have previously identified novel tetrapeptides for the three opioid receptors from a single tetrapeptide positional scanning combinatorial library [1]. The library contained over 13 million peptides from which we synthesized only 24 peptides to identify novel KOR ligands. The active sequences identified were all D amino acid peptides lacking an N-terminal tyrosine (D-Phe-D-Nal-D-Nle-D-Arg-NH$_2$). With the knowledge that the library contained additional active sequences not identified in the first screen, we have used a similar tetrapeptide library (65 amino acids versus 60 in the first library) and employed a new mixture linking analysis to assist in the library deconvolution. Positional scanning deconvolution can be prohibitive when the combination of all active amino acids requires the synthesis of a large number of peptides. We describe the use of mixture of mixtures and mixture linking analysis for the identification of three clusters of active peptides from the library.

Results and Discussion
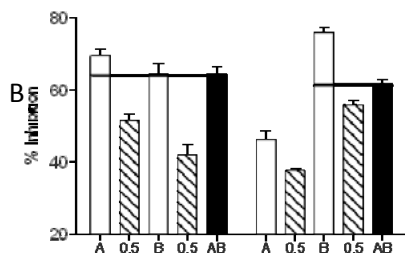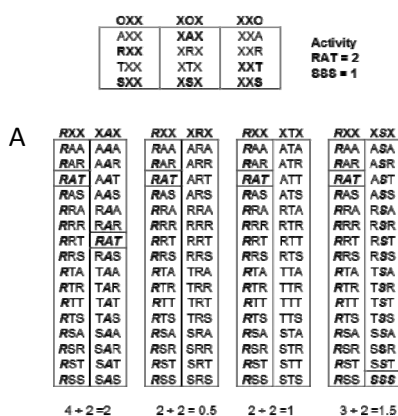
Fig. 1. A. Activities for hypothetical mixtures of mixtures. B. Activity for mixtures diluted by 2 (hatched) or the mixture of two mixtures (solid). Left: activity retained Right: activity lost. Inhibition of the mixture of mixtures is compared to most active undiluted parent mixture.

Discussed below is a theoretical example of how mixtures of mixtures would enable the detection of amino acid linkages. If a hypothetical compound, RAT, has an activity value of 2 and a second compound, SSS, had an activity of 1 and all other compounds in the library had no activity, since mixture activity is driven by the most active component [1] a mixture containing RAT will have an activity of ~2. Adding an equal volume of 2 mixtures together each containing RAT will result in an activity of (2+2)/2=2; mixtures containing one representation of RAT will have an activity of (2+0)/2=1 and a mixture containing both RAT and SSS will have an activity of (2+1)/2=1.5.

The tetrapeptide positional scanning library was screened in a receptor binding assay for the kappa opioid receptor. The library was composed of over 16,253,055 tetrapeptides containing four sublibraries, in which each one of the four positions was defined with one of 65 amino acids (O) and the three remaining positions are a mixture of 65 different L-, D-, and unnatural amino acids (X). In a routine deconvolution of this library, the most active mixtures at each of the four positions were chosen to determine IC$_{50}$ values and all combinations of the most active amino acids found at each position were synthesized as individual compounds.

To test the feasibility of using mixtures of mixtures to determine linkage of active amino acids at different positions addition screening of the most actives mixtures was undertaken. Linkages were explored for D-Phe and L-Dimethyltyrosine at position 1 and *p*-nitro-L-Phe at position 3. Thus the mixture fXXX was combined with the most active mixtures from positions 2-4 and the percent activity to the most active individual mixture was determined. Mixtures of mixtures were tested using percent inhibitions to save on compound. Each mixture of mixtures was tested using five sample tubes (Figure

Table 1. Activity at kappa opioid receptors for individual peptides identified using mixture of mixture analysis or direct positional scanning deconvolution

Mixture Analysis Deconvolution

				K_i nM	STD					K_i nM	STD					K_i nM	STD
D-Phe	D-Phe	D-Ile	D-Arg	3 ±	0.4	L-Tyr	D-Ser	*L-NOF*	L-LFF	11 ±	3	*L-DMT*	D-FF	D-Leu	D-Arg	8 ±	5
D-Phe	D-Phe	D-Ile	D-Phe	171 ±	80	*D-Thi*	D-Ser	*L-NOF*	L-LFF	14 ±	0.3	*L-DMT*	D-Lys	D-Leu	D-Cha	10 ±	2
D-Phe	D-Phe	D-Ile	L-Trp	420 ±	19	D-Nle	D-Ser	*L-NOF*	L-LFF	345 ±	151	*L-DMT*	D-FF	D-Leu	D-Cha	52 ±	5
D-Phe	D-Nve	D-Ile	D-Arg	816 ±	97	L-Tyr	D-Ser	*L-NOF*	D-Phe	373 ±	11	*L-DMT*	D-Lys	L-Trp	L-FF	69 ±	34
D-Phe	D-Phe	L-Trp	D-Arg	3995 ±	1242	D-Thi	D-Ser	*L-NOF*	D-Phe	504 ±	119	*L-DMT*	D-FF	D-Leu	D-Phe	105 ±	1
D-Phe	D-Phe	L-Trp	D-Phe	5448 ±	670	L-Tyr	D-Phe	*L-NOF*	L-LFF	514 ±	167	*L-DMT*	D-FF	L-Trp	L-FF	109 ±	41
D-Phe	D-Nve	L-Trp	L-Trp	7305 ±	120	D-Thi	D-Phe	*L-NOF*	L-LFF	1079 ±	423	*L-DMT*	D-FF	D-Leu	L-FF	125 ±	24
D-Phe	D-Nve	L-Trp	D-Phe	8198 ±	6000	D-Nle	D-Phe	*L-NOF*	L-LFF	1220 ±	375	*L-DMT*	D-Lys	D-Leu	D-Phe	144 ±	9
D-Phe	D-Phe	D-Ile	D-Phe	>10000		D-Nle	D-Phe	*L-NOF*	D-Phe	5769 ±	926	*L-DMT*	D-Lys	D-Leu	L-FF	309 ±	138
D-Phe	D-Nve	L-Trp	D-Arg	>10000		L-Tyr	D-Phe	*L-NOF*	D-Phe	8247 ±	8076	*L-DMT*	D-FF	L-Trp	D-Arg	321 ±	98
D-Phe	D-Phe	L-Trp	L-Trp	>10000		D-Nle	D-Ser	*L-NOF*	D-Phe	9506 ±	1109	*L-DMT*	D-FF	L-Trp	D-Cha	507 ±	50
D-Phe	D-Nve	D-Ile	L-Trp	>10000		D-Thi	D-Phe	*L-NOF*	D-Phe	18170 ±	3635	*L-DMT*	D-Lys	D-Leu	D-Arg	508 ±	48
												L-DMT	D-Lys	L-Trp	D-Phe	997 ±	61
												L-DMT	D-Lys	L-Trp	D-Cha	1207 ±	434
												L-DMT	D-Lys	L-Trp	D-Arg	2298 ±	109
												L-DMT	D-FF	L-Trp	D-Phe	4680 ±	109

Positional Scan Deconvolution

				K_i nM	STD					K_i nM	STD					K_i nM	STD
L-DMT	D-Nal	D-Leu	D-Arg	89 ±	7	L-DMT	D-Nve	D-Leu	D-Arg	23 ±	8	L-DMT	D-Pyr	D-Leu	D-Arg	5 ±	1
L-DMT	D-Nal	D-Leu	D-Cha	130 ±	17	L-DMT	D-Nve	D-Leu	D-Cha	10 ±	1	L-DMT	D-Pyr	D-Leu	D-Cha	17 ±	8
L-DMT	D-Nal	D-Leu	L-FF	439 ±	217	L-DMT	D-Nve	D-Leu	L-FF	75 ±	16	L-DMT	D-Pyr	D-Leu	L-FF	43 ±	19
L-DMT	D-Nal	L-Trp	D-Arg	635 ±	54	L-DMT	D-Nve	L-Trp	D-Arg	80 ±	8	L-DMT	D-Pyr	L-Trp	D-Arg	341 ±	32
L-DMT	D-Nal	L-Trp	D-Cha	3161 ±	550	L-DMT	D-Nve	L-Trp	D-Cha	444 ±	55	L-DMT	D-Pyr	L-Trp	D-Cha	131 ±	43
L-DMT	D-Nal	L-Trp	L-FF	607 ±	121	L-DMT	D-Nve	L-Trp	L-FF	7 ±	3	L-DMT	D-Pyr	L-Trp	L-FF	13 ±	5
D-Phe	D-Nal	D-Leu	D-Arg	3 ±	0.2	D-Phe	D-Nve	D-Leu	D-Arg	222 ±	11	D-Phe	D-Pyr	D-Leu	D-Arg	1 ±	0.5
D-Phe	D-Nal	D-Leu	D-Cha	27 ±	6	D-Phe	D-Nve	D-Leu	D-Cha	5026 ±	126	D-Phe	D-Pyr	D-Leu	D-Cha	15 ±	5
D-Phe	D-Nal	D-Leu	L-FF	205 ±	103	D-Phe	D-Nve	D-Leu	L-FF	4738 ±	234	D-Phe	D-Pyr	D-Leu	L-FF	270 ±	87
D-Phe	D-Nal	L-Trp	D-Arg	1290 ±	132	D-Phe	D-Nve	L-Trp	D-Arg	>10000		D-Phe	D-Pyr	L-Trp	D-Arg	4386 ±	2067
D-Phe	D-Nal	L-Trp	D-Cha	1593 ±	422	D-Phe	D-Nve	L-Trp	D-Cha	7881 ±	2369	D-Phe	D-Pyr	L-Trp	D-Cha	9732 ±	691
D-Phe	D-Nal	L-Trp	L-FF	>10000		D-Phe	D-Nve	L-Trp	L-FF	>10000		D-Phe	D-Pyr	L-Trp	L-FF	>10000	

1B): (A) mixture 1 alone, (B) mixture 2 alone, (C) 0.5 volume mixture 1 + 0.5 volume mixture 2, (D) 0.5 volume mixture 1 + 0.5 volume assay buffer, and (E) 0.5 volume mixture 2 + 0.5 volume assay buffer. All combinations were carried out in quadruplicate and tested in at least 4 separate experiments. Each assay tube contained 0.5 ml of membrane suspension, 2 nM [^{3}H]U69,593, and 0.02 mg/ml mixture in a total volume of 0.65 ml. Assay tubes were incubated for 2h at 25°C. Mixtures of mixtures were compared to the most active parental mixture (Figure 1B). Statistical analysis for percentage of parental activity was analyzed with one-way ANOVA using Tukey's post hoc test for comparison of the two parent mixtures, the parent mixtures diluted by 2 and mixture of mixtures. Statistical analysis was performed with GraphPad Prism Version 5.0 (San Diego, CA).

Individual compounds were made using combinations of the mixtures of the more active pairings and tested in kappa opiate receptors (Table 1). Mixture linkage identified tetrapeptides previously shown to have activity (those with D-Phe at position 1). Dimethyltyrosine was not in the original library and both methods identified active peptides with L-DMT at the first position. Mixture linkage identified active peptides with D-Lys at position 2 that would not have been identified from positional scanning. Likewise we had chosen to determine linkages for p-nitro-L-Phe at position 3 which would not have been chosen in the top amino acids for positional scanning deconvolution, active peptides were identified using this method. Therefore, we have determined mixture of mixtures can identify additional peptides to those identified from positional scanning data. It is particularly useful in determining linkage between amino acids not ranked in the top 2-3 in positional scanning data. In conclusion, mixture of mixtures may be more useful as an add-on method using this analysis after the initial active compounds from positional scanning data have been synthesized rather than a stand-alone analysis to determine which sequences to make directly following screening.

References

1. Dooley, C.T., Ny, P., Bidlack, J.M., Houghten, R.A. *J. Biol. Chem*. **273** (30), 18848-18856 (1998).
2. Santos, R.G., Giulianotti, M.A., Dooley, C.T., Pinilla, C., Appel, J.R., Houghten, R.A. *ACS Comb. Sci.* **13**(3), 337-344 (2011).

Cyclic Fluorescent Opioid Peptides from a Combinatorial Library

Jaime A. Misler, Yangmei Li, Margaret E. Cazares, Gina Debevec, Marc A. Giulianotti, Richard A. Houghten, and Colette T. Dooley

Torrey Pines Institute for Molecular Studies, Port Saint Lucie, FL, 34987, U.S.A.

Introduction

Fluorescent ligands for G-coupled receptors such as the opioid receptors are needed for imaging and FRET based binding studies. We desired fluorescent labels for the μ-opioid receptor and we wished to identify antagonists to the receptor and be able to orientate the fluorescent label. For the latter requirement, we chose to confine our efforts to cyclic peptides. We have previously identified rhodamine labeled linear peptides from a mixture based library, and while successful at identifying active ligands for kappa opioid receptors, the mixtures were difficult to handle and the library was very expensive to synthesize [1]. In this study we chose to synthesize and screen a cyclic peptide library with a smaller and less expensive fluorescent label and use the compounds identified from the initial screen as leads for synthesis of peptides labeled with the more expensive fluorescent dyes.

Results and Discussion

A positional scanning library of 30,420 cyclic peptides was prepared using a pentapeptide thioester scaffold on mercaptomethylphenyl-functionalized silica gel. Positions R^1 and R^3 were fixed with glycine and Dap (diaminopropionic acid; for subsequent addition of 2-amino benzoic acid). Positions R^2 and R^4 contained 36 L- and D- amino acids and position R^5 contained 19 L-amino acids. Boc-amino acids were coupled on the resin by using the PyBOP/DIEA activation method. Glycine was defined at the first position as R1=H. 19 L- and 17 D-amino acids were used as a mixture at the second and fourth positions as R2 and R4. 19 L-amino acids were used as a mixture at the fifth position as R5. A Boc-Dap(Alloc) was incorporated into the linear peptide at the third position. Its side chain was reacted with 2-nitrobenzoic acid to form a resin bound peptide. After being reduced by $SnCl_2$ and treated with anhydrous HF, the linear anthraniloyl fluorescent peptide was cyclized in a mixture solution of 1.5 M aqueous imidazole and acetonitrile (1:7 in volume) at a concentration of 1 mM for 72h, resulting in the fluorescent cyclic peptide.

The mixture library was screened in a radioreceptor binding assay for the μ-opioid receptor. Membrane suspensions were prepared and used on the same day. Rat brains, minus the cerebellum, were homogenized using 50 mM Tris-HCl, pH 7.4, and centrifuged and rewashed. Each assay tube contained 0.5 ml of membrane suspension, 1.9 nM [^{3}H]-DAMGO, 1 mg/ml mixture, and 50 mM Tris-HCl in a final volume of 0.65 ml. The reaction was terminated by filtration through GF-B filters, bound radioactivity was counted.

Screening data determined the most active amino acids at positions 2, 4, and 5 (Table 1). Sixty combinations of the most active mixtures were synthesized as individual peptides and their activities determined in the μ-opioid receptor binding assay. The only peptides showing significant activity possessed D-Lys at R4 and L-Tyr at R5 (K_i are given in Table 2).

Table 1. Deconvolution of screening data at μ-opioid receptor

R1	R2	R3	R4	R5
	D-Phe		D-Lys	L-Tyr
	L-Trp		L-Arg	L-Trp
	D-Met		L-Trp	L-Ile
	L-Tyr		L-Tyr	
	L-Phe			

Lysine in the R4 position for peptide #1 yielded two possible cyclic peptides, N^ε-amino cyclization (19 membered ring) and N^α-amino cyclization (15 membered ring). The two peaks were isolated and treated with 2,4-dinitro-1-fluorobenzene (Sanger's reagent) and hydrolyzed to determine which peak is the α and ε. RP-HPLC showed that peak 1 is cyclized on the N^ε-amino cyclized product and peak 2 is the N^α-amino cyclized product (Figure 1).

Table 2. Most active individual compounds

Peptide #	R1	R2	R3	R4	R5	K_i (nM)	STD
1	Gly	L-Tyr	Dap	D-Lys	L-Tyr	16	1
2	Gly	L-Phe	Dap	D-Lys	L-Tyr	20	1
3	Gly	D-Phe	Dap	D-Lys	L-Tyr	144	37
4	Gly	L-Typ	Dap	D-Lys	L-Tyr	505	25

Both peaks were highly selective for the μ-opioid receptor (Table 3). Opiate receptors couple to G_i proteins, their activation blocks the production of cAMP. Forskolin (4 μM) was used to stimulate cAMP levels and inhibition of cAMP stimulation is determined at each concentration of opioid ligand. Delta F% is inversely related to the amount of cAMP made. cAMP experiments determined Peptide 1 peaks 1 and 2 did not exhibit significant agonist activity. Antagonist activity was determined by evaluating the peptides ability to prevent DAMGO (1 μM) inhibition of cAMP production. Both Peaks 1 and 2 exhibited antagonist activity at the μ-opioid receptor.

Fig. 1. Compounds of peak 2 and 1.

While many cyclic peptides have been described for all three opioid receptors, most cyclizations involve the amino acid at the second position (e.g. Tyr-c(S-CH_2-S)[D-Cys-Phe-2-Nal-Cys]-NH_2 [2]), corresponding to R1 in Table 1. This study revealed a preference for cyclization through lysine side chain at position 3 (R4 in Table 1) for binding affinity. The affinity of these cyclic peptides is somewhat lower than other cyclic peptides described for the μ-opioid receptor. Replacement of the N-terminal tyrosine (R5) with dimethyltyrosine should increase binding affinity, however it may also convert the peptides to an agonist. The same synthetic process will be used to create rhodamine and fluorescein labeled analogs of Peptide 1, Peak 1.

Table 3. Selectivity of Peptide 1, Peaks 1 and 2 for the three opiate receptors

Peptide 1	MOR K_i (nM)	KOR K_i (nM)	DOR K_i (nM)
Peak 1	14	3231	865
Peak 2	39	3197	1221

Acknowledgements

References

1. Houghten, R.A., Dooley, C.T., Appel, J.R. *Bioorg. Med. Chem. Lett.* **19**, 14(8); 1947-1951 (2004).
2. Purington, L.C., Pogozheva, I.D., Traynor, J.R., Mosberg, H.I. *J. Med. Chem.* **10**, 52(23); 7724-7731 (2009).

Analgesic Effects of Novel Hexapeptide Analogues as Nociceptin Receptor Ligands

Emilia D. Naydenova[1], Nikola D. Pavlov[1], Petar T. Todorov[1], Elena B. Dzhambazova[2], and Adriana I. Bocheva[3]

[1]*University of Chemical Technologies and Metallurgy, Department of Organic Chemistry, Sofia, 1756, Bulgaria;* [2]*Sofia University, Faculty of Medicine, Department of Physiology, Sofia, 1407, Bulgaria;* [3]*Medical University, Faculty of Medicine, Department of Pathophysiology, Sofia, 1431, Bulgaria*

Introduction

Nociceptin/Orphanin FQ (N/OFQ) is an endogenous ligand of the nociceptin opioid peptide (NOP) receptor, structurally and functionally related to the classical opioid receptors [1]. The hexapeptides with formula Ac-RYYR/KW/IR/K-NH$_2$ have been identified as least peptide sequence with high NOP receptor affinity, selectivity and marked analgesic effect [2,3]. With a view to developing ligands for the NOP receptor with more potent analgesic activity and lower enzymatic degradation, new series of N-modified analogues of the Ac-RYYRWK-NH$_2$ were synthesized. The aim of the present study was to examine the effects of naloxone (Nal) and JTC-801 (NOP receptor antagonist) in the analgesic activity of newly synthesized hexapeptide analogues.

Results and Discussion

We have recently described the preparation of newly synthesized peptide analogues with N-terminal aminophosphonates moiety as NOP - receptor ligands [4]. The phosphonopeptides (Figure 1) were obtained by solid phase peptide synthesis – Fmoc-strategy using TBTU, an efficient peptide coupling reagent. In order to elucidate the influence of Arg and acetyl group we decided to introduce the 1-[(methoxyphosphono)-methylamino]cyclopentanecarboxylic acid to the N-side of Arg, compound **6**. The crude peptides were purified on a reversed-phase high-performance liquid chromatography (HPLC) and the molecular weights determined using electrospray ionization mass-spectrometry.

Because pain is a frequently observed symptom of various diseases and development of analgesic drugs is one of the greatest achievements in medicine we investigated N-modified analogues of the H-Arg-Tyr-Tyr-Arg-Trp-Lys-NH$_2$ with aminophosphonates moiety during acute pain in male Wistar rats. Antinociceptive effects were evaluated by two nociceptive tests - paw-pressure (PP) and hot-plate (HP) and statistically accessed by ANOVA.

Fig. 1. Newly synthesized Ac-RYYRWK-NH$_2$ analogues.
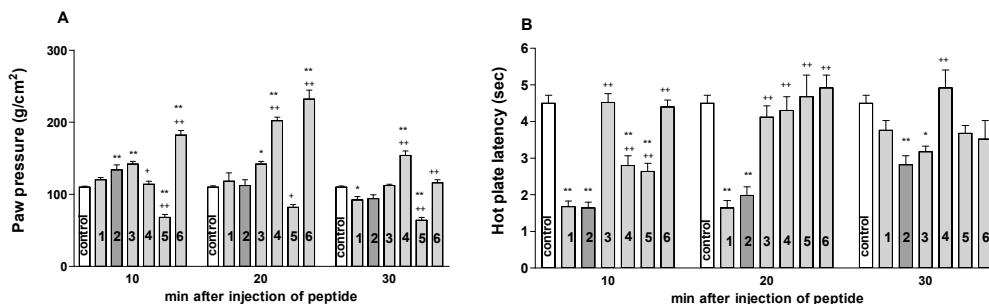
Fig. 2. Effects of H-Arg-Tyr-Tyr-Arg-Trp-Lys-NH$_2$ (1) and it's analogues (all in dose 10 µg/kg, i.p) estimated by A. PP test and B. HP test in male Wistar rats. Data are presented as mean ±S.E.M.; *P<0.05, **P<0.01 vs. control; +P<0.05, ++ P<0.01 vs. parent hexapeptide.
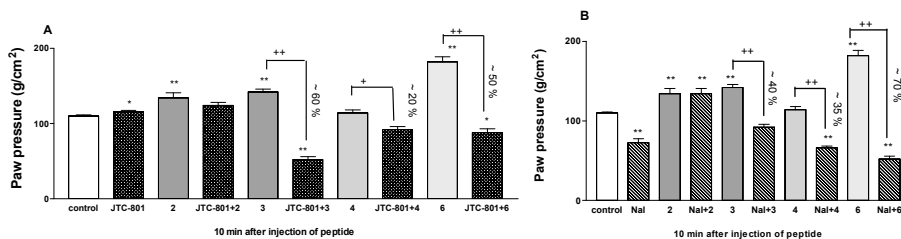
*Fig. 3. Effects of Ac-Arg-Tyr-Tyr-Arg-Trp-Lys-NH$_2$ (**2**) and newly synthesized analogues **3, 4** and **6** (all in dose 10 µg/kg, i.p) pretreated with A. JTC-801 (0.5 mg/kg, i.p.) or B. Nal (1 mg/kg, i.p.) estimated by PP test in male Wistar rats. Data are presented as mean ± S.E.M.; *P<0.05, **P<0.01 vs. control; ++P<0.01 vs. respective hexapeptide.*

The investigations started 10 min after intraperitoneal (i.p.) injection of hexapeptide. Applied alone H-Arg-Tyr-Tyr-Arg-Trp-Lys-NH$_2$ (compound **1**, 10 µg/kg, i.p.) had no analgesic effect in PP test and significantly decreased HP latency (p < 0.01). Ac-Arg-Tyr-Tyr-Arg-Trp-Lys-NH$_2$ (compound **2**, 10 µg/kg, i.p.) showed significant analgesic effect only on 10th min in PP test (p < 0.01), while it's effect in HP test was the opposite – significant decrease HP latency (p < 0.01) during the whole investigated period (Figure 2A, 2B). Only analogues **3, 4** and **6** significantly increased analgesic effects compared to the control and compound **2** (p < 0.01) in PP test mainly on 20th min from the beginning of the experiment. The effect was more pronounced for analogue **6** (Figure 2A).

For our second experimental series we used JTC-801, N-(4-amino-2-methylquinolin-6-yl)-2-(4-ethylphenoxymethyl) benzamide monohydrochloride, NOP receptor antagonist and Nal as classical opioid receptor antagonist. JTC-801 (0.5 mg/kg, i.p.) applied alone in PP test showed significant analgesic effect compared to the control (p < 0.05). JTC-801 (0.5 mg/kg, i.p.) applied 10 min before the injection of small peptide analogues significantly decreased (p < 0.01) the pain threshold of compounds **3** (60%)**, 4** (20%) and **6** (50%) during the 30th min investigated period. The effect was more pronounced, about 60%, for compound **3**. The analgesic effect of partial agonist of NOP receptor Ac-Arg-Tyr-Tyr-Arg-Trp-Lys-NH$_2$ (**2**) was decreased but not significantly from the NOP receptor antagonist JTC-801 (Figure 3A). Similar effects were observed when the non-competitive antagonist of opioid receptors Nal (1 mg/kg, i.p.) was applied 20 min before the investigated compounds **2, 3, 4** or **6** in PP test. Pretreatment with Nal significantly decreased the pain threshold of all investigated analogues, with exception of compound **2**. The effect was more pronounced, about 70%, for compound 6 (p < 0.01) (Figure 3B).

Naloxone or JTC-801 pretreatment significantly decreased (p < 0.01) HP latency only of compounds **3** and **6** in HP test approximately 50%. They didn't show any effect on decreased HP latency of compounds **2** and **4** (none shown on the figure).

The obtained results showed that incorporation of 1-[(methoxyphosphono)methylamino] cycloalkane-carboxylic acid in position 1 of hexapeptide molecule increases the analgesic effects of the newly synthesized peptide analogues **3** and **4**, while enlargement of the cycle (with 8 carbon atoms) in compound **5** diminished its analgesic effect. The analgesic effect of newly synthesized small peptides was more pronounced in compound **6** where the Arg^1 was preserved.

Our results showed that JTC-801 inhibited the analgesic effects of compounds **3, 4** and **6** in PP test, while Nal reversed them to hyperalgesic with exception of compound **3**. These data suggest the involvement of nociceptin and opioid neuromediatory systems in their mechanisms of action during acute pain.

Acknowledgments

References

1. Heinricher, M. *Life Sci.* **73**, 813-822 (2003).
2. Dooley, C., Spaeth, C., Berzetei-Gurske, I., et al. *J. Pharmacol. Exp. Ther.* **283**(2), 735-741 (1997).
3. Ambo, A., Kohara, H., Kawano, S., Sasaki, Y. *J. Pept. Sci.* **13**, 672-678 (2007).
4. Naydenova, E., Todorov, P., Mateeva, P., et al. *Amino Acids* **39**(5), 1537-1543 (2010).

Synthesis and Investigations of Peptidic-Non-Peptidic Bivalent Ligands for Treatment of Pain

R. Vardanyan[1]*, Y.S. Lee[1], J.P. Cain[1], P. Davis[2], T.W. Vanderah[2], J. Lai[2], F. Porreca[2], and V.J. Hruby[1]

[1]*Department of Chemistry, and Biochemistry, University of Arizona, Tucson, AZ, 85721, U.S.A.;*
[2]*Department of Pharmacology, University of Arizona Health Sciences Center, Tucson, AZ, 85724, U.S.A.;*
E-mail:vardanyr@email.arizona.edu

Introduction

Opioid analgesics are the mainstay for treatment of moderate to severe pain, but they still have significant disadvantages. In attempts to avoid them as well as to try to find compounds for relief of untreatable pain, our research in the last years has been devoted to the design and synthesis of new bifunctional ligands, which combine the structure of the strong opioid - Fentanyl with an adjuvant analgesic. A series of compounds - representatives of mixed peptidic-non-peptidic bivalent ligands in which the two ligands are merged into a single entity that can hit multiple targets have been synthesized. Among them are mixed μ- and δ-opioid agonists; μ-opioid agonist- δ-opioid antagonists; μ-opioid agonist-NK1 antagonists; μ-opioid agonist-MC modulators and μ-opioid agonist-COX inhibitors. Different functionalized Fentanyl derivatives like carboxy-, amino-, and hydrazino-Fentanyls have been designed and synthesized as lipophilic scaffolds with novel chemical/physical properties and with log Ps consistent with drugable properties. Entities with very high binding affinities (0.4 nM) at μ- and δ- receptors with an increased hydrophobicity were found among the novel compounds (Figure 1).
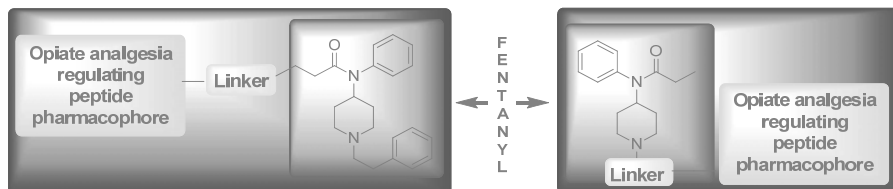
Fig. 1. Design of novel compounds.

Previously we designed, synthesized and investigated different new μ-/δ-bivalent ligands with coupling them at the propionyl moiety of Fentanyl and showed that these compounds have approximately equal binding affinity and bioactivity [1] (Figure 2).
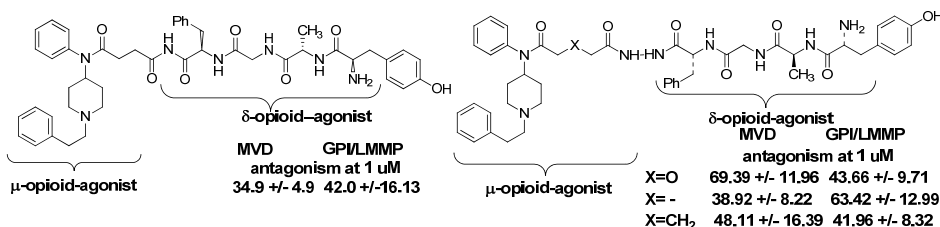
Fig. 2. Early results on attempts of creation of new μ-agonist/δ-agonist compounds.

Results and discussion

Our systematic work on creation of novel bifunctionl ligands have led us to a "generation" of novel compounds, a "matrix" able to occupy MOR and DOR receptors simultaneously in nanomolar/picomolar concentrations. Thus, replacing the δ-agonists - enkephalin-like tetrapeptides from the 4-th position of piperidine ring to the 1-th position, a ~100 fold increase in μ- and δ- binding has been observed. Moreover, taking in consideration that lipophilicity is a key factor in determining the rate at which a drug crosses the BBB and previous findings from our laboratory [2,3], that halogenation on the Phe[4] residue of DPDPE led to a significant increase in cell permeability in both *in vivo* and *in vitro* studies, new 4-anilinopiperidine

(Fentanyl) series preparations with very high binding affinities (~0.4 nM) at μ-and δ- receptors with an increased hydrophobicity, with aLog Ps 3.01-4.74 consistent with drugable properties, have been synthesized in attempts to develop a new generation of safer, more effective opioid drugs [4,5].

Our preliminary experiments demonstrate that obtained ligands have potent *in vitro* and *in vivo* antihyperalgesic and antiallodynic effects (Figure 3).

IC50 of 0.37 and 0.26 nM in theMVD and GPI assays, respectively) with excellent efficacy (EC50=0.07 nM, Emax=48% at hDOR; EC50=0.29 nM, Emax = 98% at rMOR) at both receptors.
The binding affinity at the μ receptor was subnanomolar (Ki=0.02 nM), and the Emax at rMORin the [35S]GTP-ã-S binding assay was 98% which represents high efficacy.
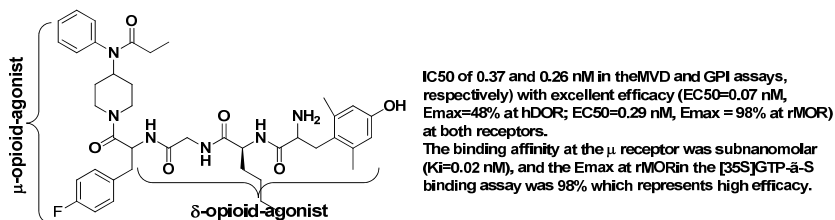
Fig. 3. New μ-agonists/δ-agonists compounds.

Functional synergism between MORs and DORs could become a milestone to improve pain management, and to clarify mechanisms of opioid action.

Acknowledgement

References

1. Petrov, R., Vardanyan, R.S., Lee, Y.S., Ma, S-W., Davis, P., Begay, L.J., Lai, J.Y., Porreca, F., Hruby, V.J. *Bioorg. Med. Chem. Lett.* **16**(18), 4946-4950 (2006).
2. Weber, S.J., Greene, D.L., Sharma, S.D., Yamamura, H.I., Krammer, T.H., Burks, T.F., Hruby, V.J., Hersh, L.B., Davis, T.P. *J. Pharmacol. Exp. Ther.* **259**, 1109-1117 (1991).
3. Weber, S.J., Abbruscato, T.J., Brownson, E.A., Lipkowski, A.W., Polt, R., Misicka, A., Haaseth, R.C., Bartosz, H., Hruby, V.J., Davis, T.P. *J. Pharmacol. Exp. Ther.* **266**, 1649-1655 (1993).
4. Lee, Y.S., Nyberg, J., Moye, S., Agnes, R.S., Davis, P., Ma, S-W., Lai, J., Porreca, F., Vardanyan, R., Hruby, V.J. *Bioorg. Med. Chem. Lett.* **17**(8), 2161-2165 (2007).
5. Lee, Y.S., Kulkarani, V., Cowell, S.M., Ma, S.-W., Davis, P., Hanlon, K.E., Vanderah, T.W., Lai, J., Porreca, F., Vardanyan, R., Hruby, V.J. *J. Med. Chem.* **54**(1), 382-386 (2011).

Energy Balance Studies and Cancer

Joel Nyberg, Minying Cai, Kimberly Osesky, and Victor Hruby

Department of Chemistry, University of Arizona, Tucson, AZ, 85721, U.S.A.

Introduction

The melanocortin system currently has five known receptors and these 5 receptors regulate a remarkably vast array of physiological processes in our bodies. Everything from inflammation and pigmentation (MC1), adrenal gland function (MC2), energy partitioning (MC3), feeding and sexual behavior (MC4) to exocrine gland function (MC5) [1-4]. This research has been mostly concerned with energy partitioning and feeding behavior, especially in its application to cancer. Cachexia is a clinical syndrome of wasting that accompanies many chronic diseases including cancer, renal failure, and heart failure. Evidence from animal models suggests a compelling link between cachexia and inflammation, and a variety of pro-inflammatory cytokines such as TNF-α play an integral role in wasting syndrome. This condition is marked by an increase in energy expenditure and preferential loss of lean body mass, creating a striking catabolic state. Few treatments have proved to be of significant benefit to patients suffering from cachexia. One new treatment that shows promise is pharmacological blockade of the central melanocortin system. The importance of this system is in maintaining normal body weight. In humans it is highlighted by the finding that disordered melanocortin signaling results in early-onset morbid obesity or dramatic decreases in lean body mass in humans. Emerging evidence suggests that blocking this system via pharmacological antagonists of the type 4 melanocortin receptor (MC4R) may restore appetite and lean body mass in subjects with cachexia caused by a variety of underlying disorders. The basic template for these are bifunctional drugs involving a MC4 antagonist portion coupled with various linkers to the core sequence of the endogenous peptide α-MSH believed to be involved in inflammation, Lys-Pro-Val. Comparatively little attention has been given to obtaining selective ligands for the hMC3R owing to the dearth of specific evidence on their physiological functions. However, recent reports have demonstrated that inactivation of the mouse MC3R leads to increased fat mass, reduced lean mass, and higher feed efficiency than their wild type littermates. Furthermore, studies have shown that peripheral injections of a hMC3R selective agonist can stimulate food intake in mice, suggesting an important role of this receptor subtype in the regulation of feeding and energy partitioning. In addition, possible involvement of the hMC3R in the regulation of inflammatory responses and cardiovascular function has also been proposed. Finally, the emerging evidence points to a potential role of the hMC3R in regulation of erectile function and sexual behavior, which provides further impetus for the development of highly selective hMC3R agonists and antagonists. Results of testing a series of hMC4/TNF-α antagonists on the four of the five known melanocortin receptors (MCR) is seen in Table 1.

Results and Discussion

Several of these peptides have been subjected to bioassays expressing melanocortin receptors and although the MC4R selective portion results from the first series of compounds (shown in Table 1) have not been ideal, however, some very promising MC3 selective antagonist ligands have resulted in this series of peptides as well as an additional series of peptides. Of the four MC receptors tested in the additional series, those peptides show the most antagonistic effects on MC3 based on the % max effect which will be presented at a later date. Developing ligands that are selective for MC3R over MC4R has become one of our major goals. In Table 1 the IC_{50} values for five of the compounds are shown. Compound **1** appears to show a greater selectivity towards the MC3R over the MC4R as does compound **2**. We see less selectivity in the remaining three compounds. In this table it appears that a succinic anhydride linker and shorter, smaller amino acids such as glycine and alanine connecting to the KPV sequence are the most promising lead compounds.

Table 1. IC$_{50}$ values for five of the tested compounds

Compound	IC$_{50}$ (nM)			
	hMC1R	hMC3R	hMC4R	hMC5R
Ac-Nle-*c*[D-H-DPhe-R-W-K]-NH$_2$ (control) MT-II	3.1	1.1	0.18	1.6
1. c[CO(CH$_2$)$_2$CO-DNal-R-W-K]-G-K-P-V-NH$_2$	3.1	1.1	35	11
2. c[CO(CH$_2$)$_2$CO-DNal-R-W-K]-A-K-P-V-NH$_2$	51	2.2	42	17
3. c[CO(CH$_2$)$_2$CO-DNal-R-W-K]-A-G-K-P-V-NH$_2$	390	2.8	17	6.5
4. c[CO(CH$_2$)$_2$CO-DNal-R-W-K]-β-A-K-P-V-NH$_2$	2.7	5.0	1.9	3.4
5. Ac-Nle-c[D-H-DNal-R-W-K]-G-K-P-V-NH$_2$	4.6	2.7	0.88	4.5

References

1. Butler, A.A., Kesterson, R.A, Khong, K., et al. *Endocrinology* **141**(9), 3518-3521 (2000).
2. Ellacott, K.L.J., Murphy, J.G., Marks, D.L., et al. *Endocrinology* **148**(12), 6186-6194 (2007).
3. Sutton, G.M., Perez-Tilve, D., Nogueiras, R., et al. *Journal of Neuroscience* **28**(48), 12946-12955 (2008).
4. Getting, S.J., Di Filippo, C., Christian, H.C. *J. Leukocyte Biology* **76**, 1-91 (2004).

Comparative Study of Computer Modeling and Biological Testing of New Kyotorphin Analogues

Tatyana Dzimbova[1], P. Milanov[2], and Tamara Pajpanova[1]

[1]*Institute of Molecular Biology "Roumen Tsanev", Bulgarian Academy of Sciences, 1113, Sofia, Bulgaria;*
[2]*South-West University "Neofit Rilski", 2700, Blagoevgrad, Bulgaria*

Introduction

The most important thing is to know with which receptor kyotorphin, respectively its analogues, interacts. Kyotorphin (KTP) was isolated from bovine brain by Takagi and co-workers [1,2]. This endogenous dipeptide (L-Tyr-L-Arg) belongs to the neuropeptide family due to its opiate-like activity. The Tyr-Arg motif exists widely through-out the brain, not only as KTP, but also as the N-terminal part of several endogenous analgesic peptides [3,4]. This peptide is very rapidly degraded by aminopeptidases [5]. Many of these properties are typical for neurotransmitters, and it is not surprising that KTP has also nonopioid action independent of enkephalin release [6]. There is evidence suggesting that KTP does not bind the opiate receptors (μ, δ, κ), but that it exerts Met-enkephalin-release force [7]. These results led to the suggestion that the dipeptide bind to a specific receptor (KTP receptor, KTPr) [8], triggering a cascade of events that leads to strong analgesia in the brain [9,10]. Despite the fact that several studies [7,11,12] confirm the existence of a KTPr, it has not yet been identified. There is still the question of whether the KTPr is specific [11], or the result of mixed oligomerization of μ- and δ-opioid receptors [13]. The L-Tyr residue at first position of the peptide presented in most of the opioid peptides. It is believed to be crucial for receptor recognition [14,15] due to both π-stacking [16] and hydrogen-bonding with the alcohol of the phenol group [17]. A protonable N-terminal group is also present in KTP and, when protonated, can form a salt bridge with an anionic group in the receptor, which is typical for the morphine/μ-receptor interaction [17]. Another important aspect of the KTP-receptor interaction is orientation. By fitting the KTP conformations to the structure of morphine, Machuqueiro et al. [18] tried to exclude the hypothesis that the KTPr pocket is similar to that of the μ-receptor. They observed exactly opposite. The best-fitted KTP conformations revealed several nonobvious aspects: 1) there was no preference for any N-terminus charge or cis/trans conformation in the set; and 2) the predominance of the extended conformations (both cis and trans) results in the Arg side chain not invading the vicinities of the phenol group of the Tyr. That allowed it to be presented to the receptor without any hindering effects. These results suggest that, despite the fact that KTP does not bind to the opioid receptors, there is no indication for the KTPr pocket to be very different from those of the opioid receptors. Using all this data we can consider that the receptor pocket is the same as in μ-receptor, and to try to explain biological effect of analogues using computational methods.

Fig. 1. New KTP analogues.

Results and Discussion

Synthesis. The synthesis of the four new analogues of KTP was realized by synthetical approaches based on methods of peptide synthesis in solution – mixed anhydride and activated esters method. For Nα-protection Z- and Tos-groups were used, and for carboxyl protection benzyl and methyl ester, respectively. Strategy for minimal side chain protection was applied – phenol hydroxyl group in Tyr and sulfo-guanidino group in NsArg were unprotected during the coupling reaction. Synthetic schemes were presented previously [19].

Biological activity. Male Wistar rats (180-200 g) and male albino mice (25-28 g) were used. Two methods were applied – Paw-pressure and Hot plate test. Norsulfoarginine (1 mg/kg, i.p.), NsArg-Tyr, Tyr-NsArg, Tyr-NsArgNH$_2$ and Tyr-NsAr-OBzl (all at a dose of 5 mg/kg, i.p.) applied alone exerted well-pronounced antinociceptive effect in PP test and they significantly

increased HP latency. Obtained results showed that only Tyr-NsArg-OBzl increase significantly the pain threshold vs. native peptide KTP on 15th minute. On the 30th minute only Tyr-NsArg had analgesic effect compared to the control and KTP [19].

Computer modeling. With a help of computer modeling we tried to explain the activity of the kyotorphin analogues synthesized by us. As a model of µ-receptor we used published in PBDe (2iqo). Docking studies were performed by using GOLD 4.1 (Genetic Optimization for Ligand Docking) [17], run on Linux operating system. Energy minimization, Molecular Dynamics, and visualizations were made on MOE (Molecular Operating Environment).
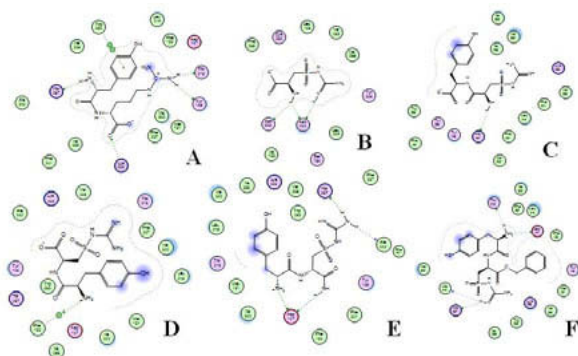
Fig. 2. Interactions in receptor surface.

The amino acid residue Asp 147 was predicted to be a key binding site of the cationic amino group in the µ selective ligands. Aromatic ring in ligand interact with Tyr 299 and hydrogen bonding interaction between the phenolic hydroxyl group of ligand, and both the amino group of Lys303, and hydroxyl group of Tyr 148 were proposed to be major forces for binding. In the case of KTP (**A**) interaction of guanidino group with Asp 147, and Thr 218 and Tyr 148 occurs. Free carboxyl group binds Lys 233 residue, and His 297 forms H-bond with free amino group of Tyr residue. Additional stabilization of this complex is ensured by aromatic interaction between aromatic rings of Trp 293 and Tyr. Interaction between receptor and NsArg (**B**) is very week – there is no conformational fitting. Replacement of Arg with NsArg in KTP (**C**) makes molecule very different. Protonation of sulfoguanidino-group does not occur under physiological conditions, and all interactions due to this effect are not possible. In the case of reversed KTP (**D**) analogue situation is completely different. Interactions occur between different residues in the receptor. Better ligand-receptor interaction appears in the case of Tyr-NsArg-OBzl (**E**). Binding of the free amino group with Asp 147 and Thr 218, interaction between Tyr 148, and aromatic ring of benzyl ester, donor-acceptor interactions as well as H-bond formation – all this shows that the binding is very strong. Tyr-NsArgNH$_2$ (**F**) interacts with a receptor by forming H-bond (His 297 and sulfoguanidino group), side chain interactions, and acidic-basic interaction (Asp 147 and protonated amino group).

Acknowledgments

References

1. Takagi, H., Shiomi, H. Ueda, H. Amano. H. *Eur. J. Pharmacol.* **55**, 109-111 (1979).
2. Ueda, H., Shiomi, H., Takagi, H. *Brain Res.* **198**, 460-464 (1980).
3. Fukui, K., et al. *Neuropharmacology* **22**, 191-196 (1983).
4. Amano, H., Morimoto, Y. Kaneko, S., Takagi, H. *Neuropharmacology* **23**, 395-400 (1984).
5. Ueda, H., Ming, G., Hazato, T., Katayama, T., Takagi, H. *Life Sci.* **36**, 1865-1871 (1985).
6. Ueda, H., Inoue, M., Weltrowska, G., Schiller, P.W. *Peptides* **21**, 717-722 (2000).
7. Takagi, H., Shiomi, H. Ueda, H., Amano, H. *Nature* **282**, 410-412 (1979).
8. Ueda, H., Yoshihara, Y., Takagi, H. *Biochem. Biophys. Res. Commun.* **137**, 897-902 (1986).
9. Ueda, H., et al. *J. Biol. Chem.* **262**, 8165-8173 (1987).
10. Ueda, H., Inoue, M. *Mol. Pharmacol.* **57**, 108-115 (2000).
11. BoËrjesson, U., HuËnenberger, P.H. *J. Chem. Phys.* **114**, 9706-9719 (2001).
12. Shiomi, H., Ueda, H., Takagi, H. *Neuropharmacology* **20**, 633-638 (1981).
13. George, S.R., et al. *J. Biol. Chem.* **275**, 26128-26135 (2000).
14. Lapalu, S., et al. *FEBS Lett.* **417**, 333-336 (1997).
15. Lapalu, S., Moisand, C., Butour, J.L., Mollereau, C., Meunier, J.C. *FEBS Lett.* **427**, 296-300 (1998).
16. Zacharias, N., Dougherty, D.A. *Trends Pharmacol. Sci.* **23**, 281-287 (2002).
17. Patrick, G.L. *An Introduction to Medicinal Chemistry*, Oxford University Press, New York, 511 (2001).
18. Machuqueiro, M., Baptista, A.M. *Biophysical Journal* **92**, 1836-1845 (2007).
19. Bocheva, A., et al. *Compt. Rend. Akad. Bulg. Sci.* **59 (2)**, 219-222 (2006).

Enhancement of HIV-1 Infectivity by Amyloid Peptides

John T.M. DiMaio[1], David Easterhoff[2], Todd M. Doran[1], Stephen Dewhurst[2], and Bradley L. Nilsson[1]

[1]*Department of Chemistry, University of Rochester;* [2]*Department of Microbiology and Immunology, University of Rochester Medical Center, Rochester, NY, 14627, U.S.A.*

Introduction

Semen-derived enhancer of viral infection (SEVI) is an amyloid material formed from the 248–286 fragment of prostatic acidic phosphatase [PAP(248–286)] that dramatically enhances HIV-1 infectivity [1]. It has been postulated that SEVI, which is highly cationic, increases HIV-1 infectivity by shielding charge repulsion between HIV virions and target cells [2]. We tested this hypothesis using non-SEVI amyloid-like fibrils derived from simple peptides of general sequence Ac-$K_n(XKXE)_y$-NH_2 with varying degrees of positive charge appended to the *N*-terminus [3]. Ac-$(XKXE)_y$-NH_2 peptides self-assemble into soluble fibril-like structures with a bilayer architecture; the hydrophobicity of the X residues can be exploited to tune the self-assembly propensity of the resulting sequence [4,5]. We found that cationic Ac-$K_n(XKXE)_2$-NH_2 peptides (Figure 1), where X is phenylalanine (Phe) or cyclohexylalanine (Cha), were able to form soluble fibrils that increased HIV-1 infectivity in a SEVI-like manner [3]. The degree to which HIV-1 infectivity was enhanced by these fibrils varied as a function of X and the number of Lys residues appended to the *N*-terminus. In order to gain additional insight into the varying effects of these materials on HIV-1 infectivity we conducted studies to characterize the equilibrium between monomer and fibril for each of these peptides.

Results and Discussion

In our initial report, it was observed that the ability of Ac-$K_n(XKXE)_2$-NH_2 fibrils to enhance HIV infectivity was dependent on peptide sequence and fibril concentration [3]. At fibril concentrations of 1 μM (fibrils were formed in water with sufficient NaCl to induce self-assembly and then diluted into phosphate buffered saline) the order of enhancement of infectivity was

Fig. 1. Chemical structures of self-assembling peptides.

observed to be Ac-$K_4(FKFE)_2$-NH_2 > Ac-$K_4(ChaKChaE)_2$-NH_2 > Ac-$K_2(ChaKChaE)_2$-NH_2 > Ac-$K_2(FKFE)_2$-NH_2 > SEVI. At higher concentrations of fibril (> 10 μM), fibrils of the tetra-Lys peptides had a weaker effect on infectivity relative to the other peptides. We concluded that these variations in infectivity effects were partly due to differences in fibril solubility; we have since hypothesized that the equilibrium between monomer and fibril for each fibril type may also be a contributing factor.

Peptide self-assembly is a dynamic process in which fibrils exist in equilibrium with peptide monomer. This equilibrium can be described for any given peptide as a function of the critical concentration of monomer (C_r) once fibril formation is complete. Solution state-NMR is useful to study this dynamic equilibrium because fibril signal cannot be observed due to anisotropic line broadening; monomer that is unincorporated into fibril can be quantified by integration of ^1H-NMR signal against an internal standard. We analyzed each Ac-$K_n(XKXE)_2$-NH_2 peptide by ^1H-NMR in simple aqueous (D_2O) solutions with sufficient NaCl to induce self-assembly (500 μM peptide, 300 mM NaCl) and in d_6-DMSO (in which each peptide is unassembled); monomer concentrations were determined by integration of ^1H-signal and correlation to an internal standard of DMF (Table 1). Under these conditions, nearly all Ac-$K_4(ChaKChaE)_2$-NH_2, Ac-$K_2(ChaKChaE)_2$-NH_2, Ac-$K_2(FKFE)_2$-NH_2 peptides are incorporated into fibril, although the Phe-containing peptide had a small amount of unincorporated monomer. These results indicate thermodynamically favorable self-assembly for

these peptides. ^{1}H NMR analysis of Ac-K$_4$(FKFE)$_2$-NH$_2$ showed a substantial amount of unincorporated monomer (66.6%). This is consistent with our published data that indicates that Ac-K$_4$(FKFE)$_2$-NH$_2$ assembles more efficiently at higher [NaCl] [3]. Collectively, this data indicates that self-assembly of peptides is dependent on balancing repulsive charge effects with attractive hydrophobic effects. The less hydrophobic Phe-containing sequences thus self-assemble less efficiently than the Cha-containing counterparts.

Table 1. Tabulated ^{1}H NMR data for peptide self-assembly studies. Percent assembled was inferred by the reduction in integrated peak area of chemical signal between monomeric (DMSO) and assembled (D$_2$O, 300 mM NaCl) peptide samples relative to an internal standard. The percent assembly was used to determine the [monomer] compared to the total [peptide].

Peptide	[Total Peptide]	[Monomer]	Percent Assembled
Ac-K$_2$(FKFE)$_2$-NH$_2$	500 μM	25 μM	99.5%
Ac-K$_4$(FKFE)$_2$-NH$_2$	500 μM	333 μM	33.3%
Ac-K$_2$(ChaKChaE)$_2$-NH$_2$	500 μM	Not detectable	>99%
Ac-K$_4$(ChaKChaE)$_2$-NH$_2$	500 μM	Not detectable	>99%

These data are in agreement with our earlier report which states that the Cha containing Ac-K$_n$(XKXE)$_2$-NH$_2$ peptides more efficiently self-assemble than the Phe counterparts [3]. The thermodynamic order of self-assembly clearly follows a trend (Ac-K$_2$(ChaKChaE)$_2$-NH$_2$ ≈ Ac-K$_4$(ChaKChaE)$_2$-NH$_2$ > Ac-K$_2$(FKFE)$_2$-NH$_2$ > Ac-K$_4$(ChaKChaE)$_2$-NH$_2$) that indicates that increased peptide hydrophobicity results in more efficient assembly that counteracts the repulsive Coulombic effects of increasing positive charge. It is interesting to compare the effects of these peptides in HIV-1 infectivity [3] with the comparative thermodynamic effects reported herein. As stated earlier, Ac-K$_4$(FKFE)$_2$-NH$_2$ fibrils elicit the greatest enhancement on HIV infectivity of the reported materials at low concentrations, but this enhancement disappears at higher concentrations. A similar drop in enhancement in HIV infectivity is observed for all of the previously reported peptides, including SEVI. This trend is interesting since one might assume that dilution of these fibrils to low concentrations might result in loss of infectivity enhancement due to fibril disassembly at concentrations below the C_r value at which self-assembly occurs. This is clearly not the case in our previous report. It should be noted that the NMR characterization here is in simple salt solutions; dilution into more complex phosphate buffers will perturb the thermodynamic equilibrium between fibril and monomer due to relative differences in counterions and ionic strength. In addition, while disassembly of fibrils does occur upon dilution, the kinetics of disassembly is often slow. Thus, the data reported herein confirm the influence of hydrophobicity on peptide self-assembly processes and also indicate the complexity of these processes. Thermodynamic effects must be considered in the design of biomaterials derived from self-assembled peptides in order to accurately explain the behavior of these materials in dynamic environments.

Acknowledgments

References

1. Münch, J., Kirchhoff, F., et al. *Cell* **131**, 1059-1071 (2007).
2. Roan, N.R., Münch, J., Kirchhoff, F., Greene, W.C., et al. *J. Virol.* **83**, 73-80 (2009).
3. Easterhoff, D., DiMaio, J.T.M., Doran, T.M., Dewhurst, S., Nilsson, B.L. *Biophys. J.* **100**, 1325-1334 (2011).
4. Bowerman, C.J., Ryan, D.M., Nissan, D.A., Nilsson, B.L. *Mol. Biosyst.* **5**, 1058-1069 (2009).
5. Bowerman, C.J., Liyanage, W., Federation, A.J., Nilsson, B.L. *Biomacromolecules* **12**, 2735-2745 (2011).

Probing the Effect of Turn Nucleation on Amyloid Self-Assembly Using *β*-Turn Peptidomimetics

Todd M. Doran and Bradley L. Nilsson

Department of Chemistry, University of Rochester, Rochester, NY, 14627, U.S.A.

Introduction

Peptide and protein self-assembly has been proposed to underlie the pathophysiology of Alzheimer's disease (AD), Parkinson's disease, Huntington's disease, and related amyloid disorders [1]. The mechanism by which peptides misfold to form fibrils is nucleation dependent, as evidenced by an observable lag phase prior to self-assembly [2]. Turn nucleation has been proposed to be an early critical step during the lag phase of A*β* self-assembly and is a potential rate-limiting step leading to amyloid fibrils [3-5]. Based on the hypothesis that turn nucleation is a rate-limiting step in A*β* self-assembly, we extended the A*β*(16–20) peptide, a component of *β*-breaker inhibitors of A*β* self-assembly, and added a turn nucleation motif at a position that would interact with the turn region of full-length A*β* if these peptides were incubated with full-length A*β* [6]. We prepared two peptides that terminate with the D-ProGly (^{D}PG) dipeptide motif, an effective type II′ turn nucleator; these peptide sequences are Ac-KLVFFAED^{D}PG-NH$_2$ (peptide **1**) and Ac-KLVFFAEDVG^{D}PG-NH$_2$ (peptide **2**) [7]. We found that co-incubation of these peptides with A*β*42 promoted more rapid self-assembly of the A*β*42 peptide.

Results and Discussion

Turn nucleation has been hypothesized to be a rate-limiting step during A*β* self-assembly [3-5]. Based on this hypothesis, we sought to determine if placing a turn motif onto an A*β* fragment that in some contexts kinetically inhibits A*β* self-assembly would impede or promote self-assembly of the full-length peptide. While a high-resolution structure of the turn region of A*β* is not available, models indicate that the putative turn exists between an internal salt bridge formed by D23 and K28 [8]. Therefore, two peptides that included both the A*β*(16–20) fragment and a *C*-terminal ^{D}PG turn motif were designed in which the ^{D}PG dipeptide would interact with the turn region of A*β*42 if the peptides bind to the full length peptide in a parallel orientation (peptides **1** and **2**). We hypothesized that if turn nucleation is rate-limiting, and peptides **1** and **2** interacted with the turn region of A*β*, then self-assembly rates would be accelerated.
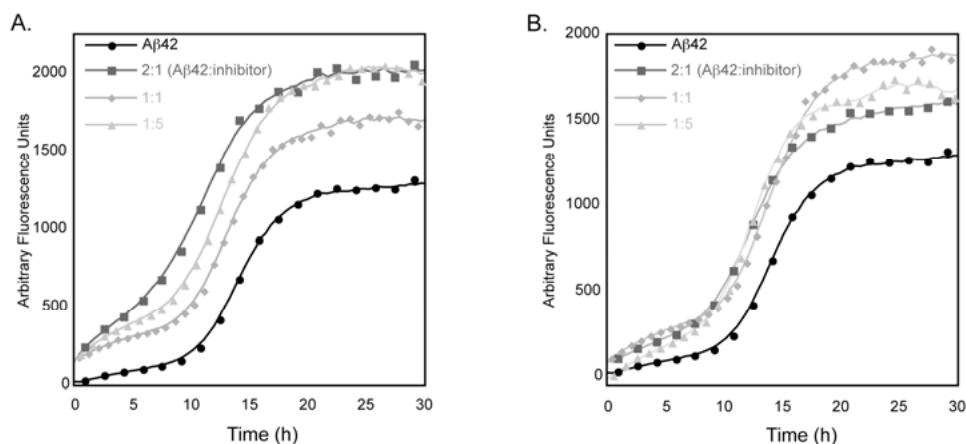
*Fig. 1. Self-assembly kinetics of 10 µM Aβ42 in phosphate-buffered saline (pH 7.4) in the presence or absence of A. peptide **1** or B. peptide **2**.*

The kinetics of self-assembly were monitored using a thioflavin T (ThT) binding assay. ThT is a benzothiazole derivative that undergoes a red shift in the emission spectrum from 430 nm to 482 nm when bound to amyloid fibrils [9]. When Aβ42 is incubated in the presence or absence of peptides **1** or **2**, the kinetics of amyloid fibril formation can be measured over time by monitoring fluorescence at 485 nm. By fitting these self-assembly kinetic curves to a sigmoid equation, it is possible to derive the $t_{1/2}$, a measure of the time it takes for the emission signal to reach half its maximum value; k, the apparent rate constant; and the lag time, which is the time it takes for nucleation to occur before fibril formation enters an exponential growth phase [10]. Addition of peptide **1** or peptide **2** accelerated the rate of self-assembly for Aβ42 (Figure 1). The kinetic parameters derived from this curve indicate that the addition of peptide **1** or peptide **2** decreased the lag phase and $t_{1/2}$ for self-assembly by ~1–2 hours at all concentrations (Table 1). This effect is likely mediated by the interaction of the [D]PG motif with the turn region of the full-length Aβ42 peptide. These results are consistent with turn nucleation as an important early step in Aβ42 self-assembly.

*Table 1. Kinetic self-assembly parameters derived from co-assembly of Aβ42 with peptides **1** and **2***

Peptides	Inhibitor **1**			Inhibitor **2**		
	$t_{1/2}$ (h)	k (h^{-1})	lag time (h)	$t_{1/2}$ (h)	k (h^{-1})	lag time (h)
Aβ42[a]	13.5 ± 0.4	0.50 ± 0.03	9.5 ± 0.4	13.5 ± 0.4	0.50 ± 0.03	9.5 ± 0.4
2:1[b]	10.4 ± 0.4	0.36 ± 0.03	4.8 ± 0.3	12.4 ± 0.6	0.45 ± 0.08	7.8 ± 0.6
1:1[b]	11.3 ± 3.0	0.63 ± 0.03	7.6 ± 0.3	12.3 ± 1.3	0.42 ± 0.03	7.6 ± 1.6
1:5[b]	12.3 ± 0.3	0.42 ± 0.04	7.6 ± 0.6	11.7 ± 0.6	0.41 ± 0.07	6.8 ± 1.5

[a][Aβ42] = 10μM; [b]X:Y refers to X equivalents of Aβ42 to Y equivalents of inhibitor

We have shown that incorporation of a [D]PG turn motif into a short fragment of Aβ42 provides peptides that accelerate the rate of Aβ42 self-assembly, even at substoichiometric concentrations. The increase in self-assembly rate is presumably caused by interaction of the [D]PG turn motif with the turn region of the full-length Aβ42 peptide. This interaction leads to turn nucleation of Aβ42, increasing the rate of self-assembly. These results provide additional evidence for a role for turn nucleation during Aβ self-assembly.

Acknowledgments

References

1. Chiti, F., Dobson, C. *Annu. Rev. Biochem.* **75**, 333-366 (2006).
2. Hamley, I. *Angew. Chem., Int. Ed.* **46,** 8128-8147 (2007).
3. Lazo, N., et al. *Protein Sci.* **14,** 1581-1596 (2005).
4. Sciaretta, K., et al. *Biochemistry* **44,** 6003-6014 (2005).
5. Sandberg, A., et al. *Proc. Natl. Acad. Sci. U.S.A.* **107,** 15595-15600 (2010).
6. Tjernberg, L., et al. *J. Biol. Chem.* **271,** 8545-8548 (1996).
7. Haque, T., Little, J., Gellman, S. *J. Am. Chem. Soc.* **116,** 4105-4106 (1994).
8. Petkova, A., et al. *Proc. Natl. Acad. Sci. U.S.A.* **99,** 16742-16747 (2002).
9. LeVine, H. *Methods in Enzymol.* **309,** 274-284 (1999).
10. Nielsen, L. et al. *Biochemistry* **40,** 6036-6046 (2001).

Inhibition of Human Islet Amyloid Polypeptide Aggregation and Membrane Damage in β-Islet Cell Mimics

Brenan Wilson and Deborah L. Heyl

Department of Chemistry, Eastern Michigan University, Ypsilanti, MI, 48197, U.S.A.

Introduction

Human Islet Amyloid Polypeptide (hIAPP) is a 37-amino acid polypeptide co-secreted with insulin in response to elevated blood glucose levels [1]. In non-diabetics, hIAPP remains soluble [2]. In more than 95% of individuals with type II diabetes, however, hIAPP is found in dense insoluble fibril aggregations on the β-islet cells [3]. The formation of these aggregations is thought to be responsible for β-islet cell membrane disruption and cell death [4]. Insulin has been found to act against the actions of hIAPP. The internal sequence of insulin, HLVEALYLV, recognizes and binds the 10-19 region of hIAPP [5]. Since insulin reportedly blocks the formation of amyloid fibers, insulin analogs may protect cell membranes from damage.

Results and Discussion
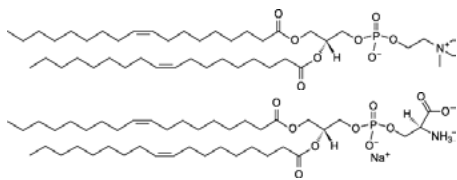
Fig. 1. 1,2-Dioleoyl-sn-Glycero-3-Phosphocholine (DOPC, top) and 1,2-Dioleoyl-sn-Glycero-3-[Phospho-L-Serine](Sodium Salt) (DOPS, bottom).

Fragments of insulin were synthesized and tested to determine their effects on hIAPP (purchased from SynBioSci) aggregation and induced membrane damage. Insulin is a known kinetic inhibitor of hIAPP aggregation [6], so penta- to nonapeptide fragments of the sequence believed to interact with hIAPP were selected for synthesis. These included the following: ALYLV, EALYV, VEALYLV, LVEALYV, and HLVEALYLV. The peptides were synthesized by standard fluorenylmethyl-oxycarbonyl (Fmoc)-based solid phase techniques and purified by reverse-phase high performance liquid chromatography (RP-HPLC). Carboxyfluorescein-encapsulating vesicles which mimic the β-cell were created using a 7:3 ratio of the lipids 1,2-dioleoyl-sn-glycero-3-phosphocholine (DOPC) and 1,2-dioleoyl-sn-glycero-3-(phospho-L-serine) (DOPS), respectively (Figure 1), and the percent leakage of fluorescent dye from the vesicles in the presence of 10 μM hIAPP and varying concentrations of the peptides (in inhibitor:hIAPP ratios of 0.2:1, 1:1, 5:1, and 10:1) was calculated as compared to a 100% Triton-X detergent-treated control. Assays were run in triplicate in a 96-well plate, and average values were calculated. Fluorescence values were recorded by an FLx fluorescence microplate reader. The activity of the truncated analogs was compared to that of insulin (purchased from Sigma Aldrich) under the same conditions. The effects of the inhibitors on hIAPP aggregation were similarly determined using the same peptide and vesicle concentrations with Thioflavin T fluorescence assays to determine the $t_{1/2}$ for conversion to fibers.

Data obtained were converted to relative changes as compared to hIAPP-treated vesicles without inhibitor (i.e., without insulin or synthesized peptide) and are provided in Figure 2. All inhibitor sequences tested were most effective in slowing hIAPP aggregation at a concentration ratio of 10:1 inhibitor:hIAPP. Most sequences demonstrated the ability to mimic approximately half of insulin's aggregate inhibitory activity despite being much shorter fragments, implying that the correct binding piece is being used. However, increased fragment length did not always result in slower aggregation. Only one inhibitor, EALYLV, exhibited a reduction in membrane damage at all concentration ratios and this reduction was minimal. Most inhibitors actually increased membrane damage, with more damage occurring at higher concentration ratios. Most importantly, slowing hIAPP aggregation did not correlate to reduced membrane destruction as expected. On the contrary, slower aggregation was associated with increased membrane damage in most cases.
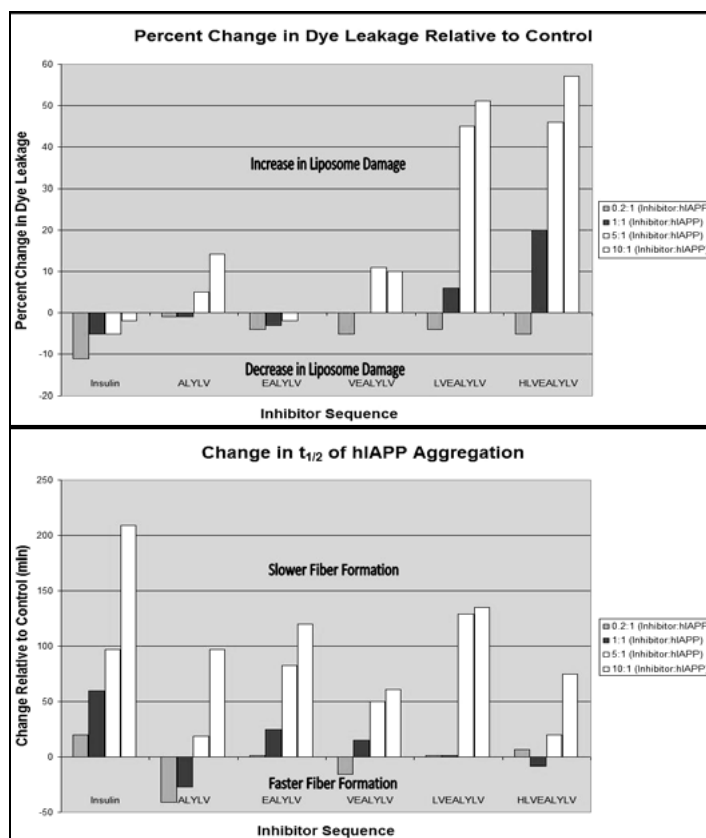
Fig. 2. (Top) Summary of dye leakage assay results for all inhibitors tested. Inhibitors which decreased liposome damage at a given concentration ratio are represented by negative bars while increased liposome damage is represented by positive bars. (Bottom) Summary of thioflavin T assay results for all inhibitors tested. Inhibitors which slowed aggregation at a given concentration ratio are represented by positive bars while the hastening of aggregation is represented by negative bars.

The results of this study indicate that something more than just aggregation must be occurring as the mechanism of membrane damage, possibly the formation of pores, disordering or puncturing of the membrane, or induction of membrane curvature. Alternatively, slowing the aggregation process actually may be prolonging the presence of a cytotoxic intermediate species.

Acknowledgments

References

1. Scrocchi, L.A., Chen, Y, Wang, F., Han, K., Ha, K., Wu, L., Fraser, P.E. *Lett. Peptide Sci.* **10**, 545-551 (2004).
2. Smith, P.E.S., Brender, J.R., Ramamoorthy, A. *J. Am. Chem. Soc.* **131**, 4470-4478 (2008).
3. Azriel, R., Gazit, E. *J. Biol. Chem.* **276**(36), 34156-34161 (2001).
4. Brender, J.R., Lee, E.L., Cavitt, M.A., Gafni, A., Steel, D.G., Ramamoorthy, A. *J. Am. Chem Soc.* **130**, 6424-6429 (2008).
5. Gilead, S., Wolfenson, H., Gazit, E. *Angew. Chem.* **45**, 6476- 6480 (2006).
6. Cui, W., Ma, J.W., Lei, P., Wu, W.H., Yu, Y.P., Xiang, Y., Tong, A.J., Zhao, Y.F., Li, Y. M. *FEBS Journal* **276**, 3365-3371 (2009).

Stabilization of the Amyloid β-Peptide in a Helical Conformation Reduces Aβ Toxicity

Dmytro Honcharenko[1], Partha P. Bose[1], Jan Johansson[2], and Roger Strömberg[1]

[1]*Department of Biosciences and Nutrition;* [2]*Department of Neurobiology, Care Sciences & Society, Alzheimer Centre, Karolinska Institute, Huddinge, S-14183, Sweden*

Introduction

The term amyloid was originally proposed for tissue deposits found in association with disease, and later found to be composed of proteins with fibrillar, cross-β-sheet structures [1]. The 40-42 residues long Aβ peptide is invariably present in amyloid plaques found in association with Alzheimer's disease. The formation of Aβ fibrils, through aggregation of peptides in β-strand conformation, is thought to be a major part of the cause of this devastating disease [2].

The Aβ peptide is generated by proteolytic cleavage of the transmembrane amyloid precursor protein, APP [3], and it initially harbour α-helices which are strongly predicted to form β-strands (discordant helices) [4]. Evidence is accumulating that prefibrillar soluble aggregates, including species referred to as protofibrils, may be more toxic than the mature fibrils [5-7]. The structure of amyloid fibrils was recently established and supports the indication that a region around positions 17-20 is essential for Aβ fibril formation [8]. Recent molecular dynamics studies also show that the α-helical propensity of the three nonpolar residues (18, 19, and 20) is the main factor for the stability of the Aβ central helix and that their hydrophobicity plays a secondary role [9].

Inhibition of fibril and/or oligomer/protofibril formation could prevent the occurrence or progression of Alzheimer's disease. Several ways are being explored to prevent fibril toxicity [10] including active or passive immunisation. These attempts have given promising results, in both animal models and humans, but have also given serious side-effects in clinical trials. Several low molecular weight inhibitors of Aβ aggregation have also been identified, including chemically diverse compounds such as curcumin, inositol, and nicotine [11]. Many of these compounds are predicted to bind to Aβ in an elongated, β-strand-like conformation and prevent its polymerization. However blocking of the later stages of fibril formation may increase accumulation of potentially cytotoxic prefibrillar oligomers. Another disadvantage of this strategy is the lack of specificity and difficulty to target oligomeric Aβ forms by rational design because of the lack of their structural determination. An alternative possible approach to prevent Aβ aggregation is stabilization of the native α-helical structure in a state similar to its perceived structure in membrane embedded APP.

Results and Discussion

We have shown that by using small designed ligands, directed towards the discordant region of Aβ (residues 13-23), it is possible to stabilize a helical structure and reduce Aβ aggregation *in vitro* [12]. Oral administration of such compounds in *Drosophila melanogaster* Alzheimer's disease model expressing human $Aβ_{1-42}$ in the central nervous system increases longevity, decreases locomotor dysfunction and reduces neuronal damage. These compounds also reduce Aβ toxicity to cells and prevent Aβ-induced reduction of γ oscillation in hippocampal slices, which is connected to memory and cognition and reduced in Alzheimer's patients.

Encouraged by the success of the first generation of ligands we are extending our design and synthesizing a new generation of compounds in order to screen them *in vitro* and in *Drosophila* and other animal models, primarily transgenic mouse models of Alzheimer's disease. The second generation of ligands is designed to give improved binding affinity to Aβ (Figure 1). Synthesis of the new ligands requires non-natural amino acid building blocks, some of which are previously unknown. Several new peptoid ligands containing these amino acids have been synthesized (Figure 1).
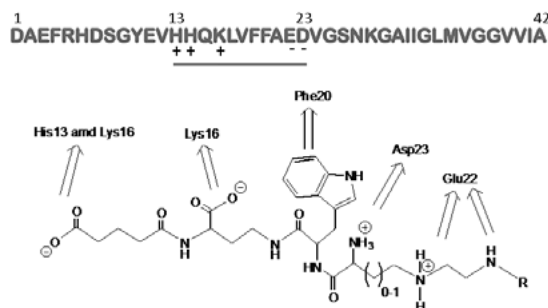
Fig. 1. Examples of ligands designed for binding to the α-helical form of the 13-23 region of the Aβ$_{1-42}$ peptide. Arrows indicate the amino acids in Aβ peptide with which the different groups are designed to interact.

The ligands have, in general, been designed so that versatile and well working peptide/amide chemistry can be used to construct them. The synthesis development involves both solution and solid phase methodology which allows for substantial variation of substituents and more ready production of libraries where the different parts of the peptoid that interact with the Aβ-peptide can be optimized. We have worked out methodology for the synthesis, produced one set of compounds and are currently investigating their properties and ability to inhibit Aβ-aggregation.

Alzheimer's disease is the most common cause of dementia among elderly people and at present there is no curative treatment available against this condition. In light of these circumstances and based on our results this approach holds promise for the development of orally available compounds against Alzheimer's disease.

Acknowledgments

References

1. Westermark, P. *FEBS J.* **272**, 5942-5949 (2005).
2. Goedert, M., Spillantini, M.G. *Science* **314**, 777-781 (2006).
3. Esler, W.P., Wolfe, M.S. *Science* **293**,1449-1454 (2001).
4. Kallberg, Y., Gustafsson, M., Persson, B., Thyberg, J., Johansson, J. *J. Biol. Chem.* **276**, 12945-12950 (2001).
5. Walsh, D.M., Klyubin, I., Fadeeva, J.V., Cullen, W.K., Anwyl, R., Wolfe, M.S., Rowan, M.J., Selkoe D.J. *Nature* **416**, 535-539 (2002).
6. Nilsberth, C., Westlind-Danielsson, A., Eckman, C.B., Condron, M.M., Axelman, K., Forsell, C., Stenh, C., Luthman, J., Teplow, D.B., Younkin, S.G., et al. *Nat. Neurosci.* **4**, 887-893 (2001).
7. Lesné, L., Koh, M.T., Kotilinek, L., et al. *Nature* **440**, 352-357 (2006).
8. Janek, K., Rothemund, S., Gast, K., Beyermann, M., Zipper, J., Fabian, H., Bienert, M., Krause, E. *Biochemistry* **40**, 5457-5463 (2001).
9. Ito, M., Johansson, J., Strömberg, R., Nilsson, L. *PLoS One* **6**, e17587 (2011).
10. Roberson, E.D., Mucke, L. *Science* **314**, 781-784 (2006).
11. LeVine III, H. *Amyloid* **14**, 185-197 (2007).
12. Nerelius, C., Sandegren, A., Sargsyan, H., Raunak, R., Leijonmarck, H., Chatterjee, U., Fisahn, A., Imarisio, S., Lomas, D.A., Crowther, D.C., Strömberg, R., Johansson, J. *PNAS* **106**, 9191-9196 (2009).

Peptides Derived from the Central Domain of the Human SAA Protein are Forming Amyloid-Like Fibrils *in vitro*

Emanuel Perugia and Mati Fridkin

Department of Organic Chemistry, Weizmann Institute of Science, Rehovot, 76100, Israel

Introduction

Serum amyloid A is an acute phase protein associated with pathological amyloid deposit [1]. A growing number of studies in the past years have demonstrated that the amyloid cascade can be triggered by short (five to ten amino-acids long) aggregation-prone sequences also known as "consensus sequences" or "consensus motifs" [2]. The objective of the present work was to ascertain the existence of such motifs inside the human Serum Amyloid A protein (SAA), their structure and their role in SAA aggregation. This knowledge may lead to the development of compounds for the treatment of Amyloidosis A.

Results and Discussion

The major amyloidogenic domain of the human SAA protein was identified by Westermark and colleagues in 1992 in the N-terminus of the protein (SAA 2→12) [3]. In 2007, Liu, et al. reported that the highly conserved domain SAA 29→42 was forming amyloid-like fibrils that were lacking seeding activity and were incapable of inducing amyloidosis in experimental animals [4]. Here we report for the first time that other peptides derived from the central domain of the human Serum amyloid A protein, namely SAA 50→59, 48→64 and 47→76, (Table 1) are forming amyloid-like fibrils *in vitro*. Synthetic peptides were prepared according to the Fmoc solid-phase strategy and purified by reverse-phase HPLC, their M.W. was confirmed by mass spectrometry. Amyloid formation was induced by dissolving the peptides at a concentration of 10 mg/ml in 10% v/v acetic acid and fibers characterization was performed by TEM, ThT and FT-IR. Interestingly, we've noticed that the SAA 50→59 shares a consensus sequence remarkably similar to a common one identified in Synuclein, Aβ 1-42, the prion protein and the IAPP. The
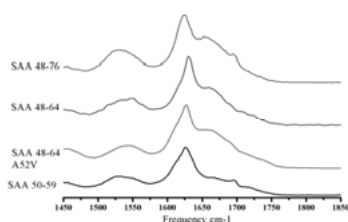
Fig. 1. FT-IR of SAA-derived peptides.
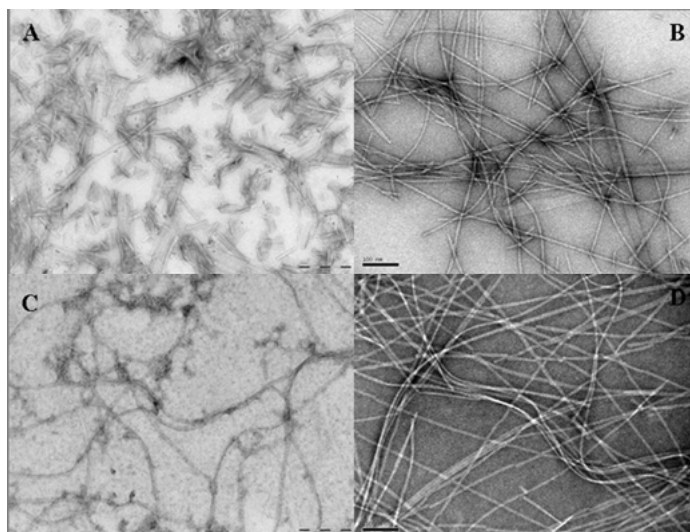
Fig. 2. TEM micrographs of SAA-derived peptides: A) SAA 50→59; B) SAA 48→64; C) SAA 47→76; D) SAA 48-64 A52V. Scale: 200 nm A) and C); 100 nm B) and D).

Table 1. SAA derived peptides tested positive for amyloid formation (ThT, TEM, FT-IR)

Peptide Sequences	Name	Mass
1. GGAWAAEVIS	SAA 50→59	959
2. GPGG∇WAAEVISDARE	SAA 48→64 A52V	1614
3. GPGGAWAAEVISDARE	SAA 48→64	1586
4. GPGGAWAAEVISDARENIQRFFGHGAEDS	SAA 48→76 (hSAA1β)	3045

significance of this finding in the context of the formation of the Amyloid A is not yet fully understood. Other studies demonstrated via site directed mutagenesis that removal of the first twelve amino-acids of the human SAA effectively inhibits amyloid formation and even proper folding of the protein, implying a primary and essential amyloidogenic domain in the N-terminus [5]. Bearing this in mind, we've decided to adopt an opposite strategy from our initial minimalistic approach and to elongate the middle amyloidogenic domain to encompass a large portion of the protein. To determine if indeed amyloid could be obtained from a substantial segment of SAA even without the N-terminal, we synthesized first the SAA 48→64 and then, via Microwave-assisted synthesis the SAA 47→76. Interestingly, amyloidogenicity was retained. An explanation for this behavior may be found in the intrinsic hydrophobic nature of these peptides and in the folding of the protein itself: this portion of the protein is in fact usually hidden in the internal core which in its physiological state is also buried inside the HDL particle. It may be also possible that this domain becomes important for amyloid formation only upon proteolysis and subsequent exposure.

The TEM morphology of the three peptides is, as expected [6], quite different (Figure 2). The SAA 50→59 showed heterogeneity in the shape of the fibers with two preponderant profiles – thin and elongated (8nm thickness, several microns length) vs. thick and short profile (15nm thick, 200nm length). This suggests a complex pattern of aggregation. It is noteworthy that the FT-IR profile exhibits only a very small component at $1695cm^{-1}$ (Figure 1) that can suggest a conformation with a parallel β-sheet.

The SAA 48→64 and 48→64 A52V derived amyloids are the most regular and homogeneous. The fibers have a thickness of 10 to 15 nm and a considerable length up to several μm. Substitution of the Alanine with the Valine seems to influence the twisting although the FT-IR trace is remarkably similar.

The SAA 47→76 shows the widest fibers in the group that can reach up to 40 nm and as well considerable length up to several μm. The FT-IR pattern shows a strong component at $1695cm^{-1}$ (Figure 1) suggesting the formation of an antiparallel β-sheet.

To summarize, the contribution of the present study can be recapitulated in three points:
1. We were able to identify a previously unknown highly amyloidogenic domain inside the SAA molecule: the SAA 50→59. The consensus motif isolated in this peptide may be used as target for the development of β-sheet breaker compounds.
2. The importance of this domain is further substantiated by the fact that even upon elongation of the sequence (i.e SAA 48→64 and SAA 48→76), amyloidogenicity is preserved. Stable Amyloid A fibrils can therefore be generated without the presence of the N-terminal region of the SAA.
3. We believe that this central domain becomes important for amyloid formation only after being exposed upon proteolysis.

Acknowledgments

References

1. Ulhar, C.M., Whitehead, A.S. *Eur. J. Biochem.* **265**, 501-523 (1999).
2. Ventura, et al. *Proc. Natl. Acad. Sci. U.S.A.* **101**, 7258-7263 (2004).
3. Westermark, G.T., Engstrom, U., Westermark, P. *Biochem. Biophys. Res. Commun.* **182**, 27-33 (1992).
4. Liu, Y., Cui, D., Hoshii, Y., Gondo, Y., Ishihara, T. *Scand. J. Immunology.* **66**, 495-500 (2007)
5. Patel, H., Bramall, J., Waters, H., De Beer, M.C., Woo, P. *Biochem. J.* **318,** 1041-1049 (1996).
6. Rubin, N., Perugia, E., Wolf, S.G., Klein, E., Fridkin, M., Addadi, L. *JACS* **132,** 4242-4248 (2010).

A Dual-Acting Heterodimer Peptide

Graeme Kelly, Tanya Smith, Marcus Sims, and Marc Devocelle

Department of Pharmaceutical and Medicinal Chemistry, Royal College of Surgeons, 123 St. Stephens green, Dublin, 2., Ireland

Introduction

Sequences of pro- and anti-apoptotic proteins can recapitulate the activity of their parent proteins. Synthetic peptides derived from pro-apoptotic proteins can therefore potentially be used as anticancer drugs. The BH3 domain of Bid, for example, has the ability to enhance the apoptotic response of cancer cells to chemotherapy but unfortunately is susceptible to *in vivo* instability and is unable to translocate the cell membranes. To enhance the cellular uptake of this peptide, permanent modifications of the sequence with fatty acids or cell-penetrating peptides have been performed [1].

Host defence peptides, such as buforin, are molecular mediators of innate immunity in multi-cellular organisms [2,3]. Their ability to induce mitochondria-dependent apoptosis in cancer cells and to overcome drug resistance has made them attractive anti-cancer leads. Furthermore, host defence peptides do not easily select resistant mutants and are active against both dividing and non-dividing cells. Interestingly, these peptides have also the ability to translocate cellular membranes and promote the uptake of a conjugated moiety. However, their capacity to act as vectors has not been exploited to date and it is proposed here to use buforin not only as an anticancer candidate in its own right, but also as a carrier for a BH3 peptide.

The aim of this project is therefore to synthesise a heterodimeric peptide including the BH3 and buforin sequences (Figure 1). Both sequences can be synthesised with a cysteine residue at their N-termini to cross-link them through a disulfide bond. They are both amenable to assembly by Solid Phase Peptide Synthesis (SPPS) according to the Fmoc/*t*-Bu strategy. As the activity of some membrane active peptides is independent of the stereochemistry of their constitutive residues, the buforin sequence can be used as an all-D peptide, while the BH3 sequence is assembled from natural amino acids. The use of the cross-linking reagent 2,2'-dithiol-bis(5-nitropyridine) (DTNP) was chosen to favour the formation of the heterodimer over its homodimeric counterparts [4].
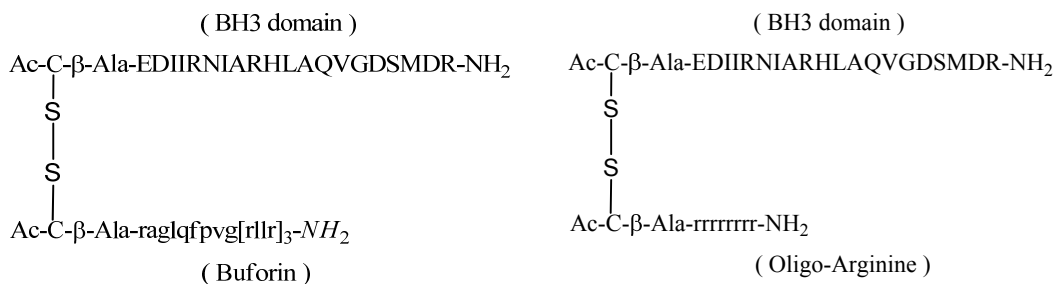
Fig. 1. Structure of the heterodimeric BH3-Buforin and BH3-oligo-Arginine peptides.

Results and Discussion

Peptides were synthesized by automated SPPS on as Applied Biosystems 433A from a MBHA Rink Amide resin. They were purified by RP-HPLC and characterized by Mass Spectrometry (Maldi-Tof MS) using an a-cyano-4-hydroxy-cinnamic acid matrix. Formation of the heterodimer was performed in solution using DTNP activation of the BH3 sequence in 3:1 acetic acid/water under an argon atmosphere. The reaction was monitored by RP-HPLC on a C18 Gemini column.

Achieving high yields and purities of both individual cysteine-modified sequences is a prerequisite in the present study, as the assembled sequences do not constitute end products, but intermediates. Preliminary studies for the assembly of the BH3 and buforin sequences by HBTU/HOBt/DIEA coupling chemistry showed the formation of truncated sequences and assembly of the BH3 sequence from Ile[7] and of the buforin sequence from Pro[7] were performed by a double coupling procedure. During the activation procedure of the BH3 peptide with DTNP, the number of equivalents of DTNP was increased to 20 to drive the reaction to completion. The reaction time was also extended from 5 hours to 24 hours with conversion going from 35% to 65%. The large excess of DTNP also favoured ultimately the asymmetric disulfide bond formation.

The conjugation of the two peptides after activation was attempted under 2 different conditions. The reaction was either performed in 0.1M acetic acid or in 1M ammonium acetate. In the first case, the formation of the heterodimer only occurred to a small extent with concomitant formation of several impurities. The low recovery of desired product by semi-preparative RP-HPLC didn't warrant future scale-up of this approach. Reaction in 1M ammonium acetate resulted in increased formation of product by asymmetric disulfide bond formation.

Table 1. Mass Spectrometry and RP-HPLC Analysis of peptides and peptide conjugates

Peptide	M/Z	Purity %
Ac-Cys-b-Ala Buforin	2775	96.7
Ac-Cys-b-Ala-BH3	2524	77.8
Ac-Cys-b-Ala-Buforin conjugated to Ac-Cys-b-Ala-BH3	5302	64.9
Ac-Cys-b-Ala-OligoArginine	1482	90.0
Ac-Cys-b-Ala-BH3 conjugated to Ac-Cys-b-Ala-OligoArginine	4006	78.1

A synthetic route has been developed for the production of a heterodimeric peptide allowing the delivery and release of two anticancer peptide sequences in cancer cells. This strategy capitalises on the selectivity of buforin for cancer cells and its ability to promote the cellular uptake of a conjugated cargo. Alternative conjugation strategies of the two sequences will also be evaluated if the stability of the disulfide bond in the heterodimer is not adequate for scale-up production and testing.

Acknowledgments

References

1. Francisco, J., Mendoza, et al. *Arch. Immuno. Ther. Exp.* **53**, 47-60 (2005).
2. Mader, J.S., Hoskin, D.W. *Expert Opin. Investig. Drugs* **15**, 933-946. (2006).
3. Takeshima, K., et al. *J. Biol. Chem.* **278,** 1310-1315 (2003).
4. Rabanal, F., et al. *Tetrahedron Letters* **37,** 1347-1350 (1996).

Truncation of a 20-mer Wild Type Bim BH3 Domain Peptide: Identification of the Minimum Sequence Necessary for Promoting Cell Death of Prostate Cancer (PC3) Cells

Mohamed Elsawy*, Lorraine Martin, and Brian Walker*

School of Pharmacy, Faculty of Medicine, Health and Life Sciences, The Queen's University of Belfast, Belfast, BT9 7BL, UK
Address correspondence to: melsawy01@qub.ac.uk, brian.walker@qub.ac.uk

Introduction

Cancer cells become resistant to mitochondrial-driven apoptosis, through the up-regulation of anti-apoptotic Bcl-2 family proteins. Based on a published study showing the functional activation of the pro-apoptotic Bcl-2 protein Bax by Bim BH3 20-mer peptides [1], we have carried out systematic truncation studies on the 20-mer wild-type sequence to identify the minimal domain that can cause Bax activation and promote apoptosis in PC3 prostate cancer cells.

Results and Discussion

The disruption of the normal balance in the ratio between pro- and anti-apoptotic Bcl-2 family members is one of the resistance mechanisms displayed by cancer cells [2]. Inhibition of the over-expressed anti-apoptotic proteins is a frequently suggested strategy to overcome this resistance [3], albeit that this would not be successful unless an activator of the effector pro-apoptotic proteins (Bax, Bak) is present [4]. Recently, Gavathiotis et al. discovered a novel activation site of Bax, which they proved to be activated by stabilized α-helix Bim BH3 domain (SAHB) 20-mer peptides [1]. This interaction causes functional activation of Bax, and consequent release of cytochrome c from mitochondrial intermembrane space, which initiates the apoptotic cascade and self-digestion of the cell.

Previous studies employing single site substitutions identified the *C*-terminal 20 residues of Bim BH3 20-mer peptides as being functionally critical for activation of Bax [1]. Consequently, a series of truncated linear peptides derived from this so-called Bim BH3 domain were synthesized by SPPS, purified by RP-HPLC and were examined for their ability to promote apoptosis in prostate cancer PC3 cells, in order to identify the minimum active sequence. Cell viability assays for PC3 cells treated with the truncated peptides (10 μM) showed that 10-mer peptide was the most active truncated candidate that caused ~ 50% reduction in viability compared to the Bim BH3 wild sequence 20-mer peptide that caused only ~ 40% reduction at the same concentration level (Figure 1). The same study performed on breast cancer MDA-MB-231cells revealed the same pattern of activity, where the 10-mer peptide showed slightly higher potency than the BIM BH3 wild sequence 20-mer peptide in reducing cell viability (data not shown).
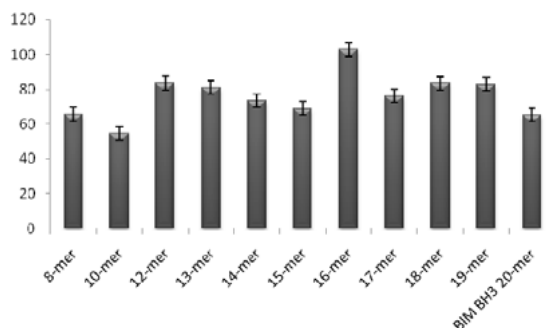
Fig. 1. Percentage viability assay results compared to untreated control for PC3 cells treated with10μM Bim BH3 20-mer peptide and Bim BH3 truncated 10-mer peptide for 72 hours.

Western blotting studies performed on PC3 cells demonstrated that treatment with 10 µM 10-mer and BIM BH3 wild type 20-mer resulted in cytochrome c release into the cytoplasm of these cells (Figure 2), further supporting our contention that the loss of cell viability is most likely the result of the induction of apoptosis. Thus, we hypothesize that the truncated Bim BH3 10-mer peptide represents the minimum sequence required for Bax activation and promotion of apoptosis in cancer cells and represents a lead compound for cancer therapeutics.
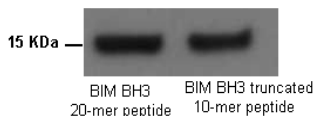
Fig. 2. Western blotting for cytochrome c extracted from PC3 cells cytoplasm lysates treated with 10µM Bim BH3 20-mer peptide and Bim BH3 truncated 10-mer peptide for 72 hours.

Further studies are currently in progress to determine the binding affinity of the 10-mer to recombinant Bax protein and to identify key functional residues within this sequence. These studies will identify approaches aimed at enhancing the apoptotic activity of the 10-mer through increasing its conformational and proteolytic stabilities.

Acknowledgments

References

1. Gavathiotis, E., Suzuki, M., Davis, M., Pitter, K., Bird, G., Katz, S., Tu, H.-C., Kim, H., Cheng, E., Tjandra, N., Walensky, L. *Nature* **455**, 1076-1082 (2008).
2. Paul, K., Mukhopadhyay, A. *Biologia, Bratislava* **62** (4), 371-380 (2007).
3. (a) Sadowsky, J., Schmitt, M., Lee, H.-S., Umezawa, N., Wang, S., Tomita, Y., Gellman, S. *J. Am. Chem. Soc.* **127**(34), 11966-11968 (2005); (b) Sadowsky, J., Murray, J., Tomita, Y., Gellman, S., *ChemBioChem* **8**, 903-916 (2007); (c) Sadowsky, J., Fairlie, W., Hadley, E., Lee, H.-S., Coleska, Z., Wang, S., Huang, D., Tomita, Y., Gellman S. *J. Am. Chem. Soc.* **129**(1), 139-154 (2007); (d) Horne, W., Boersma, M., Windsor, M., Gellman, S. *Angew. Chem. Int. Ed.* **47**, 2853-2856 (2008).
4. Kuwana, T., Bouchier-Hyas, L., Chipuk, J., Bonzon, C., Sullivan, B., Green, D., Newmeyer, D. *Molecular Cell* **17**, 525-535 (2005).

NMR Analysis of Synthetic Peptides Agonist to PTPRJ, a Receptor-Type Protein Tyrosine Phosphatase with Tumor Suppressor Activity

Diego Brancaccio[1], Alfonso Carotenuto[1], Antonio Limatola[1], Pietro Campiglia[2], Francesco Trapasso[3], and Ettore Novellino[1]

[1]*Department of Medicinal and Toxicological Chemistry, University of Naples "Federico II", Naples, 80131, Italy;* [2]*Department of Pharmaceutical Sciences, University of Salerno, Fisciano, 84084, Italy;* [3]*Department of Experimental and Clinical Medicine, University Magna Graecia of Catanzaro, Catanzaro, 88100, Italy*

Introduction

The Protein Tyrosine Phosphatase Receptor J (PTPRJ) is negatively involved in cellular proliferation. It represents a new interesting target for anticancer drugs [1]. Recently five PTPRJ cyclic 9-mer peptide ligands have been identified by means of phage display library screening. After synthesis and purification, all compounds have been tested *in vitro*. In particular, two peptides reported an interesting anti-proliferative activity after interaction to the target. The conformational properties of all compounds have been evaluated by means of NMR studies. NMR data suggested a 2:1 stoichiometry target recognition for those peptides showing anti-proliferative activity.

Results and Discussion

To isolate PTPRJ ligands, we screened a 9-mer cyclic random phage display library against a PTPRJ-tagged recombinant protein. After three rounds of panning, we isolated by immunoscreening 25 phage clones reactive against the PTPRJ-His6 recombinant protein. Among the twenty-five isolated clones, four of them (PTPRJ-pep5: c[C^1-N^2-S^3-H^4-N^5-H^6-H^7-T^8-C^9], PTPRJ-pep19: c[C^1-H^2-H^3-N^4-L^5-T^6-H^7-A^8-C^9], PTPRJ-pep23: c[C^1-L^2-K^3-Q^4-L^5-Q^6-R^7-G^8-C^9], and PTPRJ-pep24: c[C^1-L^2-H^3-H^4-T^5-H^6-G^7-S^8-C^9]) were studied for further characterization based on the ELISA absorbance. Two PTPRJ-interacting peptides, PTPRJ-pep19 and PTPRJ-pep24, induced cell growth inhibition and apoptosis of cancer cells compared to controls (25% vs 1.5%).
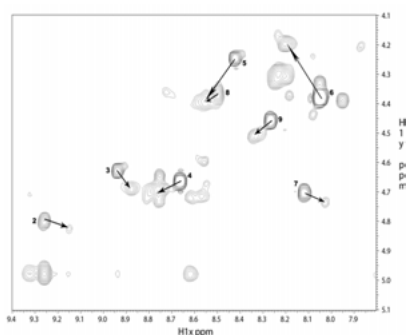
Fig. 1. "Finger print" region of the TOCSY spectrum of PTPRJ-pep19. Arrows indicate signal shifts.

Peptides conformational preferences were investigated by solution NMR spectroscopy. NMR analysis was performed in water at different pH's and temperatures, at a peptide concentration of about 2 mM. For peptide PTPRJ-pep19, all the spectra showed splitting of the signals. Following the most intense signal pattern, complete ^{1}H NMR chemical shift assignments were achieved according to the Wüthrich procedure *via* the usual systematic application of DQF-COSY, TOCSY, and NOESY experiments. Considering the main system, all NMR parameters indicated structural flexibility. For example, no standard α-helix or β-sheet structure from H_α CSI (chemical shift index) values, and no unambiguous medium- or long-range backbone NOE connectivities were found in the NOESY spectrum of the peptide. Only strong $d_{\alpha N}(i, i+1)$ NOEs, which are generally observed in random structures, appeared along the entire length of the peptide. Considering the secondary signals, some interesting features were observed: a) these signals were broadened compared to the others, indicating that aggregation phenomena occurred; b) H_α resonances of all residues but Thr^6 shift down-fields, which indicated a β-hairpin peptide folding with a turn structure encompassing residue 6 (Figure 1).

Table 1. Results from DOSY and STD-NMR experiments

Peptide	R_h^a	N^b	STD^c
PTPRJ-pep5	-	-	2.4
PTPRJ-pep19	8.4 (11.3)[d]	10 (18)[d]	0.7
PTPRJ-pep23	14.7	28	3.2
PTPRJ-pep24	8.5 (11.7)[d]	9 (19)[d]	0.7

[a] R_h = Hydrodynamic radius (Å) from DOSY experiment (2 mM, pH = 4, T = 5° C); [b] N = Calculated number of residues in the oligomer; [c] STD = relative STD effect (%). [d] Secondary signal pattern values are in parentheses.

Peptide PTPRJ-pep24 spectra also showed splitting of the signals. Again, the analysis of the main system revealed a random coil conformation. Secondary signals were relatively broadened as for peptide PTPRJ-pep19. Nevertheless, due to overlapping, only partial assignments of these signals could be achieved and thus we were not able to formulate any hypothesis about the peptide structure in the aggregate form. For PTPRJ-pep5 and PTPRJ-pep23, only broad signals were observed in the ^{1}H NMR spectra and only partial assignment could be done. This result indicated a higher tendency of these peptides to aggregation or chemical exchange phenomena.

To check the aggregation state of the peptides under the NMR conditions, DOSY experiments [2] were recorded. In fact, pulse field gradient NMR methods can be used to determine diffusion coefficients and from these the effective hydrodynamic radii of polypeptides. Moreover, empirical relationships between the hydrodynamic radius (R_h) and the number of residues (N) in a polypeptide were proposed [3]. The calculated hydrodynamic radii and number of residues of peptides PTPRJ-pep19, PTPRJ-pep23 and PTPRJ-pep24 are reported in Table 1. Monomeric (N ~ 9, signal pattern-1) or dimeric (N ~ 18, secondary signal patterns) states were found for PTPRJ-pep19 and PTPRJ-pep24. For PTPRJ-pep23, decay rates associated to any proton resonance pointed to higher aggregate states (on average, a trimer). Low solubility of PTPRJ-pep5 prevented to obtain good quality DOSY spectra for this peptide.

It is also possible that observed oligomers undergo chemical exchange with higher molecular weight aggregates which cannot be observed directly by solution state NMR methods since their NMR resonances are broadened beyond the detection level. To confirm this hypothesis STD-NMR experiments were also performed [4]. On-resonance irradiation induces higher intensity STD signals in the case of PTPRJ-pep5 and PTPRJ-pep23 compared to PTPRJ-pep19 and PTPRJ-pep24 (Table 1) suggesting that high molecular weight aggregation states of the formers are present in solution.

In conclusion, two PTPRJ ligands have been identified by means of innovative biochemical and biological approaches. NMR studies have been carried out in order to investigate conformational properties of compounds. NMR analysis of our peptides suggest that active peptides PTPRJ-pep19 and PTPRJ-pep24 can form dimers in aqueous solution, the first folding as β-hairpin around Thr[6]. On the other hand, the same studies reveal that PTPRJ-pep5 and PTPRJ-pep23 have a tendency to aggregate in higher molecular weight aggregates which could account for their biological inactivity.

Taking into account the reported information, further study, still in progress, are involved for identifying novel more potent, peptide and/or peptidomimetic ligands for PTPRJ.

References

1. Ostman, A., et al. *Nat. Rev. Cancer* **6**, 307-320 (2006).
2. Wu, D., et al. *J. Magn. Res. Ser. A* **115**, 260-264 (1995).
3. Wilkins, D.K., et al. *Biochemistry* **38**, 16424-16431 (1999).
4. Mayer, M., Meyer, B. *Angew. Chem. Int. Ed.* **38**, 1784-1788 (1999).

Enhancement of VEGF-Binding Peptide Potency by α-Helical Extensions

Yanwen Fu, Jie Huang, Bin Liu, Ping Jin, Joel Desharnais, Bryan Oates, Jing-Yu Lai, Venkata R. Doppalapudi, David Tumelty, Curt W. Bradshaw, and Abhijit Bhat

CovX, Pfizer Biotherapeutics Research and Development, San Diego, CA, 92121, U.S.A.

Introduction

Vascular endothelial growth factor (VEGF)-mediated angiogenesis plays a critical role in tumor growth and metastasis and VEGF inhibition has been actively investigated as a potential anti-cancer therapy. We have been investigating structure-based modifications of known VEGF-binding peptides in an attempt to improve their affinity. The phage-derived VEGF-binding peptide is a disulfide-constrained 19-mer (VEPNCDIHVMWEWECFERL) [1]. Previous studies indicated that these peptides have defined solution structures upon binding to VEGF and that a short helical fragment at the peptide C-terminus (EWECFERL) is critical for its binding [2]. We have examined whether enhanced interactions could be induced between the trapping peptides and VEGF by extending the peptides at their C-termini. A series of two and four residues were added to the end of the helical fragment generating an amphipathic helical pattern. We found that the modified peptides gained a 2-8 fold increase over the original motif in inhibition of the interaction between VEGF and its receptor.

Results and Discussion

We have designed a C-terminal extension to the original motif v114 based on the existing helical fragment (Figure 1). Residue 20 and 21, a hydrophobic and hydrophilic amino acid respectively, were added to the peptide C-terminus, generating an amphipathic pattern. Lys or Arg was placed at sequence position 21 in an attempt to form a salt bridge with Glu^{17} (*i* to *i +4*). Residue 22 and 23 were added following the same rule. The peptides were synthesized and evaluated for their ability to inhibit the interaction between human VEGF and its receptor VEGF2 using competitive ELISA (Table 1). The addition of Ala-Lys (A) and Phe-Lys (B) to the peptide C-terminus did not improve the potency, while addition of Met-Lys (C) lead to an 8-fold increase of inhibition IC50 over the original motif. It was unlikely that peptide C adopted a more helical structure than A and B and thus induced enhanced activity. Ala and Phe could possess similar propensity as Met in stabilizing the helical structure as elucidated by circular dichroism experiments (data not shown). To study whether additional extensions would increase the trapping peptide's potency, we have added two more residues to the C-terminus of A and B (Table 1, peptide D-I). It was observed that five out of six designed compounds had improved inhibitory efficacy over both the parental peptides and the original motif. There were
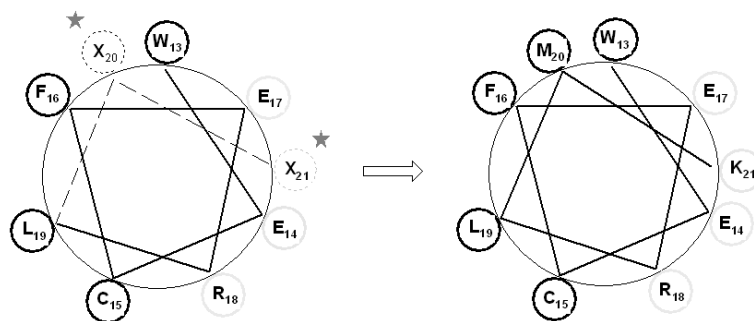
Fig. 1. Helical wheel of the peptide C-terminus fragment.

Table 1. Peptide potency in VEGF/VEGFR2 competitive binding ELISA

Peptide	Sequence	IC50 (nM)[a]
v114[b]	VEPNCDIHVMWEWECFERL	195
A	VEPNCDIHVMWEWECFERL<u>AK</u>	362
B	VEPNCDIHVMWEWECFERL<u>FK</u>	265
C	VEPNCDIHVMWEWECFERL<u>MK</u>	25
D	VEPNCDIHVMWEWECFERL<u>AKEM</u>	68
E	VEPNCDIHVMWEWECFERL<u>AKEL</u>	72
F	VEPNCDIHVMWEWECFERL<u>AKEF</u>	115
G	VEPNCDIHVMWEWECFERL<u>FKEA</u>	51
H	VEPNCDIHVMWEWECFERL<u>FKEL</u>	79
I	VEPNCDIHVMWEWECFERL<u>FKEW</u>	325

[a] *Average value of n=1-4;* [b] *Literature peptide [2]*

two factors that might contribute to the enhanced activity of the VEGF trapping peptides. Firstly, the C-terminal extension stabilized the helical fragment, thus strengthening existing interactions between the peptides and VEGF, and secondly, the added residue(s) participated in the intermolecular interactions, either binding to VEGF or blocking the VEGF-VEGFR2 interface, therefore inducing an enhanced inhibitory activity.

In summary, we have optimized a phage-derived, VEGF-binding peptide through structure-based chemical modifications. Further structural studies of the extended peptide-VEGF interaction are being carried out to elucidate this enhanced activity effect.

Acknowledgments

References

1. Fairbrother, W.J., et al. *Biochemistry* **37**, 17754-17764 (1998).
2. Pan, B., et al. *Journal of Molecular Biology* **316**, 769-787 (2002).

Development of Readthrough Peptides from Dipeptidic Antibiotics (+)-Negamycin for Duchenne Muscular Dystrophy Chemotherapy

Yoshio Hayashi[1,2], Akihiro Taguchi[1], Mayuko Ina[1], Yuri Yamazaki[1], Fumika Yakushiji[1], Thomas Regnier[2], Shigenobu Nishiguchi[2], Yoshiaki Kiso[2], Masataka Shiozuka[3], and Ryoichi Matsuda[3]

[1]*Department of Medicinal Chemistry, Tokyo University of Pharmacy and Life Sciences, Tokyo, 192-0392, Japan;* [2]*Department of Medicinal Chemistry, Kyoto Pharmaceutical University, Kyoto, 607-8412, Japan;* [3]*Department of Life Sciences, University of Tokyo, Tokyo, 153-8902, Japan*

Introduction

Duchenne muscular dystrophy (DMD) is the most common children's muscular dystrophy, which primarily affects males and is characterized by progressive skeletal muscle weakness. A part of this genetic disease is caused by the defect in the muscle protein "dystrophin" by the nonsense mutation, which is a point mutation with a premature termination codon (PTC), namely stop codon, in the DNA sequence. Recently, it was reported that both the aminoglycoside antibiotic, gentamicin, and the less toxic (+)-negamycin **1** [1] restore dystrophin expression in skeletal and cardiac muscles of *mdx* mice, an animal model of DMD with the nonsense mutation in the dystrophin gene [2]. Hence, these compounds are recently designated as "readthrough compounds" that can skip PTC during protein biosynthesis and produce a functional protein with the full protein sequence. We focused on the dipeptidic antibiotics (+)-**1** (Figure 1) as a promising new therapeutic lead compound for the development of a DMD or other genetic disease drug caused by nonsense mutation.
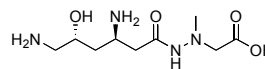
*Fig. 1. Structure of (+)-negamycin **1**.*
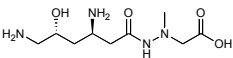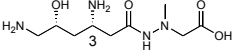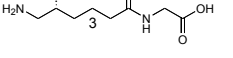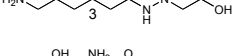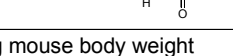
Results and Discussion

We recently developed a new synthetic route for (+)-**1** from commercially available achiral Boc-Gly-H using modern organic chemistry techniques, including asymmetric allylboration, microwave-assisted ruthenium catalyzed cross-metathesis and asymmetric Michael addition to afford (+)-**1** with an overall yield of 41% in 8 steps [3].

Current efforts with this synthetic approach have been expanded into Medicinal Chemistry to discover new peptidomimetic drug candidates with a suitable readthrough activity for chemotherapy of DMD. We synthesized several derivatives with the functional groups removed and substituted or with the different stereochemistry, via our new synthetic route. The readthrough activity of some synthetic derivatives was showed in Table 1 with the ratios of the activity against a positive control gentamycin. A 3-desamino- and glycine-derivative **N3** exhibited a slightly higher readthrough activity than (+)-**1**, although no antimicrobial activity was observed. This suggests that the readthrough activity in eukaryotic cells could be distinguished from the antimicrobial activity against prokaryote cells.

To understand the further biological properties of **N3** *in vivo*, the serum creatine kinase (CK) level, which is a clinical indicator of muscular dystrophy, was measured in *mdx* mice after subcutaneous injection of **N3** (1 mg) for 3 weeks. As a result, a significant decrease of the CK level in **N3**-treated *mdx* mice was observed in comparison to the untreated controls. This suggests that **N3** protects the muscle tissues collapse in *mdx* mice (Figure. 2). In addition, partial dystrophin expression in the skeletal muscle of *mdx* mice was confirmed by the immunohistochemical analysis (data not shown). Moreover, the acute toxicity of **N3** was evaluated by the body weight change in *mdx* mice. During the s.c. administration of the compounds (1 mg/ day) for 4 weeks, **N3** exhibited a slight slowing-down of the body weight increase, while (+)-**1** exhibited a marked decrease (Figure. 3). Therefore, it can be concluded the lower toxic compound **N3** than (+)-**1** might have a potential for the long-term treatment for DMD. Development of more potent derivatives is currently under investigation.

Table 1. In vivo readthrough activity of negamycin derivatives

Compound	Structure	Relative Read-through Activity (READ mice)	Anti-microbial Activity
Gentamicin		1.00 ± 0.24	+
N1 (+)-Negamycin		1.00 ± 0.25	+
N2		1.01 ± 0.16	±
N3		1.36 ± 0.14	—
N4		0.83 ± 0.13	—
N5		1.01 ± 0.07	NT

0.1 mg/day/20 g mouse body weight   NT = not tested
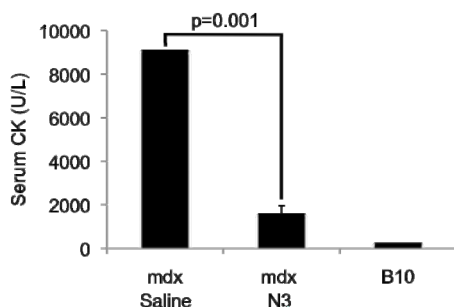
Fig. 2. Effect of N3 on serum creatine kinase level in mdx mice.
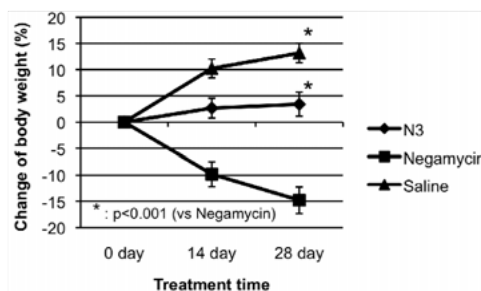
Fig. 3. Effect of negamycin or N3 on body weight change of mdx mice.

Acknowledgments

References

1. (a) Hamada, M., Takeuchi, T., Kondo, S., Ikeda, Y., Naganawa, H., Maeda, K., Okami, Y., Umezawa, H. *J. Antibiot.* **23**, 170-171 (1970); (b) Uehara, Y., Hori, M., Umezawa, H. *Biochim. Biophys. Acta.* **374**, 82-95 (1974).
2. Arakawa, M., Shiozuka, M., Nakayama, Y., Hara, T., Hamada, M., Kondo, S., Ikeda, D., Takahashi, Y., Sawa, R., Nonomura, Y., Sheykholeslami, K., Kondo, K., Kaga, K., Kitamura,T., Suzuki-Miyagoe, Y., Takeda, S., Matsuda, R., et al. *J. Biochem.* **134**, 751-758 (2003).
3. (a) Hayashi, Y., Regnier, T., Nishiguchi, S., Sydnes, M. O., Hashimoto, D., Hasegawa, J., Katoh, T., Kajimoto, T., Shiozuka, M., Matsuda, R., Node, M., Kiso, Y. *Chem. Commun.* 2379-2381 (2008); (b) Nishiguchi, S., Sydnes, M. O., Taguchi, A., Regnier, T., Kajimoto, T., Node, M., Yamazaki, Y., Yakushiji, F., Kiso, Y., Hayashi, Y. *Tetrahedron* **66**, 314-320 (2010).

Polymeric Combination Therapy Based on Host Defence Peptides Targeting Cancer Cells

Graeme Kelly[1], Angnieszka Foltyn-Afria Kai[2], Siobhan McClean[2], Yvonne Smith[c], Judy Harmey[3], and Marc Devocelle[1]

[1]*Pharmaceutical and Medicinal Chemistry, Royal College of Surgeons, 123 St. Stephens green, Dublin 2., Ireland;* [2]*Centre of Microbial Host Interaction, Institute Technology Tallaght, Dublin 24, Ireland;* [3]*Department of Molecular and Cellular Therapeutics, Royal College of Surgeons, 123 St. Stephens green, Dublin 2., Irleland*

Introduction

Chemotherapy combinations have being the mainstays in the treatment of most types of cancer in the past half century [1]. Multi-drug therapies may circumvent mechanisms of tumour resistance to single agents and potentially provide greater therapy benefits if the selected agents act synergistically in combination. The aim of the project is to develop a multi component drug delivery system by combining a classical cytotoxic drug, doxorubicin (DOX), and a host defence peptide (P18) to a polymeric carrier [2]. A polymer of ethylene glycol (PEG) was chosen as the carrier because of its non-toxic and non-immunogenic properties. Pegylation of a peptide can also improve its pharmacokinetic properties and enhance its accumulation in tumour tissue by the "enhanced permeability and retention (EPR) effect". A method for the reversible pegylation of P18 (H-kwkflkklpflkhalkkf-NH$_2$), a hybrid sequence of cecropin A (1-8) and magainin 2 (1–12) with known anticancer activity and its conjugation and/or combination with a classical anticancer agent was originally developed. In this approach, the P18 sequence assembled from D-amino acids is elongated at its N-terminus by a short peptide linker Gly-L-Phe-L-Leu-Gly. This GFLG sequence is a substrate of the endo-lysosomal cathepsin B enzyme, a protease over-expressed in cancer cells. The N-terminal amino group of this linker is amidated with a bi-functional PEG (H$_2$N-PEG-COOH) in which the amino group is modified with a hydrazide linker for conjugation of doxorubicin via a hydrazone bond. The latter is stable at neutral pH, but can be hydrolysed in the lysosome at pH < 4.5. Pegylation of doxorubicin can be used to prevent its toxicity and target its delivery to malignant cells by the EPR effect. Following passive accumulation in the tumour and cellular uptake by endocytosis, it is proposed that release of the anticancer peptide and classical agent could occur in the lysosome of cancer cells, thereby allowing their combined and selective delivery. While the synthetic feasibility study for the production of these conjugates was successfully completed, the linear multi-step synthetic strategy implemented was not amenable to convenient scale-up. Furthermore, the design of these polymeric prodrugs limit their application to a 1:1 doxorubicin-peptide ratio, which might not be adequate due to the significant difference in the anticancer activities of these two candidates (nanomolar range for doxorubicin, micromolar range for P18). An alternative approach based on the combination of individually pegylated peptide and doxorubicin was therefore developed to study their potential synergistic/additive effects.

Results and Discussion

Peptides were synthesized by Solid Phase Peptide Synthesis (SPPS) according to the Fmoc/tBu strategy from a Rink Amide MBHA PEGA resin. The sequences of P18 and the cathepsin B-sensitive linker were assembled by automated synthesis on an Applied Biosystems 433A. A pegylated peptide containing a di-glycine motif in place of the cathepsin B-sensitive linker was also synthesized as a negative control. The mono-functional PEG was added manually using HATU coupling chemistry. The peptides and their pegylated counterparts were characterized by Mass Spectrometry (Maldi-Tof MS) using a-cyano-4-hydroxy-cinnamic acid matrix. The peptides/ PEGylated peptides were purified by reverse-phase or size-exclusion chromatography, respectively, and analyzed by RP-HPLC semi preparative on a C18 Gemini/C5 Jupiter columns respectively, using a buffer system Acetonitrile/Water containing 0.1% TFA). Their purity was analyzed by RP-HPLC (Analytical C18 Gemini Column, buffer system Acetonitrile/Water containing 0.1% TFA).Doxorubicin was pegylated by formation of a hydrazone bond with a hydrazide PEG reagent. The latter was synthesized by attachment of a Fmoc-protected

bi-functional PEG (H_2N-PEG-COOH) on Rink Amide MBHA PEGA resin. After Fmoc deprotection, the amino group was amidated with *S*-benzyl-thiosuccinic acid, followed by reaction with hydrazine. The hydrazide PEG was then cleaved from the solid support and reacted in solution with doxorubicin. Cells were cultured in 96-well plates (10,000 cells/well) in a complete medium [Dulbecco's modified eagle medium (DMEM)] with 10% FBS for 4T1.2Luc cells, ovarian human non-malignant cells, SKOV3 ovarian cancer cells, and RPMI 1640 with 10% FBS for A2780P ovarian cancer cell. After 24h of incubation, cells were treated with peptides (0-200 lg/ml) and incubated for another 24h or 72h (cell line dependent). Cell viability was measured with the MTT or MTS assay using the CellTiter 96-cell proliferation assay kit (Promega, Madison, WI), and the IC_{50} value was calculated as the concentration of peptide that induced 50% growth inhibition compared to a untreated control (Table 1).

Table 1. Activities (IC_{50}) of prepared conjugates

	P18	*MeO-PEG$_{5000}$-GFLG-P18*	*MeO-PEG$_{2000}$-GFLG-P18*	*MeO-PEG$_{2000}$-GG-P18*	*NH$_2$-PEG$_{5000}$-DOX*	*MeO-PEG$_{2000}$-GFLG-P18 PEG$_{5000}$-DOX*	*DOX*
4t1.2 Luc Breast Cancer *	16µM	59 µM	NT	NT	NT	NT	NT
A2780P Ovarian Cancer Cell *	2.2µM	NT	6.3 µM	87 µM	29.8 µM	2.93 µM	98nM
Hs832 Ovarian Non-malignant cell **	5.8µM	42.3 µM	19 µM	51.8 µM	>100	NT	>100
SKOV3 Ovarian Cancer Cell **	17.4µM	65.3 µM	39.4 µM	77.9 µM	>100	NT	>100

The activity differentials between MeO-PEG$_{2000}$-GFLG-P18 and MeO-PEG$_{2000}$-GG-P18 indicate that the former pegylated peptide can constitute a cathepsin B-sensitive polymeric prodrug. The results obtained with MeO-PEG$_{2000}$-GFLG-P18 and MeO-PEG$_{5000}$-GFLG-P18 show that better reactivation can be achieved with a shorter PEG length. Preliminary results (n=1) of a combination study involving MeO-PEG$_{5000}$ DOX and MeO-PEG$_{2000}$ GFLG-P18 indicates that there is an additive/synergistic effect between the compounds. Poor reactivation of doxorubicin appears to be achieved from PEG$_{5000}$ DOX and alternative pegylation method of this agent will be investigated. The two compounds PEG$_{5000}$-DOXO and MeO-PEG$_{2000}$-GFLG-P18 were synthesized in high yields and in high purity. Preliminary results indicate that additive/synergistic effect can be achieved by the combination of these two polymeric prodrugs and warrant further combination studies.

Acknowledgments

References

1. Mader, J.S., Hoskin, D.W. *Expert Opin. Investig. Drugs* **15**, 933-946 (2006).
2. Takeshima, K., et al. *J. Biol. Chem*. **278**,1310-1315 (2003).

Potent VEGF Trapping CovX-Body with Antitumor Activity

Dingguo Liu*, Venkata R. Doppalapudi, Jie Huang, Ping Jin, Bin Liu, Lingna Li, Joel Desharnais, Jing-Yu Lai, Gang Chen, Nancy Levin, Abhijit Bhat, Curt W. Bradshaw, Gary Woodnutt, and Rodney W. Lappe

CovX Research, Biotherapeutics Division of Pfizer, San Diego, CA, 92121, U.S.A.

Introduction

CovX-Body[TM] technology enables covalent fusion of a targeting agent including a peptide, protein or a small molecule to the Fab binding site of a specially designed antibody via proprietary linkers. The resulting CovX-Body retains both the pharmacologic properties of the targeting agent and the pharmacokinetic properties of monoclonal antibodies.

As one of the most important endothelial cell specific mediator of angiogenesis and vasculogenesis, vascular endothelial growth factor (VEGF) plays an essential role in both physiological and pathological angiogenesis. Due to its involvement in numerous pathological conditions including tumor growth, diabetic retinopathy, rheumatoid arthritis and psoriasis, VEGF has become an important therapeutic target.

Herein, we would like to present the discovery of a potent VEGF trapping CovX-Body, **CVX-51**, which was identified through lead optimization of a known anti-VEGF peptide and the subsequent optimization of the CovX-Body. **CVX-51** showed favorable PK in rodents, reduced pVEGF expression in colo-205 tumor and demonstrated efficacy in multiple xenograft models.

Results and Discussion

V114 (CVX-2207) is a known anti-VEGF peptide identified through phage display showing decent binding affinity and competing with VEGFR2 [1,2]. NMR study of VEGF binding to v107, a structurally related peptide to v114, revealed its binding site similar to those of Flt-1D2 and its C-terminal is critical for VEGF binding. Therefore, we envision that C-terminal extension of lead peptide CVX-2207 might be a viable strategy to improve the binding potency by picking up some interaction sites shown in the complex of VEGF-Flt-1D2.

Table 1. Peptide optimization

Compd #	Sequence	VEGF binding IC_{50} (nM)
v107	GGNECDIARMWEWECFERL	
2207	VEPNCDIHVMWEWECFERL	107
2793	VEPNCDIHVMW**V**WECFERL	50
2838	VEPNCDIHVMW**V**WECFERL**YG**	43
2839	VEPNCDIHVMW**V**WECFERL**YGG**	32
2840	VEPNCDIHVMW**V**WECFERL**YGGG**	22
2872	VEPNCDIHVMW**V**WECFERL**YGLT**	10
2869	VEPNCDIHVMW**V**WECFERL**YGIT**	5.2
2875	VEPNCDIHVMW**V**WECFERL**YGLE**	3.1

The specially designed AZD linker was first attached to the N-terminal of lead peptide CVX-2875 and then the tethered compound was fused with our antibody scaffold CVX-2000 to generate the CovX-Body, which was observed with enhanced binding affinity (IC_{50} = 0.2 nM). To improve the PK of CovX-Bodies, tether walk (moving the linker attachment point along the peptide sequence) was implemented, which identified residue 10 as the optimal tethering point with enhancement of $T_{1/2}$ in mouse PK study while retaining the VEGF binding potency. Additionally, C-terminal stabilization via D-AA mutation further improved the PK, which led to the identification of our candidate CovX-Body **CVX-51**.
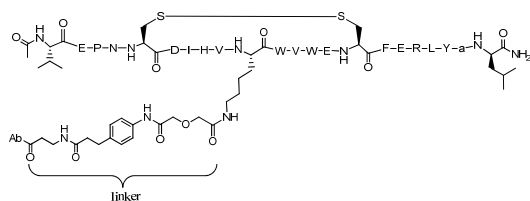
Fig. 1. Structure of CVX-51.
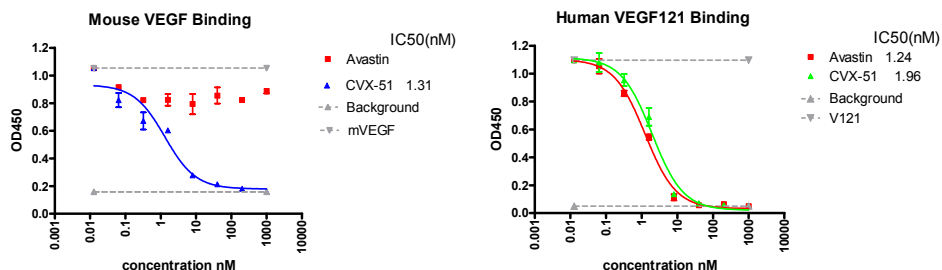
Fig. 2. CVX-51 binds to both human and mouse VEGF.
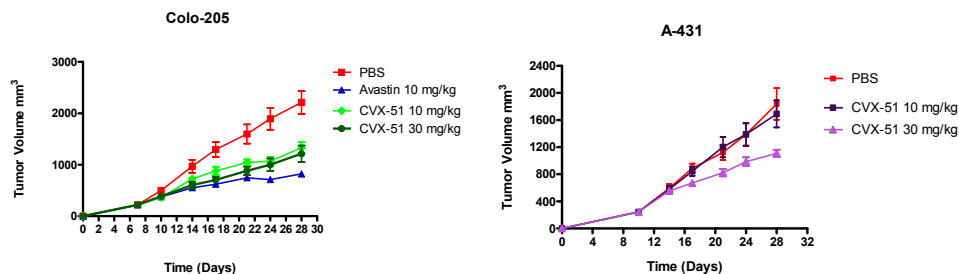
Fig. 3. CVX-51 treatment reduces tumor growth in multiple models.
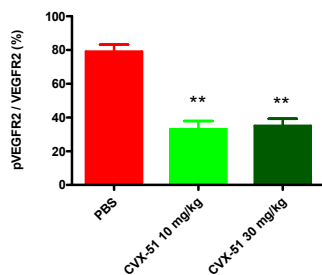
Fig. 4. CVX-51 treatment reduces pVEGFR2 in colo-205 tumor.

In summary, we demonstrated:
- C-terminal extension and optimization effectively enhanced the binding affinity of lead peptide CVX-2207.
- Tether walk and C-terminal stabilization effectively improved the PK of CovX-Body.
- Candidate CovX-Body **CVX-51** binds to both mouse and human VEGF in high affinity.
- **CVX-51** exerts tumor growth inhibition effect on Colo-205 and A-431 xenografts.

References

1. Pan, B., et al. *J. Mol. Biol.* **316**, 769-787 (2002).
2. Fairbrother, W.J., et al. *Biochemistry* **37**, 17754-17764 (1998).

Optimization of Glioblastoma-Targeting Peptide Ligand LXY1 Using One-Bead One-Compound Focused Library Approach

Ruiwu Liu[1], Wenwu Xiao[1], Harry Tseng[1], Yanlei Liu[2], Eduardo Sanchez[1], Anisha Mazloom[1], Jia Lin[1], Fernanda C. Bononi[1], and Kit S Lam[1]

[1]*Department of Biochemistry and Molecular Medicine;* [2]*Department of Pathology, University of California Davis, 2700 Stockton Blvd., Suite 2301, Sacramento, CA, 95817, U.S.A.*

Introduction

Glioblastoma, the most common type of brain tumor in adults, remains largely incurable, and surgical resection followed by radiation and chemotherapy has been shown to increase patient survival only slightly. New diagnostic and therapeutic agents against this cancer are needed. Cancer-targeting peptide ligands can be used as vehicles for the delivery of radionuclides or cytotoxic agents to tumors. Using the "one-bead one-compound" (OBOC) combinatorial library method [1], we previously identified a specific ligand LXY1 (Figure 1, cyclic cdGLG-Hyp-Nc) which targets the α3β1 integrin of U-78 MG glioblastoma cell line. *In vivo* optical [2] and radio-imaging studies demonstrated that LXY1 targets tumors well. We have recently used a focused OBOC library approach to further optimize LXY1. Some of these new α3β1 integrin ligands could be used as efficient vehicles for the delivery of imaging probes and therapeutic agents against glioblastoma.

Results and Discussion

The focused OBOC libraries were designed by fixing the motif cdG-G--c, randomizing other positions with 30-34 amino acids, including L-, D-, and other unnatural amino acids, and extending 1-2 random amino acids at the *N*-terminus and/or *C*-terminus of LXY1. This approach enabled us to probe for additional contact residues adjacent to the ligand binding site occupied by LXY1. Three focused OBOC libraries were synthesized on TentaGel resin beads and the structures were shown in Figure 1. The OBOC libraries were synthesized using a split-mix synthesis approach [1]. On-bead cell binding assay against U-87 MG cells was used to screen the libraries. Twelve positive beads, which were covered with a monolayer of U-87 cells, were identified from Library 1. Three out of the twelve positive ligands have one added L-amino acid at the *C*-terminus of LXY1. Extension of additional residues at the *N*-terminus (Libraries 2 and 3) did not yield any positive beads.
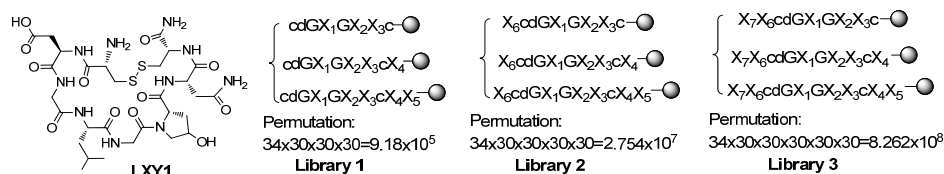
Fig. 1. Structures of three focused OBOC libraries.

A series of new ligands were designed based on screening result and previous SAR [3,4]. The sequences and biological activities of those ligands are shown in Table 1. Six new ligands (LXY5, LXY6, LXY7, LXY9, LXY14 and LXY15) showed stronger binding against U-87 cells than the lead ligand LXY1. Among them, LXY7 was the best, so it was selected for further *in vivo* targeting evaluation. Introduction of a positively charged-amino acid at the X_4 position of the C-terminal increased binding. In contrast, a negatively-charged amino acid decreased binding. At the X_1 position, the order of ligand binding affinity is Phe(3,5-diF)>Phe(3,4,5-triF)>Phe(3,4-diF). The potent ligands were synthesized in biotinylated form and their binding against U-87 cells was confirmed with flow cytometry. In addition, the tumor-targeting potential of LXY7 was confirmed *in vivo* using optical imaging. In this experiment, ligand-biotin/streptavidin-Cy5.5 tetravalent conjugate was injected via tail vein into mice bearing U-87 MG

Table 1. Resynthesized ligands and their biological activities

Ligand	X_1	X_2	X_3	X_4	Relative binding affinity[a]	IC_{50}[b] (μM)
LXY1	L	Hyp	N		1.00	3.5
LXY4	Phe(3,5-diF)	Hyp	N		1.36	0.41
LXY5	Phe(3,4,5-triF)	Hyp	N	D-T	1.45	
LXY6	Phe(3,5-diF)	Hyp	N	W	1.17	
LXY7	Phe(3,4,5-triF)	Hyp	N	R	1.62	0.13
LXY8	L	Hyp	N	D	0.22	
LXY9	Phe(3,5-diF)	Hyp	N	D-S	1.44	
LXY10	L	Hyp	D	G	0.64	
LXY11	Phe(3,4-diF)	Hyp	N	D-K	1.01	
LXY12	Phe(3,4-diF)	Hyp	N	S	0.47	
LXY13	Phe(3,4,5-triF)	Hyp	N	D	0.57	
LXY14	Phe(3,4,5-triF)	Hyp	N	D-S	1.35	
LXY15	Phe(3,5-diF)	Hyp	N	D-K	1.31	0.23
LXY16	Phe(3,5-diF)	Hyp	N	S	0.61	
LXY17	Phe(3,4-diF)	Hyp	N	G	0.65	
LXY18	Phe(3,4-diF)	Hyp	N	W	0.10	
LXY19	Phe(3,5-diF)	Hyp	S		0.84	
LXY20	L	Hyp	D-2-Thi		0.15	
LXY21	Phe(3,5-diF)	Hyp	Y		0.62	
LXY22	L	Hyp	R		0.93	

[a]Each peptide at 0.4 μM was used to compete 0.5 μM biotinylated LXY1 binding with U-87 MG cells. The relative competition effect compared to LXY1 was evaluated with the following formulation: ($_{MFI}$Positive -$_{MFI}$Sample) / ($_{MFI}$Positive -$_{MFI}$LXY1)

Positive: 0.5 μM biotinylated LXY1 only without competition. Competition: 0.5 μM biotinylated LXY1 mixed well with 0.4 μM free peptide, incubated with U-87 MG cells for 30 min. After washing, then cells were incubated with streptavidin-PE (1:500), finally samples analyzed with flow cytometry.
[b]Series of concentration of free peptides competing 0.5 μM biotinylated LXY1 binding to U-87MG cells. IC_{50} (concentration of 50% inhibition) was determined.

xenograft. After 6.5h, ex vivo near infra-red imaging was conducted. LXY7 exhibited a higher tumor targeting effect than LXY1.

Evaluation of glioblastoma-targeting of LXY7 in an orthotopic model is under way. We expect LXY7 to show good tumor targeting as well because the lead ligand, LXY1, has shown that characteristic in both models.

In summary, several more potent ligands, other than LXY1, which targeted the α3β1 integrin of glioblastoma U-87 MG cells have been identified through an OBOC focused library approach and, later, medicinal chemistry modification. LXY7 has shown good glioblastoma targeting effects *in vitro* and *in vivo*. Important SAR information has been obtained for further optimization of LXY7 to reduce the nonspecific uptake in normal organs, such as the kidney.

Acknowledgments

References

1. Lam, K.S., et al. *Nature* **354**, 82-84 (1991).
2. Xiao, W., Yao, N., Peng, L., Liu, R., Lam, K.S. *Eur. J. Nucl. Med. Mol. Imaging* **36**, 94-103 (2009).
3. Yao, N., et al. *J. Med. Chem.* **52**, 126-133 (2009).
4. Yao, N., Xiao, W., Meza, L., Tseng, H., Chuck, M., Lam, K.S. *J. Med. Chem.* **52**, 6744-6751 (2009).

A Synthetic 83 Amino Acid Long Peptide Corresponding to the Minimal Metacaspase Catalytic Domain Induces Cell Death in *Leishmania major*

Servis Catherine, Zalila Habib[*], Gonzalez Iveth, Lozano Leyder, and Fasel Nicolas

Department of Biochemistry, University of Lausanne, Epalinges, Switzerland
*Corresponding author: habib.zalila@unil.ch

Introduction

Despite a lot of controversy during the last decade, there is increasing experimental evidence that cell death (CD) is genetically programmed in lower eukaryotes. In the CD proteolytic cascade of plants and protozoa, caspases are likely replaced by metacaspases that are cysteine peptidases recognizing arginines or lysines in P1-position. Metacaspases have been found to control cell death in plants. The human protozoan parasite *Leishmania major* expresses a single metacaspase (LmjMCA) harboring a central domain with the catalytic dyad histidine and cysteine as found in caspases. Metacaspase could therefore be one of the executioners of the death pathway in *Leishmania*.

In a previous study [1] we showed that, in stress conditions, LmjMCA precursor forms were extensively processed into soluble forms containing the catalytic domain and this domain was sufficient to enhance sensitivity of parasites to hydrogen peroxide by impairing the mitochondrion function.

Results and Discussion

We tested different lengths of the LmjMCA catalytic domain and found that the overexpression of the polypeptide corresponding to amino acids 136-218 was sufficient to sensitize *L. major* mitochondria to oxidative stress as measured by the loss of mitochondrial membrane potential (Figure 1).
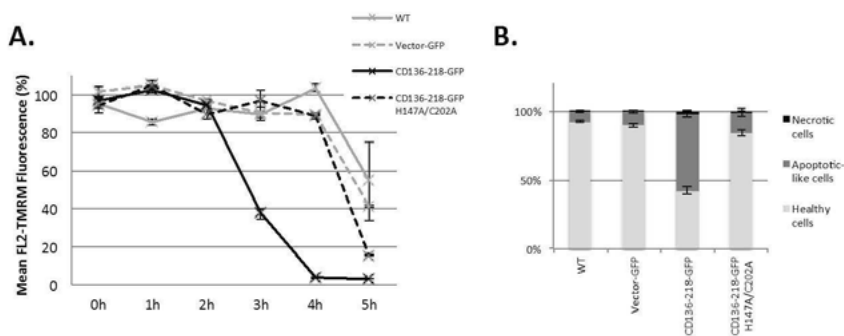
Fig. 1. In vivo characterization of CD136-218 polypeptide. (A) Mitochondrial membrane potential: parasites (WT, GFP, CD136-218-GFP and CD136-218-GFP H147A/C202A) were exposed to 0.5 mM H_2O_2, harvested every hour, incubated with the TMRM dye and analysed by flow cytometry to detect the loss of mitochondrial membrane potential. (B) Mitochondrial membrane potential (TMRM) and cell integrity (Live/Dead) analysis after 3h H_2O_2 treatment of parasites expressing wild type (WT), GFP (Vector-GFP), CD136-218-GFP or CD136-218-GFP H147A/C202A. Percentages of healthy (TMRM-positive, Live/Dead-negative), necrotic (TMRM-negative, Live/Dead-positive) and apoptotic-like cells (TMRM-negative, Live/Dead-negative) are represented by stacked columns.

We synthetized an 83aa long peptide corresponding to the minimal metacaspase catalytic domain (aa136-218). Circular dichroism studies revealed a typical α-helical structure (Figure 2) and *in vitro* enzymatic tests showed specific metacaspase activity (Figure 3).
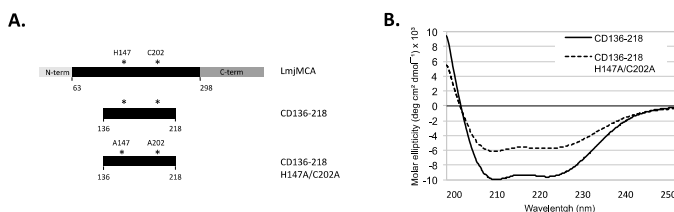
Fig. 2. Synthetic metacaspase catalytic domain CD136-218. (A) Schematic representation of LmjMCA domain composition: the central catalytic domain is shown in black. A synthetic peptide corresponding to the minimal catalytic domain (CD136-218) and its catalytically inactive version (CD136-218 H147A/C202A) have been synthesized in vitro. (B) Circular dichroism spectra of CD136-218 and CD136-218 H147A/C202A peptides.
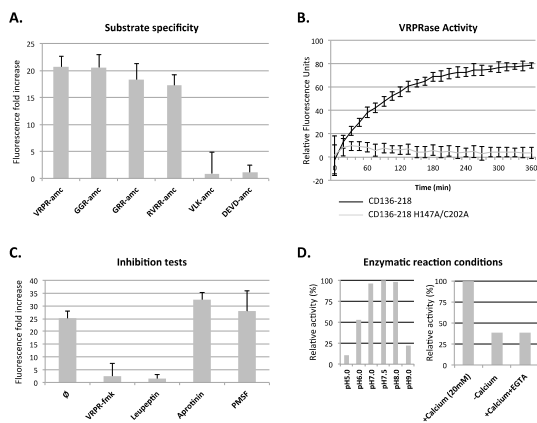
Fig. 3. In vitro characterization of CD136-218 synthetic peptide. (A) Substrate specificity of CD136-218 peptide was tested in vitro using various fluoreogenic substrates with arginine (VRPR-amc, GGR-amc, GRR-amc and RVRR-amc) or lysine (VLK-amc) in P1 position. Activity towards the caspase-3/7 substrate DEVD-amc was also tested. (B) VRPRase activity was monitored over time with CD136-218 peptide and its catalytically inactive form CD136-218 H147A/C202A. (C) VRPRase activity was measured upon pre-incubation with various inhibitors. The metacaspase specific inhibitor VRPR-fmk, the cysteine protease inhibitor Leupeptin, the trypsin inhibitor Aprotinin and the serine protease inhibitor PMSF. (D) VRPRase activity was measured in various conditions to determine the optimal pH (left panel) and assess the calcium dependency (right panel).

We are currently investigating CD136-218 peptide activity on possible metacaspase target proteins, which have been identified in a yeast two-hybrid screen or described for other organisms such as Tudor Staphylococcal Nuclease (TSN) for plant metacaspase [2] (Figure 4).
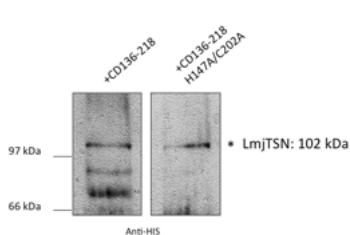
Fig. 4. CD136-218 in vitro activity towards metacaspase substrates. The Leishmania homologue of the plant metacaspase physiological substrate Tudor Staphylococcal Nuclease (LmjTSN) has been expressed in bacteria with a C-terminal His-tag and purified using affinity Nickel-columns. Purified LmjTSN was then incubated in vitro with CD136-218 or CD136-218 H147A/C202A peptides. Processing pattern was then revealed upon immunoblotting using anti-HIS antibodies. (Preliminary result).

Identifying proteins involved in the metacaspase signaling pathway will shed light on the understanding of cell death in *Leishmania* and open new perspectives in drug target investigation to fight leishmaniasis and other major infectious diseases.

Acknowledgements

References

1. Zalila, et al. *Molecular Microbiology* (2011).
2. Sundström, et al. *Nature Cell Biology* (2009).

In vitro Assessment of the Cytotoxic Effects of Hydrazide Derivatives of Unnatural Amino Acids

Tatyana Dzimbova[1], Ivan Iliev[2], Kaloyan Georgiev[3], Roumyana Detcheva[1], Anelia Balacheva[1], and Tamara Pajpanova[1]

[1]*Institute of Molecular Biology "Acad. R. Tsanev", Bulgarian Academy of Sciences, 1113, Sofia, Bulgaria;* [2]*Institute of Experimental Morphology and Anthropology with Museum, Bulgarian Academy of Sciences, 1113, Sofia, Bulgaria;* [3]*Medical University of Varna, Varna, Bulgaria*

Introduction
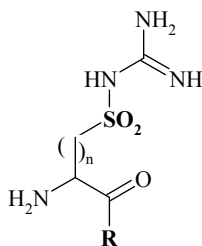
Fig. 1. Structures of sulfoarginine (n=2) (sArg) and nor-sulfoarginine (n=1) (NsArg) and their derivatives. R=NHNH₂, NHN(CH₂CH₂Cl)₂, NHNC₆H₅.

The significance of the guanidine moiety's importance in many biologically active compounds cannot be disputed. The guanidine moiety often causes significant changes in the biological activity of organic molecules.

Following our current interest in application of non-protein amino acids in preparative peptide synthesis, we have synthesized several amino acid derivatives as structural analogs of arginine and canavanine (Cav) [1,2]. Their effects on the growth of microorganisms, model plant systems and cultured tumor cells have been evaluated as well as their antitumor activity *in vivo*. We reported that modification of Cav at the carboxyl group selectively changed toxicity against bacteria, plants and leukemia cells [3,4].

In this study, the cytotoxic activities of arginine analogues sArg, NsArg, and their hydrazide derivatives (Figure 1) sArg-$CONHNH_2$, sArg-$CONHN(CH_2CH_2Cl)_2$, sArg-$CONHNC_6H_5$, NsArg-$CONHNH_2$ and NsArg-$CONHN(CH_2CH_2Cl)_2$, NsArg-$CONHNC_6H_5$ on **3T3** (standard mouse embryonic fibroblast cell line) and **HepG2** (human liver hepatocellular carcinoma cell line) cells were examined.

Results and Discussion

The synthesis of sulfoarginines and their hydrazides has been described previously [5]. The 3T3 (standard mouse embryonic fibroblast cell line) and HepG2 (human liver hepatocellular carcinoma cell line) cells were cultured as described [6]. 24 hours post seeding, the cultivated cells were treated with amino acid analogues in a wide concentration range (0.015 – 2 mM). MTT assay was performed 24 hours after treatment as described elsewhere [7]. Optical density was determined at a wavelength of 540 nm and a reference wavelength of 620 nm. PrizmaPlot.4 (ANOVA-test) was used for statistical analysis.

The cytotoxic activities of NsArg and its analogue NsArg-$CONH_2$ on 3T3 and HepG2 cells were examined (results not shown) but only the highest concentration used (2 mM) revealed cell growth inhibitory effect (42% and 17%, respectively). Some lower concentrations of sArg showed cell growth stimulating effects on 3T3 cells - statistically significant for sArg concentrations 1, 0.5 and 0.125 mM. The sArg analogues sArg-$CONHNH_2$ and especially sArg-$CONHN(CH_2CH_2Cl)_2$ exhibited higher cell growth inhibitory effects on both cell lines in comparison with the parent compound. IC_{50} for sArg-$CONHNH_2$ in 3T3 cells and HepG2 cells was 0.82 mM and 1.38 mM, respectively.

The sArg-$CONHN(CH_2CH_2Cl)_2$ showed clear cell growth inhibitory effect on both cell lines, considerably higher with the tumor cells HepG2, where statistically reliable results were achieved for the concentrations: 0.25, 0.5, 1 and 2 mM (Figure 2). Its IC_{50} values for 3T3 and HepG2 cells were 1.09 mM and 0.63 mM, respectively.
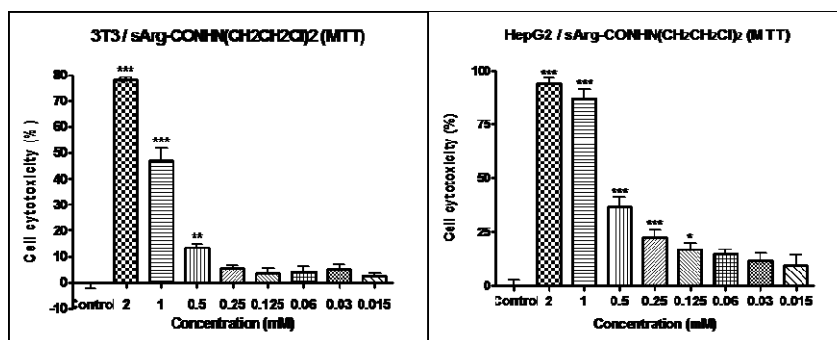
Fig. 2. Effect of sArg-CONHN(CH₂CH₂Cl)₂ on growth of 3T3 and HepG2 cells after 24 h treatment. Cell cytotoxicity determined by MTT assay is expressed as per cent of dead cells and presented as mean ± SD (n=6), **P<0.001, **P< 0.01, *P<0.05, ANOVA-test, versus the control group.

The cytotoxic activities of NsArg and its analogues NsArg-CONHNH₂, and NsArg-CONHN(CH₂CH₂Cl)₂ (Figure 3) on 3T3 and HepG2 cells were also examined. Their effects on cell growth were lower in comparison with sArg and its analogues, but an increase of the cell growth inhibitory effects was also observed with the modification of the carboxyl group.

It may be concluded that the substitution in the carboxylic group of sArg increases the cell growth inhibitory effects of the compounds, especially in the case of the *bis*-(2-
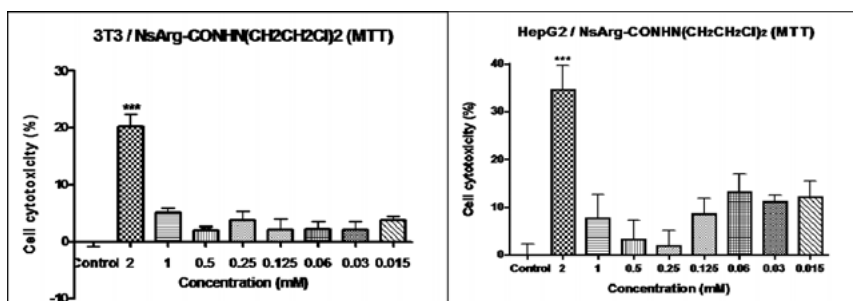
Fig. 3. Effect of sArg-CONHN(CH₂CH₂Cl)₂ growth of 3T3 and HepG2 cells after 24 h treatment. Cell cytotoxicity determined by MTT assay is expressed as per cent of dead cells and presented as mean ± SD (n=6), **P<0.001, **P< 0.01, *P<0.05, ANOVA-test, versus the control group.

chloroethyl)hydrazide substitute. The same correlation was observed in the case of NsArg and its analogues.

The results confirm our previous findings that the cell growth inhibitory effect of the compounds depends mainly on the modification in the carboxylic group.

Acknowledgments

References

1. Pajpanova, T., Stoev, S., Golovinsky, E., Krauss, G.-J., Miersch, J. *Amino Acids* **12**, 191- 204 (1997).
2. Dzimbova, T., Pajpanova, T., Golovinsky, E. *Collection Symposium Series* **6**, 12-14 (2003).
3. Pajpanova, T., Grancharov, K., Golovinsky, E., Kazakov, L., Miersch, J., Krauss, G.-J., In Ramage, R. and Epton, R. (Eds.) *Peptides 1996*, Mayflower Scientific Ltd, 1998, p. 705.
4. Miersh, J., Grancharo , K., Pajpanova, T., Neumann, D., Tabakova, S., Stoev, S., Krauss, G.-J., Golovinsky, E. *Amino Acids* **18**, 41-59 (2000).
5. Dzimbova, T., Pajpanova, T., Tabakova S., Golovinsky, E., In Cordopatis, P.A., Manessi-Zoupa, E., Pairas, G.N. (Eds.) *5th Hellenic Forum on Bioactive Peptides,* TYPORAMA, Patras, 2007, p. 223.
6. Cory, A.H., Owen, T.C., Barltrop, J.A., Cory, J.G. *Cancer Communications* **3**, 207-212 (1991).
7. Fotakis, G., Timbrell, J.A. *Toxicology Letters* **160**, 171-177 (2006).

Development of Biotin-Tagged Plinabulin Chemical Probes towards the Elucidation of Binding Mechanism of a Diketopiperazine Based Anti-Microtubule Agent

Yuri Yamazaki[1], Yui Kido[1], Yurika Masuda[1], Koushi Hidaka[2], Hiroyuki Yasui[2], Yoshiaki Kiso[2], Fumika Yakushiji[1], and Yoshio Hayashi[1]

[1]School of Pharmacy, Tokyo University of Pharmacy and Life Sciences, Hachioji, Tokyo, 192-0392, Japan; [2]Kyoto Pharmaceutical University, Kyoto, 607-8412, Japan

Introduction

'Plinabulin' (**1**, NPI-2358/KPU2), designed and synthesized previously by us from a natural diketopiperazine phenylahistin (PLH), is a potent anti-microtubule agent [1]. It was also recently shown that plinabulin functions as a strong 'vascular disrupting agent' to induce tumor-selective vascular collapse, and now under Phase II clinical trials in four countries including US as an anti-cancer drug. Although PLH exhibits colchicine-like tubulin depolymerizing activity, the chemical structure of plinabulin is different from natural colchicine-binding molecules: it has a relatively hydrophilic diketopiperazine (DKP) skeleton. Moreover, several biological assays have shown that plinabilin displays properties that are distinct from those of colchicine. Hence, it was attractive to explore the precise binding mode and microtubule depolymerization mechanism of our dehydroDKP-type inhibitor, plinabulin. To understand the binding mode of plinabulin on tubulin, we decided to perform a photoaffinity labeling study using biotin tagged plinabulin chemical probes derived from a benzophenone-containing potent derivative, KPU-244 (**2**).

Results and Discussion

Based on the structure of potent plinabulin derivative **2** including the photoreactive benzophenone group, we have successfully synthesized three chemical probes (KPU-244-B2 (**3**), KPU-244-B3 (**4**) and KPU-252-B1 (**5**)) possessing a biotin-tag on a benzophenone moiety or an oxazole ring at the opposite side (Figure 1). Since these probes all showed a significant binding ability to tubulin and cytotoxicity, we performed tubulin photoaffinity labeling study. These three probes photolabeled tubulin in a dose- or UV irradiation-time-dependent manner, and labeling was inhibited by addition of colchicine or plinabulin (Figure 2). Interestingly, probe **4** labeled tubulin as two clearly separated bands, while probe **3**, which has a shorter linker, labeled tubulin as an ambiguous broad band (Figure 2B). The immunoblot analysis
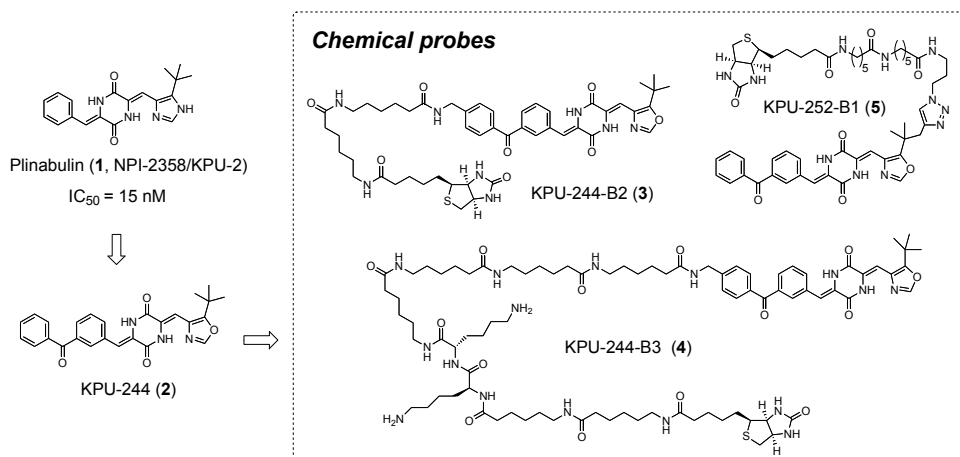
*Fig. 1. Structures of plinabulin (**1**), KPU-244 (**2**) and plinabulin chemical probes **3**–**5**.*
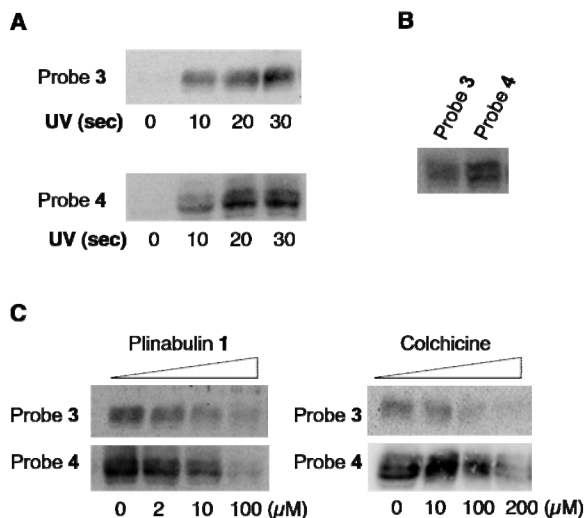
Fig. 2. Photoaffinity labeling of tubulin. (A) Photoaffinity labeling by probe **3** or **4** at different irradiation time. (B) Comparison of tubulin photoaffinity labeling between photoaffinity probes **3** and **4**. (C) Photoaffinity labeling of tubulin with probe **3** or **4** (2 μM) in the absence or presence of plinabulin **1** (2-100 μM) or colchicine (10-200 μM).

indicated that the upper and lower bands were found to be derived from α- and β-tubulin, respectively, indicating that probe **4** bound in the boundary region between α- and β-tubulin around the colchicine binding site, where it could photolabel both α- and β-tubulin subunits. In addition, probes **3** and **5** photolabeled tubulin in a similar manner, although their biotin tags are on the opposite side each other. Taken together, these results revealed that the probes serve as effective chemical probes for our diketopiperazine-type anti-microtubule agents, and their recognition sites are located around the intradimer space between the α- and β-tubulin units, near the colchicine binding site. Further analysis using the photoaffinity probes is now under way to identify the modified amino acid residues that react with the photoaffinity probe. These findings would help us understand the mechanism of binding between plinabulin derivatives and tubulin [2-4].

Acknowledgments

References

1. Nicholson, B., Lloyd, G.K., Miller, B. R., Palladino, M.A., Kiso, Y., Hayashi, Y., Neulteboom, S.T.C. *Anti-Cancer Drugs* **17**, 25-31 (2006).
2. Yamazaki, Y., Kohno, K., Yasui, H., Kiso, Y., Akamatsu, M., Nicholson, B., Deyanat-Yazdi, G., Neuteboom, S., Potts, B., Lloyd, G.K., Hayashi, Y. *ChemBioChem* **9**, 3074-3081 (2008).
3. Yamazaki, Y., Sumikura, M., Hidaka, K., Yasui, H., Kiso, Y., Yakushiji, F., Hayashi, Y. *Bioorg. Med. Chem.* **18**, 3169-3174 (2010).
4. Yamazaki, Y., Kido, Y., Hidaka, K., Yasui, H., Kiso, Y., Yakushiji, F., Hayashi, Y. *Bioorg. Med. Chem.* **19**, 595-692 (2011).

Loop Mutations in a CFTR Transmembrane Helical Hairpin

Vincent G. Nadeau[1,2] and Charles M. Deber[1,2]

[1]*Division of Molecular Structure & Function, Research Institute, Hospital for Sick Children, Toronto, M5G 1X8;* [2]*Department of Biochemistry, University of Toronto, Toronto, M5S 1A8, Ontario, Canada*

Introduction

Mutations in membrane proteins can lead to severe diseases in humans. Cystic fibrosis is such a disease, wherein a single mutation in a 1,480-residue anion channel – the cystic fibrosis transmembrane conductance regulator (CFTR) - disrupts water homeostasis across epithelial membranes [1]. CFTR is a member of the ABC transporter superfamily, and is composed of 12 transmembrane (TM) segments distributed in two TM domains, two nucleotide-binding domains (NBD), and a regulatory region. More than 300 different CF-phenotypic mutations in the TM domains of CFTR have been observed in patients [2]. A number of these mutations are found in the several membrane-embedded segments and are thought to affect protein-protein or protein-lipid interactions [3,4]. On the other hand, numerous mutations can also be found in the short extracellular loops (ECLs) of CFTR TM domains - regions with lower hydrophobicity than TM segments and potentially containing sequence specific elements that allow proper packing of TM helices. Indeed, preliminary work has shown that loop mutations in CFTR can alter the fold of adjacent helices [5]. However, data on the effect of protein sequence in this region on folding of the rest of membrane protein domains remain scarce.

Results and Discussion

To address this issue, we have mutated a CF-phenotypic position in the loop of a helix-loop-helix ('hairpin') construct of CFTR TM segments 3 and 4 (sequence: GSGMKETAAAKFER-QHMDSPDLGTDDDDKAM<u>GLALAHFVWIAPLQVALLMGLI**WELLQA**SAFAGLGFLIV-LALFQAGLG</u>LEHHHHHH, containing CFTR residues 194-241 (underlined), along with an S-tag, thrombin cleavage site, and His-tag for affinity purification; loop residues between TM helices 3 and 4 are bolded. Hairpin constructs were expressed in *E. coli* and purified according to previous protocols [4]. The Glu residue at loop position 217 was changed to residues with varying charge, size and polarity and the effect(s) of these mutations on hairpin folding were compared to the wild-type sequence, and to the previously characterized [2] E217G (CF-phenotypic) and E217S TM3/4. SDS-PAGE analysis of variants of these TM3/4 hairpins showed that mutation at E217 induced changes in the rates of migration. Indeed, charged-to-non-polar mutations (E217F, E217V) and the charge-switch mutation (E217K) increased the migration rate on PAGE, an indication that these mutations increase the number of SDS molecules bound to the hairpin construct [4] (Figure 1A). Conversely, a shortening of E217 side chain mutation decreases the E217D-SDS particle size. This relative measure of size can also be understood in terms of percent change in molecular weight versus WT (dMW%-WT) [5]. Residue variation at position E217 can change hairpin-detergent particle size by *ca.* 50% (-6.8% to 46.7%; Figure 1B). This situation is further displayed by the negative correlation observed between hydropathy and percent change in MW versus WT (Figure 1C).

The size of this membrane protein model in a membrane mimetic environment thus appears very sensitive to mutations in its loop, indicating a propensity for this small region to modify the fold of the helices it connects. The large variation in migration due to point mutations in such a short segment of this membrane protein model suggests that the wild-type sequence of this region is constrained, and has been evolved to allow proper TM domain folding. Thus, modification of an "insulator region" such as an ECL that is sensitive to changes in sequence could be sufficient to destabilize a TM domain. In the case of CF, a destabilized CFTR channel could correspondingly lead to loss of function and disease due to a mutation in the insulating loop region.
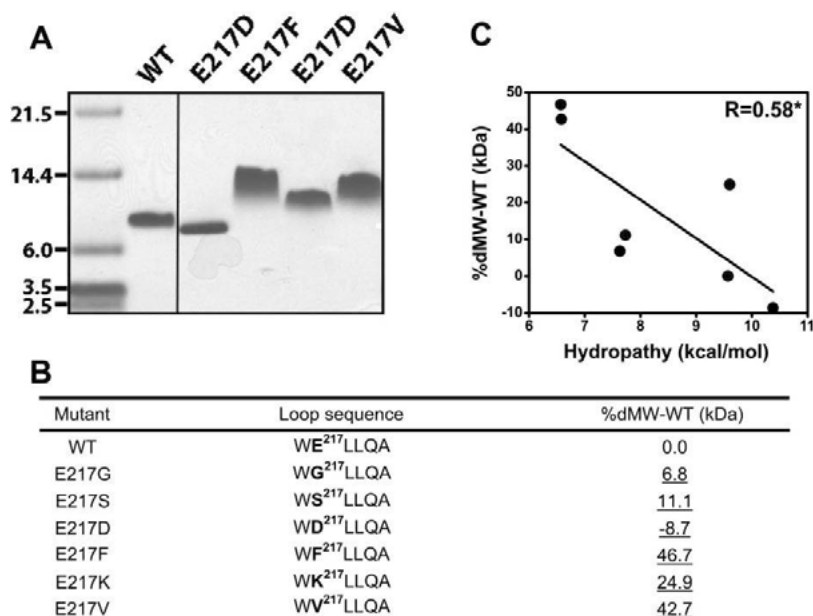
Fig. 1. Analysis of CFTR TM3/4 variants at E217. (A) SDS-PAGE migration of several TM3/4 hairpin constructs. MW markers are indicated on the right. Apparent MW according to MW markers ranges from ca. 9.0 to 14.5 kDa while the theoretical MW of these mutants varies between 9.1 and 9.6 kDa. (B) Percent change in MW versus WT values (dMW%-WT) for each mutant at position E217. Values underlined are statistically different than WT (p<0.05). Loop sequence of each TM3/4 construct is shown. (C) Correlation between the hydropathy of each mutant and their dMW%-WT values. This correlation is statistically significant (*, p<0.05). The von Heijne-Hessa biological hydrophobicity scale [6] was used to calculate the hydropathy of each TM3/4 mutant.

Acknowledgements

References

1. Gadsby, D.C., Vergani, P., Csanády, L. *Nature* **440**, 477-483 (2006).
2. Cheung, J.C., Deber, C.M. *Biochemistry* **47**, 1465-1473 (2008).
3. Choi, M.Y., Partridge, A.W., Daniels, C., Du, K., Lukacs, G.L., Deber, C.M. *J. Biol. Chem.* **280**, 4968-4974 (2005).
4. Rath, A., Glibowicka, M., Nadeau, V.G., Chen, G., Deber, C.M. *Proceedings of the National Academy of Sciences* **106,** 1760-1765 (2009).
5. Wehbi, H., Rath, A., Glibowicka, M., Deber, C.M. *Biochemistry* **46,** 7099-7106 (2007).
6. Hessa, T., Meindl-Beinker, N.M., Bernsel, A., Kim, H., Sato, Y., Lerch-Bader, M., Nilsson, I., White, S.H., von Heijne, G. *Nature* **450,** 1026-1030 (2007).

Cell Penetration Properties of Pituitary Adenylate Cyclase-Activating Polypeptide

Ngoc-Duc Doan, Thi Tuyet Mai Nguyen, Myriam Létourneau, David Chatenet, and Alain Fournier*

Laboratoire International Associé Samuel de Champlain (INSERM – INRS-Université de Rouen);
INRS - Institut Armand-Frappier 531 boulevard des Prairies, Ville de Laval, QC, H7V 1B7, Canada

Introduction

The Pituitary Adenylate-Cyclase Activating Polypeptide (PACAP), a C-terminally α-amidated neuropeptide, exists as two equiactive isoforms PACAP27 and PACAP38 that exert pleiotropic activities, including functions as a hypophysiotropic hormone, neuromodulator, and neurotrophic factor [1,2], all mediated through the activation of their receptors (PAC1, VPAC1 and VPAC2) [3]. Recently, the presence of intracellular PACAP receptors was reported [4] raising the possibility that PACAP could act as an intracrine factor. Based on its propensity to interact with the cellular membrane, its amphipatic character, and the numerous basic residues dispersed throughout its C-terminal helical domain, it is highly possible that PACAP could cross the plasma membrane in a receptor-independent manner. In this present work, we demonstrated the propensity of both PACAP isoforms to reach the intimal cell compartment by a receptor-independent mechanism. Moreover, the presence of functional PACAP receptors in nuclear fractions of various rat tissues was also observed.

Results and Discussion

Using confocal microscopy on living cells, we demonstrated that both PACAP isoforms penetrate into CHO-K1 cells non-expressing PACAP receptors and that the fluorescent signal was detected in the cytoplasm and the nucleus (Figure 1). Similar distribution was also observed in HEK 293 and HeLa cells giving evidence that they can enter into different cell types. Surprisingly, the highly basic segment PACAP(28-38), which also possesses a helical secondary structure, showed no cell-penetrating property. Using flow cytometry, we showed that the uptake potency of fluorescent-labeled PACAP27 was comparable to TAT(48-60), the well known CPP. Interestingly, PACAP38-associated fluorescence was 3-times higher than for TAT(48-60) (Figure 2). Altogether, these results provide evidence that PACAP38 and PACAP27 cellular uptake could not only be a receptor-mediated event.
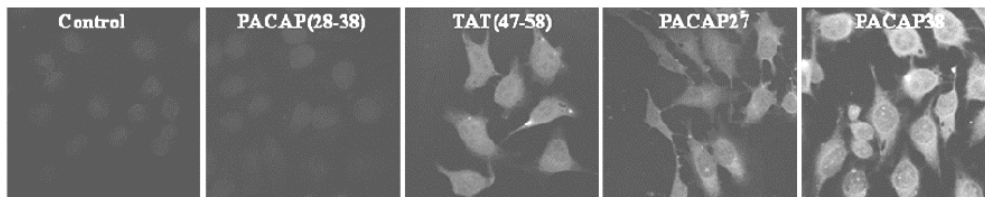
Fig. 1. Distribution of FITC-conjugated PACAP(28-38), TAT(48-60), PACAP27, and PACAP38 in living untransfected CHO-K1 cells as observed by confocal microscopy. Nuclei were stained with DRAQ5^TM.

When incubated at 4°C, both isoforms were still able to translocate within the internal compartment of CHO-K1 cells. However, the cellular uptake, as observed by flow cytometry analysis, was significantly reduced by up to 80% in all cell lines thus suggesting that both direct translocation and endocytosis pathways are involved in the internalization process of these peptides. Exploration of the mechanisms involved in PACAP cellular uptake was performed using specific inhibitors of endocytosis. Treatment of cells with nystatin, MβCD, NH$_4$Cl, chloroquine or maleimide had no noticeable impact on PACAP isoforms cellular uptake. However, when treated with clathrin-coated endocytosis inhibitors such as hypertonic sucrose, chlorpromazine, a significant decrease in cellular uptake of both PACAP isoforms was observed. Finally, pre-treatment with amiloride, a commonly used macropinocytosis inhibitor,

caused a high diminution in cellular uptake of both PACAP isoforms. These results indicated that the cellular uptake of these peptides are dependent of the clathrin-dependent endocytosis and macropinocytosis pathways.
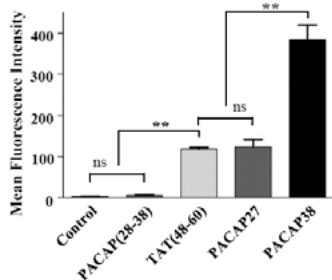
Fig. 2. Transduction efficiency of FITC-labelled peptides in CHO-K1 cells. Cells were incubated for 1h with fluo-rescent peptides $(10^{-6}M)$ before FACS analysis.

From kinetic studies of PACAP cellular uptake, we suggested that both peptides could also possess the ability to exit the cells by crossing the plasma membrane. To test this possibility, exit kinetic of radioactive materials was determined. We found that the percentage of cytosolic radioactive species cells decreased with time. A similar phenomenon was also observed by flow cytometry with a decrease of cellular fluorescence in CHO-K1 cells. Next, following the incubation of CHO-K1 cells with PACAP38 $(10^{-5}M)$ and the subsequent removal of membrane-bound peptide, cells were re-suspended in FBS-free media. MS and RP-HPLC analysis of the existing materials showed the presence of intact PACAP38, as the main peptide species, as well as 13 other fragments including PACAP27. These data strongly indicated that even though the neuropeptide can be degraded in the cytoplasm, a significant amount of not only PACAP38 but also PACAP27 can also exit the cells in order to activate neighboring cells.

In addition, the presence of PACAP nuclear binding sites was evaluated in five different nuclear extracts from rat brain, spleen, adrenal gland, kidneys and testis. Photolabeling experiments on rat nuclear fractions showed the presence of only one protein specifically and covalently labelled by the [Bpa^0]PACAP27 analog in all preparations except kidney isolated nuclei. Noteworthy, using CHO-PAC1 transfected cells as a control, a similar band at 67 kDa was also detected. Binding experiments were then used to further evaluate the specificity of these binding sites for PACAP. We found that, with the exception of the kidney, PACAP27 was able to significantly displace the radioligand from nuclear binding sites. Interestingly, using isolated testis nuclei incubated with a Fura-red:Fluo-4 indicator mixture, an increase of the FL-1/FL-2 ratio was noticed following the addition of PACAP38 $(10^{-7}M)$. A significant release of intranuclear calcium was still observed at 10^{-9} M, indicating a concentration-dependent effect of PACAP on calcium release. Moreover, our results showed that PACAP27 and PACAP38 but not VIP were able to upregulate de novo DNA synthesis in testis nuclei and that this effect was abolished by PACAP(6-38). Altogether, these results suggest that the receptor present at the nuclear membrane is functional and might be related to PAC1 receptors.

In conclusion, we demonstrated for the first time the propensity of PACAP isoforms to reach the intimal cellular space in a receptor-independent manner in order to probably activate its cytosolic and nuclear binding sites. These cell-penetrating properties of the neuropeptide PACAP were never reported and might explain in part the subnanomolar activities often associated with PACAP. Although the physiological role of intracellular PACAP receptors remains to be investigated, our findings suggest that this intracellular GPCR could be associated with specific biological activities that should be taken into account during the development of PACAP-based drug.

Acknowledgments

References

1. Miyata, A., et al. *Biochem. Biophys. Res. Commun.* **164**, 567-574 (1989).
2. Miyata, A., et al. *Biochem. Biophys. Res. Commun.* **170**, 643-648 (1990).
3. Vaudry, D., et al. *Pharmacol. Rev.* **61**, 283-357 (2009).
4. Li, M., et al. *Endocrine.* **23**, 59-75 (2004).

Influence of Epitope Multiplicity, Attachment Mode and Orientation on the Immune Response of Multiple Antigenic Peptides

M. Monsó[1], E. Blanco[2], C. Cubillos[2], N. Moreno[2], F. Sobrino[3], D. Andreu[1], and B.G. de la Torre[1]

[1]Department of Experimental and Health Sciences, Pompeu Fabra University, Barcelona, Spain; [2]CISA-INIA, Valdeolmos, Spain; [3]Severo Ochoa Center for Molecular Biology-CSIC, Madrid, Spain

Introduction

Multiple presentation of antigenic sequences as MAP dendrimers [1-3] can significantly enhance immunogenicity over monomeric peptides and result in improved immunogens and synthetic vaccines [4]. We have recently reported a vaccine candidate of this type (B_4T), with a T-cell epitope branching out into 4 copies of a B-cell epitope, conferring total protection against foot-and-mouth disease virus [5]. Here we inspect how B epitope multiplicity, the N- or C-terminal attachment of the B epitope to the branching core, as well as the type of linkage used to this end, affect the immunogenicity of the dendrimeric construct.

Results and Discussion

Mono- (BT), di- (B_2T) and tetravalent (B_4T) constructs (Table 1) were made by thioether ligation (Figure 1a) to evaluate the effect of epitope multiplicity on immunogenicity. For each
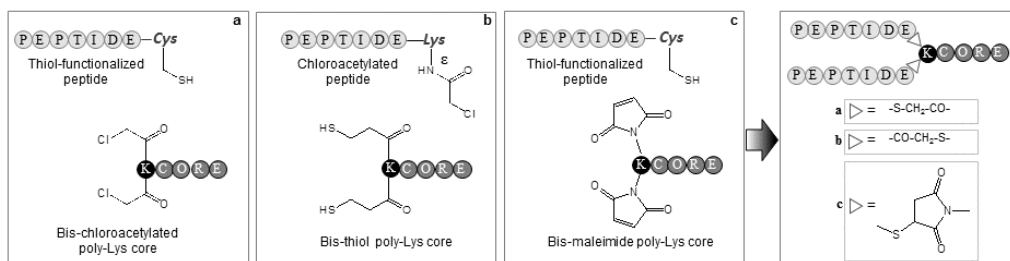
Fig. 1. Ligation approaches to MAP constructs. a) Standard thioether, b) reverse thioether, c) maleimide.

construct, nine mice were immunized with two 100 μg doses (day 0, complete Freund's adjuvant; day 20, incomplete adjuvant). In the B_2T- and B_4T-immunized groups, 100% of the mice showed an immune response, whereas BT- and B-immunized mice gave 33% and 55% response, respectively. Interestingly, the antibody response was better for B_2T than for B_4T-vaccinated animals (Figure 2a), and the population of IFNγ-producing spleen cells was also higher for the B_2T group (Figure 2c) upon stimulation with cognate peptide. For

Table 1. Dendrimeric constructions synthesized

MAP[a]	Linkage	N/C terminal attachment	Multiplicity
BT		C-terminal	1 copy
B_2T	Standard thioether		
D1		N-terminal	2 copies
D2	Reverse thioether		
D3	Maleimide	C-terminal	
B_4T	Standard thioether		4 copies

[a]B epitope is PVTNVRGDLQVLAQKAART; T epitope is KKAAIEFFEGMVHDSIK

FMDV-stimulated splenocytes, however, best performers were mice vaccinated with the B_4T dendrimer.

To evaluate the effect of the linkage used for epitope-to-core ligation, a dimeric model was chosen and the ligation chemistries outlined in Figures 1a-c, standard thioether (B_2T), reverse thioether (D2) and maleimide (D3), were examined. *In situ* TCEP reduction in the reverse thioether ligation (Figure 1b) is advantageous in preserving continuously reactive thiols, with low enough TCEP levels to pose no risk to ClAc groups. Standard ligation [4], in contrast, suffers from substantial dimerization of the thiol-bearing B epitope. The maleimide approach (Figure 1c) is valuable in that its pH<7 conditions also avoid dimerization, hence reduce B epitope requirements. ELISA showed D3 to be the best immunogen, followed by B_2T (Figure 2b). Despite its synthetic appeal, the D2 (reverse thioether) construct was the poorest immunogen.

To assess the influence of either N- or C-terminal orientation of the B epitope, a dendrimer (D1) with the B epitope linked to the Lys core via an N-terminal Cys was compared to B_2T. A clear advantage for C-terminal attachment (B_2T) was found, D1 being the only immunogen for which no antibody response was found after a single dose (Figure 2b). On the other hand, D3 and D1 performed better than B_2T and D2 in terms of IFNγ production (Figure 2d).

On the basis of these results we conclude that (i) multimeric presentation enhances peptide immunogenicity only to a certain extent, as shown by the slightly better response of B_2T over B_4T; (ii) the type of linkage between the B epitope and the branched Lys-T epitope core does influence immunogenicity, maleimide and standard thioether linkages performing best; (iii) while appendage of the B epitope by the N-terminus has a slight improvement on the cellular immune response, it has an adverse effect on the humoral response, with significant antibody titers detectable only after a booster.
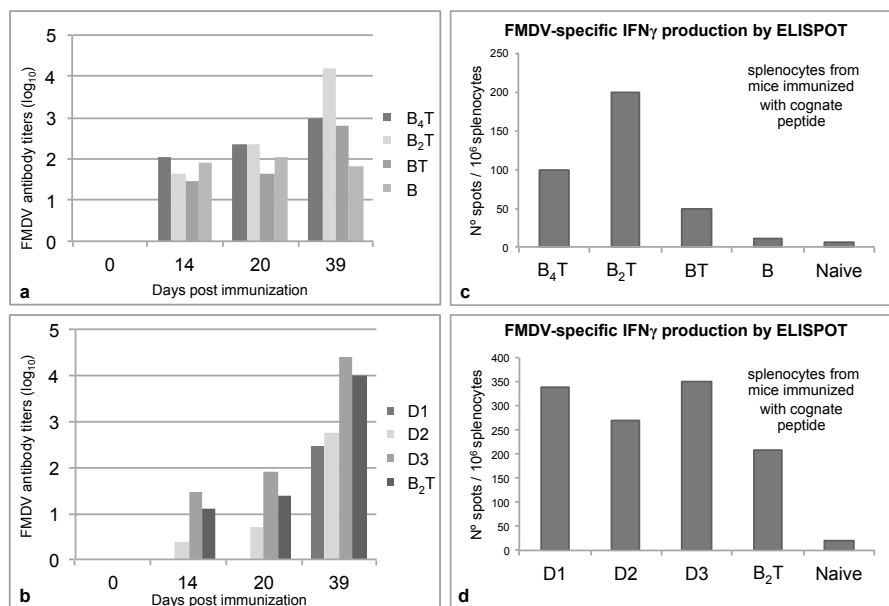
Fig. 2. Antibody (panels a,b) and interferon γ production (panels c,d) responses of mice vaccinated with dendrimeric constructs.

Acknowledgments

References

1. Tam, J.P. *Proc. Natl. Acad. Sci. U.S.A.* **85**, 5409-5413 (1988).
2. Mezö, G., Mihala, N., Andreu, D., Hudecz, F. *Bioconj. Chem.* **11**, 484-491 (2000).
3. Krikorian, D., et al. *Biopolymers* **84**, 383-399 (2006).
4. Lu, Y.A., et al. *Mol. Immunol.* **28**, 623-630 (1991).
5. Cubillos, C., et al. *Journal of Virology* **82**, 7223-7230 (2008).

Chemical Generation of Bispecific Antibodies from Peptide Pharmacophores

B. Liu*, V. Doppalapudi, J. Huang, D. Liu, P. Jin, L. Li, J. Desharnais, C. Hagen, N. Levin, M. Shields, M. Parish, R. Murphy, J. Rosario, B. Oates, J. Lai, M. Matin, Z. Ainekulu, A. Bhat, C. Bradshaw, G. Woodnutt, G. Chen, Y. Fu, D. Tumelty, J. Rizzo, and R. Lappe

CovX Research, Biotherapeutics Division of Pfizer, San Diego, CA, 92121, U.S.A.

Introduction

Bispecific antibodies have been pursued by the research community over the last two decades. However, most technology platforms are highly complex, suffering from challenging manufacture and lacking of product homogeneity issues. In addition, any modifications to the antibody constructs are quite difficult and time consuming, therefore slow down the process of optimizing the bispecific agents to reach desirable properties.

Recently we developed a novel bispecific CovX-Body platform which provided a versatile solution to those problems. Two different targeting peptides are joined together by a branched azetidinone linker to construct a heterodimer moiety, which is subsequently programmed to a scaffold antibody under mild conditions in a site-specific manner to form the bispecific CovX-Body. While the peptide pharmacophores are responsible for target functions, the antibody scaffold imparts IgG like long half-life and distribution properties to the CovX-Body.

A unique feature of this platform is that the peptide heterodimer pharmacophores can be

Fig. 1. Generation of bispecific CovX-Body.

chemically modified for the desired binding affinity, potency and pharmacokinetics based on the therapeutic requirement. Furthermore, different combination of targeting peptides leads to completely new bispecific agents. The integration of medicinal chemistry with recent advances in bioconjugation techniques and recombinant antibody technology allows rapid generation, optimization and production of bispecific antibodies (Figure 1 and 2).

Results and Discussion

Fig. 2. Synthesis of peptide heterodimer with azetidinone linker.

Here, we present CVX-241, an angiopoietin2 (Ang2) and vascular endothelial growth factor (VEGF) targeting bispecific CovX-Body, as an example of this technology. VEGF and Ang2 are two important tumor angiogenesis growth factors which are over-expressed in renal, skin, colon, breast and many other cancers. The increased expression of both VEGF and Ang2 has also been shown to correlate with poor survival rate in patients. Thus, inhibition of both pro-angiogenic factors simultaneously may provide better benefit to cancer patients with elevated expression levels of both factors.

Optimization of the peptide heterodimer pharmacophores plays a critical role in generating the bispecific CovX-Body with balanced target binding affinity and desired pharmacokinetic profile. Intensive trials on the composition of each peptide pharmacophore, the site of linker attachment, and the composition and length of the spacers finally lead to CVX-241, a bispecific CovX-Body with optimal pharmacodynamic and pharmacokinetic properties. The resulting CVX-241 binds both VEGF and Ang2 with sub-nanomolar affinity, demonstrates excellent half-life in rodents and non-human primates, exhibits efficacy equivalent to the combination of the corresponding monospecific CovX-Bodies and shows profound synergy with chemotherapy in tumor xenograft models (Table 1, Figure 3). This novel synthetic biologic combines clinically validated VEGF inhibition with Ang2 inhibition into one molecule and is currently in phase-1 clinical trials.

Table 1. Optimization of peptide pharmacophores plays a critical role

CVX	VEGF* C-Modif.	Tether position		PEG length VEGF, Ang2	IC$_{50}$ (nM)		Simu. Binding (VEGF)	Mouse T$_{1/2}$ (hr)	
		VEGF	Ang2		VEGF	Ang2		VEGF	Ang2
3067		K1		4,4	0.36	0.44	Fair	18	51
3027	(dL)K(Ac)	K10		4,4	7.1	0.50	Poor	-	-
3025		K12		4,4	31.4	0.60	ND	-	-
241			K11	4,4	0.7	0.6	Fair+	116	115
3129	Y(dA)(dL)	K10		4,0	1.1	0.5	Fair	90	52
3130				0,0	2.9	0.6	Fair	109	73
3131				0,4	2.3	0.5	Fair	144	98
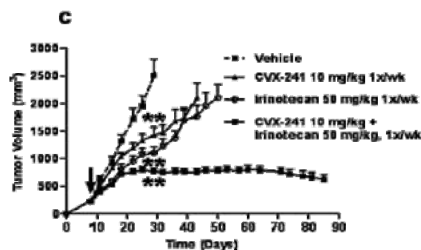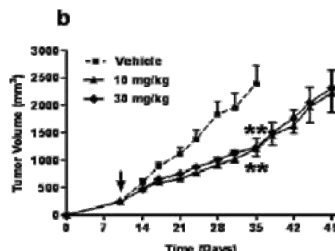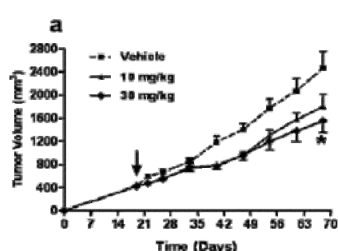
CVX-241 (i.p., once weekly) significantly inhibits tumor growth in staged MDA-MB-435 breast carcinoma (a) and A431 skin carcinoma (b) xenograft models. (c) Combination of CVX-241 and irinotecan displays greater antitumor effect and dramatically delayed tumor growth compared with the single agents alone

Fig. 3. CVX-241 Shows profound synergy with chemotherapy.

References

1. Doppalapudi, V.R., et al. *Proc. Natl. Acad. Sci. U.S.A.* **107**(52), 22611-22616 (2010).
2. Huang, H., et al. *Clin. Cancer Res.* **17**(5), 1001-1011 (2011).

Preparation of Anti-β-Functionalized γ,δ-Unsaturated Amino Acids via Asymmetric Thio-Claisen Rearrangement and Using Them for the Synthesis of Novel Cyclic Melanocortin Analogues

Zhihua Liu, Sukeshi J. Mehta, Kwang-Soo Lee, Bryan Grossman, and Victor J. Hruby

Department of Chemistry & Biochemistry, 1306 E. University Blvd, University of Arizona, Tucson, AZ 85721, U.S.A.

Introduction

Amino acids carrying unsaturations are important building blocks in peptide design and synthesis [1-3]. The versatile reactivities of the double bond offer unprecedented convenience to chemically modify peptides. Therefore, they are extremely useful chemical tools in peptide sciences. Among the efforts of adding tools into the peptide chemistry box, we report here a synthesis of anti-β-functionalized γ,δ-unsaturated amino acids via a Claisen rearrangement with $FeBr_3$ catalyzed allylation. This reaction has very mild reactions condition and is highly selective for anti isomers. Amino acids generated were used for the synthesis of a cyclic peptide via ring-closing metathesis [4], and a novel Melanocortin cyclic carba analogue was prepared.
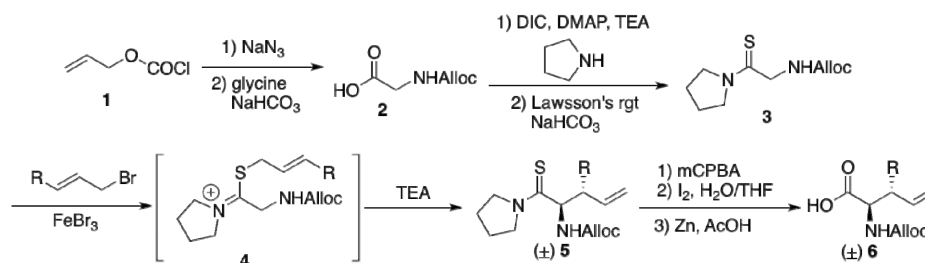
Fig. 1. Asymmetric synthesis of thioamide derivatives via thio-Claisen rearragement.

Table 1. Results of amino acids generation

Entry	Product	anti/syn[a]	Yields[b]
6a		15/1	53
6c		>49/1	80

[a]*Determined by ^{1}H-NMR.* [b]*Isolated yield of total isomers.*

Results and Discussion

The N^α-alloc glycine is not commercially available, and was prepared by reacting freshly prepared alloc azide with glycine [5]. Subsequent amide formation and thionation reaction afforded thioamide compound **3**. The thioamide was then treated with allyl bromide in the presence of $FeBr_3$, for 24-48 h at 45°C, then cooled to -78°C and 1.2 equivalent of TEA was added [6]. Presumably, this afforded the thio-enol ether, which rearranged upon raising the reaction temperature. Rearrangement product **5** was isolated with excellent anti/syn selectivities. Noticeably, since only TEA is required in this reaction, the reaction condition is a lot milder as compared with LDA/nBuLi treatment in our previous studies [6,7]. Amino acid generation was achieved by an oxidation-iodolactonization-reduction method. Thioamide **5** was converted to amide with mCPBA treatment, and subsequent hydrolysis removed the pyrollidine auxiliary and afforded an iodolactone. A Zn reductive elimination reaction opened the lactone ring and

furnished the desired amino acid with no loss of asymmetry. Results of the last three-step reaction were summarized in Table 1.

With alloc-protected β-substituted γ,δ-unsaturated amino acids in hand, we decided to investigate the synthesis of cyclic melanocortin peptide dicarba analogues. The synthesis was carried out via standard solid phase peptide synthesis methods using the Fmoc strategy. The alloc group was removed via a Pd(PPh$_3$)$_4$ treatment. The last amino acid was used as Boc protected for the convenient concomitant Boc removal during the peptide cleavage step. After the assembly of the linear peptide sequence **7** and **8**, peptides were subjected to a microwave assisted ring-closing metathesis condition for 1h. Peptides were cleaved from resin and deprotected by using 95% TFA with 2.5% H$_2$O and 2.5% TIPS. We successfully isolated the 21-membered ring cyclic peptide products **9**, which contain cis/trans isomers as expected. However, there were no cyclic products observed with peptide **8**, only starting material was recovered after cleavage. We assume ring strains might be one of the factors to prevent the cyclization since forming an 11-membered ring is highly disfavored. We also consider using a DPhe in the peptide may facilitate the ring closure in the case of 7, because our previous studies suggested this D-amino acid induces a β-turn structure in the peptide backbone, making the two terminal double bonds spatially close.

Scheme 1. Synthesis of melanocortin peptide cyclic dicarba analogues.
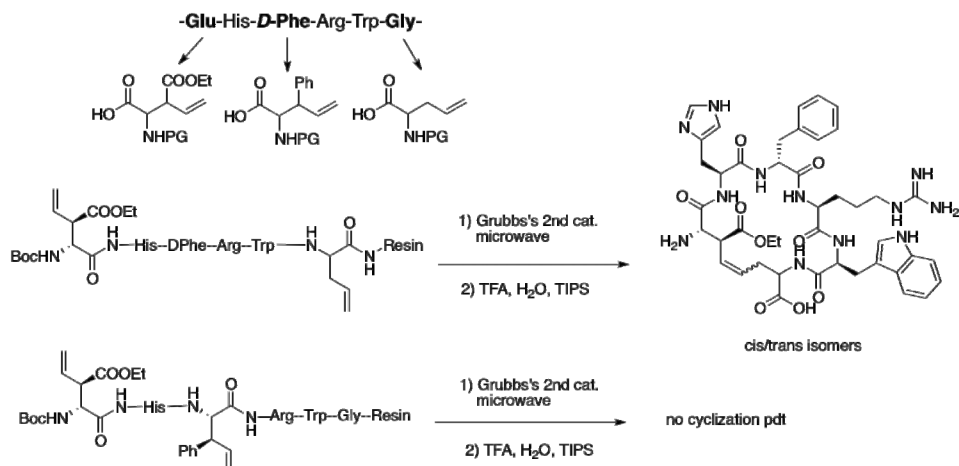
In summary, we have developed a novel methodology for synthesizing β-substituted γ,δ-unsaturated amino acids via asymmetric thio-Claisen rearrangement. This new method also uses much milder conditions, which offered excellent anti/syn ratios and functional group compatibility. Novel amino acids obtained were successfully applied in the synthesis of melanocortin peptide cyclic analogues via ring-closing metathesis.

Acknowledgments

References

1. Sawyer, T.K. In *Peptidomimetic and Nonpeptide Drug Discovery: Impact of Structure-Based Drug Design*; Veerapandian, P., Ed.; Marcel Dekker: New York, 1997, pp 559-634.
2. Lin, Y.A., Chalker, J.M., Davis, B.G. *J. Am. Chem. Soc.* **132**, 16805-16811 (2010).
3. Blackwell, H.E., Sadowsky, J.D., Howard, R.J., Sampson, J.N., Chao, J.A., Steinmetz, W.E., O'Leary, D.J., Grubbs, R. H. *J. Org. Chem.* **66**, 5291-5302 (2001).
4. Chatterjee, A.K., Choi, T.L., Sanders, D.P.,Grubbs, R. H. *J. Am. Chem. Soc.* **125**, 11360-11370 (2003).
5. Cruz, L.J., Beteta, N.G., Ewenson, A., Albericio, F. *Org. Process Res. Dev.* **8**, 920-924 (2004).
6. Liu, Z.H., Qu, H.C., Gu, X.Y., Lee, K.S., Grossman, B., Kumirov, V.K., Hruby, V.J. *Tetrahedron Lett.* **51**, 3518-3520 (2010).
7. Liu, Z., Qu, H., Gu, X., Min, B.J., Nichol, G.S., Nyberg, J., Hruby, V.J. *Org. Lett.* **10**, 4105-4108 (2008).

Solid-Phase Peptide Synthesis: State of the Art

Fernando Albericio,[1,2,3] Ayman El-Faham,[1,4] Myriam Gongora-Benitez,[1,3] Ramon Subirós-Funosas,[1,3] and Judit Tulla-Puche[1,3]

[1]*Institute for Research in Biomedicine, Barcelona Science Park, 08028, Barcelona, Spain;* [2]*Department of Organic Chemistry, University of Barcelona, 08028, Barcelona, Spain;* [3]*CIBER-BBN, Networking Centre on Bioengineering, Biomaterials and Nanomedicine, Barcelona Science Park, 08028, Barcelona, Spain;* [4]*Department of Chemistry, Faculty of Science, Alexandria University, Alexandria, Egypt;*

Introduction

The last years have witnessed the so-called peptide revolution. Peptides have moved from just biochemical tools to a consistent alternative to small organic molecules as therapeutic drugs. Lately, peptides are becoming cornerstones of emerging fields such as drug delivery, nanotechnology or new functional materials. However, this revolution could not be possible without the extraordinary creativity and work of a large number of synthetic peptide chemists. Herein, we would like to pay honor to two outstanding scientists, the Nobel Laureate Bruce Merrifield and Louis Carpino. Whereas Bruce was the inventor of the Solid-Phase approach and greatly contributed to development of the Boc/Bzl chemistry, Louis introduced the two most important α-amino protecting groups, Boc and Fmoc groups, as well as a second generation of coupling reagents based on HOAt.

Results and Discussion

The basis for solid-phase peptide synthesis are the solid support, a proper combination of protecting groups, and a right choice of coupling reagent.

Although, polystyrene is still the most employed solid support, the use of more hydrophilic ones such as the ChemMatrix® resin is advisable for the synthesis of large and/or complex peptides. ChemMatrix®, which is totally based in polyethyleneglycol chains and presents excellent swelling in a broad range of solvents, facilitates the incorporation of the incoming residues as well as the removal of the Fmoc protecting group [1]. Even when using ChemMatrix® resin, the synthesis of well structured peptides could be problematic. In these cases, the concourse of pseudoPro dipeptides, which prevent the interchain aggregation, results in improved purity of the final product. Thus, peptides which are not amenable to synthesis employing polystyrene resins, can be prepared combining both ChemMatrix® resin and pseudoPro dipeptides [2].

Although Boc/Bzl strategy is more suited than the Fmoc/tBu one for the synthesis of large peptides, the latter is more convenient for conventional laboratories as well as for large scale synthesis due to the fact that it implies less hazardous reagents. Moreover, the synthesis of cyclic and/or branched peptides requires a third orthogonal protecting group, which is usually based on the allyl chemistry. In addition, synthesis of sophisticated and/or fragile peptides depend on additional protecting groups such as pNZ, removable by tin chloride [3].

Special consideration is required by Cys, which is a key residue for the preparation of a large number of biologically active peptides as well as bioconjugates finding broad applications in the nanotechnology field. Nonetheless, Trt and Acm, the most common Cys protecting groups, show several drawbacks. To begin with, they are not orthogonal to each other, and additionally, the Acm removal conditions (I_2) may result in scrambling if other disulfide bridges are already formed and/or in modification of other residues such as Tyr or Trp. With the aim of introducing more suitable Cys protecting groups, Phenylacetamidomethyl (Phacm), which is compatible with both Boc and Fmoc synthetic strategies, has been recently reported [4]. Phacm is eliminated in similar conditions that Acm and, in addition, by the action of the penicillin amidohydrolase (PGA, E.C.3.5.1.11) enzyme. The combination of Phacm and a PGA from *E. coli*, covalently immobilized on an amino acrylic resin, exhibits promising applications in peptide synthesis and opens new perspectives for further purposes [5].

Coupling reagents or "there's more than one way to skin a cat". What is the best coupling reagent? Could just a single coupling reagent be used for all amide and ester bond formations? These are recurrent questions, proposed very often by students, conference attendees, and even oneself. In this matter, the answer is definitely "no". Unfortunately, a coupling reagent that can

be used for all couplings does not exist, and even in the same synthesis different coupling reagents are employed. In addition to the price, it is important to consider several parameters, such as: (i) manual or automatic synthesis; (ii) use excess or defect of coupling reagents; and (iii) presence of other functional groups in the molecule(s) involved in the reaction.

Activation of the carboxyl group is normally carried out by carbodiimides in the presence of hydroxyl-containing molecules or by stand-alone reagents such as onium salts, which also present a hydroxyl-based moiety. Both strategies act through active ester formation. *N*-Hydroxylamines are the most common hydroxyl-containing additives/components used in peptide couplings. In this sense, benzotriazole-based additives and derived coupling reagents have prevailed in the past decades over other templates such as benzotriazines, triazoles, succinimides or pyridinones. However, the presence of consecutive nitrogens in these structures derive in explosive profiles. After September 11, these properties have seriously compromised their overseas transport and consequently, their commercial availability. Alternatively, recently introduced oxime-based templates such as ethyl 2-cyano-2-(hydroxiimino)acetate (Oxyma Pure®) stand as a reliable, efficient, and safe family of coupling reagents, showing in many cases enhanced solubility and reactivity than HOAt in demanding sequences [6]. COMU®, the uronium salt derived from Oxyma Pure®, containing a morpholine moiety in its carbon skeleton, and PyOxim®, the corresponding tris-pyrrolidinophosphonium analogue, have superseded HOBt derivatives in terms of yield and absence of racemization. Furthermore, Oxyma Pure® can be used to minimize some of the most frequent side-reactions that occur during peptide synthesis (aspartiimide formation and double incorporation of a residue due to the premature Fmoc removal from the incoming Pro at the *N*-terminal).

In conclusion, continuous work in peptide chemistry methodology will be translated in new peptide based drugs and other biochemical tools.

Acknowledgments

References

1. García-Martín, F., Quintanar-Audelo, M., García-Ramos, Y., Cruz, L.J., Gravel, C., Furic, R., Côté, S., Tulla-Puche, J., Albericio, F. *J. Comb. Chem.* **8**, 213-220 (2006).
2. García-Martín, F., White, P., Steinauer, R., Côté, S., Tulla-Puche, J., Albericio, F. *Biopolymers (Peptide Science)* **84**, 566-575 (2006).
3. Isidro-Llobet, A., Guasch-Camell, J., Álvarez, M., Albericio. F. *Eur. J. Org. Chem.* 3031-3039 (2005).
4. Royo, M.. Alsina, J., Giralt, E., Slomcyznska, U., Albericio, F. *J. Chem. Soc. Perkin Trans.* **1**, 1095-1102 (1995).
5. Góngora-Benítez, M., Basso, A., Bruckdorfer, T., Tulla-Puche, J., Albericio. This volume.
6. Subirós-Funosas, R., Prohens, R., Barbas, R., El-Faham, A., Albericio, F. *Chem. Eur. J.* **15,** 9394-9403 (2009).
7. Subirós-Funosas, R., El-Faham, A., Albericio, F. This volume.

Author Index

Keyword Index